



Universitat Autònoma de Barcelona

**ADVERTIMENT.** L'accés als continguts d'aquesta tesi queda condicionat a l'acceptació de les condicions d'ús establertes per la següent llicència Creative Commons:  [http://cat.creativecommons.org/?page\\_id=184](http://cat.creativecommons.org/?page_id=184)

**ADVERTENCIA.** El acceso a los contenidos de esta tesis queda condicionado a la aceptación de las condiciones de uso establecidas por la siguiente licencia Creative Commons:  <http://es.creativecommons.org/blog/licencias/>

**WARNING.** The access to the contents of this doctoral thesis it is limited to the acceptance of the use conditions set by the following Creative Commons license:  <https://creativecommons.org/licenses/?lang=en>



**Biological assessment of novel series of  
Multitarget-Directed Ligands based on  
donepezil to be used in  
Alzheimer's disease therapy**

**Gerard Esteban Conde**

**PhD Thesis**

Bellaterra, 2015





Universitat Autònoma de Barcelona  
Departament de Bioquímica i de Biologia Molecular  
Unitat de Bioquímica de Medicina

Mercedes Unzeta López, professor at the Universitat Autònoma de Barcelona and José Luis Marco Contelles, professor at the Instituto de Química Orgánica General (CSIC),

CERTIFY:

That the thesis entitled “**Biological assessment of novel series of Multitarget-Directed Ligands based on donepezil to be used in Alzheimer’s disease therapy**” presented by Gerard Esteban Conde to obtain the PhD degree in Neurosciences from the Universitat Autònoma de Barcelona, has been conducted under the direction of the Institute of Neurosciences and the Department of Biochemistry and Molecular Biology at the Universitat Autònoma de Barcelona, which is able to be reviewed and evaluated by the corresponding academic committee.

PhD student

Thesis supervisor

Thesis supervisor

Gerard Esteban Conde

Mercedes Unzeta López

José Luis Marco Contelles

Bellaterra (Cerdanyola del Vallès), 2015  
Barcelona



This thesis has been conducted under the following funding sources:

- Proyecto SAF referencia: SAF2009-0727 (Secretaría de Estado e Investigación, MICIN) titulado “Diseño, síntesis y evaluación farmacológica de nuevas propargilaminas neuroprotectoras para el tratamiento de la enfermedad de Alzheimer”.
- Proyecto SAF referencia: SAF2012-33304. Ministerio de Economía y Competitividad. Dirección General de Investigación Técnica) titulado “Moléculas basadas en donepecilo con capacidad para interactuar con los sistemas monoaminérgico, colinérgico y secuestrador de metales pesados para la enfermedad de Alzheimer”.
- Project COST Action CM1103, funded by the COST European Commission Directorate-General for Science, Research and Development (2011-2015).



---

**TABLE OF CONTENTS**

<b>INDEX.....</b>	<b>i</b>
<b>LIST OF ABBREVIATIONS.....</b>	<b>vii</b>
<b>RESUM.....</b>	<b>xi</b>
<b>ABSTRACT.....</b>	<b>xiii</b>
<b>I. INTRODUCTION.....</b>	<b>1</b>
<b>1. Ageing, neurodegeneration and Alzheimer’s disease.....</b>	<b>3</b>
<b>i. Familial Alzheimer’s disease.....</b>	<b>6</b>
<b>ii. Sporadic Alzheimer’s disease.....</b>	<b>7</b>
<b>2. Pathophysiology of Alzheimer’s disease.....</b>	<b>7</b>
<b>i. Cholinergic hypothesis.....</b>	<b>7</b>
a. Acetylcholinesterase.....	9
b. Butyrylcholinesterase.....	11
<b>ii. Amyloid hypothesis.....</b>	<b>14</b>
a. Amyloid precursor protein and presenilins.....	17
<b>iii. Tau hypothesis.....</b>	<b>18</b>
<b>iv. Oxidative stress.....</b>	<b>19</b>
<b>v. Biometal dyshomeostasis.....</b>	<b>22</b>
a. Role of copper.....	23
b. Role of zinc.....	24
c. Role of iron.....	26
<b>vi. Monoaminergic neurotransmission impairment.....</b>	<b>29</b>
a. Monoaminergic systems.....	29
i. DAergic system in AD.....	31
ii. NAergic system in AD.....	32

---

iii.	Serotonergic system in AD.....	33
iv.	Monoamine oxidases.....	34
<b>vii.</b>	<b>Neuroinflammation.....</b>	<b>37</b>
<b>3.</b>	<b>Therapeutic strategies against Alzheimer’s disease.....</b>	<b>39</b>
<b>i.</b>	<b>FAD-approved drugs.....</b>	<b>39</b>
a.	Cholinergic agents: Cholinesterase inhibitors (ChEI)....	40
i.	Tacrine.....	40
ii.	Donepezil.....	40
iii.	Rivastagmine.....	41
iv.	Galantamine.....	42
b.	Glutamatergic agents: NMDA receptor antagonists.....	42
i.	Memantine.....	42
<b>ii.</b>	<b>Drugs under development.....</b>	<b>43</b>
a.	Secretase modulators.....	43
i.	Tarenflurbil.....	43
ii.	EVP-0962.....	43
iii.	Avagacestat.....	44
iv.	Etazolate.....	44
b.	Amyloid-based approaches.....	44
i.	TC-6683.....	44
ii.	Affitope AD02.....	45
iii.	Bapineuzumab.....	45
iv.	Solaneuzumab.....	45
v.	Gantenerumab.....	46
vi.	Crenezumab.....	46
c.	Muscarinic receptor antagonists.....	46
d.	Glutamatergic agents.....	47

---

e. Serotonergic agents: 5-HT receptor modulators.....	47
f. Anti-tau therapies.....	48
i. Rember.....	48
ii. Epithilone D.....	48
iii. T-817MA.....	49
g. Monoamine oxidase inhibitors (MAOI).....	49
i. Selegiline or <i>l</i> -deprenyl.....	53
ii. Rasagiline.....	53
iii. Safinamide.....	54
iv. PF9601N.....	55
h. Other single-target approaches.....	55
i. Multi-Target-Directed Ligands (MTDL).....	55
i. Ladostigil.....	57
ii. M-30 and M-30D.....	59
iii. Clioquinol.....	62
iv. PBT2.....	63
v. ASS234.....	63
vi. Other MTDLs.....	65
i. Berberine-derived ligands.....	65
ii. Memoquin.....	66
vii. Natural products for use in AD.....	66
i. Huperzine A.....	67
ii. EGCG.....	67
iii. Resveratrol.....	68
iv. Curcumin.....	68
<b>II. AIMS.....</b>	<b>69</b>
<b>III. MATERIAL AND METHODS.....</b>	<b>73</b>

---

<b>IV. RESULTS</b> .....	85
<b>Chapter I.</b> “Kinetic and structural analysis of the irreversible inhibition of human monoamine oxidases by ASS234, a multi-target compound designed for use in Alzheimer’s disease”.....	87
<b>Chapter II.</b> “ <i>In vitro</i> and <i>in vitro</i> modulation of the monoaminergic neurotransmitters by multi-target compound ASS234”.....	101
<b>Chapter III.</b> “Multipotent cholinesterase/monoamine oxidase inhibitors for the treatment of Alzheimer's disease: design, synthesis, biochemical evaluation, ADMET, molecular modeling, and QSAR analysis of novel donepezil-pyridyl and donepezil-indolyl hybrids”.....	132
<b>Chapter IV.</b> “Donepezil + propargylamine + 8-hydroxyquinoline hybrids as new multifunctional metal-chelators, ChE and MAO inhibitors for the potential treatment of Alzheimer's disease”.....	167
<b>Chapter V.</b> “Biological assessment of the novel multi-target compound DPH-4, a donepezil-propargylamine+8-hydroxyquinoline hybrid with anti-A $\beta$ aggregation, antioxidant, anti-inflammatory and anti-apoptotic properties for potential use in Alzheimer’s disease”.....	211
<b>V. DISCUSSION</b> .....	241
<b>VI. CONCLUSIONS</b> .....	249
<b>VII. LIST OF REFERENCES</b> .....	253
<b>VIII. ANNEXES</b> .....	293

---

<b>Annex I.</b> “Synthesis, biological assessment and molecular modelling of new multipotent MAO and cholinesterase inhibitors as potential drugs for the treatment of Alzheimer’s disease” .....	295
<b>Annex II.</b> “A therapeutic approach to cerebrovascular diseases based on indole-substituted hydrazides and hydrazines able to interact with human vascular adhesion protein-1, monoamine oxidases (A and B), AChE and BuChE” .....	301
<b>Annex III.</b> “Catecholaminergic and cholinergic systems of mouse brain are modulated by LMN diet, rich in theobromine, polyphenols and polyunsaturated fatty acids” .....	311
<b>Annex IV.</b> “Protective effect of the multitarget compound DPH-4 on human SSAO/VAP-1-expressing hCMEC/D3 cells under oxygen-glucose deprivation conditions, an <i>in vitro</i> experimental model of cerebral ischemia” .....	323



## LIST OF ABBREVIATIONS

3D-QSAR	3-dimensional quantitative structure-activity relationship
5-HIAA	5-hydroxyindoleacetic acid
5-HT	5-hydroxytryptamine, serotonin
6-OH	6-hydroxydopamine
8-OHG	8-hydroxyguanosine
AAAD	Aromatic <i>L</i> -amino acid decarboxylase
ACh	Acetylcholine
AChE	Acetylcholinesterase
AD	Alzheimer's disease
ADMET	Absorption, distribution, metabolism, excretion and toxicity
ALS	Amyotrophic lateral sclerosis
AMPA	<i>D, L</i> - $\alpha$ -amino-3-hydroxy-5-methyl-isoxazolpropionic acid
AP-1	Activator protein-1
ApoE	Apolipoprotein E
APP	Amyloid precursor protein
ARE	Antioxidant response elements
ATCC	American Type Culture Collection
ATP	Adenosine triphosphate
A $\beta$	Beta amyloid
BACE-1	Beta site APP-cleaving enzyme-1
Bad	Bcl-2-associated death promoter
Bax	Bcl-2-like protein 4
BBB	Blood-brain barrier
Bcl-2	B-cell lymphoma-2
Bcl-XL	B-cell lymphoma-extra large
BDNF	Brain-derived neurotrophic factor
BuSCh	Butyrylthiocholine
BuChE	Butyrylcholinesterase
CaMKII	Calmodulin-dependent protein kinase II
CAS	Catalytic site
CDK-5	Cyclin-dependent kinase-5
ChAT	Choline acetyltransferase
ChEI	Cholinesterase inhibitor
CHO	Chinese hamster ovary
CLK-1	Dual specificity protein kinase

CNS	Central nervous system
Cnt	Control
COX-1/2	Cyclo-oxygenase-1/2
CQ	Clioquinol
CSF	Cerebrospinal fluid
COMT	Catechol-O-methyl transferase
DA	2-(3,4-dihydroxyphenyl)ethylamine, dopamine
DAT	Dopamine transporter
DBH	Dopamine $\beta$ -hydroxylase
DLB	Dementia Lewy bodies
DPH	Donepezil + propargylamine + 8-hydroxyquinoline
DMSO	Dimethylsulfoxide
DNA	Deoxyribonucleic acid
DOPAC	3,4-dihydroxyphenylacetic acid
EGCG	Epigallocatechin-gallate
EPO	Erythropoietin
ERK	Extracellular signal-regulated kinase
fAD	Familial Alzheimer's disease
FAD	Falvin adenine dinucleotide
FBS	Foetal bovine serum
FDA	Food and Drug Administration
FTD	Frontotemporal dementia
GABA	Gamma-aminobutyric acid
GAPDH	Glyceraldehyde-3-phosphate dehydrogenase
GDNF	Glial cell-derived neurotrophic factor
GPR39	G-protein coupled receptor 39
GPx	Glutathione peroxidase-1
GSK-3	Glycogen synthase kinase 3
H <sub>2</sub> O <sub>2</sub>	Hydrogen peroxide
HA	Histamine
HD	Huntington's disease
HFIP	1,1,1,3,3,3-hexa-fluoro-2-propanol
HIF-1 $\alpha$	Hypoxia inducible factor-1 $\alpha$
HO-1	Heme oxygenase-1
HRE	Hormone response element
HRP	Horseradish peroxidase
HupA	Huperzine A

HVA	Homovanillic acid
IFN- $\gamma$	Interferon-gamma
IRE	Iron response element
LC	Locus coeruleus
LDH	Lactate dehydrogenase
L-DOPA	<i>L</i> -3,4-dihydroxyphenylalanine
LPS	Lipopolysaccharid
LTP	Long-term potentiation
mAChR	Muscarinic acetylcholine receptor
MAO	Monoamine oxidase
MAOI	Monoamine oxidase inhibitor
MAPK	Mitogen-activated protein kinase
MCI	Mild cognitive impairment
MHPG	3-Methoxy-4-hydroxyphenylglycol
MP	Metalloprotease
MPP <sup>+</sup>	1-methyl-4-phenylpyridine
MPTP	1-methyl-4-phenyl-1,2,3,6-tetrahydropyridine
MTDL	Multi-target-Directed Ligand
MTT	3-(4,5-dimethylthiazol-2-yl)-2,5-diphenyltetrazolium bromide
mRNA	Messenger ribonucleic acid
NA	Noradrenaline
nAChR	Nicotinic acetylcholine receptor
NF-K $\beta$	Nuclear factor kappa-light-chain-enhancer of activated B cells
NFTs	Neurofibrillary tangles
NGF	Nerve growth factor
NMDA	N-methyl- <i>D</i> -aspartate
NO	Nitric oxide
Nrf-2	Nuclear factor (erythroid-derived 2)-like 2
ORAC	Oxygen radical absorbance capacity
OS	Oxidative stress
PARP	Poly ADP ribose polymerase
PAS	Peripheral anion site
PBS	Phosphate-buffered saline
PCR	Polymerase chain reaction
PD	Parkinson's disease
PET	Positron emission tomography
PGE <sub>2</sub>	Prostaglandin E <sub>2</sub>

PKA	Protein kinase A
PI3K	Phosphatidylinositol-4,5-bisphosphate 3-kinase
PS1/2	Presenilin 1/2
RNS	Reactive nitrogen species
ROS	Reactive oxygen species
sAD	Sporadic Alzheimer's disease
SN	Substantia nigra
SOD-1	Superoxide dismutase-1
Tf	Transferrin
TGF $\beta$ 1	Transforming growth factor beta 1
TH	Tyrosine hydroxylase
THA	Tetrahydroaminoacride
TNF $\alpha$	Tumour necrosis factor $\alpha$
TPH	Tryptophan hydroxylase
UTR	Untranslated region
UV-VIS	Ultraviolet visible
VTA	Ventral tegmental area
VEGF	Vascular endothelial growth factor
VMA	Vanillylmandelic acid
ZnT-3	Zinc transporter-3

## RESUM

En l'actualitat, el tractament de la malaltia d'Alzheimer es basa principalment en l'ús d'inhibidors de colinesterases, els quals, juntament amb un antagonista de receptor NMDA han estat aprovats per la FDA. Tanmateix, l'ús d'aquests fàrmacs no només ha resultat terapèuticament ineficaç, sinó que a més el benefici simptomàtic que aquests compostos produeixen és temporalment. En el context d'una malaltia multifactorial com l'Alzheimer, la recerca de nous fàrmacs capaços de produir un efecte modulador de llarga durada és urgentment necessària.

Una de les aproximacions farmacològiques més acceptades recentment pel tractament de l'Alzheimer és l'ús dels lligands dirigits multidiana o MTDL. Aquests compostos multifuncionals són capaços de presentar diverses activitats farmacològiques amb la finalitat d'actuar simultàniament sobre diferents dianes terapèutiques.

En aquesta tesi s'ha realitzat l'estudi i avaluació del compost ASS234 i de diverses sèries de compostos MTDL de nova síntesi derivats del donepezil com a agents potencialment actius en la teràpia d'Alzheimer. Primerament, l'estudi s'ha dirigit en la millora de la caracterització del compost ASS234, un MTDL àmpliament descrit pel nostre grup com a agent amb diverses propietats que inclouen una potent capacitat inhibidora de les activitats MAO i ChE, un efecte neuroprotector i antiagregant de la proteïna beta amiloide *in vitro* i *in vivo* i una activitat antioxidant i antiapoptòtica. S'ha dut a terme la caracterització el mecanisme i cinètica del compost ASS234 com a inhibidor de les MAO i s'ha estudiat mitjançant HPLC el seu efecte modulador en el sistema monoaminèrgic en cultius cel·lulars i per microdiàlisi i UHPLC en rates tractades amb una única dosi d'aquesta molècula. Seguidament, compostos derivats de l'ASS234, com a híbrids de donepezil i propargilamines, han estat evaluats farmacològicament com a molècules potencials per l'Alzheimer. D'entre aquests compostos, s'han identificat potents inhibidors (en rang nanomolar) duals de les MAO i colinesterases com a estructures útils per al disseny i síntesi de futurs derivats millorats.

Finalment, s'ha seleccionat el compost DPH-4, d'entre una nova sèrie de compostos MTDL amb activitat quelant de metalls. Amb aquesta molècula s'han identificat múltiples propietats d'interès farmacològic en l'Alzheimer incloent una capacitat d'inhibició equimolar de les activitats MAO i ChE, un potent efecte quelant per complexar coure, ferro i zinc, una habilitat per restablir dels dèficits cognitius en rates tractades amb escopolamina, i efectes antioxidants, antiagregants de proteïna beta amiloide i antiinflamatoris *in vitro*.

En general, els resultats d'aquesta tesi reafirmen els potencials beneficis en l'ús farmacològic dels MTDLs en la teràpia d'Alzheimer, i proposen la molècula DPH-4 com a *lead* d'especial interès pel seu ús contra aquest transtorn neurològic.



## ABSTRACT

The current treatment of Alzheimer's disease is essentially based on the use of cholinesterase inhibitors that together with a NMDA receptor antagonist have been approved by the FDA. Nevertheless, the use of these drugs in therapy has been reported ineffective accompanied with temporary symptomatic benefits. In the context of a multifactorial disorder such as Alzheimer's disease, the search for new pharmacological approaches able to produce real long-term modulator effects is urgently encouraged.

A well-accepted recent pharmacological approach for the treatment of Alzheimer's disease is the so-called Multi-target directed ligands or MTDLs, as multifunctional compounds exhibiting multiple pharmacological activities to simultaneously interact with several therapeutic targets.

In this thesis, the study and evaluation of compound ASS234 and other series of novel donepezil-derived MTDLs has been carried out as potentially active ligands for use in Alzheimer's disease. First, a study focused on the improvement of the biochemical characterisation of compound ASS234 has been undertaken. This widely described MTDL by our group is a molecule bearing multiple properties including potent dual MAO and ChE inhibition, neuroprotective and anti-A $\beta$  aggregating effect *in vivo* and *in vitro* and antioxidant and anti-apoptotic capacities. With ASS234, the mechanism and kinetics as MAO inhibitor was studied and its modulator effect on the monoaminergic system in both cell culture by HPLC and *in vivo* by microdialysis and UHPC was also assessed. Subsequently, novel ASS234-derived compounds as donepezil and propargylamine hybrids, were pharmacologically evaluated as potential drugs for potential use in Alzheimer's disease therapy. Among the tested compounds, some potent dual MAO/ChE inhibitors were identified (nanomolar range) as scaffolds for further design a synthesis of new derivatives.

Finally, compound DPH-4 was selected among a new series of MTDLs with metal-chelating properties. Multiple interesting activities were identified with this molecule for use in Alzheimer's disease including a moderate equimolar capacity to dually inhibiting MAO/ChE activities, an ability to complex metals copper, iron and

zinc, an effect to restore the cognitive deficits in scopolamine-treated rats and antioxidant, anti-A $\beta$  aggregating and anti-inflammatory properties *in vitro*.

Overall, the results obtained in this thesis reinforce the potential pharmacological benefits of MTDLs for use in Alzheimer's disease and suggest molecule DPH-4 as a lead compound for the treatment of this neurologic disorder.

# **I. INTRODUCTION**



## **I. INTRODUCTION**

### **1. Ageing, neurodegeneration and Alzheimer's disease**

Ageing is an irreversible process that combines predictable and random effects leading to cellular damage and weakening cell repair and compensatory mechanisms (Kirkwood TB 2003), including physical, psychological and social changes. The variation in ageing is accounted for by lifestyle and environment, with genes representing only 25% of variability (Kirkwood TB 2003).

Ageing is a major risk factor of neurodegeneration, and brain cells are particularly susceptible to the neuronal death occurring throughout the ageing process, in which cellular and molecular changes interact with genes and environmental factors to determine the progression of the neurodegenerative course. Nevertheless, during ageing, compensatory protective strategies against cell damage rise including mitochondrial oxygenation, ubiquitination and proteolysis by proteasomes and activity of chaperones and lysosome-mediated autophagy. In fact, ageing is closely associated with mitochondrial dysfunction, increase in free radical production and oxidative stress (OS), which lead to DNA instability and reduced survival (Migliore L 2009).

Ageing not only makes patients more prone to neurodegenerative diseases, but also impairs their abilities of self-repair. To date, a number of signalling pathways involved in the regulation of ageing and lifespan have been identified, and an alteration of these molecular mechanisms may contribute to the pathogenesis of neurodegenerative diseases (Bishop NA 2010). Many age-related neurodegenerative diseases are characterised by accumulation of specific misfolded proteins in the central nervous system (CNS) (van Ham TJ 2009), including amyloid peptides or phosphorylated tau protein in Alzheimer's disease (AD),  $\alpha$ -synuclein in Parkinson's disease (PD), superoxide dismutase in amyotrophic lateral sclerosis (ALS) or mutant huntingtin in Huntington's disease (HD).

The association between age and protein misfolding is not clear yet, but it might be related to cellular changes that occur during the ageing process (Gaczynska M 2001; Reznick AZ 1979). Neurodegenerative diseases comprise a range of conditions that primarily affect neurons in the human brain. At present, they are incurable debilitating conditions that result in progressive degeneration and/or death of nerve cells, leading to movement problems or ataxias and/or mental malfunctioning or dementias.

Dementias are responsible for the greatest burden of disease, with AD representing approximately 60-70% of all cases. Other neurodegenerative disorders include PD, HD, ALS, prion disease, motor neuron disease, stroke, spinocerebellar ataxia or spinal muscular atrophy, among others.

AD is one of the most common neurodegenerative diseases accounting for more than 80% of total dementia cases in elderly people. It is estimated that currently 47 million victims of AD exist worldwide and that number is expected to grow up to more than 130 million cases by 2050 as a result of life expectancy increase over the next decades (Thies W 2012; Thies W 2013). It is predicted that by 2050, one new case of AD will appear every 33 seconds, or nearly a million new cases per year.

In 2015, the World Alzheimer Report estimated that the current annual societal and economic cost of dementia was US \$818 billion worldwide and that amount is expected to rise up to 1 trillion by 2018. The findings also show that the cost associated with dementia has increased by 35% since 2010. The clinical manifestations of AD are characterised by the malfunctioning and gradual death of neuron resulting in a progressive memory deterioration and cognitive decline. The anatomopathology of AD has been described by a progressive loss of synaptic neurons that triggers atrophy in the hippocampus and frontal and tempopareital cortex. Two distinctive hallmarks of AD include the presence of accumulated amyloid beta ( $A\beta$ ) plaques around neurons (Glennner GG 1989) and hyperphosphorylated microtubules associated with tau protein in the form of neurofibrillary tangles (NFT) (Goedert M 2006) within the cells (Fig. 1).

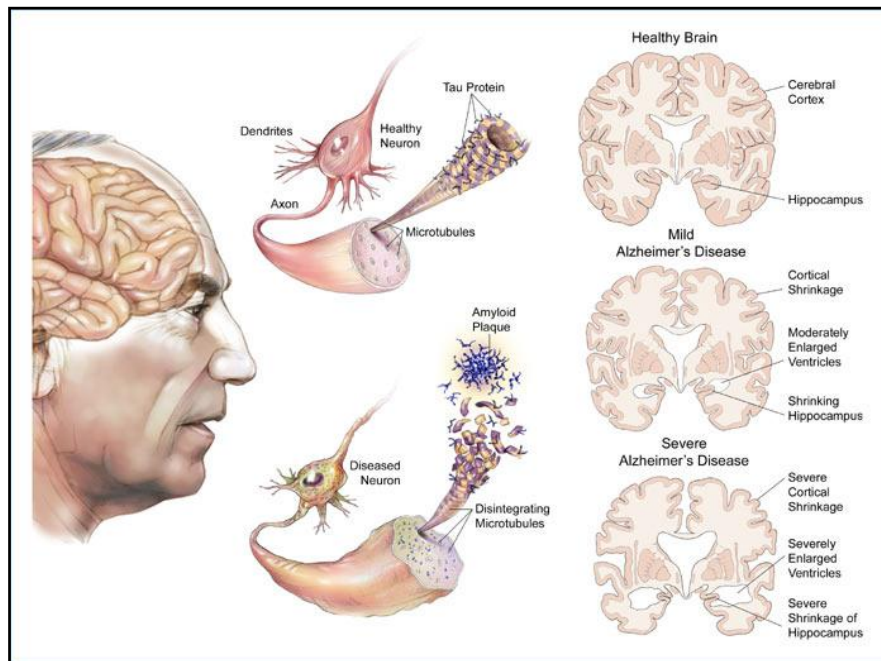


**Fig. 1.** Distinctive presence of amyloid plaques and NFTs within the neurons and brain anatomical alterations during AD progression (from the American Health Assistance Foundation 2014).

According to the Global Deterioration Scale or Reisberg Scale, the progression of AD can be split into seven stages:

- **Stage 1: No impairment.** Memory and cognitive abilities appear normal.
- **Stage 2: Minimal Impairment.** Memory lapses and changes in thinking rarely detected by close people.
- **Stage 3: Mild Cognitive Impairment (MCI).** Subtle difficulties begin to impact function. Difficulty with retrieving words, planning, organization, misplacing objects, and forgetting recent learning. Depression and other changes in mood can also occur at this stage. Duration: 2 to 7 years.
- **Stage 4: Mild AD.** Problems handling finances, forgetfulness in conversations, problems carrying out sequential tasks, withdrawal from social situations. Accurate diagnosis of AD is possible at this stage. Lasts roughly 2 years.
- **Stage 5: Early Dementia/Moderate AD.** Decline is more severe and requires assistance. No longer able to manage independently. Frequently disoriented. There is a severe decline in numerical abilities and judgment skills. Problems in basic daily living tasks. Duration: an average of 1.5 years.
- **Stage 6: Middle Dementia/Moderately Severe AD.** Total lack of awareness of present events and inability to accurately remember the past. Progressive loss of the ability to take care of daily living activities. Appearance of agitation, hallucinations and dramatic personality change. Lasts approximately 2.5 years.

- **Stage 7: Late or Severe Dementia.** Speech becomes severely limited, as well as the ability to walk or sit. Total support around is needed for daily functions. Duration is impacted by quality of care and average length is 1 to 2.5 years.

AD can be divided into two types: Familial AD (fAD) and sporadic AD (sAD), both differing from genetic occurrence and onset time of clinical symptoms (Fig. 2).

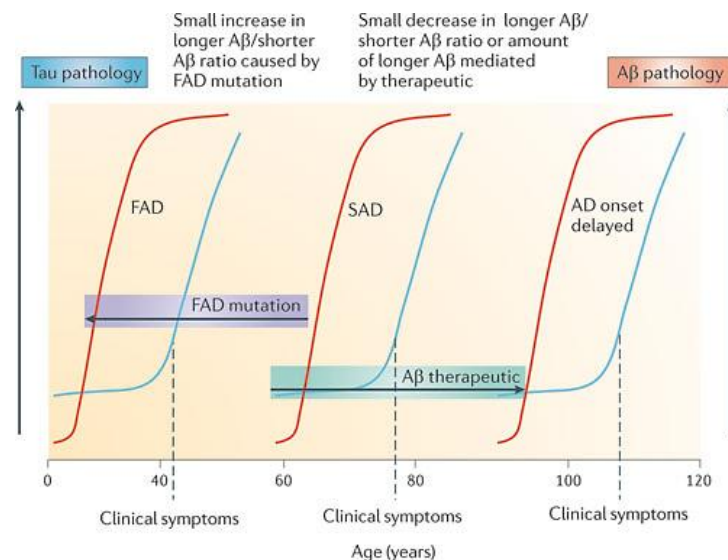


**Fig. 2.** Comparison in the age of the onset of AD hallmarks A $\beta$  and tau pathologies and clinical symptoms between fAD and sAD (Karran E 2011).

### i. Familial Alzheimer's disease

Familial AD (fAD) or early onset AD is an uncommon form of the disease affecting less than 3% of total AD cases (Harvey RJ 2003), which typically strikes earlier in life, defined as before the age of 65, usually between 50 and 65, although it can appear as early as 15.

This type of AD is inherited in an autosomal dominant fashion and identified by genetic mutations in the amyloid precursor protein (APP) or presenilin-1 and -2 (PS1 and PS2) genes (Levy-Lahad E 1995; Bayer TA 1999), a family of multi-pass transmembrane proteins constituting the catalytic subunits of the  $\alpha$ -secretase intramembrane protease complex. Of these, mutations occurring on PS1 account for most fAD, while those on APP and PS2 are less common.

## **ii. Sporadic Alzheimer's disease**

The late-onset form of AD (sAD) is the most common, cause of disease cases, and its onset still remains unclear. While age constitutes the main risk factor for sAD, environmental and genetic elements have been observed to also influence on the manifestation of the pathology.

The most relevant genetic factor is the inheritance of the  $\epsilon 4$  allele of the apolipoprotein E (ApoE), which enhances the proteolytic breakdown of A $\beta$  peptide within and between cells. At least one allele is present in 40-80% of sAD cases (Mahley RW 2006) and its presence increases the risk of AD by three times in heterozygosis and by 15 in homozygosis (Blennow K 2006).

Recently, genome-wide association studies have found 19 areas in genes related to AD risk (Lambert JC 2013). Other risk factors linked to sAD include head trauma and vascular-related diseases such as high blood pressure, heart diseases, stroke, diabetes or high cholesterol levels. In addition, environmental agents such as diet, aluminium and viruses have also been reported as factors involved in the etiology of AD (Grant WB 2002).

## **2. Pathophysiology of Alzheimer's disease**

### **i. Cholinergic hypothesis**

The cholinergic system is based on the neurotransmitter acetylcholine (ACh), firstly described by Loewi in the 1920s (Loewi O 1921) and located in both central and peripheral nervous systems. The basal forebrain cholinergic complex contains medial septum, diagonal band of Broca and nucleus basalis of Meynert and provides the major cholinergic projections to the cerebral cortex and hippocampus. The pontine cholinergic system, however, acts through the thalamic intralaminar nuclei providing a minor innervation of the cortex (Fig. 3).

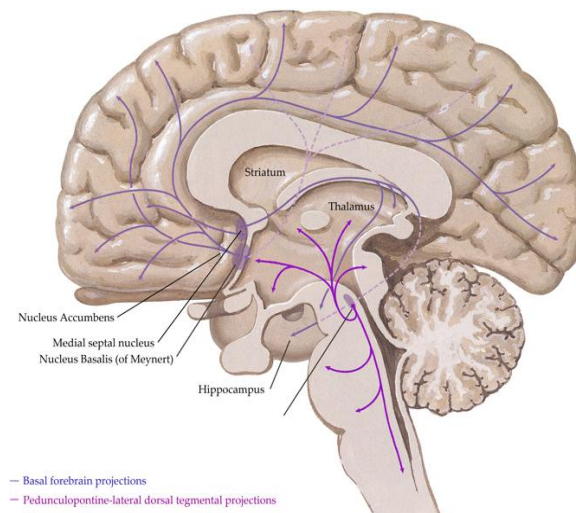


**Fig. 3.** Schematic representation of the cholinergic projections in the human brain (Scarr E 2013).

The cholinergic neurotransmission plays a key role in the control of cerebral blood flow (Biesold D 1989), cortical activity (Détári L 1999) and the sleep-wake cycle (Lee MG 2005). It also modulates the cognitive function and cortical plasticity (Arendt T 1986). In 1971, Deutsch and colleagues postulated the involvement of the cholinergic system in learning and memory, which was later corroborated in studies with animal models and humans (Fibiger HC 1991; Christensen H 1992; Schliebs R 2005).

Similarly to the ageing process, first physiological evidence of the involvement of the cholinergic system in AD pathology was found by a reduction in the presynaptic cholinergic markers such as ACh, or the expression of choline acetyltransferase (ChAT), responsible for the ACh synthesis. In addition, it has been reported a decrease in the binding of both muscarinic acetylcholine receptors (mAChR) and nicotinic acetylcholine receptors (nAChR), which are located in the nervous system, neuromuscular junctions and expressed in multiple cells including endothelial and some types of immune cells (Wessler I 2008), as well as cell atrophy.

These findings exhibit a direct link between cholinergic neurotransmission and AD, and constitute the premises for the so-called “cholinergic hypothesis of AD” (Deutsch JA 1971), which has been used to establish the primary therapeutic approach to date to address the cognitive loss associated with AD.

### Cholinesterases

Cholinesterases (ChE) are a family of enzymes that catalyse the hydrolysis of ACh into choline and acetic acid, a process required in the cholinergic neurotransmission. There are two types of cholinesterases: acetylcholinesterase (AChE, EC 3.1.1.7) and butyrylcholinesterase (BuChE, EC 3.1.1.8). Both enzymes are type  $\alpha/\beta$  hydrolases folded with an  $\alpha$ -helix bound with  $\beta$ -sheet containing a catalytic domain (Ollis DL 1992) (Fig. 4).

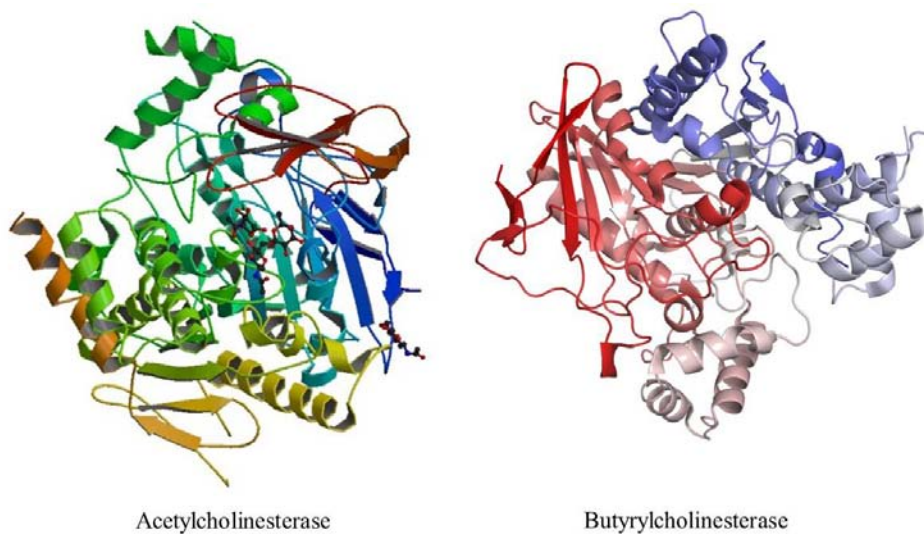


**Fig. 4.** Three-dimensional structures of AChE and BuChE enzymes (extracted from the PDB).

#### a. Acetylcholinesterase

Although AChE and BuChE are structurally similar, resembling each other by more than 50%, both their significance and location are substantially different. AChE is expressed in cholinergic neurons and neuromuscular junctions and relatively high activity levels of this enzyme can also be found in blood cells, responsible for the degradation of ACh in plasma (Fujii T 1997).

The primary function of AChE is the rapid breakdown of the neurotransmitter ACh during the cholinergic neurotransmission (Fig. 5).

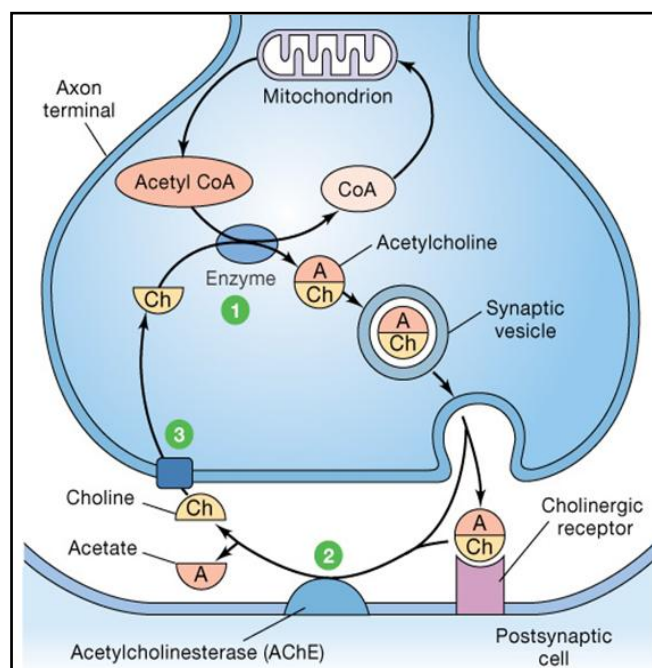


**Fig. 5.** Scheme of the AChE role in the synaptic cleft of cholinergic neurotransmission. (1) ACh is synthesised from choline and acetylCoA by ChAT. (2) ACh is rapidly broken down to acetate and choline by AChE. (3) Choline is reuptaken into the axon terminal for the ACh synthesis.

When inhibited or knocked out, over-stimulation of ACh receptor has been observed in mice as well as an increase of up to 60-fold of the extracellular levels of ACh compared to control animals (Fukuto TR 1990). The structure of AChE has been widely studied since the 1990s. Both the structure and the active site of this enzyme have remained evolutionary conservative, sharing numerous regions with other serine hydrolases. The active site of AChE lies on a bottom of long and narrow cavity of 20 Å deep. The active site contains a catalytic triad within an esterase site with amino acid positions Ser 200, His 440 and Glu 327. The anionic site or  $\alpha$ -anionic site is another part of the active site that interacts with ACh quaternary ammonium atom and is responsible for its correct orientation. Closely located, the esterase site hydrolyses the ester bond (Fig. 6).

Substrate penetration is allowed by cation  $-\pi$  interactions between ACh atom and  $\pi$  electrons of phenylalanine, tryptophan and tyrosine aromatic cores. The peripheral anionic site or  $\beta$ -anionic site is located on the enzyme surface, around the cavity entrance. This site was first recognised in the 1960s as a target for multiple AChE activity modulators (Sussman JL. 1991) such as toxins and promising drugs, as it plays an important role in AD. A $\beta$  peptide interacts with the peripheral anionic site resulting in the contribution of the formation of amyloid plaques by accelerating the aggregation process. This site is inhibited by propidium iodide.

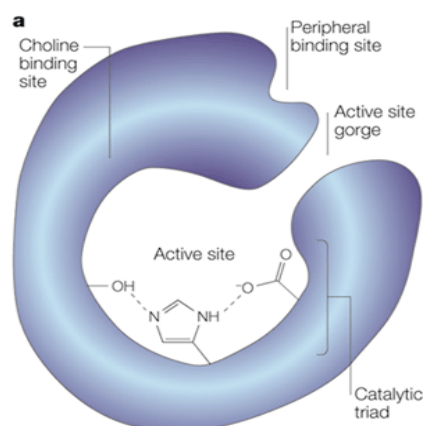


**Fig. 6.** Structure of AChE displaying the active site at the bottom of a narrow gorge, lined with hydrophobic amino-acid side chains within the catalytic triad, the choline binding site and the peripheral binding site (Soreq H 2001).

Cholinesterases conformation can be monomeric, dimeric or tetrameric. In monkey brains, 83% of AChE molecules are tetramers, 10% dimers and 5% monomers (Liao J 1993). Different abilities between AChE and BuChE to split substrates have been reported. While AChE is not able to hydrolyse high molecular weight esters as BuChE, it exhibits higher affinity for ACh. These differences in substrate affinity may be due to specific changes in the aromatic gorge disposition.

Since the 1970s, one of the most consistent changes associated with AD has been the degeneration of neurons from the cholinergic nuclei in the basal forebrain region and their terminals in the hippocampus (Struble RG 1982). More recently, the neuronal atrophy has been associated with a loss of cholinergic markers, occurring specifically in the nucleus basalis of Meynert (Vogels OJ 1990). The cholinergic system function, responsible for the storage and retrieval of items in memory, is therefore highly impaired in AD pathology.

#### b. Butyrylcholinesterase

In AD brain, neuritic plaques and neurofibrillary tangles (NFT) contain large amounts of AChE and BuChE, the latest present in the neuroglia (Wright CI 1993), possessing different histochemical properties from the analogous enzymes in intact neuronal cell bodies and axons. Moreover, these two enzymes may play a role in the processing of APP (Wright CI 1993), though it is unclear whether inhibition could influence the pathogenic course of AD. Butyrylcholinesterase (BuChE, EC 3.1.1.8),

also known as pseudocholinesterase or plasma cholinesterase, is an enzyme that hydrolyses different choline esters.

While AChE is expressed in nerve and blood cells hydrolysing ACh, the biological significance of BuChE still remains not well understood, even though it has been described to be able to partially modulate or compensate the diminished AChE activity in the deficient animals (Xie W 2000).

Similarly to AChE, neurotransmitter ACh can also be metabolised to choline by glial BuChE (Mesulam M 2002; Daikhin Y 2000) but with different kinetic behaviour. While AChE predominates in neurons and exhibits high affinity for ACh with low  $K_M$  values, BuChE is present in endothelia, glia and neuronal cells with low affinity for ACh and high  $K_M$  values (Soreq H 2001).

Enzyme BuChE is expressed in the hippocampus and temporal neocortex, but at lower levels than AChE, and it is associated with glial cells (Mesulam M 2002). However, Darvesh and colleagues reported that, in the hippocampal formation, AChE is present in both neurons and neuropil, while BuChE is only detected in neurons, suggesting that these enzymes may colocalize. In the amygdala, the number of BuChE-positive neurons is reported to exceed the number of AChE-positive neurons, with BuChE residing predominantly in the neurons and their dendritic processes and AChE residing in the neuropil (Darvesh S, Grantham DL, and DA 1998). The distinct distribution of AChE and BuChE within the brain suggests that these enzymes may both play interactive central biological roles.

In addition to its role in the hydrolysis of ACh, non-enzymatic functions have also been attributed to BuChE. As previously mentioned, while AChE may accelerate amyloid deposition in the AD brain, BuChE can associate with A $\beta$  protein possibly delaying the onset and rate of neurotoxic A $\beta$  fibril formation *in vitro* (Diamant S 2006). Furthermore, since neurotransmitter ACh has been reported to display anti-inflammatory properties, the activity of both AChE and BuChE might also be considered as a potential marker of low-grade systemic inflammatory conditions such as AD (Das UN 2007).

In certain AD brain regions, BuChE activity has been found unaltered or increased (Perry EK 1978; Ciro A 2012), which has been associated with amyloid plaques and NFTs (Geula C 1989; Guillozet AL 1997). In addition to changes in activity, changes in AChE and BuChE protein expression also occur over the progression of AD. Furthermore, an increase in the levels of glial-derived BuChE and decreases in synaptic AChE have also been observed, triggering a dramatic increase in the BuChE: AChE ratio in cortical regions from 0.6 in healthy conditions to 11 in AD (Giacobini E 2003).

High levels of BuChE in gray matter have been correlated with annual cognitive decline in a prospective, autopsy-confirmed population with dementia with Lewy bodies (Perry E 2003). However, high CSF BuChE activity may be associated with greater levels of cognitive function in patients with AD (Darreh-Shori T 2006). It has been hypothesized that low levels of BuChE in the CSF may correlate with high levels of BuChE/AChE/A $\beta$ /ApoE complexes (BA $\beta$ AC) in the vicinity of, or trapped within, plaques, along with cerebral amyloid angiopathy, increased neurotoxicity, and greater central neurodegeneration (Darreh-Shori T 2011).

The observed changes in BuChE activity and expression throughout the course of AD, and its relationship with cognitive function, emphasize the potential value of BuChE and AChE inhibition as a therapeutic target in AD patients.

Thus, cholinesterase inhibitors (ChEIs) have provided a dose-dependent increase in ACh levels, enhancing cholinergic transmission in AD patients and providing relief from symptoms of cholinergic deficits. A number of ChEIs have been developed with varying potency against AChE and BuChE, many of which are close analogues of the same pharmacophore. The selectivity (AChE-selective, BuChE-selective, or dual inhibitor) of some of the available ChEIs, based on their inhibitory potency against human erythrocyte AChE and plasma BuChE is shown in Table 1. Several of these compounds are BuChE-selective, while others show inhibitory potency against both AChE and BuChE.

**Table 1.** Some available selective and dual ChE inhibitors.

<i>AChE-selective inhibitors</i>	<i>BuChE-selective inhibitors</i>	<i>Dual inhibitors</i>
BW284c51	Bambuterol	Eptastigmine
Donepezil	Bisnorcymserine	(-)-Heptyl-physostigmine
Diisopropylfluorophosphate	Cymserine	Metrifonate
Echothiophate	Ethopropazine	Physostigmine
Edrophonium	(-)-4'-Isopropylphenyl	Rivastigmine
Galantamine	Carbamate of thiaphysovenol	Tacrine
Huperzine-A	Iso-OMPA	
Neostigmine	MF-8622	
Phenserine		

To date, no large-scale randomized controlled trials of a BuChE-selective inhibitor in patients with AD have been performed. Studies in patients with mild-to-moderate AD would be unlikely to highlight treatment advantages of BuChE inhibitors (Ballard C 2003). BuChE-selective inhibitors may be more effective than AChE-selective inhibitors in patients with severe AD, although this remains to be tested clinically.

Mounting preclinical and clinical evidence suggests that BuChE may be significant in maintaining normal cholinergic function and in neurologic conditions in AD and that this role may become more pronounced during the disease course. Available data on the effect of BuChE genotype are limited and are largely based on prospective or retrospective analyses of clinical trial databases. Moreover, these analyses are generally based on reduced patient numbers, and the studies are not powered to detect differences in efficacy between treatment groups stratified according to genotype. However, further investigation in more severe disease stages and advantages of dual inhibitors in specific patient populations is necessary. An increased understanding of AD pathology, including the role of BuChE, will enable physicians to make best use of the available therapeutic options for those patients.

## **ii. Amyloid hypothesis**

The amyloid cascade hypothesis postulates that the neurodegeneration in AD is caused by abnormal accumulation of A $\beta$  plaques in various areas of the brain (Hardy JA 1992; Evin G 2002). This accumulation acts as a pathological trigger for a cascade that includes neuritic injury, formation of NFTs via tau protein to neuronal dysfunction and cell death (Hardy JA 1992; Selkoe DJ 1999). Genetic, biochemical and pathological evidences support this hypothesis as the primary cause of AD (Kayed R 2003).

The A $\beta$  senile plaques are composed by A $\beta$  peptides, which consist of 39-43 amino acid residues proteolytically derived from the sequential enzymatic action of  $\beta$ - and  $\gamma$ -secretases of transmembrane APP (Coulson EJ 2000). The length of A $\beta$  peptides varies at C-terminal according to the cleavage pattern of APP, being the A $\beta$ <sub>1-40</sub> the most prevalent form followed by A $\beta$ <sub>1-42</sub>, an hydrophobic form that aggregates faster (Perl DP 2010). Within plaques, A $\beta$  peptides and  $\beta$ -sheet conformation assemble and polymerise into structurally distinct forms such as fibrillar, protofibrils and polymorphic oligomers (Selkoe DJ 1994).

The kinetics of aggregation process of A $\beta$  peptide follows a sigmoidal curve due to the presence of  $\beta$ -sheets in its structure (LeVine H 1993), and it can be monitored *in vitro* by the use of dye molecules. The aggregating process comprises two main phases: lag phase and elongation phase. During the lag or nucleation phase, soluble monomers or dimers with random-coil structures form a nucleus that proceeds rapidly to the formation of fibrils. At the end of this phase, low-weight soluble oligomeric species are formed, which are spherical, globular and described as micelles or amorphous aggregates. The molar mass of these species varies between 25 and 50 KDa (Lambert MP 1998). Throughout the elongation phase, the

oligomeric species link together to form high-molecular weight oligomers of up to 1,000 KDa approximately (Huang TH 2000). These prefibrillar species transform into protofilaments or protofibrils, which are short, flexible and fibrillar. The protofibrils are the precursors of full-length fibrils by simple lateral association and structural organisation. Mature fibrils are straight, unbranched, twisted and can reach up to 10  $\mu\text{m}$  in length (Dobson J 2004) (Fig. 7).

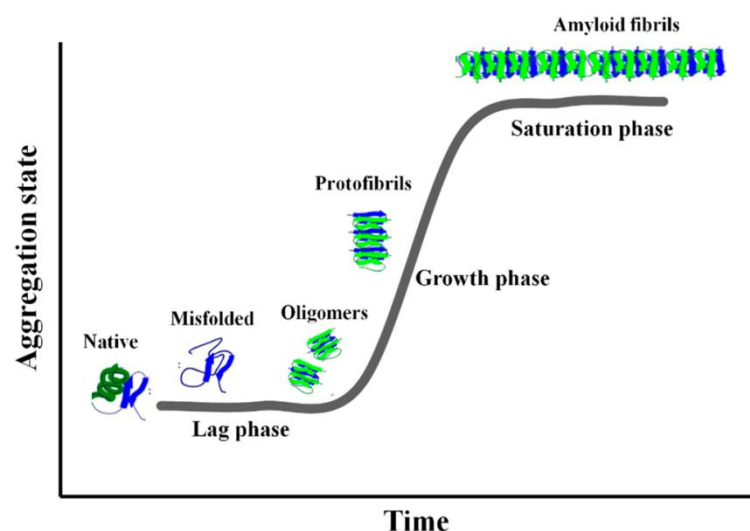


**Fig. 7.** Nucleation-dependent fibril formation process The sequence of events along the fibril formation pathway includes: (Lag phase) aggregation of misfolded monomers into small intermediate oligomers; (Growth phase) re-arrangement of these oligomers into an organized conformation containing the cross beta structure; (Saturation phase) association of beta structured oligomers into proto-fibrils and finally into fibrils (Iannuzzi C 2015).

The  $A\beta$  aggregation process is highly susceptible to many factors including pH, ionic strength of the solvent, purification process or temperature, which are responsible for complications in reproducibility when experimentally assayed *in vitro*. Distinct oligomerisation and assembly processes between  $A\beta_{1-40}$  and  $A\beta_{1-42}$  have been described (Bitan G 2003). While  $A\beta_{1-42}$  exhibits higher neurotoxicity and is able to form hexamers, heptamers or octamers,  $A\beta_{1-40}$  reach equilibrium from monomers to tetramers. These differences are related to differences in the Ile-41-Ala-42 dipeptide at the C-terminus of  $A\beta$ . Until recently, it was assumed that fibrillary  $A\beta$  deposits were the responsible agents for the neuronal injury and neurodegenerative process of AD (Selkoe DJ 1994; Hardy JA 1992). However, later findings showed that soluble oligomeric species were able to disrupt synaptic function (Lambert MP 1998) and recent data support the belief that soluble dimeric species are highly toxic (Jin M 2011). The mechanism by which  $A\beta$  induce cell damage have been reported to be by ROS production (Schubert D 1995), altered

signalling pathways (Mattson MP 1997), mitochondrial dysfunction (Shoffner JM 1997) and interaction with biometals (Jin L 2011).

The A $\beta$  deposition and plaque formation also lead to local microglia activation, cytokine release, reactive astrocytosis and multi-protein inflammatory response (Rogers J 1996) (Fig. 8). Also, the multifaceted biochemical and structural changes in surrounding axons, dendrites and neuronal cell bodies, induce the synapse loss, and a remarkable cerebral atrophy in AD (Braak H 1994).

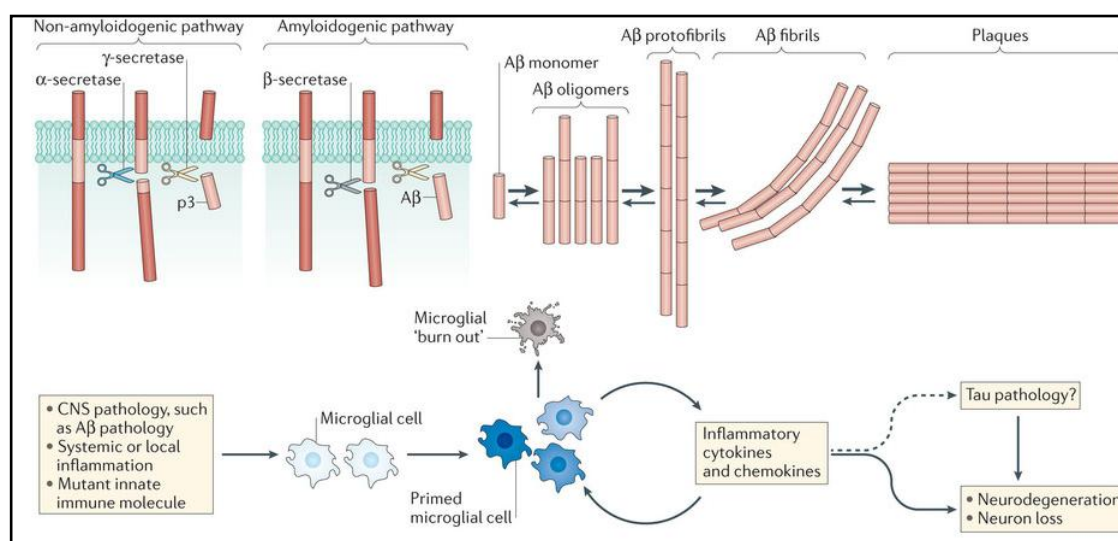


**Fig. 8.** Role of APP cleavage processing in AD and microglial activation (Heppner FL 2015).

Nonetheless, no correlation between the A $\beta$  accumulation with extent of neuronal loss and cognitive dysfunction has been reported so far. In addition, the direct A $\beta$ -peptide neurotoxicity has been difficult to prove in animal models, revealing the existence of key intermediate between amyloidosis and neurodegeneration (Nelson PT 2012; Serrano-Pozo A 2013). Despite these studies, genetic research has suggested that neurodegenerative processes in AD are the consequence of an imbalance between A $\beta$  peptide production and clearance.

Since the postulation of the “amyloid hypothesis of AD”, tremendous efforts have been undertaken in clinical research in order to develop novel therapeutics and this hypothesis has continued to gain support over the last two decades, particularly from genetic studies.

a. Amyloid precursor protein and presenilins

APP is a poorly understood type I membrane glycoprotein that present multiple isoforms derived by alternative splicing. APP gene is located on chromosome 21, and individuals suffering from Down's syndrome are reported to develop fAD (Ling Y 2003). The Swedish mutation in APP gene ( $APP_{swe}$ ) allows changes in amino acid residues 670 and 671 that increase  $A\beta$  peptide generation by increasing  $\beta$ -secretase processing activity (Citron M 1992). This mutation has been widely used to generate AD animal models.

As aforementioned, APP can be proteolytically processed through two pathways: the non-amyloidogenic and the amyloidogenic pathways (Fig. 9). In the non-amyloidogenic pathway, APP is cleaved by  $\alpha$ - and  $\gamma$ -secretases activity resulting the production of soluble form of APP ( $sAPP\alpha$ ), which has been reported to possess several neuroprotective properties (Selkoe DJ 2003). In the amyloidogenic pathway, APP is cleaved by  $\beta$ -secretase generating a membrane-bound C-terminal fragment (C99) which is subsequently cleaved by  $\gamma$ -secretase activity to produce  $A\beta$  peptide (Selkoe DJ 2003). The enzymes  $\beta$ -secretases 1 and 2 (BACE1 and BACE2) are also capable to cleave APP at  $\beta$  site. It was shown that  $\gamma$ -secretase cleaves APP near the boundary of the cytoplasmic membrane and middle of the membrane called  $\epsilon$ -cleavage and  $\gamma$ -cleavage, respectively (Weidemann A 2002).

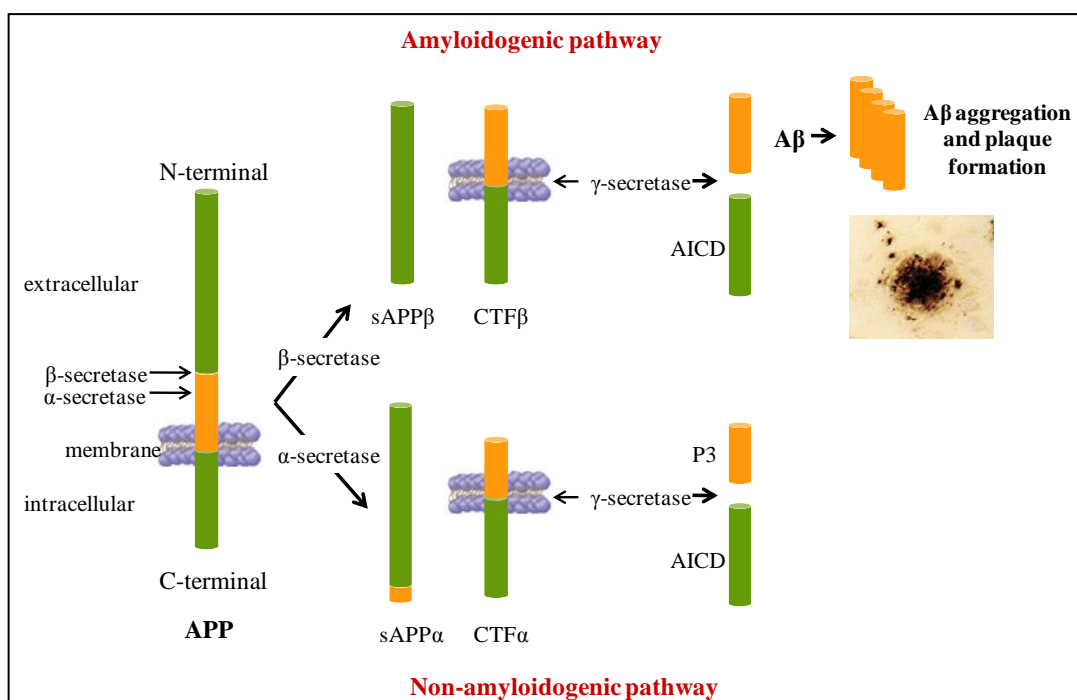


**Fig. 9.** Scheme of the APP processing through either non-amyloidogenic or amyloidogenic pathways. Modified from (Bush AI 2008).

Presenilins 1 and 2 (PS1, PS2) proteins are mainly located in the endoplasmic reticulum and Golgi subcellular compartment, but also in the nucleus, endosomal system and plasma membrane (De Strooper B 1997). Although the functions of PS have not been understood yet, some observations pointed that they might be involved in protein trafficking and Notch signalling (Mercken M 1996). To date, several mutations in both PS have been identified as the cause of fAD (Bertram L 2008). In addition, specific mutations in PS1 are responsible for an alteration in cleavage pattern of  $\gamma$ -secretase triggering higher  $A\beta_{1-42}$  levels. However, only few mutations on PS2 cause fAD (Herreman A 1999).

### **iii. Tau hypothesis**

Neuropathologically, AD is defined as the presence of intraneuronal neurofibrillary lesions consisting of tau proteins (Forman MS 2004). Tau proteins are mainly found in the axons of neurons and belong to the family of microtubule-associated proteins (Tucker RP 1990).

In the adult brain six isoforms of tau protein have been identified which derived through alternative splicing from single gene located on chromosome 17 (Neve RL 1986). They play an important role in microtubule assembly and stabilisation of neuronal microtubule network (lee 1989). Tau is composed by a microtubule binding domain integrated by three or four conserved repeats of 18 amino acids on the C-terminal half of the protein.

In AD, tau protein is abnormally phosphorylated, resulting from an imbalance between kinases and phosphatase activities. This phosphorylation occurs at serine and threonine by protein kinases cyclin-dependent kinase-5 (CDK-5), glycogen synthase kinase-3 (GSK-3) and mitogen-activated protein kinase (MAPK). Other kinases including Akt, Fyn, protein kinase A (PKA), calcium-calmodulin protein kinase-2 (CaMKII) and microtubule affinity-regulating kinase (MARK) are also involved in the tau phosphorylation process (Fig. 9).

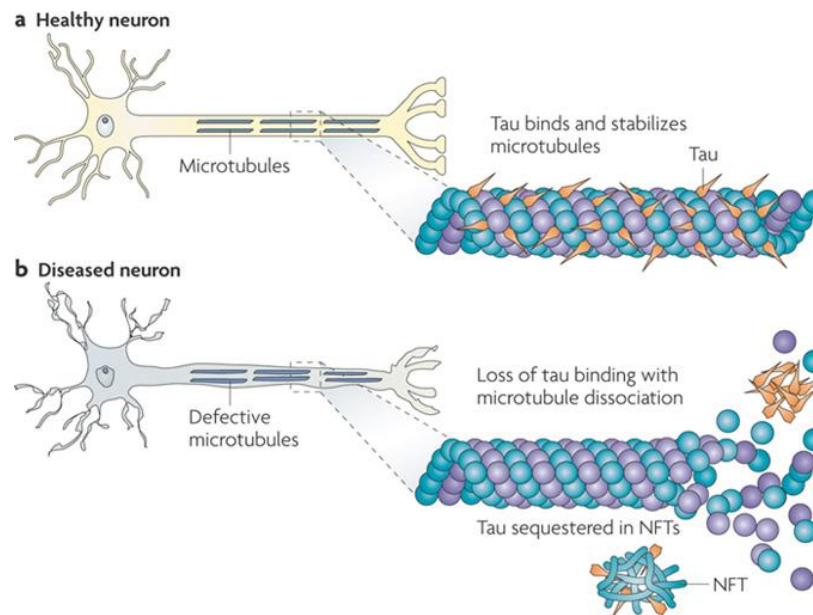


**Fig. 9.** (A) Tau facilitates microtubule stabilisation within cells and is particularly abundant in neurons. Microtubules are essential for normal trafficking of cellular cargo along the lengthy axonal projections of neurons. (B) In AD and other tauopathies, tau function is compromised as a result of its hyperphosphorylation into NFTs, which reduce the amount of tau that is available to bind microtubules. The loss of tau function leads to microtubule instability and reduced axonal transport, which could contribute to neuropathology (Brunden KR 2009).

The hyperphosphorylation of tau induce a destabilisation of microtubules (Alonso AC 1994) that leads to loss of neural cytoskeletal architecture and plasticity (Mandelkow EM 1998) and to an impaired neuronal transport which finally leads to cell death by the formation and accumulation of NTFs (Trojanowski JQ 1993).

Several pathogenic events have been reported to contribute to tau hyperphosphorylation including tau gene mutation as a cause of frontotemporal dementia and Parkinsonism (Goedert M 2005) or dysregulation of tau kinases and phosphatases (Mazanetz MP 2007). Consequently, recent therapeutic approaches against tau hyperphosphorylation have been addressed to the inhibition of kinases to block tau deposition (Mazanetz MP 2007) or the upregulation of tau phosphatases (Gong CX 2008), however their role under pathophysiological conditions is not yet clear.

#### iv. Oxidative stress

Within any functional aerobic cell, the process involved in respiration inevitably generates reactive oxygen species (ROS) (Petersen RB 2007). In particular, redox reactions are necessary for the generation of ATP and free radical intermediates are produced via the establishment of a proton gradient in oxidative phosphorylation.

Multiple damaging mechanisms coexist in AD pathology, affecting each other at multiple levels (von Bernhardt R 2012). In this respect, oxidative stress (OS), which could be secondary to several other pathophysiological events, appears to be a major determinant in case of AD pathogenesis and progression. Experimental evidence indicates that at a dysregulation of the redox state strongly participates in an early stage of AD, including and activating multiple cell signalling pathways that contribute to the initial progression of the neurodegenerative process (Feng Y 2012).

Constant evidence of ROS and reactive nitrogen species (RNS) mediated injury is observed in AD (Praticò D 2008). Increased levels of oxidative markers of biomolecules including proteins, lipids, carbohydrates, and nucleic acids, have been detected in a number of studies (Sultana R 2011; Moreira PI 2008; Fukuda M 2009). In addition, levels of antioxidant enzymes were found to be altered in specific AD brain regions (Sultana R 2010). Consequently, the “oxidative stress hypothesis of AD” emerged as a key event in both the onset and progression of this disease. OS is a widespread cellular process that currently lacks a specific treatment target such as a receptor or a single major metabolic pathway (Galasko DR 2012). The wide variety of sources and sites of OS production goes along with an even higher heterogeneity in the antioxidant response.

Specifically, the activity of cytochrome oxidase and the pyruvate and  $\alpha$ -ketoglutarate dehydrogenase complexes have been observed reduced as a result of oxidative damage (Aliev G 2011). In AD, there are established connexions between OS and other key AD events, which amplify its complexity (Fig. 10).

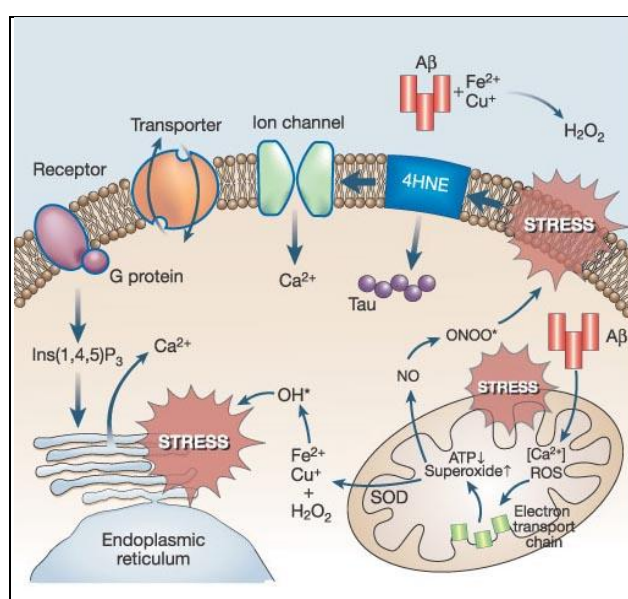


**Fig. 10.** Prevailing connections between OS and other key players in AD (Mattson MP 2004).

The aforementioned presence of oxidation markers indicates that OS in fact precedes these other hallmarks. Moreover, the accumulation of oxidative active modification products, such as 8-hydroxyguanosine (8-OHG) and nitrotyrosine, in the cytoplasm of cerebral neurons from Down's syndrome patients temporary has reported to precede amyloid deposition (Nunomura A 2000; Odetti P 1998). This was also demonstrated in an APP transgenic mice model of AD (Praticò D 2001; Smith MA 1998). In post-mortem brains of MCI patients, CSF, plasma urine, showed increased levels of lipid peroxidation, nuclear acid oxidation and diminished levels of antioxidant enzymes (Butterfield DA 2006; Keller JN 2005). Besides, heme oxygenase-1 (HO-1) levels were also reported to be increased in both AD and MCI post-mortem brain tissues (Schipper HM 2006).

Although A $\beta$  and its aggregated senile plaques are undoubtedly involved in the neurodegenerative process of AD, the chronology of its presence has been now deemed secondary by many studies (Castellani RJ 2006; Zhu X 2007). Evidence suggests that secretion and deposition of A $\beta$  within the neurons are compensatory measures taken by cells in effort to protect themselves against damage triggered by OS (Hayashi T 2007; Nakamura M 2007).

Mitochondrial abnormalities, initially caused by gradual oxidative disturbances are an enormous contributor of ROS to the cell (Bonda DJ 2010). Oxidative perturbances in mitochondrial operations create damaged metabolic capacity (Wang X 2009) that would prevent the effective transferring of electrons during oxidative phosphorylation, thus generating excessive ROS. This abnormality creates a vicious positive feedback cycle where ROS produce OS that eventually yields more ROS, along with other cellular detriments. ROS gradually accumulates in the cell over the years and once a threshold is reached, the cell is no longer able to control the debilitating cycle propagation and a compensatory "steady state" is unavoidably initiated in order to regain control of its environment (Zhu X 2007). This state that intends to prolong cell life increases its vulnerability to additional insults such as A $\beta$  peptides, and therefore becoming subject to oxidative damage produced by oligomerisation and aggregation (Wang X 2008), and, in turn, leading to neuroinflammation, mitochondrial damage, and further ROS generation.

In addition, cellular oxidative damage has also been linked to tau hyperphosphorylation and formation of NFTs (Lee YJ 2004). As a consequence of this aberrant cycle, cells succumb to neurodegeneration, exhibiting the common cognitive decline and dementia descriptive of AD (Zhu X 2007). Altogether, the primary role of OS in AD onset and progression has been overwhelmingly confirmed, offering the chance to develop specific disease-modifying antioxidant approaches to confronting the disease.

## v. Biometal dyshomeostasis

Numerous studies in AD and other neurodegenerative disorders have described an increase in the levels of oxidative stress reflected by a dysregulated content of metals iron, copper and zinc in the brain of patients. Recent findings have strongly pointed to brain oxidative stress as one of the earliest changes in AD pathogenesis that might play a central role in the disease progression (Guglielmotto M 2010; Lee HP 2010). Redox-active metals, especially  $\text{Fe}^{2+}$ ,  $\text{Cu}^{2+}$  and  $\text{Zn}^{2+}$ , are capable of stimulating free radical formation via Fenton reaction (Fig. 11), increasing protein and DNA oxidation and enhancing lipid peroxidation.

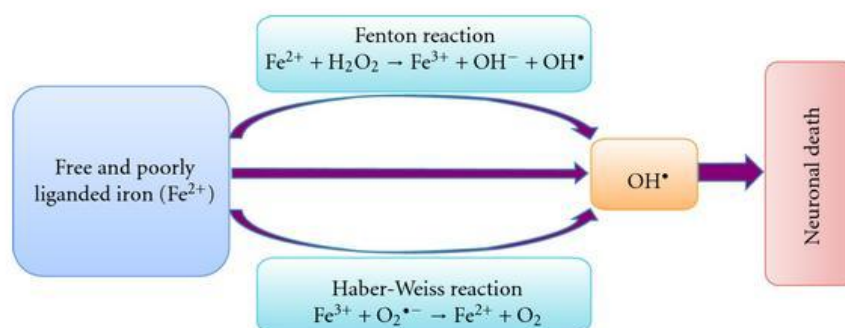


**Fig. 11.** Free iron reacts through the Fenton reaction with hydrogen peroxide, leading to the generation of reactive and damaging hydroxyl radicals ( $\text{OH}^\bullet$ ) through the Fenton reaction. Superoxide can also react with ferric iron by the Haber-Weiss reaction leading to the production of  $\text{Fe}^{2+}$ , which affects redox cycling. The highly hydroxyl radicals lead to OS-induced lipid peroxidation, mitochondrial dysfunction and increase in intracellular free-calcium concentration, causing neuronal death (Khalil M 2011).

Biometals have also shown to mediate  $\text{A}\beta$  toxicity in AD (Duce JA 2010). It has been described that  $\text{A}\beta$  peptide itself is a strong redox-active metalloprotein able to directly produce hydrogen peroxide and  $\text{OH}^\bullet$  in the presence of copper or iron, which, in turn, are enriched in the amyloid cores of senile plaques (Huang X, LE, and Tanzi RE 1999; Huang X et al. 1999). Also, metal ions can interact with  $\text{A}\beta$  peptide enhancing its self-aggregation and oligomerisation at low physiological concentrations or at mildly acidic conditions (Huang X, LE, and Tanzi RE 1999; Huang X et al. 1999). Moreover, metals can promote tau hyperphosphorylation and subsequent formation of neurofibrillary tangles (NFTs) inducing its aggregation upon interaction with  $\text{A}\beta$  (Yamamoto A and Yoshimasu F 2002).

The presence of iron-responsible element (IRE) in the 5' untranslated region (UTR) of  $\text{A}\beta\text{PP}$  mRNA was revealed as another link between iron metabolism and AD

(Rogers JT, H, and Lahiri DK 2002; Silvestri L 2008). Iron closely upregulates the intracellular levels of A $\beta$ PP holo-protein by a mechanism that is similar to the translational control of ferritin L- and H- mRNAs through an IRE in their 5' UTR (Rogers JT, H, and Lahiri DK 2002; Silvestri L 2008).

a. The role of copper

Copper is an essential trace element for all living animals. In humans, this biometal is essential to the proper functioning of organs and metabolic processes and it is constantly controlled by homeostatic mechanisms to prevent an excess or deficiency of it, which may trigger a unique set of adverse health effects. Copper can undergo redox cycling between Cu<sup>1+</sup> and Cu<sup>2+</sup> and the activity of some copper-containing enzymes including SOD, cytochrome c oxidase, ceruloplasmin or tyrosinase, are linked to important biological functions. However, copper is also involved in the formation of free radicals by the Fenton reaction, in which free copper catalyses the formation of toxic hydroxyl radicals from physiologically available hydrogen peroxide (Barnham KJ 2004). Two classic disorders related to copper metabolism are Menkes and Wilson diseases, and neurodegeneration is a common complication present in both disorders (Kodama H 1999; Merle U 2007).

In AD pathology, copper is mislocalised in brains, where decreased levels of this metal have been reported in affected regions (Deibel MA 1996; Magaki S 2007), with enrichment in amyloid plaques and tangles (Lovell MA 1998). Copper is released into the glutamatergic synaptic cleft facilitated by ATP7A at concentrations of 15 $\mu$ M approximately (Hopt A 2003; Hartter DE 1988). There, it causes S-nitrosylation of NMDA receptors inhibiting their activation (Schlief ML 2005; Schlief ML 2006).

The central theory of A $\beta$  toxicity is well-established to be linked with the presence of redox metals, especially the binding of copper and non-redox zinc (Tougu V 2008; Hou L 2006), whose precise mechanism is still a subject of investigation (Minicozzi V 2008; Syme CD 2004; Alies B 2011; Ma QF 2006).

The copper binding site of A $\beta$ <sub>1-42</sub> has an affinity of log $K_{app}$  of 17.2, whereas that of A $\beta$ <sub>1-40</sub> is 10.3 (Atwood CS 2000) when measured by competitive metal-capture analysis. Moreover, copper is reported to modify and accelerate A $\beta$  aggregation. Purified human plaques contain fewer histamine and tyrosine residues by the copper-mediated oxidation (Tanzi RE 1992). Copper promotes dityrosine cross-linking of A $\beta$ , and therefore accelerating A $\beta$  aggregation (Atwood CS 2004; Ali FE 2005). Copper-induced A $\beta$  oligomer contains membrane-penetrating structure with histamine bridging (Curtain CC 2001; Smith DP 2006). This remarks the importance

of histidine in the copper- A $\beta$  interaction, which, unlike zinc, forms oligomers rather than fibrils (Jiao Y 2005; Jiao Y 2007).

The copper-A $\beta$  complex has been reported to exhibit cytotoxic properties (You H 2012) as this binding ameliorates A $\beta$ -induced cell death in cell culture (Wu W 2008; Perrone L 2010). A hypothesis for this finding is the potential inhibition of cytochrome c (Crouch PJ 2005). Additionally, the increase of oxidative stress triggered by the generation of hydrogen peroxide by A $\beta$  and copper via a catalytic cycle is another assumption (Huang X et al. 1999; Huang X 1999).

APP also interacts with copper by binding to it between residues 142 and 166 (White AR 1999; Barnham KJ 2003; Cappai R 2004) and catalytically reducing Cu<sup>1+</sup> to Cu<sup>2+</sup> (Multhaup G 1996). Copper promotes APP internalisation, and its deficiency promotes A $\beta$  secretion, but not APP cleavage (Acevedo KM 2011). Therefore, APP may not directly influence copper homeostasis, but inappropriate interaction with copper could result neurotoxic.

Tau phosphorylation and aggregation may also be induced by copper. Certain fragments in the four-repeat microtubule-binding domain of tau were shown to aggregate in the presence of copper *in vitro* (Ma QF 2005; Zhou LX 2007). Besides, copper binding to tau induces *in vitro* a hydrogen peroxide production (Su XY 2007), and NFTs have also been shown to bind copper in a redox-dependent manner, as a source of ROS within the neuron (Sayre LM 2000). In addition, copper exposure induces tau hyperphosphorylation promoting tau pathology in a mouse model of AD (Kitazawa M 2009).

#### b. The role of zinc

The brain is the main pool of zinc within the body (Frederickson 1989). Zinc is an essential component for hundreds of enzymes and transcription factors. In healthy conditions, most of zinc content is compartmentalised in membrane-bound metalloproteins (MP I, II and III), loosely bound zinc within the cytoplasm, and vesicular zinc enriched in synapses. Synapse transmission releases high concentrations of zinc (Vogt K 2000; Qian J 2005; Frederickson CJ 2006) into the synapse, where it acts as a GABA (Molnar P 2001; Ruiz 2004) and NMDA receptors antagonist (Vogt K 2000; Paoletti P 1997; Traynelis SF 1998) and activates GPR39 (Besser L 2009), which underlies its functional roles in signal transmission. Zinc levels in AD have been reported inconsistently over the years. Early surveys of brain tissue found no difference in zinc levels between AD and controls (Hershey LA 1984). Later studies showed a decrease in zinc levels in the neocortex (Danscher G 1997), in the superior frontal and parietal gyri, the medial

temporal gyrus and thalamus (Panayi AE 2002), and the hippocampus (Panayi AE 2002; Corrigan FM 1993). However, conflicting reports have shown elevated zinc levels in AD-affected amygdala (Danscher G 1997), hippocampus (Danscher G 1997; Deibel MA 1996), cerebellum (Danscher G 1997), olfactory areas (Samudralwar DL 1995), and superior temporal gyrus (Religa D 2006).

The cause of zinc dysregulation remains unknown, but may be involved in the failure of proteins such as metallothionein III, found in neurons and reduced in AD brains (Uchida Y 1991; Yu WH 2001). In contrast, metallothionein I/II is increased in astrocytes of post-mortem and preclinical AD brains (Adlard PA 1998). In AD pathogenesis, enriched zinc levels have been found in amyloid plaques (Bush AI 1994c), also reported from studies using microparticle-induced X-ray emission tomography, in which 3-fold zinc concentrations were found in plaques surrounding neuropil in the amigdala (Lovell MA 1998). These findings were later corroborated by histochemistry (Suh SW 2000), autometallographic tracing (Stoltenberg M 2005) and synchrotron-based infrared and X-ray imaging (Miller LM 2006).

A $\beta$  binds zinc at residues 6-28 (Bush AI 1994c; Bush AI 1993; Bush AI 1994a, 1994b), with up to three zinc ions bound to histidines 6, 13 and 14 (Damante CA 2009), inducing the aggregation of A $\beta$  into soluble precipitates (Bush AI 1994c). Therefore, zinc, like copper, accelerates A $\beta$ -induced toxicity and zinc sequestration into amyloid deposits (Bush AI 1994c) (Fig. 12), inducing loss of functional zinc in the synapses. This loss may contribute to cognitive decline in AD due to ZnT-3 depletion (Adlard PA 2010).

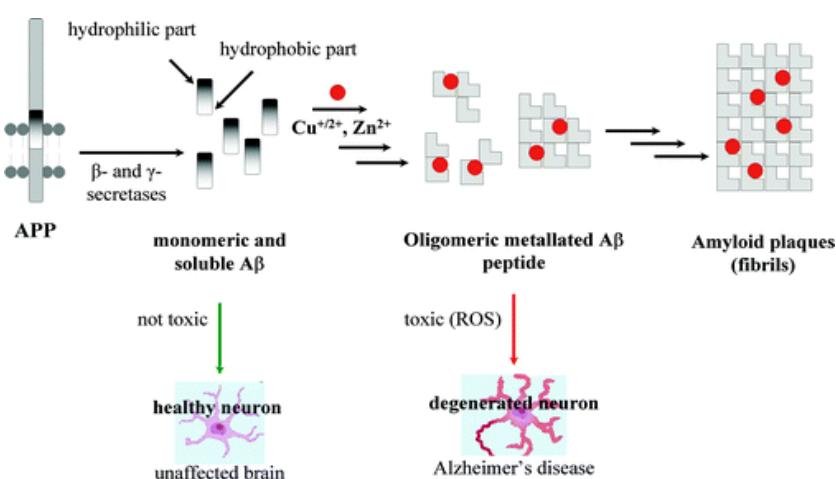


**Fig. 12.** The role of copper and zinc in the amyloid cascade hypothesis (Faller P 2013).

Zinc may also interfere with APP processing and function as these processes are coordinated by secretases under the zinc regulation. This metal increases the synthesis of PS-1 (Park IH 2001); however, the  $\gamma$ -secretase activity is inhibited by  $Zn^{2+}$  (Hoke DE 2007). Zinc binds directly to A $\beta$ , hiding its proteolytic cleavage site (Bush AI 1994b) and therefore inhibiting its degradation by matrix metalloproteases (Crouch PJ 2009). Secreted A $\beta$  is normally degraded by proteases such as neprilysin within a short period of time. However, zinc and other metals enhance the oligomerisation and accumulation of the amyloid protein. After being incorporated into the membrane, the conformation of A $\beta$  changes and aggregates on the membranes. These aggregates are able to form channels, which unlike endogenous  $Ca^{2+}$  channels, are not regulated by standard channel blockers. Thus, a continuous flow of  $Ca^{2+}$  is initiated and disruption of calcium homeostasis triggers several apoptotic pathways, including free radical formation and tau phosphorylation leading to cell death. Conversely, secreted zinc into synaptic clefts, inhibits A $\beta$ -induced  $Ca^{2+}$  entry, and thus confers a protective function in AD (Kawahara M 2014).

In agreement with these findings, *in vivo* studies revealed that high intake of dietary zinc triggered elevated expression of APP and enhanced amyloidogenic APP cleavage and A $\beta$  deposition in APP/PS1 transgenic mice (Wang CY 2010; Borchardt T and Beyreuther K 2000; Cuajungco MP 2003). Finally, zinc may also be involved in tau pathology as it is enriched in tangle-containing neurons (Suh SW 2000). Zinc moderates translation of tau and modulates its phosphorylation by affecting the activities of GSK-3 $\beta$ , protein kinase B, ERK1/2, and c-Jun N-terminal kinase (An WL 2005; Pei JJ 2006; Lei P 2011). In addition, zinc can also bind to tau monomers, altering its conformation (Boom A 2009) and inducing both aggregation and fibrillation of this protein (Mo ZY 2009).

### c. The role of iron

Iron is a fundamental element in biology for energy metabolism. It is a transition element that exists in oxidative states from -2 to +8, though in biological systems only ferrous ( $Fe^{2+}$ ) and ferric ( $Fe^{3+}$ ) states exist. The cycling between ferric to ferrous states is used in biology for various redox reactions essential to life. However, deleterious reactions with oxygen, such as Fenton reaction, are a source of oxidative stress (Zigler Jr JS 1985).

In the brain, iron is involved in development (Beard J. 2003), neurotransmitter systems (Agarwal KN. 2001), and myelination (Schulz K 2012). It is therefore regulated by multiple proteins and involved in different cellular functions. In AD

brains, iron is enriched in both NFTs (Smith MA 1997) and senile plaques (Goodman L. 1953) with an estimated concentration of 3-fold higher than that of the normal neuropil levels (Lovell MA 1998). Iron accumulation occurs in the cortex but not in the cerebellum (Duce JA 2010; Andrasik E 1995). The iron storage protein ferritin binds most iron within the brain (Collingwood JF 2005) and its levels increase with age and AD (Bartzokis G 2000). Transferrin (Tf) is an extracellular iron-transporting protein expressed in the brain that exchanges iron between cells. The complex Fe-Tf is endocytosed (Eckenroth BE 2011) and iron is reduced to its ferrous state by an unknown ferrireductase.

Recently, AD-associated APP was identified as a neuronal ferroxidase (Duce JA 2010). APP-knockout mice exhibit iron accumulation in the brain and peripheral tissues, and loss of APP ferroxidase activity in AD brains is coincident with iron retention in the tissues (Duce JA 2010). It has been lately reported that iron-export capability of APP requires tau protein (Lei P 2012), which is involved in axonal transport (Lei P 2010) and binds to APP (Islam K 1997). Moreover, the loss of tau in mice is reported to cause age-related iron accumulation (Lei P 2012). In AD brains, iron-regulatory system is disturbed. Ferritin has been reported to be elevated and co-localised with senile plaques (Connor JR 1992), found to be expressed in astrocytes (Connor JR 1992) and increased in frontal cortex of AD brains (Loeffler DA 1995). However, the amount of APP was not significantly reduced in cortex (Duce JA 2010) but both ferroxidase activity and soluble tau protein level were observed to be decreased (Duce JA 2010; Shin RW 1992; van Eersel J 2009; Zhukareva V 2001; Khatoon S 1994). Genetic factors have also been linked to higher susceptibility to iron burden in AD (Bertram L 2008; Blazquez L 2007; Percy M 2008). Iron burden enriches around the senile plaques region (Meadowcroft MD 2009) and promotes A $\beta$  aggregation *in vitro* (Mantyh PW 1993). Furthermore, iron-aggregated A $\beta$  toxicity in cell culture (Schubert D 1995) is mediated by ROS production (Rottkamp CA 2001) or by the activation of Bcl-2/Bax-related apoptosis pathway (Kuperstein F 2003). As mentioned, iron also binds to tau, but only Fe<sup>3+</sup> has been reported to induce aggregation of hyperphosphorylated tau, which can be reversed by reducing Fe<sup>3+</sup> to Fe<sup>2+</sup> (Yamamoto A 2002) or by the use of iron-chelators (Amit T 2008). In AD brain, NFTs bind iron, which acts as a source of ROS within the neurons (Sayre LM 2000). In hippocampal neurons treated with Fe<sup>3+</sup> a decrease of tau phosphorylation was observed (Egaña JT 2003), which corresponds with a decrease in CDK5 activity. Conversely, treatment with Fe<sup>2+</sup> also shows hyperphosphorylation (Lovell MA 2004) without inducing aggregation, possibly caused by upstream activation of the ERK1/2, MAPK pathway (Huang X 2007; Muñoz P 2006). Recently, oxygen tension-dependent transcriptional factor, hypoxia inducible factor-1 $\alpha$  (HIF-1 $\alpha$ ) has emerged as a potential target in

neurodegenerative diseases. This protein regulates intracellular iron by binding to HIF-responsive elements (HREs) that are located within the genes of iron-related proteins such as Tf receptor and heme oxygenase-1 (Fig. 13).

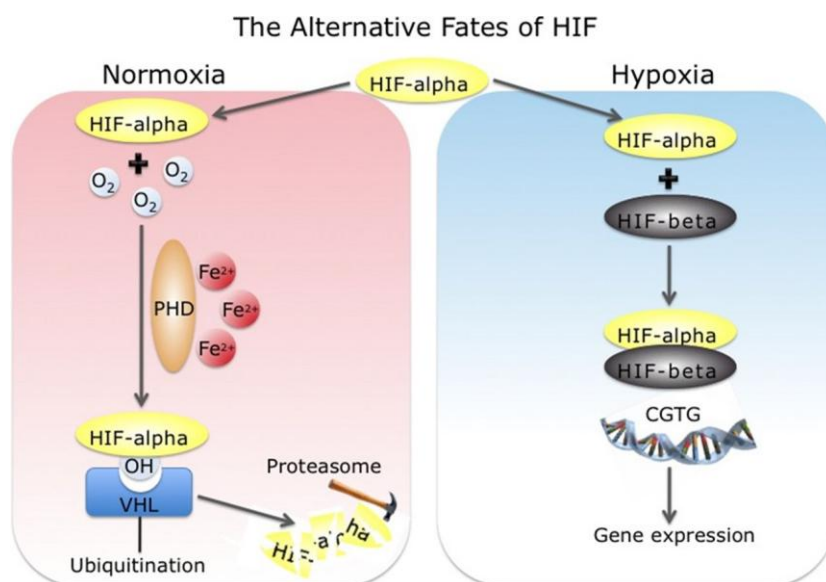


**Fig. 13.** Schematic representation of the regulation of HIF-1 $\alpha$  pathways. Under normoxia, HIF-1 $\alpha$  accumulates, dimerises with HIF- $\beta$ , binds to DNA, and transcriptionally regulates hypoxia-responsive genes. In presence of oxygen and Fe<sup>2+</sup>, prolyl hydroxylase domain (PHD) enzymes hydroxylate specific proline residues in HIF- $\alpha$  for ubiquitination and mediates its proteosomal degradation (Petousi N 2014).

Particularly in AD, recent research and clinical trials have confirmed that HIF-1 $\alpha$  activation may be a potent strategy to postpone the pathogenesis and ameliorate the outcomes of AD. In this context, the use of iron chelators such as M30, has reported an increased of the levels of this protein by elevating the expression of its target genes VEGF and EPO. Overexpression of HIF-1 $\alpha$  has been shown to protect cultured cortical neurons from A $\beta$ -induced neurotoxicity, through activating glycolytic and hexose monophosphate shunt-related enzymes. Therefore, an additional use of iron-chelators to overexpress HIF-1 $\alpha$  may contribute to prevent neuron death and ameliorate symptomatology of AD by inducing the expression of neuroprotection-related genes (Benkler C 2010).

Overall, in the context of AD pathology, the role of both OS and metal ions dyshomeostasis in brain (Fig. 14) confirms the use of antioxidant-chelators as potential beneficial agents in the prevention and treatment of the disease by scavenging free radicals and, more importantly, blocking their production, as well as restoring metal dyshomeostasis.

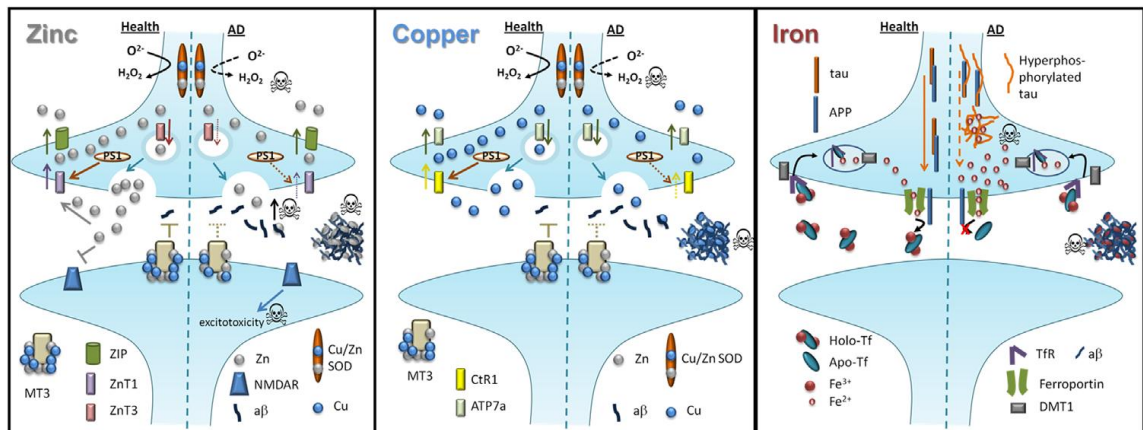


**Fig. 14.** Overview of the role of metals dyhomeostasis (zinc, copper and iron) in AD leading to neurodegeneration (Ayton S 2013).

## vi. Monomnergic neurotransmission impairment

### a. Monoaminergic systems

The monoaminergic neurotransmission comprises four pathways with specific locations in the brain and neurotransmitters: dopaminergic (DAergic), noradrenergic (NAergic), serotonergic and histaminergic (HAergic) pathways (Fig. 15).

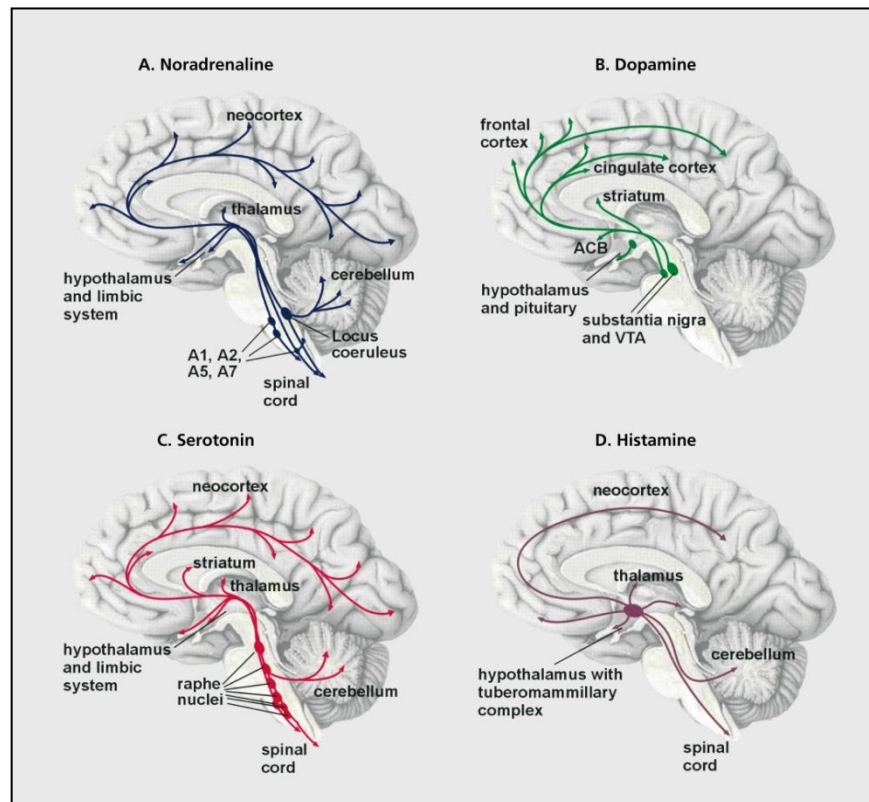


**Fig. 15.** Schematic representation of the monoaminergic systems (NAergic, DAergic, serotonergic and HAergic) and their projections in human brain (Fuchs E 2004).

Monoamines are able to induce modulatory and trophic effects on a large number of neighboring cells through diffusion to distant extra-synaptic sites (Fuxe K 2007). By using wire and volume transmission, the monoaminergic systems impose a strong modulatory influence on most of the regions of the brain. In many instances, different monoaminergic systems share similar input and output regions and directly project to each other (Bolte TJ 1998). The interaction between various monoaminergic systems is complex and site and receptor specific (Gonzalez-Burgos I 2008).

Selective vulnerability of brainstem nuclei monoaminergic cells has been described in AD. While the rostral raphe complex is especially susceptible to tangle formation, other monoaminergic nuclei frequently exhibit both pathological markers (plaques and tangles) (Parvizi J 2001). An additional link between the monoaminergic systems and the pathophysiology of AD stems from genome-wide association studies. Polymorphisms in mDNA have been linked to a higher incidence of AD, though the precise role of them is yet to be fully understood (Kazuno AA 2006).

i. DAergic system in AD

DA is a catecholamine synthesised from L-tyrosine by the sequential action of tyrosine hydroxylase (TH) and aromatic L-aminoacid decarboxylase (AADC). It is metabolised by DA-hydroxylase (DBH) into NA, and, by catechol-O-methyltransferase (COMT) and preferably by MAO B in humans to homovanillic acid (HVA). The main DAergic regions are located in the midbrain. The DAergic neurons arising from SN and VTA together form mesencephalic DAergic system. DAergic neurons play a central role in reward-oriented behaviours (Schultz W 2007). By improving DA signalling, a reinforcement of motivating actions was observed, while when those levels are reduced, these actions are suppressed (Bromberg-Martin ES 2009).

In AD pathology, significantly lower levels of DA, its precursor L-3,4-dihydroxyphenylalanine (L-DOPA) and its metabolite DOPAC have been found in the cingulate gyrus, amygdala, striatum, and raphe nuclei in AD brains (Storga D 1996). In addition, lower levels of this neurotransmitter have also been reported in CSF (Tohgi H 1992) and urine. This reduction may correlate with both the loss of DA transporter (DAT) (Allard P 1990) and the duration of the disease in AD (Pinessi L 1987). In addition, D<sub>1</sub> receptor has been described to be reduced in the putamen and hippocampus (Cortes R 1988) as well as in striatum together with D<sub>2</sub> receptors (Kempainen 2000) in AD brains. Conversely, D<sub>3</sub> receptors were found to be selectively increased in AD subjects with psychosis (Sweet RA 2001). A reciprocal relationship between severity of AD and the status of the DAergic system seems to exist as accumulation of A $\beta$  oligomers impair memory by possibly promoting long-term depression and inhibiting long-term potentiation (Lacor PN 2007).

It has been shown that by stabilising monomeric state of amyloid aggregation pathway, COMT inhibitors were able to reduce A $\beta$  oligomerisation (Di GS 2010). Moreover, amyloid oligomers have been observed to affect synaptic function by altering the internalisation of AMPA and NMDA receptors. In APP-expressing mice, a significant reduction in the density of TH-positive fibers in the vicinity of amyloid deposits has been reported (Diez M 2003). Interestingly, a restoration of the cognitive function was also reported after L-DOPA injections in those mice (Ambree O 2009). In this context, the use of MAO B inhibitors have been considered as promising clinical interventions in AD, even if the results have been inconsistent to date (Filip V 1999).

In conclusion, degeneration of the DAergic system and deficits in its modulatory effects on cortical regions play a significant role in both cognitive and non-cognitive

symptoms associated with AD. Therefore, more successful clinical intervention targeting this system would be achieved.

ii. NAergic system in AD

NA is produced from DA by DBH and is metabolised through various pathways involving MAO A and COMT, into vanillylmandelic acid (VMA) and 3-methoxy-4-hydroxyphenylglycol (MHPG). NAergic cells in the brain are found in the LC, the periaqueductal grey area, the paragigantocellular nucleus and in the ventral nucleus of the lateral lemniscus. The majority of ascending fibers from the NAergic system start in the LC. These ascending fibers reach the olfactory bulb, the neocortex, the hippocampus, thalamus, striatum, basal forebrain, preoptic area, and the hypothalamus. LC neurons are characterised by extensive arborisation. Ascending NA system plays an important role in attention, stress, and in navigational and contextual memory regulation (van Stegeren AH 2008). LC neurons send extensive projections to hippocampal and cortical regions.

In AD, diminished levels of NA have been detected in regions receiving LC terminals including the hippocampus, the frontal and temporal cortices, and the cingulate gyrus in AD (Reinikainen KJ 1988). Interestingly, NA reduction was found to be more severe in early-onset rather than in late onset cases of AD (Arai H 1992). Reduced levels of NA in AD have also been detected in the CSF and urine of individuals with AD as compared to non-demented controls (Martignoni E 1992). In addition, the enzymes involved in the biosynthesis of NA have also been shown to undergo alterations in AD, as significant reduction in the density of TH and dopamine-beta-hydroxylase-positive terminals has been found in the hippocampus in AD (Iversen LL 1983).

Morphological alterations of LC neurons in AD include swelling of cell body and shortening and thickening of dendrites (Chan-Palay V 1989). It has been shown that the severity of cell loss and NFT degeneration in the LC correlates well with the duration and severity of dementia (Bondareff W 1987) and with the occurrence of aggressive behaviour (Matthews KL 2002). Recent therapeutic approaches combining long-term treatment with NA reuptake inhibitors and NA prodrugs have shown to significantly improve cognitive function in mouse models of AD (Kalinin S 2012).

Both DA and NA systems have reciprocal and mutual connections to the frontal cortex, therefore exhibiting a high interdependency. Moreover, there are striking similarities between the factors that govern the activity of DA and NA neurons, suggesting that both neurotransmitters are released simultaneously. NA has multiple

effects on targeting neurons membrane potential, cellular excitability, intracellular cascade and synaptic plasticity and it is able to enhance or block excitatory responses to glutamate, depending on its concentration. Furthermore, NA has recently been reported to play an important role regarding the new concept of “cognitive reserve”, a set of variables that include intelligence, education, mental stimulation, social networking and which allow the brain to adapt to underlying pathologies such AD by maintaining cognitive function (Robertson IH 2013).

### iii. Serotonergic system in AD

Neurotransmitter 5-HT is an indolamine produced from L-tryptophan by the sequential action of tryptophan hydroxylase (TPH) and AAAD and is metabolised by MAO A into 5-hydroxyindoleacetic acid (5-HIAA). Ascending serotonergic fibers arise predominantly from the dorsal raphe nucleus and median raphe nucleus, both targeting the cortex and projecting to the hippocampus, septum, and hypothalamus, and the striatum. 5-HT has been proposed to encode aversive stimuli and signals to achieve behavioural inhibition, alerting about punishment or rewarding outcomes (Boureau YL 2011).

The 5-HT levels are severely affected in AD brains (Gottfries CG 1986). These alterations might be attributed to a combination of neuronal loss and a failure in compensating turnover mechanisms. In fact, both 5-HT and 5-HIAA cortical levels correlate negatively with the number of NFTs, suggesting that the impairment of the serotonergic system parallels disease progression (Palmer AM 1987).

Later studies confirmed that 5-HT is significantly decreased in AD in the amygdala, striatum, SN, and raphe nuclei. Some authors found reduced levels of 5-HT and 5HIAA in the cortex (superior frontal gyrus, insula, temporal cortex, occipital cortex, cingulate gyrus), globus pallidus, amygdala, the hippocampus, and lateral nucleus of the thalamus of AD patients (Arai H 1984). Interestingly, alterations in 5-HT levels have been found to be more pronounced in early onset familial forms of AD. Decreased 5-HT levels and have also been detected in platelets in AD (Koren P 1993), leading to their altered physiology. It has been shown that platelets in AD exhibit higher MAO B activity levels (Saura J 1996). Since platelets constitute the primary source of A $\beta$  in the blood, they may play a significant role in AD pathophysiology (Prodan CI 2011).

Patients with AD plus depression show significant decrease in 5-HTT binding in the midbrain, nucleus accumbens, and thalamus. As for the 5-HT receptors, while the density of hippocampal 5-HT<sub>1A</sub> receptors is significantly reduced in AD, individuals with amnesic MCI show increased level of 5-HT<sub>1A</sub> (Truchot L 2007) which has

been suggested to be due to a compensatory mechanism (Dickerson BC 2005). It appears that various 5-HT receptors are altered differently in the course of AD. While the density of 5-HT<sub>1A</sub> receptors diminishes in the neocortex, hippocampus and amygdala along with progression of AD, 5-HT<sub>2</sub> receptor density reduction occurs early in the course of the disease and correlates with the number of NFTs (Perry G 1987). Medial temporal cortex also shows a significant reduction in 5-HT<sub>1A</sub> receptor density in AD (Lanctot KL 2007), which correlates with aggression and dementia severity in this disease (Lai et al., 2003). The 5-HT<sub>4</sub> receptor, implicated in learning and memory, has been shown to mediate ACh release and increase the secretion of non-amyloidogenic soluble products of APP *in vitro* (Robert PH 2008).

These studies suggest that targeting the serotonergic system might improve non-cognitive and to some extent cognitive symptoms in AD (Henry G 2011).

#### iv. Monoamine oxidases

Monoamine oxidases (MAO, EC 1.4.3.4) are a family of flavin adenine dinucleotide (FAD)-containing enzymes that catalyse the oxidative deamination of primary, secondary or tertiary amines, producing hydrogen peroxide, ammonia and the corresponding aldehyde (Fig. 16).

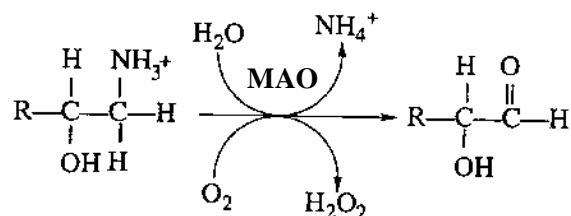


**Fig. 16.** Oxidative deamination of amines by MAO activity.

There are two isoforms of MAO present in mammals: MAO A and MAO B, which share approximately 70% sequence identity and are encoded by separate genes located on the X chromosome. Both rat MAO isoforms crystallise as dimers with similar monomer-monomer interactions while human MAO A does as a monomer for the presence of a lysine that lies at the dimer interface (De Colibus 2005).

The C-terminal regions of MAOs are transmembrane  $\alpha$ -helices that anchor the enzymes to the mitochondrial outer membrane as the rest of the protein is exposed to the cytoplasm. The entry of a substrate or inhibitor into the active site of MAOs is

predicted to occur near the intersection of the enzyme with the surface of the membrane (Fig. 17).

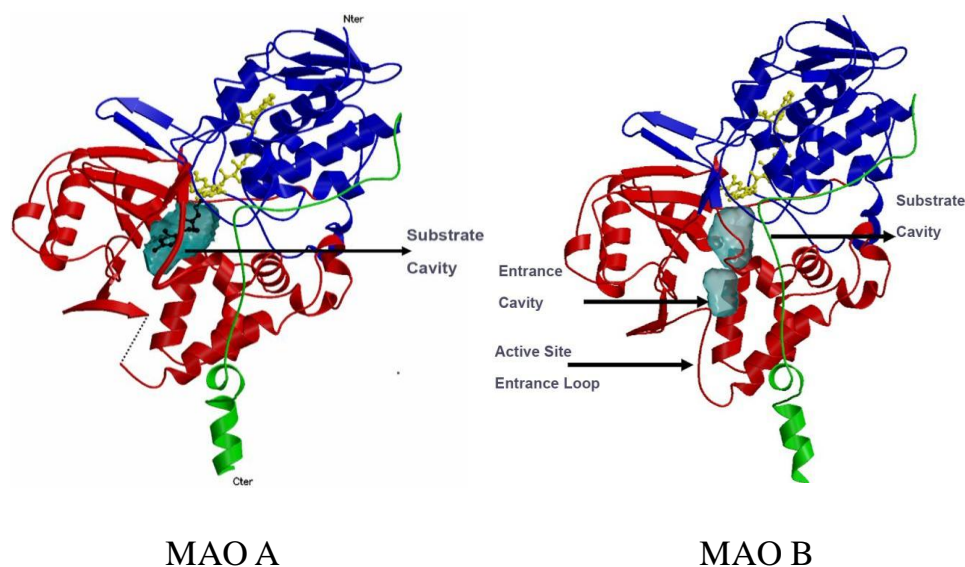


**Fig. 17.** Ribbon diagrams of monomeric units of human MAO A (A) and MAO B (B) structures. In yellow, the covalent flavin moiety is shown. In blue, the flavin binding domain. In red, the substrate domain and in green, the membrane binding domain (Edmondson DE 2007).

In selective MAO-knockout mice, the two MAO isoforms were found to significantly differ in both metabolism and behaviour. While the lack of MAO A triggered aggressive phenotypes as a result of elevated levels of 5-HT and NA and lesser of DA (Chester DS 2015), only the levels of 2-phenylethylamine were increased in MAO B-knockout mice, which exhibited traits such as sensation seeking, impulsiveness and extraversion. MAO A and MAO B were originally distinguished by their sensitivity to nanomolar concentrations of the acetylenic inhibitors clorgyline and *l*-deprenyl, respectively as well as by their substrate specificities. The content of MAO varies over time as MAO A appears before MAO B, which levels dramatically increases in the brain after birth (Nicotra A 2004; Tsang D 1986; Strolin-Benedetti M 1992) and throughout lifetime and in AD. In the rat peripheral nervous system, MAO is localised in the endothelial cells of the endoneurial vessels, Schwann cells and in the unmyelinated axons of some neurons (Matsubayashi K 1986).

In the human brain, MAO activity differs among regions. While the highest levels are found in basal ganglia and hippocampus, the lowest are observed in the cerebellum and neocortex (O'Carroll AM 1983). The anatomical distribution of MAO isoforms in human brains were confirmed by positron-emission topography

(PET) using intravenous  $^{11}\text{C}$ -labelled irreversible inhibitors (Fowler JS 1987; Saura J 1992).

Immunohistochemical studies have revealed that serotonergic neurons and astrocytes are rich in MAO B whereas catecholaminergic neurons contain mainly MAO A (Westlund KN). Caudate dopaminergic nerve endings contain only MAO A and small amounts of this isoform is also found in the serotonergic nerve terminals (O'Carroll AM 1987).

Some differences in the dopamine metabolism have been observed between species. For instance, only MAO A isoform is involved in the rat brain whereas MAO B is primary responsible for dopamine metabolism in human brain (Fornai F 1999).

Some MAO substrates include indolamines 5-HT or HA and catecholamines DA, NA and adrenaline, exhibiting different specificities as shown in Table 2.

**Table 2.** MAO substrates and their specificities in the cerebral cortex (Youdim MH 2006).

Substrate	MAOA			MAOB		
	$K_m$ ( $\mu\text{M}$ )	$V_{\max}$ ( $\text{pmol min}^{-1}$ $\text{mg protein}^{-1}$ )	$V_{\max}/K_m$ ( $\mu\text{mol M}^{-1} \text{min}^{-1}$ $\text{mg protein}^{-1}$ )	$K_m$ ( $\mu\text{M}$ )	$V_{\max}$ ( $\text{pmol min}^{-1}$ $\text{mg protein}^{-1}$ )	$V_{\max}/K_m$ ( $\mu\text{mol M}^{-1} \text{min}^{-1}$ $\text{mg protein}^{-1}$ )
Adrenaline	125 $\pm$ 42	379 $\pm$ 54	3.03 $\pm$ 1.11	266 $\pm$ 9	465 $\pm$ 61	1.75 $\pm$ 0.23
Dopamine	212 $\pm$ 33	680 $\pm$ 123	3.21 $\pm$ 0.77	229 $\pm$ 33	702 $\pm$ 158	3.07 $\pm$ 0.82
5-Hydroxytryptamine	137 $\pm$ 24	228 $\pm$ 31	1.66 $\pm$ 0.37	1093 $\pm$ 20	6.6 $\pm$ 1.3	0.006 $\pm$ 0.001
Noradrenaline	284 $\pm$ 17	561 $\pm$ 42	1.98 $\pm$ 0.19	238 $\pm$ 30	321 $\pm$ 13	1.35 $\pm$ 0.18
2-Phenylethylamine	140 $\pm$ 22	20 $\pm$ 8	0.14 $\pm$ 0.06	4 $\pm$ 2	309 $\pm$ 24	77.3 $\pm$ 39.1
Tryptamine	35 $\pm$ 6	58 $\pm$ 5	1.66 $\pm$ 0.32	35 $\pm$ 8	108 $\pm$ 2	2.84 $\pm$ 0.60
Tyramine	127 $\pm$ 18	182 $\pm$ 28	1.43 $\pm$ 0.30	107 $\pm$ 21	343 $\pm$ 48	3.21 $\pm$ 0.77

Since MAO activity is involved in neurotransmission, specific MAO A inhibitors have been therapeutically used as effective antidepressants to increase the diminished levels of affection-related amines such as 5-HT or NA. Conversely, specific MAO B inhibitors have been widely used in PD therapy as enhancers of the levels of DA, which is preferably metabolised by this isoform in human brain (Riederer P 2011). In addition, MAO inhibitors provide additional benefits in these neurologic disorders by reducing the formation of neurotoxic products such as hydrogen peroxide and aldehydes, which are derived from MAO activities and promote ROS generation contributing to increase neuronal damage. In neurodegeneration, MAO inhibitors, especially those containing a propargylamine group, have been reported to possess multiple beneficial activities including neuroprotective, anti-apoptotic and antioxidant properties (Sanz E 2004, Bar-Am O 2005; Jenner P 2004; Sanz E 2008).

## vii. Neuroinflammation

Inflammation is a defensive mechanism of the body against multiple threats such as infections and injury. It is a complex event that involves both soluble factors and specialised cells (Brown KL 2007). Similar inflammatory processes occur in the brain and peripheral tissues. In the brain, glial cells, including astrocytes and microglia, undergo activation under pro-inflammatory conditions, by the increase in the production of inflammatory cytokines in the CNS, which become deleterious leading to progressive tissue damage in degenerative diseases (Fig. 18).

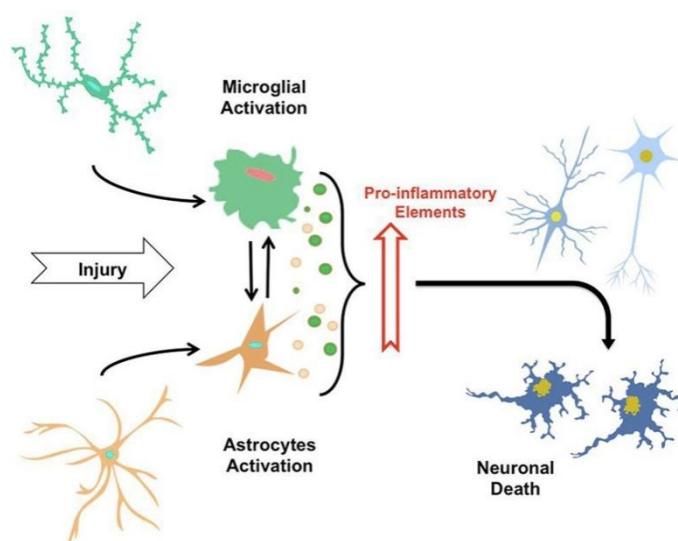


**Fig. 18.** The neuroinflammatory process. Both astrocytes and microglia suffer a gradual activation triggered by damage or injury leading to secretion of pro-inflammatory elements such as cytokines, cytotoxic elements or ROS. The constant exposure to factors causing injuries induces a neuroinflammatory process that eventually triggers neuronal death (Morales I 2014).

In chronic disorders such as AD pathology, inflammation plays a critical role. It has been reported that insoluble fibrillar A $\beta$  surrounding microglia, reactive astrocytes and dystrophic neurites contributes to the neuronal process of degeneration by initiating a series of cellular events which are able to elicit an immune response. Moreover, A $\beta$  deposition in parenchyma and blood vessels has been described to trigger microglial migration and mediation of acute and chronic inflammatory response against the aggregates, thus inducing the production of nitric oxide (NO), ROS, pro-inflammatory cytokines such as tumour necrotic factor  $\alpha$  (TNF $\alpha$ ) or interleukins-1 $\beta$  and -6 (IL-1 $\beta$ , IL-6) and prostaglandin E2 (PGE2), which eventually may promote neuronal death (Kitazawa M 2004) (Fig. 19).

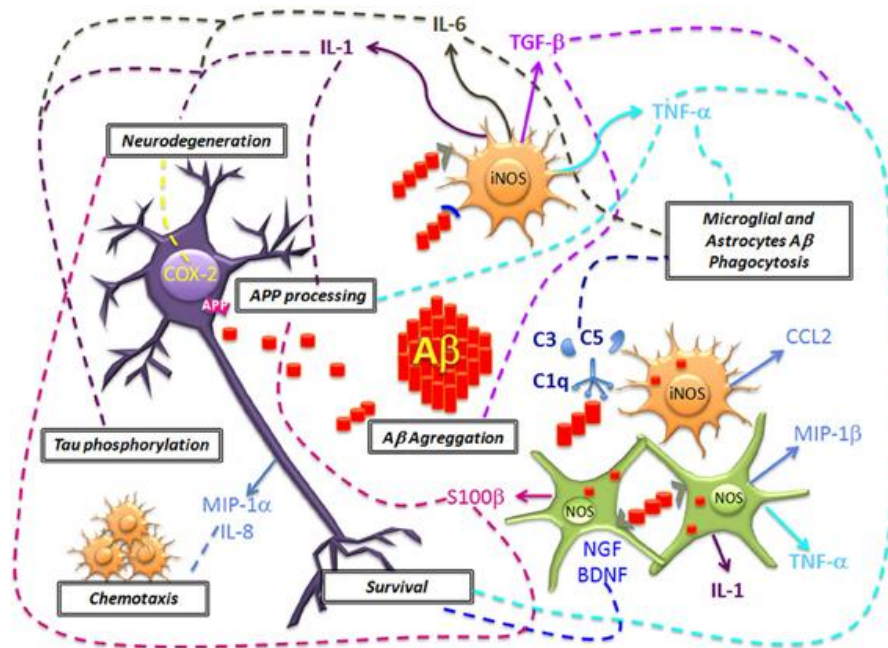


**Fig. 19.** Neuroinflammation in AD condition. Neuronal damage and A $\beta$  deposition triggers microglial and astrocytes activation and generation of inflammation molecular mediators such as complement system, cytokines, chemokines that induce NO and OS, favouring the production of COX-2 and leading to cell death (Meraz-Rios MA 2013).

Although the role of A $\beta$  as a potential initiator of neuroinflammation is not obvious, its accumulation exerts an indirect effect by activating caspases and transcriptional factors such as NF- $\kappa$ B and AP-1, which produce numerous inflammation amplifiers. Furthermore, APP, BACE1 and PS expression is governed by transcription factors such as NF- $\kappa$ B. The genes encoding these proteins have sites in their promoter regions, which are recognized by NF- $\kappa$ B, and in turn, the expression of these factors is upregulated by the presence of pro-inflammatory cytokines. Inflammatory mediators acting on neurons contribute to an increase in amyloid production and activate microglia-mediated inflammation. The microglia-neuron communication amplifies the production of factors that contribute to AD-type pathology. However, the neural response is specific for the receptor type expressed in the different neuronal populations.

Therefore, the slow but steady inflammation state generated for long periods in the AD brain eventually may destroy neurons and contribute to the clinical symptoms observed in this disease. Consequently, both the current lack of clinical trials on anti-inflammatory treatments and the limited safety of immunotherapy have recently prompted the development and implement of novel effective strategies for AD immunological treatments.

Overall, the aforementioned multifaceted nature of AD, in which multiple pathological events occur in the brain, has become a global medical challenge for this century that urgently requires novel effective therapeutic disease-modifying approaches.

## 1. Therapeutic strategies against AD

The abovementioned complexity of AD pathology has encouraged the development of multiple therapeutic approaches targeting several pathological events occurring in this multifaceted pathology (Fig. 20).

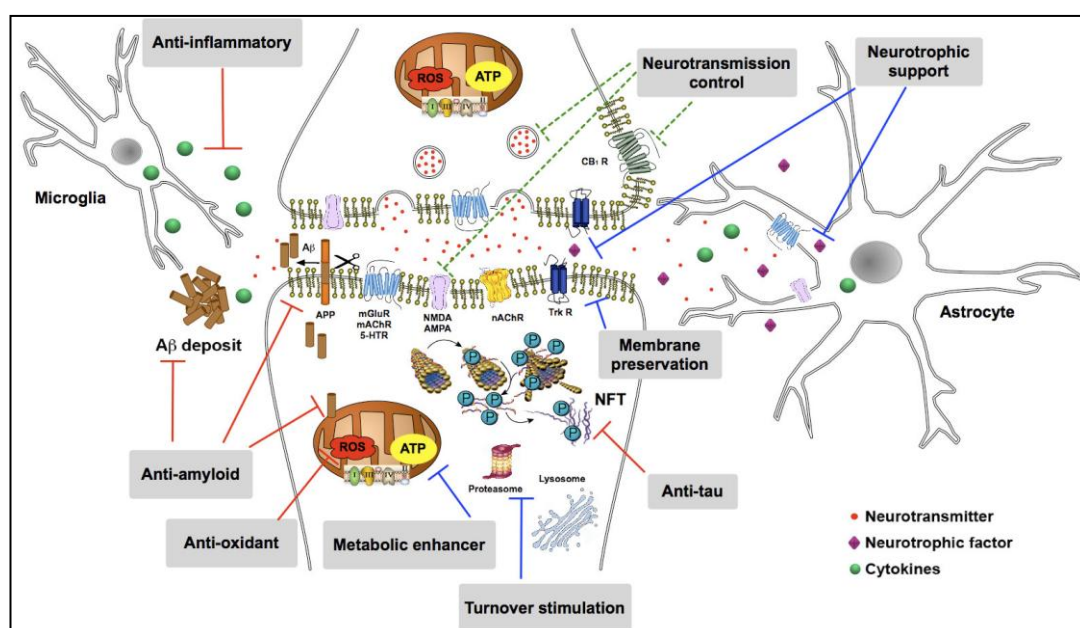


**Fig. 20.** Schematic representation of the main cellular targets that are currently under development to prevent and/or delay the progression of AD (Aso E 2013).

### i. FDA-approved drugs

To date, only five drugs (Fig. 21) have been approved by the U.S. Food and Drug Administration (FDA, USA) for use in the treatment of AD. Four of them are cholinesterase inhibitors (tacrine, rivastigmine, donepezil and galantamine) and memantine, an NMDA receptor antagonist.

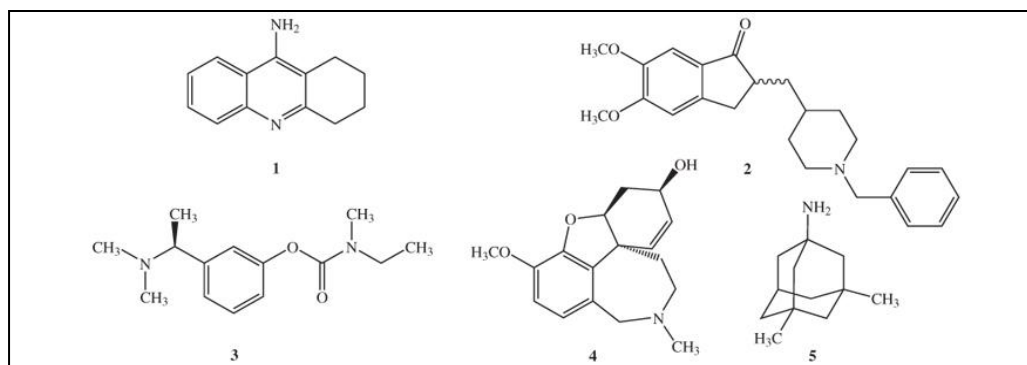


**Fig. 21.** Chemical structures of FDA-approved agents for use in AD: (1) Tacrine, (2) Donepezil, (3) Rivastigmine, (4) Galantamine, (5) Memantine.

#### a. Cholinergic agents: Cholinesterase inhibitors

Cholinergic neurotransmission is highly impaired in AD pathology due to a progressive loss of cholinergic neurons in the nucleus basalis of Meynert, and hence cholinergic activity (Davies P 1976). In this context, the “cholinergic hypothesis” was the first theory postulated to describe the onset of AD. This finding led to the development of drugs specifically designed to treat the distinctive hallmarks of this neurologic disorder by increasing the reduced levels of the neurotransmitter ACh in AD: the acetylcholinesterase inhibitors (Bartus RT. 2000; Bartus RT 1982).

There are currently three FDA-approved ChE inhibitors being used to treat mild-to-moderate AD, with reported similar effectiveness.

##### i. Tacrine

Tacrine or tetrahydroaminoacridine (THA) was the first drug approved for use in AD by the FDA in 1993 marketed as *Cognex*<sup>®</sup>. It is a competitive AChE inhibitor with high lipid solubility (Nielsen JA 1989) able to interact with muscarinic receptors (Adem A 1993) and MAO A and B (Adem A 1989). Despite the relatively small proportion of benefits on cognition, tacrine was withdrawn from the market in 2013 due to the high incidence of side effects, mostly from hepatotoxicity (Qizilbash N 1998).

##### ii. Donepezil

Donepezil, marketed under the trade name of *Aricept*<sup>®</sup> in 1996, is a brain-permeable reversible non-competitive ChE inhibitor approved for use in AD (Birks J. and R.J.

2006) and currently the most widely prescribed drug for the treatment of this disease. It is a piperidine derivative soluble in water, chloroform and glacial acetic acid highly selective for AChE over BuChE activity (405:1) (Nochi S 1995).

Compared to other approved AChE inhibitors, donepezil is similarly effective in ameliorating cognitive and functional decline in AD with comparable safety and tolerability. Moreover, beneficial effects have been observed at lower doses (5 mg/day), which is valuable preventing adverse reactions.

Although clinical trials with donepezil have reported modest but reproducible improvements in cognition and global functioning in treated patients compared to placebo, these effects were not permanent as patients continue exhibiting a decline in cognitive functioning over time (Doody RS 2001). Besides its AChE-inhibitory activity, donepezil has also been reported as a moderate NMDAR antagonist in the synaptic membranes of rat cerebral cortex (Wang XD 1999) while in a later study, contradictory findings were revealed describing it as an enhancer of NMDA currents (Narahashi T 2004). It has also shown to be muscarinic M1 receptor antagonist (Snape MF 1999).

In recent years, the costs of donepezil have considerably dropped, which has contributed to being favoured among prescribing physicians compared with other AChE inhibitors. Moreover, it is proven to be effective as antedementia drug.

In recent years, the consistent failure of pharmaceutical approaches targeting traditional AD targets such as A $\beta$  and tau protein together with the existing number of drugs to be tested in pre-dementia stages of the disease has left no effective disease-modifying treatment of AD at the horizon. Thus, additional benefits of donepezil might be achieved with the use of this molecule in combination with other active moieties.

### iii. Rivastigmine

Rivastigmine was marketed under the trade name of *Exelon*<sup>®</sup> since 1998. It is a non-selective pseudoreversible ChE inhibitor reported to produce enhanced benefits over AChE inhibition alone (Touchon J 2006; Bullock R 2007). Moreover, a recent study using a transdermal patch reported a reduction in the prevalence of side effects as well as positive results after administering rivastigmine to mild-to-moderate AD patients, in which, in comparison with placebo group, better outcomes were observed for rate of decline of cognitive function and activities of daily living (Birks JS 2015).

#### iv. Galantamine

Galantamine (*Razadyne*<sup>®</sup>) is a well-studied drug approved in 2001 by the FDA for the treatment of AD possessing a dual mechanism of action to attenuate the symptoms of cognitive decline in AD. It is a reversible selective competitive AChE inhibitor (Greenblatt HM 1999) able to simultaneously modulate nAChERs (Dajas-Bailador FA 2003 ). The main mechanism of action of this molecule is the ability to increase the content of ACh, enhancing the cholinergic neurotransmission and therefore improving cognition in AD patients. Moreover, galantamine has also demonstrated to directly interact with the nAChER as low-affinity agonist allosterically binding to a distinct binding site from where nicotinic agonists, such as ACh, choline or carbachol, bind (Akk G 2005). Moriguchi and colleagues (Moriguchi S 2003) also showed that galantamine potentiates the activity of NMDARs, so that the dual mechanism of action on both the cholinergic and glutamatergic systems in AD patients may be the reason of the improvement in cognition, memory and learning found in the clinical trial with this drug (Wilkinson D 2001).

#### b. Glutamatergic agents: NMDA receptor antagonists

##### i. Memantine

Memantine, marketed as *Namenda*<sup>®</sup> or *Ebixa*<sup>®</sup>, was the first and only NMDAR antagonist up-to-date approved by FDA in 2003 for the treatment of moderate-to-severe AD and dementia. In clinical trials, memantine has showed significant benefits on cognition, function, and global status of AD patients. Moreover, it is safe and well-tolerated, with a safety profile compared to placebo (Doody RS 2007). Moreover, memantine possesses highly low-affinity binding to NMDARs with a low-micromolar IC<sub>50</sub> value. Furthermore, it has poor selectivity among NMDARs subtypes, with under micromolar IC<sub>50</sub> values for NR2A, NR2B, NR2C and NR2D receptors expressed in *Xenopus* oocytes (Parsons CG1 1999).

Thus, memantine was initially regarded as a poor drug candidate for AD therapy; however the mechanisms by which it exerts clinical benefits with safe profile have attracted a great interest in the field of medicinal chemistry (Lipton SA 2006). Accumulating evidence has indicated that memantine can also bind to many other CNS targets and modulate their activities, such as neuronal nAChRs at potencies similar to the NMDA receptors and 5-HT<sub>3</sub> receptors non-competitively (Rammes G 2001). Furthermore, memantine possesses agonist action at dopamine D2<sup>high</sup> receptors (Seeman P 2008).

In addition, memantine also exhibits neuroprotective activities against A $\beta$  toxicity (Tremblay R 2000; Hu M 2007; Miguel-Hidalgo JJ 2002), tau phosphorylation (Song MS 2008), neuroinflammation (Willard LB 2000), and oxidative stress (Liu W 2013; Figueiredo CP 2013).

## **ii. Drugs under development**

### **a. Secretase modulators**

The rationale for the development of agents able to modify secretase activity or processing stems from the idea that the increase of these enzymes is related to the conversion of APP into non-toxic by-products. Therefore, by inhibiting  $\beta$ - and  $\gamma$ -secretases a decrease in amyloidogenic APP processing is expected. Ligands binding at the cell surface receptors including muscarinic/GABA agonists, and activation of signalling cascades such as protein kinase C, regulates the activation of  $\alpha$ -secretase strongly.

### **i. Tarenflurbil**

Tarenflurbil, an enantiomer of flurbiprofen, modulates  $\gamma$ -secretase activity and thereby reduce A $\beta$  levels (Eriksen JL 2003). A Phase II trial of the drug showed genuine promise, whereas Phase III trials proved to be a considerable failure and so, is no longer used. Subsequent analyses of the study results demonstrated the reasons for tarenflurbil fiasco. In the study, CSF levels of tarenflurbil attained were much lower than the predicted concentrations from the preclinical evidence; in addition, there was no change in CSF A $\beta$  levels (Galasko DR 2007). The apparent benefits of tarenflurbil in Phase II trials were, in fact, due to an accelerated cognitive worsening in the placebo arm. The anti-inflammatory actions of tarenflurbil could also be a contributory reason for the observed failure (Imbimbo BP 2009).

### **ii. EVP-0962**

Although technically an amyloid-related approach, EVP-0962 is a  $\gamma$ -secretase modulator that decreases the generation of A $\beta_{1-42}$  in favour of shorter A $\beta$  proteins while allowing for cleavage of the Notch substrate, preventing many of the toxic side effects typically associated with  $\gamma$ -secretase inhibitors. In preclinical animal studies, this drug reduced A $\beta_{1-42}$ , decreased neuroinflammation and lowered the hippocampal plaque load as well as reversed memory deficits in fear conditioning

tests. At last report, EVP-0962 is in a single-centre Phase II trial to evaluate safety, tolerability, pharmacokinetics and pharmacodynamics (EnVivo Pharmaceuticals).

iii. Avagacestat

Avagacestat or BMS-708163 is a  $\gamma$ -secretase inhibitor that was recently discontinued in Phase II. In Phase I trials, avagacestat decreased both  $A\beta_{1-40}$  and  $A\beta_{1-42}$  in CSF by 30% for lower doses and 60% for higher doses. However, in a trial of 209 patients with 5 dosage groups (25, 50, 100, 125 mg/day and placebo), equal numbers of patients discontinued in the treatment cohorts compared with placebo. Additionally, patients on higher dosages indicated a faster cognitive decline compared with lower dosages and the placebo, causing the discontinuation of any development for this drug (Coric V 2012).

iv. Etazolate

Etazolate, also called EHT 0202, is hypothesized to stimulate the  $\alpha$ -secretase pathway while inhibiting  $A\beta$ -induced neuronal death. By redirecting APP processing away from amyloid pathways, this is supposed to both reduce symptoms and to slowdown/stop disease progression.

This drug showed only ‘precognitive’ properties in rodent trials but is undergoing human safety studies to investigate potential viability as a supplement to standard treatments, even though it is not suitable as a singular therapy in and of itself. Etazolate is currently in Phase II testing (Vellas B 2011).

b. Amyloid-based approaches

i. TC-6683

An  $\alpha 4\beta 2$  nicotinic receptor activator, TC-6683 was hypothesized to activate the  $\alpha 4\beta 2$  nicotinic receptor to enhance the release of ACh; although agonist binding to  $\alpha 4\beta 2$  nAChR has been shown to attenuate  $A\beta$  production *in vitro*, the Phase II trials for TC-6683 was concluded due to poor enrolment without conclusive results (Mousavi M 2009).

ii. Affitope AD02

This drug is a synthetic peptide composed of six amino acids designed to allow for the production of A $\beta$  antibodies without triggering an inflammatory response. The Phase I safety study showed a favourable profile for both safety and tolerability after 1 year. Phase II trials of affitope AD02 are currently underway (AFFiRiS AG).

iii. Bapineuzumab

Bapineuzumab is a humanized monoclonal antibody that acts on the nervous system and may have potential therapeutic value for the treatment of AD and possibly glaucoma (Sample I 2007). However, in a 2012 study, no significant cognitive improvements were observed in patients in two major trials, despite lowering key biomarkers of AD: amyloid brain plaque and phosphorylated tau protein in CSF.

Bapineuzumab is an A $\beta$  antibody believed to underlie AD neuropathology. In previous clinical trials for vaccination against human beta amyloid, called AN-1792, AD patients using active immunization experienced positive outcomes with plaques removal, but 6% of subjects developed aseptic meningitis and the trial was stopped (Woodhouse A 2007).

iv. Solanezumab

Solanezumab is a monoclonal antibody directed against the mid-domain of the A $\beta$  peptide. It recognizes soluble monomeric, not fibrillary A $\beta$ . The therapeutic rationale is that it may exert benefit by sequestering A $\beta$  and removing small soluble species of A $\beta$  that are synaptotoxic. In two Phase III clinical trials, people with mild-to-moderate AD were randomized to receive intravenous infusions of solanezumab or placebo once a month. Solanezumab was noted to be safe, but treatment showed no improvement on the primary outcome (Doody RS 2014). However, in a subgroup analysis, a trend to improved cognition with solanezumab in people with mild AD was observed, but with missed statistical significance. Statistically significant benefit was seen in a pooled analysis of patients with mild AD in both trials (Doody RS 2014). In mid-2013, a Phase III clinical trial was started with mild AD patients whose results are expected in late 2016.

v. Gantenerumab

Gantenerumab is a monoclonal antibody designed to bind to a conformational epitope on fibrillary A $\beta$  (Bohrmann B 2012). The therapeutic rationale for this antibody is that it acts centrally to disassemble and degrade amyloid plaques by recruiting microglia and activating phagocytosis. Gantenerumab preferentially interacts with aggregated brain A $\beta$ , both parenchymal and vascular. In a Phase II clinical trial, gantenerumab was injected subcutaneously into a number of participants and in 2012 the study was expanded to a Phase II/III.

A futility analysis led to halting a trial in December 2014 due to lack of perceived efficacy as compared to placebo. Besides removal of A $\beta$ , another approach in AD therapeutic development has been to reduce production of A $\beta$  (Rafii MS 2015). Recent genetic evidence shows that mutations near the  $\beta$ -secretase cleavage site, that prevent such cleavages, lead to decreased production of A $\beta$  and are, indeed, protective against developing AD dementia, despite ApoE4 status (Jonsson T 2012).

vi. Crenezumab

Crenezumab or MABT102A is a form of passive immunotherapy. It is a humanized monoclonal antibody designed to bind to human A $\beta_{1-40}$  and A $\beta_{1-42}$  in the brain and to remove it to the periphery. In addition to Phase II testing, this drug will be evaluated in a trial against placebo for the prevention of cognitive decline in presymptomatic carriers of autosomal dominant genetic mutations. Crenezumab was proven to be safe in Phase I trials, and Phase II trials have been completed for treatment of mild-to-moderate AD (Adolfsson O 2012).

c. Muscarinic receptor antagonists

Nicotinic receptor antagonists are mainly developed as modulators of the nicotinic receptors  $\alpha 7$ ,  $\alpha 2\beta 2$ ,  $\alpha 4\beta 2$ ,  $\alpha 6\beta 2$  to influence on several neurotransmitters including ACh, NA, DA, GABA or glutamate.

AZD-3480 is a modulator of nicotinic receptors  $\alpha 2\beta 2$  and  $\alpha 4\beta 2$ . No evidence of benefit was observed in a Phase II trial with mid-to-moderate AD patients (Frolich L 2010). Other trials with this compound are being undertaken.

EVP-6124 is a modulator of the  $\alpha 7$  receptor that showed positive results in a Phase IIb trial in cases of mild-to-moderate AD patients (Hilt D 2012). Two Phase III trials with mild-to-moderate patients are currently ongoing.

d. Glutamatergic agents

Besides well-reported memantine, some other NMDA receptor antagonists are currently under clinical trials for their potential use in AD therapy.

DAOI-B is a NMDA enhancer in Phase II trial with MCI and mild AD patients (results not published) and AVP923 or dextromethorphan is in Phase II for use with mild-to-moderate AD patients.

e. Serotonergic agents: 5-HT receptors modulators

A number of serotonomimetic compounds being used in clinical are under consideration in AD as monotherapy or along with AChE inhibitors (Rodriguez JJ 2012). Many novel ligands with agonistic or antagonistic properties targeting different 5-HT receptors (5-HT<sub>1A</sub>, 5-HT<sub>4</sub> and 5-HT<sub>6</sub>) are currently available (King MV 2008).

A 5-HT<sub>1A</sub> antagonist, lecozotan, proved to be safe and effective in Phase I (Patat A 2009) and Phase II clinical trials. Further studies with this molecule are under investigation. 5-HT<sub>4</sub> agonists such as PRX-03140, Velusetrag, TD-8954, RQ-00000009, SUVN-D1003019 or SUVN-1004028 have exhibited cognitive benefits in preclinical studies with potential effects on amyloid processing (Shen F 2011). The safety and pharmacokinetic potential of Velusetrag are known as this drug is currently used for gastrointestinal disorders (Long DD 2012).

The novel 5-HT<sub>6</sub> agonist SB-422457 has also shown positive results in Phase II clinical trials as a monotherapy or combined with donepezil (Maher-Edwards G 2011; Maher-Edwards G 2010). 5-HT<sub>6</sub> antagonists RO-4368554, SB-258585 or SB-399885 have also exhibited cognition enhancing properties in animal experiments (Gravius A 2011; Hirst WD 2006), hence the clinical utility of these ligands needs to be fully comprehended.

Inverse agonists of 5-HT<sub>2A</sub> receptors may improve cognitive and non-cognitive processes. Pimavanserin successfully reversed psychosis-like features in PD animal models (Price DL 2012) and in PD patients (Meltzer HY 2010). Finally, the role of 5-HT<sub>7</sub> receptor has been recently characterised in learning and memory processes, and its therapeutic interest is currently under consideration (Cifariello A 2008).

f. Anti-tau therapies

In AD pathology, it is believed that NFTs are formed in later stages of the disease following A $\beta$  accumulation, while in frontotemporal dementia (FTD), no A $\beta$  is present.

Despite its critical role in neurodegenerative diseases, therapies targeting tau have not progressed as quickly as those targeting A $\beta$ , certainly because tau aggregates are found intracellularly (Golde TE 2010). Recent anti-tau therapies have emerged as approaches targeting phosphorylation (Yang Y 2013; Claxton A 2013), microtubules stabilisation (Gozes I. 2011), prevention of oligomerisation (Badiola N 2013), enhancement of degradation (Ma QL 2013), or immunotherapy (Rosenmann 2013).

i. Rember

Rember or methylthioninium chloride, methylene blue or LMTX is a drug that is supposed to be an inhibitor of tau protein aggregation. As an inhibitor of tau aggregation, Rember may be able to halt or reverse the progression of AD. Furthermore, it is able to enhance mitochondrial biochemical pathways and, as such, can activate and increase complex IV, which is correlated with AD when inhibited. In Phase IIB clinical trials, Rember was able to slow down the development of AD symptoms in patients by 81%. This drug is currently in Phase III trials (Gerald Z 2013).

ii. Epothilone D

Epothilone D, also known as BMS-241027, is presently undergoing Phase I trials for its tolerability and efficacy following successful preclinical animal studies. BMS-241027 unlike Epothilone D compounds is studied for application in oncology and in that it can both cross the BBB and is relatively safe. Epothilone D is a small-molecule microtubule stabilizer. Hyperphosphorylated tau dissociates from microtubules and is potentially related to neurodegeneration and cognitive decline; although no specific tau mutation is currently associated with AD. It is hypothesized that epothilone D will prevent this dissociation by stabilizing the microtubules (Brunden KR 2010), thus counteracting tau abnormalities.

In animal studies on mice expressing human mutant tau, epothilone D reduced hippocampal neuronal loss and restored spatial memory. In both young and old tauopathy animals wherein tau pathology was either developing or well established, epothilone D cleared tau pathology, curbed neuron loss and reversed behavioural as

well as cognitive deficits. Additionally, epothilone D can be used in both preventative and interventional treatment depending on disease stage (Zhang B 2012).

iii. T-817MA

T-817MA is a Phase II neurotrophic/neuroprotective agent that prevents A $\beta$ -induced cell loss in the dentate gyrus and increases hippocampal neurogenesis when intracerebroventricularly infused.

In animal studies with P301L mice displaying tau pathology, administration of T-817MA decreased spatial memory impairment, increased synaptic terminal density in the hippocampal gyrus, improved cognition and decreased tau-related neurodegeneration (Fukushima T 2011).

g. Monoamine oxidase inhibitors

MAO inhibitors (MAOI) have been reported to possess a range of potential therapeutic uses. The first MAOI developed were iproniazid, an antidepressant initially developed for treatment of tuberculosis, and some hydrazine derivatives such as phenelzine, whose use was discontinued due to reported major side effects such as hepatotoxicity.

Non-hydrazine-derived inhibitors tranylcypromine and pargyline were later developed to avoid liver toxicity, yet numerous cases of hypertensive crises were reported. This side-effect, commonly known as 'cheese effect reaction', occurs after the ingestion of foods rich in tyramine and other sympathomimetic amines such as cheese (Da Prada M 1988), causing a potentiation of the sympathetic cardiovascular activity by inducing NA release from vesicles (Fig. 22).

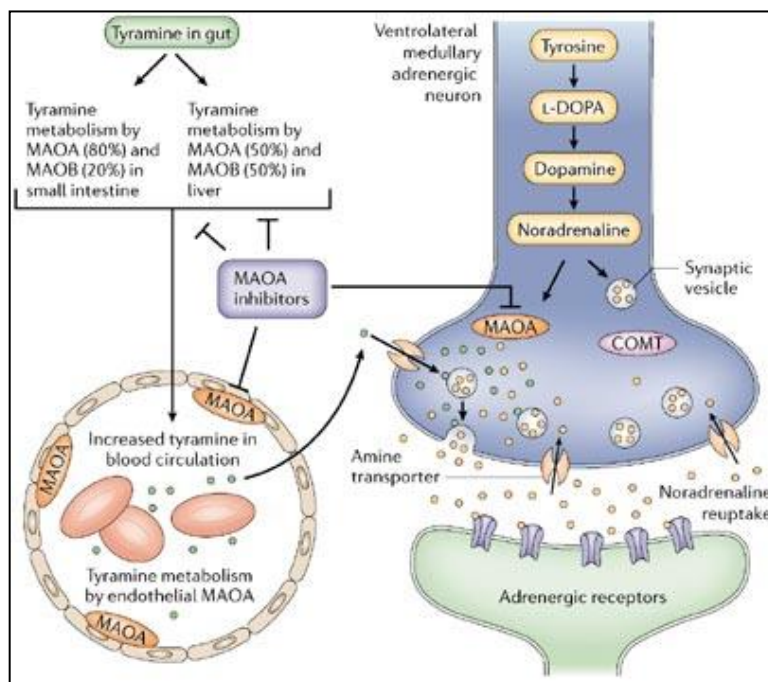


**Fig. 22.** Potentiation of cardiovascular effects of tyramine by the use of MAO A inhibitors: the 'cheese effect' reaction (Youdim MBH 2006).

This undesirable outcome only occurs when MAO A is irreversibly inhibited, as it is the most abundant isoform in the intestine (Knoll J 2000; Youdim MBH 2004), where tyramine is effectively metabolised by this isoenzyme (Hasan F 1988).

The development of reversible MAO A inhibitors, such as moclobemide or lazabemide (Knoll J 2000; Youdim MBH 2004), has emerged as a suitable pharmacological approach to avoid the 'cheese effect reaction'. The use of these inhibitors can sufficiently block MAO A in the CNS to achieve an antidepressant effect while dietary tyramine is able to displace the reversible inhibitor from the peripheral MAO A allowing its metabolism (Anderson MC 1993).

Alternatively, brain-selective irreversible MAO A inhibitors such as Ladostigil or M-30 can also be used to prevent the 'cheese effect reaction' by using a precursor that is activated by L-amino acid decarboxylase together with a peripheral inhibitor of that enzyme (Palfreyman MG 1985).

There is a wide array of MAOIs (Table 3) available for use in different conditions such as neurodegenerative diseases (PD or AD), cerebral ischemia, affective diseases or ageing.

**Table 3.** List of some MAOI and their current and therapeutic potential uses (Youdim MH 2006).

Compound	MAO selectivity	Inhibition type	Application
Befloxadone	A	Reversible	Antidepressant
Brofaromine	A	Reversible	Antidepressant
CGP 3466	Not inhibitory	Not inhibitory	Antiparkinson
Clorgyline	A	Irreversible	Antidepressant
l-Deprenyl (Selegiline)	B	Irreversible	Antiparkinson
2-HMP (and other aliphatic propargylamines)	B	Irreversible	Antiparkinson
Iproniazid	A and B	Irreversible	Antidepressant
Isocarboxazid	A and B	Irreversible	Antidepressant
Ladostigil	A and B (brain selective)	Irreversible	Antidepressant, antiparkinson and anti-Alzheimer
Lazabemide	B	Reversible	Antiparkinson
M30	A and B (brain selective)	Irreversible	Antidepressant, antiparkinson and anti-Alzheimer
Moclobemide	A	Reversible	Antidepressant
Nialamide	A and B	Irreversible	Antidepressant
PF 9601N	B	Irreversible	Antiparkinson
Phenelzine	A and B	Irreversible	Antidepressant
Rasagiline	B	Irreversible	Antiparkinson
Safinamide	B	Reversible	Antiparkinson
Toloxatone	A	Reversible	Antidepressant
Tranylcypromine	A and B	Irreversible	Antidepressant

2-HMP, N-(2-heptyl)-N-methylpropargylamine; MAO, monoamine oxidase.

The use of MAOIs in AD pathology has been mainly focused on the contribution of these enzymes to produce oxidative stress, through its own catalytic action, especially since the activity of MAO B is increased in the brain of such patients (Kennedy BP 2003) and the inhibition of MAO A may alleviate the depressive-like symptoms also present in some stages of this disorder. Nevertheless, a combined treatment with MAOIs plus one of the FDA-approved drugs for use in AD might enhance their single therapeutic effect.

#### *Neuroprotective propargylamine-containing monoamine oxidase inhibitors*

Propargylamines have been defined as potent anti-apoptotic and neuroprotective agents in both *in vitro* and *in vivo* studies. Propargylamines are presumably able to maintain glyceraldehyde-3-phosphate dehydrogenase (GAPDH) as a dimer and thereby preventing its nuclear translocation to block the upregulation of pro-apoptotic proteins. Also, in several studies using propargylamine-containing molecules, it has been observed an induction of cell survival in response to serum withdrawal or neurotoxins in cell culture through the activation of Bcl-2 and Bcl-XL and the downregulation of Bad and Bax (Tatton WG 2002; Bar-Am 2005; Wadia JS 1998; Akao Y 2002; Youdim MBH 2005).

In addition, propargylamines have been also described to interact with the mitochondrial membrane (Wadia JS 1998; Youdim MBH 2005), by avoiding the formation of the mitochondrial pore, preventing the collapse of the mitochondrial membrane potential and inducing the expression of antioxidant enzymes such as catalase or superoxide dismutase 1 (SOD-1) (Kitani K 2000) (Fig. 23).

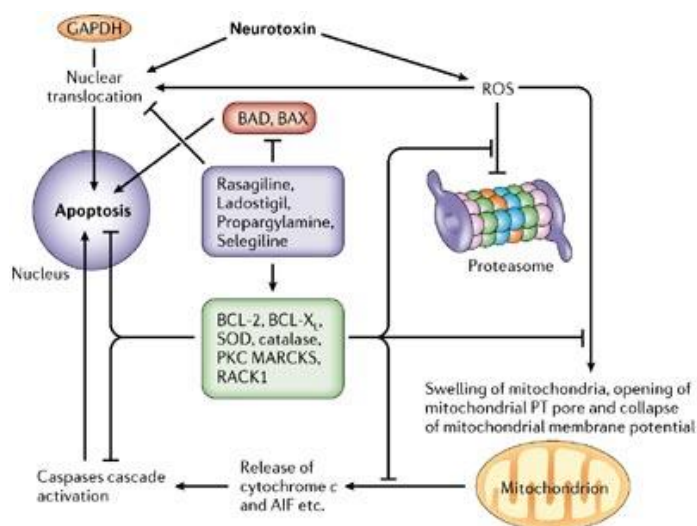


**Fig. 23.** Mechanism of neurotoxin-induced neuronal death and its prevention by propargylamine (Youdim MBH 2006).

Since the discovery of the neuroprotective activity and anti-apoptotic properties of propargylamines, numerous molecules bearing this moiety have been designed and developed for use in different neurodegenerative diseases such as PD or AD (Fig. 24).

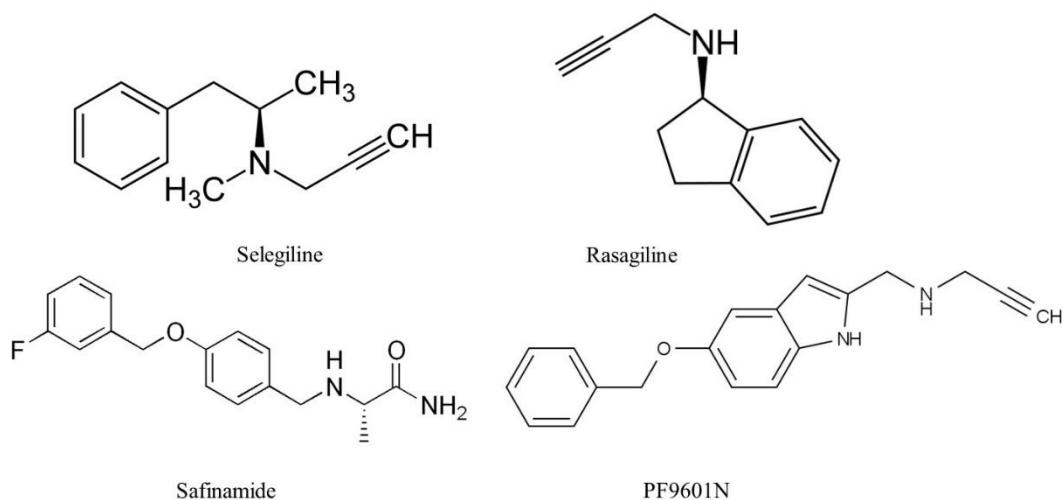


**Fig. 24.** Chemical structures of some propargylamine-containing compounds with neuroprotective properties for use in the treatment of neurodegenerative diseases.

#### i. Selegiline or l-deprenyl

Selegiline is an irreversible MAO B inhibitor approved by the FDA for use in PD therapy (Birkmayer W 1984; Birkmayer W 1983) since dopamine is preferably metabolised by this isoenzyme in humans (Kaseda S 1999) as well as to potentiate the pharmacological action of L-DOPA (Heinonen EH 1989).

The therapeutic use of selegiline has been limited since methamphetamine and L-amphetamine were identified as a result of its metabolism (Heinonen EH 1994), hence potentially damaging and hampering the reported neuroprotective properties of selegiline (Bar Am O 2004; Moszczynska A). Yet, beneficial properties have been reported with this molecule from several clinical trials in PD (Pálhagen S 2006; Przuntek H 1999; Zhao YJ 2011).

Moreover, selegiline was also described to prevent from the extrapyramidal symptoms induced by the neurotoxin MPTP, which is selectively metabolised by MAO B, to generate the toxic metabolite  $MPP^+$  in striatal microglia and hence producing degeneration by oxidative stress (Wu RM 1993).

#### ii. Rasagiline

Rasagiline is a selective irreversible MAO B inhibitor approved by the FDA in 2006 as a second-generation agent for the treatment of PD.

It is dosed daily and can be administered alone or in combination with other PD medications without causing significant side effects (Finberg JP 2002). The efficacy of rasagiline has been demonstrated in a number of Phase III-IV randomised double-blind placebo-controlled trials (Olanow CW 2009; Group. 2005, 2002; Rascol O 2005).

Rasagiline has been conclusively demonstrated to improve motor function in PD pathology over at least 5 years, but to date any potential neuroprotective benefit has been confirmed.

### iii. Safinamide

Safinamide is another potently selective MAO B inhibitor (Cattaneo C 2003) recently approved by the European Commission as an add-on to levodopa or in combination with other PD medications in mid-to-late stage PD patients with motor fluctuations. It is currently under review by the FDA for use in both early and mid-to-late stage PD. Safinamide presents additional properties such as the ability to blocking voltage-dependent sodium channels and the inhibition of glutamate release (Chazot PL 2007).

The efficacy of safinamide has been established for early and advanced PD in phase II and phase III trials. Two phase III clinical trials have been conducted in early PD with patients receiving dopamine agonists and two in mid-to-late stage PD for patients receiving levodopa with motor fluctuations (Stocchi F 2012; Barone P 2013; Schapira AH 2013; Borgohain R 2014). A potential advantage of safinamide over the other MAO-B inhibitors is a purported antidyskinetic effect, which is thought to be related to its anti-glutamate activity (Caccia C 2006). The antidyskinetic properties have been demonstrated in MTPP-lesioned dyskinetic macaque monkeys, which were pre-treated with safinamide and both reduced dyskinesias and prolonged the duration of the antiparkinsonian effect of levodopa (Gregoire L 2013).

As with the other MAO-B inhibitors, safinamide possesses neuroprotective properties *in vitro* and *in vivo*. It has been shown to prevent neuronal cell death in animal and tissue culture models (Caccia C 2006). Therefore, both laboratory and clinical evidence confirmed that safinamide is mechanistically different than other MAO-B inhibitors. These findings could provide significant advantages over selegiline and rasagiline, especially whether the potential of safinamide as a neuroprotective and anti-dyskinetic agent is fully comprehended.

#### iv. PF9601N

PF9601N or FA-73 is a propargylamine-containing irreversible selective MAO B inhibitor identified in our group amongst an extensive series of acetylenic and alenic tryptamine derivatives (Balsa D 1991; Avila M 1993; Perez V 1996). It is a potent selective MAO B inhibitor endorsed with numerous benefits including the lack of amphetamine-like products from its metabolism (Dragoni S 2007).

PF9601N was reported to block the responses elicited by endoplasmic reticulum (ER) stress (Sanz E 2009), as one of the factors underlying the pathogenesis of several diseases such as AD (Scheper W 2009). It was also been reported to attenuate the MPTP-induced striatal dopamine depletion in young adult and old adult C57/BL6 mice (Perez V 2003) and to reduce the loss of tyrosine hydroxylase (TH)-positive neurons after nigrostriatal injection of 6-hydroxydopamine (6-OH) in rats (Cutillas B 2002). The antiapoptotic effects of PF9601N might be attributed to the prevention of transcription factor p53 stabilisation and its subsequent transcriptional activity (Sanz E 2008). The protective effects observed with PF9601N led to consider it as a potential therapeutic agent for use in neurodegenerative disorders involved in neurotoxicity such as PD and AD.

#### h. Other single-target approaches

The complexity of AD has encouraged the development of a massive number of diverse pharmacological approaches in recent years. In addition to the above mentioned therapeutic strategies, others including neurotrophic agents NGF (Bruno MA 2009), BDNF (Cattaneo A 2008) or TGF $\beta$ 1 (Zhang H 2005) or metabolic enhancers (targeting reduced glucose metabolism (Bomfim TR 2012) or the use of alternative energy sources (Yao J 2011) are currently under development.

#### i. Multi-target approaches

Both the multifactorial nature of AD and the lack of therapeutic effectiveness of the current FDA-approved drugs (Opar A. 2008), which are based on the single-target paradigm, has inexorably prompted to the rational design and development of a novel and improved pharmacological approach against AD: the Multi-Target-Directed Ligands (MTDL) or 'dirty drugs'. These molecules are conceived to directly interact with multiple targets associated with AD by the molecular hybridisation of different pharmacophoric subunits from identified bioactive molecules.

To date, the therapeutic potential of MTDLs for the treatment of complex neurodegenerative diseases and age-related cognitive impairment has been partially realised since desired responses are difficult to insure for the particular targets. From studies carried out over the last decade, the efficacy of single-target drugs for the treatment of cognition and memory decline has been widely limited (Buccafusco JJ 2000; Youdim MHB 2005). Moreover, the complexity of AD therapy requires addressing the diverse pathological aspects present in the disease.

Thus, in this context, although the combination of single-target drugs with diverse therapeutic activities is feasible; the development of MTDLs obviates the challenge of simultaneously administering multiple drugs with potentially different degrees of bioavailability, pharmacokinetics and metabolism. Furthermore, this pharmacological approach also provides AD patients with a simplification of the therapeutic regimen (Fig. 25).

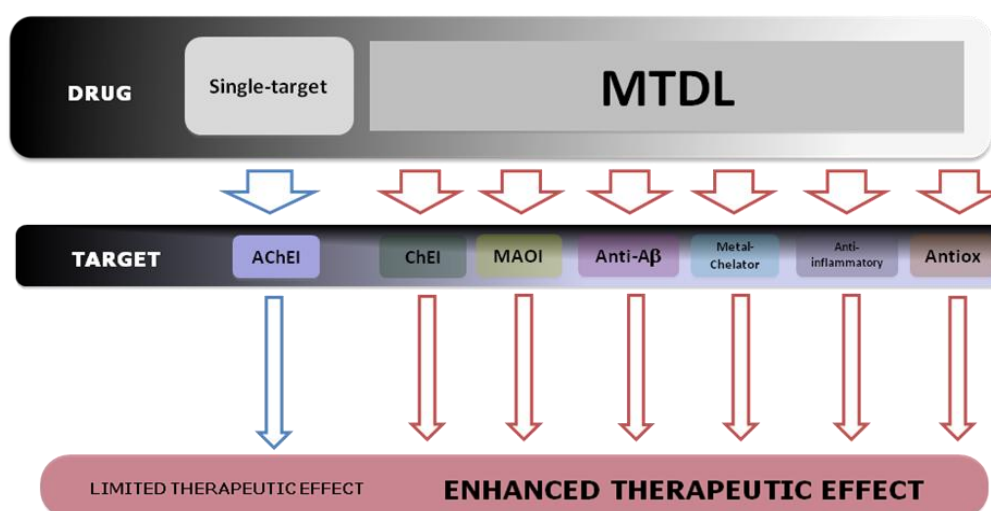


**Fig. 25.** Scheme of the therapeutic design strategy of MTDL for the treatment of the multifaceted nature of AD pathology.

Multifaceted diseases such as AD are mainly caused by perturbations of the complex intracellular network that links to tissue and organs systems. Therefore, approaches relying on targeting single proteins/mechanisms are not likely to outcome effective. Because of the existence of feedback mechanisms in biological systems, a long-term enzymatic inhibition may not be able to decrease, but instead may increase the activity as reported from the use of rapid-reversible AChE inhibitors, which significantly increased both protein activity and expression levels in the CSF of AD patients after long-term treatment (Darreh-Shori T 2010). This may contribute to the limited efficacy of these inhibitors in AD treatment as well as

the robustness of our bodies that makes drugs, in particular, single-target drugs, less effective or even ineffective (Kitano H. 2007).

Since 2005, the literature has shown several promising results from applying this innovative approach or drug design. Well-known drugs such as donepezil, tacrine or rivastigmine (Samadi A 2011; Bolognesi ML 2007) as well as bioactive natural products such as curcumin (Malar DS 2014), berberine (Shan WJ 2011; Jiang H 2011) or 8-hydroxyquinoline (Gomes LM 2014) have been used as structural scaffolds for the development and search of new chemical entities with multiple properties or MTDLs for the treatment of AD (Fig. 26).

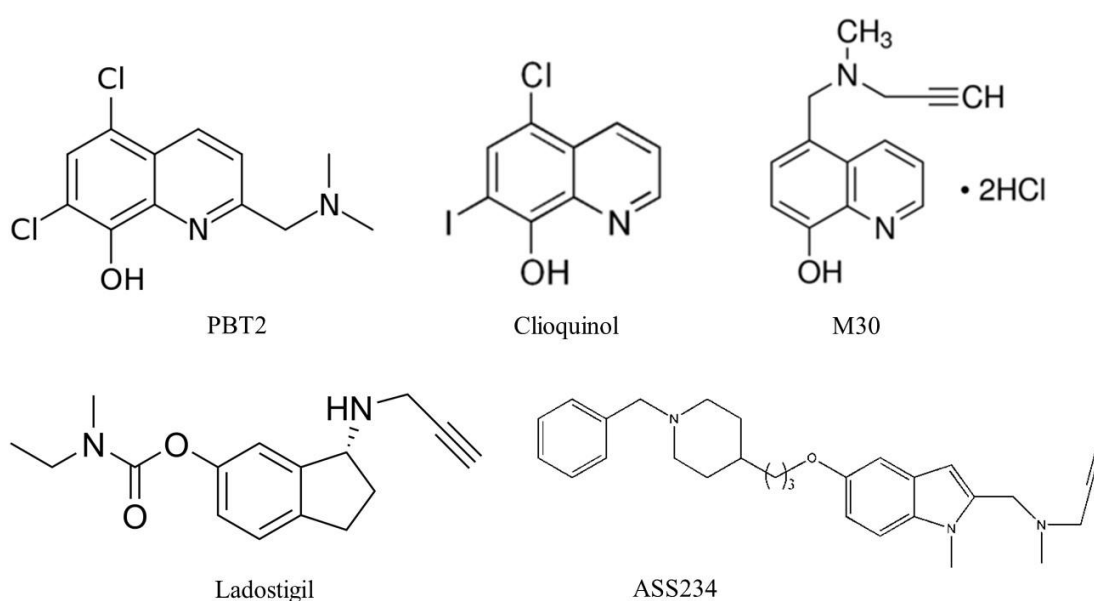


**Fig. 26.** Some MTDLs developed for use in AD and other neurodegenerative diseases: Ladostigil, M-30, Clioquinol, PBT2 and ASS234.

Although the MTDLs are not true network medicines yet, they may be considered as simplified versions or lead drugs possessing a great value as a real alternative to the current unsuccessful pharmacological therapies for effectively fighting against AD and other complex diseases.

#### i. Ladostigil

Ladostigil (TV3326) is a MTDL bearing the carbamate moiety of rivastigmine introduced into the sixth position of rasagiline, responsible for both ChE inhibition and neuroprotective activity against oxidative stress. This modification resulted in a

reduction of approximately 5-fold MAO B inhibitory activity *in vitro* compared to that of rasagiline.

Surprisingly, on repeated oral administration with different doses of ladostigil to rats and mice, brain MAO-A and -B were similarly inhibited to ChEs (Weinstock M 2000a). As a ChEI, this MTDL may enhance the cognitive function by increasing the cholinergic activity and provide symptomatic improvement of extrapyramidal symptoms by boosting nigrostriatal dopamine transmission. *In vitro*, ladostigil was found to selectively inhibit 100-fold more potently BuChE than AChE, which could be advantageous as levels of BuChE are not reduced in AD, contributing to the maintenance of ACh levels in the synaptic cleft (Giacobini E. 2001). In *in vivo* experiments, cortical ChE activity of rats was inhibited by 20-80% after oral administration of 9-200 mg/kg of ladostigil. Furthermore, ladostigil increased dose-dependently brain ACh levels in scopolamine-induced spatial memory deficits in rats (Weinstock M 2000b).

Moreover, the ability of ladostigil to inhibit both brain MAO isoforms provides it with effective antidepressant capacity. *In vivo* experiments with rats described that a single dose of 120 mg/kg of ladostigil was necessary to inhibit brain MAO isoforms activity by at least 50%. However, a daily administration of 26 mg/kg of ladostigil for two weeks, brain MAO A and MAO B were inhibited by 66% and 71%, respectively. Minor effects were observed on the MAO present in the guts under the same treatments (Weinstock M 2000a; Weinstock M 2002). The fact that ladostigil does not inhibit MAO A and MAO B *in vitro* at concentrations below 250  $\mu$ M and 1 mM, respectively, but it does in the brain isoforms *in vivo*, seems to be due to the formation of an active metabolite. One of these is produced by the hydrolysis of the carbamate moiety by ChE to yield the 6-OH derivative, a molecule able to inhibit MAO A and MAO B with  $IC_{50}$  values of 0.46  $\mu$ M and 0.35  $\mu$ M, respectively.

Therefore, patients receiving ladostigil should exhibit few symptoms related to the inhibition of MAO A in the intestine after the intake of tyramine-containing foods or beverages. This finding was observed in rabbits treated with ladostigil, in which blood pressure only increased by 30 mm Hg at doses of 30 mg/kg compared to 60-70 mg/kg in control animals. Comparatively, a reasonable equivalent daily amount of tyramine intake would be about 900 mg in humans (Da Prada M 1988). Additionally, a daily administration of ladostigil (26 mg/kg) for 14 days completely prevented the depletion of striatal dopamine and reduction of DOPAC and HVA in MPTP mice model of PD (Sagi Y 2003). Brain levels of serotonin and noradrenaline were also increased under the same experimental conditions.

On July 2014, it was announced by Avraham Pharmaceutical Ltd. (www.avphar.com) that ladostigil successful interim results in a Phase IIb clinical trial for the evaluation of its safety and efficacy in patients diagnosed with MCI. New provisional results are expected at Q3 2015 and the final results at Q3 2016. These findings suggest that like selegiline, ladostigil may possess a therapeutic value for the treatment of extrapyramidal symptoms in AD and dementia with Lewy bodies (DLB).

ii. M30 and M30D

The MTDL M30 is a potent brain-permeable propargylamine-containing metal-chelator (Fig. 27) with MAO-A/B inhibitory activities found *in vitro* and *in vivo* (Gal S 2005; Zheng H and Fridkin M 2005). In addition, it also exhibited neuroprotective and neurorestorative activities in three classical animal models of PD: MPTP (Zheng H and Fridkin M 2005), lacatcystin (Zhu W and J 2007) and 6-OH (Kupersmidt L unpublished).

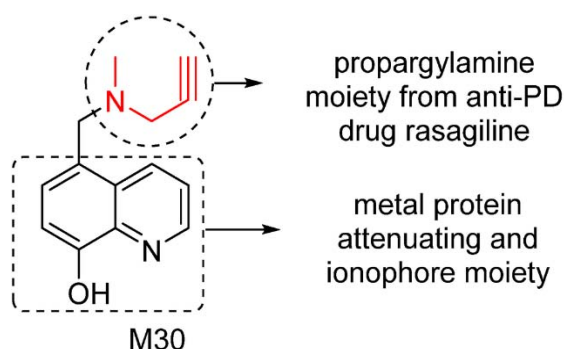


**Fig. 27.** Scheme of structure and pharmacophores of multifunctional M30.

As a potent brain-selective MAO inhibitor, M30 produces *in vivo* similar effects on increased levels of neurotransmitters DA, 5-HT and NA as those of ladostigil (Youdim MB 2013).

M30 has shown to possess a wide range of pharmacological activities, including pro-survival neurorescue effects, induction of neuronal differentiation and regulation of APP and A $\beta$  levels. M30 was also found to decrease apoptosis in a serum deprivation model using SH-SY5Y cells, via reduction of the pro-apoptotic proteins Bad and Bax, and inhibition of the apoptosis-associated phosphorylated H2A.X protein (Ser 139) and caspase-3 activation. In addition, this molecule was reported to induce the outgrowth of neurites, triggered cell cycle arrest in G(0)/G(1)

phase and to enhance the expression of growth associated protein-43. Furthermore, M-30 markedly reduced the levels of cellular APP and  $\beta$ -C-terminal fragment ( $\beta$ CTF) and the levels of the amyloidogenic A $\beta$  peptide in the medium of SH-SY5Y cells and Chinese hamster ovary (CHO) cells stably transfected with the APP<sub>swe</sub>. Levels of the non-amyloidogenic soluble APP $\alpha$  and  $\alpha$ -CTF in the medium and cell lysate respectively were coordinately increased.

The ability of this novel metal chelator to regulate APP is in line with the presence of an iron-responsive element (IRE) in the 5'-untranslated region (5'UTR) of APP. In a systemic treatment of APP/PS1 Tg mice with M30 for nine months, cognitive impairments were significantly attenuated in a variety of tasks of spatial learning and memory retention, working memory, learning abilities, anxiety levels, and memory for novel food and nesting behaviour. Furthermore, M30 reduced cerebral iron accumulation accompanied by a marked decrease in several AD-like phenotypes, including cerebral APP levels, A $\beta$  levels and plaques, phospho-APP and phospho-tau.

Additionally, the systemic chronic administration of M30 resulted in up-regulation of hypoxia inducible factor (HIF)-1 $\alpha$  protein levels in various brain regions (e.g. cortex, striatum, and hippocampus) and spinal cord of adult mice. Real-time RT-PCR revealed that M30 differentially induced HIF-1 $\alpha$ -dependent target genes, including vascular endothelial growth factor, erythropoietin, enolase-1, transferrin receptor, heme-oxygenase-1, inducible nitric oxide synthase, and glucose transporter-1. In addition, mRNA expression levels of the growth factors, BDNF and GDNF and three antioxidant enzymes (catalase, superoxide dismutase (SOD)-1, and glutathione peroxidase) were up-regulated by M30 treatment in a brain-region-dependent manner. Immunoblotting studies revealed that M30 induced a differential enhanced phosphorylation of protein kinase C, mitogen-activated protein kinase (MAPK)/ERK kinase (MEK), protein kinase B (PKB/Akt), and glycogen synthase kinase-3 $\beta$  (GSK-3 $\beta$ ). As antidepressant, similar results to those observed with ladostigil were obtained with M30 in the same animal models with 5 mg/kg dose given orally for three weeks. (Kupersmidt L, unpublished work).

Together, these results suggest that the multifunctional iron-chelator M30 is able to up-regulate a number of neuroprotective adaptive mechanisms and pro-survival signalling pathways in the brain that might function as important therapeutic targets for the drug in the context of neurodegenerative disease therapy (Fig. 28).

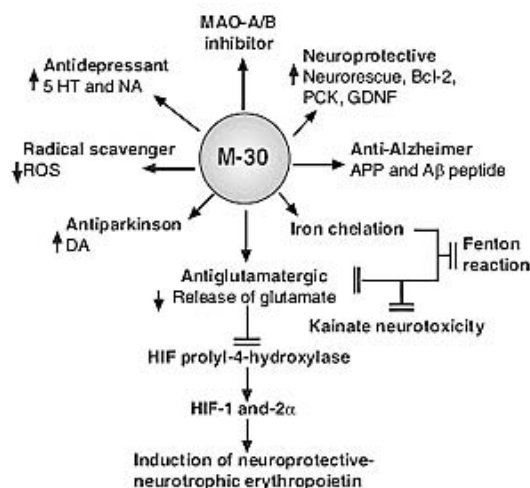


**Fig. 28.** Scheme of the multiple neuroprotective mechanisms reported with M30.

These properties, together with its brain selective MAO inhibitory and propargylamine-dependent neuroprotective effects, suggest that M30 might serve as a suitable drug for use in different neurodegenerative disorders, such as AD or PD, in which oxidative stress and iron dysregulation are highly involved.

M30D is a MTDL rationally designed as a new lead based on the structural modification of M30 (Fig. 29) to target several key disease-related enzymes/pathway of network dysfunction in AD including A $\beta$ , tau, ChEs, MAO A/B, metal dyshomeostasis, oxidative stress, and anti-inflammatory and neuroprotective pathways.

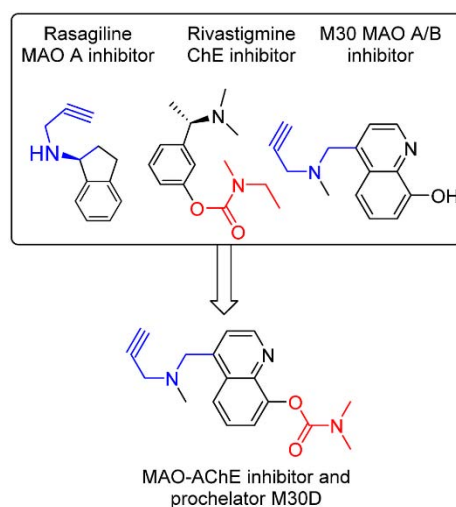


**Fig. 29.** Design strategy of M30D based on the structures of rasagiline, rivastigmine and M30 (Zheng H 2014).

Preliminary results revealed M30D as a potent pseudo-irreversible AChE inhibitor and moderate BuChE inhibitor. In addition, it is a highly potent MAO A inhibitor and weak MAO B inhibitor in rat brain homogenates. Moreover, M30D was found to possess poor metal ion chelating properties *in vitro*, however, upon incubation with AChE, it exhibited high metal-binding affinity (Meunier J 2006). In *in vivo* studies, M30D acted as a pro-chelator being metabolised to M30 following pseudo-inhibition of AChE. In human lesioned-SH-SY5Y cells, M30D was found to significantly reduce toxicity compared to M30 (Zheng H 2010).

### iii. Clioquinol

Clioquinol (CQ) is a derivative of 8-hydroxyquinoline initially designed as antiparasitic agent for intestinal amebiasis used from 1930 to 1970. The oral usage of this molecule was withdrawn from the market in 1985 due to neurotoxic side effects including subacute myelo-optic neuropathy (Tsubaki T 1971; Tateishi J. 2000). Nevertheless, later studies revealed that CQ possessed a moderate metal-chelating activity, and further investigations were carried out towards this new finding.

CQ contains two electron donor sites located at the quinoline ring nitrogen atom and phenolate oxygen atom, responsible for its chelating ability. Moreover, halogen groups help increase its lipophilicity for proper absorption to target sites in the brain (Bush AI 2003). An *in vivo* study using an AD mouse model revealed that oral treatment with CQ for nine weeks reduced brain A $\beta$  deposits by 40% (Cherny RA 2001), and another work showed that memory impairment was rescued by this molecule (Grossi C 2009). CQ has also been described as a modulator of copper efflux activities of APP (Treiber C 2004), inhibitor of the A $\beta$  oligomer formation (Mancino AM 2009; LeVine H 2009) and preventive of A $\beta$ -injection-induced cell loss (Ibach B 2005).

In neurodegeneration animal models, CQ protected against DA depletion and nigral neuronal loss MPTP-administered (Kaur D 2003) and tau knock-out mice (Lei P 2012). Positive results were also obtained in a murine model of HD disease (Nguyen T 2005). CQ was reported to attenuate the effects of aging by reducing the levels of mitochondrial hydroxylase CLK-1, required for the ubiquinone biosynthesis (Ewbank JJ 1997; Jonassen T 2001). The precise mechanism of action of CQ remains unknown, yet most studies pointed that the therapeutic effects of this molecule are related to its metal-chelating properties (Treiber C 2004; Raman B 2005; Priel T 2007).

Recent works confirmed CQ as an ionophore metal chaperone able to redistribute metals into the cell (Cherny RA 2001; Nitzan YB 2003; Adlard PA 2008; Li C 2010) (Park MH 2011; Crouch PJ 2011) hence conferring neuroprotection as iron-chelator from metal-protein interactions (Crouch PJ 2012; Tamura Z 1973; Kidani Y 1974; Ohtsuka K 1982). Additionally, this molecule can affect the PI3K pathway, and therefore upregulate matrix MP activity to promote A $\beta$  degradation (White AR 2006; Filiz G 2008a; Filiz G 2008b). A recent study also revealed that CQ restores endosomal trafficking in the vacuoles of A $\beta$ -expressing cells, and dramatically reduced A $\beta$  peptide levels by increasing degradation (Matlack KES 2014). In a phase II clinical trial, improvement in cognitive outcomes for AD patients was reported, however, this investigation was discontinued due to difficulties with large-scale manufacturing of the compound as a consequence of the presence of small amounts of a carcinogenic contaminant (Crouch PJ 2012).

#### iv. PBT2

PBT2 is a second-generation 8-hydroxyquinoline derivative developed to resolve the toxicity problem of CQ as well as to improve its solubility and ability to cross the BBB (Crouch PJ 2012). It was observed that PBT2 selectively chelates copper and zinc while forming soluble complexes able to pass through cellular membranes, leading to bioavailable delivery of these two metals into the cells (Adlard PA 2008; Crouch PJ 2011; Adlard PA 2011). PBT2 also displayed significant therapeutic effects on both AD mouse model (Adlard PA 2008) and phase II clinical trials (Lannfelt L 2008; Faux NG 2010). In a similar way to CQ, this molecule also exhibited neuroprotective activity as a copper-zinc ionophore able to induce inhibition of the phosphorylation of the GSK-3  $\alpha$ - and  $\beta$ -isoforms and subsequently lower A $\beta$  levels (Crouch PJ 2011). It is also being investigated for applications treating HD.

#### v. ASS234

ASS234 is a MTDL designed and conceived for use in AD therapy. Structurally, ASS234 is based on the hybridisation of the benzylpiperidine moiety of donepezil, responsible for the ChE inhibition, and the indolyl propargylamine of FA65, a potent MAO inhibitor and derivative of PF9601N (Fig. 30). Previous studies reported ASS234 as a potent dual inhibitor of both cholinesterases and the two MAO isoforms activities (Bolea I 2011).

More recently, new findings with this brain-permeable molecule have revealed neuroprotective properties of ASS234 against  $A\beta_{1-42}$ -associated toxicity in SH-SY5Y cells. By potently reducing  $A\beta$  self-aggregation *in vitro*, ASS234 was able to prevent the formation of fibrillary and oligomeric species. This effect was confirmed by SDS-PAGE analysis, in which amyloid species with low molecular weight such as monomers or trimers were found increased following an incubation with this molecule. This activity might be due to the direct interaction of ASS234 with the amyloid peptides during the oligomerisation process, by stabilising the less extended forms of  $A\beta$  hence preventing further assembly towards toxic species. Moreover, ASS234 was also able to block the AChE-dependent aggregation of both  $A\beta_{1-40}$  and  $A\beta_{1-42}$ , revealing its capacity to bind to the PAS (Bolea I 2013). In addition, ASS234 was also reported to protect SH-SY5Y cells from  $A\beta_{1-42}$ -mediated toxicity by decreasing the activation of caspases 3 and 9 and PARP fragmentation. These findings suggest that ASS234 might antagonise the mitochondrial pathway of apoptosis, possibly due to the well-reported neuroprotective activity of propargylamine-containing derivatives (Bolea I 2013).

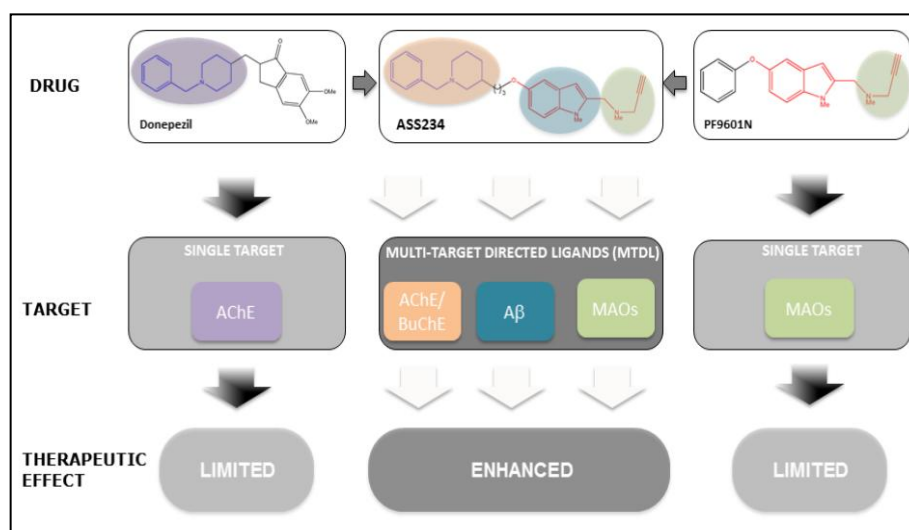


**Fig. 30.** The design strategy of multi-target ASS234 based on active moieties of donepezil and PF9601N for an enhanced use in AD therapy (Bolea I 2013).

Besides the anti-amyloid properties of ASS234, in the same study, this multi-target molecule was also reported to possess significant antioxidant activity to capture free radical species *in vitro* (ORAC-FL) as well as to increase the expression of the antioxidant enzymes catalase and superoxide dismutase-1 (SOD-1) in  $A\beta_{1-42}$ -treated SH-SY5Y cells. In ASS234-treated SH-SY5Y cells, an induction of canonical and non-canonical Wnt pathways was described as another protective mechanism by

which this molecule rescues memory loss and improves synaptic dysfunction in transgenic mice model of AD (Del Pino J 2014).

*In vivo* studies revealed ASS234 to be able to inhibit MAO and ChE activities after subcutaneous administration in rats (Stasiak A 2014). To date, several properties have been reported to ASS234 (Fig. 31), providing strong evidence to consider this molecule a promising compound for use in AD therapy that has encouraged to carry out new studies currently under investigation.

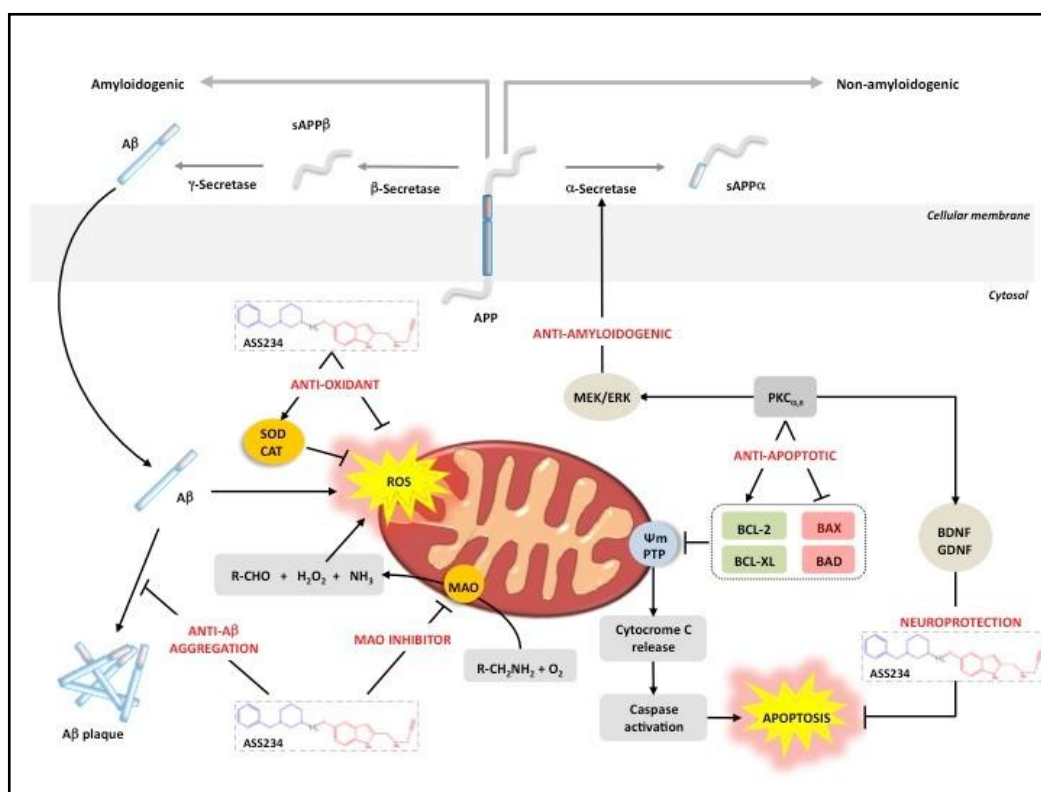


**Fig. 31.** Scheme of the multiple targets and activities reported with multi-target ASS234 for use in AD pathology (Bolea I 2013).

## vi. Other MTDLs

### i. Berberine-derived ligands

Berberine is a quaternary ammonium salt found in several plants and used in the Chinese traditional medicine for its activity against fungal infections, *Candida albicans*, yeast, parasites, and bacterial/viral infections. Berberine has been used as a scaffold for the design of hybrid compounds with molecular moieties including melatonin or ferulic acid. These derivatives have exhibited antioxidant and anti-A $\beta$

aggregation properties with weak AChE and BuChE inhibitory activity (Jiang H 2011).

ii. Memoquin

Memoquin is a quinone-bearing polyamine compound that has recently emerged as a promising drug prototype for AD (Cavalli A 2007; Cavalli A 2012). This MTDL exhibited 10-fold more potent anti-ChE activity compared to donepezil. In addition, memoquin has shown dose-dependent inhibition of spontaneous and AChE-mediated A $\beta$ <sub>1-42</sub> oligomers-induced neurotoxicity in SH-SY5Y cells (Bolognesi ML 2011).

Moreover, memoquin is also able to inhibit BACE-1 activity dose-dependently as well as to possess antioxidant properties to neutralise the formation of free radicals and ROS in sulforaphane-treated SH-SY5Y cells (Bolognesi ML 2009). In a recent *in vivo* study using two behavioural models, memoquin was able to rescue several features related to cognitive impairment (Capurro V 2013).

vii. Natural products for use in AD

Since decades ago, the beneficial properties of some natural products have been under investigation to use in AD. Among them, curcumin, EGCG, resveratrol or huperzine A, among others, have provided mounting evidence of their potential therapeutic action in neurodegeneration and age-related conditions (Fig. 32).

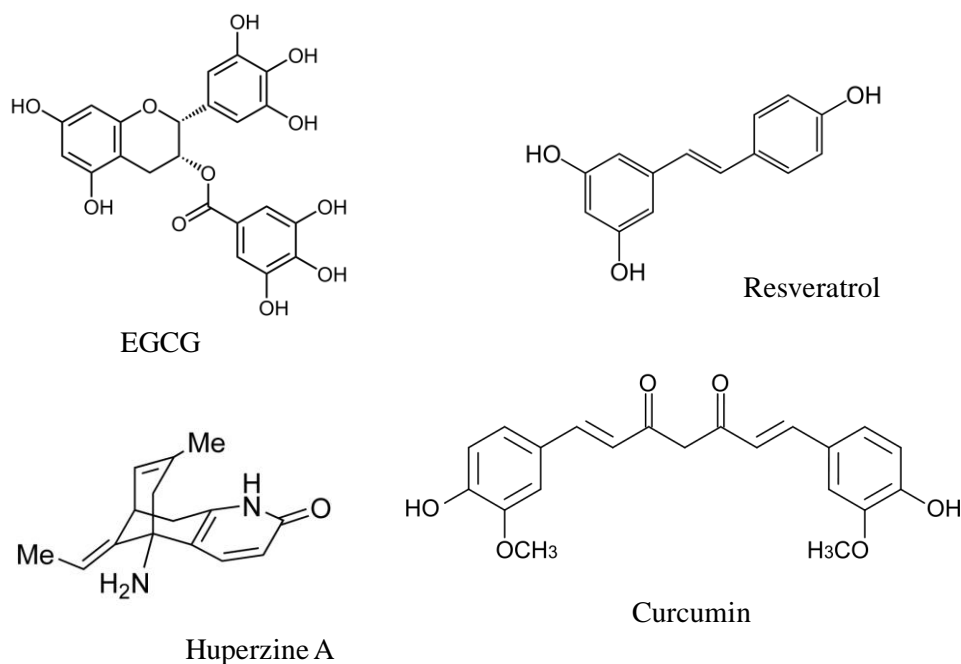


**Fig. 32.** Chemical structures of some natural products with potential use in AD therapy.

#### i. Huperzine A

Huperzine A (HupA) is a natural AChE inhibitor derived from the Chinese folk medicine *Huperzia serrata* (Ratia M 2013). It has been traditionally used to treat different disorders including bruises, strains, swelling, rheumatism, schizophrenia or fever (Ma X 2007). HupA has been licensed as anti-AD drug in China and it is available as a nutraceutical in the US (Orhan IE 2011). Recent studies have demonstrated that HupA could effectively reverse or attenuate cognitive deficits in rodents, primates and humans (Howes MJ 2011). Thus, in a meta-analysis of randomised clinical trials, HupA was concluded to improve cognitive function, daily living activity and global clinical assessment in AD patients, displaying few adverse effects (Yang Y 2014). In addition, recent findings have reported mounting evidence of non-cholinergic properties of HupA including the ability to protect neurons against A $\beta$ -induced oxidative injury and apoptosis, to ameliorate mitochondrial malfunction, to antagonize NMDA receptors, to regulate NGF, to promote non-amyloidogenic APP processing or to reduce iron in the brain (Huang XT 2014).

#### ii. EGCG

Epigallocatechin-gallate (EGCG) is a polyphenol present in green tea. Recent investigations have suggested that EGCG possesses strong antioxidant properties and induces  $\alpha$ -secretase activity and thus non-amyloidogenic APP processing (Smith

A 2010). A Phase II trial investigating the benefit of EGCG in early stages of AD is currently underway (NCT00951834).

iii. Resveratrol

Resveratrol is a polyphenol naturally produced by several plants, including grapes and berries, to avoid bacteria or fungi attack. It has been recently investigated as a cardioprotective, anticancer and anti-ageing compound (Richard T 2011; Baur JA 2006; Yao R 2013). But, to date, little evidence of beneficial effects has been proven in humans.

However, in recent years, many resveratrol-based compounds have been developed and reported to possess strong A $\beta$  antiaggregation and antioxidant activities (Sharma M 2002; Jang J 2003). Moreover, some compounds also exhibited metal-chelating properties with dual ChE and MAO inhibitory activity (Lu C 2013).

iv. Curcumin

Curcumin is currently in Phase IIb testing for AD as a neuroprotective MTDL bearing anti-inflammatory, antioxidant and anti-amyloid mechanisms. In rats, curcumin decreases inflammation, oxidation rates, inhibits tau aggregation and aids for A $\beta$  plaques clearance. Curcumin may also promote metal-chelation and neurogenesis. It is a natural polyphenol that occurs in turmeric and has been used in traditional Eastern medicinal practice for centuries; as such, it has an unusually robust safety record (Cole GM 2007).

Another action recently found with curcumin is the ability to inhibit the heat shock protein 90 (Hsp 90) (Giommarelli C 2010), a chaperone involved in folding the denatured proteins that seems to play a role in preventing tau degradation (Dickey CA 2007). Curcumin treatment alleviated tau pathology in tau transgenic mice by suppressing tangle formation as well as promoting dissolution of already formed tangles (Ma QL 2013).

## **II. AIMS**



## II. AIMS

The multifactorial nature of Alzheimer's disease (AD) together with the lack of therapeutic effectiveness of the current single-target FDA-approved drugs, prompted us to design and evaluate new MTDL molecules based on the "one drug, multiple targets" paradigm for use in this neurological disorder.

In this context, the aim of this PhD thesis has been the design and biological assessment of multiple MTDL molecules bearing the *N*-benzylpiperidine group of donepezil and the propargylamine group present in the neuroprotective MAO B inhibitor PF9601N, linked to other chemical moieties such as pyridyl, indolyl and 8-hydroxyquinoline groups. Taken together, these results will potentially contribute to improve the current pharmacological therapy of AD.

Thus, the aims of this PhD thesis have been divided into three main objectives:

1. To study the kinetic and structural mechanism of human MAO inhibition by the multi-target compound ASS234 and its effects in the monoaminergic transmission of both cell culture and rats by *in vivo* microdialysis.
2. To assess the pharmacological evaluation of novel donepezil-indolyl and donepezil-pyridyl hybrids as MTDLs derived from ASS234 for the potential design and synthesis of new derivatives to use in AD.
3. To biologically evaluate new series of MTDLs with metal-chelating properties as a promising therapeutic approach against AD condition.



### **III. MATERIAL AND METHODS**



### III. MATERIAL AND METHODS

#### *Determination of monoamine oxidase activity radiometrically*

The activities of MAO A and MAO B were determined by using specific  $^{14}\text{C}$ -labeled substrates (Perkin Elmer). Rat liver homogenates, prepared as previously described (Gomez N 1986), were used as source of MAO, loading 100-200 mg of protein, whose concentration was previously determined by the Bradford method (Bradford MM 1976). Specific MAO A activity was determined using 100 mM (0.5 mCi/mmol) [ $^{14}\text{C}$ ]-5-hydroxytryptamine (5-HT), whereas MAO B activity was determined using 20 mM (2.5 mCi/mmol) [ $^{14}\text{C}$ ]-phenylethylamine. Enzyme was pre-incubating in the presence of a range of inhibitor concentrations for 30 minutes in 50 mM phosphate buffer (pH 7.4). Inhibitor-free samples were used to determine the maximum enzyme activity. At the end of the pre-incubation, 25 ml of each substrate were added and reactions allowed for 20 minutes (MAO A) and 4 minutes (MAO B). Next, reactions were stopped by adding 2 M citric acid and radiolabeled aldehyde products extracted into toluene/ethylacetate (1:1, v/v) containing 0.6 % (w/v) 2,5-diphenyloxazole prior to scintillation counting (Tri-Carb 2810TR). From dose-response curves,  $\text{IC}_{50}$  values were accordingly determined by using GraphPad PRISM software (versions 3.0 and 4.0) as the inhibitor concentration producing half of enzyme activity.

#### *Determination of monoamine oxidase activity fluorimetrically*

Activities of human recombinant MAO A and MAO B (Sigma-Aldrich) were performed using a fluorimetric method of AmplexUltraRed<sup>®</sup>. Tyramine hydrochloride was used as substrate for both isoforms in 96-well black opaque microplates (OptiPlate-96F, Perkin Elmer) in a final volume of 200  $\mu\text{l}$ . Serial dilutions of each inhibitor were pre-incubated with 360 U/l hMAO A or 67.5 U/l hMAO B for 30 minutes at 37°C. Following the pre-incubations, enzymatic reactions were started upon the addition of 100  $\mu\text{l}$  of a mixture containing 1 mM tyramine, 40 U/l horseradish peroxidase and 25  $\mu\text{M}$  Amplex UltraRed<sup>®</sup> reagent (Life Technologies) in 250  $\mu\text{M}$  sodium phosphate buffer (pH 7.4), as final concentrations. The fluorescence production associated with peroxidase-coupled production of resorufin from the reagent was constantly measured for at least one hour at 530 nm spectrophotometrically (FluoStar OPTIMA, BMG Labtech). In control samples, inhibitor was replaced with distilled water. The possible capacity of compounds to modify the fluorescence generated by the reactions mixture due to non-enzymatic inhibition was determined by adding these compounds to solutions containing the reagent and buffer only.

#### *Assessment for reversibility of MAO inhibition*

Reversibility of MAO inhibition was determined by using two methods: consecutive washes or large dilution. By consecutive washes, rat liver MAO was first pre-incubated in presence or absence of the inhibitor for 30 minutes at 37 °C. MAO activity was then measured radiometrically before and after three consecutive washes with 50 mM phosphate buffer (pH 7.4) centrifuged at 25,000 x g for 10 minutes at 4 °C. Next, activity is expressed as a percentage of corresponding control values before and after the washes. Conversely, reversibility of human recombinant MAO inhibition was determined by the assessment of the recovery of the enzymatic activity after a large dilution of the enzyme-inhibitor complex. MAO concentration of 100-fold over that required for regular assays was used with inhibitor concentrations equivalent to 10-fold their IC<sub>50</sub> values previously determined. After 30 minute pre-incubation at 37°C, the mixture was rapidly diluted 100-fold into reaction phosphate buffer containing 40 U/l horseradish peroxidase, 25 µM Amplex UltraRed<sup>®</sup> reagent and 1 mM tyramine as final concentrations in order to initiate the enzymatic reaction in order to recover typical enzyme concentration whereas inhibitor is diluted at 0.1 x IC<sub>50</sub> value. Then, activity levels are expressed as percentage of control before and after the dilution. Standard irreversible MAO A and MAO B inhibitors clorgyline and *l*-deprenyl were used as controls in both assays, respectively.

#### *Study of time-dependent inhibition of MAO*

Time-dependent MAO inhibition was evaluated by pre-incubating varying concentrations of the inhibitor with the enzyme for different times (0-240 minutes). Then, after substrate addition, IC<sub>50</sub> values were calculated from dose-response curves as previously described.

#### *Assessment of ChE activities spectrophotometrically*

Activity of recombinant AChE from electric eel (*eeAChE*) and equine BuChE (*eqBuChE*) (Sigma-Aldrich) was assessed following a spectrophotometric method of Ellman (Ellamn GL 1961). Enzymatic reactions were allowed in 96-well plates in solutions containing 0.1 M phosphate buffer (pH 8.0), 35 mU/ml *eeAChE* or 50 mU/ml *eqBuChE* and 0.35 mM 5,5-dithiobis-2-nitrobenzoic acid (DTNB, Sigma-Aldrich). Dose-response curves were plotted after pre-incubating the mixture with serial concentrations of each inhibitor for 30 minutes. The activity in absence of compound was used to determine the maximum enzymatic activity. Following the pre-incubations, 50 µl of substrate were added to a final concentration of 0.35 mM acetylthiocholine iodide (ASCh) or 0.5 mM butyrylthiocholine iodide (BuSCh) (Sigma-Aldrich). Enzymatic reactions were followed for 5 minutes with AChE and 25 minutes with BuChE.

Changes in absorbance at 405 nm in a spectrophotometric plate reader (FluoStar OPTIMA, BMG Labtech) were detected, and IC<sub>50</sub> values accordingly calculated by using the GrapPad PRISM software (versions 3.0 and 4.0).

#### *Determination of metal-chelating properties in vitro*

Metals-compounds complex studies were performed in distilled water at room temperature using a UV-VIS spectrophotometer (Lambda25, Perkin Elmer). Spectra (220-300 nm) of compounds alone and in the presence of varying concentrations of metals CuSO<sub>4</sub>, Fe<sub>2</sub>(SO)<sub>3</sub> or Zn(SO)<sub>4</sub> (Sigma-Aldrich) were recorded in 1 cm-quartz cells. The stoichiometry of the complexes was determined by the Job's method (Job P 1928). Series of different solutions containing compounds and metals were prepared at a final concentration sum of 10 μM, ranging the proportions of both components from 0 to 100 %. Absorbance at 257 nm was then plotted versus the mole fraction of the compound for each metal.

#### *Induction of hydrogen peroxide by copper and ascorbic acid in vitro.*

The production of hydrogen peroxide was induced *in vitro* by incubating 0.2 μM Cu (II) and 10 μM ascorbic acid (Sigma-Aldrich) following an incubation of 10 minutes at room temperature with different concentrations of compound, a mixture containing horseradish peroxidase and Amplex UltraRed<sup>®</sup> reagent was added to quantify the amount of hydrogen peroxide produced. Still water was used to determine the maximum levels of hydrogen peroxide.

#### *Assessment of in vitro Aβ self- and hAChE-mediated aggregation*

The inhibition of Aβ<sub>1-42</sub> self-aggregation by compound DPH-4 was studied using the thioflavin T (ThT)-based fluorometric assay (Bolea I 2011). Briefly, Aβ<sub>1-42</sub> peptide (Bachem AG) was pre-treated with 1,1,1,3,3,3-hexafloro-2-propanol (HFIP, Sigma Chemicals), liquid removed by lyophilisation and kept at -20°C until use. For experiments, Aβ<sub>1-42</sub> peptide was resolved in 10 mM basic phosphate buffer (PBS, pH 11.2 adjusted with NH<sub>4</sub>OH). Experiments were performed by incubating the peptides (20μM) with or without the compounds with 35μM ThT. The fluorescence intensity was monitored at 485/528 nm at 37°C every 10 minutes for at least 6 hours on a Synergy HT microplate reader (Bio-Tek). Representative figures are shown in FU and expressed as percentage of control at plateau with blanks subtracted. For Aβ<sub>1-42</sub> hAChE-mediated aggregation, human recombinant AChE (Sigma-Aldrich) was co-incubated with the

peptide at ratio A $\beta$ : AChE, 100:1 in presence of absence of compounds. The same method as previously was employed for calculations.

#### *Oxygen Radical Absorbance Capacity (ORAC)*

The ORAC assay was based on the procedure previously described and partially modified by Dávalos *et al.* (Dávalos A 2004). Briefly, was used as a free radical generator and trolox as standard and melatonin as a reference compound (Sigma-Aldrich). Test compounds were diluted in 75 mM PBS pH 7.4 and measured at eight different concentrations (0.1-1  $\mu$ M), whereas trolox calibration solutions (1-8  $\mu$ M) were prepared for the standard curve. Samples were pre-incubated 15 minutes at 37°C with 70nM fluorescein. Then, upon the addition of 12 mM APPH, fluorescence intensity at 485/520 nm was monitored every minute for 80 minutes by using a Polaris Galaxy plate reader (BMG Labtechnologies). The area under the curve (AUC) of the fluorescence decay was calculated by subtracting AUC for the sample or standard from that for the blank. A calibration curve was made from the net AUC values of trolox standard solutions. The ORAC value for each compound was expressed as trolox equivalents, in which ORAC value for trolox was assigned as 1.

#### *Determination of antioxidant activity by DPPH radical method*

In a 96-well plate and a final volume of 200 $\mu$ l per well, a methanol 2,2-diphenyl-1-picrylhydrazyl (DPPH) (Sigma-Aldrich) solution at 135 $\mu$ M final concentration was added and mixed with different DPPH-4 or trolox concentrations (1-100 $\mu$ M). The resulting mixture was then incubated for 2 hours at room temperature in the dark. Then, the absorbance was measured at 517 nm in a spectrophotometric plate reader (Labsystems Multiscan RC). Reactions were prepared in triplicate and the antioxidant activity was determined as the percentage of radical scavenger activity (RSA) calculated as follows:  $RSA\% = 100[(A_0 - A_i)/A_0] \times 100$ , where  $A_0$  and  $A_i$  are the DPPH absorbance in absence or presence of added compound concentration  $i$ , respectively.

#### *Inhibition of linoleic acid lipid peroxidation*

Production of conjugated diene hydroperoxide by oxidation of linoleic acid in an aqueous dispersion was monitored at 234 nm. AAPH was used as a free radical generator. 10 $\mu$ l of 16 mM linoleic acid sodium salt were added to the UV-VIS cuvette containing 0.93 ml of 50 mM phosphate buffer pH 7.4 at 37°C. The oxidation reactions were initiated under air by adding 50 $\mu$ l of 40 mM APPH solution. Oxidation was carried out in the presence of aliquots. DMSO was used to measure the lipid peroxidation without antioxidant activity. The rate of oxidation at 37°C

was monitored and by recording the increase in absorption caused by conjugated diene hydroperoxides. Trolox was used as an appropriate standard.

#### *Cell culture and treatments*

Human neuroblastoma SH-SY5Y cell line was obtained from the European Collection of Cell Cultures (ECACC). Cells were grown in Dulbecco's modified Eagle medium/Ham's F-12 (DMEM/F-12) containing 15 % (v/v) FBS, non-essential aminoacids (Sigma-Aldrich), 100 U/ml penicillin, 100 µg/ml streptomycin and 2 mM l-glutamine (PAN Biotech) maintained at 37°C with 5 % CO<sub>2</sub>. Cells were seeded at a density of 250,000 cells/ml onto 24-well plates for both cell viability assays and Hoechst staining, and onto 60 mm-diameter dishes for western blot analyses. After 24 hours from seeding, cells were starved with serum-free medium overnight and then pre-treated with compounds for one hour prior to 24-hour treatments.

PC12 cell line was purchased from the American Type Culture Collection and grown in DMEM media supplemented with 7% FBS, 7% FHS, 1.14 mM HEPES pH 6.8 and penicillin/streptomycin. Both cell lines were maintained at 37 °C in a saturating humidity atmosphere containing 5% CO<sub>2</sub>. For treatments, cells were seeded at a density of  $2.5 \cdot 10^4$  cells/mL onto rat tail collagen type I-coated plates until 70-80% confluence was reached.

For HPLC analyses, cells were treated either with PBS (cnt) or 1 µM inhibitor (clorgyline or ASS234) for 3 or 24 hours. For activity assays, at the end of treatments, cells were washed twice with PBS, scrapped, and collected in 50 mM phosphate buffer pH 7.4. Then, lysates were sonicated for 10 seconds on ice and kept at -80 °C prior to measurement of MAO activity. For monoamine analysis, treated cells were washed twice with PBS, scrapped and centrifuged at 3,000 x g for 5 minutes. Then, pellets were resuspended in homogenisation solution containing 0.25 M perchloric acid, 100 µM sodium bisulphite and 250 µM EDTA and lysates sonicated for 10 seconds on ice and kept at -80 °C prior to analysis.

Murine microglial BV-2 cells were obtained from the European Collection of Cell Cultures (ECACC). Cells were grown in RPMI medium (LifeTechnologies) containing 10 % FBS and 0.1% penicillin/streptomycin at 37°C with 5 % CO<sub>2</sub>. Cells were seeded into 24-well plates at a density of 10<sup>5</sup> cells/ml onto collagen type-I-coated plates (BD Biosciences). Once 60-70 % confluence was reached, medium was replaced to 0.5 % FBS final concentration. After 16 hours, cells were pre-treated with compounds for 1 hour prior to 24-hour treatments.

### *MTT reduction assay*

The mitochondrial activity of cells was measured by quantitative colorimetric assay with 3-[4,5-dimethylthiazol-2-yl]-2,5-diphenyl-tetrazolium bromide (MTT) (Sigma-Aldrich) as previously described (Plumb JA 1989). Briefly, 50  $\mu$ l of the MTT reagent were added into each well to a final concentration of 0.5 mg/ml at the end of each treatment time. Then, the plate was placed in a humidified incubator at 37°C with 5 % CO<sub>2</sub> and 95% air (v/v) for at least 30 minutes. Next, the insoluble formazan was dissolved with DMSO and colorimetric determination was carried out at 540/620 nm in a microplate reader (Labsystems Multiscan RC). Untreated cells were used as control of 100 % cell viability.

### *LDH release assay*

Cell viability was assessed by the quantification of lactate dehydrogenase (LDH) activity in cells using the TOX7 kit (Sigma-Aldrich). Briefly, after treatments cell media was collected and centrifuged at 800 x g for 10 minutes at 4°C to discard the dead cells. The supernatants were collected and directly used for LDH determination. The LDH mixture was first prepared by mixing equal volumes of substrate solution, LDH assay dye solution and 1X LDH assay cofactor preparation. Next, the sample media were transferred to a clean flat-bottom plate and lactate dehydrogenase assay mixture was added to each sample in a volume equal to twice that of the sample media. The plate was then covered to protect it from light and incubated at RT for 20-30 minutes. Absorbance was spectrophotometrically measured at 490/690 nm in a microplate reader (Labsystems Multiscan RC).

### *Hoechst staining*

After treatments, cells washed with PBS (pH 7.4) and fixed with 4 % paraformaldehyde (Sigma-Aldrich) in PBS for 10 minutes at 25°C. Cell were then stained with 0.5  $\mu$ g/ml Hoechst 33258 (Sigma-Aldrich) for 30 minutes at 25°C. Stained nuclei were visualised under an inverted microscope (Nikon Eclipse TE2000-E, Nikon) and quantitative image analysis was performed by counting six fields from each well. Data was expressed as the percentage of total nuclei per field relative to untreated cells.

### *Determination of intracellular ROS and O<sub>2</sub><sup>-</sup> levels*

Intracellular accumulation of ROS levels after treatment with H<sub>2</sub>O<sub>2</sub> was assessed using 2,7-dichlorofluorescein diacetate (DCFH-DA) staining. SH-SY5Y cells were incubated with 10  $\mu$ M DCFH-DA in HEPES-buffered saline solution for 20 minutes. Next, cells were washed and the

basal DCF fluorescence levels were measured in a fluorimeter at 485/530 nm. Then, DPH-4 (5 $\mu$ M or 10 $\mu$ M) or vehicle was pre-incubated for 1 hour and 250 $\mu$ M or 500 $\mu$ M H<sub>2</sub>O<sub>2</sub> added for an additional hour. After this time, fluorescence levels were measured and basal values were subtracted. The intracellular levels of superoxide anion (O<sub>2</sub><sup>•-</sup>) were monitored by the selective oxidation of dihydroethidium (DHE) to ethidium. Cells were loaded with 10 $\mu$ M DHE for 10 minutes. Next, basal fluorescence levels were measured at 485/590 nm in a fluorimeter. Next, cells were treated with DPH-4 (5 $\mu$ M or 10 $\mu$ M) or vehicle for 30 minutes and then H<sub>2</sub>O<sub>2</sub> (250 $\mu$ M or 500 $\mu$ M) was added for an hour. Fluorescence was measured, and basal levels subtracted. In both assays, ROS and O<sub>2</sub><sup>•-</sup> levels were expressed as percentage of those in non-treated cells.

#### *Western blot analysis*

For A $\beta$ <sub>1-42</sub> aggregation experiments, peptide samples were removed from the microplate at the end of the ThT aggregation assays, heated at 95°C for 2 minutes and 50 ng loaded into 10% SDS-PAGE pre-cast gels (BioRad) and electrophoresed for 1.5 hours at 100V using a running gel containing 2.5 mM Tris, 19.2 mM glycine and 0.1 % SDS pH 8.3 (Sigma-Aldrich). Resolved bands were then transferred onto a PVDF membrane using 10 mM CAPS pH 11.0 as transfer buffer and blocked in PBS pH 7.4 containing 10 % non-fat milk and 0.1 % BSA for one hour. Membranes were then incubated with mouse monoclonal anti-A $\beta$  6E10 antibody (Covance; 1:500) at 4°C overnight. Then, blots were exposed to horseradish peroxidase-conjugated rabbit anti-mouse (DAKO; 1: 2000) for one hour at room temperature. Membranes were rinsed with peroxidase/luminol solution and bands were analysed and quantified using ChemiDoc<sup>®</sup>MP Imaging System (BioRad) and ImageLab software.

For the rest of enzyme determination, cells were collected in 50 mM Tris-HCl pH 7.5 buffer containing 10 mM EDTA and 1 % (v/v) Triton X-100 after treatments. Protein concentration was determined by the Bradford protein assay. Samples were then diluted in SDS sample buffer containing 70 mM Tris-HCl, 10 %  $\beta$ -mercaptoethanol and 0.1 % (w/v) bromophenol blue. Protein samples (20-30  $\mu$ g) were heated at 96°C for 4 minutes, resolved in SDS-PAGE gels and then transferred onto nitrocellulose membranes (Whatman-Schleicher & Schuell). Transferred membranes were then blocked with 5 % (w/v) non-fat dry milk in Tris-buffered saline (TBS) containing 0.1 % (v/v) tween-20 for one hour and then incubated with primary antibodies anti-APP 20.1 (W.E. Van Nostrand, Stony Brook University, NY, USA; 1: 1000), anti-SOD-1 (SantaCruz; 1: 1000), anti-GPx-1 (Abcam; 1:1000), anti-Nrf-2 (SantaCruz; 1:1000), anti-full-length PARP (Upstate; 1:1000), anti-COX-2 (SantaCruz; 1: 1000), anti- $\beta$ -actin (Sigma-Aldrich; 1: 5000) and anti-GAPDH (glyceraldehyde-3-phosphate dehydrogenase) (Ambion-Invitrogen; 1:20000) for 16 hours at 4°C. Then, blots were exposed to horseradish peroxidase-conjugated goat anti-rabbit (BD Biosciences; 1: 2000) or rabbit anti-mouse (DAKO; 1: 2000) for one hour

at room temperature. Membranes were rinsed with peroxidase/luminol solution and bands were analysed and quantified using ChemiDoc<sup>®</sup>MP Imaging System (BioRad) and ImageLab software.

#### *DEDV-directed caspase-like activity assay*

Caspase activity in lysates from 250 $\mu$ M H<sub>2</sub>O<sub>2</sub>-treated SH-SY5Y cells for 24 hours was determined by DEVD-directed caspase-like activity method. Quantitative caspase-like activity in cell lysates were performed as previously described with minor modifications (Gozzelino R 2008). Briefly, after the indicated treatments, cells were collected and assays were performed using 25  $\mu$ g of protein in the specific buffer containing 100 mM Tris (pH 7.2–7.4), 4 mM EDTA, 4 mM EGTA, 20% sucrose, 10 mM dithiothreitol, 1 mM PMSF plus 40  $\mu$ M of the fluorogenic substrate Ac-DEVD-afc. The resulting 96-multiwell microplates were incubated at 35°C, and caspase activity was monitored for at least one hour in a BIO-TEK Synergy HT fluorimeter at 360/530 nm. For each condition, triplicates of each sample were used.

#### *Determination of nitrite content*

The nitrite content was measured in the culture medium as an indicator of the NO production process in BV-2 cells by the method of Griess following manufacturer's instructions (Molecular Probes). Briefly, after treatments, 50  $\mu$ l of medium were incubated with the equal volume of the Griess reagent and the absorbance was determined at 570 nm using a microplate reader.

#### *HPLC analysis*

Levels of 5-HT and 5-HIAA in SH-SY5Y cells and levels of DA, NA, DOPAC and HVA in PC12 cell lysates were determined by high-performance liquid chromatography (HPLC) with electrochemical detection. The Elite LaChrom system from Hitachi (Tokyo, Japan) with L-2130 pump and L-2200 autosampler and the Coulochem 5100A electrochemical detector from ESA (Chelmsford, USA) with a Model 5011 dual-electrode analytical cell with porous graphite electrodes were used. Both SH-SY5Y and PC12 cell lysates were thawed and centrifuged at 12,000 x g for 10 minutes at 4 °C. Next, the supernatants of each sample were placed in the autosampler, cooled at 10 °C and 20  $\mu$ L was injected. DHBA was used as standard external control. The mobile phase contained 99% v/v of a buffered aqueous solution (50 mM citric acid, 0.05 mM EDTA and 1.2 mM sodium octanesulfonate, adjusted to pH 2.75 with triethylamine)

and 1% v/v acetonitrile. Elution was performed on a Chromolith Performance RP-18e monolithic column (100 x 4.6 mm) from Merck (Darmstadt, Germany) at room temperature (20-25°C) using a flow rate of 1 mL/min. The potentials of the electrodes were set at -50 mV and +400 mV. Instrument control and data acquisition were carried out by EZChromElite version 3.1.7 of Scientific Software (Pleasanton, California). GraphPad PRISM version 4.03 was employed for statistical analyses, with the  $\alpha$  level chosen at 0.05.

#### *Statistical analysis*

Data are shown as the mean  $\pm$  S.E.M. All statistical analyses were completed using GraphPad PRISM software (versions 3.0 or 4.0). Differences were established by one-way ANOVA followed by the Bonferroni post-test with \* $p$ <0.05, \*\* $p$ <0.01 and \*\*\* $p$ <0.001.



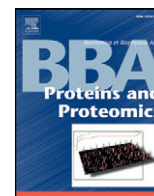
## **IV. RESULTS**



## **Chapter I.**

**“Kinetic and structural analysis of the irreversible inhibition of human monoamine oxidases by ASS234, a multi-target compound designed for use in Alzheimer’s disease”**





## Kinetic and structural analysis of the irreversible inhibition of human monoamine oxidases by ASS234, a multi-target compound designed for use in Alzheimer's disease



Gerard Esteban <sup>a,1</sup>, Jennifer Allan <sup>b,1</sup>, Abdelouahid Samadi <sup>c</sup>, Andrea Mattevi <sup>d</sup>, Mercedes Unzeta <sup>a</sup>, José Marco-Contelles <sup>c</sup>, Claudia Binda <sup>d,\*</sup>, Rona R. Ramsay <sup>b,\*\*</sup>

<sup>a</sup> Departamento de Bioquímica i Biología Molecular, Institute of Neuroscience, Facultat de Medicina, Universitat Autònoma de Barcelona, 08193 Bellaterra, Barcelona, Spain

<sup>b</sup> Biomedical Sciences Research Complex, University of St Andrews, North Haugh, St Andrews KY16 8QP, UK

<sup>c</sup> Laboratorio de Química Medica (IQOG, CSIC), C/Juan de la Cierva 3, 28006 Madrid, Spain

<sup>d</sup> Department of Biology and Biotechnology, University of Pavia, Pavia 27100, Italy

### ARTICLE INFO

#### Article history:

Received 29 January 2014

Received in revised form 4 March 2014

Accepted 10 March 2014

Available online 16 March 2014

#### Keywords:

Multi-target drug

Flavin adduct

Alzheimer's disease

ASS234

PF9601N

Crystal structure

### ABSTRACT

Monoamine oxidases (MAO) and cholinesterases are validated targets in the design of drugs for the treatment of Alzheimer's disease. The multi-target compound *N*-((5-(3-(1-benzylpiperidin-4-yl)propoxy)-1-methyl-1*H*-indol-2-yl)methyl)-*N*-methylprop-2-yn-1-amine (ASS234), bearing the MAO-inhibiting propargyl group attached to a donepezil moiety that inhibits cholinesterases, retained activity against human acetyl- and butyryl-cholinesterases. The inhibition of MAO A and MAO B by ASS234 was characterized and compared to other known MAO inhibitors. ASS234 was almost as effective as clorgyline ( $k_{inact}/K_i = 3 \times 10^6 \text{ min}^{-1} \text{ M}^{-1}$ ) and was shown by structural studies to form the same N5 covalent adduct with the FAD cofactor.

© 2014 Elsevier B.V. All rights reserved.

### 1. Introduction

Alzheimer's disease (AD) is a complex neurodegenerative disorder with a multifaceted pathogenesis. The neurodegeneration and accumulation of the characteristic plaques in AD is accompanied by loss of cholinergic function important for cognition and by decreases in serotonergic and noradrenergic transmission [1]. Despite the recent advances in the knowledge of the factors involved in the etiology of AD, slowing or halting the neurodegenerative process has not yet been accomplished. The lack of effectiveness of the current anticholinergic therapies (such as donepezil, rivastigmine or galanthamine) may be related to the multifactorial and complex nature of AD, which makes one single drug hitting a single pathway or target, inadequate as treatment [2–4]. In this context, it is now widely accepted that a more effective therapy would result from the use of compounds able to target the multiple

mechanisms underlying the etiology of AD in multi-target drug design strategy [4,5].

Both acetylcholinesterase (EC 3.1.1.7, AChE) and butyrylcholinesterase (EC 3.1.1.8, BuChE) are important in the breakdown of the neurotransmitter acetylcholine, with butyrylcholinesterase becoming more important as acetylcholinesterase decreases in AD so that inhibition of both may be needed in the treatment of neurodegeneration [6,7]. The isoenzymes MAO A and MAO B (EC 1.4.3.4) metabolize serotonin (mainly MAO A) and dopamine and noradrenaline (both MAO A and MAO B), but only MAO B increases with age [8,9]. Starting from dual inhibitors of cholinesterases (ChE) and monoamine oxidases (MAO) to combat the neurotransmitter deficits [2–4], other capabilities can be added [10–12]. Youdim and co-workers pursued this idea by developing (R)-3-(prop-2-yn-1-ylamino)-2,3-dihydro-1*H*-inden-5-yl ethyl(methyl)carbamate (ladostigil), which combines brain-specific MAO and non-selective ChE inhibition with the neuroprotective action of the propargyl group [11,13,14]. That this strategy can be successful is demonstrated, for example, by the antagonism of scopolamine-induced spatial memory impairment exerted by ladostigil [11].

MAO A and MAO B share 70% sequence identity and the same FAD cofactor covalently attached at a conserved cysteine residue [15,16].

\* Corresponding author. Tel.: +39 0382 985534.

\*\* Corresponding author. Tel.: +44 1334 463411.

E-mail addresses: [claudia.binda@unipv.it](mailto:claudia.binda@unipv.it) (C. Binda), [rrr@st-and.ac.uk](mailto:rrr@st-and.ac.uk) (R.R. Ramsay).

<sup>1</sup> These authors contributed equally.

Their deep active site cavities are different in volume and shape [17] conferring very different substrate and inhibitor specificities [15,18,19]. The majority of MAO inhibitor drugs in current use are mechanism-based irreversible inhibitors [16,20], including *L*-deprenyl which is selective for MAO B and whose adduct formed with the N5 of the flavin ring has been identified both chemically [21] and in the crystal structure of MAO B [22,23]. Clorgyline, selective for MAO A, forms the same N5 adduct with MAO A [23]. Chronic treatment with either drug giving >85% inhibition of one isoform results in decreased breakdown of the neurotransmitters normally metabolized by that isoform, either MAO A (serotonin, noradrenaline, dopamine) or MAO B (dopamine). Restoration of the activity is slow because human MAO turnover in the brain has a half-life of 30 days [24].

Using the same propargyl group that is present in clorgyline and deprenyl, a new MAO A-selective dual-target compound, *N*-((5-(3-(1-benzylpiperidin-4-yl)propoxy)-1-methyl-1*H*-indol-2-yl)methyl)-*N*-methylprop-2-yn-1-amine (ASS234, Fig. 1), was developed and patented (Reference: PCT/ES070186; WO 2011/113988 A1) to address the need to inhibit the cholinesterases and MAOs in one molecule [25]. This compound derives from the acetylcholinesterase inhibitor, donepezil, and the MAO B inhibitor *N*-((5-(benzyloxy)-1*H*-indol-2-yl)methyl)prop-2-yn-1-amine (PF9601N, Fig. 1) [26–28]. In addition to enzyme inhibition, ASS234 inhibits A $\beta$ 1–42 self-aggregation *in vitro*, prevents depletion of the antioxidant enzymes, catalase and superoxidase-1, and is able to cross the blood brain barrier [29]. In this work we report the mechanism of inhibition of human MAOs by ASS234 and compare the efficacy of ASS234 to that of the established isoform-specific propargyl MAO inhibitors, clorgyline and *L*-deprenyl, highlighting the selectivity of ASS234 for MAO A and the nature of the adduct.

## 2. Material and methods

### 2.1. Materials

Kynuramine, tyramine, benzylamine, Ampiflu™ Red, horseradish peroxidase (Type II), and 5,5'-dithiobis-2-nitrobenzoic acid (DTNB) were purchased from Sigma-Aldrich and  $\beta$ -octylglucoside from Melford Laboratories Ltd, Ipswich, UK. Plastic-ware items (tips, microfuge tubes and 96-well plates) free from the contaminants known to inhibit monoamine oxidase [30] were purchased from Eppendorf UK Ltd (Stevenage, UK). Human recombinant AChE and BuChE (lyophilized powder) were purchased from Sigma Aldrich (Madrid, Spain). Human MAO A was prepared from yeast cells (*Saccharomyces cerevisiae*) as before [31,32]. Some membrane-bound MAO A was reserved from the preparation to allow measurement of the inactivation in membranes where the lipophilicity of the inhibitor can alter association with the target. Human MAO B was purified from yeast cells after expression in *Pichia pastoris* [33]. Compounds PF9601N [28] and ASS234 [25] were synthesized as previously described.

### 2.2. Kinetic assessment of the compounds as cholinesterase (ChE) inhibitors

Cholinesterase activities were assessed using the spectrophotometric method of Ellman [34] using human recombinant AChE and BuChE (lyophilized powder). Enzymatic reactions took place in 96-well plates in a final volume of 300  $\mu$ l containing 0.1 M phosphate buffer (pH 8), 0.035 U/ml AChE or 0.05 U/ml BuChE and 0.35 mM of 5,5'-dithiobis-2-nitrobenzoic acid (DTNB). Inhibition curves were obtained by pre-incubating this mixture with serial dilutions of each compound for 30 min at 37 °C. The activity in absence of compound was used to determine the 100% of enzyme activity. At the end of the pre-incubation period, 50  $\mu$ l of substrate was added to a final concentration of 0.35 mM acetylthiocholine iodide or 0.5 mM butyrylthiocholine iodide (Sigma-Aldrich, Madrid, Spain) and the reaction followed for 30 min. Changes in absorbance were measured at 405 nm in an absorbance plate reader (FluoStar OPTIMA, BMG Labtech). IC<sub>50</sub> values were calculated using the GraphPad PRISM software (version 3.0). Data were expressed as means  $\pm$  S.E.M. of at least three different experiments in quadruplicate.

### 2.3. Kinetic assessment of the compounds as MAO inhibitors

Continuous assays for MAO were used: a) the spectrophotometric (direct assay in duplicate) for purified MAO [35,36], and b) a plate reader assay (triplicate wells) where production of hydrogen peroxide is coupled *via* horseradish peroxidase to a dye producing the fluorescent resorufin for membrane-bound MAO [37,38]. For the reversible inhibition, multiple data sets obtained at varied inhibitor and substrate concentrations were analyzed in Graphpad PRISM for the best global fit to the Michaelis–Menten equation for a competitive inhibitor, using  $Y = V_{max} * X / (K_M(1 + [I]/K_i) + X)$  where Y is the measured activity, X is substrate concentration, and K<sub>M</sub> is the Michaelis constant for the substrate.

The IC<sub>50</sub> values for the irreversible inactivation of MAO A and MAO B by these inhibitors were determined from the activity remaining after 30 min of incubation. The remaining activity was determined using the coupled assay with 1 mM tyramine as the substrate. To determine the kinetic parameters K<sub>fi</sub> and K<sub>inact</sub>, spectrophotometric assays were used to determine the remaining activity after various incubation times (0–20 min) and the data analyzed by a non-linear version of the Kitz–Wilson analysis [39] as shown in Supplementary Fig. S1. Pre-incubations were carried out at 30 °C in quartz cuvettes in a volume of 200  $\mu$ l containing 50 nM membrane-bound MAO A and inhibitor in 50 mM potassium phosphate buffer, pH 7.5, containing 0.05% Triton X-100 and 10% glycerol. The range of inhibitor concentrations used was from 2.5  $\mu$ M to 200  $\mu$ M for PF9601N, from 50  $\mu$ M to 500  $\mu$ M for *L*-deprenyl and from 100nM to 1  $\mu$ M for ASS234 and clorgyline. At the end of each incubation period, kynuramine in 800  $\mu$ l of buffer was added to give a final concentration of 0.75 mM, and the product formation followed at 314 nm in a Shimadzu UV2101 spectrophotometer.

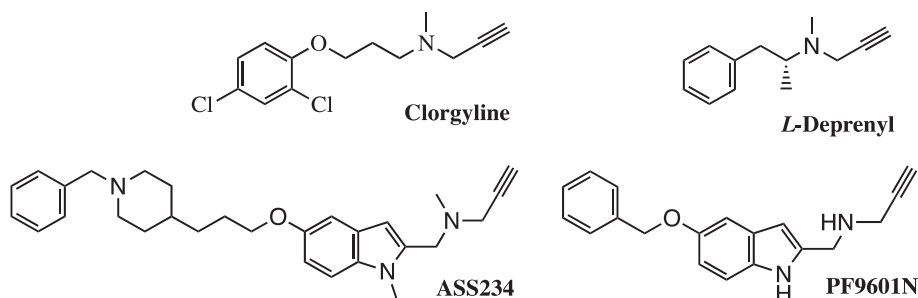


**Fig. 1.** Structures of propargyl inhibitors: clorgyline, *L*-deprenyl, *N*-((5-(benzyloxy)-1*H*-indol-2-yl)methyl)prop-2-yn-1-amine (PF9601N), *N*-((5-(3-(1-benzylpiperidin-4-yl)propoxy)-1-methyl-1*H*-indol-2-yl)methyl)-*N*-methylprop-2-yn-1-amine (ASS234).

Inhibitory rates were determined as a percentage of the control assay rate (no inhibitor) at each reaction time. The  $k_{obs}$  value was determined as the slope of the semilog plot, log of % remaining activity against preincubation time as shown in Supplementary Fig. S1A. Fitting a rectangular hyperbola (Michaelis–Menten equation, using non-linear regression in PRISM) to the rate constants at several inhibitor concentrations (shown as the linearized Kitz–Wilson plot, Fig. S1B) gave the irreversible kinetic parameters,  $K_i$  and  $k_{inact}$  [39,40]. The partition ratio (PR), defined as the number of product species being generated per formation of covalently modified enzyme was determined from the plot of the percentage of activity remaining (no inhibitor as control) after 20 min against  $[I]/[E]$  as shown in Fig. S1C.

#### 2.4. Characterization of the MAO-ASS234 adduct by visible spectroscopy and mass spectrometry

Spectra were collected in a Shimadzu 2101PC spectrophotometer in 50 mM HEPES pH 7.4 [31]. Adduct formation was complete within 20 min for each addition at the micromolar concentrations required for spectrophotometry. Samples were sent for mass analysis after centrifugal filtration and overnight dialysis against 50 mM potassium phosphate pH 7.4 to remove the  $\beta$ -octylglucoside detergent present in the purified enzyme preparation. For whole protein mass spectrometry using ESI-TOF, the protein sample (20  $\mu$ l, 10  $\mu$ M) was desalted on-line through a Waters MassPrep on-line desalting column (2.1  $\times$  10 mm), eluting with an increasing acetonitrile concentration (from 2% acetonitrile, 98% aqueous 1% formic acid to 98% acetonitrile 2% aqueous 1% formic acid) and delivered to the electrospray ionization mass spectrometer (LCT, Micromass, Manchester, U.K.) which had previously been calibrated using myoglobin. An envelope of multiply charged signals was obtained and deconvoluted using MaxEnt1 software to give the molecular mass of the protein.

#### 2.5. Crystallographic studies

A pure and homogeneous sample of human MAO B (MAO B) was incubated with 1 mM ASS234 (or either analog) for 1 h and crystallized following published protocols [41]. UV/Visible measurements on the inhibited protein showed the spectral modification corresponding to the covalent adduct formed by propargyl inhibitors. Crystals were soaked in a cryoprotectant solution containing 18% (v/v) glycerol and flash-cooled in a stream of gaseous nitrogen at 100 K. X-ray diffraction data were collected at the X06DA beamline of the Swiss Light Source (Villigen, Switzerland). Data processing and scaling (Table S1) were carried out using MOSFLM [42] and programs of the CCP4 package [43]. The structure of MAO B in complex with *L*-deprenyl [17] deprived of water and inhibitor atoms was used as initial model and inspection of the unbiased 2Fo-Fc and Fo-Fc maps indicated the presence of the ASS234 molecule bound in the MAO B active site. Whereas the *N*-benzylpiperidine moiety of the inhibitor was only partly visible in the electron density, the ASS234 propargyl unit was unambiguously found forming a covalent adduct with the N5 atom of the flavin. Crystallographic refinement (Supplementary Table S1) was performed with Refmac5 of the CCP4 package [43] and figures of the crystal structure were made using CCP4mg [44].

### 3. Results and discussion

#### 3.1. Enzyme inhibition

A previous study on ASS234 inhibition of the target enzymes used equine and fish sources for the cholinesterases and rat brain mitochondria for MAO [26]. To provide a molecular basis for its potential use in AD treatment, the inhibition mechanism of this compound has now been evaluated in human enzymes by using purified samples of these proteins. The design of ASS234 aimed to maintain inhibition of both

**Table 1**  
Inhibition of purified human cholinesterases.

	IC <sub>50</sub> ( $\mu$ M) <sup>a</sup>	
	AChE	BuChE
ASS234	0.81 $\pm$ 0.06	1.82 $\pm$ 0.14
PF9601N	>100	>100
Donepezil	0.011 $\pm$ 0.001	6.22 $\pm$ 0.77

<sup>a</sup> Expressed as means  $\pm$  standard error of the mean (S.E.M.) of at least three different experiments using quadruplicate assays.

AChE and BuChE in the dual compound. This ChE inhibitory profile was confirmed using purified human enzymes (Table 1) with the standard AChE inhibitor, donepezil, for comparison. Whereas the parent MAO B inhibitor PF9601N did not inhibit either ChE, ASS234 inhibited both AChE and BuChE.

To demonstrate that the desired MAO inhibitory properties are maintained in the presence of the additional structural features required for effective inhibition of the other target, ASS234 was compared with PF9601N and the known drugs, cloglyline and *L*-deprenyl (Fig. 1), for consistency in mechanism and for efficacy and selectivity. Cloglyline (MAO A-selective) and *L*-deprenyl (MAO B-selective) are extensively used *in vivo* [45,46], so this information will be a useful background for future *in vivo* profiling of the new compounds. Kinetic studies were performed for the human MAO isoenzymes both in the purified form necessary for spectra and crystallography and in the membrane because differences in the kinetics of MAO after extraction from the membrane have been reported [47]. First, a coupled assay [48] measuring H<sub>2</sub>O<sub>2</sub> production was used to compare the selectivity of the irreversible inhibition of MAO A and MAO B by the four inhibitors. The IC<sub>50</sub> values for the inhibition of MAO A and MAO B by all four inhibitors (Table 2) confirmed the previously reported selectivity of ASS234 for MAO A and PF9601N for MAO B [25,28]. ASS234 and cloglyline inactivate purified MAO A at sub-nanomolar concentrations whereas the IC<sub>50</sub> values with MAO B are in the micromolar range (Table 2A). Using membrane-bound enzymes (Table 2B), the selectivity of ASS234 and cloglyline for MAO A is almost 10<sup>5</sup>, with ASS234 almost 4-fold more selective than cloglyline. The excellent selectivity of PF9601N and *L*-deprenyl for MAO B can be seen in the low MAO B IC<sub>50</sub> to MAO A IC<sub>50</sub> ratios in Table 2. In membranes, PF9601N was almost 3-fold less selective than *L*-deprenyl.

The IC<sub>50</sub> data performed on human enzymes confirmed the selectivity of ASS234 for MAO A with respect to MAO B. We then focused on MAO A to perform a more in-depth kinetic analysis on this compound and to characterize its mechanism of MAO inactivation by UV/visible spectroscopy. Cloglyline and *L*-deprenyl form covalent adducts with the N5 group of the FAD moiety of MAO [17,22]. To determine whether the new compounds form the same adduct, the spectral changes upon inhibitor binding were compared for all four inhibitors (Fig. 2). In all cases, the MAO A

**Table 2**  
IC<sub>50</sub> values for irreversible inhibition of human MAO A and MAO B.<sup>a</sup>

	IC <sub>50</sub> (nM)		MAO A selectivity IC <sub>50</sub> B/IC <sub>50</sub> A
	MAO A	MAO B	
<i>A. Purified enzymes</i>			
ASS234	5.44 $\pm$ 1.74	177 $\pm$ 25	32
Cloglyline	0.23 $\pm$ 0.05	1436 $\pm$ 377	6243
PF9601N	3830 $\pm$ 795	3.1 $\pm$ 1.0	0.00105
<i>L</i> -deprenyl	16990 $\pm$ 440	3.2 $\pm$ 1.1	0.00018
<i>B. Membrane enzyme preparations</i>			
ASS234	0.17 $\pm$ 0.03	15830 $\pm$ 1040	93118
Cloglyline	0.42 $\pm$ 0.08	10660 $\pm$ 953	25380
PF9601N	790 $\pm$ 105	11 $\pm$ 2	0.0139
<i>L</i> -deprenyl	630 $\pm$ 86	3.0 $\pm$ 0.9	0.0048

<sup>a</sup> Activity was measured after 30 minutes incubation with the inhibitor using 1 mM tyramine as substrate for both MAO A and MAO B.

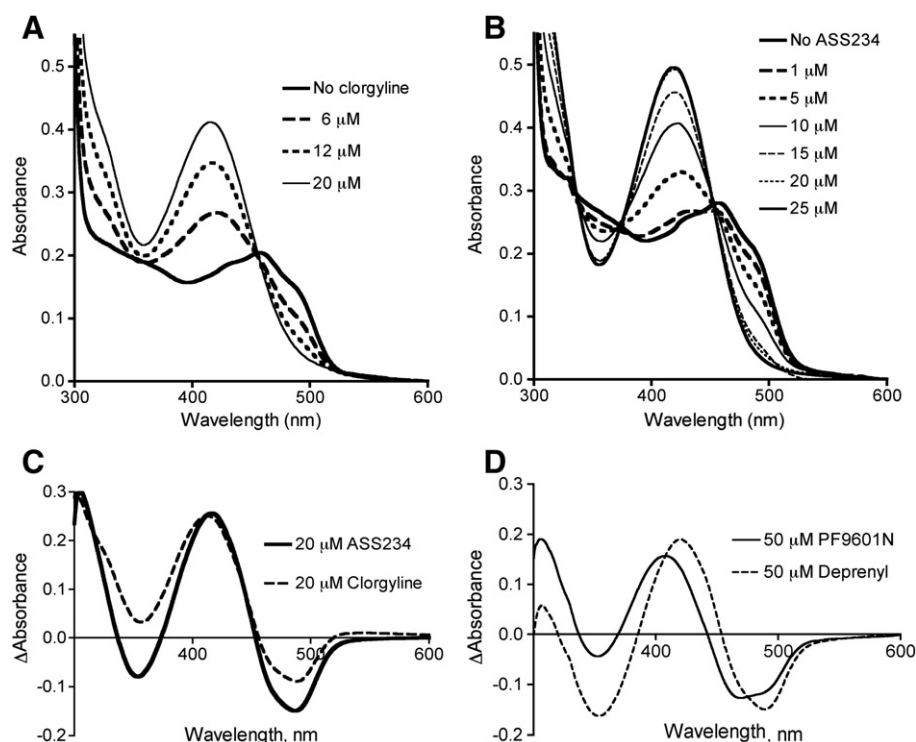


**Fig. 2.** Spectral changes in MAO-A after modification with ASS234 and clorgyline. (A) Oxidized MAO A (17.4  $\mu\text{M}$ ) alone and after 15 min incubation at 20  $^{\circ}\text{C}$  with clorgyline (6–20  $\mu\text{M}$ ). (B) Oxidized MAO A (21.5  $\mu\text{M}$ ) alone and after 15 min incubation at 20  $^{\circ}\text{C}$  with ASS234 (5–25  $\mu\text{M}$ ). (C) The change induced in the spectrum of MAO A after inactivation by each inhibitor. The difference spectra were calculated by subtracting the absorbance of the purified MAO A from the absorbance of the inactivated MAO A inhibitor complex. (D) The difference spectra after inactivation by PF9601N and *L*-deprenyl are included for comparison.

flavin absorbance above 456 nm was bleached and the absorbance at 415 nm increased proportionally. The concentration required to induce the maximum increase at 415 nm varied with the inhibitor. Following the addition of a slight excess (20  $\mu\text{M}$ ) of either ASS234 or clorgyline, MAO A was fully inactivated and there was no further change in the spectrum. The difference spectra (Fig. 2C) were calculated by subtracting the pure MAO A spectrum from the spectrum of the complex with inhibitor. There is no significant difference at 415 nm between clorgyline and ASS234, which is consistent with full modification of the flavin and suggests formation of the same covalent adduct form at the N5 of the FAD molecule. PF9601N and *L*-deprenyl gave similar spectral changes (Fig. 2D) indicating that the adduct formed is likely to be the same for all four compounds.

We then evaluated the inhibitors for their reversible and irreversible modes of MAO A inhibition. When the assay was initiated by adding purified MAO A, all four compounds acted as competitive inhibitors. Concentrations of inhibitor in the micromolar range were required to see inhibition and this inhibition was reversible by immediate dilution with excess substrate. Both clorgyline and ASS234 gave sub-micromolar  $K_i$  values for the reversible inhibition of purified human MAO A (Table 3). For membrane-bound MAO A, the competitive  $K_i$  values were 14 nM

for clorgyline and 53 nM for ASS234, whereas those for PF9601N and *L*-deprenyl were 1000-fold higher (Table 3).

After pre-incubation with the enzyme, the inhibition by all four compounds was irreversible and the activity was not restored by the addition of excess substrate (5-fold  $K_M$ ) nor after overnight dialysis. The kinetic parameters for the mechanism-based irreversible inactivation of purified and membrane-bound MAO-A, termed  $K_i$  and  $k_{\text{inact}}$  [39], determined as shown in Supplementary Fig. S1, are presented in Table 4. The specificity constant ( $k_{\text{inact}}/K_i$ ) for inactivation of purified MAO A by clorgyline and ASS234 (Table 4A) revealed that ASS234 was less effective than clorgyline as an irreversible inhibitor, mainly because the  $K_i$  value of 220 nM for clorgyline was 16-fold lower than the  $K_i$  value for ASS234 (3.54  $\mu\text{M}$ ). Nevertheless, this difference in  $K_i$  disappeared in the membrane bound MAO A (Table 4B) and the rates of inactivation were similar for either compound in both purified and membrane-bound enzyme. The  $k_{\text{inact}}/K_i$  values also indicate that ASS234 and clorgyline are >1000-fold better at forming an irreversible adduct with MAO A than are the MAO B-selective inactivators. Clorgyline inactivated MAO A with a partition ratio close to 2, meaning that two product molecules were formed per inactivation event. The partition ratio for inactivation by ASS234 was 9 (7 for the membrane-bound MAO A), suggesting that adduct formation after the enzyme-catalyzed oxidation is only slightly less likely than that occurring with clorgyline.

When membrane-bound MAO A was assayed, ASS234 was highly effective as an irreversible inhibitor with a  $K_i$  value of 45 nM, 78-fold lower than that determined with purified MAO A. However, a comparable  $k_{\text{inact}}$  (0.133  $\text{min}^{-1}$ ) and partition ratio (7) were found (Table 4B), showing that the mechanism-based reaction and adduct formation were the same in both membrane-bound and purified MAO A. The increased association with the membrane-bound MAO A with respect to purified MAO A could be due to differences in ligand access into the enzyme active site between the free and membrane-associated states [47] as well as to the partition of ASS234 into the membrane itself. In comparison to ASS234 and clorgyline, *L*-deprenyl and PF9601N gave

**Table 3**  
Reversible inhibition of human MAO A by acetylenic inhibitors.<sup>a</sup>

	$K_i$ ( $\mu\text{M}$ )	
	Purified MAO A	Membrane-bound MAO A
ASS234	0.20 $\pm$ 0.06	0.053 $\pm$ 0.013
Clorgyline	0.040 $\pm$ 0.004	0.014 $\pm$ 0.001
PF9601N	n.d. <sup>b</sup>	25 $\pm$ 5
<i>L</i> -deprenyl	n.d. <sup>b</sup>	75 $\pm$ 11

<sup>a</sup> From initial rates of kynuramine oxidation where MAO A was added last.

<sup>b</sup> n.d., not determined.

**Table 4**  
Kinetic parameters for the irreversible inhibition of MAO A.

	$K_i$ ( $\mu\text{M}$ )	$k_{\text{inact}}$ ( $\text{min}^{-1}$ )	$k_{\text{inact}}/K_i \times 10^3$ ( $\text{min}^{-1} \text{M}^{-1}$ )	Partition ratio
<i>A. Purified MAO A</i>				
ASS234	$3.54 \pm 1.46$	$0.216 \pm 0.093$	61	9
Clorgyline	$0.22 \pm 0.08$	$0.126 \pm 0.047$	570	2
PF9601N	159	0.036	0.2	6981
<i>L</i> -deprenyl	106	0.157	1.3	245
<i>B. Membrane-bound MAO A</i>				
ASS234	$0.045 \pm 0.008$	$0.133 \pm 0.041$	3000	7
Clorgyline	$0.031 \pm 0.009$	$0.157 \pm 0.018$	5100	<2
PF9601N	$118 \pm 28$	$0.97 \pm 0.11$	8.25	35
<i>L</i> -deprenyl	$193 \pm 41$	$0.252 \pm 0.04$	1.31	482

much higher  $K_i$  values against membrane-bound MAO A (193  $\mu\text{M}$  and 118  $\mu\text{M}$ , respectively, Table 4B), indicating a poor affinity for the active site of MAO A. The  $k_{\text{inact}}$  values of 0.252  $\text{min}^{-1}$  for *L*-deprenyl and 0.973  $\text{min}^{-1}$  for PF9601N are of the same order as those for ASS234 and clorgyline, suggesting that MAO A can catalyze the reaction with any of these acetylenic inhibitors. However, the high PRs for inactivation by PF9601N and *L*-deprenyl indicate that very few turnovers result in inactivated MAO A.

### 3.2. Structural studies of ASS234 inhibition

Co-crystallization experiments with ASS234 were carried out with both human MAO A and MAO B, but diffracting crystals were obtained only with the latter, so this isoform was selected for the structural analysis of the mode of MAO inhibition by ASS234. The crystal structure of human MAO B in complex with ASS234 was determined at 1.8 Å resolution (Fig. 3A–C; Table S1). Inspection of the electron density map

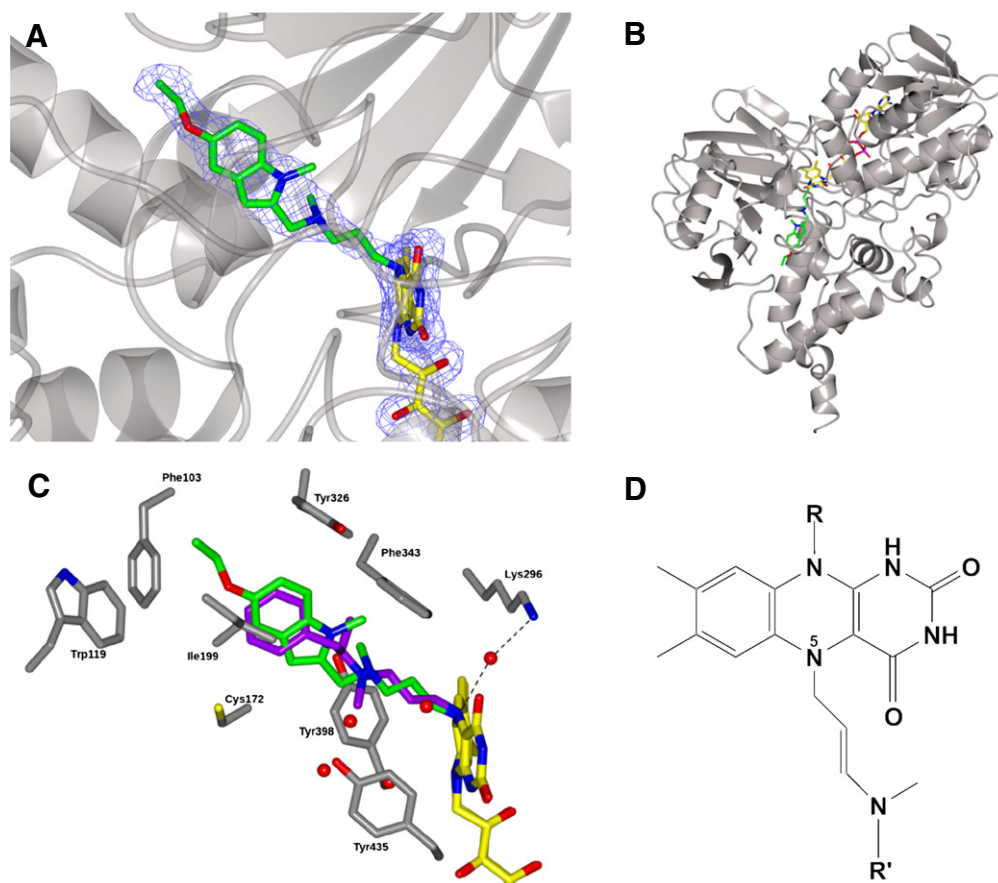


**Fig. 3.** Crystal structure of the ASS234 adduct with human MAO B. (A) Stick model and unbiased electron 2Fo-Fc density map (in blue, contoured at 1.2  $\sigma$ ) for the ASS234-flavin adduct buried in the MAO B structure (in gray ribbon semi-transparent representation). Atoms are colored as follows: carbon in yellow and green, for FAD and ASS234, respectively; nitrogen in blue; oxygen in red. The model includes all ASS234 atoms except for the *N*-benzylpiperidine moiety which was not visible in the electron density map. (B) Ribbon representation (in gray) of the overall structure of MAO B in complex with ASS234. The molecule is rotated of approximately 90° clockwise with respect to the orientation in Fig. 3A, with phosphorous atoms in magenta. (C) Stick representation of the active site of MAO B in complex with ASS234 (orientation as in Fig. 3A). Color code is as in Fig. 3A, with protein carbon atoms colored in gray and water molecules represented as red spheres. Hydrogen bonds are highlighted as dashed lines. The structure of the deprenyl-flavin covalent adduct (PDB code 2BYB) is superposed (*L*-deprenyl carbon atoms colored in purple). (D) Chemical formula of the covalent adduct formed by ASS234 with the MAO flavin N5 atom. R stands for the adenosine-phosphoribityl moiety of FAD, whereas to simplify the drawing the inhibitor molecule is represented by R' and only the acetylenic adduct formed with the flavin ring is highlighted.

(Fig. 3A) revealed that the inhibitor is undoubtedly bound in the active site of the enzyme with the acetylenic moiety forming a covalent adduct with the N5 atom of the flavin (Fig. 3D), as was hypothesized on the basis of UV/visible spectra measurements (Fig. 2). The ASS234 methylindole ring lies in the active site cavity inducing the gating residue Ile199 to adopt the open conformation (Fig. 3C) that has been observed in all human MAO B crystal structures in complex with bulky inhibitors including *L*-deprenyl [23]. The propoxy chain of the inhibitor extends towards the rear of the cavity in proximity to the protein surface (Fig. 3B), but no full electron density for the terminal *N*-benzylpiperidine moiety was detected so this part of the molecule was not included in the final model. This raised the question whether ASS234 is partly disordered or it undergoes degradation upon binding to the enzyme, the latter being a process that may occur enzymatically as MAOs are known to oxidize tertiary amines. To investigate this issue mass analysis was performed on intact MAO A and B before and after incubation with ASS234. The results for MAO A modified with ASS234 or clorgyline showed the expected increases in mass of 446 Da for ASS234 and 267 Da for clorgyline (Table 5). Similarly, with MAO B, ASS234 inactivation gave a mass increase of 446 Da and *L*-deprenyl inactivation resulted in an increase of 182 Da. This demonstrates that intact ASS234 binds to MAO B in solution and, presumably, this binding mode is retained also in the crystals with the whole compound incorporated into the adduct.

Beside the covalent linkage to the flavin cofactor, ASS234 binding to MAO B relies on van der Waals contacts with the protein active site residues and does not involve any hydrogen bond (Fig. 3C). Apart from inducing the open conformation of Ile199 as occurs with many other MAO B inhibitors, the enzyme active site structure is not perturbed by ASS234 binding and even the position of the water molecules is highly conserved. Comparison with the human MAO B structure in complex with *L*-deprenyl (Fig. 3C) showed that ASS234 fills the active site cavity, a feature which generally correlates with tighter binding [23]. In contrast, although extending enough to move Ile199 in the open conformation, *L*-deprenyl leaves the entrance cavity space essentially unoccupied by the inhibitor.

#### 4. Conclusions

A biochemical and structural analysis was performed in order to characterize the effects of the multi-target inhibitor ASS234. The kinetic studies demonstrate that ASS234 is not only a reversible inhibitor of both acetyl- and butyryl-cholinesterases with  $\mu\text{M}$  affinity, but is also a highly potent irreversible inhibitor of MAO A similar to clorgyline. In contrast, PF9601N and *L*-deprenyl are effective against MAO B. Although the mechanism of inactivation is the same, the selectivity of ASS234 for MAO A indicated by the  $\text{IC}_{50}$  values for both purified and membrane-bound protein samples is clear and is consistent with the data previously reported [25,28]. Although ASS234 and clorgyline share the same propylamine structure, ASS234 is much larger and more hydrophobic. The initial reversible binding parameter ( $K_i$  0.4  $\mu\text{M}$ ) indicates that ASS234 has a slightly lower affinity for MAO A than clorgyline ( $K_i$  0.02  $\mu\text{M}$ ), and this is also reflected in the higher  $K_i$  for the irreversible reaction. Nevertheless, these data demonstrate that the addition of the donepezil moiety, which endowed ASS234 with desirable multi-target

inhibitory properties in the context of AD treatment (namely ChE enzyme inhibition in the same affinity range as for MAO A), did not affect significantly the MAO inhibition properties of ASS234. The UV/visible spectral analysis showed that ASS234 irreversible modification of the flavin gives an absorbance profile highly similar to that found with the other propargyl MAO inhibitors. The crystal structure of human MAO B in complex with ASS234 highlights the covalent adduct formed with the flavin N5 atom which, based on the spectral changes, occurs also with the MAO A cofactor. Although the *N*-benzylpiperidine moiety is not fully visible in the electron density, the mass determinations demonstrate that ASS234 binds as the intact molecule to the MAO B active site, which rules out the possibility that the inhibitor may undergo degradation in the cellular context.

Overall, we have demonstrated the efficacy of ASS234 as inhibitor of both the “classic” AD-targeting ChE enzymes and MAOs, the latter being oxidative enzymes whose expression increased significantly with age. These data indicate that ASS234 is a promising compound in the context of neurodegenerative diseases and a model for further development of multi-target inhibitors.

#### Acknowledgements

We thank our funding sources: COST Action CM1103 STSM10483 (GE); School of Biology at the University of St. Andrews (JA); MIUR (Italy) for PRIN09 (grant number 20098FYZW002 to CB); and MINECO (Gobierno de España) for SAF2012-33304 (JMC and MU). This collaborative work was enabled by COST Action CM1103, *Structure-based drug design for diagnosis and treatment of neurological diseases*. For the whole protein mass determinations, we thank Dr Catherine Botting, the BSRC mass spectrometry facility at the University of St Andrews, and the Wellcome Trust for instrument funding.

#### Appendix A. Supplementary data

Supplementary data to this article can be found online at doi: <http://dx.doi.org/10.1016/j.bbapap.2014.03.006>.

One supporting figure and the table with the crystallographic details are reported in this Supporting Information.

PDB ID codes: coordinates and structure factors for the MAOB-ASS234 complex structure were deposited in the Protein Data Bank with the ID codes 4crt and r4crtsf, respectively.

#### References

- [1] Y. Xu, J. Yan, P. Zhou, J. Li, H. Gao, Y. Xia, Q. Wang, Neurotransmitter receptors and cognitive dysfunction in Alzheimer's disease and Parkinson's disease, *Prog. Neurobiol.* 97 (2012) 1–13.
- [2] J. Sterling, Y. Herzig, T. Goren, N. Finkelstein, D. Lerner, W. Goldenberg, I. Miskolczi, S. Molnar, F. Rantal, T. Tamas, G. Toth, A. Zagyva, A. Zekany, G. Lavian, A. Gross, R. Friedman, M. Razin, W. Huang, B. Kraiss, M. Chorev, M.B. Youdim, M. Weinstock, Novel dual inhibitors of AChE and MAO derived from hydroxy aminoindan and phenethylamine as potential treatment for Alzheimer's disease, *J. Med. Chem.* 45 (2002) 5260–5279.
- [3] M.B.H. Youdim, J.J. Buccafusco, Multi-functional drugs for various CNS targets in the treatment of neurodegenerative disorders, *Trends Pharmacol. Sci.* 26 (2005) 27–35.
- [4] J.J. Buccafusco, A.V. Terry, Multiple central nervous system targets for eliciting beneficial effects on memory and cognition, *J. Pharmacol. Exp. Ther.* 295 (2000) 438–446.
- [5] W.J. Geldenhuys, C.J. Van der Schyf, Rationally designed multi-targeted agents against neurodegenerative diseases, *Curr. Med. Chem.* 20 (2013) 1662–1672.
- [6] N.H. Greig, T. Utsuki, D.K. Ingram, Y. Wang, G. Pepeu, C. Scali, Q.S. Yu, J. Mamczarz, H. W. Holloway, T. Giordano, D.M. Chen, K. Furukawa, K. Sambamurti, A. Bossi, D.K. Lahiri, Selective butyrylcholinesterase inhibition elevates brain acetylcholine, augments learning and lowers Alzheimer beta-amyloid peptide in rodent, *Proc. Natl. Acad. Sci. U. S. A.* 102 (2005) 17213–17218.
- [7] A. Venneri, W.J. McGeown, M.F. Shanks, Empirical evidence of neuroprotection by dual cholinesterase inhibition in Alzheimer's disease, *Neuroreport* 16 (2005) 107–110.
- [8] N. Mahy, N. Andres, C. Andrade, J. Saura, Age-related changes of MAO-A and -B distribution in human and mouse brain, *Neurobiology (Bp)* 8 (2000) 47–54.
- [9] J. Saura, J.M. Luque, A.M. Cesura, M. Daprada, V. Chanpalay, G. Huber, J. Löffler, J.G. Richards, Increased monoamine-oxidase-B activity in plaque-associated astrocytes

**Table 5**

Mass changes after adduct formation with MAO A and MAO B.

Sample	Intact protein mass (Da)	Mass change (Da)
MAO A	60092	
MAO A-ASS234	60538	446
MAO A-Clorgyline	60359	267
MAO B	59467	
MAO B-ASS234	59913	446
MAO B- <i>L</i> -deprenyl	59648	182

- of Alzheimer brains revealed by quantitative enzyme autoradiography, *Neuroscience* 62 (1994) 15–30.
- [10] M.B.H. Youdim, Multi target neuroprotective and neurorestorative anti-Parkinson and anti-Alzheimer drugs ladostigil and m30 derived from rasagiline, *Exp. Neurobiol.* 22 (2013) 1–10.
- [11] O. Bar-Am, O. Weinreb, T. Amit, M.B.H. Youdim, The novel cholinesterase–monoamine oxidase inhibitor and antioxidant, ladostigil, confers neuroprotection in neuroblastoma cells and aged rats, *J. Mol. Neurosci.* 37 (2009) 135–145.
- [12] O. Weinreb, T. Amit, O. Bar-Am, M. Youdim, Ladostigil: a novel multimodal neuroprotective drug with cholinesterase and brain-selective monoamine oxidase inhibitory activities for Alzheimer's disease treatment, *Curr. Drug Targets* 13 (2012) 483–494.
- [13] O. Weinreb, T. Amit, O. Bar-Am, M.B.H. Youdim, Ladostigil: a novel multimodal neuroprotective drug with cholinesterase and brain-selective Monoamine Oxidase inhibitory activities for Alzheimer's Disease treatment, *Curr. Drug Targets* 13 (2012) 483–494.
- [14] O. Weinreb, T. Amit, O. Bar-Am, M.B.H. Youdim, A novel anti-Alzheimer's disease drug, ladostigil: neuroprotective, multimodal brain-selective monoamine oxidase and cholinesterase inhibitor, *Monoamine Oxidases and Their Inhibitors*, vol. 100, 2011, pp. 191–215.
- [15] W. Weyler, Y.P.P. Hsu, X.O. Breakefield, *Biochemistry and genetics of monoamine oxidase*, *Pharmacol. Ther.* 47 (1990) 391–417.
- [16] M.B.H. Youdim, D. Edmondson, K.F. Tipton, The therapeutic potential of monoamine oxidase inhibitors, *Nat. Rev. Neurosci.* 7 (2006) 295–309.
- [17] L. De Colibus, M. Li, C. Binda, A. Lustig, D.E. Edmondson, A. Mattevi, Three-dimensional structure of human monoamine oxidase A (MAO A): relation to the structures of rat MAO A and human MAO B, *Proc. Natl. Acad. Sci. U. S. A.* 102 (2005) 12684–12689.
- [18] C.J. Fowler, K.F. Tipton, On the substrate specificities of 2 forms of monoamine oxidase, *J. Pharm. Pharmacol.* 36 (1984) 111–115.
- [19] A.S. Kalgutkar, N. Castagnoli, B. Testa, Selective inhibitors of monoamine-oxidase (MAO-A and MAO-B) as probes of its catalytic site and mechanism, *Med. Res. Rev.* 15 (1995) 325–388.
- [20] R.R. Ramsay, Inhibitor design for monoamine oxidases, *Curr. Pharm. Des.* 19 (2013) 2529–2539.
- [21] H.Y.K. Chuang, D.R. Patek, L. Hellerma, Mitochondrial monoamine oxidase – inactivation by pargyline – adduct formation, *J. Biol. Chem.* 249 (1974) 2381–2384.
- [22] C. Binda, P. Newton-Vinson, F. Hubalek, D.E. Edmondson, A. Mattevi, Structure of human monoamine oxidase B, a drug target for the treatment of neurological disorders, *Nat. Struct. Biol.* 9 (2002) 22–26.
- [23] D.E. Edmondson, C. Binda, J. Wang, A.K. Upadhyay, A. Mattevi, Molecular and mechanistic properties of the membrane-bound mitochondrial monoamine oxidases, *Biochemistry* 48 (2009) 4220–4230.
- [24] C.D. Arnett, J.S. Fowler, R.R. Macgregor, D.J. Schlyer, A.P. Wolf, B. Langstrom, C. Halldin, Turnover of brain monoamine-oxidase measured *in vivo* by positron emission tomography using L-[C-11]deprenyl, *J. Neurochem.* 49 (1987) 522–527.
- [25] I. Bolea, J. Juarez-Jimenez, C. de los Rios, M. Chioua, R. Pouplana, F. Javier Luque, M. Unzeta, J. Marco-Contelles, A. Samadi, Synthesis, biological evaluation, and molecular modeling of donepezil and N-[(5-(benzyloxy)-1-methyl-1H-indol-2-yl)methyl]-N-methylprop-2-yn-1-amine hybrids as new multipotent cholinesterase/monoamine oxidase inhibitors for the treatment of Alzheimer's Disease, *J. Med. Chem.* 54 (2011) 8251–8270.
- [26] A. Samadi, C. de los Rios, I. Bolea, M. Chioua, I. Iriepa, I. Moraleda, M. Bartolini, V. Andrisano, E. Galvez, C. Valderas, M. Unzeta, J. Marco-Contelles, Multipotent MAO and cholinesterase inhibitors for the treatment of Alzheimer's disease: synthesis, pharmacological analysis and molecular modeling of heterocyclic substituted alkyl and cycloalkyl propargyl amine, *Eur. J. Med. Chem.* 52 (2012) 251–262.
- [27] E. Sanz, A. Quintana, V. Battaglia, A. Toninello, J. Hidalgo, S. Ambrosio, M. Valoti, J.L. Marco, K.F. Tipton, M. Unzeta, Anti-apoptotic effect of MAO-B inhibitor PF9601N[N-(2-propynyl)-2-(5-benzyloxy-indolyl) methylamine] is mediated by p53 pathway inhibition in MPP(+)-treated SH-SY5Y human dopaminergic cells, *J. Neurochem.* 105 (2008) 2404–2417.
- [28] V. Perez, J.L. Marco, E. Fernandez-Alvarez, M. Unzeta, Relevance of benzyloxy group in 2-indolyl methylamines in the selective MAO-B inhibition, *Br. J. Pharmacol.* 127 (1999) 869–876.
- [29] I. Bolea, A. Gella, L. Monjas, C. Pérez, M.I. Rodríguez-Franco, J.L. Marco-Contelles, A. Samadi, M. Unzeta, The multipotent, permeable drug ASS234 inhibits A $\beta$  aggregation, possesses antioxidant properties and protects from A $\beta$ -induced apoptosis, *Curr. Alzheimer Res.* 10 (2013) 797–808.
- [30] G.R. McDonald, A. Olivieri, R.R. Ramsay, A. Holt, On the formation and nature of the imidazoline I(2) binding site on human monoamine oxidase-B, *Pharmacol. Res.* 62 (2010) 475–488.
- [31] R.M.G. Hynson, J. Wouters, R.R. Ramsay, Monoamine oxidase A inhibitory potency and flavin perturbation are influenced by different aspects of pirlindole inhibitor structure, *Biochem. Pharmacol.* 65 (2003) 1867–1874.
- [32] W. Weyler, J.I. Salach, Purification and properties of mitochondrial monoamine-oxidase type-A from human-placenta, *J. Biol. Chem.* 260 (1985) 3199–3207.
- [33] P. Newton-Vinson, F. Hubalek, D.E. Edmondson, High-level expression of human liver monoamine oxidase B in *Pichia pastoris*, *Protein Expr. Purif.* 20 (2000) 334–345.
- [34] G.L. Ellman, K.D. Courtney, V. Andres, R.M. Featherstone, A new and rapid colorimetric determination of acetylcholinesterase activity, *Biochem. Pharmacol.* 7 (1961) 88–95.
- [35] H. Weissbach, T.E. Smith, J.W. Daly, B. Witkop, S. Udenfriend, A rapid spectrophotometric assay of monoamine oxidase based on the rate of disappearance of kynuramine, *J. Biol. Chem.* 235 (1960) 1160–1163.
- [36] R.R. Ramsay, Kinetic mechanism of monoamine oxidase-A, *Biochemistry* 30 (1991) 4624–4629.
- [37] M.J. Zhou, Z.J. Diwu, N. PanchukVoloshina, R.P. Haugland, A stable nonfluorescent derivative of resorufin for the fluorometric determination of trace hydrogen peroxide: applications in detecting the activity of phagocyte NADPH oxidase and other oxidases, *Anal. Biochem.* 253 (1997) 162–168.
- [38] A. Holt, M.M. Palcic, A peroxidase-coupled continuous absorbance plate-reader assay for flavin monoamine oxidases, copper-containing amine oxidases and related enzymes, *Nat. Protoc.* 1 (2006) 2498–2505.
- [39] R. Kitz, I.B. Wilson, Esters of methanesulfonic acid as irreversible inhibitors of acetylcholinesterase, *J. Biol. Chem.* 237 (1962) 3245–3249.
- [40] J.S. Yang, M. Jamei, K.R. Yeo, G.T. Tucker, A. Rostami-Hodjegan, Kinetic values for mechanism-based enzyme inhibition: assessing the bias introduced by the conventional experimental protocol, *Eur. J. Pharm. Sci.* 26 (2005) 334–340.
- [41] C. Binda, A. Mattevi, D.E. Edmondson, Structure–function relationships in flavoenzyme-dependent amine oxidations. A comparison of polyamine oxidase and monoamine oxidase, *J. Biol. Chem.* 277 (2002) 23973–23976.
- [42] A.G.W. Leslie, Integration of macromolecular diffraction data, *Acta Crystallogr. D Biol. Crystallogr.* 55 (1999) 1696–1702.
- [43] S. Bailey, The CCP4 suite – programs for protein crystallography, *Acta Crystallogr. D Biol. Crystallogr.* 50 (1994) 760–763.
- [44] S. McNicholas, E. Potterton, K.S. Wilson, M.E.M. Noble, Presenting your structures: the CCP4mg molecular-graphics software, *Acta Crystallogr. D Biol. Crystallogr.* 67 (2011) 386–394.
- [45] K. Magyar, The pharmacology of selegiline, *Monoamine Oxidases and Their Inhibitors*, vol. 100, 2011, pp. 65–84.
- [46] J.S. Fowler, J. Logan, N.D. Volkow, G.J. Wang, Translational neuroimaging: positron emission tomography studies of monoamine oxidase, *Mol. Imaging Biol.* 7 (2005) 377–387.
- [47] A.K. Upadhyay, J. Wang, D.E. Edmondson, Comparison of the structural properties of the active site cavities of human and rat monoamine oxidase A and B in their soluble and membrane-bound forms, *Biochemistry* 47 (2008) 526–536.
- [48] M.J. Zhou, N. PanchukVoloshina, A one-step fluorometric method for the continuous measurement of monoamine oxidase activity, *Anal. Biochem.* 253 (1997) 169–174.

## **Chapter II.**

***“In vitro and in vitro modulation of the monoaminergic neurotransmitters by multi-target compound ASS234”***



Manuscript Number:

Title: In vitro and in vivo evaluation of the modulatory effects of the multi-target compound ASS234 on the monoaminergic system

Article Type: Research Paper

Keywords: monoamine oxidase modulation; ASS234; multi-target-directed ligand; Alzheimer's disease; microdialysis

Corresponding Author: Ms. Jolien Van Schoors,

Corresponding Author's Institution: Vrije Universiteit Brussel

First Author: Jolien Van Schoors

Order of Authors: Jolien Van Schoors; Gerard Esteban; Ping Sun, PhD; Ann Van Eeckhaut, PhD; José Marco-Contelles; Ilse Smolders, PhD; Mercedes Unzeta, PhD

Manuscript Region of Origin: BELGIUM

Abstract: Alzheimer's disease (AD) is a neurodegenerative disorder frequently accompanied by psychiatric alterations caused by a monoaminergic dysfunction. The aim of the present work is to evaluate the in vitro and in vivo effects of ASS234, a promising multi-target-directed ligand (MTDL) to use in AD therapy, on the monoaminergic neurotransmission. In vitro, ASS234 exhibited a modulatory effect on the monoaminergic metabolism in both SH-SY5Y and PC12 cell lines, similar to the effect of clorgyline. ASS234 induced a significant increase of serotonin (5-HT) levels in SH-SY5Y cells. The catecholaminergic metabolism in PC12 cells was modulated by ASS234 with a significantly increased ratio of dopamine (DA) over the sum of its metabolites homovanillic acid (HVA) and 3,4-dihydroxyphenylacetic acid (DOPAC), though no apparent differences in noradrenaline (NA) could be observed. Furthermore, in vivo microdialysis showed a significant increase in the extracellular levels of 5-HT and NA in the hippocampus and those of DA and NA in the prefrontal cortex of freely moving Wistar rats following s.c. administration of ASS234. In conclusion, this study reveals that MTDL ASS234 is able to enhance the monoaminergic neurotransmission supporting its potential in AD therapy.

## Abstract

Alzheimer's disease (AD) is a neurodegenerative disorder frequently accompanied by psychiatric alterations caused by a monoaminergic dysfunction. The aim of the present work is to evaluate the *in vitro* and *in vivo* effects of ASS234, a promising multi-target-directed ligand (MTDL) for use in AD therapy, on the monoaminergic neurotransmission. *In vitro*, ASS234 exhibited a modulatory effect on the monoaminergic metabolism in both SH-SY5Y and PC12 cell lines, similar to the effect of clorgyline. ASS234 induced a significant increase of serotonin (5-HT) levels in SH-SY5Y cells. The catecholaminergic metabolism in PC12 cells was modulated by ASS234 with a significantly increased ratio of dopamine (DA) over the sum of its metabolites homovanillic acid (HVA) and 3,4-dihydroxyphenylacetic acid (DOPAC), though no apparent differences in noradrenaline (NA) could be observed. Furthermore, *in vivo* microdialysis showed a significant increase in the extracellular levels of 5-HT and NA in the hippocampus and those of DA and NA in the prefrontal cortex of freely moving Wistar rats following s.c. administration of ASS234. In conclusion, this study reveals that the MTDL ASS234 is able to enhance the monoaminergic neurotransmission supporting its potential in AD therapy.

1 ***In vitro* and *in vivo* evaluation of the modulatory effects of the multi-target compound**  
2 **ASS234 on the monoaminergic system**

3  
4 Gerard Esteban<sup>a\*</sup>, Jolien Van Schoors<sup>b\*</sup>, Ping Sun<sup>a</sup>, Ann Van Eeckhaut<sup>b</sup>, José Marco-  
5 Contelles<sup>c</sup>, Ilse Smolders<sup>b1§</sup>, Mercedes Unzeta<sup>a2§</sup>

6  
7  
8 <sup>a</sup>Institute of Neurosciences, Departament de Bioquímica i Biologia Molecular, Facultat de  
9 Medicina, Universitat Autònoma de Barcelona, 08193 Bellaterra (Cerdanyola del Vallès),  
10 Spain.

11 <sup>b</sup>Department of Pharmaceutical Chemistry and Drug Analysis (FASC), Experimental  
12 Pharmacology, Center for Neurosciences (C4N), Vrije Universiteit Brussel, Laarbeeklaan  
13 103, 1090 Jette, Belgium.

14 <sup>c</sup>Laboratory of Medicinal Chemistry (IQOG, CSIC), C/Juan de la Cierva 3, 28006 Madrid,  
15 Spain.

16  
17  
18 \*equally contributing first authors

19 §equally contributing last authors

20  
21  
22 Double family names: Van Schoors, Van Eeckhaut, Marco-Contelles

23  
24  
25 Corresponding authors:

26  
27 <sup>1</sup>**Ilse Smolders:**

28 Laarbeeklaan 103, 1090 Jette

29 Belgium

30 Ilse.Smolders@vub.ac.be

31 Tel.: +32 24774447

32  
33 <sup>2</sup>**Mercedes Unzeta:**

34 08193 Bellaterra (Cerdanyola del Vallès)

35 Spain

36 Mercedes.Unzeta@uab.cat

37 Tel.: +34 935811523

38

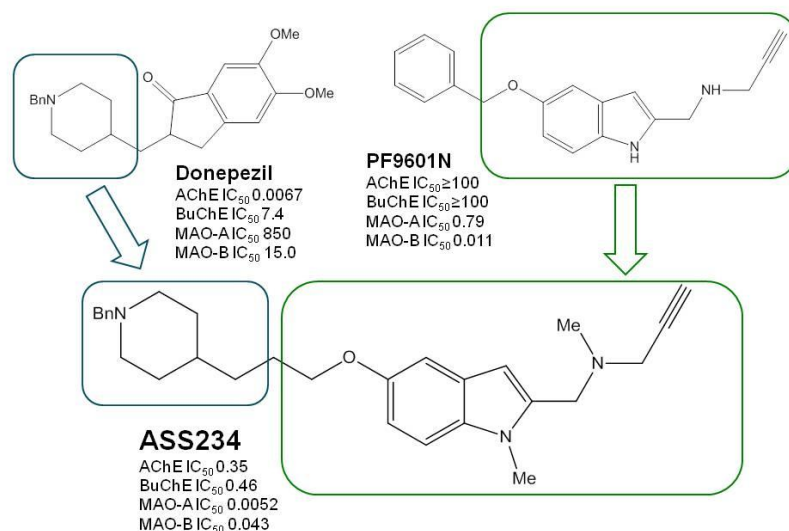
## 39 1. Introduction

40

41 Alzheimer's disease (AD) is the most common cause of dementia in the elderly population  
42 affecting over 30 million individuals worldwide (Wimo et al., 2011). Despite the widely  
43 described dysfunction of the basal forebrain cholinergic neurons (Davies and Maloney, 1976;  
44 Geula and Mesulam, 1999), the accumulation of hyperphosphorylated tau protein (Ballatore  
45 et al., 2007) and the presence of amyloid-beta peptide (Palop and Mucke, 2010), the  
46 pathogenesis of AD is not yet fully understood, though a wide consensus in describing it as a  
47 multifaceted neurological disorder exists (Kumar et al., 2015; Perl, 2010). In AD, specific  
48 brain areas such as the basal forebrain, hippocampus and neocortex closely associated with  
49 learning and memory are highly affected. Besides the distinctive cognitive deficits, AD  
50 symptoms are frequently accompanied by psychiatric alterations caused by a dysfunction of  
51 the monoaminergic transmission (Ballard et al., 2008; Rossor and Iversen, 1986). In a  
52 reported study including 100 autopsy-confirmed AD cases, depression, mood change and  
53 social withdrawal were diagnosed two years prior to the onset of AD (Jost and Grossberg,  
54 1996). In depression, levels of noradrenaline (NA) and serotonin (5-hydroxytryptamine, 5-  
55 HT) are affected, and the disturbance of dopamine (DA) metabolism in patients suffering  
56 endogenous depression has been widely reported (Birkmayer and Riederer, 1975; van Praag  
57 and Korf, 1975). The onset and progression of AD might thus be triggered by several factors  
58 including cholinergic dysfunction, excessive protein misfolding and aggregation, oxidative  
59 stress, biometal dyshomeostasis, excitotoxic and neuroinflammatory processes, as well as  
60 disturbances in the monoaminergic systems.

61 Current Food and Drug Administration-approved drugs for the treatment of the cognitive  
62 deficits featured in AD are based on the cholinergic hypothesis, exhibiting a limited  
63 therapeutic efficacy (Davies and Maloney, 1976; Geula and Mesulam, 1999). In view of this  
64 lack of therapeutic effectiveness of anti-cholinergic therapies together with the multifactorial  
65 nature of AD, some authors have proposed a new paradigm, the so-called multi-target-  
66 directed ligand (MTDL) approach, which supports the beneficial use of compounds bearing  
67 multiple pharmacological profiles able to interact with various cellular targets (Buccafusco  
68 and Terry, 2000; Youdim and Buccafusco, 2005). In this context, ASS234, a MTDL molecule  
69 resulting from the juxtaposition of the benzylpiperidine moiety of donepezil, an  
70 acetylcholinesterase (AChE) inhibitor, and the indolopropargylamine moiety of PF9601N, a  
71 potent and selective monoamine oxidase (MAO)-B inhibitor, was designed, synthesised and  
72 evaluated for the potential treatment of AD, and exhibits an interesting pharmacological  
73 profile (Bolea et al., 2011; del Pino et al., 2014) (Fig. 1). *In vitro* studies have described  
74 ASS234 as a dual inhibitor of cholinesterase (AChE and BuChE) and monoamine oxidase  
75 (MAO-A and MAO-B) activities, with anti-aggregating amyloid-beta antioxidant and anti-  
76 apoptotic properties (Bolea et al., 2013). Moreover, an effective blood-brain barrier (BBB)  
77 permeability was reported (Bolea et al., 2013). Reduced activities of MAO-A, MAO-B,

78 AChE and histamine N-methyltransferase and increased cerebral concentrations of the  
79 monoamines 5-HT, DA, NA and histamine examined in post-mortem samples of rats were  
80 reported following administration of ASS234. Moreover, in the latter study, improved  
81 working and reference memory in rats with experimental vascular dementia were observed  
82 (Stasiak et al., 2014).  
83



84  
85 **Fig. 1.** Design strategy of MTDL ASS234. Inhibitory concentrations (IC<sub>50</sub>, in μM) of cholinesterases and MAOs  
86 by donepezil, PF9601N and ASS234 are shown (Bolea et al., 2011).  
87

88 Taking into account the widely reported data on the involvement of psychiatric disorders in  
89 AD, the aim of the present work was to study the modulatory effect of the MTDL ASS234 on  
90 the monoaminergic system. The *in vitro* modulation of the monoaminergic metabolism by  
91 ASS234 was assayed in SH-SY5Y and PC12 cells. Clorgyline, a standard irreversible  
92 inhibitor of MAO-A, was used for comparative purposes. Next, *in vivo* investigation of the  
93 possible effect of ASS234 on the extracellular levels of the neurotransmitters 5-HT, DA and  
94 NA in hippocampus and prefrontal cortex of freely moving Wistar rats was assessed by  
95 microdialysis.

## 96 **2. Material and methods**

97

### 98 *2.1 Chemicals and reagents*

99 ASS234 was synthesised as previously described (Bolea et al., 2011). Clorgyline, (D)L-  
100 noradrenaline hydrochloride, dopamine hydrochloride, serotonin hydrochloride, 5-  
101 hydroxyindoleacetic acid (5-HIAA), 4-hydroxy-3-methoxyphenylacetic acid (homovanillic  
102 acid, HVA), 3,4-dihydroxyphenylacetic (DOPAC) and 2,5-dihydroxybenzoic acid (DHBA)  
103 were purchased from Sigma-Aldrich (Madrid, Spain or Steinem, Germany). Radiolabelled  
104 substrates [<sup>14</sup>C]-(5-hydroxytryptamine) and [<sup>14</sup>C]-phenylethylamine were purchased from  
105 Perkin Elmer (USA). Toluene, ethylacetate and 2,5-diphenyloxazol were purchased from  
106 Sharlab (Spain). Dulbecco's modified Eagle's medium/Ham's F12 medium (DMEM/F-12)  
107 was purchased from Gibco (Alcobendas, Spain). Cell culture reagents fetal bovine serum  
108 (FBS), fetal horse serum (FHS), HEPES, glutamine, non-essential amino acids, penicillin,  
109 streptomycin and phosphate buffered saline (PBS) were purchased from Sigma-Aldrich  
110 (Madrid, Spain). Rat-tail collagen type I was purchased from BD Biosciences (Spain). EDTA,  
111 sodium bisulphite, perchloric acid and acetonitrile were purchased from Sigma-Aldrich  
112 (Israel), bovine serum albumin (BSA) from Sigma-Aldrich (USA), citric acid from Sharlab  
113 (Germany), sodium octanesulfonate from Romil (USA) and triethylamine from Fluka (Spain).  
114 Diazepam 10 mg/2 mL was purchased as Valium from Roche (Cenexi, Fontenay-sous-Bois,  
115 France), ketamine 1000 mg/10 mL as Ketamine 1000 from Ceva (Libourne, France),  
116 Ketoprofen 1% as Ketofen from Merial (Toulouse, France) and NaCl 0.9% from Baxter  
117 (Lessines, Belgium). L-ascorbic acid, citric acid monohydrate, sodium acetate trihydrate,  
118 sodium chloride, sodium decanesulfonate and sodium hydroxide pellets were purchased from  
119 Sigma-Aldrich (Steinheim, Germany). Potassium chloride was supplied by Merck  
120 (Darmstadt, Germany). Calcium chloride hexahydrate and disodium edetate (EDTA) were  
121 purchased from Fluka (Steinheim, Germany). Purified water was obtained via an Arium pro  
122 UV system of Sartorius Stedim Biotech (Vilvoorde, Belgium). Hydrochloric acid 37% was  
123 from Acros Organics (Geel, Belgium), glacial acetic acid from Fisher Scientific  
124 (Loughborough, Leics, United Kingdom) and acetonitrile for ULC-MS from Biosolve  
125 (Valkenswaard, The Netherlands).

126

### 127 *2.2 Cell cultures and treatments*

128 Human neuroblastoma SH-SY5Y cell line was purchased from the European Collection of  
129 Cell Cultures and grown in DMEM/Ham's F-12 media supplemented with 15% FBS, 200  
130 mM glutamine, non-essential amino acids and penicillin/streptomycin. PC12 cell line was  
131 purchased from the American Type Culture Collection and grown in DMEM media  
132 supplemented with 7% FBS, 7% FHS, 1.14 mM HEPES pH 6.8 and penicillin/streptomycin.  
133 Both cell lines were maintained at 37 °C in a saturating humidity atmosphere containing 5%  
134 CO<sub>2</sub>. For treatments, both SH-SY5Y and PC12 cells were seeded at a density of 2.5·10<sup>4</sup>

135 cells/mL onto rat tail collagen type I-coated plates until 70-80% confluence was reached.  
136 Cells were treated with PBS (control) or 1  $\mu$ M inhibitor (clorgyline or ASS234) for 3 or 24  
137 hours.

138 For activity assays, at the end of treatments, cells were washed twice with PBS, scrapped, and  
139 collected in 50 mM phosphate buffer pH 7.4. Then, lysates were sonicated for 10 seconds on  
140 ice and kept at -80 °C prior to measurement of MAO activity.

141 For monoamine analysis, treated cells were washed twice with PBS, scrapped and centrifuged  
142 at 3,000 x g for 5 minutes. Then, pellets were resuspended in homogenisation solution  
143 containing 0.25 M perchloric acid, 100  $\mu$ M sodium bisulphite and 250  $\mu$ M EDTA and lysates  
144 sonicated for 10 seconds on ice and kept at -80 °C prior to analysis.

145

### 146 *2.3 Measurement of MAO activity*

147 The specific activity of MAO-A and MAO-B in lysates of SH-SY5Y and PC12 cells was  
148 determined radiometrically (Fowler and Tipton, 1981) using 100 mM (0.5 mCi/mmol) [ $^{14}$ C]-  
149 (5-hydroxytryptamine) and 20 mM (2.5 mCi/mmol) [ $^{14}$ C]-phenylethylamine, respectively.  
150 Enzymatic reactions were allowed for 20 min (MAO-A) and 5 min (MAO-B) in a bath at 37  
151 °C and stopped by adding 2 M citric acid. Radiolabelled aldehyde products were extracted  
152 into toluene/ethylacetate (1/1, v/v) containing 0.6% (w/v) 2,5-diphenyloxazole prior to liquid  
153 scintillation counting (Tri-Carb 2810TR). Specific activity is expressed in pmol/min/mg of  
154 protein. Total protein amount was measured by the method of Bradford (Bradford, 1976)  
155 using BSA as standard.

156

### 157 *2.4 Microdialysis experiment*

158 *In vivo* experiments were carried out according to the national guidelines on animal  
159 experimentation and approved by the Ethical Committee for Animal Experiments of the  
160 Faculty of Medicine and Pharmacy of the Vrije Universiteit Brussel (VUB). Male albino  
161 Wistar rats (250-300 g) purchased from Charles River Laboratories (Cedex, France) were  
162 anaesthetised with a ketamine/diazepam mixture (60/4.5 mg/kg) i.p. and received ketoprofen  
163 (3 mg/kg) s.c. prior to surgery. Intracerebral guide cannulas were implanted in the  
164 hippocampus of the left hemisphere and in the prefrontal cortex of the right hemisphere, with  
165 stereotactic coordinates respectively AP -5.6, L -4.6, V +4.1 and AP +2.2, L +0.6, V +1.2  
166 relative to bregma, according to the atlas of Paxinos and Watson (Paxinos and Watson, 1986),  
167 and fixed with dental cement. After recovery, a microdialysis probe (MAB 6.14.3, 0.6 mm  
168 outer diameter, 3 mm length, 15 kDa cut-off) of Microbiotech (Stockholm, Sweden) was  
169 inserted into each cannula. The probes were continuously perfused with modified Ringer's  
170 solution (147 mM NaCl, 4 mM KCl and 2.3 mM CaCl<sub>2</sub>) at a flow rate of 2  $\mu$ L/min.

171 The day after surgery, microdialysis samples were collected with a temporal resolution of 20  
172 min and 10  $\mu$ L of an antioxidative mixture (100 mM acetic acid, 0.27 mM EDTA and 12.5  
173  $\mu$ M ascorbic acid) was added to 40  $\mu$ L microdialysate (Van Schoors et al., 2015). Six baseline

174 samples were collected, followed by a sham injection of 500  $\mu$ L 0.9% NaCl (saline) s.c. and  
175 another six dialysis collections. Subsequently, ASS234 was injected s.c. in a dose of 5 (n = 7),  
176 15 (n = 9) or 30 (n = 7) mg/kg. Doses and route of administration are based on previous work  
177 (Stasiak et al., 2014). Nine more samples were collected during three hours after  
178 administration of the compound.

179

### 180 *2.5 Chromatographic methods*

181 Levels of 5-HT and 5-HIAA in SH-SY5Y cells and levels of DA, NA, DOPAC and HVA in  
182 PC12 cell lysates were determined by high-performance liquid chromatography (HPLC) with  
183 electrochemical detection. The Elite LaChrom system from Hitachi (Tokyo, Japan) with L-  
184 2130 pump and L-2200 autosampler and the Coulochem 5100A electrochemical detector  
185 from ESA (Chelmsford, USA) with a Model 5011 dual-electrode analytical cell with porous  
186 graphite electrodes were used. Both SH-SY5Y and PC12 cell lysates were thawed and  
187 centrifuged at 12,000 x g for 10 minutes at 4 °C. Next, the supernatants of each sample were  
188 placed in the autosampler, cooled at 10 °C and 20  $\mu$ L was injected. DHBA was used as  
189 standard external control. The mobile phase contained 99% v/v of a buffered aqueous solution  
190 (50 mM citric acid, 0.05 mM EDTA and 1.2 mM sodium octanesulfonate, adjusted to pH 2.75  
191 with triethylamine) and 1% v/v acetonitrile. Elution was performed on a Chromolith  
192 Performance RP-18e monolithic column (100 x 4.6 mm) from Merck (Darmstadt, Germany)  
193 at room temperature (20-25°C) using a flow rate of 1 mL/min. The potentials of the electrodes  
194 were set at -50 mV and +400 mV. Instrument control and data acquisition were carried out by  
195 EZChromElite version 3.1.7 of Scientific Software (Pleasanton, California).

196 For quantification of 5-HT, DA and NA in the microdialysis samples, ultra-high performance  
197 liquid chromatography (UHPLC) with electrochemical detection was used. The ALEXYS  
198 neurotransmitter analyzer from Antec (Zoeterwoude, The Netherlands) consisted of an AS  
199 110 autosampler, an OR 110 degasser unit, an LC 110S pump and a DECADE Elite  
200 electrochemical detector equipped with a SenCell electrochemical cell (2 mm glassy carbon  
201 working electrode, ISAAC reference electrode, spacing distance 12  $\mu$ m), kindly provided by  
202 Antec. The sample tray in the autosampler was cooled at 4°C and the injection volume was 5  
203  $\mu$ L. The mobile phase consisted of 92.5% v/v of a buffered aqueous solution (150 mM  
204 sodium acetate trihydrate, 20 mM citric acid monohydrate, 12 mM sodium decanesulfonate, 8  
205 mM KCl and 0.5 mM EDTA, pH adjusted to 5.5 with sodium hydroxide 8 M) and 7.5% v/v  
206 acetonitrile and was pumped at a flow rate of 60  $\mu$ L/min. Separations were performed on an  
207 Acquity UPLC BEH C<sub>18</sub> column (100 x 1.0 mm, 1.7  $\mu$ m) (Waters, Milford, Massachusetts,  
208 USA). The separation and detection temperature was set at 50°C. The applied potential was  
209 +340 mV and Fast Fourier Transformation was applied on the unfiltered chromatograms.  
210 Instrument control and data acquisition were carried out by Clarity Chromatography Software  
211 version 5.0.5 (Data Apex, Prague, The Czech Republic).

212

213 *2.6 Data analysis and statistical procedures*

214 GraphPad Prism version 4.03 was employed for statistical analyses, with the  $\alpha$  level chosen at  
215 0.05.

216 Significant *in vitro* effects of treatment groups versus the control group were analysed  
217 applying one-way ANOVA followed by Dunnett's multiple comparison test, separately for  
218 the 3 hours and 24 hours incubation groups. Differences in incubation time were evaluated by  
219 two-way ANOVA followed by Bonferroni post hoc test.

220 Some *in vivo* microdialysis data sets had to be discarded because of technical problems during  
221 the microdialysis experiment or due to low probe recovery resulting in undetectable  
222 monoamine levels in the samples. Microdialysis data were analysed applying one-way  
223 ANOVA for repeated measures and the Dunnett's multiple comparison test was used as post  
224 hoc test.

225

226

227

228 **3. Results**

229

230 *3.1 In vitro study*

231

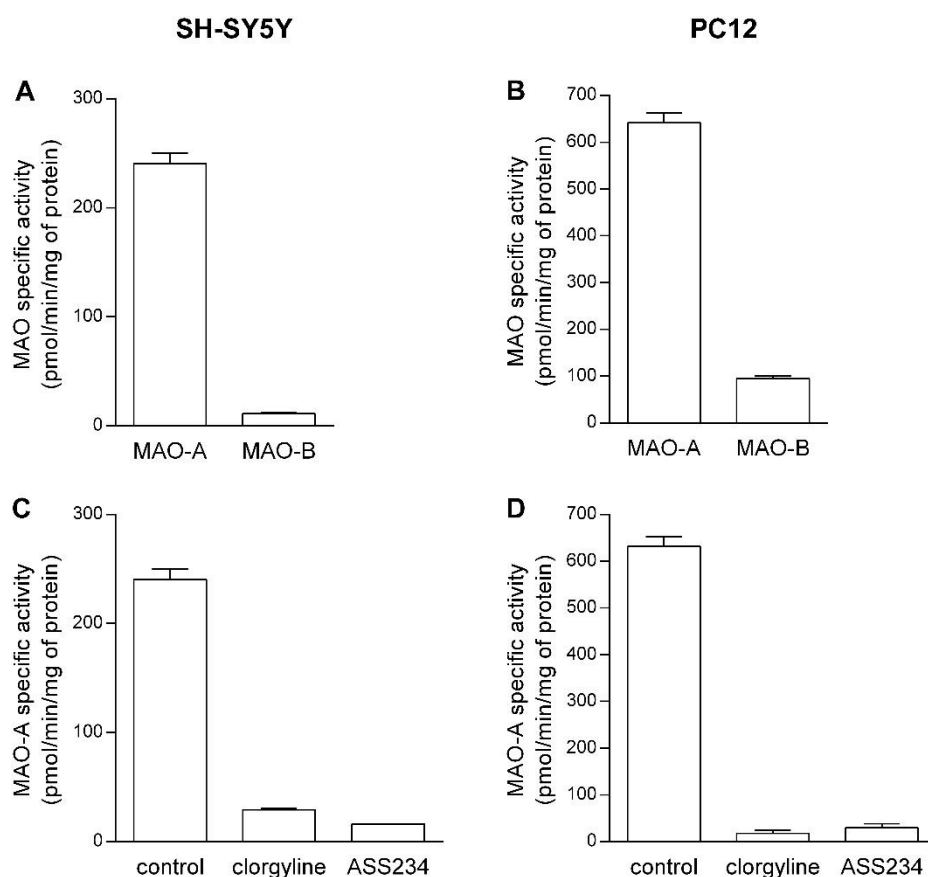
232 *3.1.1 Characterisation of MAO in SH-SY5Y and PC12 cell lines*

233 The presence of both MAO isoforms was characterised in monoaminergic cell lines of human  
234 neuroblastoma SH-SY5Y and undifferentiated PC12. To assess the corresponding activities,  
235 [<sup>14</sup>C]-labelled 5-HT and [<sup>14</sup>C]-labelled phenylethylamine were used as specific substrates for  
236 MAO-A and MAO-B activities, respectively. In both cell lines, MAO-A activity was revealed  
237 as the predominant isoform responsible for the monoaminergic metabolism (Fig. 2A and 2B).  
238 These findings are in agreement with those previously reported (Maruyama et al., 1997).

239

240 *3.1.2 Inhibition of MAO-A by ASS234 in SH-SY5Y and PC12 cells*

241 The inhibition of MAO-A activity by the multi-target compound ASS234 and clorgyline was  
242 studied in both SH-SY5Y and PC12 cell lines treated with 1  $\mu$ M of either inhibitor. The  
243 activity of MAO-A was fully inhibited following 3 hours of treatment with either ASS234 or  
244 clorgyline in both cell lines (Fig. 2C and 2D). Similar results were observed when cells were  
245 incubated for 24 hours (data not shown). Comparatively, the rapid inhibition of MAO-A  
246 exerted by both inhibitors is in agreement with previously reported work (Esteban et al.,  
247 2014). These treatment conditions were selected to further investigate the monoaminergic  
248 effect resulting from selective inhibition of MAO-A activity by both ASS234 and clorgyline.



249  
 250 **Fig. 2.** Activity levels of MAO-A and MAO-B in SH-SY5Y (A) and PC12 (B) cells using 5-HT and  
 251 phenylethylamine as substrates, respectively. Activity of MAO-A was inhibited by 1  $\mu$ M clorgyline or ASS234  
 252 in SH-SY5Y cells (C) and PC12 cells (D) treated for 3 hours. Values are the mean of specific activity expressed  
 253 in pmol/min/mg of protein  $\pm$  SEM of two independent experiments in duplicate.

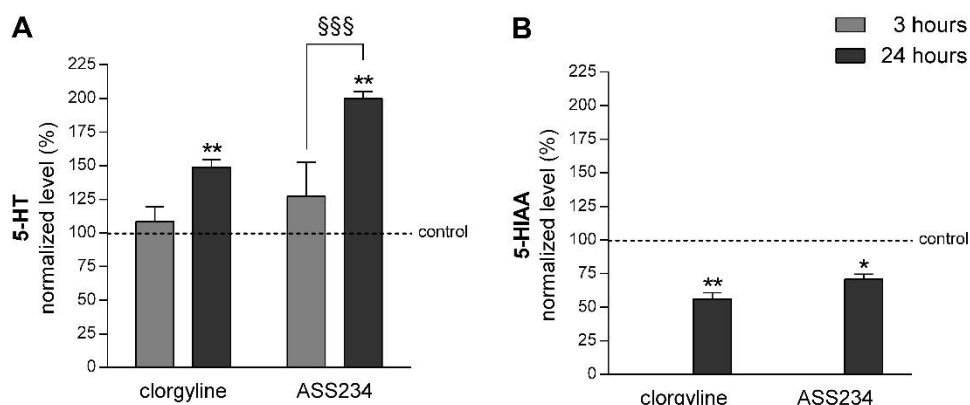
254

### 255 3.1.3 Effect of ASS234 on the serotonergic metabolism of SH-SY5Y cells

256 To study the effect of ASS234 on the serotonergic metabolism, human neuroblastoma SH-  
 257 SY5Y cells were used since elevated levels of 5-HT were detected in this cell line under the  
 258 described experimental conditions (data not shown).

259 Compared to control conditions, 5-HT levels were only increased after 24 hours of incubation  
 260 with both compounds, but this effect was more pronounced for ASS234. Indeed, the 5-HT  
 261 increase at the 24 hour incubation time point compared to the 3 hour incubation was only  
 262 significant for ASS234 (Fig. 3A). Concurrently, levels of 5-HIAA after 3 hours of incubation  
 263 could not be measured while those at 24 hours were found significantly reduced with both  
 264 inhibitors compared to control (Fig. 3B). These *in vitro* findings reveal ASS234 as a 5-HT-  
 265 enhancing agent.

266



267  
 268 **Fig. 3.** Effect of clorgyline or ASS234 on levels of 5-HT (A) and 5-HIAA (B) in SH-SY5Y cells after 3 (light  
 269 gray) and 24 (dark gray) hours of incubation. Values are expressed as the mean percentage of non-treated cells  
 270 (control)  $\pm$  SEM from at least three independent experiments in triplicate. \*  $P < 0.05$ , \*\*  $P < 0.01$  significant data  
 271 compared to control group by Dunnett's multiple comparison test. §§§  $P < 0.001$  significant data by Bonferroni  
 272 post test.

273

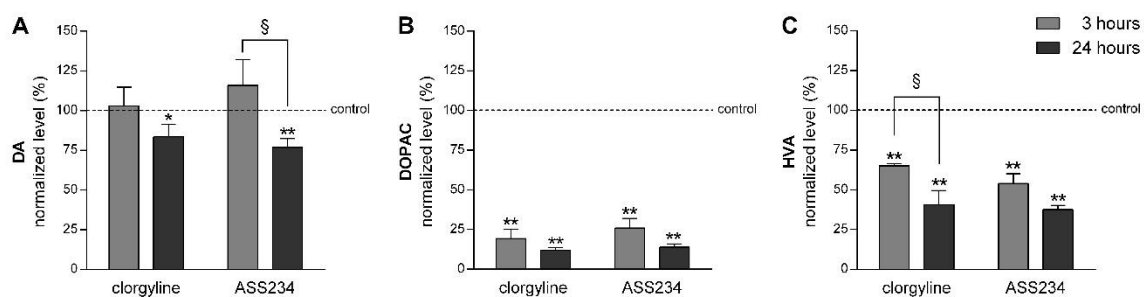
#### 274 3.1.4 Effect of ASS234 on the catecholaminergic metabolism of PC12 cells

275 The modulation of the catecholaminergic system through the selective inhibition of MAO-A  
 276 activity by ASS234 or clorgyline was studied in undifferentiated PC12 cells, since high levels  
 277 of catecholaminergic metabolites were detected in this cell line under the described  
 278 experimental conditions (data not shown).

279 The levels of DA remained nearly unaltered after 3 hours of treatment with either compound  
 280 and significantly decreased at 24 hours of incubation compared to the control group. Yet, only  
 281 with ASS234 a significant difference between both incubation times was observed (Fig. 4A).

282 Not surprisingly, the levels of DA metabolites DOPAC (Fig. 4B) and HVA (Fig. 4C)  
 283 decreased significantly following the treatment with either inhibitor, triggered by the  
 284 inhibition of MAO activity, which mediates the enzymatic breakdown of DA into DOPAC  
 285 and HVA.

286

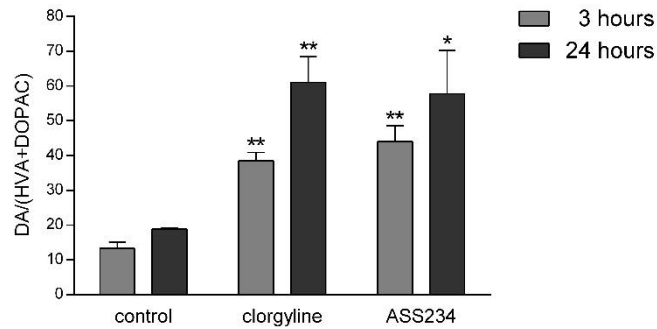


287  
 288 **Fig. 4.** Effect of clorgyline or ASS234 on levels of DA (A), DOPAC (B) and HVA (C) in PC12 cells after 3  
 289 (light gray) and 24 (dark gray) hours of incubation. Values are expressed as the mean percentage of non-treated  
 290 cells (control)  $\pm$  SEM from at least three independent experiments in triplicate. \*  $P < 0.05$ , \*\*  $P < 0.01$

291 significant data compared to control group by Dunnett's multiple comparison test. § P < 0.05 significant data by  
292 Bonferroni post test.

293 In order to confirm the prevention of DA breakdown via MAO inhibition, the ratio  
294 DA/(HVA+DOPAC), an index inversely related to the oxidative metabolism of DA by MAO,  
295 was determined. Compared to control values, the ratio was significantly increased after 3 and  
296 24 hours of incubation with ASS234 or clorgyline (Fig. 5).

297



298

299 **Fig. 5.** Effect of clorgyline or ASS234 on the ratio DA/(HVA+DOPAC) in PC12 cells after 3 (light gray) and 24  
300 (dark gray) hours of incubation. Values are expressed as the mean ratio  $\pm$  SEM from at least three independent  
301 experiments in triplicate. \* P < 0.05, \*\* P < 0.01 significant data compared to control group by Dunnett's  
302 multiple comparison test.

303

304 For NA, no significant changes were observed after incubation with either clorgyline or  
305 ASS234 (data not shown).

306

307

### 308 **3.2 *In vivo* microdialysis study**

309

310 Average basal extracellular concentrations in the hippocampal microdialysis samples were  
311 115 pM, 164 pM and 228 pM for 5-HT, DA and NA, respectively. Monoamine levels after  
312 sham injections were not significantly different from these mean basal levels (P > 0.05).  
313 Effects of ASS234 treatment on extracellular monoamine concentrations in hippocampus are  
314 expressed as percentages of baseline (Fig. 6). Results of the statistical analysis are given in  
315 Table 1.

316 No significant changes on the levels of monoamines were observed in the rats receiving 5  
317 mg/kg ASS234. However, at a dose of 15 or 30 mg/kg ASS234, significant increases in  
318 hippocampal 5-HT (Fig. 6A) and NA (Fig. 6C) levels were obtained. Though, we cannot  
319 explain why no consistent dose-response effects could be observed at these dose regimens. *In*  
320 *vivo* DA concentrations in hippocampus were not significantly altered following the  
321 administration of ASS234 (Fig. 6B).

322

323 **Table 1**  
 324 Statistical analysis (one-way ANOVA for repeated measures) of the monoamine levels in hippocampus after  
 325 ASS234 treatment for the three tested doses, compared to mean levels after sham injection.  
 326

neurotransmitter	dose ASS234 (mg/kg)	n	F	P
5-HT	5	5	$F_{9,36} = 1.047$	$P = 0.4235$
	15	7	$F_{9,54} = 5.077$	$P < 0.0001$ ***
	30	4	$F_{9,27} = 12.24$	$P < 0.0001$ ***
DA	5	4	$F_{9,27} = 0.5777$	$P = 0.8034$
	15	6	$F_{9,45} = 1.159$	$P = 0.3439$
	30	3	$F_{9,18} = 0.9154$	$P = 0.5337$
NA	5	7	$F_{9,54} = 1.724$	$P = 0.1059$
	15	7	$F_{9,54} = 4.003$	$P = 0.0006$ ***
	30	6	$F_{9,45} = 13.43$	$P < 0.0001$ ***

327 \*\*\* P < 0.001 significant data compared to mean level after sham injection  
 328

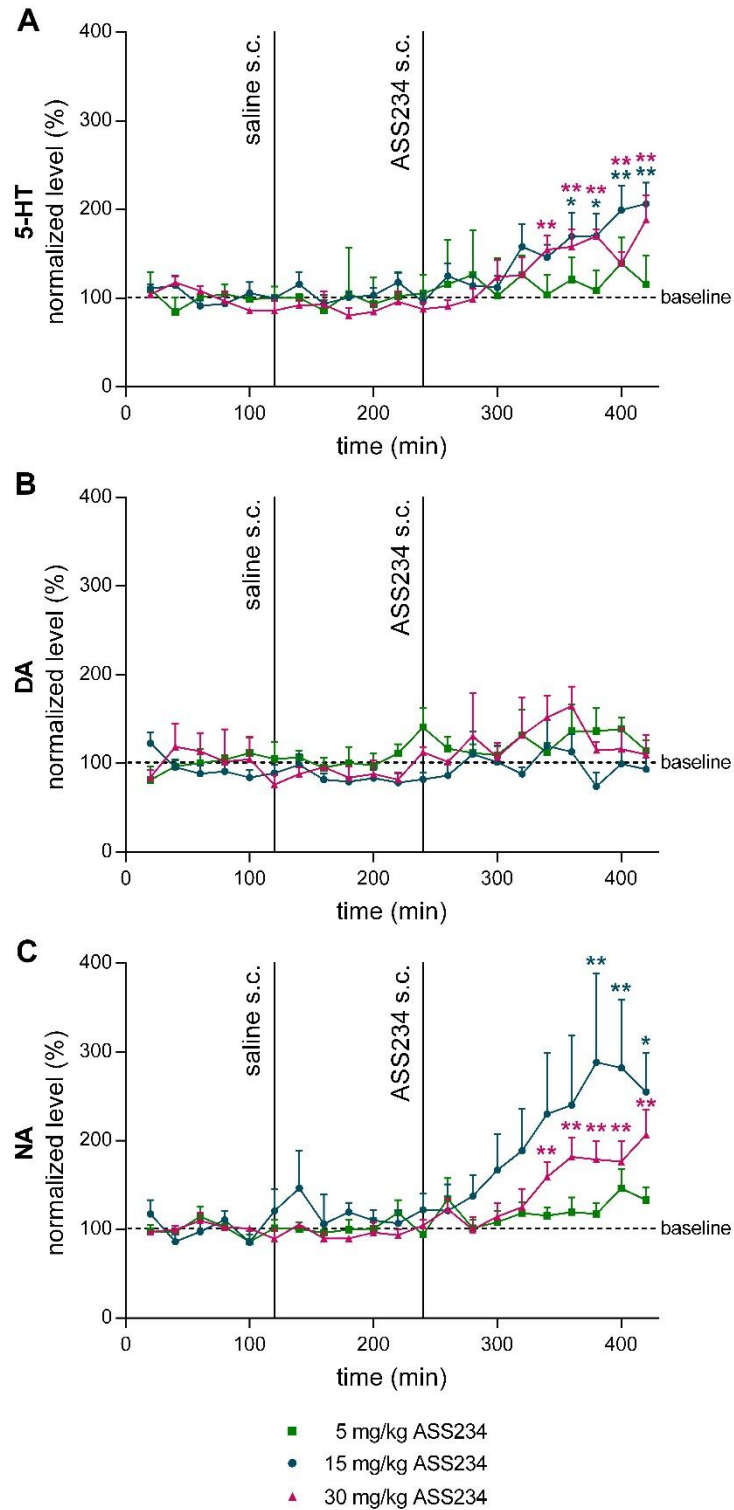
329 In the microdialysis samples of the prefrontal cortex, average concentrations of 225 pM 5-HT,  
 330 355 pM DA and 312 pM NA were found under basal conditions. After sham injections,  
 331 monoamine levels were not significantly different from these mean basal levels ( $P > 0.05$ ).  
 332 Effects of ASS234 treatment on extracellular monoamine concentrations in prefrontal cortex  
 333 are expressed as percentages of baseline levels (Fig. 7). Results of the statistical analysis are  
 334 given in Table 2.

335 The most pronounced effect was found on the extracellular levels of NA. Administration of  
 336 ASS234 indeed enhanced dose-dependently the *in vivo* NA levels in prefrontal cortex of  
 337 conscious rats (Fig. 7C). ASS234 also significantly increased DA levels after doses of 5 or 30  
 338 mg/kg (Fig. 7B). On the other hand, levels of 5-HT in the prefrontal cortex were only slightly  
 339 affected (5 mg/kg group) by the MTDL ASS234 (Fig. 7A).

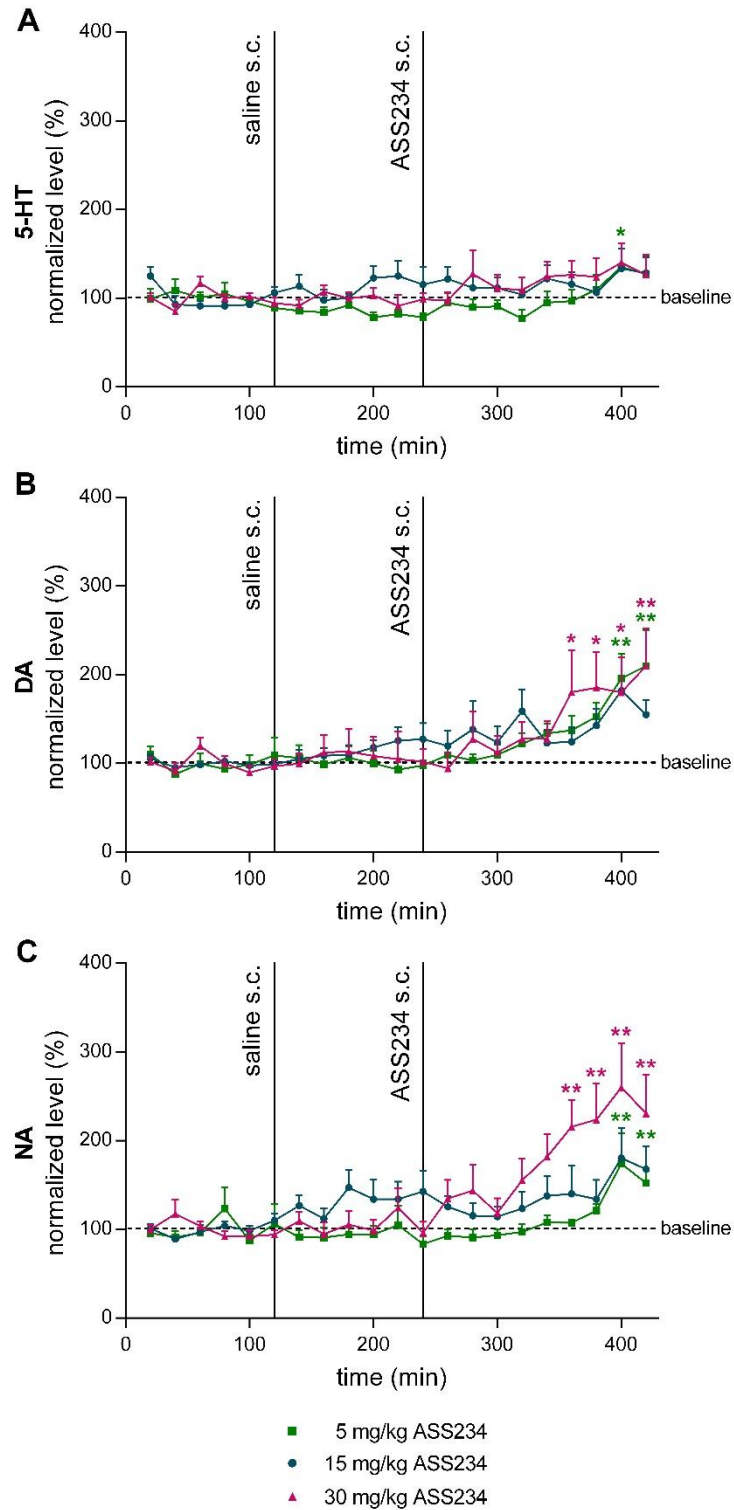
340  
 341 **Table 2**  
 342 Statistical analysis (one-way ANOVA for repeated measures) of the monoamine levels in prefrontal cortex after  
 343 ASS234 treatment for the three tested doses, compared to mean levels after sham injection.  
 344

neurotransmitter	dose ASS234 (mg/kg)	n	F	P
5-HT	5	6	$F_{9,45} = 2.358$	$P = 0.0281$ *
	15	7	$F_{9,54} = 0.5355$	$P = 0.8422$
	30	6	$F_{9,45} = 0.7872$	$P = 0.6293$
DA	5	6	$F_{9,45} = 5.858$	$P < 0.0001$ ***
	15	7	$F_{9,54} = 1.817$	$P = 0.0861$
	30	7	$F_{9,54} = 5.164$	$P < 0.0001$ ***
NA	5	6	$F_{9,45} = 5.679$	$P < 0.0001$ ***
	15	9	$F_{9,72} = 2.332$	$P = 0.0229$ *
	30	7	$F_{9,54} = 5.888$	$P < 0.0001$ ***

345 \* P < 0.05, \*\*\* P < 0.001 significant data compared to mean level after sham injection



346  
 347 **Fig. 6.** Effect of ASS234 on the extracellular levels of 5-HT (A), DA (B) and NA (C) in the hippocampus. Three  
 348 doses of ASS234 were tested: 5 mg/kg (green squares), 15 mg/kg (blue circles) and 30 mg/kg (pink triangles).  
 349 Data are presented as the mean percentage of the basal level (baseline)  $\pm$  SEM. Vertical lines indicate sham  
 350 (saline s.c.) and treatment (ASS234 s.c.) injection. \*  $P < 0.05$ , \*\*  $P < 0.01$  significant data compared to mean  
 351 level after sham injection by Dunnett's multiple comparison test.



352

353 **Fig. 7.** Effect of ASS234 on the extracellular levels of 5-HT (A), DA (B) and NA (C) in the prefrontal cortex.  
 354 Three doses of ASS234 were tested: 5 mg/kg (green squares), 15 mg/kg (blue circles) and 30 mg/kg (pink  
 355 triangles). Data are presented as the mean percentage of the basal level (baseline) ± SEM. Vertical lines indicate  
 356 sham (saline s.c.) and treatment (ASS234 s.c.) injection. \* P < 0.05, \*\* P < 0.01 significant data compared to  
 357 mean level after sham injection by Dunnett's multiple comparison test.

358

359

#### 360 4. Discussion

361

362 Psychiatric alterations such as depression underlying AD symptoms are possibly caused by  
363 monoaminergic dysfunction. The therapeutic efficacy of clinically used antidepressant drugs  
364 is based on the selective inhibition of MAO-A, as the main isoform responsible for the  
365 metabolism of 5-HT, NA, DA and/or on the blockage of the corresponding reuptake systems  
366 at the pre-synaptic nerve endings. Both approaches induce an enhancement of the  
367 neurotransmitter concentrations at the synaptic cleft and hence are able to re-establish the  
368 deficient monoaminergic neurotransmission in brain regions such as for instance prefrontal  
369 cortex.

370 In this context, both *in vitro* and *in vivo* analyses have been carried out with the aim of  
371 investigating the possible modulation of the monoaminergic neurotransmission and  
372 metabolism by the multi-target compound ASS234, as a potent selective MAO-A inhibitor.

373 Incubation of ASS234 in SH-SY5Y cells for 24 hours produced a significant increase in the  
374 levels of 5-HT associated with a significant reduction in the levels of its metabolite 5-HIAA  
375 as a result of a prolonged irreversible inhibition of MAO-A. For comparative purposes,  
376 clorgyline, a selective MAO-A inhibitor, was assessed under the same experimental  
377 conditions and similar, though less pronounced effects were revealed, possibly due to the  
378 potential inhibition of the residual MAO-B activity by ASS234.

379 The results concerning the catecholaminergic metabolism in PC12 cells are less apparent. The  
380 content of DA decreased significantly after 24 hours of incubation with ASS234 compared to  
381 the control group. This unpredicted effect might be elucidated by the modulation of the  
382 enzymes tyrosine hydroxylase (TH) and aromatic L-amino acid decarboxylase (AAAD), both  
383 required for the synthesis of DA. Previous studies described that elevated levels of DA are  
384 responsible for a reduction of both activity and expression of these two enzymes following an  
385 acute administration of selective MAO-A inhibitors in mouse striatum (Cho et al., 1996). The  
386 reduced levels of DA found after longer incubations may apparently be the cause of a  
387 prolonged depletion of its own synthesis triggered by a reduced activity of either TH or  
388 AAAD.

389 Besides, it is obvious that the DA metabolites DOPAC and HVA decreased versus control  
390 after both incubation times. Considering the ratio  $DA/(HVA+DOPAC)$ , DA is relatively  
391 increased versus its metabolites via MAO-A oxidation. These findings correlate again with  
392 those obtained with clorgyline, suggesting beneficial characteristics of ASS234 concerning  
393 MAO-A inhibition.

394 Since it is shown that the MTDL ASS234 specifically inhibits MAO-A activity *in vitro*, the  
395 significant effects on the monoaminergic levels *in vivo* are most likely attributable to MAO-A  
396 inhibition. The obtained results reveal for the first time that compound ASS234 is able to alter  
397 the extracellular levels of monoamines *in vivo* in both hippocampus and prefrontal cortex, the  
398 two main cerebral regions affected in AD. Indeed, this technique is the pre-eminent tool to

399 monitor extracellular neurotransmitter levels after administration of a test compound in freely  
400 moving rats. Despite three doses of ASS234 tested, not all microdialysis results are univocal.  
401 In hippocampus, significant increases in the levels of 5-HT and NA were observed; while in  
402 prefrontal cortex, levels of DA and NA markedly increased. Differences at this stage might be  
403 attributed to the different neuronal presence of various metabolising enzymes in both brain  
404 areas as well as to the complex *in vivo* neurochemical interactions between monoamines in  
405 different cerebral regions. The possibility that ASS234 interacts with other neurobiological  
406 targets (such as acetylcholine, histamine) cannot be dismissed at this stage. What is shown, is  
407 the final effect on monoaminergic neurotransmitters *in vivo* which is probably not solely due  
408 to MAO-A inhibition.

409 Overall, the observed *in vivo* monoaminergic effects reinforce the findings of Stasiak et al.  
410 who reported post-mortem cerebral increases for 5-HT, DA and NA after administration of  
411 ASS234 on five consecutive days in a rat model of vascular dementia, induced by permanent  
412 bilateral occlusion of the common carotid arteries (Stasiak et al., 2014). Nevertheless, the  
413 present work is distinguished from the former work since time-dependent effects on  
414 extracellular neurotransmitter levels are revealed after administration of a single dose of  
415 ASS234. It is noticeable that the significant elevated extracellular monoamine levels are only  
416 apparent more than one hour following ASS234 administration, which can be explained by  
417 multiple causes. Firstly, the lag time inherent to the microdialysis experiment is in the range  
418 of a few minutes. Secondly, the subcutaneous administration route and pharmacokinetic  
419 aspects probably delay the availability of the tested compound at the site of action.  
420 Furthermore, enzymatic inhibition is a relatively slow process for the accumulation of  
421 neurotransmitters. Lastly, the possible existence of active metabolites of ASS234 can explain  
422 the delay of the effects *in vivo* and may be the underlying rationale for differences with the  
423 results obtained *in vitro*. Ultimately the delayed effects can be correlated to the effects  
424 observed by Stasiak et al. where the animals were sacrificed prior to analysis two hours after  
425 subcutaneous administration of the compound.

426 It has been reported that in AD patients the levels of DA and NA are decreased in cortex and  
427 hippocampus, while those of 5-HT are decreased in hippocampus (Reinikainen et al., 1988).  
428 Furthermore, characteristic clinical symptoms of AD including depressive disorders,  
429 psychosis and memory impairment are related to alterations in serotonergic,  
430 catecholaminergic and cholinergic neurotransmissions (Vermeiren et al., 2015). Although we  
431 are not able to explain all the *in vivo* effects, it is clear that the presented increased  
432 monoaminergic levels in hippocampus and prefrontal cortex of the rat are the observed net  
433 effects of ASS234. In this study, the MTDL ASS234 is described as a compound able to alter  
434 the monoaminergic neurotransmission besides multiple beneficial effects reported to date  
435 (Bolea et al., 2013; Stasiak et al., 2014), which may confirm the relevance of this molecule  
436 for future use in AD. However, it is worth mentioning that the observed differences cannot be  
437 explained by the investigation of the effects on MAO alone and further functional studies may

438 be addressed to elucidate the underlying mechanism of action of ASS234 on the  
439 monoaminergic neurotransmission.

440 **5. Conclusions**

441

442 The results herein reported confirm for the first time that the multi-target compound ASS234  
443 modulates the monoamine levels both in cell cultures and in hippocampus and prefrontal  
444 cortex of freely moving rats. In addition to the well-reported properties of ASS234 as a  
445 promising compound for the therapy of AD, the current study unveils additional benefits of  
446 this molecule to ameliorate the clinical symptoms of AD related to the serotonergic and  
447 catecholaminergic neurotransmissions dysfunction and hence to potentially improve the  
448 neurological outcome and delay of AD progression.

449

450

451 **Acknowledgements**

452

453 This work was financially supported by the Fund for Scientific Research Flanders (FWO)  
454 grant 1.5.240.15N, the Spanish Ministry of Economy and Competitiveness (MINECO, Spain)  
455 grant SAF2012-33304 and COST Action CM-1103. Gerard Esteban and Jolien Van Schoors  
456 are grateful for the grants received from this COST Action. Jolien Van Schoors is a doctoral  
457 research fellow funded by a Ph.D. grant of the Agency for Innovation by Science and  
458 Technology in Flanders (IWT). Gino De Smet is acknowledged for his technical assistance in  
459 the *in vivo* experiments and Susana Benítez for the monoamine determination in the *in vitro*  
460 experiments. Antec is kindly thanked for providing the SenCell and the DECADE Elite.

461

462

463 **Conflicts of Interest**

464

465 The authors declare no conflicts of interest.

466

467

468 **References**

- 469 Ballard, C., Day, S., Sharp, S., Wing, G., Sorensen, S., 2008. Neuropsychiatric symptoms in  
470 dementia: importance and treatment considerations. *International review of psychiatry* 20,  
471 396-404.
- 472 Ballatore, C., Lee, V.M., Trojanowski, J.Q., 2007. Tau-mediated neurodegeneration in  
473 Alzheimer's disease and related disorders. *Nature reviews. Neuroscience* 8, 663-672.
- 474 Birkmayer, W., Riederer, P., 1975. Biochemical post-mortem findings in depressed patients. *J*  
475 *Neural Transm* 37, 95-109.
- 476 Bolea, I., Gella, A., Monjas, L., Perez, C., Rodriguez-Franco, M.I., Marco-Contelles, J.,  
477 Samadi, A., Unzeta, M., 2013. Multipotent, permeable drug ASS234 inhibits Abeta  
478 aggregation, possesses antioxidant properties and protects from Abeta-induced apoptosis in  
479 vitro. *Current Alzheimer research* 10, 797-808.
- 480 Bolea, I., Juarez-Jimenez, J., de Los Rios, C., Chioua, M., Pouplana, R., Luque, F.J., Unzeta,  
481 M., Marco-Contelles, J., Samadi, A., 2011. Synthesis, biological evaluation, and molecular  
482 modeling of donepezil and N-[(5-(benzyloxy)-1-methyl-1H-indol-2-yl)methyl]-N-  
483 methylprop-2-yn-1-amine hybrids as new multipotent cholinesterase/monoamine oxidase  
484 inhibitors for the treatment of Alzheimer's disease. *Journal of medicinal chemistry* 54, 8251-  
485 8270.
- 486 Bradford, M.M., 1976. A rapid and sensitive method for the quantitation of microgram  
487 quantities of protein utilizing the principle of protein-dye binding. *Analytical biochemistry*  
488 72, 248-254.
- 489 Buccafusco, J.J., Terry, A.V., Jr., 2000. Multiple central nervous system targets for eliciting  
490 beneficial effects on memory and cognition. *The Journal of pharmacology and experimental*  
491 *therapeutics* 295, 438-446.
- 492 Cho, S., Duchemin, A.M., Neff, N.H., Hadjiconstantinou, M., 1996. Modulation of tyrosine  
493 hydroxylase and aromatic L-amino acid decarboxylase after inhibiting monoamine oxidase-A.  
494 *European journal of pharmacology* 314, 51-59.
- 495 Davies, P., Maloney, A.J., 1976. Selective loss of central cholinergic neurons in Alzheimer's  
496 disease. *Lancet* 2, 1403.
- 497 del Pino, J., Ramos, E., Aguilera, O.M., Marco-Contelles, J., Romero, A., 2014. Wnt  
498 signaling pathway, a potential target for Alzheimer's disease treatment, is activated by a novel  
499 multitarget compound ASS234. *CNS neuroscience & therapeutics* 20, 568-570.
- 500 Esteban, G., Allan, J., Samadi, A., Mattevi, A., Unzeta, M., Marco-Contelles, J., Binda, C.,  
501 Ramsay, R.R., 2014. Kinetic and structural analysis of the irreversible inhibition of human  
502 monoamine oxidases by ASS234, a multi-target compound designed for use in Alzheimer's  
503 disease. *Biochimica et biophysica acta* 1844, 1104-1110.
- 504 Fowler, C.J., Tipton, K.F., 1981. Concentration dependence of the oxidation of tyramine by  
505 the two forms of rat liver mitochondrial monoamine oxidase. *Biochemical pharmacology* 30,  
506 3329-3332.

- 507 Geula, C., Mesulam, M.M., 1999. Cholinergic Systems in Alzheimer's Disease, in: Terry  
508 R..D, K.R., Bick K.L., Sisodia S.S. (Ed.), Alzheimer Disease, 2 ed. Williams & Wilkins,  
509 Lippincott, Philadelphia, pp. 269-292.
- 510 Jost, B.C., Grossberg, G.T., 1996. The evolution of psychiatric symptoms in Alzheimer's  
511 disease: a natural history study. *Journal of the American Geriatrics Society* 44, 1078-1081.
- 512 Kumar, A., Singh, A., Ekavali, 2015. A review on Alzheimer's disease pathophysiology and  
513 its management: an update. *Pharmacological reports* : PR 67, 195-203.
- 514 Maruyama, W., Naoi, M., Kasamatsu, T., Hashizume, Y., Takahashi, T., Kohda, K., Dostert,  
515 P., 1997. An endogenous dopaminergic neurotoxin, N-methyl-(R)-salsolinol, induces DNA  
516 damage in human dopaminergic neuroblastoma SH-SY5Y cells. *Journal of neurochemistry*  
517 69, 322-329.
- 518 Palop, J.J., Mucke, L., 2010. Amyloid-beta-induced neuronal dysfunction in Alzheimer's  
519 disease: from synapses toward neural networks. *Nature neuroscience* 13, 812-818.
- 520 Paxinos, G., Watson, C., 1986. The rat brain in stereotaxic coordinates, second edition ed.  
521 Academic Press, San Diego, California, USA.
- 522 Perl, D.P., 2010. Neuropathology of Alzheimer's disease. *The Mount Sinai journal of*  
523 *medicine, New York* 77, 32-42.
- 524 Reinikainen, K.J., Paljarvi, L., Halonen, T., Malminen, O., Kosma, V.M., Laakso, M.,  
525 Riekkinen, P.J., 1988. Dopaminergic system and monoamine oxidase-B activity in  
526 Alzheimer's disease. *Neurobiology of aging* 9, 245-252.
- 527 Rossor, M., Iversen, L.L., 1986. Non-cholinergic neurotransmitter abnormalities in  
528 Alzheimer's disease. *British medical bulletin* 42, 70-74.
- 529 Stasiak, A., Mussur, M., Unzeta, M., Samadi, A., Marco-Contelles, J.L., Fogel, W.A., 2014.  
530 Effects of novel monoamine oxidases and cholinesterases targeting compounds on brain  
531 neurotransmitters and behavior in rat model of vascular dementia. *Current pharmaceutical*  
532 *design* 20, 161-171.
- 533 van Praag, H.M., Korf, J., 1975. Central monoamine deficiency in depressions: causative of  
534 secondary phenomenon? *Pharmakopsychiatrie, Neuro-Psychopharmakologie* 8, 322-326.
- 535 Van Schoors, J., Lens, C., Maes, K., Michotte, Y., Smolders, I., Van Eeckhaut, A., 2015.  
536 Reassessment of the antioxidative mixture for the challenging electrochemical determination  
537 of dopamine, noradrenaline and serotonin in microdialysis samples. *Journal of*  
538 *chromatography. B, Analytical technologies in the biomedical and life sciences* 998-999, 63-  
539 71.
- 540 Vermeiren, Y., Van Dam, D., Aerts, T., Engelborghs, S., Martin, J.J., De Deyn, P.P., 2015.  
541 The monoaminergic footprint of depression and psychosis in dementia with Lewy bodies  
542 compared to Alzheimer's disease. *Alzheimer's research & therapy* 7, 7.
- 543 Wimo, A., Jonsson, L., Gustavsson, A., McDaid, D., Ersek, K., Georges, J., Gulacsi, L.,  
544 Karpati, K., Kenigsberg, P., Valtonen, H., 2011. The economic impact of dementia in Europe  
545 in 2008-cost estimates from the Eurocode project. *International journal of geriatric psychiatry*  
546 26, 825-832.

547 Youdim, M.B., Buccafusco, J.J., 2005. CNS Targets for multi-functional drugs in the  
548 treatment of Alzheimer's and Parkinson's diseases. *J Neural Transm* 112, 519-537.

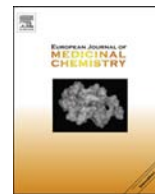
549



### **Chapter III.**

**“Multipotent cholinesterase/monoamine oxidase inhibitors for the treatment of Alzheimer's disease: design, synthesis, biochemical evaluation, ADMET, molecular modeling, and QSAR analysis of novel donepezil-pyridyl and donepezil-indolyl hybrids”**





## Original article

# Design, synthesis, pharmacological evaluation, QSAR analysis, molecular modeling and ADMET of novel donepezil–indolyl hybrids as multipotent cholinesterase/monoamine oxidase inhibitors for the potential treatment of Alzheimer's disease



Oscar M. Bautista-Aguilera<sup>a,1</sup>, Gerard Esteban<sup>b,1</sup>, Irene Bolea<sup>b</sup>, Katarina Nikolic<sup>c</sup>, Danica Agbaba<sup>c</sup>, Ignacio Moraleda<sup>d</sup>, Isabel Iriepa<sup>d</sup>, Abdelouahid Samadi<sup>a</sup>, Elena Soriano<sup>e</sup>, Mercedes Unzeta<sup>b</sup>, José Marco-Contelles<sup>a,\*</sup>

<sup>a</sup>Laboratorio de Química Médica (IQOG, CSIC), C/Juan de la Cierva 3, 28006 Madrid, Spain

<sup>b</sup>Departament de Bioquímica i Biologia Molecular, Facultat de Medicina, Universitat Autònoma de Barcelona, 08193 Bellaterra, Barcelona, Spain

<sup>c</sup>Institute of Pharmaceutical Chemistry, Faculty of Pharmacy, University of Belgrade, Vojvode Stepe 450, 11000 Belgrade, Serbia

<sup>d</sup>Departamento de Química Orgánica, Facultad de Farmacia, Universidad de Alcalá, Ctra. Barcelona, Km. 33.5, 28817 Alcalá de Henares, Spain

<sup>e</sup>SEPCO, (IQOG, CSIC), C/Juan de la Cierva 3, 28006 Madrid, Spain

## ARTICLE INFO

## Article history:

Received 22 October 2013

Received in revised form

11 December 2013

Accepted 22 December 2013

Available online 27 January 2014

## Keywords:

Donepezil

Donepezil–indolyl hybrids

EeAChE

eqBuChE

hMAO A

hMAO B

Inhibitors

3D-QSAR

Molecular modeling

ADMET

## ABSTRACT

The design, synthesis, and pharmacological evaluation of donepezil–indolyl based amines **7–10**, amides **12–16**, and carboxylic acid derivatives **5** and **11**, as multipotent **ASS234** analogs, able to inhibit simultaneously cholinesterase (ChE) and monoamine oxidase (MAO) enzymes for the potential treatment of Alzheimer's disease (AD), is reported. Theoretical studies using 3D-Quantitative Structure–Activity Relationship (3D-QSAR) was used to define 3D-pharmacophores for inhibition of MAO A/B, AChE, and BuChE enzymes. We found that, in general, and for the same substituent, amines are more potent ChE inhibitors (see compounds **12**, **13** versus **7** and **8**) or equipotent (see compounds **14**, **15** versus **9** and **10**) than the corresponding amides, showing a clear EeAChE inhibition selectivity. For the MAO inhibition, amides were not active, and among the amines, compound **14** was totally MAO A selective, while amines **15** and **16** were quite MAO A selective. Carboxylic acid derivatives **5** and **11** showed a multipotent moderate selective profile as EeACE and MAO A inhibitors. Propargylamine **15** [*N*-((5-(3-(1-benzylpiperidin-4-yl)propoxy)-1-methyl-1*H*-indol-2-yl)methyl)prop-2-yn-1-amine)] resulted in the most potent hMAO A ( $IC_{50} = 5.5 \pm 1.4$  nM) and moderately potent hMAO B ( $IC_{50} = 150 \pm 31$  nM), EeAChE ( $IC_{50} = 190 \pm 10$  nM), and eqBuChE ( $IC_{50} = 830 \pm 160$  nM) inhibitor. However, the analogous *N*-allyl and the *N*-morpholine derivatives **16** and **14** deserve also attention as they show an attractive multipotent profile. To sum up, donepezil–indolyl hybrid **15** is a promising drug for further development for the potential prevention and treatment of AD.

© 2014 Elsevier Masson SAS. All rights reserved.

## 1. Introduction

Alzheimer's disease (AD) is a neurodegenerative disorder characterized by dementia and other cognitive impairments [1]. From the biochemical point of view, amyloid- $\beta$  (A $\beta$ ) and hyperphosphorylated  $\tau$ -protein aggregates [2], oxidative stress [3] and low levels of acetylcholine (ACh) [4] play, among other, key roles in the progress and development of AD.

Acetylcholinesterase inhibitors, such as donepezil, galanthamine, and rivastigmine, increase the ACh concentration in the synaptic cleft, but with limited success and efficiency in the current clinical therapy for AD [5–7].

Similarly, some symptoms of AD are due to alterations in the dopaminergic, serotonergic and monoaminergic neurotransmitter systems [8–10]. In particular, monoamine oxidases (MAO) A and B are the enzymes that catalyze the oxidative deamination of biogenic amines [11], rendering the corresponding aldehyde, ammonia and hydrogen peroxide as metabolic products. Thus, MAO inhibitors (MAOI) might increase amine neurotransmission and reduce reactive oxygen species affording potential valuable effect

\* Corresponding author.

E-mail address: [iqoc21@iqog.csic.es](mailto:iqoc21@iqog.csic.es) (J. Marco-Contelles).

<sup>1</sup> These authors have equally contributed to this work.

for the treatment of AD [11,12] by decreasing the neuronal damage [13,14]. Recent studies have shown that the propargylamine group present on MAOIs, such as rasagiline and ladostigil, is the responsible for the neuroprotective, anti-apoptotic [15–17], and A $\beta$  aggregation inhibition power of these compounds [18].

Unfortunately, and despite the recent advances reported, no efficient therapy has been implemented for the treatment of AD patients. This is possibly due to the multifactorial and complex nature of AD, which makes inadequate the use of magic bullets targeted to a single receptor or enzymatic system for the efficient treatment of the disease [7,15].

However, it is now widely accepted that a more effective therapy would result from the use of multipotent compounds able to intervene in the different pathological events underlying the etiology of AD [19,20].

In the last years our laboratory has been particularly active in this area, and very recently we have described a number of multipotent MAO/ChE inhibitors [21,22]. These drugs, exemplified by compound **ASS234** {*N*-[5-(3-(1-benzylpiperidin-4-yl)propoxy)-1-methyl-1*H*-indol-2-yl]methyl}-*N*-methylprop-2-yn-1-amine} [22] (Chart 1), are hybrids of donepezil, an AChE inhibitor, and **PF9601N** [*N*-((5-(benzyloxy)-1*H*-indol-2-yl)methyl)prop-2-yn-1-amine] (Chart 1) [23], a potent and selective MAO B inhibitor [23]. **PF9601N** is also an effective neuroprotective agent in several *in vivo* models of Parkinson's disease, attenuates the MPTP-induced striatal dopamine depletion in young-adult and old-adult C57/BL mice, reduces the loss of tyrosine hydroxylase (TH)-positive neurons after nigrostriatal injection of 6-hydroxydopamine in rats [24], and enhances the duration of L-3,4-dihydroxyphenylalanine (L-DOPA)-induced contralateral turning in 6-hydroxydopaminelesioned rats [25].

Compound **ASS234** inhibits both MAO A/B, AChE and BuChE enzymes. In addition, recent studies have shown that hybrid **ASS234** retains the anti-apoptotic and antioxidant properties observed by the parent compound **PF9601N**, and possesses a favorable blood–brain barrier permeability [26]. These findings suggest that **ASS234** is a new promising multitarget drug candidate for the potential treatment of AD.

Now, in this context, we have designed, synthesized and submitted to pharmacological evaluation the new multipotent ChE + MAO inhibitors of type **I** and **II** (Chart 1). The structure of inhibitors of type **I**, such as **5–10** (Chart 2), is based on **donepezil** (**1**) and **ASS234** (**2**), by fixing the *N*-benzylpiperidine motif linked by a three methylene carbon chain to the oxygen at C5 in the indole nucleus, while the methylene group at C2 becomes a carbonyl group, resulting in ester **5**, carboxylic acid **6**, amides **7–10**, or a

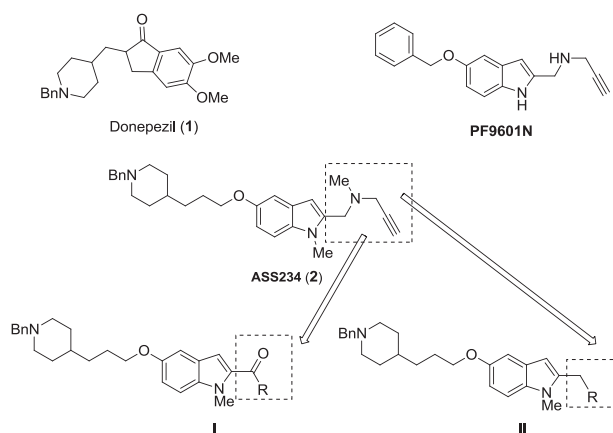


**Chart 1.** General structure of donepezil, **ASS234**, **PF9601N**, and the novel MAOI/ChE hybrids **I** and **II**, described in this work.

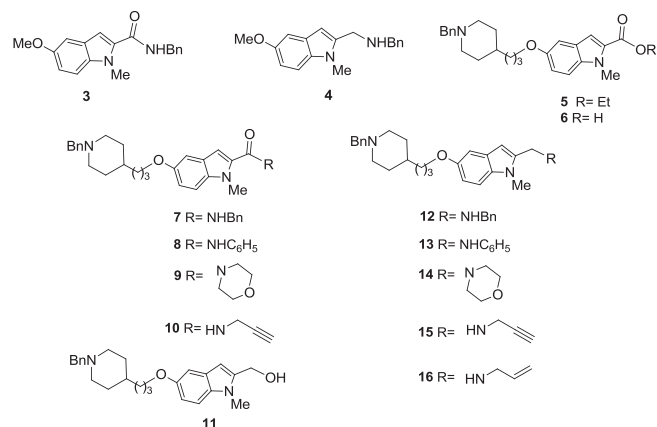


**Chart 2.** New multipotent ChE + MAO inhibitors **3–16** described in this work.

primary alcohol in **11**. Precedents that support this selection are known in the recent literature [27]. Similarly, **ASS234** analogs of type **II** have been considered, resulting in the secondary amines **12–16** (Chart 2) when substituting the *N*(Me)propargylamine motif by *N*(H)benzyl, *N*(H)phenyl, morpholino, *N*(H)propargyl and *N*(H)allyl derivatives, respectively. Note that the use of the *morpholino* motif is not casual, as it is found in moclobemide, a well-known selective MAO A reversible, non-covalent inhibitor [28]. Finally, simple *O*-methyl ethers **3** and **4** (Chart 2) have been prepared in order to evaluate the pharmacological effect of the donepezil-like motif present in related compounds **7** and **12** (Chart 2).

In this work we have also applied and described the 3D-QSAR approach in order to design potent inhibitors of ChEs and MAO, with optimal selectivity profile. The main aim of the 3D-QSAR study was to define specific molecular determinants for MAO A/B, AChE, and BuChE inhibition and to create QSAR models for evaluation of MAO A/B, AChE, and BuChE activity of the designed multipotent inhibitors.

## 2. Results and discussion

### 2.1. Chemistry

The synthesis of the target molecules **3–16** has been carried out as shown in Schemes 1–3 (see Experimental part).

The synthesis of *N*-benzyl-5-methoxy-1-methyl-1*H*-indole-2-carboxamide (**3**) is shown in Scheme 1. Thus, the reaction of ethyl 5-methoxy-1-methyl-1*H*-indole-2-carboxylate (**17**) [29] with sodium hydroxide in ethanol, at reflux, gave the corresponding carboxylic acid **18** [30], whose reaction with benzylamine, in the presence of DDC/HOBT, to afford amide **3**, followed by reduction with lithium aluminum hydride (LiAlH<sub>4</sub>), provided amine **4** in 79% yield.

Reaction of 1-benzyl-4-(3-chloropropyl)piperidine (**19**) [22] and ethyl 5-hydroxy-1-methyl-1*H*-indole-2-carboxylate (**20**) [31], in the presence of potassium carbonate, in DMF, gave product 5-(3-(1-benzylpiperidin-4-yl)propoxy)-1-methyl-1*H*-indole-2-carboxylate (**5**) in 63% yield, which after hydrolysis with lithium hydroxide, yielded 5-(3-(1-benzylpiperidin-4-yl)propoxy)-1-methyl-1*H*-indole-2-carboxylic acid (**6**), whose reaction with phosphorus pentachloride provided acid chloride (**21**) (Scheme 2). This intermediate, without further purification or isolation, was reacted with the selected amines, such as benzylamine, aniline, morpholine and propargylamine, under the usual conditions, to give amides **7–10** in good yields (Scheme 2).

Next, {5-[3-(1-benzylpiperidin-4-yl) propoxy]-1-methyl-1*H*-indol-2-yl} methanol (**11**) was obtained by reduction of the ester **5** with LiAlH<sub>4</sub> in dry THF (Scheme 3).

All the amines **12–16** were prepared from the corresponding amides **7–10** by reaction with  $\text{LiAlH}_4$  (Scheme 2).

Interestingly, in the case of the reduction of 5-(3-(1-benzylpiperidin-4-yl)propoxy)-1-methyl-*N*-(prop-2-yn-1-yl)-1*H*-indole-2-carboxamide (**10**), besides the expected amine **15** (51%), the *N*-allylamine **16** (29%) was also isolated. The structure of this product was easily deduced by inspection of its analytic and spectroscopic data. In particular, the presence of signals at  $\delta$  5.91 (m, 1H,  $\text{NCH}_2\text{CH}=\text{CH}_2$ ), 5.21 (dd,  $J = 17.1$  and  $1.5$  Hz, 1H,  $\text{NCH}_2\text{CH}=\text{CH}_2$ ), 5.12 (dd,  $J = 10.3$  and  $1.5$  Hz, 1H,  $\text{NCH}_2\text{CH}=\text{CH}_2$ ), and at  $\delta$  136.6 (NHCH= $\text{CH}_2$ ) and 116.2 (NHCH= $\text{CH}_2$ ), in the  $^1\text{H}$  and  $^{13}\text{C}$  NMR spectra, respectively, corresponded to a double bond in an *N*-allylamine, obtained as the result of further reduction of the acetylenic bond in the corresponding propargylamine.

All new compounds showed analytical and spectroscopic data were in good agreement with their structure, and data reported in the literature for similar compounds (see Experimental part).

## 2.2. Pharmacological evaluation

The *in vitro* activity of these new indoles **3–16** against *EeAChE* and eqBuChE was determined using Ellman's method [32].

In order to test their multipotent profile, compounds **3–16** have also been evaluated as human MAO A/B inhibitors following a fluorometric method [33], giving the  $\text{IC}_{50}$  values shown in Table 1, with donepezil (**1**) and ASS234 (**2**) as reference compounds.

Regarding the ChEs inhibition, the active indole derivatives here analyzed are from moderate to potent, in the low micromolar range, *EeAChE* inhibitors. For the selectivity, *EeAChE* is in general more strongly inhibited than eqBuChE. Compounds **5**, **6**, **9–11** are *EeAChE* selective, while indoles **12–16** show a remarkable eqBuChE inhibition power. Note also that amides **3**, **7** and **8** do not inhibit the ChEs. The most potent and selective AChE inhibitor was amine **13** ( $\text{IC}_{50} = 0.084 \pm 0.016$   $\mu\text{M}$ ), bearing a *N*-phenyl residue in the aminomethyl chain at C2. Compared to donepezil (**1**), indole **13** results 6.6-fold less active for the AChE inhibition and almost equipotent for BuChE. We found that, in general, and for the same substituent, amines are more potent (see compounds **12**, **13** versus **7** and **8**) or equipotent (see compounds **14**, **15** versus **9** and **10**) than the corresponding amides. While this is not surprising taking into account that amide **3** is not a donepezil-like derivative, the results observed for amides **7** and **8** allowed us to conclude that the presence of a *N*-benzyl or *N*-phenyl substituent at the aminomethyl chain at C2 is detrimental for the ChE activity.

Comparing compounds **3** and **4**, the effect of the amide ("CONHR") versus the corresponding amine ("CH<sub>2</sub>NHR") is clear and positive, rendering now amine **4** a moderately active and selective AChEI. Note also that the moclobemide-like compound **14** is a potent and moderately selective AChE inhibitor, while the moclobemide-like amide **9** is totally AChE selective. Compared with ASS234 (**2**), the *N*-propargylated analogs **10** and **15** are 2.6 and 1.8-fold, respectively, more potent for the inhibition of AChE. However, and regarding the BuChE inhibition, amide **10** is inactive, but compound **15** is 1.8-fold less active than ASS234 (**2**). The observed values for *N*-propargylamine **15** and *N*-allylamine **16** deserve also some comment, as compound **16** shows a similar *EeAChE* inhibition power, but a slightly better eqBuChE inhibitory profile, in the same

range that ASS234 (**2**). Finally, it was very interesting to find that the alcohol **11**, ester **5** and carboxylic acid **6** are selective and potent AChEI, in the 0.24–0.40  $\mu\text{M}$  range.

Regarding the MAO inhibition (see Table 1), unfortunately, most of the indoles proved inactive. This is the case of amides **3**, **4**, **7–10**, or amines **12** and **13**, while only amines bearing the morpholino (**14**), the *N*-propargylamino (**15**) or the *N*-allylamino (**16**) groups were potent and selective MAO A inhibitors. Note also that again the alcohol **11** and the ester **5**, but not the acid **6**, were quite potent and selective MAO A inhibitors. Particularly, and not surprisingly, indole **15** is a potent MAO A inhibitor [ $\text{IC}_{50} = 5.5 \pm 1.4$  nM], in the same range that ASS234 (**2**), but 3.5-fold less potent than ASS234 (**2**) for the inhibition of hMAO B.

To sum up, and looking for new multipotent ChE/MAO inhibitors for AD, and concerning our effort to improve the pharmacological results with ASS234 (**2**) [22], we can conclude that donepezil-like indole derivative **15**, bearing the *N*(1)Me/*N*(H)propargylamine structural motif, is a very potent and selective *EeAChE* and hMAO A inhibitor showing also a non-negligible eqBuChE and hMAO B activities, comparing very favorably with hybrid ASS234 (**2**) regarding the *EeAChE* and MAO A inhibition, but showing a poorer eqBuChE and MAO B inhibition profile than ASS234 (**2**).

## 2.3. QSAR Analysis of novel donepezil–indolyl hybrids

In Supplementary material, a 3D-QSAR study has been carried out on these new indoles to explain and predict the binding on the active sites of the enzymes based on the pharmacological activities observed on these derivatives.

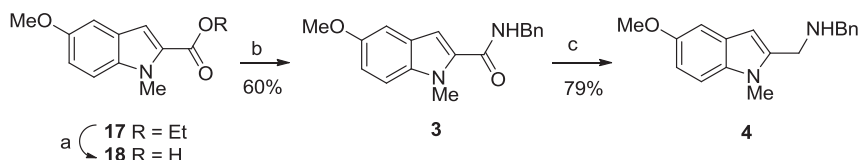
The created 3D-pharmacophore models are further applied in order to design novel multipotent inhibitors and for the selection of new promising ligands (Chart 2). The designed donepezil–indolyl hybrids have been synthesized and examined for MAO/ChE inhibiting activity (Tables 2 and 3). As shown, the agreement between predicted and measured MAO/ChE inhibiting activity for the novel ligands confirmed the predicting capacity of the formed 3D-QSAR models. Therefore the 3D-QSAR models could be further used for designing and the evaluation of novel donepezil–indolyl hybrids.

## 2.4. Molecular modeling

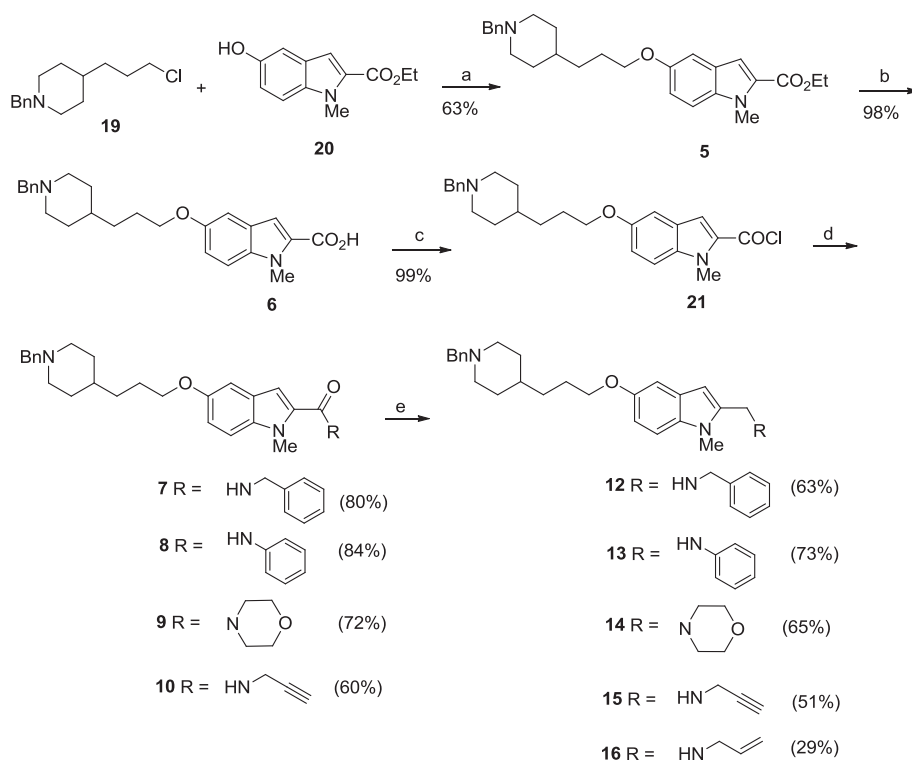
### 2.4.1. Molecular modeling of compound 15. Inhibition of AChE and BuChE

To shed light onto the putative orientation of the cholinesterase inhibitor **15** in both cholinesterases, molecular modeling studies were carried out using the Autodock Vina software [34]. A structure of *EeAChE* (PDB: 1C2B) was used for the *in silico* studies and exploited in the *in vitro* biochemical assays presented above. The binding site for docking was designed such that the entire receptor molecule was included within the selection grid. Eight side chains, Trp286, Tyr124, Tyr337, Tyr72, Asp74, Thr75, Trp86 and Tyr341 are allowed to change their conformations at the same time as the ligand that is being docked.

The binding mode for **15** (−11.9 kcal/mol) confirmed that the indole fragment was bound to near the bottom of the gorge (Fig. 1). The propargylamine scaffold of inhibitor **15** exerted strong parallel  $\pi$ – $\pi$  stacking to Trp86. In the middle of the gorge, the aliphatic



Scheme 1. Reagents and conditions: (a) NaOH 10 N, EtOH, reflux (93%); (b) HOBt, DIPEA, DCC, benzylamine, DMF; (c)  $\text{LiAlH}_4$ , THF.



**Scheme 2.** Reagents and conditions: (a)  $K_2CO_3$ , dry DMF, reflux; (b) LiOH, EtOH, reflux; (c)  $PCl_5$ ,  $CH_2Cl_2$ ; (d)  $RNH_2$  (or morpholine) TEA,  $CH_2Cl_2$ ; (e)  $LiAlH_4$ , dry THF.

alkyl chain of compound **15** was surrounded with the phenyl rings of Tyr124, Tyr341 and Phe338 providing **15**–*EeAChE* complex, stabilization and constriction. At the rim of the gorge within peripheral anionic site, the phenyl ring is stacked between Trp286 and Tyr72 (Fig. 1).

The docking study of **15** within the active site of eqBuChE was also carried out. In the absence of X-ray structure of eqBuChE, a homology model was used. SWISS-MODEL [35–37], a fully automated protein structure homology-modeling server was used to design the receptor. A putative three-dimensional structure of eqBuChE has been created based on the crystal structure of hBuChE (pdb: 2PM8) as these two enzymes exhibited 89% sequence identity. In order to simulate the binding of compound **15** to eqBuChE, docking experiments were performed as blind dockings following the same computational protocol used for *EeAChE*. As depicted in Fig. 2, compound **15** was well accommodated inside the gorge active site. The orientation of **15** in the eqBuChE active site was different from what observed in *EeAChE*, showing a binding mode where the ligand adopted an U-shaped conformation. The indole ring faced to Ser198 and Hys438 and the nitrogen atom of the propargylamine moiety is bridged to His438 via hydrogen bonding. Besides,  $\pi$ – $\pi$  interaction can be observed within propargylamine moiety and Trp82. The phenyl group is in T-shaped orientation with respect to Trp231.

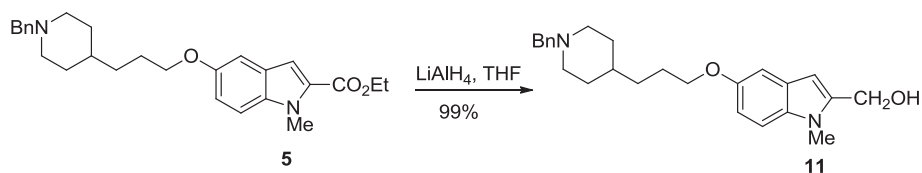
Analysis of the intermolecular interactions indicated key residues responsible for ligand binding. The propargylamine group is likely to be an important feature for these derivatives to exhibit both AChE- and BuChE-inhibitory activities.

It is significant to note that the linear conformation allows compound **15** to span both the catalytic active site (CAS) and PAS, contributing to its superior binding toward AChE.

#### 2.4.2. Molecular modeling of compound **15**. Inhibition of MAO A and MAO B

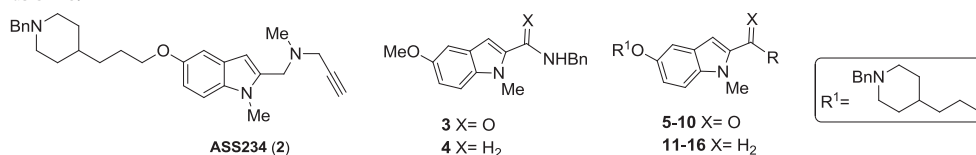
Compound **15** was docked into the active site of both MAO A and MAO B isoforms using the program Autodock Vina [34] in order to structurally understand the interactions with these biotargets together with the inhibitory profiles. Since inhibition data were determined on human MAOs, docking simulations were run on the human model of the MAO A and MAO B. The 3D structures for hMAOs were retrieved from the PDB (PDB ID: 2Z5X for hMAO A and PDB ID: 2V5Z for hMAO B).

Results from several studies have shown that it must be the neutral amine that reaches the active site of MAO A and MAO B to allow the chemistry [38–41]. The docking simulations were done with compound **15** as neutral specie despite of at physiological pH, most of the piperidine rings would be in the protonated, positively charged form.



**Scheme 3.** Synthesis of compound **11**.

**Table 1**  
Inhibition of AChE from *Electrophorus electricus* (EeAChE), equine serum butyrylcholinesterase (eqBuChE) and human monoamine oxidase (hMAO A/B) by **donepezil** (1), **ASS234** (2) and compounds **3–16**.



Compound	R	IC <sub>50</sub> (μM) <sup>a</sup>		Selectivity	IC <sub>50</sub> (μM) <sup>a</sup>		Selectivity
		EeAChE	eqBuChE	eqBuChE/EeAChE	hMAO A	hMAO B	hMAO B/hMAO A
<b>Donepezil</b> (1)		0.013 ± 0.001	0.84 ± 0.05	65	850 ± 13	15 ± 2.2	0.017
<b>ASS234</b> (2)		0.35 ± 0.01	0.46 ± 0.06	1.3	0.0042 ± 0.0005	0.039 ± 0.004	9.2
<b>3</b>		>100	>100	>1	>100	>100	>1
<b>4</b>		15.2 ± 2.1	22.9 ± 5.1	1.5	>100	>100	>1
<b>5</b>	OEt	0.27 ± 0.02	>100	>370	1.53 ± 0.21	>100	>65
<b>6</b>	OH	0.40 ± 0.04	>100	>250	>100	>100	>1
<b>7</b>		>100	>100	>1	>100	>100	>1
<b>8</b>		>100	>100	>1	>100	>100	>1
<b>9</b>		0.27 ± 0.02	>100	>370	>100	>100	>1
<b>10</b>		0.13 ± 0.02	>100	>770	>100	>100	>1
<b>11</b>	OH	0.24 ± 0.03	>100	>416	4.26 ± 0.56	>100	>23
<b>12</b>		0.14 ± 0.02	0.29 ± 0.07	2	>100	>100	>1
<b>13</b>		0.084 ± 0.016	0.85 ± 0.25	10	>100	>100	>1
<b>14</b>		0.10 ± 0.01	0.79 ± 0.077	7.9	4.40 ± 0.84	>100	>22.7
<b>15</b>		<b>0.19 ± 0.01</b>	<b>0.83 ± 0.16</b>	<b>4.4</b>	<b>0.0055 ± 0.0014</b>	<b>0.15 ± 0.031</b>	<b>27.3</b>
<b>16</b>		0.14 ± 0.01	0.46 ± 0.08	3.3	0.98 ± 0.22	15.3 ± 2.5	15.6

<sup>a</sup> Values are expressed as mean ± standard error of the mean of at least three different experiments in quadruplicate.

**Table 2**  
Experimental and QSAR activities of novel MAO A and MAO B inhibitors.

Compound	R	pIC <sub>50</sub> (hMAO A)	Pred-pIC <sub>50</sub> (MAO A)	pIC <sub>50</sub> (hMAO B)	Pred-pIC <sub>50</sub> (MAO B)
<b>Donepezil</b> (1)					
<b>4</b>		4.000	4.912	4.000	6.275
<b>12</b>		4.000	7.806	4.000	6.099
<b>13</b>		4.000	6.875	4.000	6.127
<b>15</b>		8.260	8.146	6.824	6.000
<b>16</b>		6.009	8.590	4.815	6.219

**Table 3**  
Experimental and QSAR activities of novel EeAChE and eqBuChE inhibitors.

Compound	R	pIC <sub>50</sub> (EeAChE)	Pred pIC <sub>50</sub> (EeAChE)	pIC <sub>50</sub> (eqBuChE)	Pred pIC <sub>50</sub> (eqBuChE)
<b>Donepezil</b> (1)					
<b>4</b>		4.818	6.252	4.640	4.876
<b>12</b>		6.854	7.695	6.538	6.188
<b>13</b>		7.076	6.399	6.071	6.051
<b>15</b>		6.721	7.524	6.081	6.442
<b>16</b>		6.854	8.150	6.337	6.093

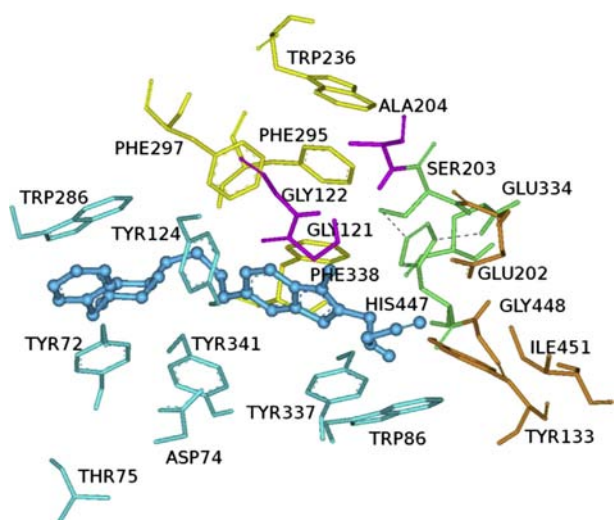


**Fig. 1.** Binding mode of inhibitor **15** at the active site of *EeAChE*. Compound **15** is illustrated in blue. Ligands are rendered as balls and sticks and the side chains conformations of the mobile residues are illustrated in the same color light as the ligand. Different subsites of the active site were colored: catalytic triad (CT) in green, oxanion hole (OH) in pink, anionic sub-site (AS) in orange, except Trp86, acyl binding pocket (ABP) in yellow, and peripheral anionic subsite (PAS) in blue. Black dashed lines are drawn among atoms involved in hydrogen bond interactions. (For interpretation of the references to color in this figure legend, the reader is referred to the web version of this article.)

As reported in our previous paper [42], a number of six structural water molecules were explicitly considered in the docking simulations. These water molecules are labeled as w72, w193, w11, w23, w15, and w53 in accordance with the numbering reported for the *hMAO B* crystallographic structure (PDB ID: 1S3E) and they are located near the FAD cofactor.

Analysis of the binding modes revealed that compound **15** could bind to *hMAO A* in two modes (Mode I and Mode II) as shown in Fig. 3. In Mode I (−9.4 kcal/mol, in red), the benzyl moiety occupies

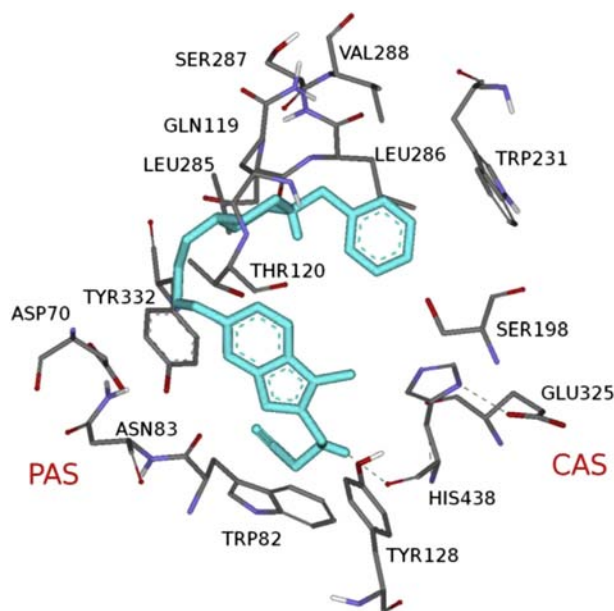


**Fig. 2.** Complex of compound **15** and eqBuChE homology built 3D-model. Compound **15** is illustrated in blue sticks. Black dashed lines are drawn among atoms involved in hydrogen bond interactions. (For interpretation of the references to color in this figure legend, the reader is referred to the web version of this article.)

the “entrance cavity”, while the indole ring is well accommodated by the catalytic cleft, leaving the propargylamine substituent facing the FAD cofactor. Glu215 contributes to the stabilization of complex, acting as a hydrogen bond acceptor with the amino group of the propargylamine moiety also involving a water molecule. Furthermore, the highly hydrophobic environment of the “entrance cavity” contributes to the stabilization of the ligand, as the *N*-benzylpiperidine moiety undergoes stable hydrophobic interactions with Val93, Leu97 and Ala111.

Slightly different binding features were revealed in analysis of the results obtained for the Mode I relative Mode II. In Mode II (−9.3 kcal/mol, in yellow), compound **15** is turned by 180° with respect to the position adopted in Mode I. The *N*-benzyl moiety binds the “entrance cavity” of the receptor with the phenyl ring directed toward Thr205, while the propargylamine motif is stably linked to the substrate cleft. On one hand, the propargyl group forms favorable  $\pi$ – $\pi$  stacking interactions with Tyr407, Tyr444 and FAD cofactor, while the amino group of the propargylamine moiety interacts with the carbonyl oxygen atom of the Gln215 via a hydrogen bond. A hydrogen bond interaction occurs between the ether oxygen of the compound **15** and the thiol group of Cys323.

It should be noticed that the propargyl group present in compound **15**, is faced to the FAD cofactor. By analogy with the propargyl containing MAO A inhibitors, such as clorgyline, able to inactivate the enzyme by covalent interactions with the N5 of FAD isoalloxazine [43], compound **15** could also establish such covalent interactions via their propargyl group, which can be considered the irreversible-enzyme inactivating moiety.

We also docked compound **15** into *hMAO B* to study the different behavior against both isoenzymes, MAO A and MAO B. Blind docking studies were done and the six structural water molecules selected for *hMAO A* were also included in the study.

Regarding MAO B binding modes, our findings revealed that unique pattern recognition is present (−8.8 kcal/mol). This inhibitor also crosses both cavities, presenting the piperidine nucleus located between the “entrance” and “catalytic” cavities, separated by the residues Ile199 and Tyr326 (Fig. 4). The substituted-indole ring is oriented toward the bottom of the substrate cavity, interacting with the FAD cofactor through  $\pi$ – $\pi$  interactions. In addition, the predicted orientation of the substituted-indole moiety allowed the interaction of the NH hydrogen of the propargylamine moiety with a water molecule, thereby preventing a hydrogen bond interaction with the enzyme. Finally, the phenyl ring is oriented to an entrance cavity, a hydrophobic sub-pocket, which is defined by Leu 88, Pro102 and Ile316.

The study confirmed the selectivity of compound **15** for MAO A. Selectivity is likely due to the orientation of the propargylamine and phenyl moieties of **15** in MAO A and in MAO B. The pose obtained in *hMAO B* for compound **15** showed a preference for the ligand to be placed in a deeper region (see Fig. 4b), resulting in an energetically less favorable complex. Compound **15** established more interactions with the MAO A active site compared to the MAO B active site which may indicate the **15** interacts more tightly with MAO A.

## 2.5. ADMET analysis

A variety of key ADMET (Absorption, Distribution, Metabolism, Excretion and Toxicity) properties has been calculated, with special emphasis on the requirements of the central nervous system (CNS). These requirements for CNS penetration by drugs are reasonably well understood and accordingly many theoretical models have been developed, although additional work still needs to be done on the effect and optimal range of molecular structure on penetration. The drugs used for neurological disorder treatment, such as AD, are

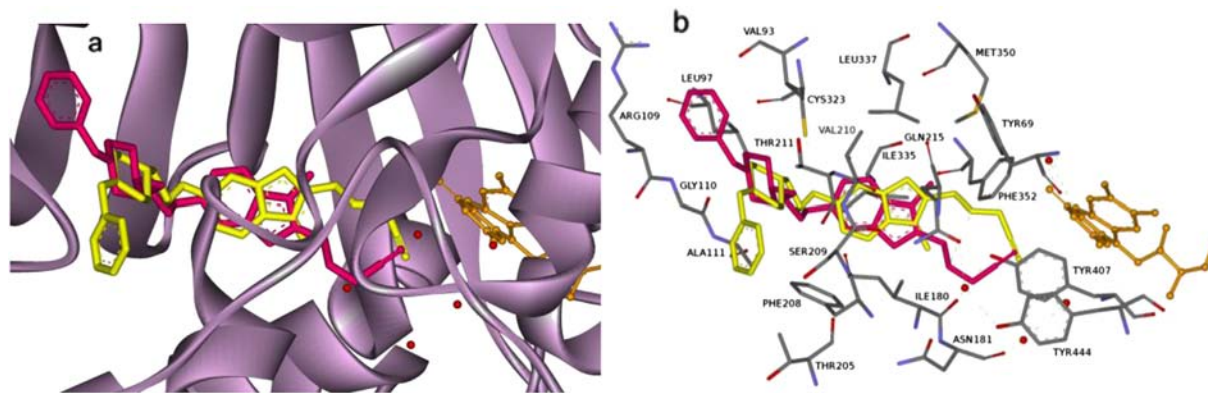


**Fig. 3.** Docking pose of inhibitor **15** into hMAO A. (a) Crystal structure of hMAO A represented in ribbon diagram. Binding modes I and II are represented as red and yellow sticks, respectively. (b) Amino acid residues of the binding site are color-coded. The flavin adenine dinucleotide cofactor (FAD) and the six water molecules are represented as an integral part of the MAO A structure model and are rendered as orange sticks and red balls, respectively. Green dashed lines are drawn among atoms involved in hydrogen bond interactions. (For interpretation of the references to color in this figure legend, the reader is referred to the web version of this article.)

generally CNS acting drugs, so factors that are important to the success of CNS drugs were analyzed. In particular, the new molecules should present a good CNS penetration profile and low toxic effects. Computer predictions were performed with ADMET Predictor 6.5 [44] and ACD/Percepta 14.0.0 [45] software packages (see Table S3, Supplementary material).

The lipophilicity (expressed as  $\log P$ ) predicted for **2**, **5**, **7**, **8**, **12** and **13** is higher than the traditionally cutoff value of 5 used in drug design ( $\log P < 5$  and/or  $m\log P < 4.1$  [46]). Therefore, these structures violate the Lipinski's rules [47]. Moreover, CNS drugs require more strict rules for a successful penetration to CNS. Thus, CNS drugs have significantly reduced molecular weights compared with other therapeutics. Van de Waterbeemd [48] has suggested that MW should be kept below 450 to facilitate brain penetration and to be lower than that for oral absorption [49]. All the structures reported herein show suitable values ( $MW < 450$ ), with the exception of the large tetracycles **7–9** and **12–14**.

As the polarity is involved as the molecule approaches the polar surface of the cell membrane and desolvates as it moves into the lipid portion, polar surface area is a key parameter to predict penetration to CNS. According to Kelder [50] and Waterbeemd [49], the drugs can be targeted to the CNS with a polar surface area less than  $60\text{--}70 \text{ \AA}^2$ , a lower range than for other kinds of therapeutics. Hence, the predicted values for **2–16** fall into the appropriate range.

The blood–brain barrier (BBB) is a separation of circulating blood and cerebrospinal fluid in the CNS. Predicting BBB

penetration means predicting whether compounds pass across the blood–brain barrier. This is crucial in drug design because CNS-active compounds must pass across it. According to the computed values [51], **3**, **4**, **6**, **7** and **10** could be CNS inactive due to low brain penetration, whereas **2**, **5**, **8**, **9** and **11–16** should be good candidates. In particular, the hybrids **2**, **5** and **13–16** show a brain penetration sufficient for CNS activity [52].

$P_{\text{eff}}$  quantifies effective permeability across the intestinal membrane, and characterizes absorption whether by passive diffusion, active transport, facilitated diffusion, paracellular diffusion, or any other mechanism [53]. MDCK models predict apparent permeability measured using the MDCK (Madin-Darby Canine Kidney) [54]. According to the predictions, all the structures show an adequate permeability to be good candidates ( $P_{\text{eff}} > 0.1$ , MDCK  $> 25$ ), and should be well absorbed compounds (%HIA) [55]. In addition, a middle Caco-2 cell permeability is suggested [56]. The percent of drug bound with plasma proteins was estimated and the compounds were predicted to bind weakly to plasma proteins, so it will be available for diffusion or transport across cell membranes and thereby finally interact with the target.

The hERG (human Ether-à-go-go Related Gene) encodes potassium channels, which are responsible for the normal repolarization of the cardiac action potential. Blockage or any other impairment of these channels in the heart cells can lead to fatal cardiac problems. Therefore, drug-induced blockage of potassium channels has been a major concern for the pharmaceutical industry. All the structures,

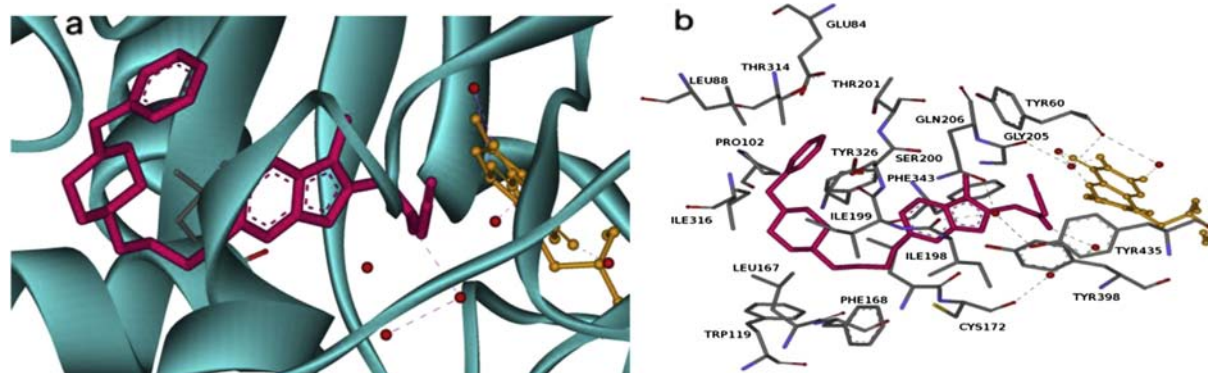


**Fig. 4.** Docking pose of inhibitor **15** into hMAO B. (a) The protein structure of hMAO B is rendered as a blue cartoon model. Compound **15** is represented as red sticks. (b) Amino acid residues of the binding site are color-coded. The flavin adenine dinucleotide cofactor (FAD) and the six water molecules are represented as an integral part of the MAO-B structure model and are rendered as orange sticks and red balls, respectively. (For interpretation of the references to color in this figure legend, the reader is referred to the web version of this article.)

except molecules **3**, **4** and **6**, show hERG liability [57]. To note that these three hybrids present the lower lipophilicity of the whole series. Many drug parameters are affected by lipophilicity. High lipophilicity frequently leads to compounds with high rapid metabolic turnover [58] and low solubility and poor absorption. As lipophilicity ( $\log P$ ) increases, there is an increased probability of binding to hydrophobic protein targets other than the desired one, and therefore, there is more potential for toxicity. So, hERG K-channel blockade is hydrophobic and bind lipophilic substrates [59]. On other hand, hybrids **3**, **4**, **7**, **8**, **12**, **13** and **16** could induce carcinogenicity in chronic mouse studies, whereas none of the molecules is predicted to present hepatotoxicity [60,61].

To sum up, despite that compounds **13**–**16** show good brain penetration profiles, it can be concluded that structure **15** presents the best drug-like characteristics and ADMET properties of the series.

### 3. Conclusions

In this paper we have reported the synthesis and pharmacological evaluation of a series of new donepezil–indolyl hybrids as multifunctional drugs for the potential treatment of AD, using the multipotent **ASS234** hybrid. We have designed amides of type **I** and amines of type **II** (Chart 1), as well as ester **5**, carboxylic acid **6** and alcohol **11** (Chart 2). We have found that, in general, and for the same substituent, the amines are more potent ChE inhibitors (see compounds **12**, **13** versus **7** and **8**) or equipotent (see compounds **14**, **15** versus **9** and **10**) than the corresponding amides, showing a clear *EeAChE* inhibition selectivity. For the MAO inhibition activity, amides were not active, and among the amines, compound **14** was totally MAO A selective, while amines **15** and **16** were quite MAO A selective. Carboxylic acid derivatives **5** and **11** showed a multipotent moderate selective profile as *EeACE* and MAO A inhibitors. As a result, we have identified *N*-((5-(3-(1-benzylpiperidin-4-yl)propoxy)-1-methyl-1*H*-indol-2-yl)methyl)prop-2-yn-1-amine (**15**), as a potent, in the nanomolar range, inhibitor of MAO A ( $IC_{50} = 5.5 \pm 1.4$  nM) and moderately potent inhibitor of MAO B ( $IC_{50} = 150 \pm 31$  nM), AChE ( $IC_{50} = 190 \pm 10$  nM), and BuChE ( $IC_{50} = 830 \pm 160$  nM).

Molecular modeling analysis suggests that inhibitor **15** is a mixed-type *EeAChE* inhibitor, and that its linear conformation allows compound **15** to span both the CAS and PAS, contributing to its superior binding toward AChE. We have also observed that the propargylamine group is likely to be an important feature for these derivatives to exhibit both AChE- and BuChE-inhibitory activities. For MAO enzymes, docking simulations have shown that the selectivity of inhibitor **15** for MAO A vs MAO B is likely due to the orientation of their propargylamine and phenyl moieties in MAO A/B. The pose obtained in hMAO B for compound **15** showed a preference for the ligand to be placed in a deeper region, resulting in an energetically less favorable complex. Compound **15** established more interactions with the MAO A active site compared to the MAO B active site which may indicate the **15** interacts more tightly with MAO A.

To sum up, and based on the best observed drug-like characteristics and ADMET properties of the series, compound **15** is a new and interesting molecule that deserves further analysis as a potential drug for the prevention and treatment of AD.

## 4. Experimental part

### 4.1. Chemistry

#### 4.1.1. General methods

Melting points were determined in a Koffler apparatus, and are uncorrected.  $^1H$  and  $^{13}C$  NMR spectra were recorded at room temperature in  $CDCl_3$  or  $DMSO-d_6$  at 300, 400 or 500 MHz and at

75.4, 100.6 or 125.6 MHz, respectively, using solvent peaks [ $CDCl_3$ : 7.27 (D), 77.2 (C) ppm and  $DMSO-d_6$  2.50 (D) and 39.7 (C) ppm] as internal references. The assignment of chemical shifts was based on standard NMR experiments ( $^1H$ ,  $^{13}C$ ,  $^1H-^1H$  COSY,  $^1H-^{13}C$  HSQC, HMBIC, DEPT). NMR values (\*) can be interchanged. Mass spectra were recorded on a GC/MS spectrometer with an API-ES ionization source. Elemental analyses were performed at the IQOG (CSIC, Spain). TLC analyses were performed on silica F254 and detection by UV light at 254 nm, or by spraying with phosphomolybdic- $H_2SO_4$  dyeing reagent. Column chromatographies were performed on silica Gel 60 (230 mesh). "Chromatotron" separations were performed on a Harrison Research Model 7924. The circular disks were coated with Kieselgel 60 PF254 (E. Merck).

#### 4.1.2. General procedure for the preparation of hydrochlorides

The hydrochlorides were prepared by dissolving the compounds in a minimum quantity of ethyl ether, and adding dropwise a saturated solution of HCl(g) in ethyl ether. A white solid was formed immediately, that was separated by filtration, washed with ether and dried.

#### 4.1.3. *N*-Benzyl-5-methoxy-1-methyl-1*H*-indole-2-carboxamide (**3**)

To a solution of known 5-methoxy-1-methyl-1*H*-indole-2-carboxylic acid (**18**), obtained for ester **17** [39] as described [30] (85 mg, 0.42 mmol) in DMF (3 mL), were added *N,N'*-dicyclohexylcarbodiimide (DCC) (103.0 mg, 0.5 mmol), hydroxybenzotriazole (HOBT) (67.6 mg, 0.5 mmol). The reaction mixture was stirred overnight. Benzylamine (92.0  $\mu$ L, 0.84 mmol) and *N,N*-diisopropylethylamine (DIPEA) (88  $\mu$ L, 0.50 mmol) were added, and the reaction was stirred for 3 h. After complete reaction (tlc analysis), the solvent was evaporated, and the residue was purified with column chromatography (1% of MeOH in  $CH_2Cl_2$ ) to give amide **3** (73 mg, 60%): mp 201–205 °C; IR (KBr)  $\nu$  3287, 2933, 2838, 1636, 1550, 1454, 1423, 1396, 1272, 1239, 1217  $cm^{-1}$ ;  $^1H$  NMR (500 MHz,  $CDCl_3$ )  $\delta$  7.38–7.31 (m, 5H, Ph), 7.28 (d,  $J = 8.7$  Hz, H-7), 7.01–6.98 (m, 2H, H-4, H-6), 6.75 (s, H-3), 6.44 (br s, 1H, NH), 4.63 (d,  $J = 5.8$  Hz, 2H,  $NHCH_2$ ), 4.06 (s, 3H,  $NCH_3$ ), 3.84 (s,  $OCH_3$ );  $^{13}C$  NMR (126 MHz,  $CDCl_3$ )  $\delta$  162.3 (CONH $_2$ Ph), 154.6 (C5), 138.1 (C'1, Ph), 134.5 (C3a), 131.9 (C2), 128.8, 127.7 (4C, C3',C5',C2',C6', Ph), 127.6 (C4', Ph), 126.1 (C7a), 115.2 (C6), 111.0 (C7), 103.1 (C3), 102.2 (C4), 55.7 ( $OCH_3$ ), 43.5 ( $NHCH_2$ ), 31.7 ( $NCH_3$ ); MS (EI)  $m/z$  (%): 146 (54) [ $C_9H_8NO$ ] $^+$ , 161 (100) [ $C_{10}H_{11}NO$ ] $^+$ , 189 (28) [ $C_{11}H_{11}NO_2$ ] $^+$ , 294 (96) [ $M$ ] $^+$ . HRMS (ESI): Calcd for  $C_{18}H_{18}N_2O_2$ : 294.1368. Found: 294.1362. Anal. Calcd. for  $C_{18}H_{18}N_2O_2$ : C, 73.45; H, 6.16; N, 9.52. Found: C, 73.20; H, 6.04; N, 9.54.

#### 4.1.4. *N*-Benzyl-1-(5-methoxy-1-methyl-1*H*-indol-2-yl) methanamine (**4**)

To a suspension of  $LiAlH_4$  (38.7 mg, 1.02 mmol) in dry THF (2 mL), at 0 °C, under argon, was added dropwise a solution of the amide **3** (100 mg, 0.33 mmol) in dry THF (3 mL) and stirring. The reaction mixture was heated for 5 h. Then, the reaction was cooled in an ice bath, and water was added carefully. The precipitate was filtered, the solution was concentrated and the crude, purified by column chromatography (5% MeOH/ $CH_2Cl_2$ ) to afford the amine **4** (75 mg, 79%): mp 101–103 °C; IR (KBr)  $\nu$  3436, 3313, 2929, 2829, 1618, 1489, 1452, 1402, 1218  $cm^{-1}$ ;  $^1H$  NMR (500 MHz,  $CDCl_3$ )  $\delta$  7.37–7.28 (m, 5H, Ph), 7.18 (d,  $J = 8.8$  Hz, 1H, H-7), 7.03 (d,  $J = 2.4$  Hz, 1H, H-4), 6.85 (dd,  $J = 8.8, 2.4$  Hz, 1H, H-6), 6.33 (s, 1H, H-3), 3.91 (s, 2H,  $CH_2NH$ ), 3.86 (s, 2H,  $NCH_2Ph$ ), 3.85 (s, 3H,  $CH_3O$ ), 3.73 (s, 3H,  $CH_3-N$ ) [the  $CH_2NHCH_2Ph$  signal was not detected];  $^{13}C$  NMR (126 MHz,  $CDCl_3$ )  $\delta$  154.0 (C5), 140.0 (C'1, Ph), 139.0 (C2), 133.2 (C7a), 128.4–128.1 (4C, C2',C3',C5',C6', Ph), 127.6 (C'4, Ph), 127.0 (C3a), 111.2 (C6), 109.6 (C7), 102.1 (C4), 100.4 (C3), 56.0 ( $OCH_3$ ), 53.1 ( $NCH_2Ph$ ), 45.2 ( $NHCH_2$ ), 29.8 ( $NCH_3$ ); MS (EI)  $m/z$  (%): 160 (28)

$[\text{C}_{10}\text{H}_{10}\text{NO}]^+$ , 175.1 (100)  $[\text{C}_{11}\text{H}_{13}\text{NO}]^+$ , 277.1 (44)  $[\text{C}_{18}\text{H}_{17}\text{N}_2\text{O}]^+$ , 280.1 (19)  $[\text{M}]^+$ . HRMS (ESI): Calcd for  $\text{C}_{18}\text{H}_{20}\text{N}_2\text{O}$ : 280.1576. Found: 280.1575. **4·HCl** was prepared using the usual manner to give a white solid (mp 224–225 °C). Anal. Calcd. for  $\text{C}_{18}\text{H}_{21}\text{ClN}_2\text{O} \cdot 1/6\text{H}_2\text{O}$ : C, 67.60; H, 6.72; N, 8.76. Found: C, 67.62; H, 6.57; N, 9.03.

#### 4.1.5. Ethyl 5-(3-(1-benzylpiperidin-4-yl)propoxy)-1-methyl-1H-indole-2-carboxylate (**5**)

To a solution of 1-benzyl-4-(3-chloropropyl)piperidine **19** [22] (0.419 g, 1.665 mmol) and ethyl 5-hydroxy-1-methyl-1H-indole-2-carboxylate (**20**) [31] (0.365 g, 1.665 mmol) in DMF (20 mL),  $\text{K}_2\text{CO}_3$  (0.92 g, 6.656 mmol, 4 equiv) was added. The reaction mixture was stirred at reflux for 24 h. After complete reaction (tlc analysis), the solvent was evaporated, the crude diluted with water, and extracted with  $\text{CH}_2\text{Cl}_2$ . The organic phase was washed with brine, dried ( $\text{MgSO}_4$ ), and evaporated at reduced pressure. The crude product was purified by flash chromatography ( $\text{CH}_2\text{Cl}_2/\text{EtOAc}$ , 10:1 to 5/1, v/v) to give compound **5** (0.452 g, 63%) as a white solid: mp 91–94 °C; IR (KBr)  $\nu$  3435, 2937, 2917, 1713, 1518, 1471, 1220, 1204, 1087  $\text{cm}^{-1}$ ;  $^1\text{H}$  NMR (500 MHz,  $\text{CDCl}_3$ )  $\delta$  7.32–7.29 (m, 5H, Ph), 7.26 (d,  $J = 8.9$  Hz, 1H, H7-indole), 7.18 (s, 1H, H3-indole), 7.04 (d,  $J = 1.9$  Hz, 1H, H4-indole), 7.01 (dd,  $J = 8.9, 1.9$  Hz, 1H, H6-indole), 4.36 (q,  $J = 7.3$  Hz, 2H,  $\text{CO}_2\text{CH}_2\text{CH}_3$ ), 4.04 [s, 3H, N(1) $\text{CH}_3$ ], 3.97 [t,  $J = 6.6$  Hz, 2H,  $\text{OCH}_2(\text{CH}_2)_2$ ], 3.49 (s, 2H,  $\text{NCH}_2\text{Ph}$ ), 2.88 [d,  $J = 11.2$  Hz, 2H, N( $\text{CH}_2$ ) $_{\text{eq}}$ ], 1.93 [tm,  $J = 11.2$  Hz, 2H, N( $\text{CH}_2$ ) $_{\text{ax}}$ ], 1.83–1.79 (m, 2H,  $\text{OCH}_2\text{CH}_2\text{CH}_2$ ), 1.70–1.68 [m, 2H, N( $\text{CH}_2$ ) $_{\text{eq}}$ ], 1.44–1.37 {m, 5H [2H ( $\text{OCH}_2\text{CH}_2\text{CH}_2$ ) + 3H ( $\text{CO}_2\text{CH}_2\text{CH}_3$ )]}, 1.32–1.25 [m, 3H, N( $\text{CH}_2$ ) $_{\text{ax}}$ CH];  $^{13}\text{C}$  NMR (125 MHz,  $\text{CDCl}_3$ )  $\delta$  162.2 ( $\text{CO}_2\text{CH}_2\text{CH}_3$ ), 153.9 (C5-indole), 138.6 (C'1, Ph), 135.2 (C2-indole), 129.2 (2  $\times$  CH, Ph), 128.1 (C7a-indole), 128.0 (2  $\times$  CH, Ph), 126.8 (C3a-indole), 126.0 (C'4H, Ph), 119.9 (C6-indole), 111.0 (C7-indole), 109.3 (C3-indole), 103.5 (C4-indole), 68.8 ( $\text{CH}_2\text{CH}_2\text{CH}_2\text{O}$ ), 63.5 ( $\text{NCH}_2\text{Ph}$ ), 60.4 ( $\text{CO}_2\text{CH}_2\text{CH}_3$ ), 53.9 [2  $\times$   $\text{CH}_2$ , N( $\text{CH}_2$ ) $_{\text{eq}}$ ], 35.6 [CH, N( $\text{CH}_2$ ) $_{\text{eq}}$ ], 32.9 ( $\text{CH}_2\text{CH}_2\text{CH}_2\text{O}$ ), 32.4 [2  $\times$   $\text{CH}_2$ , N( $\text{CH}_2$ ) $_{\text{ax}}$ ], 31.7 [N(1) $\text{CH}_3$ ], 26.7 ( $\text{CH}_2\text{CH}_2\text{CH}_2\text{O}$ ), 14.3 ( $\text{CO}_2\text{CH}_2\text{CH}_3$ ); MS (EI)  $m/z$  (%): 91 (58)  $[\text{PhCH}_2]^+$ , 216 (77)  $[\text{Bn}-\text{Piperidine}-(\text{CH}_2)_3]^+$ , 343 (7)  $[\text{M} - \text{CH}_2\text{Ph}]^+$ , 389 (11)  $[\text{M} - \text{Ph}]^+$ , 434 (67)  $[\text{M}]^+$ . Anal. Calcd. for  $\text{C}_{27}\text{H}_{34}\text{N}_2\text{O}$ : C, 74.62; H, 7.89; N, 6.45. Found: C, 74.81; H, 7.94; N, 6.74.

#### 4.1.6. 5-(3-(1-Benzylpiperidin-4-yl)propoxy)-1-methyl-1H-indole-2-carboxylic acid (**6**)

To a solution of the ester **5** (1.18 g, 2.7 mmol) in EtOH (10 mL) was added a solution of lithium hydroxide (129 mg, 5.4 mmol) in EtOH (3 mL). The reaction mixture was stirred at reflux for 2 h. After complete reaction, the solvent was evaporated, water was added and acidified with cc HCl until pH 6. Then, ethyl acetate was added and the precipitate filtered, washed with ethyl acetate to afford the corresponding free acid **6** (1.082 g, 98%): mp 104–106 °C; IR (KBr)  $\nu$  3435, 3023, 2936, 1622, 1562, 1516, 1466, 1393, 1286, 1199  $\text{cm}^{-1}$ ;  $^1\text{H}$  NMR (500 MHz,  $\text{CDCl}_3$ )  $\delta$  7.47–7.45 (m, 2H, Ph), 7.38–7.35 (m, 3H, Ph), 7.21 (d,  $J = 8.9$  Hz, 1H, H7-indole), 7.18 (s, 1H, 3-indole), 7.02 (d,  $J = 2.0$  Hz, 1H, H4-indole), 6.90 (dd,  $J = 8.9, 2.0$  Hz, 1H, H6-indole), 4.08 [s, 3H, N(1) $\text{CH}_3$ ], 4.04 (s, 2H,  $\text{NCH}_2\text{Ph}$ ), 3.93 [t,  $J = 6.4$  Hz, 2H,  $\text{OCH}_2(\text{CH}_2)_2$ ], 3.36 [d,  $J = 11.3$  Hz, 2H, N( $\text{CH}_2$ ) $_{\text{eq}}$ ], 2.39 [t,  $J = 11.3$  Hz, 2H, N( $\text{CH}_2$ ) $_{\text{ax}}$ ], 1.81–1.65 (m, 6H,  $\text{OCH}_2\text{CH}_2\text{CH}_2$ , N( $\text{CH}_2$ ) $_{\text{eq}}$ ), 1.45–1.41 [m, 3H, N( $\text{CH}_2$ ) $_{\text{ax}}$ CH] [the  $\text{CO}_2\text{H}$  signal was not detected];  $^{13}\text{C}$  NMR (125 MHz,  $\text{CDCl}_3$ )  $\delta$  167.0 ( $\text{CO}_2\text{H}$ ), 153.3 (C5-indole), 134.8 (2C: C'1, Ph; C2-indole), 130.9 (2  $\times$  CH, Ph), 128.8 (C7a-indole), 128.7 (2  $\times$  CH, Ph), 126.4 (2C: C'4, Ph; C3a-indole), 115.6 (C6-indole), 110.8 (C7-indole), 107.7 (C3-indole), 103.7 (C4-indole), 68.7 ( $\text{CH}_2\text{CH}_2\text{CH}_2\text{O}$ ), 60.8 ( $\text{NCH}_2\text{Ph}$ ), 51.9 [2  $\times$   $\text{CH}_2$ , N( $\text{CH}_2$ ) $_{\text{eq}}$ ], 34.2 [N( $\text{CH}_2$ ) $_{\text{ax}}$ CH], 32.2 [ $\text{CH}_2$ –( $\text{CH}_2$ ) $_{\text{eq}}$ ], 31.6 [N(1) $\text{CH}_3$ ], 29.7 [N( $\text{CH}_2$ ) $_{\text{ax}}$ CH], 26.5 ( $\text{CH}_2\text{CH}_2\text{CH}_2\text{O}$ ); MS (EI)  $m/z$  (%): 91 (100)  $[\text{PhCH}_2]^+$ , 172 (50), 216

(32)  $[\text{Bn}-\text{piperidine}-(\text{CH}_2)_3]^+$ , 406 (11)  $[\text{M}]^+$ , EM (ESI)  $m/z$  (%): 407 (M + 1). HRMS (ESI): Calcd. for  $\text{C}_{25}\text{H}_{30}\text{N}_2\text{O}_3$ : 406.2256. Found: 406.2273.

#### 4.1.7. 5-(3-(1-Benzylpiperidin-4-yl)propoxy)-1-methyl-1H-indole-2-carbonyl chloride (**21**)

A solution of acid **6** (91.6 mg, 0.22 mmol) and phosphorous pentachloride (70.4 mg, 0.34 mmol) in dry dichloromethane (10 mL) was stirred at reflux for about 2 h. Solvent was removed in vacuum, the residue treated with a dry ethyl ether and solvent removed in vacuum again. This operation was repeated twice with ethyl ether and then twice with chloroform to obtain compound **21** (94.8 mg, 99%) as an oil, that was used immediately, without any further purification, for the synthesis of the amides **7–10**.

#### 4.1.8. General procedures for the synthesis of 5-(3-(1-benzylpiperidin-4-yl)propoxy)-1-methyl-1H-indole-2-carboxamide derivatives (**7–10**)

The crude acyl chloride (**21**) obtained was dissolved in dry  $\text{CH}_2\text{Cl}_2$  (10 mL) and the solution cooled in an ice-bath. To the solution was added dropwise with stirring, triethylamine (4 equiv) and an appropriate amine (4 equiv). The mixture was refluxed. Solvents were removed in vacuum, the residue obtained was purified by column chromatography. The following compounds were obtained.

#### 4.1.9. N-Benzyl-5-(3-(1-benzylpiperidin-4-yl)propoxy)-1-methyl-1H-indole-2-carboxamide (**7**)

Following the General procedure, reaction of 5-(3-(1-benzylpiperidin-4-yl)propoxy)-1-methyl-1H-indole-2-carbonyl chloride (**21**) (95.7 mg, 0.22 mmol) with benzylamine (50  $\mu\text{L}$ , 0.45 mmol), and triethylamine (0.12 mL, 0.88 mmol) in dry dichloromethane (10 mL), after 12 h, and column chromatography (1% of MeOH in  $\text{CH}_2\text{Cl}_2$ ) gave product **7** (89.3 mg, 80%) as a white solid: mp 165–167 °C; IR (KBr)  $\nu$  3435, 3307, 3082, 2936, 2917, 1637, 1548, 1465, 1390, 1240, 1205  $\text{cm}^{-1}$ ;  $^1\text{H}$  NMR (500 MHz,  $\text{CDCl}_3$ )  $\delta$  7.37–7.30 (m, 10H, 2  $\times$  Ph), 7.27 (d,  $J = 8.8$  Hz, 1H, H7-indole), 6.99 (d,  $J = 2.4$  Hz, 1H, H4-indole), 6.97 (dd,  $J = 8.8, 2.4$  Hz, 1H, H6-indole), 6.73 (s, H1, H3-indole), 6.40 (t,  $J = 5.4$  Hz, 1H,  $\text{CONHCH}_2\text{Ph}$ ), 4.63 (d,  $J = 5.4$  Hz, 2H,  $\text{CONHCH}_2\text{Ph}$ ), 4.05 [s, 3H, N(1) $\text{CH}_3$ ], 3.95 (t,  $J = 6.6$  Hz, 2H,  $\text{OCH}_2\text{CH}_2\text{CH}_2$ ), 3.49 (s, 2H,  $\text{NCH}_2\text{Ph}$ ), 2.88 [d,  $J = 9.7$  Hz, 2H, N( $\text{CH}_2$ ) $_{\text{eq}}$ ], 1.94 [m, 2H, N( $\text{CH}_2$ ) $_{\text{ax}}$ ], 1.83–1.80 (m, 2H,  $\text{OCH}_2\text{CH}_2\text{CH}_2$ ), 1.78–1.68 [m, 2H, N( $\text{CH}_2$ ) $_{\text{eq}}$ ], 1.43–1.39 (m, 2H,  $\text{OCH}_2\text{CH}_2\text{CH}_2$ ), 1.28–1.24 [m, 3H, N( $\text{CH}_2$ ) $_{\text{ax}}$ CH];  $^{13}\text{C}$  NMR (125 MHz,  $\text{CDCl}_3$ )  $\delta$  162.3 ( $\text{CONHCH}_2\text{Ph}$ ), 154.0 (C5-indole), 138.1 (2C, 2  $\times$  C'1, Ph), 134.5 (C7a-indole), 131.9 (C2), 129.2–126.8 (2  $\times$  5CH, 2  $\times$   $\text{NCH}_2\text{C}_6\text{H}_5$ ), 126.2 (C3a-indole), 115.7 (C6-indole), 110.9 (C7-indole), 103.3 (C4-indole), 103.0 (C3-indole), 68.8 ( $\text{OCH}_2\text{CH}_2\text{CH}_2$ ), 63.5 ( $\text{NCH}_2\text{Ph}$ ), 53.9 [2  $\times$   $\text{CH}_2$ , N( $\text{CH}_2$ ) $_{\text{eq}}$ ], 43.5 ( $\text{CONHCH}_2\text{Ph}$ ), 35.6 [N( $\text{CH}_2$ ) $_{\text{ax}}$ CH], 32.9 ( $\text{OCH}_2\text{CH}_2\text{CH}_2$ ), 32.3 [2  $\times$   $\text{CH}_2$ , N( $\text{CH}_2$ ) $_{\text{ax}}$ ], 31.7 [N(1) $\text{CH}_3$ ], 26.7 ( $\text{OCH}_2\text{CH}_2\text{CH}_2$ ); MS (EI)  $m/z$  (%): 91 (100)  $[\text{M} - \text{Bn}]^+$ , 172 (63)  $[\text{C}_{12}\text{H}_{14}\text{N}]^+$ , 202 (9)  $[\text{M} - \text{C}_{18}\text{H}_{17}\text{N}_2\text{O}_2]^+$ , 216 (41)  $[\text{M} - \text{C}_{17}\text{H}_{15}\text{N}_2\text{O}_2]^+$ , 495 (3)  $[\text{M}]^+$ . HRMS (ESI): Calcd. for  $\text{C}_{32}\text{H}_{37}\text{N}_3\text{O}_2$ : 495.2886. Found: 495.2903. Anal. Calcd. for  $\text{C}_{32}\text{H}_{37}\text{N}_3\text{O}_2$ : C, 77.54; H, 7.52; N, 8.48. Found: C, 77.17; H, 7.25; N, 8.57.

#### 4.1.10. 5-(3-(1-Benzylpiperidin-4-yl)propoxy)-1-methyl-N-phenyl-1H-indole-2-carboxamide (**8**)

Following the General procedure, reaction of 5-(3-(1-benzylpiperidin-4-yl)propoxy)-1-methyl-1H-indole-2-carbonyl chloride (**21**) (95 mg, 0.22 mmol) with aniline (41 mg, 0.44 mmol) and triethylamine (0.12 mL) in dry dichloromethane (10 mL), after overnight, and column chromatography (MeOH/ $\text{CH}_2\text{Cl}_2$  from 1%

to 3%) gave product **14** (90.4 g, 84%) as a white solid: mp 189–192 °C; IR (KBr)  $\nu$  3435, 3294, 3060, 2917, 1644, 1597, 1538, 1499, 1466, 1443, 1316, 1243, 1207  $\text{cm}^{-1}$ ;  $^1\text{H}$  NMR (500 MHz,  $\text{CDCl}_3$ )  $\delta$  7.84 (s, 1H,  $\text{NHC}_6\text{H}_5$ ), 7.62–7.59 (m, 2H, H'2, H'6,  $\text{NHC}_6\text{H}_5$ ), 7.39–7.36 (m, 2H, H'3, H'5,  $\text{NHC}_6\text{H}_5$ ), 7.32–7.17 (m, 6H,  $\text{NCH}_2\text{C}_6\text{H}_5$ , H7-indole), 7.15 (t,  $J = 7.3$  Hz, 1H, H'4,  $\text{NHC}_6\text{H}_5$ ), 7.05 (d,  $J = 2.4$  Hz, 1H, H4-indole), 7.02 (dd,  $J = 9.3, 2.4$  Hz, 1H, H6-indole), 6.89 (s, 1H, H3-indole), 4.06 [s, 3H,  $\text{N}(\text{1})\text{CH}_3$ ], 3.98 (t,  $J = 6.6$  Hz, 2H,  $\text{OCH}_2\text{CH}_2\text{CH}_2$ ), 3.50 (s, 2H,  $\text{NCH}_2\text{Ph}$ ), 2.89 [d,  $J = 10.8$  Hz, 2H,  $\text{N}(\text{CH}_2)_{\text{eq}}$ ], 1.95 [m, 2H,  $\text{N}(\text{CH}_2)_{\text{ax}}$ ], 1.83–1.80 (m, 2H,  $\text{OCH}_2\text{CH}_2\text{CH}_2$ ), 1.71–1.69 [m, 2H,  $\text{N}(\text{CH}_2)_2(\text{CH}_2)_{\text{eq}}$ ], 1.58 (m, 2H,  $\text{OCH}_2\text{CH}_2\text{CH}_2$ ), 1.44–1.42 [m, 2H,  $\text{N}(\text{CH}_2)_2(\text{CH}_2)_{\text{ax}}\text{CH}$ ], 1.30 [m, 1H,  $\text{N}(\text{CH}_2)_2(\text{CH}_2)_{\text{ax}}\text{CH}$ ];  $^{13}\text{C}$  NMR (125 MHz,  $\text{CDCl}_3$ )  $\delta$  160.4 (CONHPh), 154.1 (C5-indole), 137.7 (2C,  $2 \times \text{C}'1$ ,  $\text{CONHC}_6\text{H}_5$ ,  $\text{NHCH}_2\text{C}_6\text{H}_5$ ), 134.8 (C7a-indole), 132.1 (C2), 129.2 ( $2 \times \text{CH}$ ,  $\text{CONHC}_6\text{H}_5$ ), 129.1 ( $2 \times \text{CH}$ ,  $\text{NHCH}_2\text{C}_6\text{H}_5$ ), 128.1 ( $2 \times \text{CH}$ ,  $\text{NHCH}_2\text{C}_6\text{H}_5$ ), 126.9 (C'4,  $\text{NHCH}_2\text{C}_6\text{H}_5$ ), 126.1 (C3a-indole), 124.4 (C'4,  $\text{CONHC}_6\text{H}_5$ ), 119.9 ( $2 \times \text{CH}$ ,  $\text{CONHC}_6\text{H}_5$ ), 116.2 (C6-indole), 111.0 (C7-indole), 103.5 (C3-indole), 103.5 (C4-indole), 68.8 ( $\text{OCH}_2\text{CH}_2\text{CH}_2$ ), 63.4 ( $\text{NCH}_2\text{Ph}$ ), 53.9 [ $\text{N}(\text{CH}_2)_2(\text{CH}_2)_2\text{CH}$ ], 35.5 [ $\text{N}(\text{CH}_2)_2(\text{CH}_2)_2\text{CH}$ ], 32.9 ( $\text{OCH}_2\text{CH}_2\text{CH}_2$ ), 32.3 [ $\text{N}(\text{CH}_2)_2(\text{CH}_2)_2\text{CH}$ ], 31.7 [ $\text{N}(\text{1})\text{CH}_3$ ], 26.7 ( $\text{OCH}_2\text{CH}_2\text{CH}_2$ ); MS (EI)  $m/z$  (%): 91 (100) [ $\text{M} - \text{Bn}$ ] $^+$ , 172 (72) [ $\text{C}_{12}\text{H}_{14}\text{N}$ ] $^+$ , 216 (41) [ $\text{M} - \text{C}_{16}\text{H}_{13}\text{N}_2\text{O}_2$ ] $^+$ . HRMS (ESI): Calcd. for  $\text{C}_{31}\text{H}_{35}\text{N}_3\text{O}_2$ : 481.2729. Found: 481.2729. Anal. Calcd. for  $\text{C}_{31}\text{H}_{35}\text{N}_3\text{O}_2 \cdot 1/3\text{H}_2\text{O}$ : C, 76.35; H, 7.37; N, 8.62. Found: C, 76.68; H, 7.06; N, 8.77.

#### 4.1.11. (5-(3-(1-Benzylpiperidin-4-yl)propoxy)-1-methyl-1H-indol-2-yl)morpholinomethanone (**9**)

Following the General procedure, reaction of 5-(3-(1-benzylpiperidin-4-yl)propoxy)-1-methyl-1H-indole-2-carbonyl chloride (**21**) (162.0 mg, 0.38 mmol) with morpholine (66  $\mu\text{L}$ , 0.76 mmol) and triethylamine (0.20 mL) in dichloromethane (10 mL), after 12 h, and column chromatography (1% of MeOH in  $\text{CH}_2\text{Cl}_2$ ) gave product **9** (130 mg, 72%): as a white solid: mp 125–128 °C; IR (KBr)  $\nu$  3435, 3084, 2921, 2851, 1615, 1532, 1453, 1273, 1236, 1116  $\text{cm}^{-1}$ ;  $^1\text{H}$  NMR (500 MHz,  $\text{CDCl}_3$ )  $\delta$  7.35–7.32 (m, 5H, Ph), 7.27 (d,  $J = 9.3$  Hz, 1H, H7-indole), 7.05 (d,  $J = 2.4$  Hz, 1H, H4-indole), 6.98 (dd,  $J = 9.3, 2.4$  Hz, 1H, H6-indole), 6.52 (s, 1H, H3-indole), 3.99 (t,  $J = 6.8$  Hz, 2H,  $\text{OCH}_2\text{CH}_2\text{CH}_2$ ), 3.85 [s, 3H,  $\text{N}(\text{1})\text{CH}_3$ ], 3.84–3.80 [m, 4H,  $\text{CON}(\text{CH}_2)_2(\text{CH}_2)_2\text{O}$ ], 3.77–3.71 [m, 4H,  $\text{CON}(\text{CH}_2)_2(\text{CH}_2)_2\text{O}$ ], 3.53 (s, 2H,  $\text{NCH}_2\text{Ph}$ ), 2.92 (dm,  $J = 10.7$  Hz, 2H,  $\text{N}(\text{CH}_2)_{\text{eq}}$ ), 1.98 [m, 2H,  $\text{N}(\text{CH}_2)_{\text{ax}}$ ], 1.86–1.84 (m, 2H,  $\text{OCH}_2\text{CH}_2\text{CH}_2$ ), 1.83–1.80 [m, 2H,  $\text{N}(\text{CH}_2)_2(\text{CH}_2)_{\text{eq}}$ ], 1.46–1.44 (m, 2H,  $\text{OCH}_2\text{CH}_2\text{CH}_2$ ), 1.36–1.32 [m, 3H,  $\text{N}(\text{CH}_2)_2(\text{CH}_2)_{\text{ax}}\text{CH}$ ];  $^{13}\text{C}$  NMR (125 MHz,  $\text{CDCl}_3$ )  $\delta$  163.2 [ $\text{CON}(\text{CH}_2)_2(\text{CH}_2)_2\text{O}$ ], 153.9 (C5-indole), 138.4 (C'1, Ph), 133.4 (C7a-indole), 131.3 (C2), 129.2 ( $2 \times \text{CH}$ , Ph), 128.1 ( $2 \times \text{CH}$ , Ph), 126.9 (C'4, Ph), 126.5 (C3a-indole), 114.9 (C6-indole), 110.6 (C7-indole), 103.5 (C4-indole), 103.4 (C3-indole), 68.9 ( $\text{OCH}_2\text{CH}_2\text{CH}_2$ ), 67.0 [2C,  $\text{CON}(\text{CH}_2)_2(\text{CH}_2)_2\text{O}$ ], 63.5 ( $\text{NCH}_2\text{Ph}$ ), 53.9 [ $\text{N}(\text{CH}_2)_2(\text{CH}_2)_2\text{CH}$ ], 35.5 [ $\text{N}(\text{CH}_2)_2(\text{CH}_2)_2\text{CH}$ ], 32.9 ( $\text{OCH}_2\text{CH}_2\text{CH}_2$ ), 32.3 [ $\text{N}(\text{CH}_2)_2(\text{CH}_2)_2\text{CH}$ ], 31.9 [ $\text{N}(\text{1})\text{CH}_3$ ], 26.7 ( $\text{OCH}_2\text{CH}_2\text{CH}_2$ ); MS (EI)  $m/z$  (%): 172 (100) [ $\text{C}_{12}\text{H}_{14}\text{N}$ ] $^+$ , 202 (19) [ $\text{M} - \text{C}_{15}\text{H}_{17}\text{N}_2\text{O}_3$ ] $^+$ , 216 (89) [ $\text{M} - \text{C}_{14}\text{H}_{15}\text{N}_2\text{O}_3$ ] $^+$ , 475 (24) [ $\text{M}$ ] $^+$ . HRMS (ESI): Calcd. for  $\text{C}_{29}\text{H}_{37}\text{N}_3\text{O}_3$ : 475.2835. Found: 475.2842. Anal. Calcd. for  $\text{C}_{29}\text{H}_{37}\text{N}_3\text{O}_3 \cdot 1/3\text{H}_2\text{O}$ : C, 72.32; H, 7.88; N, 8.72. Found: C, 72.37; H, 7.56; N, 8.84.

#### 4.1.12. 5-(3-(1-Benzylpiperidin-4-yl)propoxy)-1-methyl-N-(prop-2-yn-1-yl)-1H-indole-2-carboxamide (**10**)

Following the General procedure, reaction of 5-(3-(1-benzylpiperidin-4-yl)propoxy)-1-methyl-1H-indole-2-carbonyl chloride (**21**) (63.8 mg, 0.15 mmol) with prop-2-yn-1-amine (20.0  $\mu\text{L}$ , 0.30 mmol) and triethylamine (83.0  $\mu\text{L}$ , 0.60 mmol) in dry dichloromethane (10 mL), after 12 h, and column

chromatography (MeOH/ $\text{CH}_2\text{Cl}_2$  from 1% to 3%) gave product **10** (40 mg, 60%) as a white solid: mp 163–165 °C; IR (KBr)  $\nu$  3435, 3291, 3060, 2919, 1638, 1542, 1466, 1391, 1275, 1242, 1206  $\text{cm}^{-1}$ ;  $^1\text{H}$  NMR (500 MHz,  $\text{CDCl}_3$ )  $\delta$  7.32–7.29 (m, 5H, Ph), 7.25 (d,  $J = 8.8$  Hz, 1H, H7-indole), 7.01–6.99 (m, 2H, H4-indole, H6-indole), 6.77 (s, 1H, H3-indole), 6.29 (s, 1H, CONH), 4.23 (dd,  $J = 5.4, 2.5$  Hz, 2H,  $\text{NHCH}_2\text{C}\equiv\text{CH}$ ), 4.02 [s, 3H,  $\text{N}(\text{1})\text{CH}_3$ ], 3.96 (t,  $J = 6.6$  Hz, 2H,  $\text{OCH}_2\text{CH}_2\text{CH}_2$ ), 3.50 (s, 2H,  $\text{NCH}_2\text{Ph}$ ), 2.88 [m, 2H,  $\text{N}(\text{CH}_2)_{\text{eq}}$ ], 2.29 (t,  $J = 2.5$  Hz, 1H,  $\text{NHCH}_2\text{C}\equiv\text{CH}$ ), 1.96 [m, 2H,  $\text{N}(\text{CH}_2)_{\text{ax}}$ ], 1.82–1.79 (m, 2H,  $\text{OCH}_2\text{CH}_2\text{CH}_2$ ), 1.70–1.68 [m, 2H,  $\text{N}(\text{CH}_2)_2(\text{CH}_2)_{\text{eq}}$ ], 1.43–1.41 (m, 2H,  $\text{OCH}_2\text{CH}_2\text{CH}_2$ ), 1.29–1.25 [m, 3H,  $\text{N}(\text{CH}_2)_2(\text{CH}_2)_{\text{ax}}\text{CH}$ ];  $^{13}\text{C}$  NMR (126 MHz,  $\text{CDCl}_3$ )  $\delta$  162.0 (CONH), 154.0 (C5-indole), 138.3 (C'1, Ph), 134.6 (C7a-indole), 131.2 (C2-indole), 129.3 ( $2 \times \text{CH}$ , Ph), 128.1 ( $2 \times \text{CH}$ , Ph), 126.9 (C'4, Ph), 126.1 (C3a-indole), 116.0 (C6-indole), 111.0 (C7-indole), 103.6 (C3-indole)\*, 103.3 (C4-indole)\*, 79.4 ( $\text{NCH}_2\text{C}\equiv\text{CH}$ ), 71.8 ( $\text{NCH}_2\text{C}\equiv\text{CH}$ ), 68.8 ( $\text{OCH}_2\text{CH}_2\text{CH}_2$ ), 63.4 ( $\text{NCH}_2\text{Ph}$ ), 53.8 [ $\text{N}(\text{CH}_2)_2(\text{CH}_2)_2\text{CH}$ ], 35.5 [ $\text{N}(\text{CH}_2)_2(\text{CH}_2)_2\text{CH}$ ], 32.9 ( $\text{OCH}_2\text{CH}_2\text{CH}_2$ ), 32.2 [ $\text{N}(\text{CH}_2)_2(\text{CH}_2)_2\text{CH}$ ], 31.6 [ $\text{N}(\text{1})\text{CH}_3$ ], 29.2 ( $\text{NHCH}_2\text{C}\equiv\text{CH}$ ), 26.7 ( $\text{OCH}_2\text{CH}_2\text{CH}_2$ ); MS (EI)  $m/z$  (%): 91 (100) [ $\text{M} - \text{Bn}$ ] $^+$ , 172 (68) [ $\text{C}_{12}\text{H}_{14}\text{N}$ ] $^+$ , 188 (7), 202 (9) [ $\text{M} - \text{C}_{14}\text{H}_{13}\text{N}_2\text{O}_2$ ] $^+$ , 216 (35) [ $\text{M} - \text{C}_{13}\text{H}_{11}\text{N}_2\text{O}_2$ ] $^+$ , 443 (9) [ $\text{M}$ ] $^+$ . HRMS (ESI): Calcd. for  $\text{C}_{28}\text{H}_{33}\text{N}_3\text{O}_2$ : 443.2573. Found: 443.2577. Anal. Calcd. for  $\text{C}_{28}\text{H}_{33}\text{N}_3\text{O}_2 \cdot 1/3\text{H}_2\text{O}$ : C, 74.80; H, 7.55; N, 9.35. Found: C, 74.89; H, 7.21; N, 9.46.

#### 4.1.13. (5-(3-(1-Benzylpiperidin-4-yl)propoxy)-1-methyl-1H-indol-2-yl)methanol (**11**)

Following the General procedure, reaction of ethyl 5-(3-(1-benzylpiperidin-4-yl)propoxy)-1-methyl-1H-indole-2-carboxylate (**5**) (221.8 mg, 0.51 mmol) with  $\text{LiAlH}_4$  (58.1 mg, 1.53 mmol, 3 equiv) in THF (3 mL), after 15 min, and column chromatography (MeOH/ $\text{CH}_2\text{Cl}_2$  from 1% to 5%) gave product **11** (200 mg, 99%) as a white solid: mp 93–96 °C; IR (KBr)  $\nu$  3435, 3101, 3101, 3065, 2929, 2812, 1620, 1488, 1474, 1196, 1157, 1032  $\text{cm}^{-1}$ ;  $^1\text{H}$  NMR (500 MHz,  $\text{CDCl}_3$ )  $\delta$  7.31–7.29 (m, 5H, Ph), 7.19 (d,  $J = 8.8$  Hz, 1H, H7-indole), 7.03 (d,  $J = 2.4$  Hz, 1H, H4-indole), 6.88 (dd,  $J = 8.8, 2.4$  Hz, 1H, H6-indole), 6.35 (s, 1H, H3-indole), 4.77 (s, 2H,  $\text{CH}_2\text{OH}$ ), 3.96 [t,  $J = 6.6$  Hz, 2H,  $\text{OCH}_2(\text{CH}_2)_2$ ], 3.77 [s, 3H,  $\text{N}(\text{1})\text{CH}_3$ ], 3.48 (s, 2H,  $\text{NCH}_2\text{Ph}$ ), 2.87 [d,  $J = 11.7$  Hz, 2H,  $\text{N}(\text{CH}_2)_{\text{eq}}$ ], 1.93 [tm,  $J = 11.7$  Hz, 2H,  $\text{N}(\text{CH}_2)_{\text{ax}}$ ], 1.81–1.78 (m, 2H,  $\text{OCH}_2\text{CH}_2\text{CH}_2$ ), 1.69–1.67 [m, 2H,  $\text{N}(\text{CH}_2)_2(\text{CH}_2)_{\text{eq}}$ ], 1.41–1.39 (m, 2H,  $\text{OCH}_2\text{CH}_2\text{CH}_2$ ), 1.28–1.27 [m, 3H,  $\text{N}(\text{CH}_2)_2(\text{CH}_2)_{\text{ax}}\text{CH}$ ] (the signal for  $\text{CH}_2\text{OH}$  was not detected);  $^{13}\text{C}$  NMR (125 MHz,  $\text{CDCl}_3$ )  $\delta$  153.4 (C5-indole), 139.0 (C'1, Ph), 138.6 (C2-indole), 133.5 (C7a-indole), 129.2 ( $2 \times \text{CH}$ , Ph), 128.0 ( $2 \times \text{CH}$ , Ph), 127.3 (C3a-indole), 126.8 [C'(4)H, Ph], 112.9 (C6-indole), 109.8 (C7-indole), 103.7 (C4-indole), 100.9 (C3-indole), 69.0 ( $\text{CH}_2\text{CH}_2\text{CH}_2\text{O}$ ), 63.5 ( $\text{NCH}_2\text{Ph}$ ), 57.2 ( $\text{CH}_2\text{OH}$ ), 53.9 [ $2 \times \text{CH}_2$ ,  $\text{N}(\text{CH}_2)_2(\text{CH}_2)_2\text{CH}$ ], 35.6 [ $\text{CH}$ ,  $\text{N}(\text{CH}_2)_2(\text{CH}_2)_2\text{CH}$ ], 32.9\* ( $\text{CH}_2\text{CH}_2\text{CH}_2\text{O}$ ), 32.3\* [ $2 \times \text{CH}_2$ ,  $\text{N}(\text{CH}_2)_2(\text{CH}_2)_2\text{CH}$ ], 29.9 [ $\text{N}(\text{1})\text{CH}_3$ ], 26.7 ( $\text{CH}_2\text{CH}_2\text{CH}_2\text{O}$ ); MS (EI)  $m/z$  (%): 91 (100) [ $\text{M} - \text{Bn}$ ] $^+$ , 172 (68) [ $\text{C}_{12}\text{H}_{14}\text{N}$ ] $^+$ , 202 (9) [ $\text{M} - \text{C}_{14}\text{H}_{13}\text{N}_2\text{O}_2$ ] $^+$ , 216 (35) [ $\text{M} - \text{C}_{13}\text{H}_{11}\text{N}_2\text{O}_2$ ] $^+$ , 392 (9) [ $\text{M}$ ] $^+$ . HRMS (ESI): Calcd. for  $\text{C}_{25}\text{H}_{32}\text{N}_2\text{O}_2$ : 392.2464. Found: 392.2477. Anal. Calcd. for  $\text{C}_{25}\text{H}_{32}\text{N}_2\text{O}_2$ : C, 76.49; H, 8.22; N, 7.14. Found: C, 75.9; H, 7.93; N, 7.15.

#### 4.1.14. General procedures for the synthesis of (5-(3-(1-Benzylpiperidin-4-yl)propoxy)-1-methyl-1H-indol-2-yl)methanamine derivatives (**12–16**)

A suspension of  $\text{LiAlH}_4$  in freshly distilled dioxane was cooled at 0 °C and a solution of the amides (**7–10**) in dioxane was added dropwise with stirring. The mixture was refluxed for the time indicated for each case. When the reaction was over, the mixture was cooled in an ice-bath and, water was added dropwise. The precipitate was removed by filtration. The solvent was removed,

and the residue purified by column chromatography to afford the amines.

#### 4.1.15. *N*-Benzyl-1-(5-(3-(1-benzylpiperidin-4-yl)propoxy)-1-methyl-1*H*-indol-2-yl)methanamine (**12**)

Following the General procedure, reaction of *N*-benzyl-5-(3-(1-benzylpiperidin-4-yl)propoxy)-1-methyl-1*H*-indole-2-carboxamide (**7**) (98 mg, 0.21 mmol) with LiAlH<sub>4</sub> (24 mg, 0.63 mmol) in dry dioxane (10 mL), after 7 h, and column chromatography (MeOH/CH<sub>2</sub>Cl<sub>2</sub> from 1% to 3%) gave product **12** (60 mg, 63%) as a white solid: mp 74–76 °C; IR (KBr)  $\nu$  3435, 3310, 3025, 2936, 1619, 1491, 1472, 1453, 1393, 1249, 1195, 1160 cm<sup>-1</sup>; <sup>1</sup>H NMR (500 MHz, CDCl<sub>3</sub>)  $\delta$  7.36–7.26 (m, 10H, 2Ph), 7.17 (d, *J* = 8.9 Hz, 1H, H7-indole), 7.02 (d, *J* = 2.3 Hz, 1H, H4-indole), 6.83 (dd, *J* = 8.9, 2.3 Hz, H6-indole), 6.30 (s, H1, H3-indole), 3.97 (t, *J* = 6.6 Hz, 2H, OCH<sub>2</sub>CH<sub>2</sub>CH<sub>2</sub>), 3.90 [br s, 2H, C(2)CH<sub>2</sub>NHCH<sub>2</sub>Ph]\*, 3.85 [s, 2H, C(2)CH<sub>2</sub>NHCH<sub>2</sub>Ph]\*, 3.72 [s, 3H, N(1)CH<sub>3</sub>], 3.52 (s, 2H, NCH<sub>2</sub>Ph), 2.90 [d, *J* = 10.1 Hz, 2H, N(CH<sub>2</sub>)<sub>eq</sub>], 1.97 [m, 2H, N(CH<sub>2</sub>)<sub>ax</sub>], 1.83–1.76 (m, 2H, OCH<sub>2</sub>CH<sub>2</sub>CH<sub>2</sub>), 1.71–1.69 [m, 2H, N(CH<sub>2</sub>)<sub>2</sub>(CH<sub>2</sub>)<sub>eq</sub>], 1.43–1.41 (m, 2H, OCH<sub>2</sub>CH<sub>2</sub>CH<sub>2</sub>), 1.39–1.30 [m, 3H, N(CH<sub>2</sub>)<sub>2</sub>(CH<sub>2</sub>)<sub>ax</sub>CH] (the signal for C(2)CH<sub>2</sub>NHCH<sub>2</sub>Ph could not be detected); <sup>13</sup>C NMR (125 MHz, CDCl<sub>3</sub>)  $\delta$  153.3 (C5-indole), 140.1 (2C, 2C'1, Ph), 138.9 (C7a-indole), 133.2 (C2), 129.3, 128.4, 128.1, 127.6 (10C, NCH<sub>2</sub>C<sub>6</sub>H<sub>5</sub>, NHCH<sub>2</sub>C<sub>6</sub>H<sub>5</sub>), 127.0 (C3a-indole), 111.8 (C6-indole), 109.5 (C7-indole), 103.3 (C4-indole), 100.4 (C3-indole), 69.0 (OCH<sub>2</sub>CH<sub>2</sub>CH<sub>2</sub>), 63.7 (NCH<sub>2</sub>Ph), 53.8 [C(2)CH<sub>2</sub>NHCH<sub>2</sub>Ph]\*, 53.2 [2CH<sub>2</sub>, N(CH<sub>2</sub>)<sub>2</sub>(CH<sub>2</sub>)<sub>2</sub>CH]\*, 45.2 [C(2)CH<sub>2</sub>NHCH<sub>2</sub>Ph]\*, 35.5 [N(CH<sub>2</sub>)<sub>2</sub>(CH<sub>2</sub>)<sub>2</sub>CH], 32.8 (OCH<sub>2</sub>CH<sub>2</sub>CH<sub>2</sub>), 32.1 [2 × CH<sub>2</sub>, N(CH<sub>2</sub>)<sub>2</sub>(CH<sub>2</sub>)<sub>2</sub>CH], 30.0 [N(1)CH<sub>3</sub>], 26.7 (OCH<sub>2</sub>CH<sub>2</sub>CH<sub>2</sub>); MS (EI) *m/z* (%): 172 (46), 216 (37), 283 (14), 374 (100), 383 (13), 481 (11) [M]<sup>+</sup>. HRMS (ESI): Calcd. for C<sub>32</sub>H<sub>39</sub>N<sub>3</sub>O: 481.3093. Found: 481.3111. Bis-chlorhydrate **12·2HCl** was prepared using the usual method to afford a white solid (mp 245–248 °C). Anal. Calcd. for C<sub>32</sub>H<sub>39</sub>N<sub>3</sub>O·2HCl·3/2H<sub>2</sub>O: C, 66.08; H, 7.63; N, 7.22. Found: C, 66.06; H, 7.07; N, 7.42.

#### 4.1.16. *N*-((5-(3-(1-Benzylpiperidin-4-yl)propoxy)-1-methyl-1*H*-indol-2-yl)methyl)aniline (**13**)

Following the General procedure, reaction of 5-(3-(1-benzylpiperidin-4-yl)propoxy)-1-methyl-*N*-phenyl-1*H*-indole-2-carboxamide (**8**) (174 mg, 0.36 mmol) with LiAlH<sub>4</sub> (41.2 mg, 1.1 mmol) in dry dioxane (7 mL), after 5 h, and column chromatography (MeOH/CH<sub>2</sub>Cl<sub>2</sub> from 1% to 3%) gave product **13** (123 mg, 73%) as a white solid: mp 114–116 °C; IR (KBr)  $\nu$  3412, 3022, 2941, 2905, 1624, 1599, 1501, 1476, 1424, 1312, 1250, 1197, 1026 cm<sup>-1</sup>; <sup>1</sup>H NMR (500 MHz, CDCl<sub>3</sub>)  $\delta$  7.32–7.27 (m, 5H, NCH<sub>2</sub>C<sub>6</sub>H<sub>5</sub>), 7.25–7.22 (m, 2H, H'2, H'6, CH<sub>2</sub>NHC<sub>6</sub>H<sub>5</sub>), 7.19 (d, *J* = 8.8 Hz, 1H, H7-indole), 7.03 (d, *J* = 2.4 Hz, 1H, H4-indole), 6.87 (dd, *J* = 8.8, 2.4 Hz, 1H, H6-indole), 6.78 (m, 1H, H'4, CH<sub>2</sub>NHC<sub>6</sub>H<sub>5</sub>), 6.71 (m, 2H, H'3, H'5, CH<sub>2</sub>NHC<sub>6</sub>H<sub>5</sub>), 6.39 (s, 1H, H3-indole), 4.39 [d, *J* = 4.9 Hz, 2H, C(2)CH<sub>2</sub>NHPh], 3.97 (t, *J* = 6.6 Hz, 2H, OCH<sub>2</sub>CH<sub>2</sub>CH<sub>2</sub>), 3.72 [s, 3H, N(1)CH<sub>3</sub>], 3.50 (s, 2H, NCH<sub>2</sub>Ph), 2.89 (d, *J* = 11.2 Hz, 2H, N(CH<sub>2</sub>)<sub>eq</sub>), 2.05–1.93 [m, 2H, N(CH<sub>2</sub>)<sub>ax</sub>], 1.82–1.80 [m, 2H, OCH<sub>2</sub>CH<sub>2</sub>CH<sub>2</sub>], 1.79–1.69 [m, 2H, N(CH<sub>2</sub>)<sub>2</sub>(CH<sub>2</sub>)<sub>eq</sub>], 1.44–1.40 (m, 2H, OCH<sub>2</sub>CH<sub>2</sub>CH<sub>2</sub>), 1.30–1.26 [m, 3H, N(CH<sub>2</sub>)<sub>2</sub>(CH<sub>2</sub>)<sub>ax</sub>CH] (the signal for C(2)CH<sub>2</sub>NHPh could not be detected); <sup>13</sup>C NMR (125 MHz, CDCl<sub>3</sub>)  $\delta$  153.5 (C5-indole), 147.8 (C'1, CH<sub>2</sub>NHC<sub>6</sub>H<sub>5</sub>), 138.7 (C'1, NCH<sub>2</sub>C<sub>6</sub>H<sub>5</sub>), 137.5 (C2), 133.2 (C7a-indole), 129.3 (2 × CH, C'3, C'5, CH<sub>2</sub>NHC<sub>6</sub>H<sub>5</sub>), 129.2 (2 × CH, NCH<sub>2</sub>C<sub>6</sub>H<sub>5</sub>), 128.1 (2 × CH, NCH<sub>2</sub>C<sub>6</sub>H<sub>5</sub>), 127.6 (C'4, NCH<sub>2</sub>C<sub>6</sub>H<sub>5</sub>), 126.8 (C3a-indole), 118.3 [CH, C'4, CH<sub>2</sub>NHC<sub>6</sub>H<sub>5</sub>], 113.0 (2 × CH, C'2, C'6, CH<sub>2</sub>NHC<sub>6</sub>H<sub>5</sub>), 112.4 (C6-indole), 109.6 (C7-indole), 103.5 (C4-indole), 100.8 (C3-indole), 69.1 (OCH<sub>2</sub>CH<sub>2</sub>CH<sub>2</sub>), 63.5 (NCH<sub>2</sub>Ph), 53.9 [2CH<sub>2</sub>, N(CH<sub>2</sub>)<sub>2</sub>(CH<sub>2</sub>)<sub>2</sub>CH], 41.0 [C(2)CH<sub>2</sub>NHPh], 35.5 [N(CH<sub>2</sub>)<sub>2</sub>(CH<sub>2</sub>)<sub>2</sub>CH], 32.9 (OCH<sub>2</sub>CH<sub>2</sub>CH<sub>2</sub>), 32.1 [2 × CH<sub>2</sub>, N(CH<sub>2</sub>)<sub>2</sub>(CH<sub>2</sub>)<sub>2</sub>CH], 30.1 [N(1)CH<sub>3</sub>], 26.8 (OCH<sub>2</sub>CH<sub>2</sub>CH<sub>2</sub>); MS (EI) *m/z* (%): 160 (15), 172 (23) [C<sub>12</sub>H<sub>14</sub>N]<sup>+</sup>, 216 (17) [C<sub>15</sub>H<sub>22</sub>N]<sup>+</sup>, 375 (100)

[C<sub>25</sub>H<sub>31</sub>N<sub>2</sub>O]<sup>+</sup>, 467 (12) [M]<sup>+</sup>. HRMS (ESI): Calcd. for C<sub>31</sub>H<sub>37</sub>N<sub>3</sub>O: 467.2937. Found: 467.2935. Bis-chlorhydrate **13·2HCl** was prepared using the usual method to afford a white solid (mp 166–168 °C). Anal. Calcd. for C<sub>31</sub>H<sub>37</sub>N<sub>3</sub>O·2HCl·1/2H<sub>2</sub>O: C, 67.75; H, 7.34; N, 7.65. Found: C, 67.94; H, 7.10; N, 8.07.

#### 4.1.17. 4-((5-(3-(1-Benzylpiperidin-4-yl)propoxy)-1-methyl-1*H*-indol-2-yl)methyl)morpholine (**14**)

Following the General procedure, reaction of (5-(3-(1-benzylpiperidin-4-yl)propoxy)-1-methyl-1*H*-indol-2-yl)(morpholino)methanone (**9**) (192 mg, 0.40 mmol) with LiAlH<sub>4</sub> (46.0 mg, 1.21 mmol) in dry dioxane (8 mL), after 5 h, and column chromatography (MeOH/CH<sub>2</sub>Cl<sub>2</sub> from 1% to 3%) gave product **14** (121 mg, 65%) as a white solid: mp 113–115 °C; IR (KBr)  $\nu$  3436, 3029, 2938, 2905, 2850, 2804, 2761, 1621, 1489, 1467, 1452, 1201, 1114 cm<sup>-1</sup>; <sup>1</sup>H NMR (500 MHz, CDCl<sub>3</sub>)  $\delta$  7.33–7.29 (m, 5H, Ph), 7.17 (d, *J* = 8.8 Hz, 1H, H7-indole), 7.01 (d, *J* = 2.5 Hz, 1H, H4-indole), 6.84 (dd, 1H, H6-indole), 6.27 (s, 1H, H3-indole), 3.96 (t, *J* = 6.8 Hz, 2H, OCH<sub>2</sub>CH<sub>2</sub>CH<sub>2</sub>), 3.76 [s, 3H, N(1)CH<sub>3</sub>], 3.67 [m, 4H, N(CH<sub>2</sub>)<sub>2</sub>(CH<sub>2</sub>)<sub>2</sub>O], 3.59 [s, 2H, C(2)CH<sub>2</sub>N(CH<sub>2</sub>)<sub>2</sub>(CH<sub>2</sub>)<sub>2</sub>O], 3.50 (s, 2H, NCH<sub>2</sub>Ph), 2.88 (d, *J* = 10.3 Hz, 2H, N(CH<sub>2</sub>)<sub>2</sub>(CH<sub>2</sub>)<sub>eq</sub>), 2.45 (m, 4H, N(CH<sub>2</sub>)<sub>2</sub>(CH<sub>2</sub>)<sub>2</sub>O), 1.94 [m, 2H, N(CH<sub>2</sub>)<sub>ax</sub>], 1.81–1.78 (m, 2H, OCH<sub>2</sub>CH<sub>2</sub>CH<sub>2</sub>), 1.76–1.68 [N(CH<sub>2</sub>)<sub>2</sub>(CH<sub>2</sub>)<sub>eq</sub>], 1.43–1.39 (m, 2H, OCH<sub>2</sub>CH<sub>2</sub>CH<sub>2</sub>), 1.29 [m, 3H, N(CH<sub>2</sub>)<sub>2</sub>(CH<sub>2</sub>)<sub>ax</sub>CH]; <sup>13</sup>C NMR (125 MHz, CDCl<sub>3</sub>)  $\delta$  153.3 (C5-indole), 136.3 (2C, C'1, Ph; C2-indole), 133.3 (C7a-indole), 129.2 (2 × CH, Ph), 128.1 (2 × CH, Ph), 127.4 (2C, C'4, Ph; C3a-indole), 112.0 (C6-indole), 109.5 (C7-indole), 103.3 (C4-indole), 102.1 (C3-indole), 69.1 (OCH<sub>2</sub>CH<sub>2</sub>CH<sub>2</sub>), 67.0 [2C, N(CH<sub>2</sub>)<sub>2</sub>(CH<sub>2</sub>)<sub>2</sub>O], 63.5 (NCH<sub>2</sub>Ph), 55.3 [C(2)CH<sub>2</sub>N(CH<sub>2</sub>)<sub>2</sub>(CH<sub>2</sub>)<sub>2</sub>O], 53.9 [2CH<sub>2</sub>, N(CH<sub>2</sub>)<sub>2</sub>(CH<sub>2</sub>)<sub>2</sub>CH], 53.4 [2C, N(CH<sub>2</sub>)<sub>2</sub>(CH<sub>2</sub>)<sub>2</sub>O], 35.5 [N(CH<sub>2</sub>)<sub>2</sub>(CH<sub>2</sub>)<sub>2</sub>CH], 32.9 (OCH<sub>2</sub>CH<sub>2</sub>CH<sub>2</sub>), 32.3 [2C, N(CH<sub>2</sub>)<sub>2</sub>(CH<sub>2</sub>)<sub>2</sub>CH], 29.9 [N(1)CH<sub>3</sub>], 26.8 (OCH<sub>2</sub>CH<sub>2</sub>CH<sub>2</sub>); MS (EI) *m/z* (%): 172 (86) [C<sub>12</sub>H<sub>14</sub>N]<sup>+</sup>, 188 (12) [C<sub>13</sub>H<sub>18</sub>N]<sup>+</sup>, 202 (10) [C<sub>14</sub>H<sub>20</sub>N]<sup>+</sup>, 216 (89) [C<sub>15</sub>H<sub>22</sub>N]<sup>+</sup>, 375 (100) [C<sub>25</sub>H<sub>31</sub>N<sub>2</sub>O]<sup>+</sup>, 461 (51) [M]<sup>+</sup>. HRMS (ESI): Calcd. for C<sub>29</sub>H<sub>39</sub>N<sub>3</sub>O<sub>2</sub>: 461.3042. Found: 461.3047. Bis-chlorhydrate **14·2HCl** was prepared using the usual method to afford a white solid (mp 249–252 °C). Anal. Calcd. for C<sub>29</sub>H<sub>39</sub>N<sub>3</sub>O<sub>2</sub>·2HCl·3/2H<sub>2</sub>O: C, 62.02; H, 7.90; N, 7.48. Found: C, 62.07; H, 7.20; N, 7.75.

#### 4.1.18. Reduction of 5-(3-(1-benzylpiperidin-4-yl)propoxy)-1-methyl-*N*-(prop-2-yn-1-yl)-1*H*-indole-2-carboxamide (**10**)

Following the General procedure, reduction of 5-(3-(1-benzylpiperidin-4-yl)propoxy)-1-methyl-*N*-(prop-2-yn-1-yl)-1*H*-indole-2-carboxamide (**10**) (50 mg, 0.11 mmol) with LiAlH<sub>4</sub> (12.8 mg, 0.33 mmol) in dry THF (5 mL), after 8 h, and column chromatography (MeOH/CH<sub>2</sub>Cl<sub>2</sub> from 1% to 3%) gave products **15** (24.7 mg, 51%) and **16** (14.1 mg, 29%). *N*-((5-(3-(1-Benzylpiperidin-4-yl)propoxy)-1-methyl-1*H*-indol-2-yl)methyl)prop-2-yn-1-amine (**15**): mp 89–92 °C; IR (KBr)  $\nu$  3436, 3301, 3269, 2919, 2862, 1621, 1490, 1472, 1451, 1198 cm<sup>-1</sup>; <sup>1</sup>H NMR (500 MHz, CDCl<sub>3</sub>)  $\delta$  7.33–7.26 (m, 5H, Ph), 7.17 (d, *J* = 8.8 Hz, 1H, H7-indole), 7.02 (d, *J* = 2.3 Hz, 1H, H4-indole), 6.84 (dd, *J* = 8.8, 2.3 Hz, 1H, H6-indole), 6.33 (s, 1H, H3-indole), 4.00 [br s, 2H, C(2)CH<sub>2</sub>NHCH<sub>2</sub>C≡CH], 3.96 (t, *J* = 6.6 Hz, 2H, OCH<sub>2</sub>CH<sub>2</sub>CH<sub>2</sub>), 3.73 [s, 3H, N(1)CH<sub>3</sub>], 3.54 (s, 2H, NCH<sub>2</sub>Ph), 3.45 [d, *J* = 2.4 Hz, 2H, C(2)CH<sub>2</sub>NHCH<sub>2</sub>C≡CH], 2.92 [d, *J* = 10.4 Hz, 2H, N(CH<sub>2</sub>)<sub>eq</sub>], 2.27 [t, *J* = 2.4 Hz, 1H, C(2)CH<sub>2</sub>NHCH<sub>2</sub>C≡CH], 1.99 (m, 2H, N(CH<sub>2</sub>)<sub>ax</sub>), 1.79–1.77 [m, 2H, OCH<sub>2</sub>CH<sub>2</sub>CH<sub>2</sub>], 1.76–1.72 [m, 2H, N(CH<sub>2</sub>)<sub>2</sub>(CH<sub>2</sub>)<sub>eq</sub>], 1.43–1.41 (m, 2H, OCH<sub>2</sub>CH<sub>2</sub>CH<sub>2</sub>), 1.39–1.32 [m, 3H, N(CH<sub>2</sub>)<sub>2</sub>(CH<sub>2</sub>)<sub>ax</sub>CH] (the signal for C(2)CH<sub>2</sub>NHCH<sub>2</sub>C≡CH could not be detected); <sup>13</sup>C NMR (126 MHz, CDCl<sub>3</sub>)  $\delta$  153.5 (C5-indole), 137.8 (2C, C'1, C<sub>6</sub>H<sub>5</sub>; C2-indole), 133.2 (C7a-indole), 129.4 (2 × CH, Ph), 128.2 (2 × CH, Ph), 127.5 (2C, C'4, Ph; C3a-indole), 112.0 (C6-indole), 109.5 (C7-indole), 103.3 (C4-indole), 100.9 (C3-indole), 81.8 (NCH<sub>2</sub>C≡CH), 76.6 (NCH<sub>2</sub>C≡CH), 69.0 (OCH<sub>2</sub>CH<sub>2</sub>CH<sub>2</sub>), 63.7 (NCH<sub>2</sub>Ph), 53.7 [2CH<sub>2</sub>, N(CH<sub>2</sub>)<sub>2</sub>(CH<sub>2</sub>)<sub>2</sub>CH], 44.1 [C(2)

$\text{CH}_2\text{NCH}_2\text{C}\equiv\text{CH}$ ], 37.1 [ $\text{N}(\text{CH}_2\text{C}\equiv\text{CH})$ ], 35.3 [ $\text{N}(\text{CH}_2)_2(\text{CH}_2)_2\text{CH}$ ], 32.8 ( $\text{OCH}_2\text{CH}_2\text{CH}_2$ ), 32.0 [ $\text{N}(\text{CH}_2)_2(\text{CH}_2)_2\text{CH}$ ], 29.7 [ $\text{N}(\text{CH}_2)_2$ ], 26.7 ( $\text{OCH}_2\text{CH}_2\text{CH}_2$ ); MS (EI)  $m/z$  (%): 172 (100) [ $\text{C}_{12}\text{H}_{14}\text{N}^+$ ], 188 (12) [ $\text{C}_{13}\text{H}_{18}\text{N}^+$ ], 202 (13) [ $\text{C}_{14}\text{H}_{20}\text{N}^+$ ], 216 (83) [ $\text{C}_{15}\text{H}_{22}\text{N}^+$ ], 374 (79) [ $\text{C}_{25}\text{H}_{30}\text{N}_2\text{O}^+$ ], 429 (33) [ $\text{M}^+$ ]. HRMS (ESI): Calcd. for  $\text{C}_{28}\text{H}_{35}\text{N}_3\text{O}$ : 429.278. Found: 429.2801. Bis-chlorhydrate **15·2HCl** was prepared using the usual method to afford a white solid (mp 204–205 °C). Anal. Calcd. for  $\text{C}_{28}\text{H}_{35}\text{N}_3\text{O} \cdot 2\text{HCl} \cdot 4/5\text{H}_2\text{O}$ : C, 64.05; H, 7.58; N, 8.09. Found: C, 64.15; H, 7.09; N, 8.25. *N-((5-(3-(1-Benzylpiperidin-4-yl)propoxy)-1-methyl-1H-indol-2-yl)methyl)prop-2-en-1-amine* (**16**): mp 57–60 °C; IR (KBr)  $\nu$  3435, 3076, 3060, 2912, 1620, 1490, 1473, 1452, 1203  $\text{cm}^{-1}$ ;  $^1\text{H}$  NMR (500 MHz,  $\text{CDCl}_3$ )  $\delta$  7.32–7.29 (m, 5H, Ph), 7.16 (d,  $J = 8.8$  Hz, 1H, H7-indole), 7.01 (d,  $J = 2.5$  Hz, 1H, H4-indole), 6.83 (dd,  $J = 8.8, 2.5$  Hz, 1H, H6-indole), 6.28 (s, 1H, H3-indole), 5.91 (m, 1H,  $\text{NCH}_2\text{CH}=\text{CH}_2$ ), 5.21 (dd,  $J = 17.1, 1.5$  Hz, 1H,  $\text{NCH}_2\text{CH}=\text{CH}_2$ ), 5.12 (dd,  $J = 10.3, 1.5$  Hz, 1H,  $\text{NCH}_2\text{CH}=\text{CH}_2$ ), 3.96 (t,  $J = 6.6$  Hz, 2H,  $\text{OCH}_2\text{CH}_2\text{CH}_2$ ), 3.89 [s, 2H,  $\text{C}(2)\text{CH}_2\text{NHCH}_2\text{CH}=\text{CH}_2$ ], 3.73 [s, 3H,  $\text{N}(\text{CH}_3)$ ], 3.51 (br s, 2H,  $\text{NCH}_2\text{Ph}$ ), 3.32 (m, 2H,  $\text{NHCH}_2\text{CH}=\text{CH}_2$ ), 2.90 [d,  $J = 10.2$  Hz, 2H,  $\text{N}(\text{CH}_2)_{\text{eq}}$ ], 1.97 [m, 2H,  $\text{N}(\text{CH}_2)_{\text{ax}}$ ], 1.81–1.78 (m, 2H,  $\text{OCH}_2\text{CH}_2\text{CH}_2$ ), 1.70–1.68 [m, 2H,  $\text{N}(\text{CH}_2)_2(\text{CH}_2)_{\text{eq}}$ ], 1.59 (br s, 1H,  $\text{NHCH}_2\text{CH}=\text{CH}_2$ ), 1.42–1.40 (m, 2H,  $\text{OCH}_2\text{CH}_2\text{CH}_2$ ), 1.30 [m, 3H,  $\text{N}(\text{CH}_2)_2(\text{CH}_2)_{\text{ax}}\text{CH}$ ];  $^{13}\text{C}$  NMR (126 MHz,  $\text{CDCl}_3$ )  $\delta$  153.3 (C5-indole), 139.0 (C2-indole), 136.6 ( $\text{NHCH}=\text{CH}_2$ ), 133.2 (C7a-indole), 129.3 (C1, Ph), 128.1 (2 $\times$  CH, Ph), 127.6 (C3a-indole), 126.9 (2 $\times$  CH, Ph), 116.2 ( $\text{NHCH}=\text{CH}_2$ ), 111.9 (C6-indole), 109.5 (C7-indole), 103.4 (C4-indole), 100.2 (C3-indole), 69.1 ( $\text{OCH}_2\text{CH}_2\text{CH}_2$ ), 63.4 ( $\text{NCH}_2\text{Ph}$ ), 53.8 [ $2\text{CH}_2$ ,  $\text{N}(\text{CH}_2)_2(\text{CH}_2)_2\text{CH}$ ], 51.7 [ $\text{C}(2)\text{CH}_2\text{NCH}_2\text{CH}=\text{CH}_2$ ], 45.1 [ $\text{C}(2)\text{CH}_2\text{NCH}_2\text{CH}=\text{CH}_2$ ], 35.5 [ $\text{N}(\text{CH}_2)_2(\text{CH}_2)_2\text{CH}$ ], 32.9 ( $\text{OCH}_2\text{CH}_2\text{CH}_2$ ), 32.2 [ $\text{N}(\text{CH}_2)_2(\text{CH}_2)_2\text{CH}$ ], 29.8 [ $\text{N}(\text{CH}_3)$ ], 26.8 ( $\text{OCH}_2\text{CH}_2\text{CH}_2$ ); MS (EI)  $m/z$  (%): 172 (52) [ $\text{C}_{12}\text{H}_{14}\text{N}^+$ ], 188 (7) [ $\text{C}_{13}\text{H}_{18}\text{N}^+$ ], 202.2 (6) [ $\text{C}_{14}\text{H}_{20}\text{N}^+$ ], 216 (45) [ $\text{C}_{15}\text{H}_{22}\text{N}^+$ ], 374 (100) [ $\text{C}_{25}\text{H}_{30}\text{N}_2\text{O}^+$ ], 431 (24) [ $\text{M}^+$ ]; HRMS (ESI): Calcd. for  $\text{C}_{28}\text{H}_{37}\text{N}_3\text{O}$ : 429.2937. Found: 429.2934. Bis-chlorhydrate **16·2HCl** was prepared using the usual method to afford a white solid (mp 225–226 °C). Anal. Calcd. for  $\text{C}_{28}\text{H}_{37}\text{N}_3\text{O} \cdot 2\text{HCl} \cdot 3/5\text{H}_2\text{O}$ : C, 62.91; H, 7.98; N, 7.86. Found: C, 62.72; H, 7.24; N, 8.19.

## 4.2. Pharmacology

### 4.2.1. Cholinesterase activity

Cholinesterase activities were assessed following a spectrophotometric method [32] using AChE from *Electrophorus electricus* (type V-S) and BuChE from equine serum (lyophilized powder) (Sigma–Aldrich, Madrid, Spain). Donepezil and **ASS234** were used as standard compounds. Enzymatic reactions took place in 96-well plates in a final volume of 300  $\mu\text{L}$  containing 0.1 M phosphate buffer (pH 8.0), 0.035 U/ml AChE or 0.05 U/ml BuChE and 0.35 mM of 5,5'-dithiobis-2-nitrobenzoic acid (DTNB, Sigma–Aldrich, Madrid, Spain). Inhibition curves were plotted by pre-incubating this mixture with serial dilutions of each compound for 20 min at 37 °C. The activity in absence of compound was always performed to determine the 100% of enzyme activity. At the end of the pre-incubation period, 50  $\mu\text{L}$  of substrate were added to a final concentration of 0.35 mM acetylthiocholine iodide or 0.5 mM butyrylthiocholine iodide (Sigma–Aldrich). Enzymatic reactions were allowed for 5 min incubation for AChE and 25 min for BuChE as the yellowish anion 5-thio-2-nitrobenzoic acid is continuously produced due to the DTNB oxidation along with the enzymatic degradation of both substrates. Changes in absorbance were detected at 405 nm in a spectrophotometric plate reader (FluoStar OPTIMA, BMG Labtech). Color generation is reduced as the enzymatic activities are inhibited by the compounds and  $\text{IC}_{50}$  values were calculated at the compound concentration that produces 50% of enzymatic activity inhibition by using the GraphPad 'PRISM' software

(version 3.0). Data are expressed as mean  $\pm$  SEM of at least three different experiments performed in triplicate.

### 4.2.2. Monoamine oxidase activity

Monoamine oxidase activities from recombinant human MAO A and MAO B (Sigma–Aldrich, Madrid, Spain) were performed using a fluorometric method [33]. Tyramine hydrochloride was used as substrate for both enzymes in a 96-well black opaque microplates (OptiPlate-96F, PerkinElmer) in a final volume of 200  $\mu\text{L}$ . Serial dilutions of each inhibitor were pre-incubated for 30 min at 37 °C with 0.36 U/mL hMAO A or 0.0675 U/mL hMAO B. Following the pre-incubations, enzymatic reactions were started by adding 100  $\mu\text{L}$  of a mixture containing 1 mM tyramine, 0.04 U/ml horseradish peroxidase (HRP) and 25  $\mu\text{M}$  Amplex UltraRed reagent in 0.25 mM sodium phosphate (pH 7.4) as final concentrations. The fluorescence production associated with peroxidase-coupled production of resorufin from Amplex UltraRed was continuously measured for at least one hour at 530 nm in a spectrophotometric plate reader (FluoStar OPTIMA, BM G Labtech). Control experiments were carried out simultaneously by replacing the inhibitors by distilled water. In addition, the possible capacity of compounds to modify the fluorescence generated in the reaction mixture due to non-enzymatic inhibition was determined by adding these compounds to solutions containing only the Amplex UltraRed reagent in a sodium phosphate buffer. Substrate-free samples were used as blanks. Dose–response curves were plotted by using the GraphPad 'PRISM' software (version 3.0) and  $\text{IC}_{50}$  values were accordingly calculated. Data are expressed as mean  $\pm$  SEM of at least three different experiments performed in triplicate.

## 4.3. Molecular modeling

### 4.3.1. Molecular docking into AChE and BuChE

Compound **15** was assembled as hydrochloride and free base within Discovery Studio, version 2.1, software package, using standard bond lengths and bond angles. With the CHARMM force field [62] and partial atomic charges, the molecular geometry of **15** was energy-minimized using the adopted-based Newton–Raphson algorithm. Structures were considered fully optimized when the energy changes between iterations were less than 0.01 kcal/mol [63].

### 4.3.2. Molecular docking of compound **15** into EeAChE

The coordinates of *E. electricus* AChE (PDB ID: 1C2B), were obtained from the Protein Data Bank (PDB). For docking studies, initial protein was prepared by removing all water molecules, heteroatoms, any co-crystallized solvent and the ligand. Proper bonds, bond orders, hybridization and charges were assigned using protein model tool in Discovery Studio, version 2.1, software package. CHARMM force field was applied using the receptor–ligand interactions tool in Discovery Studio, version 2.1, software package. Docking calculations were performed with the program Autodock Vina [34]. AutoDockTools (ADT; version 1.5.4) was used to add hydrogens and partial charges for proteins and ligands using Gas-teiger charges. Flexible torsions in the ligands were assigned with the AutoTors module, and the acyclic dihedral angles were allowed to rotate freely. Trp286, Tyr124, Tyr337, Tyr72, Asp74, Thr75, Trp86, and Tyr341 receptor residues were selected to keep flexible during docking simulation using the AutoTors module. Because VINA uses rectangular boxes for the binding site, the box center was defined and the docking box was displayed using ADT. For *E. electricus* AChE (PDB ID: 1C2B) the docking procedure was applied to whole protein target, without imposing the binding site ("blind docking"). Using the GridBox option, the 3-dimensional parameters for docking the ligand to the protein were determined; the grid center coordinates

were  $x = 21.5911$ ,  $y = 87.752$ ,  $z = 23.591$  and the size coordinates were  $x = 60$ ,  $y = 60$ ,  $z = 72$  with grid points separated 1 Å. Default parameters were used except num\_modes, which was set to 40. The AutoDock Vina docking procedure used was previously validated [64].

#### 4.3.3. Molecular docking of inhibitor **15** into eqBuChE

The eqBuChE model has been retrieved from the SWISS-MODEL Repository. This is a database of annotated three-dimensional comparative protein structure models generated by the fully automated homology-modeling pipeline SWISS-MODEL. A putative three-dimensional structure of eqBuChE has been created based on the crystal structure of hBuChE (PDB ID: 2PM8), these two enzyme exhibited 89% sequence identity. Proper bonds, bond orders, hybridization and charges were assigned using protein model tool in Discovery Studio, version 2.1, software package. CHARMM force field was applied using the receptor–ligand interactions tool in Discovery Studio, version 2.1, software package. Docking calculations were performed following the same protocol described before for EeAChE. All dockings were performed as blinds dockings where a cube of 75 Å with grid points separated 1 Å, was positioned at the middle of the protein ( $x = 29.885$ ;  $y = -54.992$ ;  $z = 58.141$ ). Default parameters were used except num\_modes, which was set to 40. The lowest docking-energy conformation was considered as the most stable orientation. Finally, the docking results generated were directly loaded into Discovery Studio, version 2.1.

#### 4.3.4. Molecular docking of compound **15** into human MAO A/B

Compound **15** was assembled as non-protonated amine within Discovery Studio, version 2.1, software package, following the procedure described before for cholinesterases. The crystal structures of human MAO A in complex with harmine (PDB ID 2Z5X) and human MAO B in complex with safinamide (PDB ID 2V5Z) were obtained from the Protein Data Bank. For docking studies initial proteins were prepared. First, in the PDB crystallographic structures any co-crystallized solvent and the ligand were removed. Then, proper bonds, bond orders, hybridization and charges were assigned using protein model tool in Discovery Studio, version 2.1, software package. CHARMM force field was applied using the receptor–ligand interactions tool in Discovery Studio, version 2.1, software package. Six water molecules located around the FAD cofactor were considered in the docking experiments because of their well-known role into the MAO's inhibition. Finally, atoms of the FAD cofactor were defined in their oxidized state. Docking calculations were performed following the same protocol described before for EeAChE. For MAO-A, the grid center coordinates were  $x = 54.181$ ,  $y = 160.270$ ,  $z = 22.052$  and the size coordinates were  $x = 50$ ,  $y = 40$ ,  $z = 40$  with grid points separated 1 Å; for MAO-B, the grid center coordinates were  $x = 55.743$ ,  $y = 161.175$ ,  $z = 19.420$  and the size coordinates were  $x = 46$ ,  $y = 40$ ,  $z = 40$  with grid points separated 1 Å. Default parameters were used except num\_modes, which was set to 40. According to Vina best scored poses, the most stable complex configurations were considered. The docked ligand output files was viewed and atomic distances and interactions were analyzed using Discovery Studio.

#### Acknowledgments

This work was supported by the COST action CM1103. KN acknowledge project supported by the Ministry of Education and Science of the Republic of Serbia, Contract #172033. JMC and MU thank MINECO (Spain) for support (SAF2008-07271; SAF2012-33304). OMBA thanks MINECO (Spain) for a fellowship (BES-2010-037196).

#### Appendix A. Supplementary material

Supplementary data related to this article can be found at <http://dx.doi.org/10.1016/j.ejmech.2013.12.028>.

#### References

- [1] M. Goedert, M.G.A. Spillantini, *Science* 314 (2006) 777–781.
- [2] I. Grundke-Iqbal, K. Iqbal, Y.C. Tung, M. Quinlan, H.M. Wisniewski, L.I. Binder, *Proc. Natl. Acad. Sci. U. S. A.* 93 (1986) 4913–4917.
- [3] A. Gella, N. Durany, *Cell. Adhes. Migr.* 3 (2009) 88–93.
- [4] V.N. Talesa, *Mech. Ageing Dev.* 122 (2001) 1961–1969.
- [5] J. Birks, E.J. Grimley, V. Iakovidou, *Cochrane Database Syst. Rev.* (2000) CD001191.
- [6] M. Racchi, M. Mazzucchelli, E. Porrello, C. Lanni, S. Govoni, *Pharm. Res.* 50 (2004) 441–451.
- [7] R. León, A.G. García, J. Marco-Contelles, *Med. Res. Rev.* 33 (2013) 139–189.
- [8] K.L. Davis, P. Powchick, *Lancet* 345 (1995) 625–630.
- [9] C.M. Spencer, S. Noble, *Drugs Aging* 13 (1998) 391–400.
- [10] E.L. Barner, S.L. Gray, *Ann. Pharmacother.* 32 (1998) 70–77.
- [11] M.B. Youdim, D. Edmonson, K.F. Tipton, *Nat. Rev. Neurosci.* 7 (2006) 295–309.
- [12] P. Riederer, W. Danielczyk, E. Grünblatt, *Neurotoxicology* 25 (2004) 271–277.
- [13] N. Pizzinat, N. Copin, C. Vindis, A. Parini, C. Cambon, Naunyn-Schmiedeberg's *Arch. Pharmacol.* 359 (1999) 428–431.
- [14] B.S. Kristal, A.D. Conway, A.M. Brown, J.C. Jain, P.A. Ulluci, S.W. Li, J.W. Burke, *Free Radical Biol. Med.* 30 (2001) 924–931.
- [15] J. Sterling, Y. Herzig, T. Goren, N. Finkelstein, D. Lerner, W. Goldenberg, I. Miskolczi, S. Molnar, F. Rantal, T. Tamas, G. Toth, A. Zagyva, A. Zekany, G. Lavian, A. Gross, R. Friedman, M. Razin, W. Huang, B. Kraiss, M. Chorev, M.B. Youdim, M. Weinstock, *J. Med. Chem.* 45 (2002) 5260–5279.
- [16] M. Yogeve-Falach, O. Bar-Am, T. Amit, O. Weinreb, M.B. Youdim, *FASEB J.* 20 (2006) 2177–2179.
- [17] M.B. Youdim, M. Weinstock, *Cell. Mol. Neurobiol.* 21 (2002) 555–573.
- [18] O. Bar-Am, T. Amit, O. Weinreb, M.B. Youdim, S. Mandel, *J. Alzheimers Dis.* 21 (2010) 361–371.
- [19] F.O. Brühlmann, P.-A. Carrupt, B. Testa, M. Catto, F. Leonetti, C. Altomare, A. Carotti, *J. Med. Chem.* 44 (2001) 3195–3198.
- [20] A. Cavalli, M.L. Bolognesi, M. Minarini, V. Rosini, M. Tumiatti, C. Recanatini, C. Melchiorre, *J. Med. Chem.* 51 (2008) 347–372.
- [21] A. Samadi, M. Chioua, I. Bolea, C. de los Ríos, I. Iriepa, I. Moraleda, A. Bastida, G. Esteban, M. Unzeta, E. Gálvez, J. Marco-Contelles, *Eur. J. Med. Chem.* 46 (2011) 4665–4668.
- [22] I. Bolea, J. Juárez-Jiménez, C. de los Ríos, M. Chioua, R. Pouplana, F.J. Luque, M. Unzeta, J. Marco-Contelles, A. Samadi, *J. Med. Chem.* 54 (2011) 8251–8270.
- [23] V. Pérez, J.L. Marco, E. Fernández-Álvarez, M. Unzeta, *Br. J. Pharmacol.* 127 (1999) 869–876.
- [24] B. Cutillas, S. Ambrosio, M. Unzeta, *Neurosci. Lett.* 329 (2002) 165–168.
- [25] G. Prat, V. Pérez, A. Rubí, M. Casas, M. Unzeta, *J. Neural. Transm.* 107 (2000) 409–417.
- [26] I. Bolea, A. Gella, L. Monjas, C. Pérez, M.I. Rodríguez-Franco, J. Marco-Contelles, A. Samadi, M. Unzeta, *Curr. Alzheimer Res.* 10 (2013) 797–808.
- [27] G. La Regina, R. Silvestri, V. Gatti, A. Lavecchia, E. Novellino, O. Befani, P. Turini, E. Agostinelli, *Bioorg. Med. Chem.* 16 (2008) 9729–9740.
- [28] M.L. Wu, J.F. Deng, *J. Chin. Med. Assoc.* 72 (2009) 446–449.
- [29] C. Fernández-García, J.L. Marco, E. Fernández-Álvarez, *Tetrahedron* 48 (1992) 6917–6928.
- [30] M.A. Cruces, C. Elorriaga, E. Fernández-Álvarez, O. Nieto López, *O. Eur. J. Med. Chem.* 25 (1990) 257–265.
- [31] P.C. Unangst, D.Y. Connor, S.R. Miller, R. Steven, *J. Heterocycl. Chem.* 33 (1996) 1627–1630.
- [32] G.L. Ellman, K.D. Courtney, B.J. Andrés, R.M. Featherstone, *Biochem. Pharmacol.* 7 (1961) 88–95.
- [33] M. Zhou, N. Panchuk-Valashina, *Anal. Biochem.* 253 (1997), 169–174.
- [34] O. Trott, A.J. Olson, *J. Comput. Chem.* 31 (2010) 455–461.
- [35] K. Arnold, L. Bordoli, J. Kopp, T. Schwede, *Bioinformatics* 22 (2006) 195–201.
- [36] F. Kiefer, K. Arnold, M. Künzli, L. Bordoli, T. Schwede, *Nucleic Acids Res.* 37 (2009) D387–D392.
- [37] M.C. Peitsch, *Biotechnology* 13 (1995) 658–660.
- [38] D.E. Edmonson, A. Mattevi, C. Binda, M. Li, F. Hubálek, *Curr. Med. Chem.* 11 (2004) 1983–1993.
- [39] T.Z.E. Jones, D. Balsa, M. Unzueta, R.R. Ramsay, *J. Neural. Transm.* 114 (2007) 707–712.
- [40] J. Wang, D.E. Edmonson, *Biochemistry* 50 (2011) 7710–7717.
- [41] R.A. Scerrer, A.J. Leo, *Mol. Inform.* 30 (2011) 386.
- [42] A. Samadi, C. de los Ríos, I. Bolea, M. Chioua, I. Iriepa, I. Moraleda, M. Bartolini, B. Andrisano, E. Gálvez, C. Valderas, M. Unzeta, J. Marco-Contelles, *Eur. J. Med. Chem.* 52 (2012) 251–262.
- [43] J. Ma, M. Yoshimura, E. Yamashita, A. Nakagawa, A. Ito, T. Tsukihara, *J. Mol. Biol.* 338 (1) (2004) 103–114.
- [44] AMET Predictor, v.6.5, Simulations Plus, Inc., Lancaster, CA, 2013.
- [45] ACD/Percepta 14.0.0, Advanced Chemistry Development, 2013.
- [46] I. Moriguchi, S. Hirono, Q. Liu, I. Nakagome, Y. Matsushita, *Chem. Pharm. Bull.* 40 (1992) 127–130.

- [47] C.A. Lipinski, F. Lombardo, B.W. Dominy, P.J. Feeney, *Adv. Drug Delivery Rev.* 46 (2001) 3–26.
- [48] H. Van de Waterbeemd, F. Atkinson, S. Cole, C. Green, *Curr. Med. Chem Cent. Nerv. Syst. Agents* 2 (2002) 229–240.
- [49] H. Van de Waterbeemd, G. Camenish, G. Folkers, J.R. Chretien, O.A. Raevsky, *J. Drug Target.* 6 (1998) 151–165.
- [50] J. Kelder, P.D.J. Grootenhuis, D.M. Bayada, L.P.C. Delbressine, J.-P. Ploemen, *Pharm. Res.* 16 (1999) 1514–1519.
- [51] P.A. Nielsen, O. Andersson, S.H. Hansen, K.B. Simonsen, G. Andersson, *Drug. Discov. Today* 16 (2011) 472–475.
- [52] X. Ma, C. Chen, J. Yang, *Acta Pharmacol. Sin.* 26 (2005) 500–512.
- [53] A. Sjöberg, M. Lutz, C. Tannergren, C. Wingolf, A. Borde, A.L. Ungell, *Eur. J. Pharm. Sci.* 48 (2013) 166–180.
- [54] J.D. Irvine, L. Takahashi, K. Lockhart, J. Cheong, J.W. Tolan, H.E. Selick, *J. Pharm. Sci.* 88 (1999) 28–33.
- [55] S. Yee, *Pharm. Res.* 14 (1997) 763–766.
- [56] S. Yamashita, T. Furubayashi, M. Kataoka, T. Sakane, H. Sezaki, H. Tokuda, *Eur. J. Pharm. Sci.* 10 (2000) 195–204.
- [57] L.S. Gold, N.B. Manley, T.H. Slone, L. Rohrbach, *Environ. Health Perspect.* 107 (Suppl. 4) (1999) 527–600.
- [58] H. Van de Waterbeemd, D.A. Smith, K. Beaumont, D.K. Walker, *J. Med. Chem.* 44 (2001) 1313–1333.
- [59] S. Ekins, *Drug. Discov. Today* 9 (2004) 276–285.
- [60] E.J. Matthews, N.L. Kruhlak, R.D. Benz, J.F. Contreras, *Curr. Drug. Discov. Technol.* 1 (2004) 61–76.
- [61] L.G. Valerio, K.B. Arvidson, R.F. Chanderbhan, J.F. Contreras, *Toxicol. Appl. Pharmacol.* 222 (2007) 1–16.
- [62] B.R. Brooks, R.E. Brucoleri, B.D. Olafson, D.J. States, S. Swaminathan, M. Karplus, M. Charrm, *J. Comput. Chem.* 4 (1983) 187–217.
- [63] A. Morreale, F. Maseras, I. Iriepa, E. Gálvez, *J. Mol. Graph. Modell.* 21 (2002) 111–118.
- [64] M. Bartolini, M. Pistozzi, V. Andrisano, J. Egea, M.G. López, I. Iriepa, I. Moraleda, E. Gálvez, J. Marco-Contelles, A. Samadi, *ChemMedChem* 6 (2011) 1990–1997.

# Multipotent cholinesterase/monoamine oxidase inhibitors for the treatment of Alzheimer's disease: design, synthesis, biochemical evaluation, ADMET, molecular modeling, and QSAR analysis of novel donepezil-pyridyl hybrids

Oscar M Bautista-Aguilera<sup>1,\*</sup>  
Gerard Esteban<sup>2,\*</sup>  
Mourad Chioua<sup>1</sup>  
Katarina Nikolic<sup>3</sup>  
Danica Agbaba<sup>3</sup>  
Ignacio Moraleda<sup>4</sup>  
Isabel Iriepa<sup>4</sup>  
Elena Soriano<sup>5</sup>  
Abdelouahid Samadi<sup>1</sup>  
Mercedes Unzeta<sup>2</sup>  
José Marco-Contelles<sup>1</sup>

<sup>1</sup>Laboratory of Medicinal Chemistry (Institute of General Organic Chemistry [IQOG], National Research Council [CSIC]), Madrid, Spain; <sup>2</sup>Department of Biochemistry and Molecular Biology, Institute of Neurosciences, Autonomous Barcelona University, Barcelona, Spain; <sup>3</sup>Institute of Pharmaceutical Chemistry, Faculty of Pharmacy, University of Belgrade, Belgrade, Serbia; <sup>4</sup>Department of Organic Chemistry, Faculty of Pharmacy, University of Alcalá, Ctra Barcelona, Alcalá de Henares, Spain; <sup>5</sup>Synthesis, and Structure of Organic Compounds (SEPCO) (IQOG, CSIC), Madrid, Spain

\*These authors have equally contributed to this work

Correspondence: José Marco-Contelles  
Laboratorio de Química Médica  
(IQOG, CSIC), C/Juan de la Cierva 3,  
28006-Madrid, Spain  
Fax +34 91 546 4853  
Email iqoc21@iqog.csic.es

**Abstract:** The design, synthesis, and biochemical evaluation of donepezil-pyridyl hybrids (DPHs) as multipotent cholinesterase (ChE) and monoamine oxidase (MAO) inhibitors for the potential treatment of Alzheimer's disease (AD) is reported. The 3D-quantitative structure-activity relationship study was used to define 3D-pharmacophores for inhibition of MAO A/B, acetylcholinesterase (AChE), and butyrylcholinesterase (BuChE) enzymes and to design DPHs as novel multi-target drug candidates with potential impact in the therapy of AD. DPH14 (*Electrophorus electricus* AChE [EeAChE]: half maximal inhibitory concentration [ $IC_{50}$ ] =  $1.1 \pm 0.3$  nM; equine butyrylcholinesterase [eqBuChE]:  $IC_{50}$  =  $600 \pm 80$  nM) was 318-fold more potent for the inhibition of AChE, and 1.3-fold less potent for the inhibition of BuChE than the reference compound ASS234. DPH14 is a potent human recombinant BuChE (hBuChE) inhibitor, in the same range as DPH12 or DPH16, but 13.1-fold less potent than DPH15 for the inhibition of human recombinant AChE (hAChE). Compared with donepezil, DPH14 is almost equipotent for the inhibition of hAChE, and 8.8-fold more potent for hBuChE. Concerning human monoamine oxidase (hMAO) A inhibition, only DPH9 and 5 proved active, compound DPH9 being the most potent ( $IC_{50}$  [MAO A] =  $5,700 \pm 2,100$  nM). For hMAO B, only DPHs 13 and 14 were moderate inhibitors, and compound DPH14 was the most potent ( $IC_{50}$  [MAO B] =  $3,950 \pm 940$  nM). Molecular modeling of inhibitor DPH14 within EeAChE showed a binding mode with an extended conformation, interacting simultaneously with both catalytic and peripheral sites of EeAChE thanks to a linker of appropriate length. Absorption, distribution, metabolism, excretion and toxicity analysis showed that structures lacking phenyl-substituent show better druglikeness profiles; in particular, DPHs13–15 showed the most suitable absorption, distribution, metabolism, excretion and toxicity properties. Novel donepezil-pyridyl hybrid DPH14 is a potent, moderately selective hAChE and selective irreversible hMAO B inhibitor which might be considered as a promising compound for further development for the treatment of AD.

**Keywords:** donepezil-pyridyl hybrids, ChE, MAO, 3D-QSAR, molecular modeling, ADMET

## Introduction

Alzheimer's disease (AD) is a neurodegenerative disorder characterized by dementia and other cognitive impairments.<sup>1</sup> Previous biochemical studies indicated that amyloid- $\beta$  (A $\beta$ ) deposits,<sup>2</sup> hyperphosphorylated  $\tau$ -protein aggregation,<sup>3</sup> and oxidative stress<sup>4</sup> play crucial roles in the pathophysiology of the disease. AD is characterized by a selective loss of cholinergic neurons as a consequence of decreasing levels of

acetylcholine (ACh) in specific brain regions that mediate memory and learning functions.<sup>5</sup> Inhibitors of acetylcholinesterase (AChE; EC 1.1.1.7) prevent the hydrolysis of ACh and thus increase ACh concentration in the synaptic cleft. Donepezil,<sup>6</sup> galantamine,<sup>7</sup> and rivastigmine<sup>8</sup> are US Food and Drug Administration (FDA)-approved drugs that improve AD symptoms by inhibiting AChE. Also, some symptoms of AD are related to the alterations in the dopaminergic<sup>9</sup> and serotonergic neurotransmitter systems.<sup>10</sup>

Monoamine oxidase (MAO; EC 1.4.3.4) is the enzyme that catalyzes the oxidative deamination of various biogenic amines,<sup>11</sup> rendering the corresponding aldehyde, ammonia, and hydrogen peroxide as metabolic products. Thus, MAO inhibitors might increase amine neurotransmission and exert valuable biochemical effects in the treatment of AD.<sup>11</sup> Increased levels of MAO B due to enhanced astrogliosis in the brain of AD patients has been reported,<sup>12</sup> indicating that dual inhibition of MAO A/B may be valuable AD therapy. Beneficial properties of MAO inhibitors are also related to the reduction of the formation of the reactive oxygen species, which may influence the increased neuronal damage.<sup>13,14</sup> Finally, recent biochemical and clinical studies indicated that the propargylamine group of the MAO B inhibitors, such as rasagiline and ladostigil, is responsible for neuroprotective, antiapoptotic activities,<sup>15–17</sup> and inhibitory effect on the A $\beta$  aggregation of these compounds.<sup>18</sup>

Because of the multifactorial nature of AD and diverse cerebral mechanisms implicated in the control of AD,<sup>1,11</sup> multi-target-directed ligands have been extensively examined as novel drug candidates with beneficial effects in therapy of AD.<sup>7,15,19,20</sup>

In this context, in previous communications from our laboratory, we have identified the pyridine structural and

functional motif affording molecules endowed with cholinesterase inhibition potential.<sup>21</sup>

Our recently synthesized hybrids<sup>22</sup> exerted appreciable MAO A/B, AChE, and butyrylcholinesterase (BuChE) inhibitory activity. These molecules, exemplified by the most attractive compound ASS234 (Figure 1), are hybrids of donepezil, a potent AChE inhibitor currently used to treat AD, and PF9601N, an inhibitor of MAO B,<sup>23</sup> connected through an appropriate linker to facilitate the binding of both *N*-benzylpiperidine and indole-propargylamine moieties at catalytic anionic site (CAS) and peripheral anionic site (PAS), respectively, in AChE.

With these ideas in mind, we have designed, synthesized, and submitted to biochemical evaluation donepezil-pyridyl hybrids (DPHs) of type I (Figure 1), as multipotent ChE and MAO inhibitors.

In a recent communication we have reported preliminary results on DPHs1–8 (Figure 2).<sup>24</sup> These compounds are based on donepezil and ASS234 by fixing the *N*-benzylpiperidine motif linked by a methylene carbon chain ( $n=0$  to 3) attached through an amino group to C2 of a pyridine substituted with a phenyl group or a hydrogen at C4, used now as the central heterocyclic core instead of the indole motif, while retaining the *N*(H,Me)-propargylamine moiety at C6. We have observed<sup>24</sup> that most of these DPHs showed no MAO inhibition activity, and that the only active compound (DPH5) was a very weak MAO A inhibitor (Table 1).<sup>24</sup> Consequently, more work was needed in order to improve in power and selectivity the multipotent profile of our molecules. As a result, we have synthesized new DPHs9–16 (Table 1), and report here the biochemical evaluation for the inhibition of MAO A/B, AChE, and BuChE, as well as a 3D-quantitative

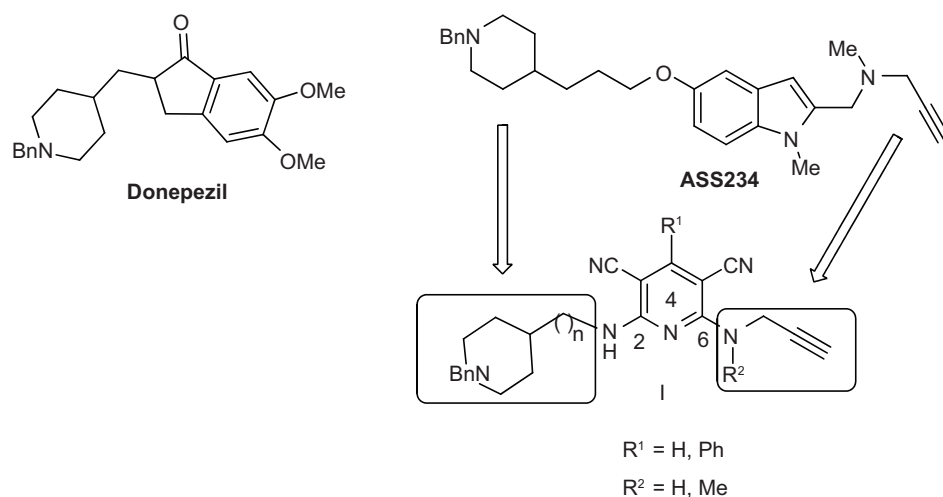


**Figure 1** General structure of donepezil, ASS234, and donepezil-pyridyl hybrids (DPHs) (I) described here. **Abbreviations:** Bn, benzyl; Me, methyl; Ph, phenyl.

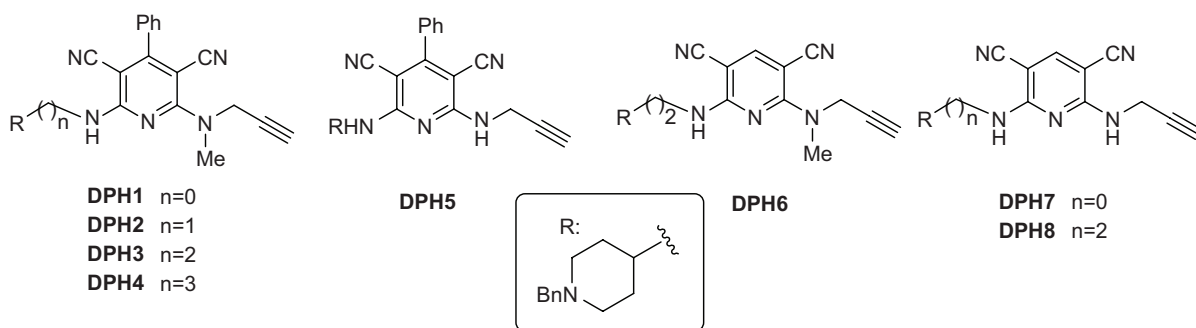


**Figure 2** Recently reported donepezil-pyridyl hybrids (DPHs1–8).

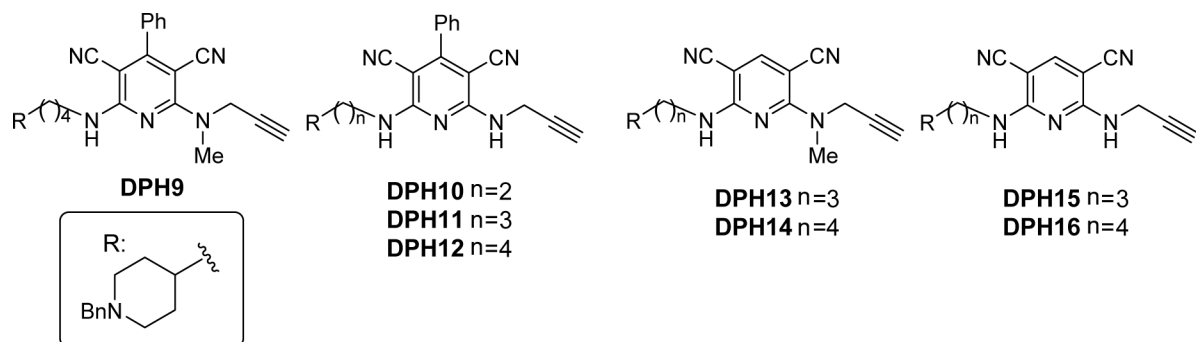
**Note:** Data from Samadi A, Chioua M, Bolea I, et al. Synthesis, biological assessment and molecular modeling of new multipotent MAO and cholinesterase inhibitors as potential drugs for the treatment of Alzheimer's disease. *Eur J Med Chem.* 2011;46(9):4665–4668.<sup>24</sup>

**Abbreviations:** Bn, benzyl; Me, methyl; Ph, phenyl.

structure-activity relationship (QSAR) study used to define specific molecular determinants for MAO A/B, AChE, and BuChE inhibition and to create QSAR models for evaluation of MAO A/B, AChE, and BuChE activity of the designed

multipotent inhibitors. From this work, we have identified the novel donepezil-pyridyl hybrid DPH14 as a moderately potent, selective AChE and MAO B inhibitor, whose molecular modeling has also been investigated.

**Table I** Inhibition ( $IC_{50}$  [ $\mu$ M]) of *Electrophorus electricus* acetylcholinesterase (EeAChE), equine serum butyrylcholinesterase (eqBuChE) and human monoamine oxidase (hMAO A and hMAO B) by ASS234, donepezil, and DPHs1–16



Drug	$IC_{50}$ (nM) <sup>a</sup>		Selectivity BuChE/AChE	$IC_{50}$ (nM) <sup>a</sup>		Selectivity MAO B/MAO A
	EeAChE	eqBuChE		hMAO A	hMAO B	
DPH1 <sup>24</sup>	1,200±200	>100	>83	>100	>100	nd
DPH2 <sup>24</sup>	270±52	5,000±700	18	>100	>100	nd
DPH3 <sup>24</sup>	16±2	1,110±30	69	>100	>100	nd
DPH4 <sup>24</sup>	14±1	230±30	16.4	>100	>100	nd
DPH5 <sup>24</sup>	4,000±100	>100	>25	14,100±3,800	>100	>7.1
DPH6 <sup>24</sup>	13±1	3,100±300	238	>100	>100	nd
DPH7 <sup>24</sup>	530±70	>100	>189	>100	>100	nd
DPH8 <sup>24</sup>	16±2	>100	>6,250	>100	>100	nd
DPH9	23±3	220±10	9.6	5,700±2,100	>100	>17
DPH10	31±7	>100	>18,083	>100	>100	nd
DPH11	19±5	>100	>5,379	>100	>100	nd
DPH12	1.7±0.3	840±100	494	>100	>100	nd
DPH13	6.2±1.4	1,120±160	181	>100	6,110±1,400 <sup>b</sup>	<0.06
DPH14	1.1±0.3	600±80	545	>100	3,950±940	<0.039
DPH15	4.7±0.5	2,030±370	434	>100	>100	nd
DPH16	1.3±0.3	530±60	408	>50	>50	nd
ASS234	350±10	460±60	1.3	4±1	39±4	9.2
Donepezil	13±10	6,910±1,250	532	>100	15,000±2,200	<0.15

**Notes:** <sup>a</sup>Values are expressed as mean ± standard error of the mean of at least three different experiments in quadruplicate. <sup>b</sup>Residual activity (10%–20%) was observed.

**Abbreviations:** Bn, benzyl; DPHs, donepezil-pyridyl hybrids; nd, not determinable;  $IC_{50}$ , concentration of compound that produces 50% activity inhibition; Me, methyl; MAO, monoamine oxidase; Ph, phenyl.

## Materials and methods

### General

Melting points were determined on a Koffler apparatus, and are uncorrected. Infrared spectra were recorded in a Perkin-Elmer apparatus ("Spectrum One"; PerkinElmer Inc., Waltham, MA, USA).  $^1\text{H}$  nuclear magnetic resonance (NMR) and  $^{13}\text{C}$  NMR spectra were recorded in deuterated chloroform ( $\text{CDCl}_3$ ) or deuterated dimethylsulfoxide ( $\text{DMSO-d}_6$ ) at 300, 400, or 500 MHz and at 75, 100, or 125 MHz, respectively, in a Bruker Avance III HD (Bruker Corporation, Billerica, MA, USA) apparatus, using solvent peaks [ $\text{CDCl}_3$ : 7.27 (D), 77.2 (C) ppm] as internal reference. The assignment of chemical shifts was based on standard NMR experiments ( $^1\text{H}$ ,  $^{13}\text{C}$ , DEPT [Distortionless Enhancement by Polarization Transfer], COSY, gHSQC, gHMBC [2D NMR correlation spectroscopy experiments]). High-resolution mass spectrometry spectra were recorded in a Hewlett-Packard (Palo Alto, CA, USA) HP-5973 mass selective detector apparatus. Mass spectra were recorded on a gas chromatography-mass spectrometry spectrometer with an electrospray ionization source in a Hewlett-Packard HP-1100 MSD apparatus. Elemental analyses were performed at Centro Química Organica (Consejo Superior de Investigaciones Científicas, Madrid, Spain) in a Carlo Erba (Milan, Italy) instrument (CHNS/O EA1108). Thin-layer chromatography were performed on silica F254 and detection by ultraviolet light at 254 nm or by charring with either ninhydrin, anisaldehyde, or phosphomolybdic- $\text{H}_2\text{SO}_4$  dyeing reagents. Anhydrous solvents were used in all experiments. Column chromatography was performed on silica gel 60 (230 mesh). All known compounds have been synthesized as reported.

### Chemistry

The synthesis of the target DPH molecules was carried out as shown in schemes 1 and 2 (Supplementary material

<http://www.iqog.csic.es/iqog/sites/default/files/public/User/Jos%C3%A9%20Luis%20Marco%20Contelles/Supplementary%20material.pdf>).

Target DPHs py(C6)*N*(Me)propargylamines 9, 13, and 14 have been synthesized starting from known intermediates 2,6-dichloro-4-phenylpyridine-3,5-dicarbonitrile (17)<sup>25</sup> and 2,6-dichloropyridine-3,5-dicarbonitrile (18),<sup>26</sup> easily prepared from readily available precursors 2-amino-6-chloro-4-phenylpyridine-3,5-dicarbonitrile<sup>27</sup> and 2-amino-6-chloropyridine-3,5-dicarbonitrile,<sup>28</sup> respectively. The reaction of pyridines 17 and 18 with *N*-methylprop-2-yn-1-amine afforded pyridines 19<sup>24</sup> and 20,<sup>24</sup> respectively, is shown in Figure 3. In the synthesis of compound 20, minor amounts of *N,N*-di(C2,6)alkylated product were isolated and characterized (Supplementary material <http://www.iqog.csic.es/iqog/sites/default/files/public/User/Jos%C3%A9%20Luis%20Marco%20Contelles/Supplementary%20material.pdf>). Next, the reaction of compound 19 with 4-(1-benzylpiperidin-4-yl)butan-1-amine (22)<sup>29</sup> gave the desired target compound DPH9 in good yield (Figure 3). Similarly, the reaction of 20 with amines 3-(1-benzylpiperidin-4-yl)propan-1-amine (21),<sup>30</sup> and 22<sup>29</sup> gave the desired target compounds DPH13 and 14 in good yields (Figure 3).

Next, we attacked the synthesis of target DPHs py(C6)*N*(H)propargylamines 10–12, 15, and 16. Thus, the reaction of 2,6-dichloropyridine 17<sup>25</sup> with propargylamine gave 2-chloro-4-phenyl-6-(prop-2-yn-1-ylamino)pyridine-3,5-dicarbonitrile (23) (Figure 4) that after coupling with amines 2-(1-benzylpiperidin-4-yl)ethanamine (24),<sup>31</sup> 21,<sup>30</sup> and 22<sup>29</sup> cleanly afforded the desired target molecules DPHs10–12 in good overall yield (Figure 4). Finally, the synthesis of DPHs15 and 16 was carried out from the key intermediate 25 (prepared as usual from precursor 18)<sup>26</sup> and reaction with amines 21 and 22, respectively (Figure 4).

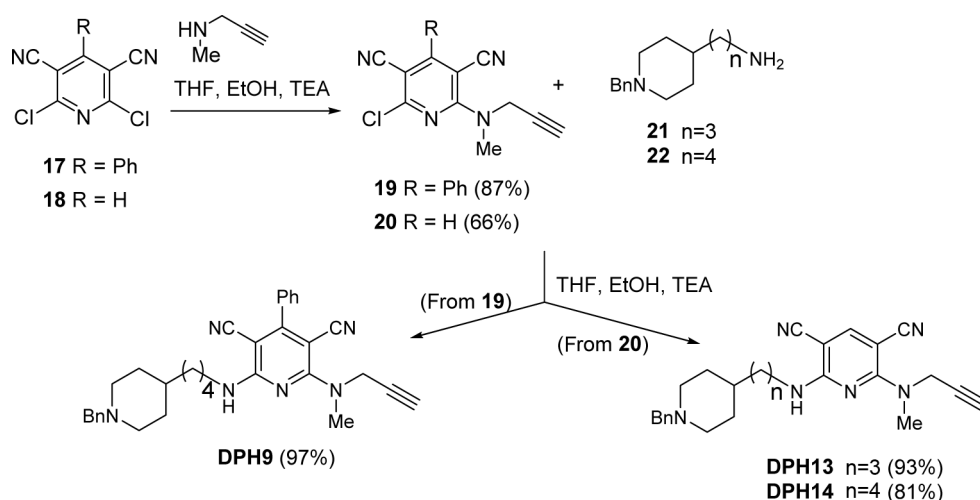


**Figure 3** Synthesis of target DPHs 9, 13, and 14.

**Abbreviation:** Bn, benzyl; DPHs, donepezil-pyridyl hybrids; EtOH, ethanol; Me, methyl; Ph, phenyl; TEA, triethylamine; THF, tetrahydrofuran.

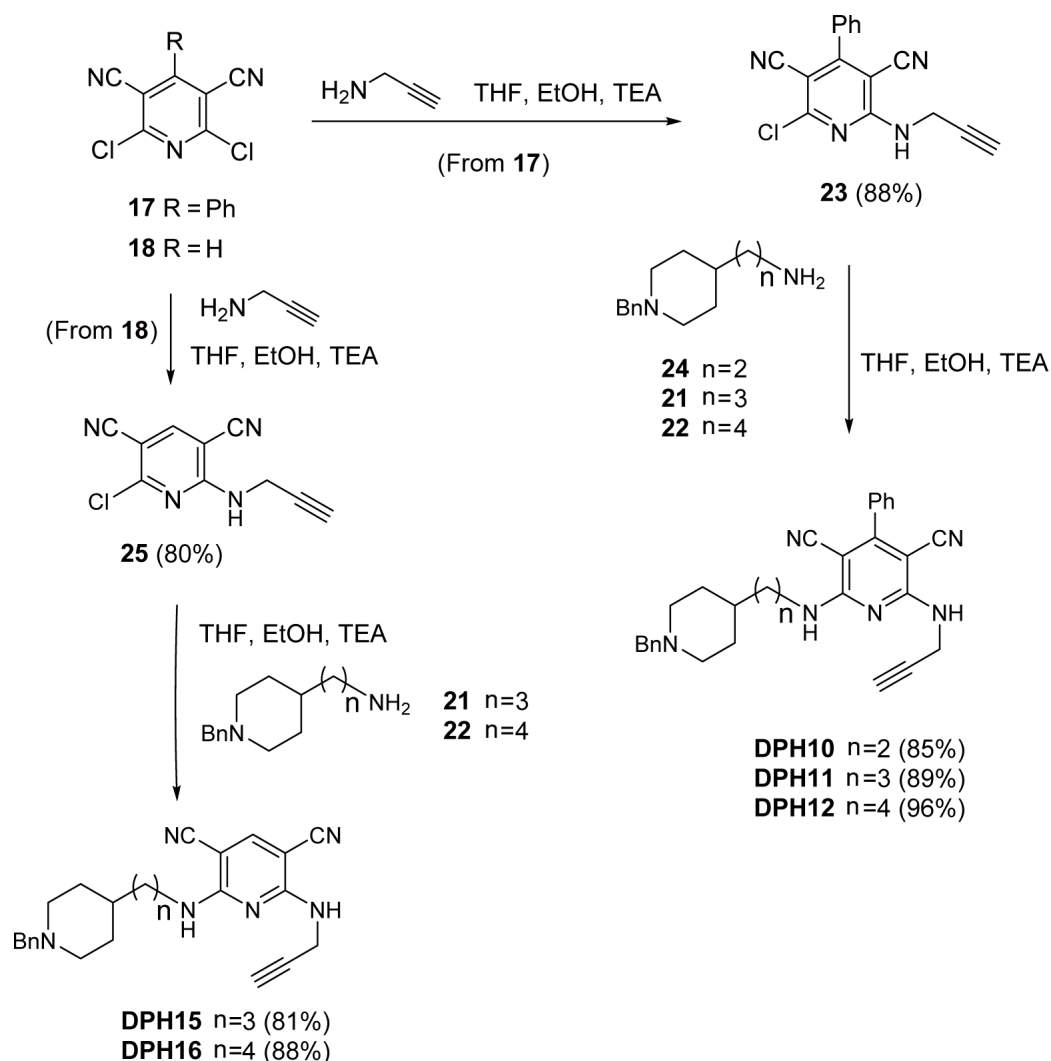


**Figure 4** Synthesis of target DPHs 10–12, 15, and 16.

**Abbreviation:** Bn, benzyl; DPHs, donepezil-pyridyl hybrids; EtOH, ethanol; Ph, phenyl; TEA, triethylamine; THF, tetrahydrofuran.

## Biochemical methods

### Inhibition experiments of AChE and BuChE

To assess the inhibition of the activities of AChE from *Electrophorus electricus* (type V-S), human recombinant AChE (hAChE) or BuChE from equine serum (lyophilized powder) and human recombinant BuChE (hBuChE) (Sigma-Aldrich Co., St Louis, MO, USA), the spectrophotometric method of Ellman was followed.<sup>32</sup> The reactions took place in a final volume of 300  $\mu$ L in a phosphate-buffered solution (0.1 M) at pH 8, containing 116.7 U/L of AChE or 166.7 U/L of BuChE and 0.35 mM of 5,5'-dithiobis-2-nitrobenzoic acid (DTNB; Sigma-Aldrich Co.). Inhibition curves were made by pre-incubating this mixture with at least nine concentrations of each compound for 20 minutes. A sample with no compound was always present to determine the 100% of the enzyme activity. After this pre-incubation period, 0.35 mM acetylthiocholine iodide or 0.5 mM butyrylthiocholine iodide (Sigma-Aldrich

Co.) were added, allowing the enzymatic reaction for 5 minutes with AChE and 30 minutes with BuChE while the DTNB produces the yellow anion 5-thio-2-nitrobenzoic acid along with the enzymatic degradation of the substrates. Changes in absorbance were detected at 405 nm in a spectrophotometric plate reader (FluoStar OPTIMA; BMG Labtech, Ortenberg, Germany). Compounds inhibiting AChE or BuChE activity would reduce the color generation, thus the half maximal inhibitory concentration ( $IC_{50}$ ) values were calculated as the concentration of compound that produces 50% activity inhibition. Data are expressed as means  $\pm$  standard error of the mean (SEM) of at least three different experiments in quadruplicate.

### Inhibition experiments of MAO A/B

MAO activities from recombinant human MAO A/B (Sigma-Aldrich Co.) were performed using a fluorometric

method.<sup>33</sup> Tyramine hydrochloride was used as substrate for both enzymes in a 96-well black opaque microplate (OptiPlate-96F, PerkinElmer Inc.) in a final volume of 200  $\mu$ L. Serial dilutions of each inhibitor were pre-incubated for 30 minutes at 37°C with 360 U/L human monoamine oxidase (hMAO) A or 67.5 U/L hMAO B. Following the pre-incubations, enzymatic reactions were started by adding 100  $\mu$ L of a mixture containing 1 mM tyramine, 40 U/L horseradish peroxidase, and 25  $\mu$ M Amplex UltraRed (Life Technologies, Eugene, OR, USA) reagent in 0.25 mM sodium phosphate pH 7.4 as final concentrations. The fluorescence production associated with peroxidase-coupled production of resorufin from Amplex UltraRed was constantly measured for at least 1 hour at 530 nm in a spectrophotometric plate reader (FluoStar OPTIMA, BMG Labtech). Control experiments were carried out simultaneously by replacing the inhibitors with distilled water. In addition, the possible capacity of compounds to modify the fluorescence generated in the reaction mixture due to nonenzymatic inhibition was determined by adding these compounds to solutions containing only the Amplex UltraRed reagent in a sodium phosphate buffer. Samples with no substrate were used as blanks.

#### Determination of $IC_{50}$ values

$IC_{50}$  values were determined from dose–response curves, plotted by using the GraphPad “PRISM” software (version 3.0; GraphPad Software, Inc., La Jolla, CA, USA), as the inhibitor concentration producing 50% of activity inhibition. Data are expressed as mean  $\pm$  SEM of at least three different experiments performed in triplicate.

#### Test of reversibility inhibition of human recombinant MAO B by DPH14

Reversibility of MAO B inhibition by DPH14 was determined by studying the recovery of the enzymatic activity after a large dilution of the complex. MAO B concentration of 100-fold over the concentration required for the activity assay was used with 50  $\mu$ M DPH14 and 0.5  $\mu$ M *R*-deprenyl (as standard irreversible MAO B inhibitor), concentrations equivalent to 10-fold their  $IC_{50}$  values previously determined. After 30 minutes pre-incubation at 37°C, the mixture was rapidly diluted 100-fold into reaction buffer containing 40 U/L horseradish peroxidase, 25  $\mu$ M Amplex UltraRed reagent, and 1 mM *p*-tyramine in order to initiate enzymatic reaction. Curves of each sample were plotted and compared to that of enzyme samples incubated and diluted in absence of inhibitor. After enzyme dilutions, enzyme concentrations were equal to that used in previous dose-curve experiments, but MAO B concentration changing from  $10\times IC_{50}$  to  $0.1\times IC_{50}$  upon dilution.

The resulting progress curves were plotted and followed for at least 1 hour reaction. Activity rates were calculated and final data were expressed as percentage of remaining enzyme activity as mean  $\pm$  SEM of at least three different experiments.

## Results and discussion

### Biochemical evaluation

The *in vitro* activity of DPHs9–16 derivatives inhibiting *E. electricus* AChE (EeAChE) and equine BuChE (eqBuChE) was determined using the Ellman’s method.<sup>32</sup> Donepezil and ASS234 were also assayed for comparative purposes. In order to test their potential multipotent profile, DPHs9–16 were also evaluated as human recombinant MAO A/B inhibitors using a fluorometric assay,<sup>33</sup> giving the values shown in Table 1, where we have incorporated the corresponding  $IC_{50}$  values of compound DPHs1–8 for comparative purposes.<sup>24</sup>

Regarding ChEs inhibition, DPHs were very active and selective EeAChE versus (vs) eqBuChE inhibitors. Particularly, DPH12, 14, and 16 were potent, in the low nanomolar range, AChE inhibitors, DPH14 being the most active (AChE:  $IC_{50}=1.1\pm 0.3$  nM; BuChE:  $IC_{50}=600\pm 80$  nM), exhibiting one of the most active ChE inhibitory potencies ever determined by us.<sup>34</sup>

DPH14 bears a hydrogen at C4, four methylene groups in the chain linker, and an *N*Me-propargylamine moiety at C6, three structural motifs that seem relevant for a strong AChE inhibition power in this family of compounds, although structural changes in these groups still afford potent acetylcholinesterase inhibitors (AChEI) (Table 1). As shown in Table 1, and compared with the reference compound ASS234,<sup>22</sup> DPH14 was 318-fold more potent for the inhibition of AChE, but 1.3-fold less active for the inhibition of BuChE, while, by comparison with donepezil, DPH14 was 11.8- and 11.5-fold more active at inhibiting AChE and BuChE, respectively.

As shown in Table 1, on-going from DPH1 to DPH4 and DPH9, by increasing the linker length (*n*) from 0 to 4, while retaining a phenyl group at C4 and an *N*Me-propargylamine at C6, the most potent AChEI was DPH4 (*n*=3) (AChE:  $IC_{50}=14\pm 1$  nM), 1.6-fold more potent than DPH9 (*n*=4), and in the same range than DPH3 (*n*=2). Concerning the selectivity (BuChE/AChE), DPH1 and DPH3 showed the highest values, while DPH9 was the most potent BuChE inhibitor ( $IC_{50}=220\pm 10$  nM), similar to DPH4.

Next, in DPHs5, 10–12 compared to DPHs1, 3, 4, and 9, the *N*Me-propargylamine at C6 was changed by an *NH*-propargylamine. In this group, the most potent AChEI was DPH12 (*n*=4) (AChE:  $IC_{50}=1.7\pm 0.3$  nM), being the only active BuChE inhibitor ( $IC_{50}=840\pm 100$  nM). DPH10 and

11 were significantly less active than DPH12. It is also remarkable that for the same value of  $n$  (0, 2, and 3), by comparing DPH1 with DPH5 ( $n=0$ ), DPH3 with DPH10 ( $n=2$ ), and DPH4 with DPH11 ( $n=3$ ), the most potent was always the DPH bearing the *N*Me-propargylamine moiety, while for  $n=4$ , by comparing DPH9 with DPH12, the most potent was the DPH bearing the *NH*-propargylamine moiety.

In compounds DPHs6–8, and 13–16 (Table 1), the same type of modifications was explored, but instead of a phenyl group at C4, a proton was incorporated at the same position.

Concerning DPHs6, 13, and 14, bearing the *N*Me-propargylamine moiety at C6, the power and selectivity increased from  $n=2$  to 4, DPH14 being the most active (AChE:  $IC_{50} = 1.1 \pm 0.3$  nM; BuChE:  $IC_{50} = 600 \pm 80$  nM). However, compared with DPH9, both bearing the same value of  $n$  (4) and an *N*Me-propargylamine moiety at C6, DPH14 was 20-fold more potent at inhibiting AChE, but 2.7-fold less active at inhibiting BuChE.

Regarding hybrids DPHs7, 8, 15, and 16, bearing an *NH*-propargylamine moiety at C6, the inhibitory potency and selectivity also increased from  $n=0, 2$  to 4, DPH16 being the most active inhibitor (AChE:  $IC_{50} = 1.3 \pm 0.3$  nM; BuChE:  $IC_{50} = 530 \pm 60$  nM). DPH12 and DPH16, both bearing the same  $n$  value (4) and an *NH*-propargylamine moiety at C6, were almost equipotent at inhibiting AChE and BuChE, respectively, but highly selective for the inhibition of AChE. Concerning AChE inhibition, it was also noticed that for the same  $n$  values ( $n=2$  or 4), DPH6 and DPH8, DPH14 and DPH16, were equipotent, whereas comparing DPH13 with DPH15 ( $n=3$ ), the most potent was the DPH15 bearing the *NH*-propargylamine moiety. However, in the BuChE inhibition, for the same  $n$  value, in the case of DPH6 and 8 ( $n=2$ ) and DPH13 and DPH15 ( $n=3$ ), the most potent was the DPH bearing the *N*Me-propargylamine moiety, while DPH14 and 16 ( $n=4$ ) were equipotent.

Based on these results, the activity of DPHs9, 12–16, possessing potent EeAChE/eqBuChE inhibitory profiles, was also determined as hAChE and hBuChE inhibitors.

As shown in Table 2, all selected compounds exhibited similar trends as previously observed in nonhuman ChEs, revealing hAChE-selectivity and displaying  $IC_{50}$  values in low nanomolar range. DPH15 ( $IC_{50} = 1 \pm 0.4$  nM) and DPH12 ( $IC_{50} = 770 \pm 140$  nM) were the most potent hAChE and hBuChE inhibitors, respectively. DPH16 showed the most satisfactory balance in terms of inhibitory activity power for both enzymes [hAChE ( $IC_{50} = 2.9 \pm 0.8$  nM); hBuChE ( $IC_{50} = 790 \pm 110$  nM)], but DPH15 was the most selective hAChE inhibitor (selectivity index: 1920). Very interestingly, DPH14 is still a potent hBuChE inhibitor, in the same range as DPH12 or DPH16, but 13.1-fold less potent than DPH15

**Table 2** Inhibition ( $IC_{50}$  [ $\mu$ M]) of human recombinant acetylcholinesterase (hAChE) and human recombinant butyrylcholinesterase (hBuChE) by DPHs9, 12–16, ASS234, and donepezil

Drug	$IC_{50}$ (nM) <sup>a</sup>		Selectivity BuChE/AChE
	hAChE	hBuChE	
DPH9	25±3	1,190±310	48
DPH12	6±1.3	770±140	128
DPH13	26.3±8.1	1,680±240	64
DPH14	13.1±2.1	835±139	64
DPH15	1±0.4	1,920±680	1,920
DPH16	2.9±0.8	790±110	275
ASS234	913±122	1,845±365	2.0
Donepezil	9.1±1	7,330±1,136	805

**Note:** <sup>a</sup>Values expressed as mean  $\pm$  standard error of the mean of at least three different experiments in quadruplicate.

**Abbreviations:** DPHs, donepezil-pyridyl hybrids;  $IC_{50}$ , concentration of compound that produces 50% activity inhibition.

for the inhibition of hAChE. Finally, note that DPH16 was 3.1- and 9.2-fold more active than donepezil for the inhibition of hAChE and hBuChE, respectively.

Concerning MAO inhibition by DPHs (Table 1), some of them (DPHs10–12, 15, 16) were inactive, or moderate inhibitors, such as DPHs9, 5, 13, and 14. Among those active, DPH9 [ $IC_{50}$  (MAO A) = 5,700  $\pm$  2,100 nM] and DPH14 [ $IC_{50}$  (MAO B) = 3,950  $\pm$  940 nM] exhibited the most interesting profile, as moderately selective MAO A/B inhibitors, respectively, in the low  $\mu$ M range.

Regarding our multi-target approach, DPH14 showed a very potent and slightly selective EeAChE inhibition, and a moderately selective hMAO B inhibition activity. DPH5 showed a potent and selective hAChE inhibition as well as a moderate, but selective hMAO A inhibition activity.

Once  $IC_{50}$  values were determined as a preliminary evaluation, DPH14 was selected as the most relevant MAO B inhibitor to next investigate its mechanism of inhibition.

Thus, the study of reversibility of hMAO B inhibition by DPH14 was assessed by pre-incubating for 30 minutes 100-fold enzyme concentration used in the experiments previously described with inhibitor concentrations equivalent to 10-fold their  $IC_{50}$  values: 50  $\mu$ M DPH14 and 0.5  $\mu$ M *R*-deprenyl, as standard irreversible MAO B inhibitor. After pre-incubations, the mixture was diluted 100-fold into a buffered solution containing 1 mM *p*-tyramine to recover previous enzyme activity levels. Figure 5 shows that initial MAO B inhibition by DPH14 (55%) was not recovered after a 100-fold dilution in saturated-substrate concentration, suggesting an irreversible MAO B inhibition by DPH14. Control tests were carried out by pre-incubating and diluting in the absence of inhibitors.

In order to further characterize the mechanism of hMAO B inhibition by DPH14, dose–response curves ( $IC_{50}$ ) were

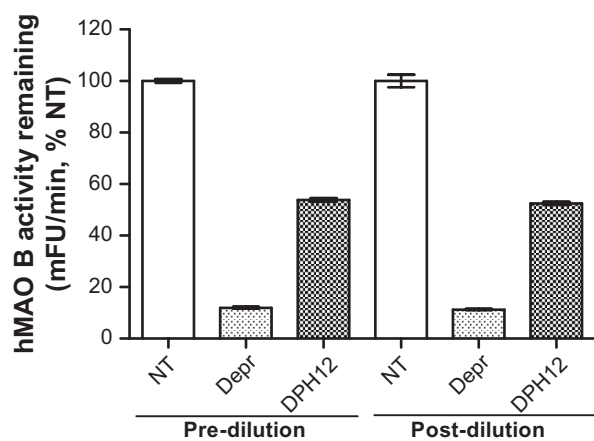


**Figure 5** Assessment of reversibility of hMAO B activity inhibited by DPH14 (50  $\mu$ M) and R-deprenyl (500 nM).

**Notes:** hMAO B was pre-incubated with each inhibitor for 30 minutes and remaining activity was measured prior and following a rapid 100-fold dilution with 1 mM tyramine. No changes were observed in enzyme inhibition by DPH14 revealing an irreversible inhibitory behavior. Bars expressed as mean  $\pm$  standard error of the mean of at least three different experiments.

**Abbreviations:** hMAO B, human monoamine oxidase B; DPH, donepezil-pyridyl hybrid; Depr, R-deprenyl; NT, non-treated.

obtained by varying pre-incubation times (15–60 minutes). A time-dependent inhibition was clearly observed since  $IC_{50}$  values were found to decrease in a pre-incubation time-dependent manner (Table 3). These findings agree with the previously determined irreversible behavior.

### 3D-QSAR study of novel DPHs

The 3D-QSAR study has been carried out on these hybrids with main goal to define structural requirements for high inhibitory activity on the enzymes involved, following the usual methods (Supplementary material <http://www.iqog.csic.es/iqog/sites/default/files/public/User/Jos%C3%A9%20Luis%20Marco%20Contelles/Supplementary%20material.pdf>).

The  $IC_{50}$  inhibition values of MAO A/B and AChE/BuChE by donepezil-pyridine hybrids (Chart S1, Supplementary material <http://www.iqog.csic.es/iqog/sites/default/files/public/User/Jos%C3%A9%20Luis%20Marco%20Contelles/Supplementary%20material.pdf>), and 37 donepezil-indole

**Table 3** Time-dependent inhibition ( $IC_{50}$ ) of human recombinant MAO B by DPH14 following different pre-incubation times

Pre-incubation time (minutes)	$IC_{50}$ (nM) <sup>a</sup>
15	64,800 $\pm$ 11,900
30	3,260 $\pm$ 860
45	205 $\pm$ 44
60	2.7 $\pm$ 0.4

**Note:** <sup>a</sup>Values expressed as mean  $\pm$  standard error of the mean of at least three different experiments in quadruplicate.

**Abbreviations:** MAO B, monoamine oxidase B; DPH, donepezil-pyridyl hybrid;  $IC_{50}$ , concentration of compound that produces 50% activity inhibition.

(Charts S2 and S3, Supplementary material <http://www.iqog.csic.es/iqog/sites/default/files/public/User/Jos%C3%A9%20Luis%20Marco%20Contelles/Supplementary%20material.pdf>)<sup>22–24</sup> derivatives were used for the 3D-QSAR study. In the examined data set, the  $pIC_{50}$  (MAO A) interval spanned 6 log units (3.07–9.10), the  $pIC_{50}$  (MAO B) interval was 6.6 log units (4.00–10.60), the  $pIC_{50}$  (AChE) activity was 4.2 log units (4.00–8.17), and  $pIC_{50}$  (BuChE) activity was 2.6 log units (4.00–6.64). Relatively wide activity interval of the training set provides extensive applicability domain for the formed 3D-QSAR models.

Hydrogen bond acceptor (HBA) properties of O-bridge create crucial favorable interactions (v892: N1-TIP) (Figure S1, Supplementary material <http://www.iqog.csic.es/iqog/sites/default/files/public/User/Jos%C3%A9%20Luis%20Marco%20Contelles/Supplementary%20material.pdf>) for MAO A inhibiting activity with steric properties of the propargylamine moiety (Donz-D4/Donz-D9, Figure S2A/B, Supplementary material <http://www.iqog.csic.es/iqog/sites/default/files/public/User/Jos%C3%A9%20Luis%20Marco%20Contelles/Supplementary%20material.pdf>). The unsaturated bond of the propargylamine moiety also forms a favorable interaction (v287: TIP-TIP, v344: TIP-TIP) with the nearest terminal hydrogen (Donz-D4/Donz-D9, Figure S2A/B, Supplementary material <http://www.iqog.csic.es/iqog/sites/default/files/public/User/Jos%C3%A9%20Luis%20Marco%20Contelles/Supplementary%20material.pdf>). The 3D-QSAR study confirmed previous experimental findings,<sup>22–23</sup> which indicated the essential role of the propargylamine moiety for the MAO A inhibiting activity. Substitution of the terminal hydrogen of propargylamine moiety (Donz-D4/Donz-D9, Figure S2A/B, Supplementary material <http://www.iqog.csic.es/iqog/sites/default/files/public/User/Jos%C3%A9%20Luis%20Marco%20Contelles/Supplementary%20material.pdf>) with bulky groups could enhance MAO A inhibiting activity of the examined compounds by facilitating the favorable interactions (v892: N1-TIP, v287: TIP-TIP, v344: TIP-TIP).

Also, HBA O-bridge forms very specific unfavorable interactions (v854: N1-TIP and v868: N1-TIP) with *N*-Me group of the indole moiety (Donz-D9, Figure S2B, Supplementary material <http://www.iqog.csic.es/iqog/sites/default/files/public/User/Jos%C3%A9%20Luis%20Marco%20Contelles/Supplementary%20material.pdf>). Furthermore, the *N*-Me group of the indole moiety forms unfavorable interactions (v301: TIP-TIP, v325: TIP-TIP, and v332: TIP-TIP) with meta/para positions of the benzyl moiety (Donz-D4/Donz-D9, Figure S2A/B, Supplementary material <http://www.iqog.csic.es/iqog/sites/default/files/>

[public/User/Jos%C3%A9%20Luis%20Marco%20Contelles/Supplementary%20material.pdf](http://www.iqog.csic.es/iqog/sites/default/files/public/User/Jos%C3%A9%20Luis%20Marco%20Contelles/Supplementary%20material.pdf)).

Finally, the HBD properties of the *N*-atom in the piperidyl or piperazinyl moiety create very specific unfavorable interactions (v783: O-TIP) with meta positions of the benzyl moiety (Donz-D4/Donz-D9, Figure S2A/B, Supplementary material <http://www.iqog.csic.es/iqog/sites/default/files/public/User/Jos%C3%A9%20Luis%20Marco%20Contelles/Supplementary%20material.pdf>).

Therefore, substitution of the methyl group with hydrogen in the *N*-Me group of the indole could enhance MAO A inhibiting activity, while bulky groups in meta/para positions of the benzyl moiety could decrease MAO A inhibiting activity.

The HBA group of compounds does not have propargylamine moiety to form essential pharmacophores (v287: TIP-TIP and v892: N1-TIP) for MAO A inhibiting activity.

Predictive potential of the developed 3D-QSAR (MAO A) model was tested by use of leave-one-out cross validation of the training set ( $Q^2$ : 0.87,  $R^2_{\text{Observed vs Predicted}}$ : 0.977, and root mean square error of estimation [RMSEE]: 0.229) and verification set ( $R^2_{\text{Observed vs Predicted}}$ : 0.804 and root mean square error of prediction [RMSEP]: 0.578) (Table S1, Supplementary material <http://www.iqog.csic.es/iqog/sites/default/files/public/User/Jos%C3%A9%20Luis%20Marco%20Contelles/Supplementary%20material.pdf>). The obtained statistical parameters indicated that the created 3D-QSAR (MAO A) model has good prognostic capacity for MAO A inhibiting activity.

Hydrogen bond donor (HBD) properties of amino groups of propargylamine and indole moieties create very specific favorable interactions (v765: O-TIP, v775: O-TIP) (Figure S3, Supplementary material <http://www.iqog.csic.es/iqog/sites/default/files/public/User/Jos%C3%A9%20Luis%20Marco%20Contelles/Supplementary%20material.pdf>) for MAO B inhibiting activity with unsaturated back chain (Donz-D3/Donz-D5, Figure S4A/B, Supplementary material <http://www.iqog.csic.es/iqog/sites/default/files/public/User/Jos%C3%A9%20Luis%20Marco%20Contelles/Supplementary%20material.pdf>). Thus, new electron-donating groups in propargylamine or indole moiety could increase electron densities of the groups and therefore selectively enhance MAO B activity of the compounds. The propargylamine group creates favorable interaction (v295: TIP-TIP, v314: TIP-TIP) with *N*-CH<sub>3</sub> group of the indole moiety, and also forms favorable interaction with meta/para positions of the benzyl moiety (Donz-D3/Donz-D5, Figure S4A/B, Supplementary material <http://www.iqog.csic.es/iqog/sites/default/files/public/User/Jos%C3%A9%20Luis%20Marco%20Contelles/Supplementary%20material.pdf>). Therefore, substitution of the methyl substituent on

*N*-atom of the indole moiety and meta/para positions of the benzyl moiety with ethyl or other bulkier group could selectively increase MAO B activity of the compounds. The 3D-QSAR study confirmed previous experimental findings<sup>15-17</sup> that propargylamine moiety has essential positive influence on the MAO B inhibiting activity.

Also, the hydrophobic part of the propargylamine moiety forms unfavorable interactions (v477: N1-DRY, v527: N1-DRY) with HBA ortho-C-atom of the benzyl moiety (Donz-D3, Figure S4A, Supplementary material <http://www.iqog.csic.es/iqog/sites/default/files/public/User/Jos%C3%A9%20Luis%20Marco%20Contelles/Supplementary%20material.pdf>). Therefore, electron withdrawing groups at meta/para positions of the benzyl moiety could enhance MAO B inhibiting activity of the examined compounds.

The HBA group of compounds does not have propargylamine moiety to form essential pharmacophores (v765: O-TIP, v775: O-TIP, v295: TIP-TIP, and v314: TIP-TIP) for MAO B inhibiting activity.

Predictive potential of the developed 3D-QSAR (MAO B) model was tested by use of leave-one-out cross validation of the training set ( $Q^2$ : 0.82,  $R^2_{\text{Observed vs Predicted}}$ : 0.956, and RMSEE: 0.314) and verification set ( $R^2_{\text{Observed vs Predicted}}$ : 0.924 and RMSEP: 0.410) (Table S2, Supplementary material <http://www.iqog.csic.es/iqog/sites/default/files/public/User/Jos%C3%A9%20Luis%20Marco%20Contelles/Supplementary%20material.pdf>). The obtained statistical parameters indicated that the created 3D-QSAR (MAO B) model has good prognostic capacity for MAO B inhibiting activity.

HBD properties of *N*-atom in the piperidine ring and secondary *N*-atom in the propargylamine group create very specific unfavorable interactions (v133: O-O) (Figure S5, Supplementary material <http://www.iqog.csic.es/iqog/sites/default/files/public/User/Jos%C3%A9%20Luis%20Marco%20Contelles/Supplementary%20material.pdf>) for AChE inhibition (DPH8, Figure S6A, Supplementary material <http://www.iqog.csic.es/iqog/sites/default/files/public/User/Jos%C3%A9%20Luis%20Marco%20Contelles/Supplementary%20material.pdf>). Thus, extension of the *N*-alkyl bridge could selectively enhance AChE inhibiting activity of the pyridine derivatives.

HBD feature of *N*-atom in piperidyl moiety creates very specific unfavorable interaction (v678: O-N1) with the cyano group (DPH4, Figure S6B, Supplementary material <http://www.iqog.csic.es/iqog/sites/default/files/public/User/Jos%C3%A9%20Luis%20Marco%20Contelles/Supplementary%20material.pdf>). The propargylamine group creates unfavorable interactions (v334: TIP-TIP) with meta/para position of benzyl moiety (DPH8 and 4, Figure S6A/B,

Supplementary material <http://www.iqog.csic.es/iqog/sites/default/files/public/User/Jos%C3%A9%20Luis%20Marco%20Contelles/Supplementary%20material.pdf>). All these results indicated that extension of the *N*-alkyl bridge could selectively decrease three very specific unfavorable interactions, v133: O-O, v334: TIP-TIP, and v678: O-N1, and therefore significantly enhance AChE inhibiting activity of the pyridine derivatives.

HBA feature of *N*-atom in the pyridine ring creates favorable interactions with meta/para position of benzyl moiety (v895: N1-TIP) for AChE inhibition (DPH8 and 4, Figure S6A/B, Supplementary material <http://www.iqog.csic.es/iqog/sites/default/files/public/User/Jos%C3%A9%20Luis%20Marco%20Contelles/Supplementary%20material.pdf>). The propargylamine moiety creates crucial favorable interaction with hydrophobic phenyl substituent of the pyridine moiety (v803: DRY-TIP) (DPH4, Figure S6B, Supplementary material <http://www.iqog.csic.es/iqog/sites/default/files/public/User/Jos%C3%A9%20Luis%20Marco%20Contelles/Supplementary%20material.pdf>). Therefore, phenyl substituent in the pyridine ring is able to selectively enhance AChE inhibiting activity. Since meta position of the phenyl substituent of the pyridine moiety forms one unfavorable interaction with *N*-atom of the pyridine ring (v909: N1-TIP), substitution of the meta position of the phenyl substituent could result in decrease of AChE inhibiting activity (DPH4, Figure S6B, Supplementary material <http://www.iqog.csic.es/iqog/sites/default/files/public/User/Jos%C3%A9%20Luis%20Marco%20Contelles/Supplementary%20material.pdf>).

HBD properties of *N*-bridge forms a very specific favorable interaction (v785: O-TIP) with the propargylamine group (DPH8 and 4, Figure S6A/B, Supplementary material <http://www.iqog.csic.es/iqog/sites/default/files/public/User/Jos%C3%A9%20Luis%20Marco%20Contelles/Supplementary%20material.pdf>).

Predictive potential of the developed 3D-QSAR (AChE) model was tested by use of leave-one-out cross validation of the training set ( $Q^2$ : 0.87,  $R^2_{\text{Observed vs Predicted}}$ : 0.979, and RMSEE: 0.203) and verification set (RMSEP: 0.574). The obtained statistical parameters indicated that the created 3D-QSAR (AChE) model has good prognostic capacity for AChE inhibiting activity.

HBD feature of *N*-atom in piperidinyl moiety creates crucial favorable interactions (v690: O-N1) (Figure S7, Supplementary material <http://www.iqog.csic.es/iqog/sites/default/files/public/User/Jos%C3%A9%20Luis%20Marco%20Contelles/Supplementary%20material.pdf>) for BuChE inhibition with the HBA properties of *N*-atom of the pyridine ring (DPH3 and 4, Figure S8A/B, Supplementary material <http://www.iqog.csic.es/iqog/sites/default/files/>

[public/User/Jos%C3%A9%20Luis%20Marco%20Contelles/Supplementary%20material.pdf](http://www.iqog.csic.es/iqog/sites/default/files/public/User/Jos%C3%A9%20Luis%20Marco%20Contelles/Supplementary%20material.pdf)).

HBA feature of *N*-atom in the pyridine ring also creates a crucial favorable interaction (v984: N1-TIP) with meta/para position of benzyl moiety (DPH3 and 4, Figure S8A/B, Supplementary material <http://www.iqog.csic.es/iqog/sites/default/files/public/User/Jos%C3%A9%20Luis%20Marco%20Contelles/Supplementary%20material.pdf>).

The propargylamine group creates two favorable interactions (v334: TIP-TIP, v351: TIP-TIP) with meta/para position of benzyl moiety (DPH3 and 4, Figure S8A/B, Supplementary material <http://www.iqog.csic.es/iqog/sites/default/files/public/User/Jos%C3%A9%20Luis%20Marco%20Contelles/Supplementary%20material.pdf>).

The propargylamine (DPH3, Figure S8A, Supplementary material <http://www.iqog.csic.es/iqog/sites/default/files/public/User/Jos%C3%A9%20Luis%20Marco%20Contelles/Supplementary%20material.pdf>) or benzyl (DPH4, Figure S8B, Supplementary material <http://www.iqog.csic.es/iqog/sites/default/files/public/User/Jos%C3%A9%20Luis%20Marco%20Contelles/Supplementary%20material.pdf>) moieties create crucial favorable interactions (v317: TIP-TIP) with phenyl substituent of the pyridine ring. Therefore, the donepezil-pyridine hybrids with phenyl substituent in the pyridine ring are good leads for further design of novel multipotent ligands. Since meta position of the phenyl substituent of the pyridine moiety forms one unfavorable interaction with *N*-atom of the pyridine ring (v884: N1-TIP), substitution of the meta position of the phenyl substituent could result in decrease of BuChE inhibiting activity (DPH3 and 4, Figure S8B, Supplementary material <http://www.iqog.csic.es/iqog/sites/default/files/public/User/Jos%C3%A9%20Luis%20Marco%20Contelles/Supplementary%20material.pdf>).

HBA properties of cyano group of compound DPH3 forms a crucial unfavorable interaction (v907: N1-TIP) with meta position of benzyl moiety, while the compounds with longer *N*-alkyl chain (such as compound DHH4) do not create the v907: N1-TIP unfavorable interaction for BuChE inhibiting activity (DPH3 and 4, Figure S8A/B, Supplementary material <http://www.iqog.csic.es/iqog/sites/default/files/public/User/Jos%C3%A9%20Luis%20Marco%20Contelles/Supplementary%20material.pdf>).

These results indicated that extension of the *N*-alkyl bridge could decrease unfavorable interaction, v907: N1-TIP, and therefore influence a modest increase of BuChE inhibiting activity.

Predictive potential of the developed 3D-QSAR (BuChE) model was tested by use of leave-one-out cross validation of the training set ( $Q^2$ : 0.78,  $R^2_{\text{Observed vs Predicted}}$ : 0.931, and

RMSEE: 0.254) and verification set ( $R^2_{\text{Observed vs Predicted}}$ : 0.619 and RMSEP: 0.550). The obtained statistical parameters indicated that the created 3D-QSAR (BuChE) model has good prognostic capacity for BuChE inhibiting activity.

The created 3D-QSAR models were further applied for design of novel multipotent inhibitors, prediction of their inhibitory activity on the enzymes, and for selection of the most promising ligands. Results of the 3D-QSAR (AChE) study were mainly applied for design of novel multipotent MAO/ChE ligands with strong AChE inhibiting activity (Figure 2). Since the QSAR (AChE) study indicated that the longer *N*-butyl bridge and phenyl substituent in the pyridine ring are crucial for enhancement of AChE inhibiting activity of the donepezil-pyridine derivatives, several new donepezil-pyridine hybrids have been designed, examined for MAO/ChE inhibiting activity. Since the designed compounds contain unique *N*-butyl bridge between two pharmacophores, while the QSAR-training set ligands contain *O*-methyl, *O*-ethyl, *O*-propyl, *N*-methyl, *N*-ethyl, and *N*-propyl, bridge, relatively good agreement was obtained between QSAR-predicted and observed MAO/ChE inhibiting activity for the novel compounds. The designed compounds with 3D-QSAR predicted  $pIC_{50}$  (AChE) >6.0 were selected for synthesis (Table 1) and examined in vitro (Tables 4 and 5).

Next, we have investigated the molecular modeling of compound DPH14 following the usual methods (Supplementary material <http://www.iqog.csic.es/iqog/sites/default/files/public/User/Jos%C3%A9%20Luis%20Marco%20Contelles/Supplementary%20material.pdf>).

## Molecular modeling of compound DPH14 Inhibition of AChE and BuChE

The ligand-enzyme binding interactions of the potent ChE inhibitor DPH14, (EeAChE  $IC_{50}$  = 0.0011 ± 0.0003 μM;

**Table 4** Experimental and QSAR activities of novel MAO A and MAO B inhibitors

ID	Data set	$pIC_{50}$ (MAO A)	Pred- $pIC_{50}$ (MAO A)	$pIC_{50}$ (MAO B)	Pred- $pIC_{50}$ (MAO B)
T1	DPH9	4.936	5.089	6.658	4.030
T2	DPH10	4.000	4.277	4.000	4.713
T3	DPH11	4.000	3.391	4.000	4.105
T4	DPH12	4.000	3.945	6.215	4.393
T5	DPH13	4.000	3.360	5.924	5.290
T6	DPH14	4.000	4.134	6.260	4.342
T7	DPH15	4.000	3.571	5.693	5.215
T8	DPH16	4.273	4.628	6.292	3.911

**Abbreviations:** QSAR, quantitative structure-activity relationship; ID; compound identification name; MAO A, monoamine oxidase A; MAO B, monoamine oxidase B; DPH, donepezil-pyridyl hybrid;  $pIC_{50}$ , predicted half maximal inhibitory concentration; Pred- $pIC_{50}$ , predicted half maximal inhibitory concentration.

**Table 5** Experimental and QSAR activities of novel EeAChE and eqBuChE inhibitors

ID	Data set	$pIC_{50}$ (EeAChE)	Pred- $pIC_{50}$ (EeAChE)	$pIC_{50}$ (eqBuChE)	Pred- $pIC_{50}$ (eqBuChE)
T1	DPH9	7.638	6.204	6.658	5.353
T2	DPH10	9.824	7.742	4.000	5.686
T3	DPH11	9.959	7.189	4.000	5.681
T4	DPH12	11.678	7.579	6.215	4.826
T5	DPH13	8.208	8.071	5.924	4.693
T6	DPH14	9.131	7.284	6.260	4.920
T7	DPH15	8.328	7.768	5.693	4.858
T8	DPH16	9.959	6.850	6.292	5.972

**Abbreviations:** QSAR, quantitative structure-analysis relationship; ID; compound identification name; Pred, predicted; DPH, donepezil-pyridyl hybrid;  $pIC_{50}$ , predicted half maximal inhibitory concentration; EeAChE, *Electrophorus electricus* acetylcholinesterase; eqBuChE, equine serum butyrylcholinesterase.

eqBuChE  $IC_{50}$  = 0.60 ± 0.08 μM) were investigated by molecular modeling studies. We have used the 3D structure of the enzyme species (EeAChE and eqBuChE), which was also used for the biochemical studies.

Docking simulations of EeAChE (Protein Data Bank [PDB]: 1C2B) and compound DPH14 were performed using Autodock Vina program (Molecular Graphics Laboratory, Scripps Research Institute, La Jolla, CA, USA).<sup>35</sup> The binding site for docking was designed so that the entire receptor molecule was included within the selection grid. Autodock Vina introduces side chain flexibility into the target macromolecule. Eight side chains, Trp286, Tyr124, Tyr337, Tyr72, Asp74, Thr75, Trp86, and Tyr341, are allowed to change their conformations at the same time as the ligand that is being docked.

The docking study of inhibitor DPH14 within EeAChE indicates that two major binding modes at the enzyme-binding site can be proposed. In Figure 6, the two most favored binding modes are presented along with the first shell of residues surrounding DPH14. In both modes, compound DPH14 showed a binding mode with an extended conformation and interacted simultaneously with both catalytic and peripheral site of EeAChE thanks to a linker of appropriate length.

In Mode I (Figure 6A; binding energy: -13.1 kcal/mol), the *N*-benzylpiperidine structural motif was oriented toward the PAS, where the benzene ring was stacked over Trp286 and Tyr124. The pyridine ring was positioned at the bottom of the active site and it was stacked between Trp86 and a tyrosine pocket comprising Tyr124, Tyr337, and Tyr341. This ligand also showed hydrophobic interactions with His447 at the choline-binding site.

In Mode II (Figure 6B; binding energy: -11.9 kcal/mol), the ligand is oriented the other way around than in Mode I. As can be seen in Figure 6B, compound DPH14 had several

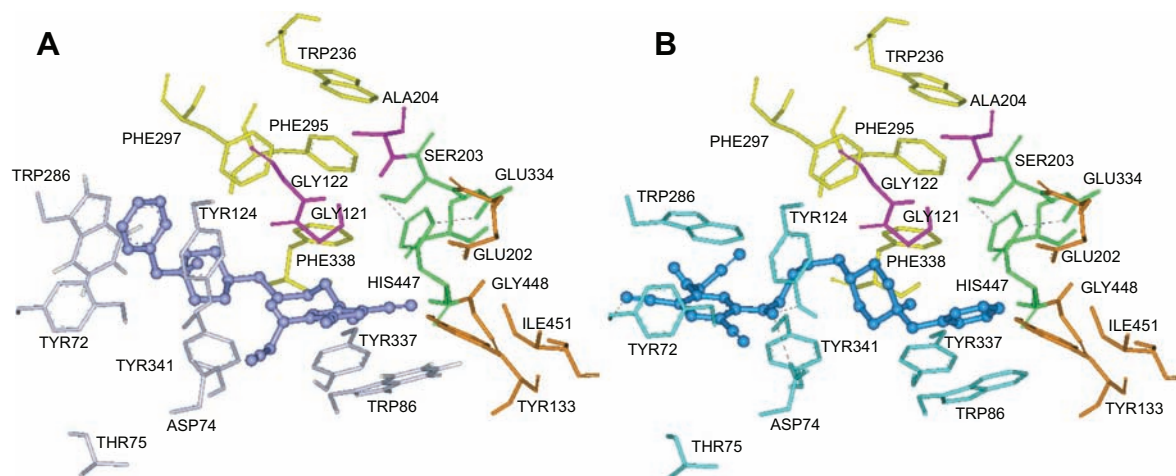


**Figure 6** Binding mode of inhibitor DPH14 at the active site of EeAChE.

**Notes:** (A) Mode I, compound DPH14 is illustrated in violet. (B) Mode II, compound DPH14 is illustrated in blue. Ligands are rendered as balls and sticks and the side chains conformations of the mobile residues are illustrated in the same color as the ligand. Different sub-sites of the active site were colored: catalytic triad (CT) in green, oxyanion hole (OH) in pink, anionic sub-site (AS) in orange, except Trp86, acyl binding pocket (ABP) in yellow, and PAS in light blue. Black dashed lines are drawn among atoms involved in hydrogen bond interactions.

**Abbreviations:** DPH, donepezil-pyridyl hybrid; PAS, peripheral anionic site; EeAChE, *Electrophorus electricus* acetylcholinesterase.

interactions along the active site of EeAChE. Near the bottom of the gorge, the phenyl ring stacked against the Trp86 indole ring. At the top of the gorge, the pyridine ring and Trp286 indole ring formed a favorable face-to-face  $\pi$ - $\pi$  interaction. The nitrogen of the cyano group was undergoing hydrogen bonding with the hydroxyl group of Tyr72. The amino-alkyl linker was positioned midway through the active site gorge and the NH group was undergoing hydrogen bonding with the hydroxyl group of Tyr124 and the carboxylate group of Asp74.

On the other hand, the docking study of DPH14 within the active site of eqBuChE was also carried out. In the absence of X-ray structure of eqBuChE, a homology model was used. SWISS-MODEL,<sup>36–38</sup> accessible via the Expasy web server (<http://swissmodel.expasy.org/>), a fully automated protein structure homology-modeling server was used to design the receptor. A putative 3D structure of eqBuChE has been created based on the crystal structure of hBuChE (pdb: 2PM8) as these two enzymes exhibited 89% sequence identity.

In order to simulate the binding of compound DPH14 to eqBuChE, docking experiments were performed as blind dockings following the same computational protocol used for EeAChE. As depicted in Figure 7, compound DPH14 was well accommodated inside the active site gorge and two major binding modes (Modes I and II) can be proposed. In both modes, compound DPH14 showed a binding mode with a U-shaped conformation. Modes I and II (Figure 7A and B) placed the substituted-pyridine moiety into the binding pocket interacting with the residues involved in catalysis. In these orientations, the phenyl moieties interact with Trp82 allowing  $\pi$ - $\pi$  stacking interactions.

In Mode I (Figure 7A; binding energy:  $-9.3$  kcal/mol), a close examination of the first shell of residues surrounding DPH14 revealed that the cyano group formed a hydrogen bond with the hydroxyl of Ser198. The NH group of the linker formed a hydrogen bond with residue Leu286. The bound ligand is also stabilized by hydrophobic interactions with the catalytic triad residue His438.

In Mode II (Figure 7B; binding energy:  $-9.8$  kcal/mol), two hydrogen bonds were observable. Compound DPH14 preserved the hydrogen bond already observed in Mode I, and it is established between the cyano group and the hydroxyl group of Ser198. The NH group of the protonated piperidine ring was also undergoing hydrogen-bonding interaction with the hydroxyl group of Tyr332.

Analysis of the intermolecular interactions indicated key residues responsible for ligand binding. The cyano group is likely to be an important feature for these derivatives to exhibit both AChE- and BuChE-inhibitory activities.

It is significant to note that the linear conformation allows DPH14 (Modes I and II) to span both CAS and PAS that contributes to its superior binding toward EeAChE.

### Inhibition of MAO A and MAO B

In order to explore the nature of the ligand-receptor interactions, the ligand was docked to the active site of both MAO A and MAO B isoforms using the program Autodock Vina.<sup>35</sup> We have focused on the compound DPH14, which showed the best hMAO B ( $IC_{50} = 3.95 \pm 0.94$   $\mu$ M) inhibitory activity, with very significant EeAChE inhibitory potency.

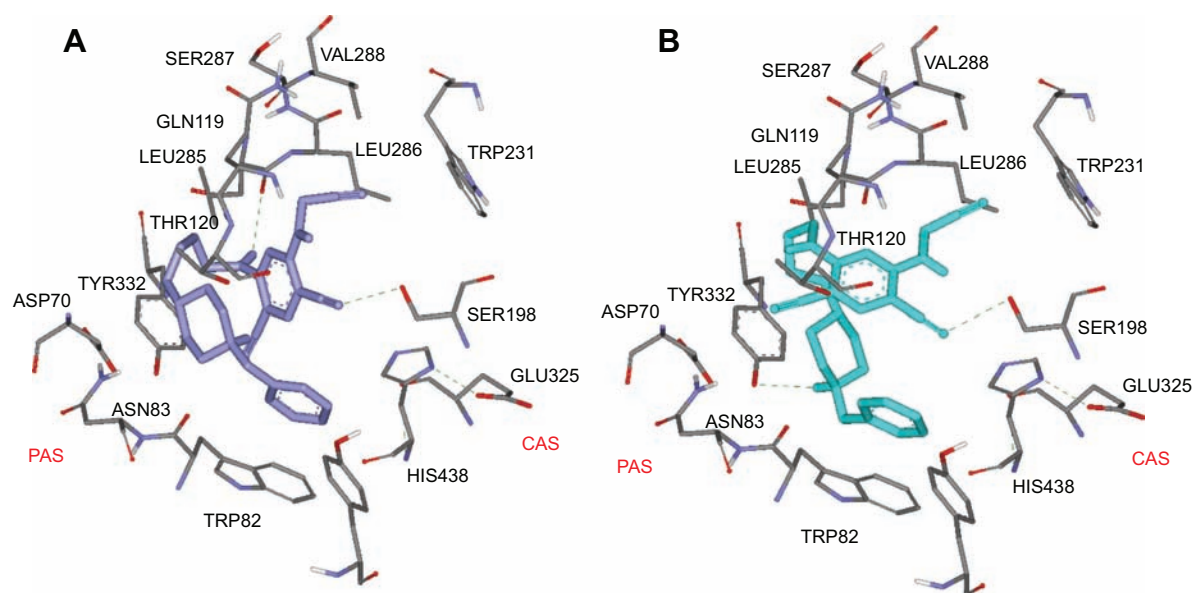


**Figure 7** Complexes of compound DPH14 and eqBuChE homology built 3D-model.

**Notes:** (A) Mode I, compound DPH14 is illustrated in violet (B) Mode II, compound DPH14 is illustrated in blue. Compound DPH14 is rendered as sticks.

**Abbreviations:** DPH, donepezil-pyridyl hybrid; eqBuChE, equine serum butyrylcholinesterase; CAS, catalytic active site; PAS, peripheral anionic site.

Since inhibition data were determined on human MAOs, docking simulations were run on the human model of the MAO A and MAO B isoforms. The 3D structures for hMAOs were retrieved from the PDB (PDB ID: 2Z5X for hMAO A and PDB ID: 2V5Z for hMAO B). Following the protocol previously described for eqBuChE, we have theoretically investigated the recognition process between compound DPH14 (chosen as reference compound) and hMAOs.

Results from several studies have shown that it must be the neutral amine that reaches the active site of MAO A and MAO B that allows the chemistry.<sup>39–42</sup> The docking simulations were done with compound DPH14 as neutral species despite that at physiological pH, most of the piperidine rings would be in the protonated, positively charged form.

As reported in our previous paper,<sup>43</sup> a number of six structural water molecules were explicitly considered in the docking simulations. These water molecules are labeled as w72, w193, w11, w23, w15, and w53 in accordance with the numbering reported for the hMAO B crystallographic structure (PDB ID: 1S3E) and they are located near the flavin adenine dinucleotide (FAD) cofactor.

Figure 8 illustrates the binding mode of DPH14 into the hMAO A binding cavity (binding energy:  $-6.5$  kcal/mol). Visual inspection of the pose of compound DPH14 into the MAO A binding site revealed that the phenyl ring placed in the “aromatic cage” framed by Tyr407, Tyr444 side chains, as well as the isoalloxazine FAD ring and the aromatic ring is oriented to establish  $\pi$ – $\pi$  stacking interactions with the carbonyl group of Gln215 residue. The pyridine moiety is located in a hydrophobic

core delimited by residues Val93, Leu97, and Ala111. Moreover, the amino group of the propargylamine moiety is also able to form a hydrogen bond with Ser209 side chain.

To rationalize the selectivity of MAO A/B, blind docking studies of compound DPH14 into the MAO B were done. The six structural water molecules selected for hMAO A were also included in the study.

Visual inspection of the pose of compound DPH14 into the MAO B binding site revealed that this inhibitor also crosses both cavities, presenting the piperidine nucleus located between the “entrance” and “catalytic” cavities, separated by the residues Ile199 and Tyr326 (Figure 9; binding energy:  $-8.3$  kcal/mol). The substituted-pyridine ring is oriented toward the bottom of the substrate cavity, interacting with the FAD cofactor as well as Tyr398, Tyr435, and Gln206 through van der Waals, hydrophobic interactions and  $\pi$ – $\pi$  interactions. In addition, the predicted orientation of the substituted-pyridine moiety allowed the interaction of the NH hydrogen of the propargylamine moiety with Cys172, showing a favorable geometry for the formation of hydrogen bond between the ligand and the receptor. Moreover, the cyano group in ortho-position with respect to the propargylamine group formed a hydrogen bond with a water molecule. Finally, the phenyl ring is oriented to an entrance cavity, a hydrophobic sub-pocket, which is defined by Pro102, Thr201, Thr314, and Ile316.

The study confirmed the selectivity of compound DPH14 for MAO B isoform. Thus, selectivity is likely due to the

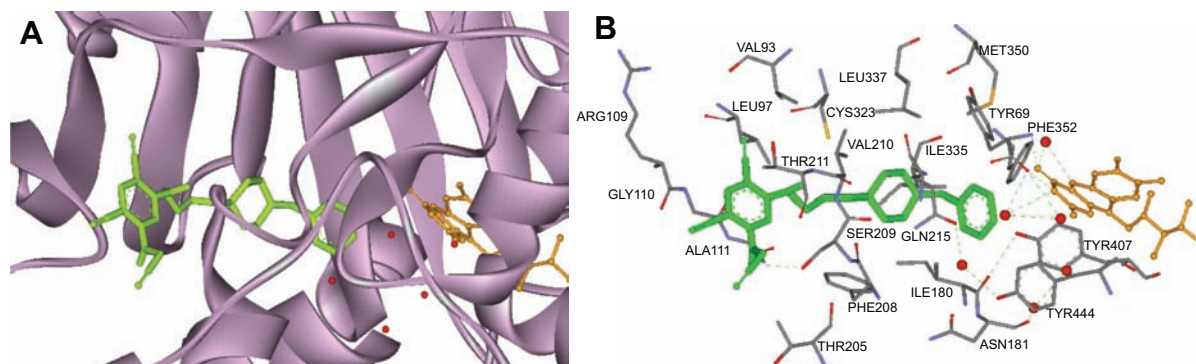


**Figure 8** Docking pose of inhibitor DPH14 into hMAO A.

**Notes:** (A) Crystal structure of hMAO A represented in ribbon diagram. Compound DPH14 is represented as green sticks. (B) Amino acid residues of the binding site are color-coded. The flavin adenine dinucleotide cofactor (FAD) and the six water molecules are represented as an integral part of the hMAO A structure model and are rendered as orange sticks and red balls, respectively. Green dashed lines are drawn among atoms involved in hydrogen bond interactions.

**Abbreviations:** DPH, donepezil-pyridyl hybrid; hMAO A, human monoamine oxidase A.

orientation of the pyridine and phenyl moieties of DPH14 in MAO A and in MAO B. For MAO A, the pyridine system was hosted in the entrance cavity and for MAO B this system occupied the substrate cavity. Compound DPH14 established more interactions with the MAO B active site than with the MAO A active site, indicating that DPH14 might interact more tightly with MAO B.

## Absorption, distribution, metabolism, excretion and toxicity analysis

Absorption, distribution, metabolism, excretion and toxicity (ADMET; ADMET Predictor, v.6.5, Simulations Plus, Inc., Lancaster, CA, USA) analysis has been carried out following the usual methods (Supplementary material <http://www.iqog.csic.es/iqog/sites/default/files/public/User/Jos%C3%A9%20Luis%20Marco%20Contelles/Supplementary%20material.pdf>).<sup>44</sup>

Drugs that penetrate the central nervous system (CNS) should have lower polar surface areas than other kinds of molecules,<sup>45</sup> namely, in the range 60–90 Å<sup>2</sup>. In our study, all the compounds present appropriate values.

The lipophilicity increases with the hydrocarbon tether chain, in such a way that DPH4, 9, and the unmethylated structures DPH11 and DPH12 show  $\log P > 5$  (and/or  $M\log P > 4.1$ ).<sup>46</sup> Similarly, the molecular weight of DPHs4, 9, and 12 fall outside the recommended range (molecular weight <500). Therefore, these structures violate the Lipinski's rule of five.<sup>47</sup> Moreover, a more rigid rule for CNS drug-like characteristics<sup>48</sup> (molecular weight  $\leq 450$ , hydrogen bond donor  $\leq 3$ , hydrogen bond acceptors  $\leq 7$ ,  $\log P \leq 5$ , polar surface area  $\leq 90$ , and number of rotatable bonds  $\leq 8$ ) is only satisfied for DPH5 and 6. DPHs13–16 also show good values despite being too flexible.

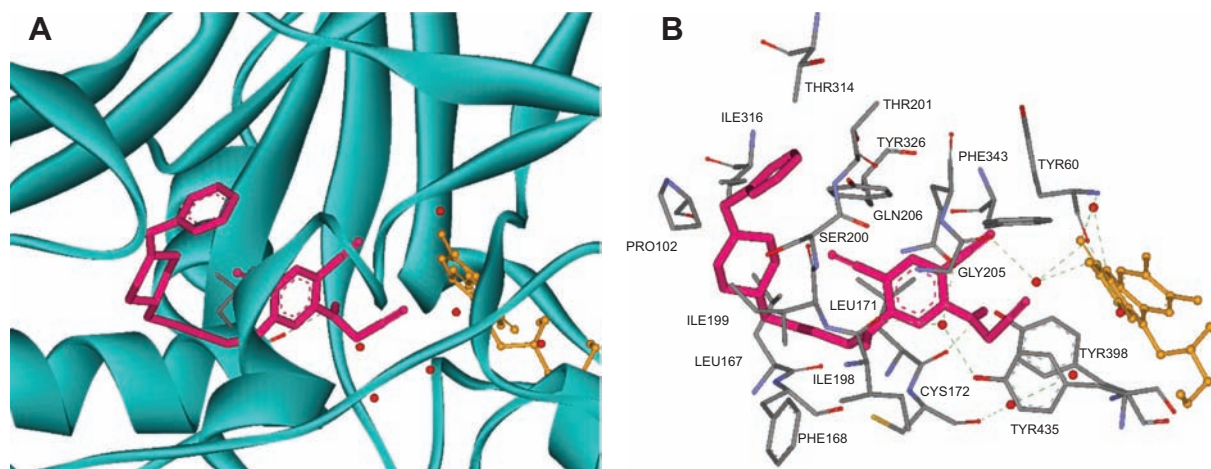


**Figure 9** Docking pose of inhibitor DPH14 into hMAO B.

**Notes:** (A) The protein structure of hMAO B is rendered as a blue cartoon model. Compound DPH14 is represented as pink sticks. (B) Amino acid residues of the binding site are color-coded. The flavin adenine dinucleotide cofactor (FAD) and the six water molecules are represented as an integral part of the hMAO B structure model and are rendered as orange sticks and red balls, respectively.

**Abbreviations:** DPH, donepezil-pyridyl hybrid; hMAO B, human monoamine oxidase B.

The blood–brain barrier (BBB) is a separation of circulating blood and cerebrospinal fluid in the CNS. Predicting BBB penetration means predicting whether compounds pass across the BBB. This is crucial in drug design because CNS-active compounds must pass across it and CNS-inactive compounds must not pass across it in order to avoid CNS side effects. According to the computed values, one of the models predicts that DPHs4, 6, 9–11, 13–16 should be good candidates. In particular, DPHs13–15 show a brain penetration sufficient for CNS activity.<sup>49,50</sup>

Peff quantifies permeability across the intestinal membrane and characterizes absorption whether by passive diffusion, active transport, facilitated diffusion, paracellular diffusion, or any other mechanism. According to the predictions, all the structures show an adequate permeability to be good candidates (Peff >0.1),<sup>51</sup> and should be well absorbed compounds (% human intestinal absorption).<sup>52</sup> Moreover, a middle Caco-2 cell permeability is suggested.<sup>53</sup>

The human Ether-à-go-go Related Gene (hERG) encodes potassium channels, which are responsible for the normal repolarization of the cardiac action potential. Blockage or any other impairment of these channels in the heart cells can lead to fatal cardiac problems. Therefore, drug-induced blockage of potassium channels has been a major concern for the pharmaceutical industry. DPHs4, 6, 9, 14 and 16 show hERG liability.<sup>54</sup> On other hand, DPHs1–5, 9–12 could induce carcinogenicity, whereas none of the molecules is predicted to present hepatotoxicity.<sup>55</sup>

To sum up, the structures lacking phenyl substituent show better druglikeness profiles; in particular, DPHs13–15 present the more suitable ADMET properties of the DPH compounds studied here (Table S3, Supplementary material <http://www.iqog.csic.es/iqog/sites/default/files/public/User/Jos%C3%A9%20Luis%20Marco%20Contelles/Supplementary%20material.pdf>).

## Conclusion

In this paper, the synthesis and biochemical evaluation of the designed novel DPHs is reported. Compound DPH9 was identified as a very potent hAChE inhibitor ( $IC_{50} = 25 \pm 3$  nM) and moderate hBuChE inhibitor ( $IC_{50} = 1,190 \pm 310$  nM) with low selectivity toward hMAO B. However, DPH14 was revealed to be an active hAChE ( $IC_{50} = 13.1 \pm 2.1$  nM) and hBuChE ( $IC_{50} = 835 \pm 139$  nM) inhibitor and a selective moderate irreversible hMAO B inhibitor ( $IC_{50} = 3,950 \pm 940$  nM). As suggested by one of the reviewers, the increased potency on BuChE inhibition might potentiate emetogenic side effects certainly, but as it is very well-known, in old AD patients, AChE levels

are decreased, and BuChE activity is elevated,<sup>56</sup> suggesting that ACh hydrolysis in AD may largely occur via BuChE catalysis.<sup>57</sup> Consequently, increased and/or specific inhibition of BuChE is important in raising ACh levels and improving cognition.<sup>58</sup>

Taking these initial results into account, and considering that in AD brain MAO B isoform is overexpressed and contributing consequently to the oxidative stress,<sup>59</sup> DPH14 was selected as the most promising candidate to be further studied.

The 3D-QSAR study of 37 donepezil-indolyl and DPHs was used to define 3D-pharmacophores for inhibition of MAO A/B, AChE, and BuChE enzymes and to design DPHs as novel multipotent ligands (Supplementary material <http://www.iqog.csic.es/iqog/sites/default/files/public/User/Jos%C3%A9%20Luis%20Marco%20Contelles/Supplementary%20material.pdf>). The 3D-QSAR study has selected structural modifications of the examined hybrids that could selectively enhance inhibiting activity on MAO A/B, AChE, and BuChE. Substitution of the terminal hydrogen of propargylamine moiety with bulky groups and replacement of the methyl substituent with hydrogen in the *N*-Me group of the indole moiety could selectively increase MAO A inhibiting activity, while bulky groups in meta/para positions of the benzyl moiety are able to decrease MAO A inhibiting activity of the examined hybrids. New electron-donating substituents in propargylamine or indole moiety and also bulky substituents on *N*-atom of the indole moiety could selectively enhance MAO B activity. Furthermore, an electron withdrawing bulky groups at meta/para positions of the benzyl moiety are able to selectively increase MAO B inhibiting activity of the examined hybrids. Extension of the *N*-alkyl bridge could selectively and strongly enhance AChE inhibiting activity, while BuChE inhibiting activity could be slightly increased too. Phenyl substituent in the pyridine ring is able to selectively enhance AChE inhibiting activity, while substitution in meta position of the phenyl group could result in decrease of AChE inhibiting activity.

In addition, we have found that the structures lacking phenyl substituent show better druglikeness profiles; in particular, DPH14 presents the more suitable ADMET properties of the series.

Molecular modeling of inhibitor DPH14 within EeAChE showed a binding mode with an extended conformation, interacting simultaneously with both catalytic and peripheral sites of EeAChE thanks to a linker of appropriate length. It is clear that the linear conformation allows DPH14 (Modes I and II) to span both CAS and PAS which contributes to its superior binding toward EeAChE. Similarly, visual

inspection of the pose of compound DPH14 into the MAO B binding site revealed that this inhibitor also crosses both cavities, presenting the piperidine nucleus located between the entrance and catalytic cavities, separated by the residues Ile199 and Tyr326. The observed MAO A/B selectivity is likely due to the orientation of the pyridine and phenyl moieties of DPH14 in MAO A and in MAO B. For MAO A, the pyridine system was hosted in the entrance cavity and for MAO B this system occupied the substrate cavity. Compound DPH14 established more interactions with the MAO B active site compared to the MAO A active site, which may indicate that DPH14 interacts more tightly with MAO B.

To sum up, donepezil-pyridyl hybrid DPH14 is a promising new multipotent molecule for the potential prevention and treatment of AD.

## Acknowledgments

This work was supported by the European Cooperation in Science and Technology (COST) action CM1103. KN and DA acknowledge project supported by the Ministry of Education and Science of the Republic of Serbia, Contract 172033. JMC and MU thank Ministerio de Economía y Competitividad (MINECO) (Spain) for support (SAF2009-07271; SAF2012-33304). OMB-A thanks MINECO (Spain) for an Formación del Personal Investigador (FPI) fellowship.

## Disclosure

The authors report no conflicts of interest in this work.

## References

- Goedert M, Spillantini MG. A Century of Alzheimer's disease. *Science*. 2006;314(5800):777–781.
- Kung HF. The  $\beta$ -amyloid hypothesis in Alzheimer's disease: seeing is believing. *ACS Med Chem Lett*. 2012;3(4):265–267.
- Ballatore C, Lee VM, Trojanowski JQ. Tau-mediated neurodegeneration in Alzheimer's disease and related disorders. *Nat Rev Neurosci*. 2007; 8(9):663–672.
- Gella A, Durany N. Oxidative stress in Alzheimer disease. *Cell Adh Migr*. 2009;3(1):88–93.
- Jakob-Roetne R, Jacobsen H. Alzheimer's disease: from pathology to therapeutic approaches. *Angew Chem Int Ed Engl*. 2009;48(17): 3030–3059.
- Sugimoto H, Yamanishi Y, Iimura Y, Kawakami Y. Donepezil hydrochloride (E2020) and other acetylcholinesterase inhibitors. *Curr Med Chem*. 2000;7(3):303–339.
- Marco-Contelles J, do Carmo Carreiras M, Rodríguez C, Villarroya M, García AG. Synthesis and pharmacology of galantamine. *Chem Rev*. 2006;106(1):116–133.
- Anand P, Singh B. A review on cholinesterase inhibitors for Alzheimer's disease. *Arch Pharm Res*. 2013;36(4):375–399.
- Barbanti P, Fabbrini G, Ricci A, et al. Reduced density of dopamine D2-like receptors on peripheral blood lymphocytes in Alzheimer's disease. *Mech Ageing Dev*. 2000;120(1–3):65–75.
- Thompson AJ, Lummis SC. The 5-HT3 receptor as a therapeutic target. *Expert Opin Ther Targets*. 2007;11(4):527–540.
- Shih JC, Chen K, Ridd MJ. Monoamine oxidase: from genes to behavior. *Annu Rev Neurosci*. 1999;22:197–217.
- Riederer P, Danielczyk W, Grünblatt E. Monoamine oxidase-B inhibition in Alzheimer's disease. *Neurotoxicology*. 2004;25(1–2):271–277.
- Pizzinat N, Copin N, Vindis C, Parini A, Cambon C. Reactive oxygen species production by monoamine oxidases in intact cells. *Naunyn Schmiedebergs Arch Pharmacol*. 1999;359(5):428–431.
- Kristal BS, Conway AD, Brown AM, et al. Selective dopaminergic vulnerability: 3,4-dihydroxyphenylacetaldehyde targets mitochondria. *Free Radical Biol Med*. 2001;30(8):924–931.
- Sterling J, Herzig Y, Goren T, et al. Novel dual inhibitors of AChE and MAO derived from hydroxy aminoindan and phenethylamine as potential treatment for Alzheimer's disease. *J Med Chem*. 2002;45(24): 5260–5279.
- Yogev-Falach M, Bar-Am O, Amit T, Weinreb O, Youdim MB. A multifunctional, neuroprotective drug, ladostigil (TV3326), regulates holo-APP translation and processing. *FASEB J*. 2006;20(12): 2177–2179.
- Youdim MB, Weinstock M. Molecular basis of neuroprotective activities of rasagiline and the anti-Alzheimer drug TV3326 [par;N-Propargyl-(3R) aminoindan-5-YL-ethyl methyl carbamate]. *Cell Mol Neurobiol*. 2002;21(6):555–573.
- Bar-Am O, Amit T, Weinreb O, Youdim MB, Mandel S. Propargylamine containing Compounds as modulators of proteolytic cleavage of amyloid protein precursor: involvement of MAPK and PKC activation. *J Alzheimer's Dis*. 2010;21(2):361–371.
- Bruehlmann C, Ooms F, Carrupt PA, et al. Coumarins derivatives as dual inhibitors of acetylcholinesterase and monoamine oxidase. *J Med Chem*. 2001;44(19):3195–3198.
- Zheng H, Fridkin M, Youdim MB. Novel chelators targeting cell cycle arrest, acetylcholinesterase, and monoamine oxidase for Alzheimer's therapy. *Curr Drug Targets*. 2012;13(8):1096–1113.
- Samadi A, Marco-Contelles J, Soriano E, et al. Multipotent drugs with cholinergic and neuroprotective properties for the treatment of Alzheimer and neuronal vascular diseases. I. Synthesis, biological assessment, and molecular modeling of simple and readily available 2-aminopyridine-, and 2-chloropyridine-3,5-dicarbonitriles. *Bioorg Med Chem*. 2010;18(16):5861–5872.
- Bolea I, Juárez-Jiménez J, de los Ríos C, et al. Synthesis, biological evaluation, and molecular modeling of donepezil and *N*-[(5-(benzyloxy)-1-methyl-1*H*-indol-2-yl)methyl]-*N*-methylprop-2-yn-1-amine hybrids as new multipotent cholinesterase/monoamine oxidase inhibitors for the treatment of Alzheimer's disease. *J Med Chem*. 2011;54(24): 8251–8270.
- Pérez V, Marco JL, Fernández-Álvarez E, Unzeta M. Relevance of benzyloxy group in 2-indolyl methylamines in the selective MAO-B inhibition. *Brit J Pharmacol*. 1999;127(4):869–876.
- Samadi A, Chioua M, Bolea I, et al. Synthesis, biological assessment and molecular modeling of new multipotent MAO and cholinesterase inhibitors as potential drugs for the treatment of Alzheimer's disease. *Eur J Med Chem*. 2011;46(9):4665–4668.
- Peinador C, Veiga MC, Vilar J, Quintela. A synthesis of heterocyclic ring systems. Pyrido[3',2':4,5]thieno[2,3-b]pyrrolizine and pyrido[6',5':4,5][3',2':4,5]dithieno[2,3-b':2,3-b]dipyrrolizine. *Heterocycles*. 1994;38(6):1299–1305.
- Vilarelle DV, Peinador C, Quintela JM. Synthesis of pyrido and pyrazinodithienodipyrimidine-4,8(3*H*,9*H*)-dione derivatives by the aza-Wittig methodology. *Tetrahedron*. 2004;60(2):275–283.
- Murray TJ, Zimmerman SC, Kolotuchin SV. Synthesis of heterocyclic compounds containing three contiguous hydrogen bonding sites in all possible arrangements. *Tetrahedron*. 1995;51(2):635–648.
- Piper JR, McCaleb GS, Montgomery JA, Kisliuk RL, Gaumont Y, Sirotnak FM. Syntheses and antifolate activity of 5-methyl-5-deaza analogs of aminopterin, methotrexate, folic acid, and N10-methylfolic acid. *J Med Chem*. 1986;29(6):1080–1087.

29. Samadi A, Estrada M, Pérez C, et al. Pyridonepezils, new dual AChE inhibitors as potential drugs for the treatment of Alzheimer's disease: Synthesis, biological assessment, and molecular modelling. *Eur J Med Chem.* 2012;57:296–301.
30. Atsushi K, Mitsuru O, Hisashi T; inventors. Fujisawa Pharmaceutical Co.; applicant. Oxadiazole derivatives having acetylcholinesterase-inhibitory and muscarinic agonist activity. Patent publication number WO9313083A1. 1993 Jul 8.
31. Contreras JM, Rival YM, Chayer S, Bourguignon JJ, Wermuth CG. Aminopyridazines as acetylcholinesterase inhibitors. *J Med Chem.* 1999;42(4):730–741.
32. Ellman GL, Courtney KD, Andres V Jr, Feather-stone RM. A new and rapid colorimetric determination of acetylcholinesterase activity. *Biochem Pharmacol.* 1961;7(2):88–95.
33. Zhou M, Panchuk-Valashina N. A one-step fluorometric method for the continuous measurement of monoamine oxidase activity. *Anal Biochem.* 1997;253(2):169–174.
34. León R, Marco-Contelles J. A step further towards multitarget drugs for Alzheimer and neuronal vascular diseases: targeting the cholinergic system, amyloid- $\beta$  aggregation and  $\text{Ca}^{2+}$  dyshomeostasis. *Curr Med Chem.* 2011;18(4):552–576.
35. Trott O, Olson AJ. AutoDock Vina: improving the speed and accuracy of docking with a new scoring function, efficient optimization, and multithreading. *J Comput Chem.* 2010;31(2):455–461.
36. Arnold K, Bordoli L, Kopp J, Schwede T. The SWISS-MODEL workspace: a web-based environment for protein structure homology modelling. *Bioinformatics.* 2006;22(2):195–201.
37. Kiefer F, Arnold K, Künzli M, Bordoli L, Schwede T. The SWISS-MODEL Repository and associated resources. *Nucl Acids Res.* 2009; 37(Database issue):D387–D392.
38. Guex N, Peitsch MC, Schwede T. Automated comparative protein structure modeling with SWISS-MODEL and Swiss-PdbViewer: a historical perspective. *Electrophoresis.* 2009;30(Suppl 1):S162–S173.
39. Edmonson DE, Mattevi A, Binda C, Li M, Hubalek F. Structure and mechanism of Monoamine Oxidase. *Curr Med Chem.* 2004;11(15): 1983–1993.
40. Jones TZ, Balsa D, Unzeta M, Ramsay RR. Variations in activity and inhibition with pH: the protonated amine is the substrate for monoamine oxidase, but uncharged inhibitors bind better. *J Neural Transm.* 2007; 114(6):707–712.
41. Wang J, Edmonson DE.  $^2\text{H}$  kinetic isotope effects and pH dependence of catalysis as mechanistic probes of rat Monoamine Oxidase A: comparisons with the human enzyme. *Biochemistry.* 2011;50(35):7710–7717.
42. Scerrera RA, Leo AJ. Multi-pH QSAR: a method to differentiate the activity of neutral and ionized species and obtain true correlations when both species are involved. *Molecular Informatics.* 2010;29(10): 687–693.
43. Samadi A, de los Ríos C, Bolea I, et al. Multipotent MAO and cholinesterase inhibitors for the treatment of Alzheimer's disease: synthesis, pharmacological analysis and molecular modeling of heterocyclic substituted alkyl and cycloalkyl propargyl amine. *Eur J Med Chem.* 2012;52:251–262.
44. ACD/Percepta 14.0.0, Advanced Chemistry Development, 2013.
45. Kragh-Hansen U. Molecular aspects of ligand binding to serum albumin. *Pharmacol Rev.* 1981;33:17–53.
46. Moriguchi I, Hirono S, Liu Q, Nakagome I, Matsushita Y. Simple method of calculating octanol/water partition coefficient. *Chem Pharm Bull.* 1992;40(1):127–130.
47. Lipinski CA, Lombardo F, Dominy BW, Feeney PJ. Experimental and computational approaches to estimate solubility and permeability in drug discovery and development settings. *Adv Drug Deliv Rev.* 2001; 46(1–3):3–26.
48. Pajouhesh H, Lenz GR. Medicinal chemical properties of successful central nervous system drugs. *NeuroRx.* 2005;2(4):541–553.
49. Ma XL, Chen C, Yang Y. Predictive model of blood-brain barrier penetration of organic compounds. *Acta Pharmacol Sin.* 2005;26(4): 500–512.
50. Cheng F, Li W, Zhou Y, et al. admetSAR: a comprehensive source and free tool for assessment of chemical ADMET properties. *J Chem Inf Model.* 2012;52(11):3099–3105.
51. Lennernas H. Human intestinal permeability. *J Pharm Sci.* 1998;87(4): 403–410.
52. Yee S. In vitro permeability across caco-2 cells (Colonic) can predict in vivo (small intestinal) absorption in man – Fact or myth. *Pharm Res.* 1997;14(6):763–766.
53. Yamashita S, Furubayashi T, Kataoka M, Sakane T, Sezaki H, Tokuda H. Optimized conditions for prediction of intestinal drug permeability using Caco-2 cells. *Eur J Pharm Sci.* 2000;10(3):195–204.
54. Gold LS, Manley NB, Slone TH, Rohrbach L. Supplement to the Carcinogenic Potency Database (CPDB): results of animal bioassays published in the general literature in 1993 to 1994 and by the National Toxicology Program in 1995 to 1996. *Enviro Health Perspect.* 1999; 107(Suppl 4):527–600.
55. Matthews EJ, Kruhlak NL, Benz RD, Contrera JF. Assessment of the health effects of chemicals in humans: I. QSAR estimation of the maximum recommended therapeutic dose (MRTD) and no effect level (NOEL) of organic chemicals based on clinical trial data. *Curr Drug Discov Technol.* 2004;1(1):61–76.
56. Arendt T, Bruckner MK, Lange M, Bigl V. Changes in acetylcholinesterase and butyrylcholinesterase in Alzheimer's disease resemble embryonic development. A study of molecular forms. *Neurochem Int.* 1992;21(3):381–396.
57. Darvesh S, Hopkins DA, Geula C. Neurobiology of butyrylcholinesterase. *Nat Rev Neurosci.* 2003;4(2):131–138.
58. Greig NH, Utsuki T, Ingram DK, et al. Selective butyrylcholinesterase inhibition elevates brain acetylcholine, augments learning and lowers Alzheimer  $\beta$ -amyloid peptide in rodent. *Proc Natl Acad Sci U S A.* 2005;102(47):17213–17218.
59. Saura J, Bleuel Z, Ultrich J, et al. Molecular neuroanatomy of human monoamine oxidases A and B revealed by quantitative enzyme radioautography and *in situ* hybridization histochemistry. *Neuroscience.* 1996;70(3):755–774.

## Supplementary material

Available from: <http://www.iqog.csic.es/iqog/sites/default/files/public/User/Jos%C3%A9%20Luis%20Marco%20Contelles/Supplementary%20material.pdf>

### Drug Design, Development and Therapy

Dovepress

### Publish your work in this journal

Drug Design, Development and Therapy is an international, peer-reviewed open-access journal that spans the spectrum of drug design and development through to clinical applications. Clinical outcomes, patient safety, and programs for the development and effective, safe, and sustained use of medicines are a feature of the journal, which

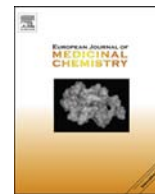
has also been accepted for indexing on PubMed Central. The manuscript management system is completely online and includes a very quick and fair peer-review system, which is all easy to use. Visit <http://www.dovepress.com/testimonials.php> to read real quotes from published authors.

Submit your manuscript here: <http://www.dovepress.com/drug-design-development-and-therapy-journal>

## **Chapter IV.**

**“Donepezil + propargylamine + 8-hydroxyquinoline hybrids as new multifunctional metal-chelators, ChE and MAO inhibitors for the potential treatment of Alzheimer's disease”**





## Original article

# Donepezil + propargylamine + 8-hydroxyquinoline hybrids as new multifunctional metal-chelators, ChE and MAO inhibitors for the potential treatment of Alzheimer's disease



Li Wang<sup>a,1</sup>, Gerard Esteban<sup>b,1</sup>, Masaki Ojima<sup>a</sup>, Oscar M. Bautista-Aguilera<sup>c</sup>, Tsutomu Inokuchi<sup>a,\*</sup>, Ignacio Moraleda<sup>d</sup>, Isabel Iriepa<sup>d</sup>, Abdelouahid Samadi<sup>c</sup>, Moussa B.H. Youdim<sup>e</sup>, Alejandro Romero<sup>f</sup>, Elena Soriano<sup>g</sup>, Raquel Herrero<sup>h</sup>, Ana Patricia Fernández Fernández<sup>h</sup>, Ricardo-Martínez-Murillo<sup>h</sup>, José Marco-Contelles<sup>c,\*</sup>, Mercedes Unzeta<sup>b,\*</sup>

<sup>a</sup> Division of Chemistry and Biotechnology, Graduate School of Natural Science and Technology, Okayama University, 3.1.1 Tsushima-Naka, Kita-ku, Okayama 700-8530, Japan

<sup>b</sup> Departament de Bioquímica i Biologia Molecular, Facultat de Medicina, Institut de Neurociències, Universitat Autònoma de Barcelona, 08193 Bellaterra, Barcelona, Spain

<sup>c</sup> Laboratorio de Química Médica (IQOG, CSIC), C/Juan de la Cierva 3, 28006 Madrid, Spain

<sup>d</sup> Departamento de Química Orgánica y Química Inorgánica, Universidad de Alcalá, Ctra. Madrid-Barcelona, Km. 33,6, 28871 Alcalá de Henares, Madrid, Spain

<sup>e</sup> Eve Topf Centers of Excellence for Neurodegenerative Diseases Research and Department of Pharmacology, Rappaport Family Research Institute, Technion-Faculty of Medicine, Haifa 31096, Israel

<sup>f</sup> Departamento de Toxicología y Farmacología, Facultad de Veterinaria, Universidad Complutense de Madrid, 28040 Madrid, Spain

<sup>g</sup> SEPCO, IQOG (CSIC), Juan de la Cierva, 3, 28006 Madrid, Spain

<sup>h</sup> Neurovascular Research Group, Department of Molecular, Cellular and Developmental Neurobiology, Instituto Cajal (CSIC) Av. Doctor Arce 37, 28002 Madrid, Spain

## ARTICLE INFO

## Article history:

Received 10 February 2014

Received in revised form

24 April 2014

Accepted 26 April 2014

Available online 29 April 2014

## Keywords:

Donepezil + Propargylamine + 8-Hydroxyquinoline hybrids

Multifunctional drugs

Fe/Cu/Zn chelators

ChE and MAO inhibitors

*In vivo* scopolamine-induced long-term memory deficit

Alzheimer's disease

## ABSTRACT

The synthesis, biochemical evaluation, ADMET, toxicity and molecular modeling of novel multi-target-directed Donepezil + Propargylamine + 8-Hydroxyquinoline (DPH) hybrids **1–7** for the potential prevention and treatment of Alzheimer's disease is described. The most interesting derivative was racemic  $\alpha$ -aminotrile-4-(1-benzylpiperidin-4-yl)-2-(((8-hydroxyquinolin-5-yl)methyl)(prop-2-yn-1-yl)amino)butanenitrile (DPH6) [MAO A (IC<sub>50</sub> = 6.2 ± 0.7 μM; MAO B (IC<sub>50</sub> = 10.2 ± 0.9 μM); AChE (IC<sub>50</sub> = 1.8 ± 0.1 μM); BuChE (IC<sub>50</sub> = 1.6 ± 0.25 μM)], an irreversible MAO A/B inhibitor and mixed-type AChE inhibitor with metal-chelating properties. According to docking studies, both DPH6 enantiomers interact simultaneously with the catalytic and peripheral site of EeAChE through a linker of appropriate length, supporting the observed mixed-type AChE inhibition. Both enantiomers exhibited a relatively similar position of both hydroxyquinoline and benzyl moieties with the rest of the molecule easily accommodated in the relatively large cavity of MAO A. For MAO B, the quinoline system was hosted at the cavity entrance whereas for MAO A this system occupied the substrate cavity. In this disposition the quinoline moiety interacted directly with the FAD aromatic ring. Very similar binding affinity values were also observed for both enantiomers with ChE and MAO enzymes. DPH derivatives exhibited moderate to good ADMET properties and brain penetration capacity for CNS activity. DPH6 was less toxic than donepezil at high concentrations; while at low concentrations both displayed a similar cell viability profile. Finally, in a passive avoidance task, the anti-amnesic effect of DPH6 was tested on mice with experimentally induced amnesia. DPH6 was capable to significantly decrease scopolamine-induced learning deficits in healthy adult mice.

© 2014 Elsevier Masson SAS. All rights reserved.

\* Corresponding authors.

E-mail addresses: [Mercedes.Unzeta@uab.cat](mailto:Mercedes.Unzeta@uab.cat), [mercedes.unzeta@uab.es](mailto:mercedes.unzeta@uab.es) (M. Unzeta).

<sup>1</sup> G.E. and L.W. have equally contributed to this work.

## 1. Introduction

Alzheimer's disease (AD) is an age-related neurodegenerative process characterized by progressive memory loss and other cognitive impairments [1]. Although its etiology has not yet been elucidated,  $\beta$ -amyloid ( $A\beta$ ) deposits [2],  $\tau$ -protein phosphorylation, oxidative stress [3] and deficits of acetylcholine (ACh) [4] are considered to play significant roles in the pathophysiology of AD [5]. Consequently, AD patients have been treated with acetylcholinesterase inhibitors (AChEI) [6] with limited therapeutic success. This might be due to the multifactorial nature of AD, a fact that has prompted the hunt for new Multi-Target-Directed Ligands (MTDL), based on the "one molecule, multiple target" paradigm [7]. Thus, in this context, multifunctional molecules able to simultaneously bind both cholinesterases and monoamine oxidases have been investigated [8,9].

Monoamine oxidase (MAO; EC 1.4.3.4) is an important target to be considered for the treatment of AD, as it catalyzes the oxidative deamination of a variety of biogenic and xenobiotic amines with the concomitant production of hydrogen peroxide, a key intermediate *via* Fenton reaction in the production of toxic radical oxygenated species implicated in the progress of AD. MAO is a FAD (Flavin-Adenine Dinucleotide)-containing enzyme bound to mitochondrial outer membranes of neuronal, glial and other cells [10]. MAO exists as two isoenzymes, MAO A/B, displaying different substrate specificity, sensitivity to inhibitors, and amino acid sequences. While MAO A preferentially oxidizes neurotransmitters norepinephrine and serotonin and it is selectively inhibited by clorgyline, MAO B preferentially deaminates  $\beta$ -phenylethylamine and it is irreversibly inhibited by l-deprenyl [11]. X-ray crystal structures of rat MAO A [12] and human MAO B have been reported [13].

Taken these facts into account, we previously reported the synthesis and biological evaluation of new multifunctional MAO/ChE inhibitor ASS234 [8,9] (Chart 1) by combining the N-benzylpiperidine and the N-propargylamine moieties present in donepezil, and PF9601N [14], ChE and MAO inhibitors, respectively.

In this work we report the design, synthesis, biochemical evaluation and molecular modeling of Donepezil + Propargylamine + 8-Hydroxyquinoline (DPH) hybrids 1–7 and the identification of the racemic  $\alpha$ -aminonitrile 4-(1-benzylpiperidin-4-yl)-2-(((8-hydroxyquinolin-5-yl)methyl)(prop-2-yn-1-yl)amino)butanenitrile (DPH6) (Table 1), as a multifunctional lead molecule for the potential treatment of AD. These hybrids are the result of the juxtaposition of donepezil, a selective AChE inhibitor currently used in the pharmacological treatment of AD, and M30 (Chart 1), a potent brain selective MAO A/B inhibitor and neuroprotective biometal-chelator [15]. HLA20A (Chart 1) is a novel pro-chelator with improved cytotoxicity exhibiting poor affinity for metal ions while not being activated to an active chelator by binding and inhibiting AChE, being able to modulate amyloid precursor protein (APP) and to reduce  $A\beta$  aggregation [16].

## 2. Results and discussion

### 2.1. Chemistry

DPHs 1–7 were prepared as shown in Schemes 1–5 by using reductive amination of suitable and different carbaldehydes bearing the N-benzylpiperidine nucleus and propargylamine, followed by N-alkylation with easily available 5-(chloromethyl)quinolin-8-ol (**8**) [17] (Experimental Part).

In the reductive amination leading to the intermediates for the preparation of DPH3, DPH5 and DPH7, we have also isolated and characterized the unexpected  $\alpha$ -aminonitriles **11**, **16** and **21** that

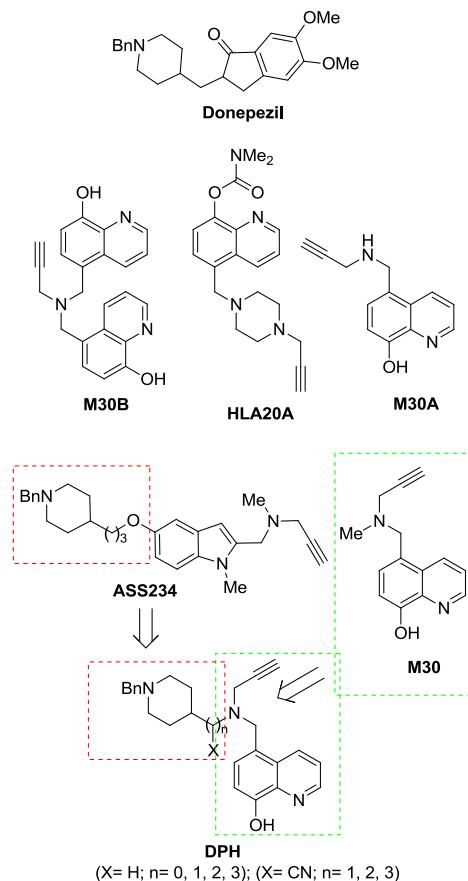


**Chart 1.** General structure of donepezil, M30, M30A, M30B, HLA20A, ASS234, and the new multifunctional ChE/MAO DPH inhibitors described in this work.

have been similarly transformed into racemic  $\alpha$ -aminonitriles **DPH2**, **DPH4** and **DPH6**. In order to confirm the structure of **DPH6**, an alternative, unequivocal synthesis of  $\alpha$ -aminonitrile **21** has been achieved from aldehyde **19** *via* Strecker-type reaction (Scheme 5), followed by standard N-alkylation as shown above.

All new compounds showed analytical and spectroscopic data, in good agreement with their structure (Experimental Part).

### 2.2. Pharmacological evaluation

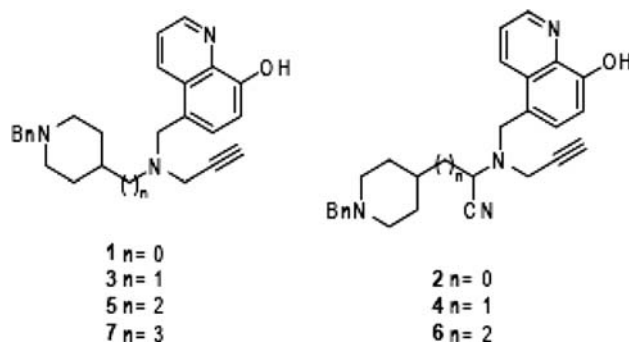
#### 2.2.1. Cholinesterase inhibition

The *in vitro* activity of DPHs 1–7 derivatives as *Ee*AChE and *eqBu*ChE inhibitors was assessed using the Ellman's method [18] (Table 1).

From these data some interesting structure–activity relationships (SAR) were obtained. DPH1, bearing no methyl in the linker connecting the N-benzylpiperidin-4'-yl residue to the N-propargyl core, was inactive. In comparison, DPHs 2–7 derivatives were non-selective moderate ChE inhibitors, DPH6 ( $n = 3$  in the linker) exhibiting the most potent profile [*Ee*AChE ( $IC_{50} = 1.8 \pm 0.1 \mu M$ ); *eqBu*ChE ( $IC_{50} = 1.6 \pm 0.25 \mu M$ )]. Regarding tertiary amines DPHs 3, 5 and 7, activity at inhibiting both cholinesterases gradually increased from DPH3 ( $n = 1$ ) to DPH7 ( $n = 3$ ), which displayed the most active profile [*Ee*AChE ( $IC_{50} = 2.7 \pm 0.4 \mu M$ ); *eqBu*ChE ( $IC_{50} = 4.5 \pm 0.3 \mu M$ )]. A similar trend was detected with the  $\alpha$ -aminonitrile series (DPHs 2, 4 and 6), with DPH6 ( $n = 3$ ) as the most potent anticholinesterasic compound. Generally, for equivalent linker length,  $\alpha$ -aminonitriles derivatives proved to be more potent than amines at inhibiting both enzymes, with the exception of

**Table 1**

Dose-response values [ $IC_{50}$  ( $\mu M$ )] of membrane-bound MAO A and MAO B from rat liver, electric eel AChE (*EeAChE*) and equine BuChE (*eqBuChE*) with DPH derivatives and standard inhibitors.



DPH	<i>EeAChE</i> <sup>a</sup>	<i>eqBuChE</i> <sup>a</sup>	SI <sup>c</sup>	ratMAO A <sup>b</sup>	ratMAO B <sup>b</sup>	SI <sup>d</sup>
<b>1</b>	≥100	≥100	–	≥100	≥100	≥1
<b>2</b>	14.5 ± 3.7	13.5 ± 1.8	0.92	22.1 ± 0.7	39.5 ± 1.4	1.7
<b>3</b>	17.0 ± 4.7	12.8 ± 1.4	0.75	85.4 ± 3.7	19.4 ± 3.2	0.22
<b>4</b>	5.5 ± 0.5	6.1 ± 0.6	1.1	9.7 ± 1.5	12.4 ± 2.5	1.2
<b>5</b>	5.0 ± 0.8	14.5 ± 3.6	2.8	≥100	50.1 ± 5.0	≥0.5
<b>6</b>	1.8 ± 0.1	1.6 ± 0.2	0.92	6.2 ± 0.7	10.2 ± 0.9	1.7
<b>7</b>	2.7 ± 0.4	4.5 ± 0.3	1.6	≥100	34.5 ± 3.5	≥0.34
<b>Donepezil</b>	0.0067 ± 0.0004	7.4 ± 0.1	1100	850 ± 13	15 ± 2.2	0.02
<b>M-30 [15]</b>	≥100	–	0.037 ± 0.02	0.057 ± 0.02	1.5	–
113.9 ± 14.05						
<b><i>l</i>-Deprenyl [14]</b>	≥500	–	3	0.02	0.0067	–
≥500						
<b>Clorgyline [22]</b>	≥500	≥500	–	0.03	8	267

end = values not determined.

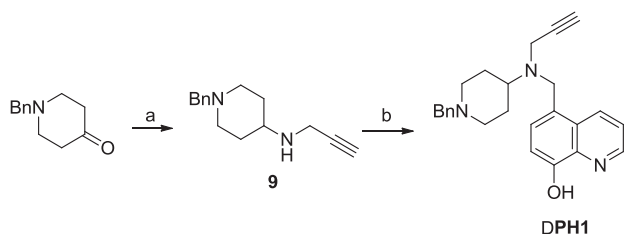
Values are expressed as mean ± standard error of the mean of at least three different experiments in quadruplicate.

<sup>a</sup> 20-min pre-incubation.

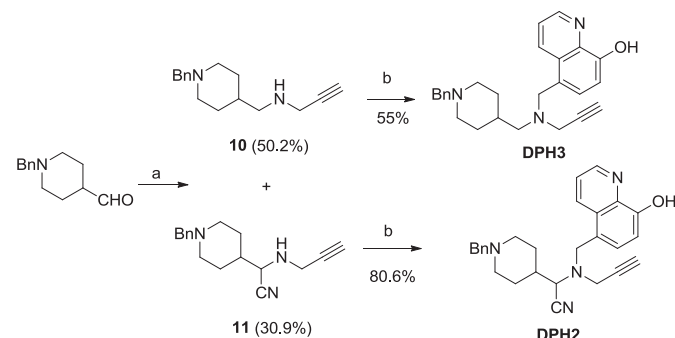
<sup>b</sup> 30-min pre-incubation.

<sup>c</sup> *eqBuChE* selectivity index =  $IC_{50}$  (*eqBuChE*)/ $IC_{50}$  (*EeAChE*).

<sup>d</sup> MAO B selectivity index =  $IC_{50}$  (MAO B)/ $IC_{50}$  (MAO A).

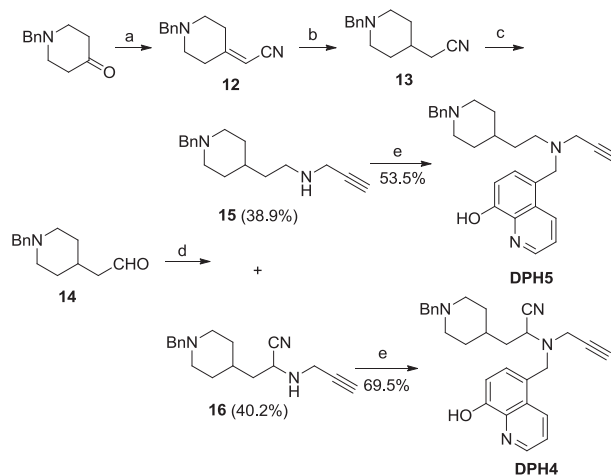


**Scheme 1.** Synthesis of **DPH1**. Reagents and conditions: (a) i. 1-Benzyl-4-piperidone, MeOH, TFA; ii.  $NaBH_3CN$  (31%); (b) 5-(chloromethyl) quinolin-8-ol (8), DCM,  $Et_3N$  (33%).

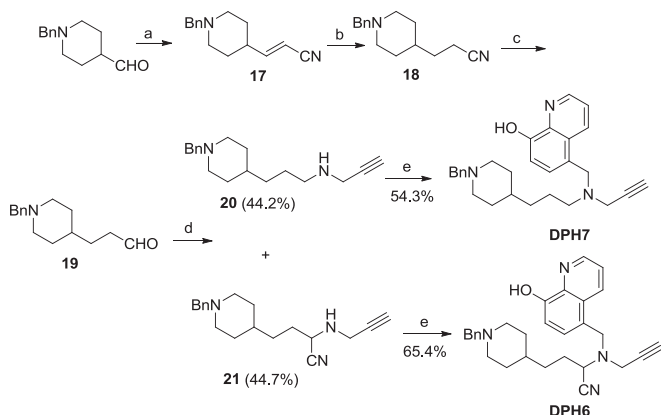


**Scheme 2.** Synthesis of **DPH2** and **DPH3**. Reagents and conditions: (a) i. Propargylamine, MeOH, TFA; ii.  $NaBH_3CN$ ; (b) 5-(chloromethyl) quinolin-8-ol (8), DCM,  $Et_3N$ .

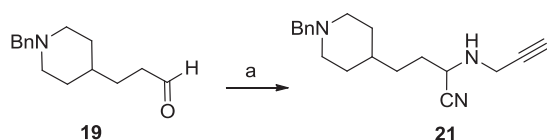
DPH4 and DPH5 exhibiting similar antiacetylcholinesterase activity. In comparison to donepezil, DPH6 was significantly less active *EeAChE* inhibitor, but more potent at inhibiting *eqBuChE* (4.5-fold). Moreover, DPH6 was 64-fold more potent inhibiting both cholinesterases than M30 (Chart 1), inactive on this enzyme.



**Scheme 3.** Synthesis of **DPH4** and **DPH5**. Reagents and conditions: (a) Diethyl(cyanomethyl)phosphonate,  $K_2CO_3$ , THF (99%); (b)  $I_2$ , Mg, MeOH (74%); (c) DIBALH, THF,  $-78^\circ C$  (27%); (d) i. Propargylamine, MeOH, TFA; ii.  $NaBH_3CN$ ; (e) 5-(chloromethyl) quinolin-8-ol (8), DCM,  $Et_3N$ .



**Scheme 4.** Synthesis of **DPH6** and **DPH7**. Reagents and conditions: (a) Diethyl(cyanomethyl) phosphonate,  $K_2CO_3$ , THF (33%); (b)  $I_2$ , Mg, MeOH (99%); (c) DIBALH, THF,  $-78^\circ C$  (28); (d) i. Propargylamine, MeOH, TFA; ii.  $NaBH_3CN$ ; (e) 5-(chloromethyl) quinolin-8-ol (8), DCM,  $Et_3N$ .



**Scheme 5.** Alternative synthesis of compound **21**. Reagents and conditions: (a) Propargylamine, TMSCN, MWI,  $125^\circ C$ , 10 min (60%)

To determine the type of AChE inhibition exerted by **DPH6**, Lineweaver–Burk reciprocal plots were obtained (Fig. 1). Increasing slopes (decreasing  $V_{max}$ ) and intercepts (increasing  $K_m$ ) with higher inhibitory concentration were determined suggesting a mixed type inhibition. Reversible inhibition constant ( $k_i$ ) of  $1.21 \pm 0.25 \mu M$  was estimated from the slopes of double reciprocal plots versus **DPH6** concentrations.

### 2.2.2. Monoamine oxidase inhibition

In order to assess their multipotent profile, the inhibitory capacity of **DPHs** 1–7 as dual MAO A and MAO B inhibitors was evaluated using [ $^{14}C$ ]-5HT and [ $^{14}C$ ]-phenylethylamine as substrates, respectively [19]. As shown in Table 1, most of **DPH** derivatives poorly inhibited MAO, except **DPH** 4 and **DPH6** that

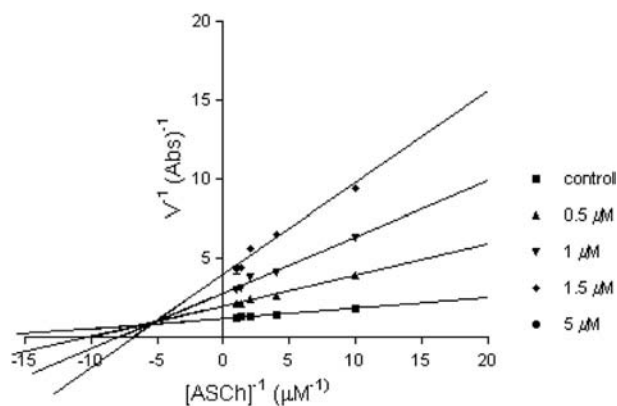


**Fig. 1.** Steady-state inhibition of *EeAChE* hydrolysis of acetylthiocholine (ASCh) by **DPH6** (0–5  $\mu M$ ). Lineweaver–Burk reciprocal plots of initial velocity and substrate concentrations (0.1–1  $\mu M$ ) are presented. Lines were derived from a weighted least-squares analysis of data.

showed moderate, almost equipotent inhibitory activity on both enzyme isoforms. Once more, **DPH6** revealed the most potent profile at inhibiting both monoamine oxidase isoforms [MAO A ( $IC_{50} = 6.2 \pm 0.7 \mu M$ ); MAO B ( $IC_{50} = 10.2 \pm 0.9 \mu M$ )]. Compared to **M30** (Chart 1) [15], **DPH6** was 166-fold and 179-fold less potent inhibiting MAO A and MAO B, respectively. Yet, **DPH6** was 138-fold more active than donepezil, showing equipotency at inhibiting MAO A and MAO B, respectively. The previously mentioned SAR also applied: for similar linker length,  $\alpha$ -aminonitriles were more potent inhibitors than their corresponding amines versus both isoenzymes, with the exception of **DPH2** as MAO B inhibitor. From dose–response curves ( $IC_{50}$ ), **DPH6** showed a non-selective MAO inhibition in comparison to standard selective MAO B and MAO A inhibitors l-deprenyl [14] and cloglyline [20], respectively.

To further characterize MAO inhibition by **DPH6**, reversibility study of this inhibitor was addressed. Irreversible inhibition was observed in both isoforms since enzyme activities were not significantly reverted after three consecutive centrifugations and washings with phosphate buffer (Fig. 2) followed by a pre-incubation with the inhibitor. Simultaneously, and for comparison purpose, the same assay was performed with irreversible MAO A inhibitor cloglyline and irreversible MAO B inhibitor l-deprenyl.

Next, the assessment of time-dependent inhibition of both MAO isoforms with **DPH6** was assessed by pre-incubating the enzyme with the inhibitor at times ranging 0–360 min (Fig. 3A). Samples with no compound were used to determine the maximum enzyme activity. Enzyme inactivation was not achieved before a pre-incubation of 180 min and 120 min for MAO A and MAO B, respectively, revealing time-dependent inhibition in both isoforms. These findings were confirmed by determining a constant variation on  $IC_{50}$  values as longer pre-incubations with **DPH6** were performed with both MAO isoforms (Fig. 3B, C and D).

### 2.2.3. Assessment of metal-chelating properties

Metal-chelating properties of compound **DPH6** were also investigated towards biometals Cu(II), Fe(III) and Zn(II) by UV–VIS spectrometry. The increase on brain levels of iron, zinc and particularly copper is reported to actively contribute to the formation of senile plaques by generating more reactive oxygen species through the  $A\beta_{1-42}$ -metal complex [21].

Upon the addition of varying concentrations of  $CuSO_4$ ,  $Fe_2(SO_4)_3$  or  $ZnSO_4$ , the maximum absorption detected at 240 nm with the compound alone shifted to 257 nm, exhibiting the formation of complexes **DPH6**-Cu(II), **DPH6**-Fe(III) and **DPH6**-Zn(II) (Fig. 4A–C). Significant variations on complexation times were observed depending on the metal. No spectral differences were identified when Cu(II) and was added after 5-min incubation whereas 1 h or O/N incubations were required to detect the formation of **DPH6**-Zn(II) and **DPH6**-Fe(III) complexes, respectively. These results confirm that **DPH6** selectively complexes Cu(II) salts. The equations obtained by the Job's method provided a solution at a mole fraction of 0.65 for compound **DPH6** complexing Cu(II) and Zn(II) and a mole fraction between 0.5 and 0.6 for the complex **DPH6**-Fe(III). This data revealed a 2:1 stoichiometry for all complexes.

## 2.3. Molecular modeling of **DPH6**

### 2.3.1. Inhibition of *EeAChE*

A modeling study was carried out through docking simulations for the purpose of gaining insights on the nature and spatial location of the key interactions of the (*R*)- and (*S*)-enantiomers of **DPH6** modulating the inhibitory activity of AChE and BuChE. As in our previous studies, we have chosen the 3D structure of the enzyme species (*EeAChE* and *eqBuChE*) used for the kinetic studies. The kinetic data provide evidence that compound **6** displays a mixed

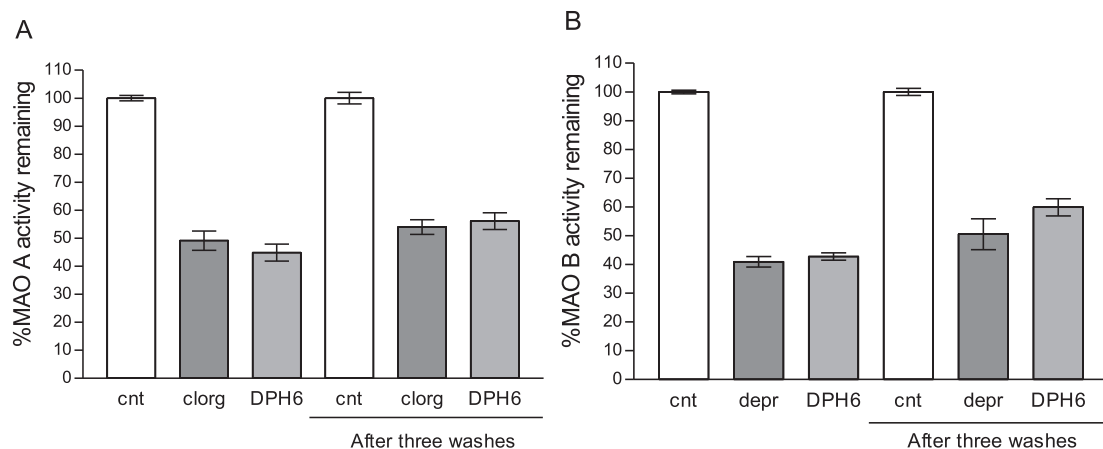


**Fig. 2.** (A) Reversibility study of MAO A inhibition by 10  $\mu\text{M}$  DPH6 and 50 nM clorgyline. (B) Reversibility study of MAO B inhibition by 20  $\mu\text{M}$  DPH6 and 20 nM l-deprenyl. MAO A and MAO B inhibition was performed following a 30-min pre-incubation. After three consecutive washes with buffer MAO activity was not significantly reverted. Data expressed as the mean  $\pm$  SEM of six independent experiments in triplicate. Kruskal–Wallis one-way analysis was used.

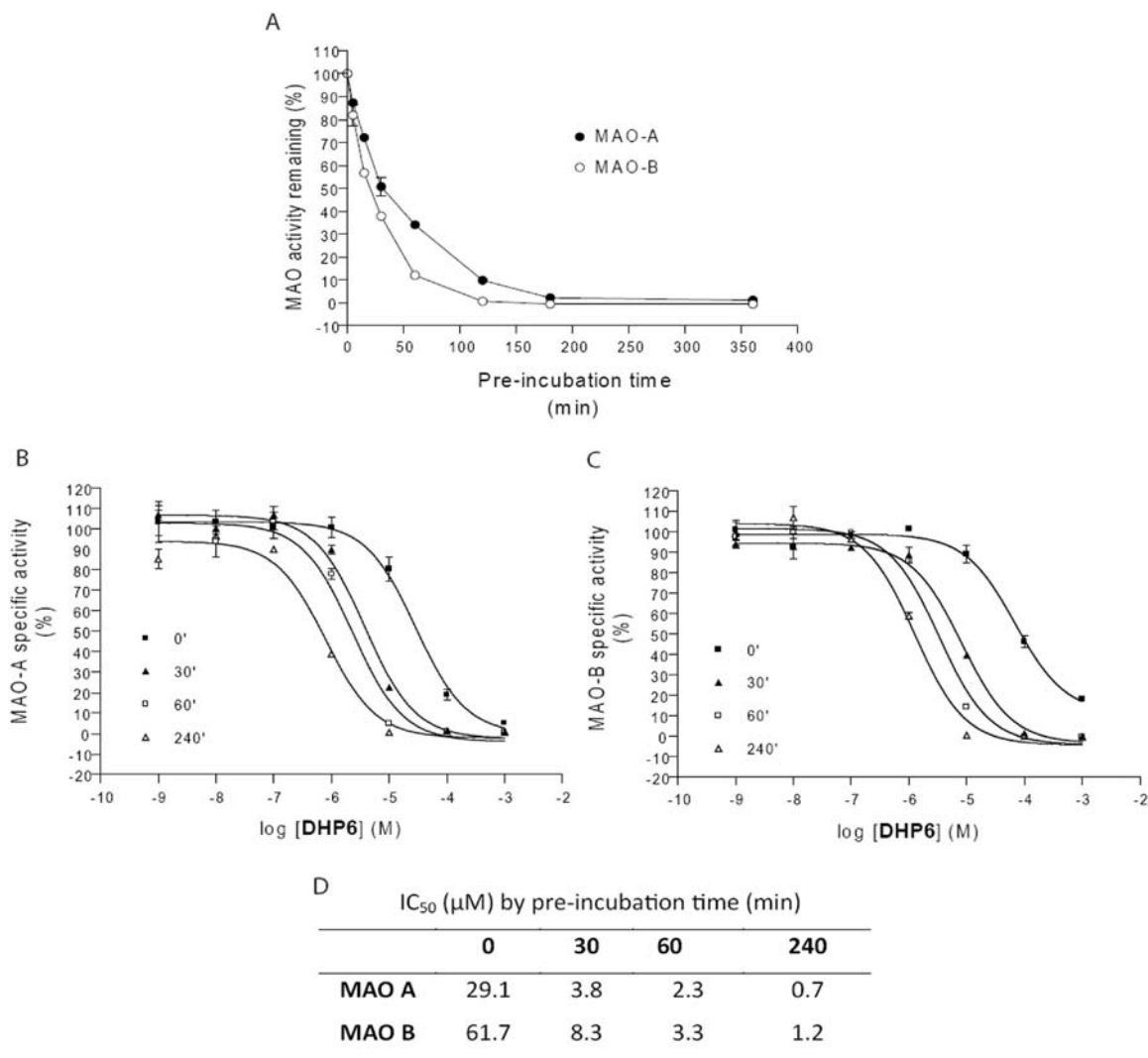


**Fig. 3.** (A) Study of time-dependent inhibition of MAO A and MAO B by DHP6 (10  $\mu\text{M}$  and 20  $\mu\text{M}$ , respectively) over different pre-incubation times (0–360 min). (B and C) Dose-response curves ( $\text{IC}_{50}$ ) following different pre-incubation times (0–240 min) with DHP6 inhibiting MAO A and MAO B. (D)  $\text{IC}_{50}$  values determined following different pre-incubations. Data are the mean  $\pm$  SEM of three independent experiments in triplicate.

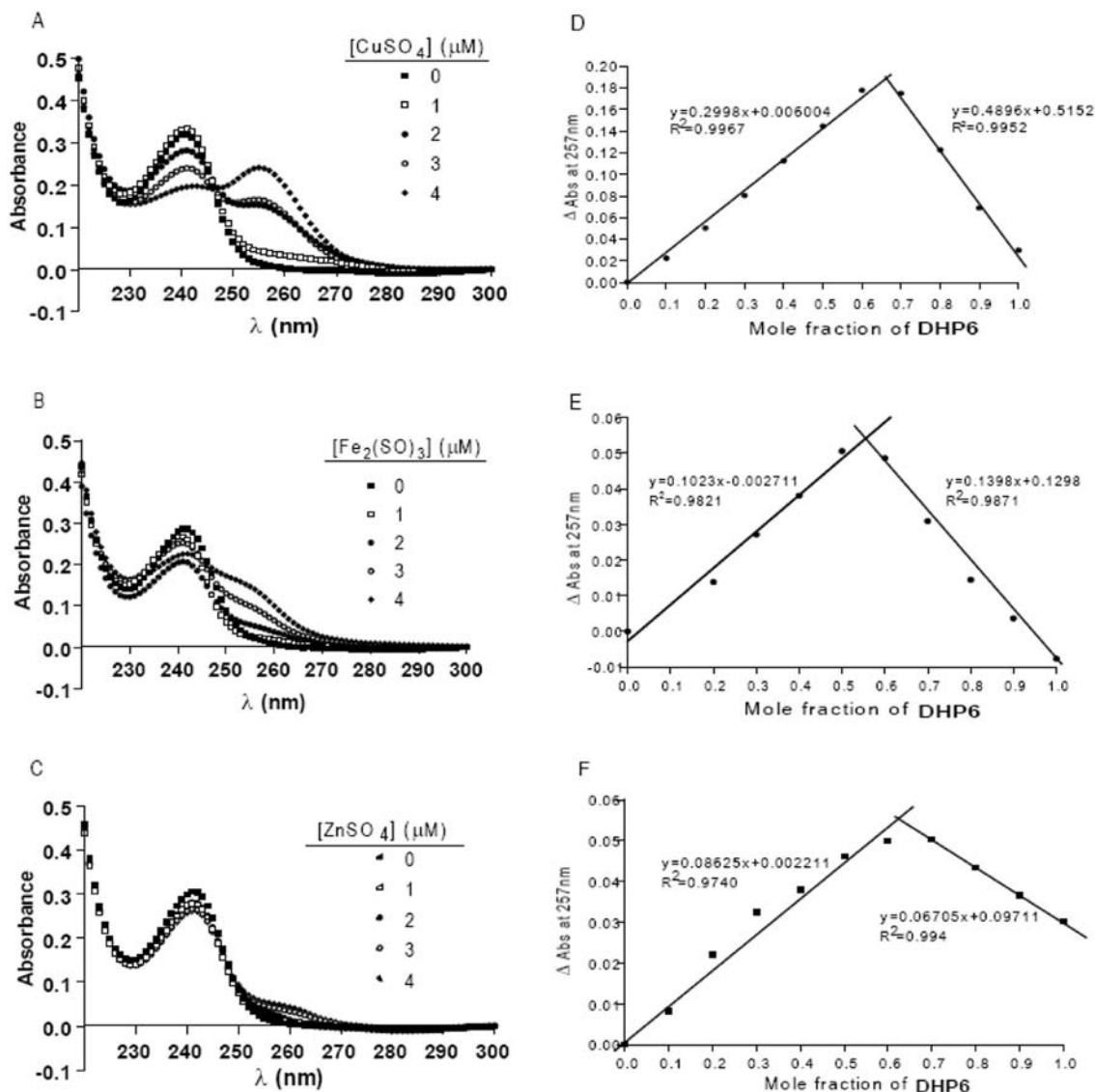


**Fig. 4.** (A) UV–VIS spectrum of a solution containing 10 μM DPH6 and 0–4 μM CuSO<sub>4</sub> following 5-min incubation. (B) UV–VIS spectrum of a solution containing 10 μM DPH6 and 0–4 μM Fe<sub>2</sub>(SO<sub>4</sub>)<sub>3</sub> following O/N incubation. (C) UV–VIS spectrum of a solution containing 10 μM DPH6 and 0–4 μM ZnSO<sub>4</sub> following 1-h incubation. (D) Determination of the stoichiometry of complex DPH6–Cu(II), (E) complex DPH6–Fe(III) and (F) complex DPH6–Zn(II) following 5-min, O/N and 1-h incubation, respectively by using the Job's method. All solutions were prepared in distilled water and incubations performed at room temperature.

type inhibition and argue in favor of interactions of DPH6 with both catalytic and peripheral binding sites of AChE. Molecular modeling studies have been carried in order to validate this assumption. Ligand docking studies were performed with Autodock Vina [22] using a single catalytic sub-unit of EeAChE (PDB: 1C2B). This docking procedure allows the docking of ligands on the entire protein surface, without prior specification of the binding site. As in previous studies, the recognition process between (R)- and (S)-enantiomers of DPH6 was theoretically investigated by flexible docking experiments. Flexible torsions in the ligands were assigned and protein side chain flexibility was incorporated allowing the rearrangement of the side chains of eight residues, Trp286, Tyr124, Tyr337, Tyr72, Asp74, Thr75, Trp86 and Tyr341. These residues delineate the shape of the gorge entry and lining and their motion may significantly enlarge the gorge to facilitate bulky ligand access to the catalytic site [23,24]. As shown in Figs. 5 and 6, it appears that both enantiomers of DPH6 interact simultaneously with both catalytic and peripheral site of EeAChE thanks to a linker of

appropriate length showing a strong correlation with the observations we have from Lineweaver–Burk plots.

**2.3.1.1. Docking studies of (R)-DPH6 with EeAChE.** Computational docking studies of (R)-DPH6 with EeAChE yielded four major binding modes at the enzyme binding site. In Fig. 7, the four most favored binding modes are presented along with the first shell of residues surrounding (R)-DPH6.

Mode I and Mode II (Fig. 5A and B) placed the quinoline moiety near the opening of the binding pocket. Mode III and Mode IV (Fig. 5C and D) placed the quinoline deep into the binding pocket next to the residues known to be involved in catalysis. The classical catalytic triad is shaded in green in all four panels. A close examination of (R)-DPH6 in Mode I revealed that the interaction with the AChE peripheral site involved a face to face  $\pi$ – $\pi$  stacking between the indole ring of Trp286 and the quinoline moiety and a T-shaped  $\pi$ – $\pi$  stacking between the phenyl ring of Tyr72 and the quinoline moiety. Besides, in this complex, a bifurcated hydrogen bond was

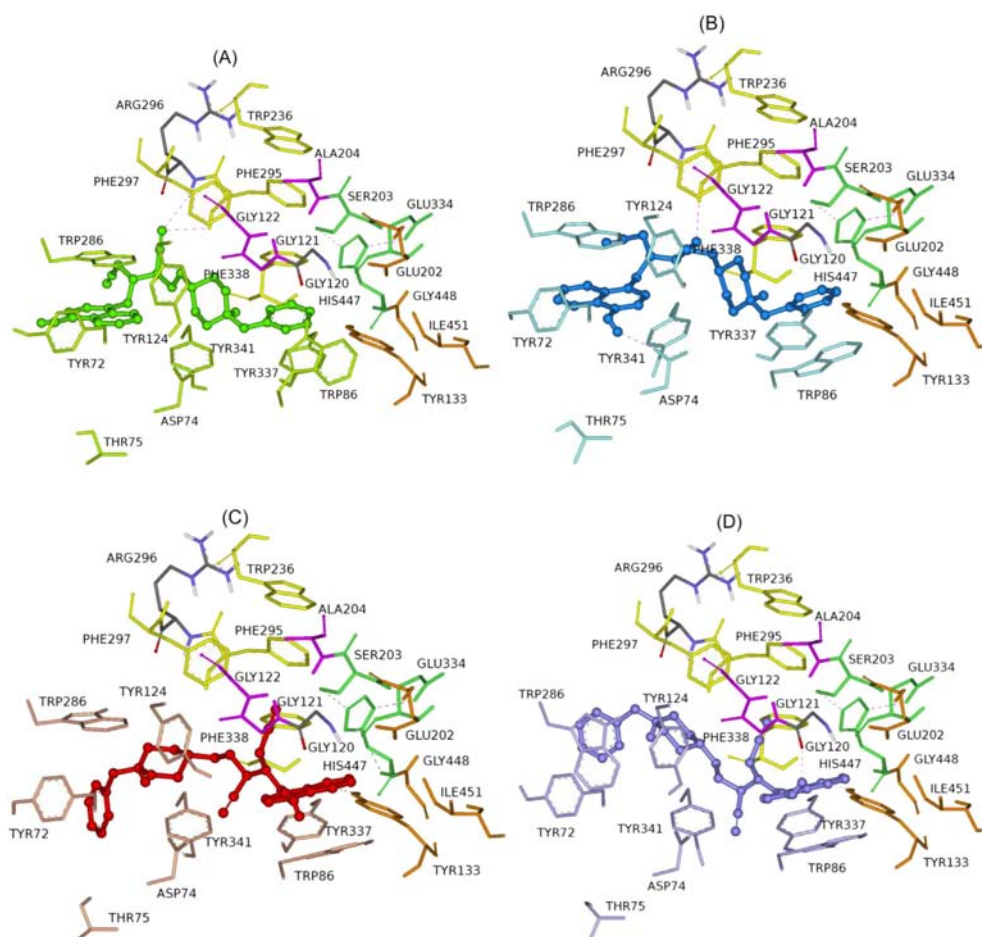


**Fig. 5.** Binding mode of inhibitor (*R*)-DPH6 at the active site of *EeAChE*. (A) Mode I, compound (*R*)-DPH6 is illustrated in green. (B) Mode II, compound (*R*)-DPH6 is illustrated in blue. (C) Mode III, compound (*R*)-DPH6 is illustrated in red (D) Mode IV, compound (*R*)-DPH6 is illustrated in violet. Ligands are rendered as sticks and the side chains conformations of the mobile residues are illustrated in the same color light as the ligand. Different subsites of the active site were colored: catalytic triad (CT) in green, oxyanion hole (OH) in pink, anionic sub-site (AS) in orange, except Trp86, acyl binding pocket (ABP) in yellow, and peripheral anionic subsite (PAS) in blue. Black dashed lines are drawn among atoms involved in hydrogen bond interactions. (For interpretation of the references to colour in this figure legend, the reader is referred to the web version of this article.)

formed between the *nitrogen atom of the cyano group and Arg296-NH and Phe295-OH*. The benzyl moiety pointed towards the bottom of the gorge and established edge-to-face  $\pi$ - $\pi$  interactions with Trp86 and face-to-face  $\pi$ - $\pi$  interactions with Tyr337. In Mode

II, the benzyl and the quinoline moieties interacted with Trp86 of the catalytic pocket and Trp286 of the peripheral site, respectively. In the middle of the gorge, the *nitrogen atom of the cyano group forms a hydrogen bond with the hydroxyl group of the Phe295*. At the

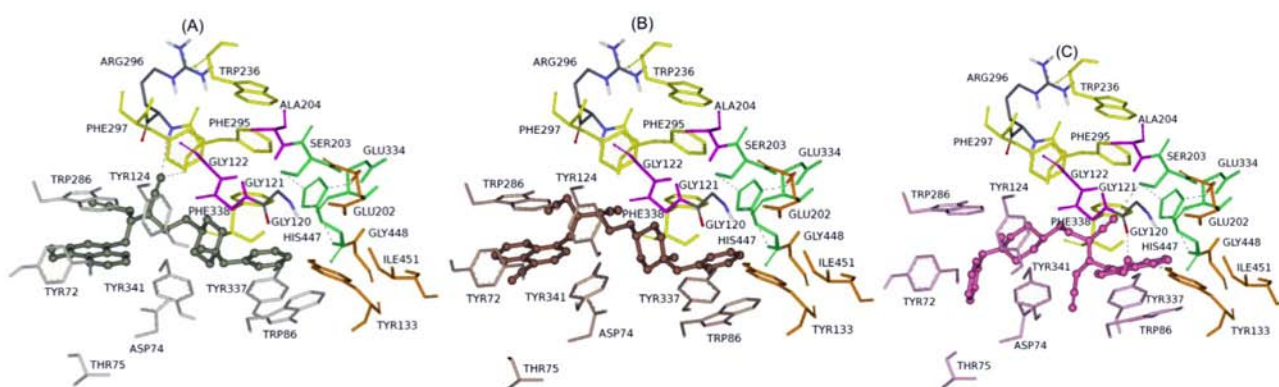


**Fig. 6.** Binding mode of inhibitor (*S*)-DPH6 at the active site of *hAChE*. (A) Mode I, compound (*S*)-DPH6 is illustrated in gray. (B) Mode II, compound (*S*)-DPH6 is illustrated in brown. (C) Mode III, compound (*S*)-DPH6 is illustrated in pink. Ligands are rendered as sticks and the side chains conformations of the mobile residues are illustrated in the same light color as the ligand. Different subsites of the active site were colored: catalytic triad (CT) in green, oxyanion hole (OH) in pink, anionic sub-site (AS) in orange, except Trp86, acyl binding pocket (ABP) in yellow, and peripheral anionic subsite (PAS) in blue. Black dashed lines are drawn among atoms involved in hydrogen bond interactions. (For interpretation of the references to colour in this figure legend, the reader is referred to the web version of this article.)

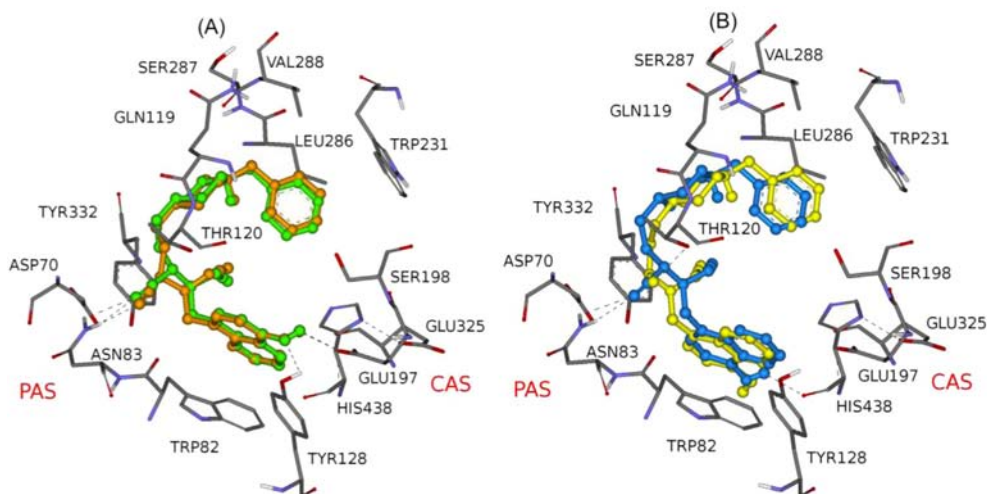


**Fig. 7.** Complex of compound (R)-DPH6 and (S)-DPH6 and eqBuChE homology built 3D-model. (A) Mode I, compound (R)-DPH6 is illustrated in orange and compound (S)-DPH6 in green. (B) Mode II, compound (R)-DPH6 is illustrated in yellow and compound (S)-DPH6 in blue. The compounds are rendered as sticks. (For interpretation of the references to colour in this figure legend, the reader is referred to the web version of this article.)

top of the gorge, the hydroxyl group of the quinoline moiety forms a hydrogen bond with the carboxylate group of Asp74. As can be seen in Fig. 5C (Mode III), (R)-DPH6 has several interactions along the active-site gorge of *EeAChE*. At the top of the gorge, the benzyl ring and Trp286 indole ring formed a favorable T-shaped  $\pi$ - $\pi$  interaction. Near the bottom of the gorge the quinoline moiety stacked against the Trp86 indole ring. In this region, the nitrogen atom of the quinoline moiety was hydrogen bonded to the hydroxyl group of Tyr133. Comparison of Mode IV (Fig. 5D) and Mode III (Fig. 5C) revealed a broadly similar interaction but with two key differences: a) a significant movement of the Trp286 indole and benzyl rings in order to establish a face-to-face  $\pi$ - $\pi$  interaction, and b) the rotation of the hydroxyl group of the quinoline moiety to form a hydrogen bond with the carbonyl group of Gly120. In both poses (Mode III and Mode IV), the three methylene units in the spacer of (R)-DPH6 were long enough to allow a proper interaction between (R)-DPH6 and both sites of the enzyme. The linker was lodged in a narrow cavity described by Asp74, Tyr124, Phe297, Tyr337, Phe338, and Tyr341. The protonated nitrogen was favorably interacting with the residues of a kind of “electrostatic cage” (Tyr124, Asp74, Tyr337 and Tyr341 side chains).

**2.3.1.2. Docking studies of (S)-DPH6 with *EeAChE*.** Docking studies of (S)-DPH6 with *EeAChE* yielded three major binding modes at the enzyme binding-site. In Fig. 6 the three most favored binding modes are presented along with the first shell of residues surrounding (S)-DPH6. Mode I and Mode II (Fig. 6A and B) placed the quinoline moiety near the opening of the binding pocket. Mode III (Fig. 6C) placed the quinoline deep into the binding pocket next to the residues involved in catalysis. In Mode I (Fig. 6A), the main stabilizing factors that keep stable the (S)-DPH6-AChE complex were found to be the hydrophobic contacts,  $\pi$ - $\pi$  interactions and hydrogen bonding interactions. Compound (S)-DPH6 can simultaneously bind at both the peripheral anionic site (PAS) and the catalytic active site (CAS) of *EeAChE*. (S)-DPH6 is able to bind in the PAS by face-to-face and edge-to-face  $\pi$ - $\pi$  interactions between the quinoline moiety of the ligand and the Trp286 indole ring and the Tyr72 phenyl ring, respectively. Other interactions like a bifurcated hydrogen bond between the nitrogen atom of the cyano group and Arg296-NH and Phe295-OH could also play an important role in positioning and stabilizing the ligand inside the active site gorge.

The benzene ring of (S)-DPH6 formed a  $\pi$ - $\pi$  stacking interaction with Trp86. In Mode II (Fig. 6B), compound (S)-DPH6 can also adopt a similar binding conformation to that in Mode I. The ligand had an orientation along the active-site gorge, extending from the anionic sub-site of the active site at the bottom, to the peripheral anionic site at the top, via aromatic stacking interactions with Trp86, Trp286 and Tyr72 residues (Mode II, Fig. 6B). Conversely, in this orientation, compound (S)-DPH6 was not able to form hydrogen bonds but a stronger stacking interaction between benzene ring and Trp86. Mode III (Fig. 6C) also placed the ligand along the active-site gorge. The quinoline ring formed a  $\pi$ - $\pi$  interaction with the indole ring of Trp86 and also established three additional hydrogen bonds, which have an important contribution to the binding potency of the ligand. The hydroxyl group of Tyr133 formed two hydrogen bonds with the nitrogen and the hydroxyl group of the quinoline moiety, the later group is also hydrogen bonded to the carbonyl oxygen from the backbone of Gly120. On the other hand, at the peripheral anionic site (PAS), the benzene ring of the ligand form edge-to-face  $\pi$ - $\pi$  interaction with the indole ring of Trp286 and with the benzene ring of Tyr72. In comparison with the other poses, the cyano residue is involved in the interactions with the catalytic triad of the active site gorge. This group is able to bind by mean of hydrogen bond with the Ser203 side chain.

On the basis of the similar orientation and the set of interactions, which were identified between the (R) enantiomer (Modes I-III, Fig. 5A–C) and (S) enantiomer (Modes I-III, Fig. 6A–C) and the protein residues within the gorge, it can be hypothesized that both enantiomers of DPH6 could simultaneously bind at both the peripheral anionic site (PAS) and the catalytic active site (CAS) of *EeAChE*.

### 2.3.2. Inhibition of eqBuChE

With respect to BuChE, in the absence of X-ray structure of eqBuChE, a homology model was used. The modeling of the 3D structure was performed by an automated homology-modeling program (SWISS-MODEL) [25–27]. A putative three-dimensional structure of human BuChE (pdb: 2PM8), as these two enzymes exhibited 89% sequence identity. In order to simulate the binding of both enantiomers of compound DPH6 to eqBuChE, docking experiments were performed as blind dockings following the same

computational protocol used for *EeAChE*. The best-ranked docking solutions revealed that BuChE can effectively accommodate both enantiomers of **DPH6** inside the active site gorge and two major binding modes can be proposed (Fig. 7). Modes I and II (Fig. 7A and B) for both enantiomers placed the quinoline moiety into the binding pocket next to the residues involved in catalysis. In this orientation, the phenyl moiety interacts with Trp231 by means of hydrophobic interactions and Trp82 allowed a  $\pi$ - $\pi$  stacking interaction with the quinoline ring of the ligand. In Mode I (Fig. 7A), a close examination of the first shell of residues surrounding (*R*)-**DPH6** and (*S*)-**DPH6** revealed that in both enantiomers the hydroxyl group of the quinoline ring formed one hydrogen bond with the carboxylate group of Glu197 and another one with the hydroxyl group of the Tyr128. Moreover, the cyano group for the (*R*)-**DPH6** enantiomer, formed a hydrogen bond with the NH<sub>2</sub> of the side chain of Asn83, this bond was bifurcated in the case of (*S*)-**DPH6** enantiomer. In this orientation, hydrophobic interactions with the catalytic triad residues, Ser198 and His438 were found. In mode II (Fig. 7B), only one hydrogen bond was observable for the (*R*) enantiomer, it was formed between the cyano group and the hydroxyl group of Thr120. The (*S*) enantiomer preserved the cyanide bifurcated hydrogen bond already observed in Mode I, and the hydroxyl group of the quinoline ring established a hydrogen bond with the catalytic triad residue His438.

Analysis of the intermolecular interactions indicated key residues responsible for ligand binding. The cyanide group is likely to be an important feature for these derivatives to exhibit BuChE inhibitory activity.

### 2.3.3. Inhibition of MAO A and MAO B

In order to explore the nature of the ligand–receptor interactions, the ligand was docked to the active site of both MAO A and MAO B isoforms using the program Autodock Vina [22]. We have focused on **DPH6**, which showed the best both MAO A (IC<sub>50</sub> = 1.8 ± 0.1 μM) and MAO B (IC<sub>50</sub> = 1.6 ± 0.25 μM) inhibitory activities, with significant *EeAChE* and eqBuChE inhibitory potencies. Although rat MAO A (rMAO A) and rat MAO B (rMAO B) are ~90% identical in sequence with human enzymes, their functional properties are similar but not identical to those of human enzymes. Given that MAO inhibition assays were carried out on rat brain mitochondria, docking experiments were carried out using the X-ray structure of rMAO A (PDB ID: 1O5W) and the homology model of rMAO B developed from a human MAO B (hMAO B) crystallographic structure (PDB ID: 1S3E) [28], as previously described for eqBuChE. The recognition process between (*R*)- and (*S*)-enantiomers of **DPH6** (chosen as reference compound) was theoretically investigated by blind docking experiments, in accordance with a protocol previously defined by us and well validated [29]. The enzyme–inhibitor interactions might allow a theoretical evaluation of which enantiomer of the inhibitor could be better accommodated into the catalytic site of MAO A and MAO B. Results from several studies have shown that it must be the neutral amine that reaches the active site of MAO A and MAO B to allow the chemistry [30–33]. Therefore, the docking simulations were done using both enantiomers of **DPH6** as neutral species despite of at physiological pH, most of the piperidine rings would be in the protonated, positively charged form. In docking with MAO A, during each run, the side chains of twenty-one residues (Tyr 69, Leu97, Gln99, Ala111, Phe112, Tyr124, Trp128, Phe173, Leu176, Phe177, Ile180, Asn181, Ile207, Phe208, Gln215, Cys323, Ileu325, Ileu335, Phe352, Tyr407 and Tyr444) were allowed to relax with the ligand, while the remainder of the enzyme was fixed in 3-D space. Six water molecules labeled as w72, w193, w11, w23, w15, and w53 in accordance with the numbering reported for the hMAO B crystallographic structure (PDB ID: 1S3E) located near the FAD cofactor

were considered as integral components of the protein structure during the docking simulation. Docking of **DPH6** was performed for both enantiomers and a sole binding mode per enantiomer was found. Fig. 8A and B illustrated the binding modes of (*R*)-**DPH6** and (*S*)-**DPH6** enantiomers into the hMAO A binding cavity. Both enantiomers showed a relatively similar localization for the hydroxy-quinoline and benzyl moieties, with the rest of the molecule easily accommodated in the relatively large cavity of MAO A.

**2.3.3.1. Inhibition of MAO A by (*R*)- and (*S*)-DPH6.** Fig. 8A showed that the optimal position for the (*R*)-**DPH6** enantiomer placed the quinoline ring in an “aromatic cage” formed by Tyr407, Tyr444 side chains, as well as the isoalloxazine FAD ring. (*R*)-**DPH6** forms  $\pi$ - $\pi$  stacking interactions with Tyr407 and the carbonyl group of Gln215 residue. The hydroxy-quinoline moiety was involved in two hydrogen bonds between the OH and the carbonyl oxygen of the FAD and the 193w molecule. The benzyl group is located in a hydrophobic core delimited by residues Phe173, Phe208, Ileu325, Ala111 Phe112 and Leu176. The cyano group is also able to form a hydrogen bond with Cys323 side chain. Compound (*S*)-**DPH6** showed a binding geometry very similar to that displayed by (*R*)-**DPH6** as for the hydroxy-quinoline and benzyl moieties (see Fig. 8B), which displayed a set of intermolecular interactions described before in the case of the (*R*)-enantiomer. The main difference with respect to the recognition of (*R*)-**DPH6** was in the spatial orientation of the propargyl, piperidine and cyano groups, the later accommodated this time to establish hydrogen bond with Thr336 residue. The docking studies rationalized the relevant inhibitory activity of **DPH6** towards MAO A, as due to the formation of several favorable interactions with the catalytic site of the enzyme.

The importance of the cyano group in properly positioning the ligand by H-bond formation is pointed out. It is worth noting that compounds lacking this CN, like in the case of **DPH7**, showed the inhibitory activity drastically lowered.

**2.3.3.2. Inhibition of MAO B by (*R*)- and (*S*)-DPH6.** To rationalize the selectivity towards MAO A and MAO B of (*R*)- and (*S*)-**DPH6**, blind docking studies of **DPH6** into the MAO B were done. Up to date, a reliable 3-D structure of rMAO B is not available and we used a 3D homology model of rMAO B for the docking studies. The six structural water molecules selected for rMAO A were also included in the model. For MAO B, the inhibitor (*R*)-**DPH6** crosses both cavities, presenting the piperidine nucleus located between the “entrance” and “catalytic” cavities, separated by the residues Ile199 and Tyr326. This complex was stabilized by hydrophobic contacts of quinoline ring with Phe103, Pro104, Trp119, His90, Val316 and Tyr115. Besides, the phenyl ring is hosted into the “aromatic cage” framed by Tyr398, Phe343, Tyr435, and the FAD aromatic ring, where it forms a number of  $\pi$ - $\pi$  interactions also including Gln206. No intermolecular H-bonds between ligand and enzyme were observed (Fig. 9A). For MAO B, the quinoline system of the inhibitor (*S*)-**DPH6** was hosted in the entrance cavity made up by lipophilic residues Phe103, Pro104, Trp119, His90, Ileu164, Val316 and Tyr115. The phenyl ring occupied the substrate cavity and was in direct contact with the Tyr398, Phe343, Tyr435, and the FAD aromatic ring. The compound established a H-bond with Tyr115 OH hydrogen by its OH oxygen (Fig. 9B). The study confirmed the selectivity of **DPH6** for MAO A isoform. Selectivity is likely due to the orientation of the quinoline and phenyl moieties of **DPH6** in MAO A and in MAO B. For MAO B, the quinoline system was hosted in the entrance cavity and for MAO A this system occupied the substrate cavity. In this disposition the quinoline moiety interacted directly with the FAD aromatic ring.

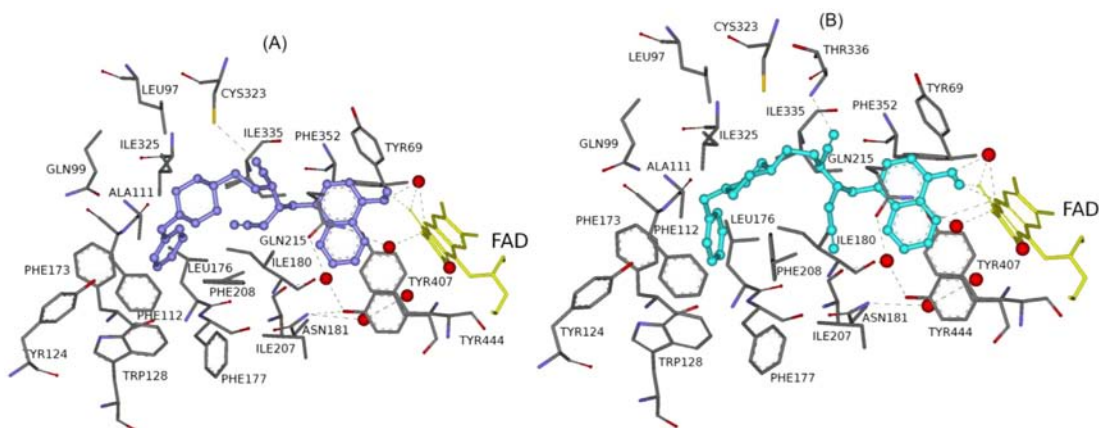


**Fig. 8.** Docking poses of inhibitor **DPH6** into rMAO A. (A) (*R*)-**DPH6** (purple sticks). (B) (*S*)-**DPH6** (blue sticks). Amino acid residues of the binding site are color-coded. The flavin adenine dinucleotide cofactor (FAD) and the six water molecules are represented as an integral part of the MAO A structure model and are rendered as yellow sticks and red balls, respectively. Green dashed lines are drawn among atoms involved in hydrogen bond interactions. (For interpretation of the references to colour in this figure legend, the reader is referred to the web version of this article.)

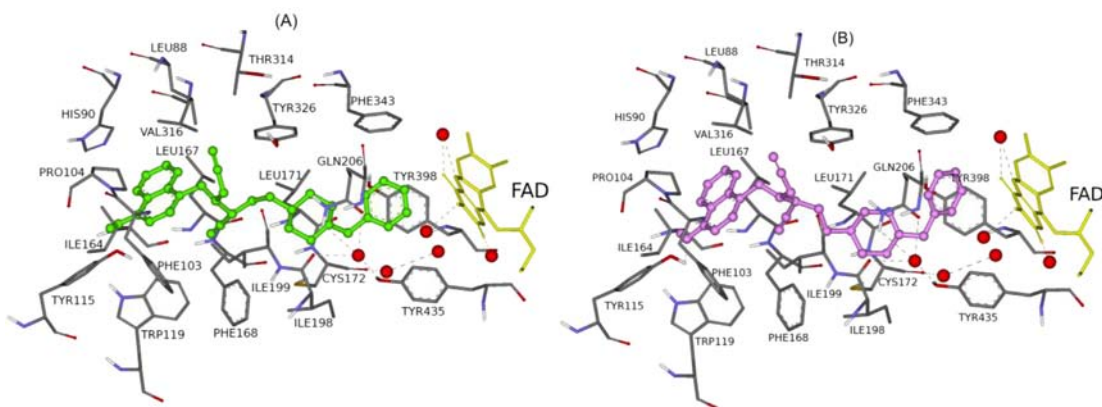


**Fig. 9.** Docking pose of inhibitor **DPH6** into rMAO B. (A) (*R*)-**DPH6** (green sticks). (B) (*S*)-**DPH6** (pink sticks). Amino acid residues of the binding site are color-coded. The flavin adenine dinucleotide cofactor (FAD) and the six water molecules are represented as an integral part of the MAO B structure model and are rendered as yellow sticks and red balls, respectively. (For interpretation of the references to colour in this figure legend, the reader is referred to the web version of this article.)

### 2.3.4. Predicted binding affinities

AutoDock Vina provides a computed binding affinity for each docking mode predicted. Binding affinity data for both enantiomers with the four enzymes are summarized in Table 2. The more negative the value, the tighter the predicted bonding. For the (*R*)-**DPH6** interaction with the AChE, predicted binding affinities were very similar for the four modes (I–IV), ranging from –11.0 to –12.3 kcal/mol. Predicted binding affinities for (*R*)-**DPH6** with BuChE (–10.4 and –10.7 kcal/mol) were slightly lower in range than those for the AChE complex (Table 2). Data for (*S*)-**DPH6** interactions gave very similar predicted binding than that for (*R*)-**DPH6** interactions: predicted binding energies of –11.5

to –12.4 kcal/mol for AChE and –9.9 and –9.7 kcal/mol for BuChE. Consistent with biological trends, both enantiomers were predicted to have similar binding interactions with AChE and BuChE. The weakest predicted binding affinities were computed for the both enantiomers interactions with the MAO A and MAO B enzymes. Very similar binding affinity values were also observed for both enantiomers with MAO A and MAO B.

### 2.4. Theoretic ADMET analysis of DPH hybrids

ADMET properties are important conditions and major parts of pharmacokinetics. Viable drugs should have proper ADMET properties to be approved as a drug in clinical tests. The drugs used for neurological disorder treatment, such as AD, are generally CNS acting drugs, so factors that are important to the success of CNS drugs were analyzed. In particular, the new molecules should present a good CNS penetration profile and low toxic effects. Current *in silico* ADMET predictions cannot fully replace well-established *in vitro* cell-based approaches or *in vivo* assays, but they can provide significant insights [34]. Computer predictions were performed with ADMET Predictor 6.53 [35] and ACD/Percepta 14.0.04 [36] software packages. According to the predictions (Table 3), the lipophilicity increases with the hydrocarbon tether

**Table 2**  
Predicted binding affinities (kcal/mol).

DPH	Mode	EeAChE	EqBuChE	MAO A	MAO B
(R)- <b>DPH6</b>	I	–11.0	–10.4	–7.8	–8.9
	II	–12.3	–10.7		
	III	–12.1			
	IV	–12.1			
(S)- <b>DPH6</b>	I	–11.9	–9.9	–7.9	–8.8
	II	–11.5	–9.7		
	III	–12.4			

**Table 3**  
Calculated physicochemical properties for DPH1–7.<sup>a,b</sup>

	Molecular weight	No. of H-bond donors	No. of H-bond acceptor	No. of rotatable Bonds <sup>a</sup>	logP (Moriguchi) <sup>a,c</sup>	logP <sup>a</sup>	TPSA	No. violations Lipinski's rule	LogBB <sup>a,d</sup>
<b>1</b>	385.51	1	4	6	3.55	3.79	39.60	0	−0.12
<b>2</b>	424.55	1	5	6	3.09	3.51	63.39	0	−0.31
<b>3</b>	399.54	1	4	7	3.75	4.16	39.60	0	0.03
<b>4</b>	438.58	1	5	7	3.29	3.76	63.39	0	−0.14
<b>5</b>	413.57	1	4	8	3.95	4.54	39.60	0	0.20
<b>6</b>	452.60	1	5	8	3.48	4.05	63.39	0	0.07
<b>7</b>	427.59	1	4	9	4.09	4.95	39.60	0	0.36
<b>Donepezil</b>	379.50	0	4	6	3.52	4.59	38.78	0	0.88
<b>M-30</b>	226.28	1	3	3	2.06	2.32	36.36	0	0.17

	LogBB <sup>b,d</sup>	logPS <sup>c</sup>	Log (PS*fu, brain) <sup>e</sup>	Peff (cm/s × 10 <sup>4</sup> )	Human intestinal absorption (%) <sup>f</sup>	In vitro Caco-2 perm (nm/sec) <sup>g</sup>	MDCK (cm/s × 10 <sup>7</sup> ) <sup>h</sup>	% Plasma protein binding (in vitro) <sup>i</sup>	Toxicity <sup>a</sup>
<b>1</b>	−0.02	−1.6	−2.8	4.47	96.79	45.66	350.7	72.68	hERG
<b>2</b>	−0.11	−1.6	−2.9	3.36	96.83	49.28	348.2	80.31	hERG
<b>3</b>	0.29	−1.5	−3.0	4.99	96.84	52.26	325.9	76.37	hERG
<b>4</b>	0.26	−1.6	−3.1	3.75	96.91	51.96	321.9	78.44	hERG
<b>5</b>	0.36	−1.4	−3.2	5.59	96.87	54.36	313.0	77.11	hERG
<b>6</b>	0.34	−1.5	−3.3	4.18	96.99	54.37	306.1	79.97	hERG
<b>7</b>	0.46	−1.4	−3.4	6.24	96.90	54.08	301.9	77.40	hERG
<b>Donepezil</b>	0.31	−1.4	−3.0	6.69	97.95	55.51	306.4	84.62	hERG
<b>M-30</b>	−0.27	−1.5	−2.1	2.5	95.86	42.90	429.3	69.02	

<sup>a</sup> ADME Predictor, v.6.5.

<sup>b</sup> ACD/Percepta 14.0.

<sup>c</sup> Moriguchi model (ref. [4]).

<sup>d</sup> According to the classification made by Ma et al. [9]: High absorption to CNS: logBB more than 0.3; Middle absorption to CNS: logBB 0.3 ~ −1.0; Low absorption to CNS: logBB less than −1.0.

<sup>e</sup> Other estimated parameters related to brain penetration were used to classify the compounds as CNS permeable or non-permeable: rate of brain penetration (LogPS) is the rate of passive diffusion/permeability; brain/plasma equilibration rate (Log(PS\*fu,brain)); fu,brain – fraction unbound in plasma.

<sup>f</sup> Human intestinal absorption is the sum of bioavailability and absorption evaluated from ratio of excretion or cumulative excretion in urine, bile, and feces. A value between 0 and 20% indicates poor absorption, 20–70% shows moderate absorption, and 70–100% indicates good absorption.

<sup>g</sup> Caco-2 cells are derived from human colon adenocarcinoma and possess multiple drug transport pathways through the intestinal epithelium. A value <4 indicates low permeability, 4–70 shows middle permeability, and >70 indicates high permeability.

<sup>h</sup> The MDCK cell system may be used as a good tool for rapid permeability screening. A value <25 indicates low permeability, 25–500 shows middle permeability, and >500 indicates high permeability.

<sup>i</sup> The percent of drug binds to plasma protein. A value <90% indicates weak binding, and >90% indicates strong binding to plasma proteins.

chain, and for the same value of  $n$ , the  $\alpha$ -aminonitriles show the expected slightly lower lipophilicity. All of the **DPH** show good values ( $\log P < 5$  and  $m\log P < 4.15$ ) [37], and as can be deduced, the whole series of structures meets the Lipinski's rule of five [38]. Moreover, a more severe rule for CNS drugs-like characteristics [39] ( $MW \leq 450$ , HB donor  $\leq 3$ , HB acceptors  $\leq 7$ ,  $\log P \leq 5$ ,  $PSA \leq 90$ , and number of rotatable bonds  $\leq 8$ ) is satisfied for all structures, although the molecular weight of **DPH6** is on the borderline. However, drugs that penetrate CNS should have lower polar surface areas (PSA) than other kinds of molecules, being the optimal range 60–70 Å<sup>2</sup> [40]. Therefore, only the  $\alpha$ -aminonitriles DPH fall in the suitable range of values.

The blood–brain barrier (BBB) is a separation of circulating blood and cerebrospinal fluid in the central nervous system (CNS), so an estimation of BBB penetration means predicting whether compounds pass across the blood–brain barrier. This is a crucial pharmacokinetic property in drug design because CNS-active compounds, such as those for AD, must pass across it. According to the computed values [41], for the same  $n$ , the  $\alpha$ -aminonitriles present slightly lower values, whereas the values increase with the chain length. In any case, the two models predict that all structures should be moderate to good candidates, showing middle to high absorption to CNS. In particular, the **DPH3** and **DPHs 5–7** show the best results suggesting a brain penetration sufficient for CNS activity [42,43].

Generally, the degree to which any drug binds to plasma protein influences not only the drug action but also its disposition and efficacy. Usually, the drug that is unbound to plasma proteins will be

available for diffusion or transport across cell membranes and thereby finally interact with the target. Herein, the percent of drug bound with plasma proteins was estimated and the compounds were predicted to be weakly bind to plasma proteins.

Other ADMET predictions of the present **DPH** compounds show satisfactory results. Thus, all of them show good intestinal absorption (HIA [44] of about 96% and effective permeability across the intestinal membrane [45],  $Pe_{eff} > 0.1$ ), moderate apparent permeability for in vitro MDCK cells (>25) [46] and middle permeability for in vitro Caco-2 cells [47]. Regarding toxicity properties, these compounds are predicted to show cardiac toxicity (hERG potassium channel blockage), but, according to the models used, they could lack carcinogenicity and hepatotoxicity [48–50].

In summary, these structures show moderate to good ADMET properties; in particular those with increasing values of  $n$  in the linker present proper drug-like properties and brain penetration capacity for CNS activity.

## 2.5. Toxicological evaluation of DPH6

Based on the predicted non hepatotoxicity (see above) of the **DHP** compounds, next we analyzed our hit **DHP6** hybrid in an in vitro toxicity test in HepG2 cells, determining the cell viability with MTT method [51], using donepezil as a reference molecule. The results shown in Table 4 are very interesting as they prove that **DPH6** is by far less toxic than donepezil at high concentrations (from 30  $\mu$ M to 1000  $\mu$ M), while at low concentrations (from 1  $\mu$ M

**Table 4**  
In vitro toxicity in HepG2 cells.<sup>a</sup>

Compounds	Viability (%) HepG2 cells						
	1 $\mu$ M	3 $\mu$ M	10 $\mu$ M	30 $\mu$ M	100 $\mu$ M	300 $\mu$ M	1000 $\mu$ M
<b>DPH6</b>	98.4 $\pm$ 1.64 <sup>ns</sup>	94.8 $\pm$ 2.42 <sup>ns</sup>	94.4 $\pm$ 1.91 <sup>ns</sup>	92.4 $\pm$ 2.20 <sup>ns</sup>	85.6 $\pm$ 4.10*	71.44 $\pm$ 3.33***	51.5 $\pm$ 3.39***
<b>Donepezil</b>	98.6 $\pm$ 0.62 <sup>ns</sup>	97.0 $\pm$ 1.77 <sup>ns</sup>	92.4 $\pm$ 1.05*	83.5 $\pm$ 2.15***	80.0 $\pm$ 2.36***	53.4 $\pm$ 1.44***	40.9 $\pm$ 1.50***

\*\*\* $P \leq 0.001$ , \*\* $P \leq 0.01$ , \* $P \leq 0.05$  and <sup>ns</sup> not significant, with respect to control group. Comparisons between drugs and control group were performed by one-way ANOVA followed by the Newman–Keuls post-hoc test.

<sup>a</sup> Cell viability was measured as MTT reduction and data were normalized as % control. Data are expressed as the means  $\pm$  s.e.m. of triplicate of four different cultures. All compounds were assayed at increasing concentrations (1–1000  $\mu$ M).

to 10  $\mu$ M) both are non toxic showing a very similar cell viability profile.

To sum up, hybrid **DPH6** preserves all the anti-cholinesterasic properties related to donepezil, but, as expected, shows an additional multipotent inhibitory activity in agreement with the in vitro results previously determined such as MAO inhibition capacity, biometal (Cu, Zn and Fe) chelating properties, favorable ADMET data and a notorious lack of hepatotoxicity. Consequently, and based on these in vitro pharmacological analyses, next we stepped forward to preliminary *in vivo* tests in order to investigate the potential biological profile of selected derivative **DPH6**.

### 2.6. Relief of scopolamine-induced long-term memory deficit in mice by DHP6

To analyze the *in vivo* effect on contextual memory, **DPH6** was administered to scopolamine-treated mice that were subjected to passive avoidance behavioral test. This task is based on contextual memory in which the hippocampus plays an important role, with the association between an environmental context that the animal learns to avoid and an aversive stimulus (foot-shock). This behavioral test has been extensively used to evaluate learning and memory in rodent models of central nervous system disorders and for screening of novel chemical entities on memory function [53,54]. Scopolamine, a well-known non-selective muscarinic antagonist that produces amnesic effects in both rodents and human, is frequently used to perform pharmacological assays for studying the effects of enhancers on cognitive functions [52]. During the training day, no significant differences in the latency time between treated groups were found (Fig. 10), even though scopolamine has been reported to influence motivational behavior [55]. In the probe session (Fig. 11), scopolamine (1 mg/kg)-induced

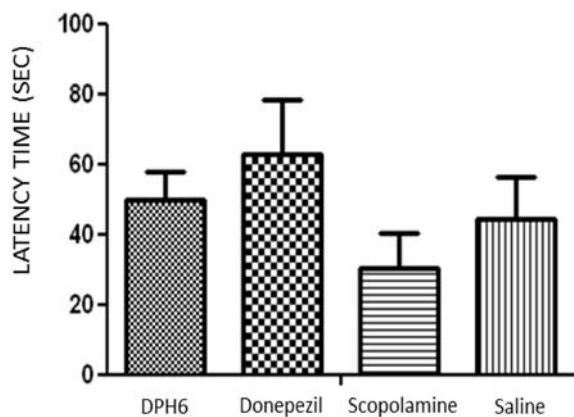


**Fig. 10.** Comparative effect of **DPH6**, donepezil and scopolamine on latency time in the training day. Bars represent the mean of latency time in seconds (sec) corresponding to each of experimental handling group. No significant differences were found between groups. Values expressed as mean  $\pm$  SEM of 8–10 independent experiments.

cognitive deficits was reflected by a decreased latency in comparison to saline (vehicle) group (\*\* $p < 0.001$ ). Not surprisingly, donepezil + scop group showed a latency time similar to that observed in the vehicle group. Likewise, scopolamine effect was widely reversed in the **DPH6** + scop group (\*\* $p < 0.001$ ). Characteristically, not statistical difference in the latency time between **DPH6** + scop and donepezil + scop groups were observed and it was similar to that exhibited by the vehicle.

When comparing individual groups between training and probe sessions (Fig. 12), it is noteworthy that in the vehicle + scop group no significant differences were observed in the latency time. In striking contrast, during the probe session, handling groups: saline, donepezil + scop (1 mg/kg) and **DPH6** + scop (35 mg/kg) remained in the brightly lit compartment for longer time than that measured in the training session, significantly increasing the latency time. The retention impairment observed in the probe session after a single dose of scopolamine (1 mg/kg), administered 30 min before training, is in good agreement with previous reports [56]. Taken these results together, we might conclude that both **DPH6** (35 mg/kg) and donepezil (1 mg/kg) are able to induce similar effects on cognition.

### 3. Conclusion

DPHs 1–7, designed as hybrids from donepezil and M30, bearing N-benzylpiperidine and a pro-chelator 8-hydroxyquinoline moieties attached to a central N-propargylamine core, have been synthesized and subjected to pharmacological evaluation. DPHs 1–7 were readily prepared in good yields, in short synthetic sequences, from easily available precursors.

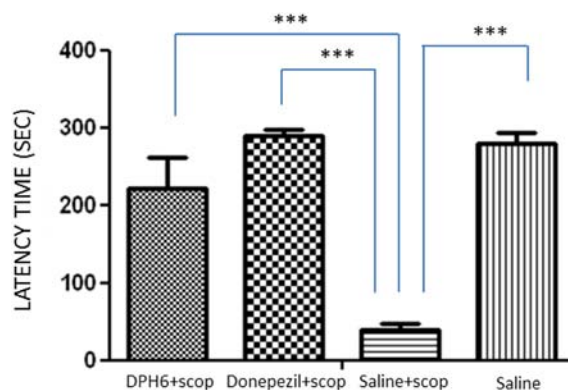


**Fig. 11.** Comparative effects on latency time of **DPH6** and donepezil on scopolamine-induced amnesia in the probe session. Bars represent the mean of latency time in seconds (sec) corresponding to each of experimental handling group. SEM is represented by error bars. Analysis of variance (ANOVA) followed by Bonferroni's post hoc test shows significant differences (\*\* $p < 0.001$ ) between groups **DPH6**, donepezil or vehicle with the scopolamine group. Values expressed as mean  $\pm$  SEM of 8–10 independent experiments.

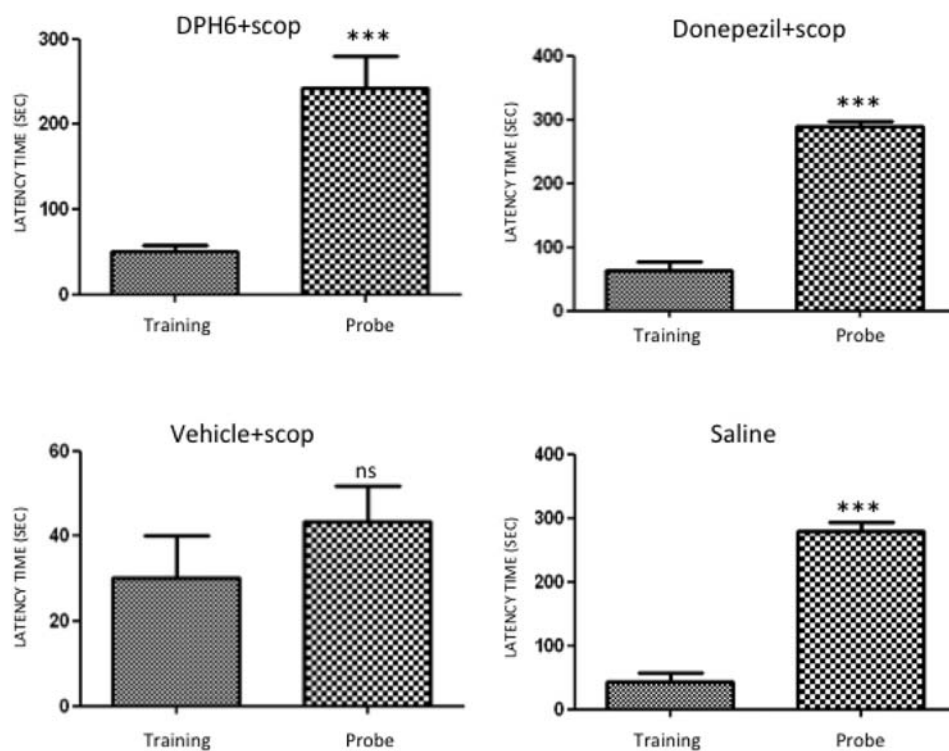


Fig. 12. Statistical differences within groups (training versus probe) determined by the Student's *t*-test (\*\**p* < 0.01; \*\*\**p* < 0.001).

The biochemical evaluation of these molecules showed DPHs 2–7 hybrids as non-selective ChE and MAO inhibitors with moderate-to-low micromolar activity. Particularly interesting resulted DPH6, an irreversible MAO A/B, mixed-type EeAChE inhibitor able to complex biometals Cu(II) and Zn(II) and Fe(III). Compared to related M30A [15] (Chart 1), the demethylated derivative of M30 [15], or M30B [39] (Chart 1), DPH6 showed a very similar MAO inhibitory profile with biometal chelating properties.

Computational docking studies of (R)- and (S)-enantiomers of **DPH6** in AChE and BuChE yielded several binding modes for each enantiomer, but we have not observed significant differences between the binding energies of the different binding patterns for each enantiomer. For both MAO A and MAO B, only one binding mode has been proposed based on the most stable complex formed between the (R)- and (S)-enantiomers of **DPH6** and the enzymes, showing also very similar binding energies. In addition, we have discovered an essential role for the cyano group in properly positioning the ligand by hydrogen-bond formation with the amino acid residues of the binding sites of AChE, BuChE and MAO A. It is worth noting that compounds lacking the cyano motif, like in the case of **DPH7**, showed drastically lowered inhibitory activity. Finally, it is worth pointing out that  $\alpha$ -aminonitriles have been seldom investigated as ChE inhibitors [40], and to the best of our knowledge, they have never been analyzed as MAO inhibitors [41]. However, some works have described nitriles as MAOIs [42], and Tipton and collaborators have reported that cyanide potentiates the inhibition of MAO by the irreversible inhibitor, phenelzine and pheniprazine [43]. One of the reviewers has kindly addressed our attention to the fact that “historically, prescribing MAO inhibitors have been reserved as a last-line of treatment because of potentially lethal effects due to drug interactions with a wide variety of therapeutic agents”. Also, donepezil produces a wide assortment of

side effects that include bradycardia, nausea, diarrhea, loss of appetite and stomach pain [44].

In addition, and according to the theoretic ADMET analysis, **DPH** compounds showed proper drug-like properties and brain penetration capacity for CNS activity. In particular, **DPH6** is less toxic than donepezil at high concentrations in an *in vitro* model of toxicity in HepG2 cells.

Finally, in terms of translational science, it is remarkable the *in vivo* effect of **DPH6** as enhancer on cognitive functions. Scopolamine induced memory deficits is greatly dependent on the cholinergic system [57]. We have found that donepezil is much more powerful than **DPH6** as cholinesterase inhibitor. This result is consistent with our own results on **ASS234** [8,9] (more potent ChEI than **DPH6**) which significantly lowers scopolamine-induced learning deficits in healthy adult mice, suggesting that product **ASS234** works as cognitive enhancer, as efficiently as donepezil at lower dosage, likely useful for the treatment of AD. Given the latter, the well-balanced anti-cholinesterasic and MAO inhibition profile in addition to the other attractive pharmacological properties of **DPH6** described here, and that **DPH6** has effect as enhancer on cognitive functions, prompt us to propose **DPH6** as the first racemic  $\alpha$ -aminonitrile identified so far as a multifunctional chelator for biometals, able to interact in two key enzymatic systems implicated in AD, and a new lead compound that deserves further investigation for the potential treatment of this disease.

To sum up, the well-balanced anti-cholinesterasic and MAO inhibition profile, in addition to the other attractive pharmacological properties described here, prompt us to propose **DPH6** as the first racemic  $\alpha$ -aminonitrile that has been identified as a multifunctional chelator for biometals, able to interact in two key enzymatic systems implicated in AD, and a new lead compound that deserves further investigation for the potential treatment of this disease.

## 4. Experimental section

### 4.1. Chemistry

#### 4.1.1. General methods

Melting points were determined on a Koffler apparatus, and are uncorrected.  $^1\text{H}$  NMR and  $^{13}\text{C}$  NMR spectra were recorded in  $\text{CDCl}_3$  or  $\text{DMSO-d}_6$  at 300, 400 or 500 MHz and at 75, 100 or 125 MHz, respectively, using solvent peaks [ $\text{CDCl}_3$ : 7.27 (D), 77.2 (C) ppm; and  $\text{DMSO-d}_6$ : 2.49 (D), 40 (C) ppm] as internal reference. The assignment of chemical shifts WAs based on standard NMR experiments ( $^1\text{H}$ ,  $^{13}\text{C}$ , DEPT, COSY, gHSQC, gHMBC). Mass spectra were recorded on a GC/MS spectrometer with an API-ES ionization source. Elemental analyses were performed at CNQO (CSIC, Spain). TLC were performed on silica F254 and detection by UV light at 254 nm or by charring with either ninhydrin, anisaldehyde or phosphomolybdic- $\text{H}_2\text{SO}_4$  dyeing reagents. Anhydrous solvents were used in all experiments. Column chromatography was performed on silica gel 60 (230 mesh). All known compounds have been synthesized as reported. All compounds were  $\geq 95\%$  purity as determined by examination of their combustion analyses.

#### 4.1.2. 5-(Chloromethyl) quinolin-8-ol (**8**) [17]

To a cooled solution of 8-hydroxyquinoline (14.6 g, 100 mmol) in conc. HCl (44 mL) at 0 °C, a 37% aqueous formaldehyde solution (20 mL) was added. Then HCl (g) was bubbled through the solution with stirring for 2 h. The mixture was allowed to warm to rt with further stirring for 6 h and without stirring for 2 h more. The product was filtered and the solid was rinsed with conc. HCl, giving product **8** [17] (19.9 g, 77.5%).

#### 4.1.3. 5-(((1-Benzylpiperidin-4-yl)(prop-2-ynyl)amino)methyl)quinolin-8-ol (DPH1)

To a solution of commercial 1-benzyl-4-piperidone (1.3 g, 7.0 mmol) and propargylamine (580 mg, 10.5 mmol) in MeOH (22 mL) at 0 °C, was added a small amount of  $\text{CF}_3\text{CO}_2\text{H}$  (5 drops). After being stirred for 1 h,  $\text{NaBH}_3\text{CN}$  (1.3 g, 19.7 mmol) was added to the solution. The mixture was stirred at 0 °C overnight and then quenched with aqueous saturated  $\text{NaHCO}_3$ . The mixture was concentrated *in vacuo* and extracted with AcOEt. The combined organic layers were dried over  $\text{MgSO}_4$  and concentrated under reduced pressure. The crude product was purified by column chromatography ( $\text{SiO}_2$ , AcOEt/MeOH = 4:1 v/v) to give 1-benzyl-N-(prop-2-ynyl)aminopiperidine (**9**) (500 mg, 31.2%) as an orange oil [ $R_f$  = 0.19 (AcOEt/MeOH = 4:1);  $^1\text{H}$  NMR (400 MHz,  $\text{CDCl}_3$ )  $\delta$  1.34–1.49 (m, 2H), 1.76–1.88 (m, 2H), 2.00–2.15 (m, 3H), 2.17–2.22 (t,  $J$  = 2.3 Hz, 1H), 2.65–2.76 (m, 1H), 2.81–2.90 (m, 2H), 3.41–3.46 (d,  $J$  = 2.3 Hz, 2H), 3.52 (s, 2H), 7.20–7.35 (m, 5H);  $^{13}\text{C}$  NMR (100 MHz,  $\text{CDCl}_3$ )  $\delta$  31.8, 34.9, 51.8, 62.7, 62.8, 71.1, 82.0, 126.8, 128.0, 128.9, 138.0]. To a solution of compound **9** (475 mg, 2.1 mmol) and quinoline **8** (387 mg, 1.5 mmol) in  $\text{CH}_2\text{Cl}_2$  (12 mL), was added  $\text{Et}_3\text{N}$  (0.84 mL, 6.0 mmol) at rt. After being stirred overnight, the mixture was quenched with aqueous saturated  $\text{NaHCO}_3$ . The product was extracted with  $\text{CH}_2\text{Cl}_2$ . The organic layer was dried over  $\text{Mg}_2\text{SO}_4$  and concentrated *in vacuo*. The product was purified by column chromatography ( $\text{SiO}_2$ , hexane/AcOEt by increasing the gradient from 5:1 to 3:1 v/v). Further purification was achieved by recrystallization (hexane/AcOEt = 1:1) to give compound DPH1 (196 mg, 33.8%) as a white solid: mp 145.5 °C; IR (KBr)  $\nu$  3289, 2958, 2914, 2805, 2754, 1582, 1510, 1422, 1360, 1281, 1229, 1186, 1152, 1107, 1069, 1001  $\text{cm}^{-1}$ ;  $^1\text{H}$  NMR (400 MHz,  $\text{CDCl}_3$ )  $\delta$  1.60–1.76 (m, 2H), 1.90–2.02 (m, 4H), 2.17 (t,  $J$  = 2.3 Hz, 1H), 2.48–2.60 (m, 1H), 2.91 (d,  $J$  = 11.5 Hz, 2H), 3.16 (d,  $J$  = 2.3 Hz, 2H), 3.46 (s, 2H), 4.00 (s, 2H), 7.00 (d,  $J$  = 7.6 Hz, 1H), 7.15–7.29 (m, 5H), 7.31–7.40 (m, 2H), 8.60 (dd,  $J$  = 8.5, 1.6 Hz, 1H), 8.69 (dd,  $J$  = 4.3, 1.5 Hz, 1H) (the OH signal

was not detected);  $^{13}\text{C}$  NMR (100 MHz,  $\text{CDCl}_3$ )  $\delta$  29.6, 38.0, 51.3, 53.0, 58.5, 63.0, 73.1, 80.0, 108.8, 121.4, 124.9, 127.1, 127.7, 128.2 (2C), 129.2, 129.3, 133.9, 138.7, 147.5, 151.8. Anal. Calcd. for  $\text{C}_{25}\text{H}_{27}\text{N}_3\text{O}$ : C, 77.89; H, 7.06; N, 10.90. Found: C, 77.88; H, 7.10; N, 10.89.

#### 4.1.4. 2-(1-Benzylpiperidin-4-yl)-2-(((8-hydroxyquinolin-5-yl)methyl)(prop-2-ynyl)amino)acetonitrile (DPH2)

To a cooled solution of 1-benzyl-4-piperidinecarboxaldehyde [58] (407 mg, 2.0 mmol) and propargylamine (165 mg, 3.0 mmol) in MeOH (6 mL) at 0 °C, a small amount of  $\text{CF}_3\text{CO}_2\text{H}$  (5 drops) was added. After being stirred for 1 h,  $\text{NaBH}_3\text{CN}$  (189 mg, 2.9 mmol) was added to the solution portionwise. The mixture was stirred at rt overnight and then quenched with aqueous saturated  $\text{NaHCO}_3$ . The mixture was concentrated *in vacuo* and then extracted with AcOEt. The combined organic layers were dried over  $\text{MgSO}_4$  and concentrated under reduced pressure to give a mixture that was purified by column chromatography ( $\text{SiO}_2$ , eluting solvent was changed from hexane/AcOEt = 5:1 to AcOEt and then AcOEt/MeOH = 4:1 v/v) to give N-[(1-benzylpiperidin-4-yl)methyl]prop-2-yn-1-amine (**10**) (232 mg, 50.2%), as an orange oil [ $R_f$  = 0.23 (AcOEt/MeOH = 4:1); IR (film)  $\nu$  3287, 3028, 2918, 2801, 2758, 1495, 1454, 1366, 1342, 1121, 1078  $\text{cm}^{-1}$ ;  $^1\text{H}$  NMR (400 MHz,  $\text{CDCl}_3$ )  $\delta$  1.15–1.55 (m, 3H), 1.72 (d,  $J$  = 12.5 Hz, 2H), 1.95–2.11 (m, 2H), 2.20 (t,  $J$  = 2.3 Hz, 1H), 2.57 (d,  $J$  = 6.6 Hz, 2H), 2.94 (d,  $J$  = 11.7 Hz, 2H), 3.33–3.65 (m, 4H), 7.19–7.40 (m, 5H) (the NH signal was not observed);  $^{13}\text{C}$  NMR (100 MHz,  $\text{CDCl}_3$ )  $\delta$  30.1, 35.8, 38.4, 53.4, 54.5, 63.1, 71.4, 82.2, 127.3, 128.3, 129.4, 137.3], and (1-benzylpiperidin-4-yl)(prop-2-yn-1-ylamino)acetonitrile (**11**) (165 mg, 30.9%) as an orange oil [ $R_f$  = 0.78 (AcOEt/MeOH = 4:1); IR (film)  $\nu$  3296, 2940, 2920, 2803, 2760, 1732, 1452, 1368, 1246, 1223, 1072  $\text{cm}^{-1}$ ;  $^1\text{H}$  NMR (400 MHz,  $\text{CDCl}_3$ )  $\delta$  1.37–1.72 (m, 4H), 1.76–1.88 (m, 2H), 1.92–2.02 (m, 2H), 2.26–2.33 (m, 1H), 2.87–2.98 (m, 2H), 3.44–3.69 (m, 5H), 7.17–7.44 (m, 5H);  $^{13}\text{C}$  NMR (100 MHz,  $\text{CDCl}_3$ )  $\delta$  28.4, 29.0, 36.8, 39.0, 53.0, 54.5, 63.0, 72.8, 80.1, 118.7, 127.1, 128.2, 129.1, 138.3].

To a solution of compound **11** (70 mg, 0.29 mmol) and  $\text{Et}_3\text{N}$  (0.085 mL, 0.58 mmol) in  $\text{CH}_2\text{Cl}_2$  (2 mL), chloride **8** (70 mg, 0.25 mmol) was added. After stirring for 30 min at rt, brine was added to the mixture. The product was extracted with  $\text{CH}_2\text{Cl}_2$ , the extract was dried over  $\text{Mg}_2\text{SO}_4$  and then concentrated *in vacuo*. The crude product was purified by column chromatography (hexane/AcOEt by increasing the gradient from 5:1 to 1:1 v/v), to give compound DPH2 (99 mg, 80.6%) as a white solid: IR (KBr)  $\nu$  3443, 3300, 3026, 2949, 2814, 1580, 1504, 1476, 1454, 1424, 1371, 1269, 1229, 1193, 1150, 1072  $\text{cm}^{-1}$ ;  $^1\text{H}$  NMR (600 MHz,  $\text{CDCl}_3$ )  $\delta$  0.68–0.70 (m, 1H), 1.17–1.22 (m, 1H), 1.65–1.95 (m, 5H), 2.41 (s, 1H), 2.65 (s, 1H), 2.81–2.83 (m, 1H), 3.23–3.29 (m, 3H), 3.34 (s, 1H), 3.45–3.48 (m, 1H), 3.68 (d,  $J$  = 13.2 Hz, 1H), 4.63 (d,  $J$  = 13.8 Hz, 1H), 7.1–7.20 (m, 1H), 7.21–7.28 (m, 5H), 7.40–7.44 (m, 2H), 8.60 (d,  $J$  = 8.4 Hz, 1H), 8.76 (d,  $J$  = 4.2 Hz, 1H) (the signal for OH was not detected);  $^{13}\text{C}$  NMR (150 MHz,  $\text{CDCl}_3$ )  $\delta$  29.4, 30.7, 36.0, 40.0, 52.5, 54.2, 57.7, 63.1, 74.0, 78.8, 84.7, 108.9, 111.8, 116.0, 121.7, 122.2, 127.2, 127.5, 128.2, 129.3, 130.0, 134.0, 138.8, 148.9, 152.6. Anal. Calcd for  $\text{C}_{27}\text{H}_{28}\text{N}_4\text{O}$ : C, 76.39; H, 6.65; N, 13.20. Found: C, 76.45; H, 6.75; N, 13.17.

#### 4.1.5. 5-(((1-Benzylpiperidin-4-yl)methyl)(prop-2-ynyl)amino)methyl)quinolin-8-ol (DPH3)

To a stirring solution of compound **10** (638 mg, 2.6 mmol) and chloride **8** (694 mg, 2.7 mmol) in  $\text{CH}_2\text{Cl}_2$  (12 mL),  $\text{Et}_3\text{N}$  (1.09 mL, 5.2 mmol) was added at rt. After being stirred overnight, the mixture was quenched with water and the product was extracted with  $\text{CH}_2\text{Cl}_2$ , dried over  $\text{Mg}_2\text{SO}_4$ , concentrated *in vacuo*, and purified by column chromatography ( $\text{SiO}_2$ , hexane/AcOEt by increasing the gradient from 5:1 to 1:1 v/v) to give amine DPH3 (572 mg, 55%) as a light brown solid: mp 128.5 °C; IR (KBr)  $\nu$  3320, 3248, 2946, 2914, 2754, 2365, 1734, 1580, 1506, 1478, 1422, 1366, 1279, 1229,

1192, 1128, 1065  $\text{cm}^{-1}$ ;  $^1\text{H}$  NMR (400 MHz,  $\text{CDCl}_3$ )  $\delta$  0.97–1.14 (m, 2H), 1.32–1.48 (m, 1H), 1.60 (d,  $J = 12.5$  Hz, 2H), 1.84 (t,  $J = 11.0$  Hz, 2H), 2.19 (s, 1H), 2.36 (d,  $J = 7.2$  Hz, 2H), 2.76 (d,  $J = 11.1$  Hz, 2H), 3.15 (d,  $J = 1.9$  Hz, 2H), 3.39 (s, 2H), 3.83 (s, 2H), 6.98 (d,  $J = 7.8$  Hz, 1H), 7.12–7.37 (m, 7H), 8.53 (dd,  $J = 8.5, 1.4$  Hz, 1H), 8.68 (dd,  $J = 4.2, 1.4$  Hz, 1H) (the signal for OH was not detected);  $^{13}\text{C}$  NMR (100 MHz,  $\text{CDCl}_3$ )  $\delta$  30.8, 33.5, 40.8, 53.6, 56.6, 59.1, 63.5, 73.4, 78.4, 108.7, 121.3, 124.9, 126.9, 127.8, 128.1, 129.1, 129.2, 134.1, 138.5, 138.7, 147.5, 151.9. Anal. Calcd for  $\text{C}_{26}\text{H}_{29}\text{N}_3\text{O}$ : C, 78.16; H, 7.32; N, 10.52. Found: C, 78.05; H, 7.36; N, 10.40.

#### 4.1.6. (1-Benzylpiperidin-4-ylidene)acetone nitrile (**12**) [59]

A solution of diethyl (cyanomethyl)phosphonate (2.13 g, 12 mmol) [prepared by heating triethylphosphite (1.0 equiv) and chloroacetone nitrile (1.0 equiv) at 150 °C for 3.5 h; the crude product was directly used in the next reaction] and  $\text{K}_2\text{CO}_3$  (1.39 g, 10 mmol) in dry THF (5 mL) was stirred for 15 min at rt. Then the mixture was heated to reflux for 20 min. After cooling down to rt, 1-benzyl-4-piperidone (1.90 g, 10 mmol) was added dropwise to this solution. Then the mixture was heated at reflux for 12 h. After cooling down to rt, 10%  $\text{K}_2\text{CO}_3$  aqueous solution was added. The reaction mixture was extracted with AcOEt, and the organic layers were dried over  $\text{MgSO}_4$  and concentrated *in vacuo* to give the crude product **12** (2.7 g, >99.0%), which was directly used in next step.

#### 4.1.7. (1-Benzylpiperidin-4-yl)acetone nitrile (**13**) [60]

To a solution of nitrile **12** (2.7 g, 10 mmol) in MeOH (100 mL), Mg (4.6 g, 191 mmol) and infinitesimal quantity of  $\text{I}_2$  was added. The mixture was stirred until it became gray gel. After conc. HCl was added, the mixture became clear solution. Then it was treated with 10 N NaOH to alkaline. The precipitate was filtered and washed with large amount of EtOAc. The filtrate was extracted with AcOEt, and the combined organic layers were dried over  $\text{MgSO}_4$  and concentrated *in vacuo* to give the product **13** (1.59 g, 74.5%).

#### 4.1.8. (1-Benzylpiperidin-4-yl)acetaldehyde (**14**) [61]

To an oven-dried and argon-purged flask were added the nitrile **13** (1.29 g, 6.0 mmol) and THF (13 mL). The mixture was cooled to –78 °C, and DIBAL-H (6.22 mL, 1 mmol/mL) was added to the reaction *via* syringe. The reaction was stirred at –78 °C for 1 h, and then quenched with aqueous saturated  $\text{NaHCO}_3$ . The precipitate was filtered and washed with large amount of EtOAc. The filtrate was extracted with EtOAc. The combined organic layers were washed with brine and dried over  $\text{MgSO}_4$ . After concentrated *in vacuo*, the crude product was purified by chromatography ( $\text{SiO}_2$ ,  $\text{CH}_2\text{Cl}_2/\text{MeOH} = 20:1$  v/v) to give product **14** (365 mg, 27.8%).

#### 4.1.9. 3-(1-Benzylpiperidin-4-yl)-2-((8-hydroxyquinolin-5-yl)methyl)(prop-2-ynyl)amino)propanenitrile (DPH4)

A solution of **14** (365 mg, 1.68 mmol) and propargylamine (187 mg, 3.4 mmol) in MeOH (10 mL) was stirred at 0 °C for 1 h; then  $\text{NaBH}_3\text{CN}$  (214 mg, 3.4 mmol) was added. The mixture was stirred at rt overnight. Water was added to the mixture and MeOH was removed under reduced pressure. Then aqueous saturated  $\text{NaHCO}_3$  was added, and the mixture was extracted with AcOEt. The separated organic layers were dried over  $\text{MgSO}_4$  and concentrated *in vacuo* to give the crude product. Further purification was achieved by column chromatography ( $\text{SiO}_2$ , eluting solvent was changed with gradient from hexane/AcOEt 5:1 to 1:5v/v and then change from AcOEt to AcOEt/MeOH 4:1 v/v) to give N-[2-(1-benzylpiperidin-4-yl)ethyl]prop-2-yn-1-amine (**15**) (168 mg, 38.9%), as an orange oil [ $R_f = 0.11$  (MeOH/AcOEt = 1:4)]; IR (film)  $\nu$  3302, 2922, 2945, 2801, 2758, 1493, 1454, 1366, 1148, 1121, 1078, 1028  $\text{cm}^{-1}$ ;  $^1\text{H}$  NMR (400 MHz,  $\text{CDCl}_3$ )  $\delta$  1.15–1.45 (m, 5H), 1.61 (d,  $J = 10.5$  Hz, 2H), 1.94 (t,  $J = 11.1$  Hz, 2H), 2.13 (t,  $J = 2.1$  Hz, 1H), 2.63

(t,  $J = 7.2$  Hz, 2H), 2.84 (d,  $J = 11.5$  Hz, 2H), 3.30–3.55 (m, 4H), 7.12–7.33 (m, 5H) (the NH signal was not observed);  $^{13}\text{C}$  NMR (100 MHz,  $\text{CDCl}_3$ )  $\delta$  32.0, 33.3, 36.3, 38.0, 45.9, 53.5, 63.1, 71.2, 82.0, 127.0, 128.0 (2C), 129.2 (2C), 137.5], and 3-(1-benzylpiperidin-4-yl)-2-(prop-2-yn-1-ylamino)propanenitrile (**16**) (190 mg, 40.2%) as an orange oil [ $R_f = 0.56$  (MeOH/AcOEt = 1:4)]; IR (film)  $\nu$  3295, 2924, 2905, 2782, 1493, 1452, 1388, 1343, 1125, 1074  $\text{cm}^{-1}$ ;  $^1\text{H}$  NMR (400 MHz,  $\text{CDCl}_3$ )  $\delta$  1.15–1.38 (m, 2H), 1.43–1.73 (m, 5H), 1.92 (t,  $J = 11.5$  Hz, 2H), 2.21 (t,  $J = 2.3$  Hz, 1H), 2.82 (d,  $J = 10.7$  Hz, 2H), 3.35–3.64 (m, 4H), 3.66–3.78 (m, 1H), 7.13–7.33 (m, 5H) (the NH signal was not observed);  $^{13}\text{C}$  NMR (100 MHz,  $\text{CDCl}_3$ )  $\delta$  31.7, 31.8, 32.2, 36.4, 39.9, 46.9, 53.2, 63.2, 72.7, 79.8 (2C), 119.6, 126.9, 128.0 (2C), 129.0 (2C), 138.1].

To a cooled mixture of **16** (84 mg, 0.3 mmol) and  $\text{Et}_3\text{N}$  (0.093 mL, 0.67 mmol) in  $\text{CH}_2\text{Cl}_2$  (6 mL), chloride **8** (77 mg, 0.3 mmol) was added at 0 °C. After being stirred at rt overnight, the reaction was quenched with aqueous 5%  $\text{NaHCO}_3$ . The reaction mixture was extracted with  $\text{CH}_2\text{Cl}_2$ , and extracts were dried with  $\text{Mg}_2\text{SO}_4$  and concentrated *in vacuo*. The crude product was purified by column chromatography (hexane: AcOEt by increasing the gradient from 5:1 to 1:1 v/v) to give compound **DPH4** (91.4 mg, 69.5%) as an orange oil: IR (film)  $\nu$  3298, 2934, 2807, 1580, 1505, 1476, 1370, 1273, 1233, 1198, 1148, 1072, 1028  $\text{cm}^{-1}$ ;  $^1\text{H}$  NMR (400 MHz,  $\text{CDCl}_3$ )  $\delta$  0.81–0.93 (m, 1H), 0.93–1.07 (m, 1H), 1.12–1.32 (m, 2H), 1.38–1.62 (m, 3H), 1.69 (ddd,  $J = 14.1, 8.8, 5.5$  Hz, 1H), 1.76–1.89 (m, 1H), 2.39–2.47 (m, 1H), 2.58 (d,  $J = 11.3$  Hz, 1H), 2.80 (d,  $J = 11.5$  Hz, 1H), 3.21–3.32 (m, 1H), 3.36–3.53 (m, 3H), 3.65–3.75 (m, 2H), 4.60 (d,  $J = 13.1$  Hz, 1H), 7.06–7.11 (m, 1H), 7.21–7.33 (m, 5H), 7.40–7.47 (m, 2H), 8.58–8.65 (m, 1H), 8.75–8.81 (m, 1H) (the signal for OH was not detected);  $^{13}\text{C}$  NMR (100 MHz,  $\text{CDCl}_3$ )  $\delta$  30.6, 31.5, 37.2, 39.8, 49.6, 52.7, 53.0, 53.6, 62.8, 74.1, 78.6, 108.9, 117.0, 121.6, 122.3, 127.2, 127.5, 128.1, 129.3, 129.8, 133.6, 138.6, 147.7, 152.5. HRMS. Calcd. for  $\text{C}_{28}\text{H}_{31}\text{N}_4\text{O}$  (M + H)<sup>+</sup>: 439.2428. Found: 439.2532 (M + H)<sup>+</sup>.

#### 4.1.10. 5-(((2-(1-Benzylpiperidin-4-yl)ethyl)(prop-2-ynyl)amino)methyl)quinolin-8-ol (DPH5)

To a cooled mixture of **15** (46 mg, 0.18 mmol) and  $\text{Et}_3\text{N}$  (0.053 mL, 0.38 mmol) in  $\text{CH}_2\text{Cl}_2$  (2.5 mL) at 0 °C, chloride **8** (47 mg, 0.18 mmol) was added. After being stirred at rt overnight, the reaction was quenched with aqueous 5%  $\text{NaHCO}_3$ . The product was extracted with  $\text{CH}_2\text{Cl}_2$ , and extracts were dried over  $\text{Mg}_2\text{SO}_4$  and then concentrated *in vacuo*. The crude product was purified by column chromatography (hexane/AcOEt by increasing the gradient from 5:1 to 1:1 v/v) to give compound **DPH5** (40 mg, 53.5%) as a yellow oil: IR (film)  $\nu$  3254, 2945, 2915, 2805, 2758, 1578, 1508, 1478, 1420, 1375, 1350, 1279, 1231, 1194, 1148, 1121  $\text{cm}^{-1}$ ;  $^1\text{H}$  NMR (400 MHz,  $\text{CDCl}_3$ )  $\delta$  1.24 (s, 3H), 1.44 (d,  $J = 33.2$  Hz, 4H), 1.82 (m, 2H), 2.67 (t,  $J = 2.40$  Hz, 1H), 2.58 (t,  $J = 7.20$  Hz, 2H), 2.83 (d,  $J = 11.20$  Hz, 2H), 3.26 (d,  $J = 2.40$  Hz, 2H), 3.48 (s, 2H), 3.92 (s, 2H), 7.08 (d,  $J = 8.00$  Hz, 1H), 7.30–7.44 (m, 7H), 8.61–8.61 (m, 1H), 8.76–8.77 (m, 1H) (the signal for OH was not detected);  $^{13}\text{C}$  NMR (100 MHz,  $\text{CDCl}_3$ )  $\delta$  32.2, 33.5, 33.9, 41.0, 50.3, 53.7, 55.9, 63.3, 72.3, 78.3, 108.7, 121.4, 124.9, 127.0, 127.9, 128.1, 129.2, 129.3, 134.0, 138.7, 147.5, 151.8. HRMS. Calcd. for  $\text{C}_{27}\text{H}_{32}\text{N}_3\text{O}$  (M + H)<sup>+</sup>: 414.2545. Found: 414.2570 (M + H)<sup>+</sup>.

#### 4.1.11. (2E)-3-(1-benzylpiperidin-4-yl)prop-2-enenitrile (**17**) [62]

A mixture of diethyl (cyanomethyl)phosphonate (2.2 g, 12 mmol) and  $\text{K}_2\text{CO}_3$  (1.4 g, 10 mmol) in dry THF (100 mL) was stirred at rt for 15 min, and then heated at reflux for 20 min. After cooling down to rt, 1-benzyl-4-piperidinecarboxaldehyde [58] (2.0 g, 10 mmol) was added. The mixture was heated to reflux for 3 h. Aqueous 10%  $\text{K}_2\text{CO}_3$  water (100 mL) was added after cooling down to rt. The product was extracted with AcOEt and dried over  $\text{MgSO}_4$ . After concentrated *in vacuum*, the crude product was

purified by column chromatography (SiO<sub>2</sub>, hexane/AcOEt from 5:1 to 1:1 v/v) to give nitrile **17** (0.74 g, 32.6%).

#### 4.1.12. 3-(1-Benzylpiperidin-4-yl)propanenitrile (**18**) [63]

To a solution of **17** (1.74 g, 7.70 mmol) in MeOH (33 mL) at rt, turning of Mg (3.70 g, 154 mmol) and infinitesimal quantity of I<sub>2</sub> was added to the mixture. The mixture was stirred until it became gray gel. After conc. HCl was added, the mixture became clear solution. Then it was treated with 10 N NaOH to alkaline. The precipitates were filtered and washed with large amount of EtOAc. The filtrate was extracted with AcOEt, and the combined organic layers were dried over MgSO<sub>4</sub> and concentrated *in vacuo* to give the crude product **18** (1.76 g, 99.9%).

#### 4.1.13. 3-(1-Benzylpiperidin-4-yl)propanal (**19**) [64]

To an oven-dried and argon-purged flask were added the nitrile **18** (1.00 g, 4.4 mmol) and THF (10 mL). The reaction was cooled to –78 °C, and DIBAL-H (4.54 mL, 1 mmol/mL) was added to the reaction *via* syringe. The mixture was stirred at –78 °C for 1 h, and then quenched with aqueous saturated NaHCO<sub>3</sub>. The precipitates were filtered and washed with large amount of EtOAc. The filtrate was extracted with EtOAc. The combined organic layers were washed with brine and dried over MgSO<sub>4</sub>. After concentrated in vacuum, the crude product was purified by chromatography (SiO<sub>2</sub>, CH<sub>2</sub>Cl<sub>2</sub>/MeOH = 20:1 v/v), to give aldehyde **19** (427 mg, 42.7%).

#### 4.1.14. 4-(1-Benzylpiperidin-4-yl)-2-(((8-hydroxyquinolin-5-yl)methyl)(prop-2-ynyl)amino)butanenitrile (DPH6)

A solution of aldehyde **19** (427 mg, 1.9 mmol) and propargylamine (204 mg, 3.7 mmol) in MeOH (6 mL) was stirred at 0 °C for 1 h, then NaBH<sub>3</sub>CN (1.3 g, 2.0 mmol) was added. The mixture was stirred at rt overnight. Water was added to the mixture and MeOH was removed under reduced pressure. Then, aqueous saturated NaHCO<sub>3</sub> was added, and the mixture was extracted with AcOEt. The separated organic layers were dried over MgSO<sub>4</sub> and concentrated *in vacuo* to give the crude products. Further purification was achieved by column chromatography (SiO<sub>2</sub>, eluting solvent was changed with gradient from hexane/AcOEt 5:1 to 1:5v/v and then change from AcOEt to AcOEt/MeOH 4:1 v/v) to give N-[3-(1-benzylpiperidin-4-yl)propyl]prop-2-yn-1-amine (**20**) (221 mg, 44.2%), as a yellow oil [*R*<sub>f</sub> = 0.19 (MeOH/AcOEt = 1:4); IR (film)  $\nu$  3304, 3028, 2922, 2847, 2794, 2758, 1495, 1452, 1386, 1343, 1119, 1028 cm<sup>-1</sup>; <sup>1</sup>H NMR (600 MHz, CDCl<sub>3</sub>)  $\delta$  1.10–1.26 (m, 5H), 1.33–1.46 (m, 2H), 1.58 (d, *J* = 9.9 Hz, 2H), 1.87 (br s, 2H), 2.13 (t, *J* = 2.3 Hz, 1H), 2.31–2.39 (m, 1H), 2.59 (t, *J* = 7.1 Hz, 1H), 2.81 (d, *J* = 10.8 Hz, 2H), 3.35 (d, *J* = 2.3 Hz, 2H), 3.43 (s, 2H), 7.13–7.29 (m, 5H) (the NH signal was not observed); <sup>13</sup>C NMR (150 MHz, CDCl<sub>3</sub>)  $\delta$  24.6, 27.0, 32.2, 32.3, 34.1, 35.6, 38.0, 48.8, 53.8, 63.4, 71.1, 82.2, 126.7, 128.0, 129.1, 138.4], and 4-(1-benzylpiperidin-4-yl)-2-(prop-2-yn-1-ylamino)butanenitrile (**21**) (234 mg, 42.7%), as a yellow oil [*R*<sub>f</sub> = 0.59 (MeOH/AcOEt = 1:4); IR (film)  $\nu$  3296, 2911, 2845, 2801, 2780, 1493, 1452, 1368, 1343, 1312, 1260, 1146, 1119, 1074; <sup>1</sup>H NMR (400 MHz, CDCl<sub>3</sub>)  $\delta$  1.18–1.69 (m, 8H), 1.70–1.83 (m, 2H), 1.85–2.02 (m, 2H), 2.23–2.37 (m, 1H), 2.87 (d, *J* = 10.5 Hz, 2H), 3.29–3.76 (m, 4H), 7.16–7.38 (m, 5H) (the NH signal was not observed); <sup>13</sup>C NMR (100 MHz, CDCl<sub>3</sub>)  $\delta$  31.0, 31.6, 32.1, 32.2, 32.3, 35.4, 36.6, 49.5, 53.7, 63.4, 72.8, 80.0, 119.4, 126.7, 127.9, 128.9, 138.1].

To a mixture of amine **21** (89 mg, 0.3 mmol) and Et<sub>3</sub>N (0.09 mL, 0.7 mmol) in CH<sub>2</sub>Cl<sub>2</sub> (6 mL) at 0 °C, chloride **8** (77 mg, 0.3 mmol) was added. After being stirred at rt overnight, the reaction was quenched with aqueous 5% NaHCO<sub>3</sub> and the product was extracted with CH<sub>2</sub>Cl<sub>2</sub>. The extracts were dried Mg<sub>2</sub>SO<sub>4</sub>, and concentrated *in vacuo*. The crude products were purified by column chromatography (SiO<sub>2</sub>, hexane/AcOEt by increasing the gradient from 5:1 to 1:1 v/v), to give compound **DPH6** (89 mg, 65.4%) as a yellow oil: IR

(film)  $\nu$  3295, 2931, 2812, 1578, 1505, 1476, 1371, 1271, 1203, 1196, 1148, 1123, 1072, 1028 cm<sup>-1</sup>; <sup>1</sup>H NMR (400 MHz, CDCl<sub>3</sub>)  $\delta$  0.99–0.77 (m, 1H), 1.40–1.38 (m, 6H), 1.53–1.40 (m, 1H), 1.84–1.60 (m, 5H), 2.42 (t, *J* = 2.4 Hz, 1H), 2.77 (ddt, *J* = 12.0, 8.3, 2.1 Hz, 1H), 3.28 (dd, *J* = 16.8, 2.4 Hz, 1H), 3.45 (s, 2H), 3.58 (dd, *J* = 16.8, 2.4 Hz, 1H), 3.75 (d, *J* = 13.1 Hz, 1H), 4.60 (d, *J* = 13.1 Hz, 1H), 7.11 (d, *J* = 7.6 Hz, 1H), 7.32–7.22 (m, 5H), 7.57–7.39 (m, 2H), 8.64 (dd, *J* = 8.5, 1.6 Hz, 1H), 8.78–8.80 (m, 1H) (the signal for OH was not detected); <sup>13</sup>C NMR (100 MHz, CDCl<sub>3</sub>)  $\delta$  28.1, 31.5, 31.9, 32.0, 34.4, 39.8, 52.3, 53.4, 53.5, 53.7, 63.3, 74.2, 78.6, 108.9, 117.2, 121.8, 122.5, 127.1, 127.6, 128.2, 129.3, 129.9, 133.7, 138.8, 147.9, 152.6. HRMS. Calcd for C<sub>29</sub>H<sub>33</sub>N<sub>4</sub>O (M + H)<sup>+</sup>: 453.2654. Found: 452.2526 (M + H)<sup>+</sup>.

#### 4.1.15. 5-(((3-(1-Benzylpiperidin-4-yl)propyl)(prop-2-ynyl)amino)methyl)quinolin-8-ol (DPH7)

To a cooled mixture of amine **20** (189 mg, 0.70 mmol) and Et<sub>3</sub>N (0.51 mL, 2.5 mmol) in CH<sub>2</sub>Cl<sub>2</sub> (15 mL) at 0 °C, chloride **8** (186 mg, 0.73 mmol) was added. After being stirred at rt overnight, the reaction was quenched with aqueous 5% NaHCO<sub>3</sub>. The product was extracted with CH<sub>2</sub>Cl<sub>2</sub>, and extracts were dried over Mg<sub>2</sub>SO<sub>4</sub> and then concentrated *in vacuo*. The crude products were purified by column chromatography (SiO<sub>2</sub>, hexane/AcOEt by increasing the gradient from 5:1 to 1:1 v/v) to give compound **DPH7** (162 mg, 54.3%) as a yellow oil: IR (film)  $\nu$  3381, 3293, 2911, 2801, 1738, 1580, 1505, 1476, 1425, 1373, 1289, 1238, 1198, 1047 cm<sup>-1</sup>; <sup>1</sup>H NMR (300 MHz, CDCl<sub>3</sub>)  $\delta$  0.99–1.33 (m, 5H), 1.42–1.66 (m, 4H), 1.86 (t, *J* = 11.3 Hz, 2H), 2.29 (t, *J* = 2.1 Hz, 1H), 2.56 (t, *J* = 7.1 Hz, 2H), 2.86 (d, *J* = 11.4 Hz, 2H), 3.26 (d, *J* = 2.2 Hz, 2H), 3.48 (s, 2H), 3.93 (s, 2H), 7.09 (d, *J* = 7.6 Hz, 1H), 7.20–7.37 (m, 5H), 7.37–7.49 (m, 2H), 8.65 (dd, *J* = 8.5, 1.3 Hz, 1H), 8.77 (dd, *J* = 4.1, 1.3 Hz, 1H) (the signal for OH was not detected); <sup>13</sup>C NMR (100 MHz, CDCl<sub>3</sub>)  $\delta$  24.4, 32.2, 34.0, 35.3, 40.9, 53.2, 53.8 (2C), 55.8, 63.4, 73.4, 78.4, 108.9, 121.4, 124.9, 127.0, 127.9, 128.2, 129.2, 129.3, 134.1, 138.7, 147.6, 152.0. Anal. Calcd for C<sub>28</sub>H<sub>33</sub>N<sub>3</sub>O: C, 78.65; H, 7.78; N, 9.83. Found: C, 76.90; H, 8.03; N, 9.98.

#### 4.1.16. 4-(1-Benzylpiperidin-4-yl)-2-(prop-2-yn-1-ylamino)butanenitrile (**21**)

3-(1-Benzylpiperidin-4-yl)propanal (**19**) (136 mg, 0.59 mmol), prop-2-yn-1-amine (47  $\mu$ L, 0.74 mmol, 1.25 equiv) and trimethylsilyl cyanide (TMSCN) (0.14 mL, 1.1 mmol, 1.85 equiv) were mixed and submitted to microwave irradiation at 125 °C for 10 min. The crude reaction was purified by column chromatography (SiO<sub>2</sub>, hexane/AcOEt from 9:1 to 1:1 v/v) to give compound **21** (104 mg, 60%) as a yellow oil, that showed identical spectroscopic data to the compound isolated in the Mannich reductive amination of aldehyde **19**.  $\alpha$ -Aminonitrile **21** was also transformed into target compound **DPH6** (see above).

## 4.2. Pharmacological evaluation

### 4.2.1. Cholinesterase inhibition

Cholinesterase activities were assessed following a spectrophotometric method [18], using purified AChE from *Electrophorus electricus* (type V–S) and purified BuChE from equine serum (lyophilized powder) (Sigma–Aldrich, Madrid, Spain). Enzymatic reactions took place in 96-well plates in solutions containing 0.1 M phosphate buffer (pH 8.0), 0.035 U/mL AChE or 0.05 U/mL BuChE and 0.35 mM of 5,5'-dithiobis-2-nitrobenzoic acid (DTNB, Sigma–Aldrich, Madrid, Spain). Inhibition curves were plotted by pre-incubating this mixture with serial dilutions of each compound for 20 min. The activity in absence of compounds was used to determine the 100% of enzyme activity. After pre-incubation times, 50  $\mu$ L of substrate were added to a final concentration of 0.35 mM acetylthiocholine iodide or 0.5 mM butyrylthiocholine iodide

(Sigma–Aldrich). Enzymatic reactions were followed for 5 min with AChE or 25 min with BuChE. Changes in absorbance at  $\lambda_{405}$  in a spectrophotometric plate reader (FluoStar OPTIMA, BMG Labtech) were detected and  $IC_{50}$  values calculated at the compound concentration inhibiting 50% of enzymatic activity by using the GraphPad 'PRISM' software (version 3.0). Data were expressed as mean  $\pm$  SEM of at least three different experiments performed in triplicate.

**4.2.1.1. Kinetic studies of AChE inhibition by DHP6.** To estimate the mechanism of action of DHP6 inhibiting AChE, reciprocal plots of  $1/V$  versus  $1/[S]$  were determined at different acetylthiocholine (ASCh) concentrations (0.1–5  $\mu$ M). The plots were assessed by a weighted least-squares analysis. Slopes of reciprocal plots were plotted against concentration of DHP6 (0–5  $\mu$ M) for AChE to determine the reversible inhibition constant ( $K_i$ ).

#### 4.2.2. Monoamine oxidase inhibition

To assess the inhibition of MAO A and MAO B by derivatives **DHPs 1–7**,  $^{14}C$ -labeled substrates were used (Perkin Elmer, USA). Rat liver homogenates were used as source of MAO [19]. MAO A activity was determined using 100  $\mu$ M (0.5 mCi/mmol) [ $^{14}C$ ]-5-hydroxytryptamine (5-HT) whereas MAO B activity was determined using 20  $\mu$ M (2.5 mCi/mmol) [ $^{14}C$ ]-phenylethylamine (PEA). Inhibition curves were plotted by pre-incubating the enzyme with several concentrations of each compound for 30 min in 50 mM phosphate buffer (pH 7.4). Inhibitor-free samples were used to determine the 100% of enzyme activity. At the end of each pre-incubation, substrate (25  $\mu$ l) was added in a final volume of 225  $\mu$ l and reactions allowed for 20 min (MAO A) or 4 min (MAO B). Reactions were stopped by adding 2 M citric acid and radiolabelled-aldehyde products extracted into toluene/ethylacetate (1:1, v/v) containing 0.6% (w/v) 2,5-diphenyloxazole prior to liquid scintillation counting (Tri-Carb 2810TR). Inhibition curves were plotted as previously mentioned. Total protein was measured by the method of Bradford (1976) using bovine-serum albumin as standard.

**4.2.2.1. Reversibility and time-dependence of MAO by DHP6.** The study of reversibility inhibition exerted by **DHP6** towards MAO A and MAO B were determined by incubating the enzyme in the presence and in the absence of the inhibitor before and after three consecutive washings with buffer. MAO A and MAO B samples were pre-incubated for 30 min at 37 °C with 10  $\mu$ M **DHP6** and 20  $\mu$ M **DHP6**, respectively. A sample of 50 nM clorgyline and 20 nM *l*-deprenyl was also used as control of irreversible MAO A and MAO B inhibition. Samples were washed with 50 mM phosphate buffer (pH 7.4) and centrifuged at 25,000 g for 10 min at 4 °C consecutively three times. Total protein was measured by the Bradford method and MAO activity determined as described above. Time-dependence inhibition of **DHP6** towards MAO A and MAO B was evaluated by pre-incubating varying concentrations of the inhibitor with the enzyme at different times (0–180 min). Dose-response curves ( $IC_{50}$ ) values were accordingly determined for each time as described above.

#### 4.2.3. Determination of metal-chelating properties

Complexing studies were performed in distilled water at room temperature using a UV–VIS spectrophotometer (Lambda25, PerkinElmer). Spectrums (220–300 nm) of DHP6 alone (10  $\mu$ M) and in presence of varying concentrations of  $CuSO_4$  (no changes observed after 5-min incubation),  $Fe_2(SO_4)_3$  (no changes observed following O/N incubation) and  $ZnSO_4$  (no changes observed after 1-h incubation) were recorded in 1 cm quartz cells. The stoichiometry of the complexes **DHP6**- $Cu(II)$ / $Zn(II)$ / $Fe(III)$  was determined by the Job's method [65]. Series of different solutions containing **DHP6** and

biometals  $CuSO_4$ ,  $ZnSO_4$  or  $Fe_2(SO_4)_3$  were prepared at a final sum of concentrations of both species of 10  $\mu$ M, varying the proportions of both components between 0 and 100%. Absorbance at 257 nm was plotted versus the mole fraction of DHP6 for each metal.

#### 4.2.4. Toxicity in human hepatoma cell line HepG2: culture of HepG2 liver cells and treatment

Human hepatoma cell line HepG2 was cultured in Eagle's minimum essential medium (EMEM) supplemented with 15 non-essential amino acids, 1 mM sodium pyruvate, 10% heat-inactivated fetal bovine serum (FBS), 100 units/mL penicillin, and 100  $\mu$ g/mL streptomycin (reagents from Invitrogen, Madrid, Spain). Cells were seeded into flasks containing supplemented medium and maintained at 37 °C in a humidified atmosphere of 5%  $CO_2$  and 95% air. For assays, HepG2 cells were subcultured in 96-well plates at seeding density of  $8 \times 10^4$  cells per well. When HepG2 cells reached 80% confluence, the medium was replaced with fresh medium containing 1–1000  $\mu$ M compounds or 0.1% DMSO as a vehicle control.

#### 4.2.5. MTT assay and cell viability

Cell viability, virtually the mitochondrial activity of living cells, was measured by quantitative colorimetric assay with 3-[4,5-dimethylthiazol-2-yl]-2,5-diphenyl-tetrazolium bromide (MTT) (Sigma Aldrich), as described previously [51]. Briefly, 50  $\mu$ l of the MTT labeling reagent, at a final concentration of 0.5 mg/ml, was added to each well at the end of the incubation time and the plate placed in a humidified incubator at 37 °C with 5%  $CO_2$  and 95% air (v/v) for an additional 2 h period. Then, the insoluble formazan was dissolved with dimethylsulfoxide; colorimetric determination of MTT reduction was measured at 540 nm. Control cells treated with EMEM were used as 100% viability.

#### 4.2.6. In vivo analysis: relief of scopolamine-induced long-term memory deficit in mice by DHP6

**4.2.6.1. Animals.** Thirty-six male C57BL/6J mice (Harlan), weighing 25 g served as subjects in order to obtain our results. Animals were housed under controlled light (with a 12-h light/12-h dark cycle, lights on at 7:00 a.m.). Procedures were carried out following the European Communities Council Directive (86/609/EEC) on animal experiments.

**4.2.6.2. Drugs and treatments.** Scopolamine hydrobromide, 1 mg/kg (Sigma, St. Louis, MO, USA), donepezil, 1 mg/kg (Tocris Bioscience, R&D Systems Inc., Minneapolis, USA), and DHP6 (35 mg/kg) were given in 10 ml/kg of saline solution (0.9% NaCl) by intraperitoneal *via*. Animals were divided into four experimental handling groups: mice administered with i) saline (vehicle,  $n = 9$ ); ii) scopolamine (vehicle + scop,  $n = 9$ ); iii) donepezil plus scopolamine (donepezil + scop,  $n = 10$ ); and iv) DHP6 plus scopolamine (DHP6 + scop,  $n = 8$ ).

**4.2.6.3. Passive avoidance task.** The test was performed using the Ugo Basile (Comerio, Italy) apparatus. Basically, the device consists of two compartments (10  $\times$  13  $\times$  15 cm) connected by a sliding door. One compartment is brightly lit (10 W) and, on the contrary, the other one is dark and equipped with an electrified grid floor. Rodents tend to prefer dark environments and will immediately enter the darkened compartment. The day before of the experiment, mice are placed in the experimental room for 1 h. The experiment is performed in two consecutive days. The first day, scopolamine or saline is administered 30 min before the training session and saline, donepezil or **DHP6** are administered 90 min prior to the administration of scopolamine or saline. During the training session, each mouse is individually placed in the

illuminated compartment with the sliding door closed. 30 sec later, the door is open so that the mouse can move freely to each room. Once the mouse gets into the dark compartment, the sliding door closes automatically and the animal receives an electric foot shock (0.5 mA, 1 s). Then, mice are returned their home cage and 24 h later, in the second day, the probe session takes place. In the second day, each individual is placed again into illuminated box. Then the sliding door opens for 5 s with the electric foot-shock switched off in the dark room. The latency in seconds taken by a mouse to enter the dark compartment after door opening during the training and the probe session was automatically determined by the computer device. A cut-off time of 5 min was defined.

**4.2.6.4. Statistical analysis.** Significance was determined using a one-way analysis of variance (ANOVA), followed by Bonferroni's post hoc test. Statistical analysis of differences within a group between training and probe sessions were determined by using the Student's *t*-test. These statistical analyses have been carried out by using GraphPad Prism 5 computer software. Results are expressed as the average of latencies  $\pm$ S.E.M. Differences are considered statistically significant at  $p < 0.05$ .

#### 4.2.7. Molecular modeling

**4.2.7.1. Molecular docking into AChE and BuChE.** (R)-DPH6 and (S)-DPH6 were assembled as hydrochlorides and free bases within Discovery Studio, version 2.1, software package, using standard bond lengths and bond angles. With the CHARMM force field [66] and partial atomic charges, the molecular geometries of (R)-DPH6 and (S)-DPH6 were energy-minimized using the adopted-based Newton–Raphson algorithm. Structures were considered fully optimized when the energy changes between iterations were less than 0.01 kcal/mol [67].

**4.2.7.2. Molecular docking of (R)-DPH6 and (S)-DPH6 into EeAChE.** The coordinates of *E. electricus* AChE (PDB ID: 1C2B), were obtained from the Protein Data Bank (PDB). For docking studies, initial protein was prepared by removing all water molecules, heteroatoms, any co-crystallized solvent and the ligand. Proper bonds, bond orders, hybridization and charges were assigned using protein model tool in Discovery Studio, version 2.1, software package. CHARMM force field was applied using the receptor–ligand interactions tool in Discovery Studio, version 2.1, software package. Docking calculations were performed with the program Autodock Vina [22]. AutoDockTools (ADT; version 1.5.4) was used to add hydrogens and partial charges for proteins and ligands using Gasteiger charges. Flexible torsions in the ligands were assigned with the AutoTors module, and the acyclic dihedral angles were allowed to rotate freely. Trp286, Tyr124, Tyr337, Tyr72, Asp74, Thr75, Trp86, and Tyr341 receptor residues were selected to keep flexible during docking simulation using the AutoTors module. Because VINA uses rectangular boxes for the binding site, the box center was defined and the docking box was displayed using ADT. For *E. electricus* AChE (PDB ID: 1C2B) the docking procedure was applied to whole protein target, without imposing the binding site (“blind docking”). A grid box of  $60 \times 60 \times 72$  with grid points separated 1 Å, was positioned at the middle of the protein ( $x = 21.5911$ ;  $y = 87.752$ ;  $z = 23.591$ ). Default parameters were used except num\_modes, which was set to 40. The AutoDock Vina docking procedure used was previously validated [23].

**4.2.7.3. Molecular docking of inhibitors (R)-DPH6 and (S)-DPH6 into eqBuChE.** The horse BuChE model has been retrieved from the SWISS-MODEL Repository. This is a database of annotated three-dimensional comparative protein structure models generated by the fully automated homology-modeling pipeline SWISS-MODEL. A

putative three-dimensional structure of eqBuChE has been created based on the crystal structure of hBuChE (PDB ID: 2PM8), these two enzyme exhibited 89% sequence identity. Proper bonds, bond orders, hybridization and charges were assigned using protein model tool in Discovery Studio, version 2.1, software package. CHARMM force field was applied using the receptor–ligand interactions tool in Discovery Studio, version 2.1, software package. Docking calculations were performed following the same protocol described before for *EeAChE*. All dockings were performed as blinds dockings where a cube of 75 Å with grid points separated 1 Å, was positioned at the middle of the protein ( $x = 29.885$ ;  $y = -54.992$ ;  $z = 58.141$ ). Default parameters were used except num\_modes, which was set to 40. The lowest docking-energy conformation was considered as the most stable orientation. Finally, the docking results generated were directly loaded into Discovery Studio, version 2.1.

**4.2.7.4. Molecular docking of compounds (R)-DPH6 and (R)-DPH7 into rat MAO A/B.** Compounds (R)-DPH6 and (R)-DPH7 were assembled as non-protonated amine within Discovery Studio, version 2.1, software package, following the procedure described before for cholinesterases. The crystal structure of rat MAO A in complex with its irreversible inhibitor MLG-709 was obtained from the Protein Data Bank (PDB ID 1O5W). The rat MAO B model has been retrieved from the SWISS-MODEL Repository. A putative three-dimensional structure of rat MAO B has been created based on the crystal structure of hMAO B (PDB ID: 1S3E), these two enzymes exhibited 89% sequence identity. For docking studies initial proteins were prepared. First, in the PDB crystallographic structure 1O5W (rat MAO A), any co-crystallized solvent and the ligand were removed; it is not necessary in the PDB MAO B model. Then, proper bonds, bond orders, hybridization and charges were assigned using protein model tool in Discovery Studio, version 2.1, software package. CHARMM force field was applied using the receptor–ligand interactions tool in Discovery Studio, version 2.1, software package. Six water molecules located around the FAD cofactor were considered in the docking experiments because of their well-known role into the MAO's inhibition. Finally, atoms of the FAD cofactor were defined in their oxidized state. Docking calculations were performed following the same protocol described before for *EeAChE*. In docking with MAO A, Tyr 69, Leu97, Gln99, Ala111, Phe112, Tyr124, Trp128, Phe173, Leu176, Phe177, Ile180, Asn181, Ile207, Phe208, Gln215, Cys323, Ileu325, Ileu335, Phe352, Tyr407 and Tyr444 receptor residues were selected to keep flexible during docking simulation using the AutoTors module. All dockings were performed as blind dockings where a cube of 40 Å with grid points separated 1 Å, was centered on the FAD N5. Default parameters were used except num\_modes, which was set to 40. According to Vina best scored poses, the most stable complex configurations were considered. At the end of the docking, the best poses were analyzed using Discovery Studio.

#### 4.3. Statistical analysis

Significance was determined using a one-way analysis of variance (ANOVA), followed by Bonferroni's post hoc test. Significant differences within group were determined with the Student's *t*-test. Results are expressed as the average of latencies  $\pm$  S.E.M. Differences are considered statistically significant at  $p < 0.05$ .

#### Acknowledgments

Supported by MINECO (SAF2012-33304 to JMC; to SAF2010-15173 RMM), MICINN for a grant (CTQ2009-10478 to ES), and EU (COST Action CM1103). Oscar M. Bautista-Aguilera thanks MINECO

(Spain) for a FPI fellowship. G.E. and L.W. have equally contributed to this work.

## Appendix A. Supplementary data

Supplementary data related to this article can be found at <http://dx.doi.org/10.1016/j.ejmech.2014.04.078>.

## References

- [1] M. Goedert, M.G. Spillantini, *Science* 314 (2006) 777–781.
- [2] A. Castro, A. Martínez, *Current Pharmaceutical Design* 12 (2006) 4377–4387.
- [3] A. Gella, N. Durany, *Cell Adhesion & Migration* 3 (2009) 88–93.
- [4] C. Geula, M.M. Mesulam, *Neuroscience* 33 (1989) 469–481.
- [5] E. Scarpini, P. Scheltens, H. Feldman, *Lancet Neurology* 2 (2003) 539–547.
- [6] V.N. Talsa, *Mechanisms of Ageing and Development* 122 (2001) 1961–1969.
- [7] A. Cavalli, M.L. Bolognesi, A. Minarini, M. Rosini, V. Tumiatti, M. Recanatini, C. Melchiorre, *Journal of Medicinal Chemistry* 51 (2008) 347–372.
- [8] I. Bolea, J. Juárez-Jiménez, C. de los Ríos, M. Chioua, R. Poupplana, F.J. Luque, M. Unzeta, J. Marco-Contelles, A. Samadi, *Journal of Medicinal Chemistry* 54 (2011) 8251–8270.
- [9] I. Bolea, A. Gella, L. Monjas, C. Perez, M.I. Rodríguez-Franco, J. Marco-Contelles, A. Samadi, M. Unzeta, *Current Alzheimer Research* 9 (2013) 797–808.
- [10] J. Mitoma, A. Ito, *Journal of Biochemistry* 111 (1992) 20–24.
- [11] T.P. Singer, *Chemistry and Biochemistry of Flavoenzymes*, F. Müller, (Ed.), CRC Press, Boca Raton, FL, USA, vol. III, pp. 437–470.
- [12] S.Y. Son, J. Ma, Y. Kondou, M. Yoshimura, E. Yamashita, T. Tsukihara, *Proceedings of the National Academy of Sciences of the United States of America* 105 (2008) 5739–5744.
- [13] C. Binda, M. Li, F. Hubalek, N. Restelli, D.E. Edmondson, A. Mattevi, *Proceedings of the National Academy of Sciences of the United States of America* 100 (2003) 9750–9755.
- [14] V. Pérez, J.L. Marco, E. Fernández-Alvarez, M. Unzeta, *British Journal of Pharmacology* 127 (1999) 869–876.
- [15] Y. Avramovich-Tirosh, T. Amit, O. Bar-Am, H. Zheng, M. Fridkin, M.B.H. Youdim, *Journal of Neurochemistry* 100 (2007) 490–502.
- [16] H. Zheng, M.B.H. Youdim, M. Fridkin, *Journal of Medicinal Chemistry* 52 (2009) 4095–4098.
- [17] V. Moret, Y. Laras, T. Cresteil, G. Aubert, D.Q. Ping, C. Di, M. Barthélémy-Requin, C. Béclin, V. Peyrot, D. Allegro, A. Rolland, F. De Angelis, E. Gatti, Ph. Pierre, L. Pasquini, E. Petrucci, U. Testa, J.L. Kraus, *European Journal of Medicinal Chemistry* 44 (2009) 558–567.
- [18] G.L. Ellman, K.D. Courtney, V. Andres, R.M. Featherstone, *Biochemical Pharmacology* 7 (1961) 88–95.
- [19] C.J. Fowler, K.F. Tipton, *Biochemical Pharmacology* 30 (1981) 3329–3332.
- [20] A. Ozaita, G. Olmos, M.A. Boronat, J.M. Lizcano, M. Unzeta, J.A. García-Sevilla, *British Journal of Pharmacology* 121 (1997) 901–912.
- [21] X. Huang, M.P. Cuanjunga, C.S. Atwood, M.A. Hartshorn, J.D. Tyndall, G.R. Hanson, K.C. Stokes, M. Leopold, G. Multhaup, L.E. Goldstein, R.C. Scarpa, A.J. Saunders, J. Lim, R.D. Moir, C. Glabe, E.F. Bowden, C.L. Masters, D.P. Fairlie, R.E. Tanzi, A.I. Bush, *The Journal of Biological Chemistry* 274 (1999) 37111–37116.
- [22] O. Trott, A.J. Olson, *Journal of Computational Chemistry* 31 (2010) 455–461.
- [23] M. Bartolini, M. Pistolozzi, V. Andrisano, J. Egea, M.G. López, I. Iriepa, I. Moraleda, E. Gálvez, J.L. Marco-Contelles, A. Samadi, *ChemMedChem* 6 (2011) 1990–1997.
- [24] C. Martins, M.C. Carreiras, R. Léon, C. de los Ríos, M. Bartolini, V. Andrisano, I. Iriepa, I. Moraleda, E. Gálvez, M.G. García, J. Egea, A. Samadi, M. Chioua, J.L. Marco-Contelles, *European Journal of Medicinal Chemistry* 46 (2011) 6119–6130.
- [25] K. Arnold, L. Bordoli, J. Kopp, T. Schwede, *Bioinformatics* 22 (2006) 195–201.
- [26] F. Kiefer, K. Arnold, M. Künzli, L. Bordoli, T. Schwede, *Nucleic Acids Research* 37 (2009) D387–D392.
- [27] M.C. Peitsch, *Bio/Technology* 13 (1995) 658–660.
- [28] C. Binda, P. Newton-Vinson, F. Hubalek, N. Restelli, D.E. Edmondson, A. Mattevi, *Nature Structural & Molecular Biology* 2 (2002) 22–26.
- [29] A. Samadi, C. de los Ríos, I. Bolea, M. Chioua, I. Iriepa, I. Moraleda, M. Bartolini, V. Andrisano, E. Gálvez, C. Valderas, M. Unzeta, J.L. Marco-Contelles, *European Journal of Medicinal Chemistry* 52 (2012) 251–262.
- [30] D.E. Edmondson, A. Mattevi, C. Binda, M. Li, F. Hubalek, *Current Medicinal Chemistry* 11 (2004) 1983–1993.
- [31] T.Z.E. Jones, D. Balsa, M. Unzeta, R.R. Ramsay, *Journal of Neural Transmission* 114 (2007) 707–712.
- [32] J. Wang, D.E. Edmondson, *Biochemistry* 50 (2011) 7710–7717.
- [33] R.A. Scerrer, A.J. Le, *Molecular Informatics* 30 (2011) 386.
- [34] F. Cheng, W. Li, G. Liu, Y. Tang, *Current Topics in Medicinal Chemistry* 13 (2013) 1273–1289.
- [35] AMET Predictor, v.6.5, Simulations Plus, Inc., Lancaster, CA, 2013.
- [36] ACD/Percepta 14.0.0, Advanced Chemistry Development, 2013.
- [37] I. Moriguchi, S. Hirono, Q. Liu, I. Nakagome, Y. Matsushita, *Chemical & Pharmaceutical Bulletin* 40 (1992) 127–130.
- [38] C.A. Lipinski, F. Lombardo, B.W. Dominy, P.J. Feeney, *Advanced Drug Delivery Reviews* 46 (2001) 3–26.
- [39] H. Pajouhesh, G.R. Lenz, *Drugs NeuroRx* 2 (2005) 541–553.
- [40] J. Kelder, P.D.J. Grootenhuys, D.M. Bayada, L.P.C. Delbressine, J.-P. Ploemen, *Pharmaceutical Research* 16 (1999) 1514–1519.
- [41] P.A. Nielsen, O. Andersson, S.H. Hansen, K.B. Simonsen, G. Andersson, *Drug Discovery Today* 16 (2011) 472–475.
- [42] X. Ma, C. Chen, J. Yang, *Acta Pharmacologica Sinica* 26 (2005) 500–512.
- [43] F. Cheng, W.L. Li, Y. Zhou, J. Shen, Z. Wu, G. Liu, P.W. Lee, Y. Tang, *Journal of Chemical Information and Modeling* 52 (2012) 3099–3105.
- [44] S. Yee, *Pharmaceutical Research* 14 (1997) 763–766.
- [45] A. Sjöberg, M. Lutz, C. Tannergren, C. Wingolf, A. Borde, A.I. Ungell, *European Journal of Pharmaceutical Sciences* 48 (2013) 166–180.
- [46] J.D. Irvine, L. Takahashi, K. Lockhart, J. Cheong, J.W. Tolan, H.E. Selick, J.R. Grove, *Journal of Pharmaceutical Sciences* 88 (1999) 28–33.
- [47] S. Yamashita, T. Furubayashi, M. Kataoka, T. Sakane, H. Sezaki, H. Tokuda, *European Journal of Pharmaceutical Sciences* 10 (2000) 195–204.
- [48] L.S. Gold, N.B. Manley, T.H. Slone, L. Rohrbach, *Environmental Health Perspectives* 107 (Suppl. 4) (1999) 527–600.
- [49] E.J. Matthews, N.L. Kruhlak, R.D. Benz, J.F. Contreras, *Current Drug Discovery Technologies* 1 (2004) 61–76.
- [50] L.G. Valerio Jr., K.B. Arvidson, R.F. Chanderbhan, J.F. Contrera, *Toxicology and Applied Pharmacology* 222 (2007) 1–16.
- [51] F. Denizot, R. Lang, *Journal of Immunological Methods* 89 (1986) 271–277.
- [52] R.A. Lenz, J.D. Baker, C. Locke, L.E. Rueter, E.G. Mohler, K. Wesnes, W. biSaab, M.D. Saltarelli, *Psychopharmacology (Berl)* 220 (2012) 97–107.
- [53] P.J. Baarendse, G.G. Van, R.F. Jansen, A.W. Pieneman, S.O. Ogren, M. Verhage, O. Stiedl, *Hippocampus* 18 (2008) 11–19.
- [54] G.R. Dawson, G. Bentley, F. Draper, W. Rycroft, S.D. Iversen, P.G. Pagella, *Pharmacology Biochemistry and Behavior* 39 (1991) 865–871.
- [55] M. Grant, *Journal of Comparative and Physiological Psychology* 86 (1974) 853–857.
- [56] R. Gupta, L.K. Gupta, P.K. Mediratta, S.K. Bhattacharya, *Pharmacological Reports: PR* 64 (2012) 438–444.
- [57] I. Izquierdo, *Trends in Pharmacological Sciences* 10 (1989) 175–177.
- [58] H. Sugimoto, Y. Iimura, Y. Yamanishi, K. Yamatsu, *Bioorganic & Medicinal Chemistry Letters* 2 (1992) 871–876.
- [59] J.M. Contreras, Y.M. Rival, S. Chayer, J.-J. Bourguignon, C.G. Wermuth, *Journal of Medicinal Chemistry* 42 (1999) 730–741.
- [60] D. Shao, C. Zou, C. Luo, X. Tang, Y. Li, *Bioorganic & Medicinal Chemistry Letters* 14 (2004) 4639–4642.
- [61] M.I. Rodríguez-Franco, M.I. Fernández-Bachiller, C. Pérez, A. Castro, A. Martínez, *Bioorganic & Medicinal Chemistry* 13 (2005) 6795–6802.
- [62] H. Takasugi, A. Kuno, M. Ohkubo, *WO* 9313083, 1993.
- [63] H. Sugimoto, Y. Tsuchiya, H. Sugumi, K. Higurashi, N. Karibe, Y. Iimura, A. Sasaki, Y. Kawakami, T. Nakamura, S. Araki, Y. Yamanishi, K. Yamatsu, *Journal of Medicinal Chemistry* 33 (1990) 1880–1887.
- [64] R. Kitbunnadaj, O.P. Zuiderveld, I.J.P. De Esch, R.C. Vollaard, R. Bakker, M. Lutz, A.L. Spek, E. Cavoy, M.-F. Deltent, W.M.P.B. Menge, H. Timmerman, R. Leurs, *Journal of Medicinal Chemistry* 46 (2003) 5445–5457.
- [65] C.Y. Huang, *Methods in Enzymology* 87 (1982) 509–521.
- [66] B.R. Brooks, R.E. Bruccoleri, B.D. Olafson, D.J. States, S. Swaminathan, M. Karplus, *Journal of Computational Chemistry* 4 (1983) 187–217.
- [67] A. Morreale, F. Maseras, I. Iriepa, E. Gálvez, *J. Mol. Graphics Modell* 2 (2002) 111–118.

Manuscript Number: EJMECH-D-15-00862R1

Title: Donepezil-like Multifunctional Agents: Design, Synthesis,  
Molecular Modeling and Biological Evaluation

Article Type: SI: Protein misfold diseases

Keywords: MAO-A; MAO-B; Human Acetylcholinesterase; Human  
Butyrylcholinesterase; Molecular Modeling; Molecular Docking; Alzheimer's  
Disease; Metal Chelating Properties; Antioxidant Properties; ADME+T  
properties.

Corresponding Author: Dr. stefania butini, Ph.D.

Corresponding Author's Institution: University of Siena

First Author: Ming-Yu Wu

Order of Authors: Ming-Yu Wu; Gerard Esteban; Simone Brogi; Masahi  
Shionoya; Li Wang; Giuseppe Campiani; Mercedes Unzeta; Tsutomu  
Inokuchi; stefania butini, Ph.D.; Jose Marco-Contelles

Manuscript Region of Origin: ITALY

Abstract: Currently available drugs against Alzheimer's disease (AD) are only able to ameliorate the disease symptoms resulting in a moderate improvement in memory and cognitive function without any efficacy in preventing and inhibiting the progression of the pathology. In an effort to obtain disease-modifying anti-Alzheimer's drugs (DMAADs) following the multifactorial nature of AD, we have recently developed multifunctional compounds. We herein describe the design, synthesis, molecular modeling and biological evaluation of a new series of donepezil-related compounds possessing metal chelating properties, and being capable of targeting different enzymatic systems related to AD (cholinesterases, ChEs, and monoamine oxidase A, MAO-A). Among this set of analogues compound 5f showed excellent ChEs inhibition potency and a selective MAO-A inhibition (vs MAO-B) coupled to strong complexing properties for zinc and copper ions, both known to be involved in the progression of AD. Moreover, 5f exhibited moderate antioxidant properties as found by in vitro assessment. This compound represents a novel donepezil-hydroxyquinoline hybrid with DMAAD profile paving the way to the development of a novel class of drugs potentially able to treat AD.

Suggested Reviewers: Rona Ramsay  
rrr@st-andrews.ac.uk

Rahime Simsek  
rsimsek@hacettepe.edu.tr

## Highlights

- Development of multifunctional compounds
- Potential therapeutic agents for the treatment of AD
- Scaffold hopping approach

# Donepezil-like Multifunctional Agents: Design, Synthesis, Molecular Modeling and Biological Evaluation

Ming-Yu Wu,<sup>a,§</sup> Gerard Esteban,<sup>b,§</sup> Simone Brogi,<sup>c,§</sup> Masahi Shionoya,<sup>a</sup> Li Wang,<sup>a</sup> Giuseppe Campiani,<sup>c</sup>  
Mercedes Unzeta,<sup>b,\*</sup> Tsutomu Inokuchi,<sup>a,\*</sup> Stefania Butini,<sup>c,\*</sup> and Jose Marco-Contelles<sup>d,\*</sup>

<sup>a</sup>*Division of Chemistry and Biotechnology, Graduate School of Natural Science and Technology, Okayama University, 3.1.1 Tsushima-Naka, Kita-ku, Okayama 700-8530, Japan.*

<sup>b</sup>*Departament de Bioquímica i Biologia Molecular, Facultat de Medicina, Institut de Neurociències, Universitat Autònoma de Barcelona, 08193 Bellaterra, Barcelona, Spain.*

<sup>c</sup>*European Research Centre for Drug Discovery and Development (NatSynDrugs) and Department of Biotechnology, Chemistry and Pharmacy, Università degli Studi di Siena Via A. Moro, 53100 Siena, Italy.*

<sup>d</sup>*Laboratory of Medicinal Chemistry (IQOG, CSIC), C/Juan de la Cierva 3, 28006-Madrid, Spain.*

\*Corresponding author. Tel. +34 93 5811523; fax +34 935811573; e-mail: [mercedes.unzeta@uab.cat](mailto:mercedes.unzeta@uab.cat)

\*Corresponding author. Tel. +81862945045; fax +81862518021; e-mail: [inokuchi@cc.okayama-u.ac.jp](mailto:inokuchi@cc.okayama-u.ac.jp)

\*Corresponding author. Tel.: +39 0577234161; fax: +39 0577 234254; e-mail: [butini3@unisi.it](mailto:butini3@unisi.it)

\*Corresponding author. Tel.: + 34 915622900; fax: +39 915644853; e-mail: [iqoc21@iqog.csic.es](mailto:iqoc21@iqog.csic.es)

§Authors equally contributed to this work

## Abstract

Currently available drugs against Alzheimer's disease (AD) are only able to ameliorate the disease symptoms resulting in a moderate improvement in memory and cognitive function without any efficacy in preventing and inhibiting the progression of the pathology. In an effort to obtain disease-modifying anti-Alzheimer's drugs (DMAADs) following the multifactorial nature of AD, we have recently developed multifunctional compounds. We herein describe the design, synthesis, molecular modeling and biological evaluation of a new series of donepezil-related compounds possessing metal chelating properties, and being capable of targeting different enzymatic systems related to AD (cholinesterases, ChEs, and monoamine oxidase A, MAO-A). Among this set of analogues compound **5f** showed excellent ChEs inhibition potency and a selective MAO-A inhibition (vs MAO-B) coupled to strong complexing properties for zinc and copper ions, both known to be involved in the progression of AD. Moreover, **5f** exhibited relevant antioxidant properties as found by *in vitro* assessment. This compound represents a novel donepezil-hydroxyquinoline hybrid with DMAAD profile paving the way to the development of a novel class of drugs potentially able to treat AD.

**Keywords:** MAO-A, MAO-B, Human Acetylcholinesterase, Human Butyrylcholinesterase, Molecular Modeling, Molecular Docking, Alzheimer's Disease, Metal Chelating Properties, Antioxidant properties, ADME+T properties.

## 1. Introduction

Alzheimer's disease (AD) represents the most prevalent pathology associated to neurodegenerative senile dementia, characterized by selective loss of cholinergic neurons and reduced level of acetylcholine (ACh) neurotransmitter, driving to memory deficit and progressive impairment of cognitive functions up to debilitating dementia before death [1, 2]. This pathology has been found to be related to many factors including ACh levels,  $\beta$ -amyloid plaques deposition, oxidative damage, free radicals formation and metal ions [3-6]. AD currently affects millions of aging people (WHO report 2012, Dementia: a public health priority) [7], a number which, with the greying of society, will lead to a dramatic increase expecting a double of patients by 2030 and triple by 2050 [8]. To date, healthcare or financial systems in developed countries are not prepared to manage this worrisome scenario [7]. Indeed the only available therapeutics for AD, focused on increasing cholinergic neurotransmission in the brain (by inhibiting cholinesterases, ChEs), have resulted in a modest improvement in memory and cognitive function and are devoid of any therapeutic potential concerning prevention and progression of neurodegeneration [9]. All the currently registered drugs for the treatment of AD are ChEIs (donepezil, **1**, rivastigmine, **2**, and galantamine, **3**, Figure 1) with the *N*-methyl-*D*-aspartate (NMDA) antagonist memantine (for the treatment of moderate to severe AD [10, 11]), while tacrine, **4** (Figure 1) the first drug approved for the treatment of AD, was withdrawn from the market [12] due to its hepatotoxicity [13, 14]. The narrowness of therapies for AD has become as the current biggest unmet medical need in neurology unless an effective disease-modifying anti-Alzheimer's drug (DMAAD) is found [15].

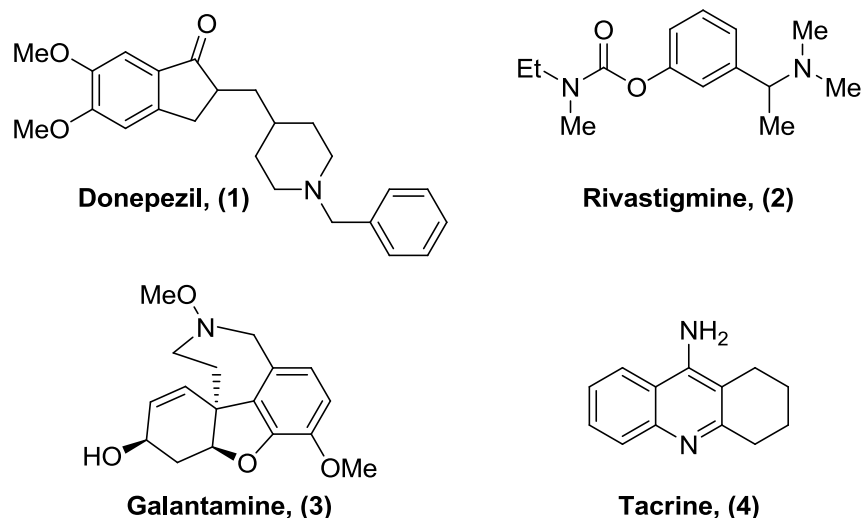


**Figure 1** Current cholinesterase inhibitors approved for the treatment of AD.

The multifactorial nature of AD has brought to “the failure of the so-called *one-drug-one-target* paradigm” [16, 17]. Besides the well-recognized symptomatic efficacy of ChEs inhibition for the treatment of AD a therapeutic potential was proposed for monoamine oxidase inhibitors (MAOIs). Indeed, among the factors that may contribute to cell death in neurodegenerative disorders such as AD, oxidative stress plays a relevant role. MAOIs capability to reduce the formation of neurotoxic products such as  $H_2O_2$  and aldehydes, which in turn, promote the generation of reactive oxygen species (ROS) [18], endorses MAOIs with strong neuroprotective properties [19].

Amyloid beta ( $A\beta$ ) aggregation and  $A\beta$  plaques formation represents the hallmark of AD, and the amyloid cascade hypothesis of AD postulates that excessive  $A\beta$  formation is one of the causes of neurodegeneration. Furthermore, the metallostasis evidence points iron, copper and zinc as relevant metals in the pathogenesis of AD, either by direct interaction with  $A\beta$ , thus increasing its aggregation, or by enhancing the production of  $H_2O_2$  and ROS. Consequently, the modulation of the homeostasis of these biometals is a potential therapeutic strategy for AD therapy [20]. In healthy people amyloid precursor protein and  $A\beta$  interact with the mentioned metal species in a subtle equilibrium. Disruption

of this balance drives to an abnormal A $\beta$  metabolism as well as an alteration in copper and zinc uptake, leading to the formation of fibrillar A $\beta$ . The formation of fibrils may induce an inflammatory reaction with consequent decrease of pH, also modifying the zinc homeostasis [21]. Zinc is thus released into the cellular environment triggering the events that lead to oxidative stress-induced cell death. Copper ions are then free to compete for zinc binding site on A $\beta$ , and these ions can catalyse H<sub>2</sub>O<sub>2</sub> production by A $\beta$ . As a consequence of the inflammatory response, a highly reactive free radical, nitric oxide is released to regulate the process [22].

Accordingly, in the last years the multifactorial etiology of AD has conducted the research to develop novel multitarget anti-AD agents [23-28]. In this frame, we have previously explored: i) multifunctional compounds able to inhibit both ChEs [29-31], ii) compounds with multifunctional profile coupling the inhibition of ChEs with A $\beta$  aggregation as well as with the disruption of preformed fibrils [32, 33], iii) compounds with acetylcholinesterase (AChE) and MAOs inhibition capacity [34, 35], and iv) compounds and AChE and MAOs inhibition capacity showing additional antioxidant properties [36, 37]. Based on our knowledge by a scaffold hopping approach, we herein report the development of novel chemical entities (compounds **5a-f**, Figure 2) which represent an improved series of our previously developed analogues typified by **DPH6** (Table 1) [38]. Compounds **5a-f** combine the *N*-benzylpiperidine moiety of **1** with a metal chelating portion represented by a 8-hydroxyquinoline system functionalized at position 2. Since **1** is a weak MAO-B inhibitor and is devoid of MAO-A affinity, for improving the MAO inhibition properties of the compounds, we also introduced the propargylamine moiety.

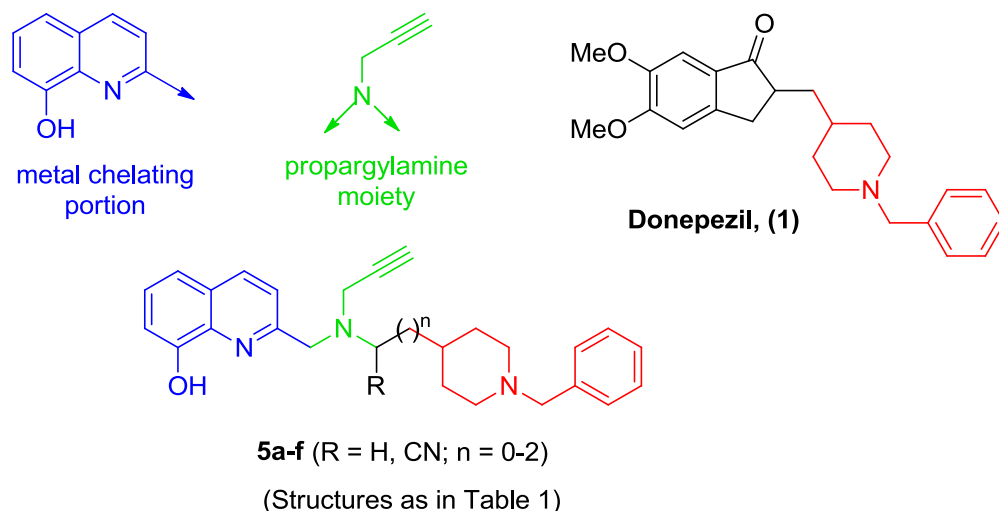


**Figure 2.** Design of the title compounds **5a-f**.

Pharmacological analysis revealed the developed compounds as potent AChE and butyrylcholinesterase (BuChE) inhibitors, with  $IC_{50}$  values in the nanomolar range combined with micromolar MAO-A selective inhibition (*vs* MAO-B), metal-chelating capability and antioxidant properties. In-depth bioinformatics analysis of the analogues with AChE BuChE and MAO-A and -B helped rationalize the observed enzyme inhibition data. Among the analogues described, compound **5f** showed the most interesting profile as multifunctional tool, thus representing an innovative scaffold for the development of improved donepezil-hydroxyquinoline hybrids as potential DMAADs.

## 2. Results and Discussion

### 2.1. Chemistry

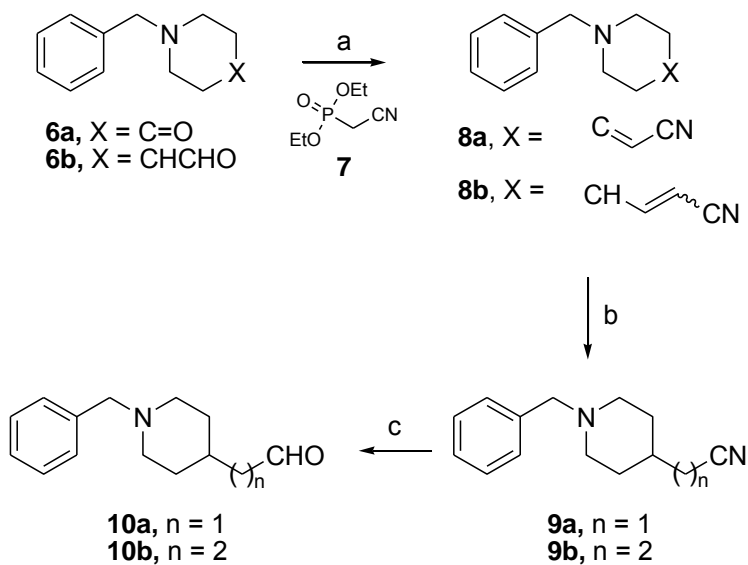
To obtain the compounds presented in this paper the following synthetic schemes 1-3 were adopted.

$\omega$ -(1-Benzylpiperidin-4-yl)alkanals **10a,b** were prepared in our previous methods [38]. Thus, two-carbon homologation of the commercial ketone **6a** and aldehyde **6b** with Horner-Wadsworth-Emmons reagent **7** (derived from Arbuzov reaction between triethyl phosphite and 1-chloroacetonitrile) gave

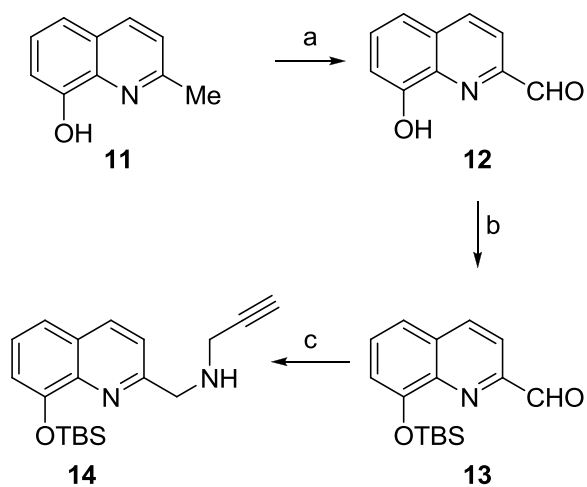
**8a,b**. On the latter olefins double bond reduction with Mg-I<sub>2</sub> in MeOH followed by DIBAL-H reduction of the resulting alkanenitriles **9a,b** gave the correspondent aldehydes **10a,b** (Scheme 1).

The secondary amine, *N*-(2-propynyl)-*N*-(quinolin-2-yl)methylamine, **14** was prepared by reductive amination of the quinoline-2-carbaldehyde **13** with propargylamine, using NaBH<sub>4</sub> under acidic conditions. For this process, **13** was derived from commercially available 2-methylquinolin-8-ol (**11**) by SeO<sub>2</sub> oxidation followed by silylation of **12** with TBSCl (Scheme 2).

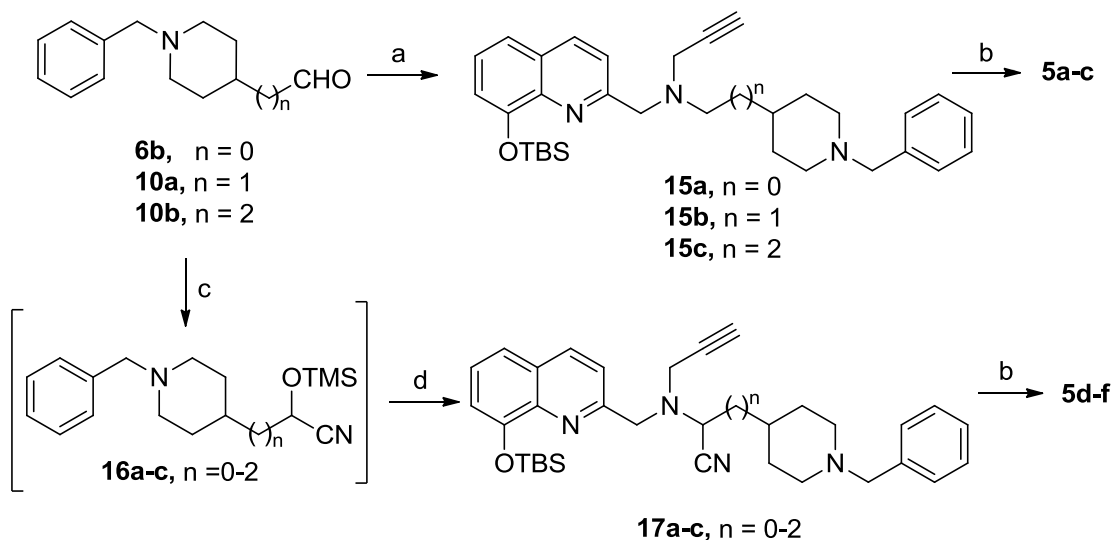
Reductive amination of **6b** and ω-(1-benzylpiperidin-4-yl)alkanals **10a,b** with the secondary amine **14**, using NaBH<sub>4</sub> under acidic conditions, afforded two component coupled tertiary amines **15a-c**, which were desilylated by treatment with Bu<sub>4</sub>NF to give the desired donepezil + propargylamine + 8-hydroxyquinoline hybrid compounds (DPHs) **5a-c** (Scheme 3). DPHs **5d-f** were prepared in short synthetic sequences through Lewis acid-catalyzed Strecker reaction as the key operation [39]. Thus, the aldehydes **6a**, **10a** and **10b** were treated with TMSCN in the presence of ZnI<sub>2</sub>, forming the corresponding cyanohydrin TMS ethers **16a-c**, which was immediately followed by addition of the secondary amine **14** to give the corresponding α-aminonitriles **17a-c**, respectively. Finally, the TBS-protective group of **17a-c** was removed by treatment with Bu<sub>4</sub>NF in THF, affording the desired DPHs **5d-f** (Scheme 3). All new molecules showed analytical and spectroscopic data in good agreement with their structures, and then submitted to biological evaluation as racemic mixtures.



**Scheme 1. Synthesis of aldehydes 1a,b.** Reagents and conditions: (a)  $\text{K}_2\text{CO}_3$ , THF, rt–reflux; (b)  $\text{Mg/I}_2$ , MeOH, 0 °C, rt; (c) DIBAL-H/toluene, -78 °C.



**Scheme 2. Synthesis of intermediate amine 14.** Reagents and conditions: (a)  $\text{SeO}_2/1,4\text{-dioxane}$ , 60 °C–reflux; (b) propargylamine, imidazole, TBSCl/DCM, 0 °C–rt; (c)  $\text{CF}_3\text{COOH/MeOH}$ , 0 °C–rt then  $\text{NaBH}_4$ , 0 °C–rt.



**Scheme 3. Synthesis of title compounds 5a-f.** Reagents and conditions: (a) compound **14**,  $\text{CF}_3\text{CO}_2\text{H}/\text{MeOH}$ ,  $0\text{ }^\circ\text{C}$ –rt then  $\text{NaBH}_4$ ,  $0\text{ }^\circ\text{C}$ –rt; (b) TBAF/THF, rt; (c) TMSCN,  $\text{ZnI}_2/\text{DCM}$ , rt; (d) compound **14**, MeOH,  $50\text{ }^\circ\text{C}$ , 3 h.

## 2.2. Pharmacological evaluation, structure-activity relationship, and molecular modeling studies

### 2.2.1. Enzyme assays

Donepezil (Aricept<sup>®</sup>) is an AChE inhibitor able to increase concentrations of ACh in the brain and improving the symptoms of disease without delaying the progression of AD. Donepezil was approved by the FDA in 1996 with the trade name of Aricept<sup>®</sup> and in 2006 the drug was also approved for treating severe dementia. As shown in Table 1, donepezil displayed an  $\text{IC}_{50}$  value in the nanomolar range AChE activity inhibition with weak selectivity for other enzymatic systems (BuChE and MAOs). In an effort to design multifunctional compounds as DMAADs the benzyl-piperidine moiety of donepezil and 8-hydroxyquinoline nucleus, were combined for maintaining both the ChEs inhibitory activity metal-chelating properties. A propargylamine moiety for inhibiting MAO was also inserted between these two moieties by a carbon chain of variable length. This approach led to the design of

compounds **5a-f** (Figure 2 and Table 1). Further in compounds **5d-f** the spacer was decorated with a cyano group as a further interacting group for potentiating enzyme inhibition. The obtained compounds were evaluated *in vitro* for assessing their inhibition properties at the human enzymes of interest (MAO-A, MAO-B, AChE, and BuChE). As shown in Table 1 the compound **5f** exhibited the most interesting profile of the series. In fact, **5f** inhibited AChE activity in the nanomolar range with an  $IC_{50}$  value of 29 nM, similar to that found for **1**. Furthermore, our prototypic multifunctional compound **5f** showed an excellent inhibitory potency ( $IC_{50} = 39$  nM) against the BuChE being more potent than reference compound **1** ( $IC_{50} = 7.5$   $\mu$ M). In addition **5f** was found to be a selective MAO-A (vs MAO-B) inhibitor in the micromolar range ( $IC_{50} = 10.1$   $\mu$ M), whereas **1** did not show appreciable MAO-A inhibitory activity and displayed MAO-B inhibition potency in the micromolar range ( $IC_{50} = 15.2$   $\mu$ M). **DPH6** (Table 1) [38], the progenitor molecule of all these compounds, when compared with **5f**, it showed similar  $IC_{50}$  values versus MAO-A, but higher affinity versus MAO-B and lower inhibition potency towards AChE and BuChE. Taken into account these data, we can assess that compound **5f** nicely challenged the *in vitro* profile of **DPH6**.



In order to provide some relevant information about the mechanism of action of **5f**, an assessment to establish the reversibility and time-dependent inhibition of *hr*MAO-A and *hChEs* was performed. In Figure 3 the output of these *in vitro* studies concerning MAO-A is shown.

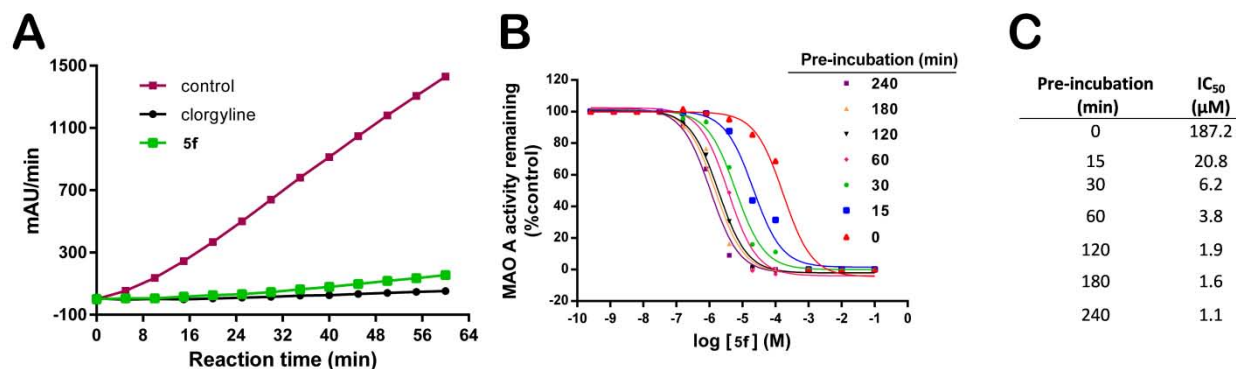


**Figure 3.** Assessment for reversibility and time-dependent inhibition of *hr*MAO-A by derivative **5f**.

Unequivocally, the lack of recovery of activity after enzyme inactivation by **5f** (Figure 3A) confirms an irreversible MAO-A inhibition similarly to that observed with the reference inhibitor clorgyline. This result is consistent with the covalent interaction between the propargylamine moiety and the flavin adenine dinucleotide (FAD) co-factor present in the MAO-A enzyme. This type of inhibition is also in agreement with molecular modelling studies discussed below (see paragraph 2.2.2 for further details). Moreover, a time-dependent inhibition mechanism of *hr*MAO-A (Figure 3B and 3C) was evidenced from the dose-response curves (IC<sub>50</sub>) when different pre-incubations times were employed.

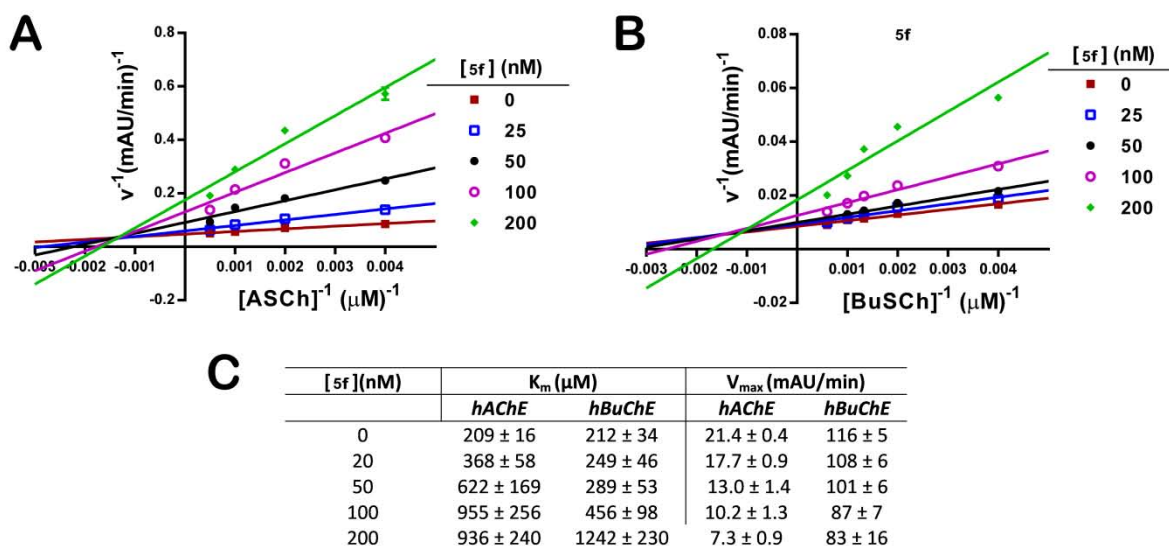


**Figure 4.** Kinetic assessment of **5f** as ChEs inhibitor. Lines were derived from a weighted least-squares analysis of data. Acetylthiocholine iodide (ASCh) and *S*-butyrylcholine iodide (BuSCh) were used as substrates.

For better characterizing compound **5f** inhibition properties at ChEs, kinetic assessments were performed as reported in Materials and Methods section. The results of this study are summarized in Figure 4. The assessment was performed by means of steady-state inhibition (Lineweaver-Burk plots of initial velocity) of *hAChE* (Figure 4A) and *hBuChE* (Figure 4B) by **5f** (0-200 nM) using acetylthiocholine iodide and *S*-butyrylcholine iodide (0.1-2 mM) as substrates, respectively. The data obtained by kinetic studies clearly showed a mixed-type inhibition for both enzymes since decreasing  $K_m$  values and increasing  $V_{\text{max}}$  values were determined as higher **5f** concentrations were used (Figure 4C). Moreover the studies performed allowed us to calculate inhibition constants ( $K_i$ ) by employing the Cheng-Prusoff equation for **5f** of 10.8 nM and 11.6 nM concerning *hAChE* and *hBuChE* inhibitions, respectively.

### 2.2.2. Structure-activity relationship and molecular modeling studies

Computational studies allowed us to rationally explain the experimentally determined different selectivity degrees of compounds **5a-f** on the *hr*MAO-A and -B enzyme isoforms. The structural requirements governing the inhibitory potency of the title compounds on *h*AChE were also investigated exploiting our experience in the field [29, 30, 40]. The potential binding modes of a subset of the analyzed compounds were found by applying the Induced Fit Docking (IFD) protocol [41] available in Schrödinger Suite [42] as already reported by us [31, 32]. The mentioned protocol involves various steps such as ligands and proteins preparation and molecular docking. In particular, in order to improve the reliability of our calculations, the ligands were prepared taking into account their protonation state at physiological pH (7.4) [33, 43-46]. In agreement with the literature data and software output, we have considered the 8-hydroxyquinoline moiety in its zwitterionic form, and the piperidine nitrogen as protonated (Table S1). Analysis of the data suggested that the presence of a CN group is relevant for improving MAO-A activity and selectivity (**5d** vs **5a**, **5e** vs **5b**, and **5f** vs **5c**, Table 1). For verifying this issue we have performed docking calculations for **5f** and **5c** in complex with *h*MAO enzymes. Results are depicted in Figure 5 for **5f** *S*-enantiomer (docking calculations of *R*-enantiomer were provided in Supporting Information in Figure S1) and Figure 6 for **5c**. As shown in Figure 5A, compound (*S*)-**5f** interacts in the active site of MAO-A with a combination of polar contacts and hydrophobic interactions, targeting the key residues of the protein [47]. In particular, (*S*)-**5f** establishes a series of H-bonds with Lys305, Tyr444 and Phe208 (backbone), and a  $\pi$ - $\pi$  stacking with Phe208 and with Phe352 (Figure 5A). In line with the experimentally determined irreversible mode of inhibition of **5f** (Figure 3), the propargylamine moiety of (*S*)-**5f** was found to lay in close proximity to the FAD molecule (3.3 Å). Accordingly, (*S*)-**5f** showed satisfactory docking score and free binding energy values (GlideXP score -10.82 kcal/mol, and  $\Delta G_{\text{bind}} = -180.03$  kcal/mol, respectively) which is consistent with good affinity for the isoform A of MAO enzyme. Notably, we observed a partial

stereoselective interaction with the enzyme. The *R*-enantiomer (Figure S1A) showed indeed a different pattern of interaction with respect to those found for the *S*-enantiomer. Although free binding energy values (GlideXP score and  $\Delta G_{\text{bind}}$  of -8.54 kcal/mol and -176.16 kcal/mol) were found slightly lower with respect to those obtained for the *S*-enantiomer, the different binding mode of (*R*)-**5f** with MAO-A, could prevent strong interactions with the enzyme. In fact, (*R*)-**5f** can establish only a  $\pi$ - $\pi$  stacking with Phe173 and polar contacts with Val210 and Thr336. However, the propargylamine moiety lies far from the FAD molecule (14.1 Å) thus precluding a potential covalent interaction with the enzyme. These findings are in agreement with the micromolar inhibition potency found for the racemic mixture (the *S*-enantiomer showed an excellent predicted affinity with a binding mode that could allow a correct interaction within the enzyme, while the *R*-enantiomer appeared to possess a reduced predicted affinity).

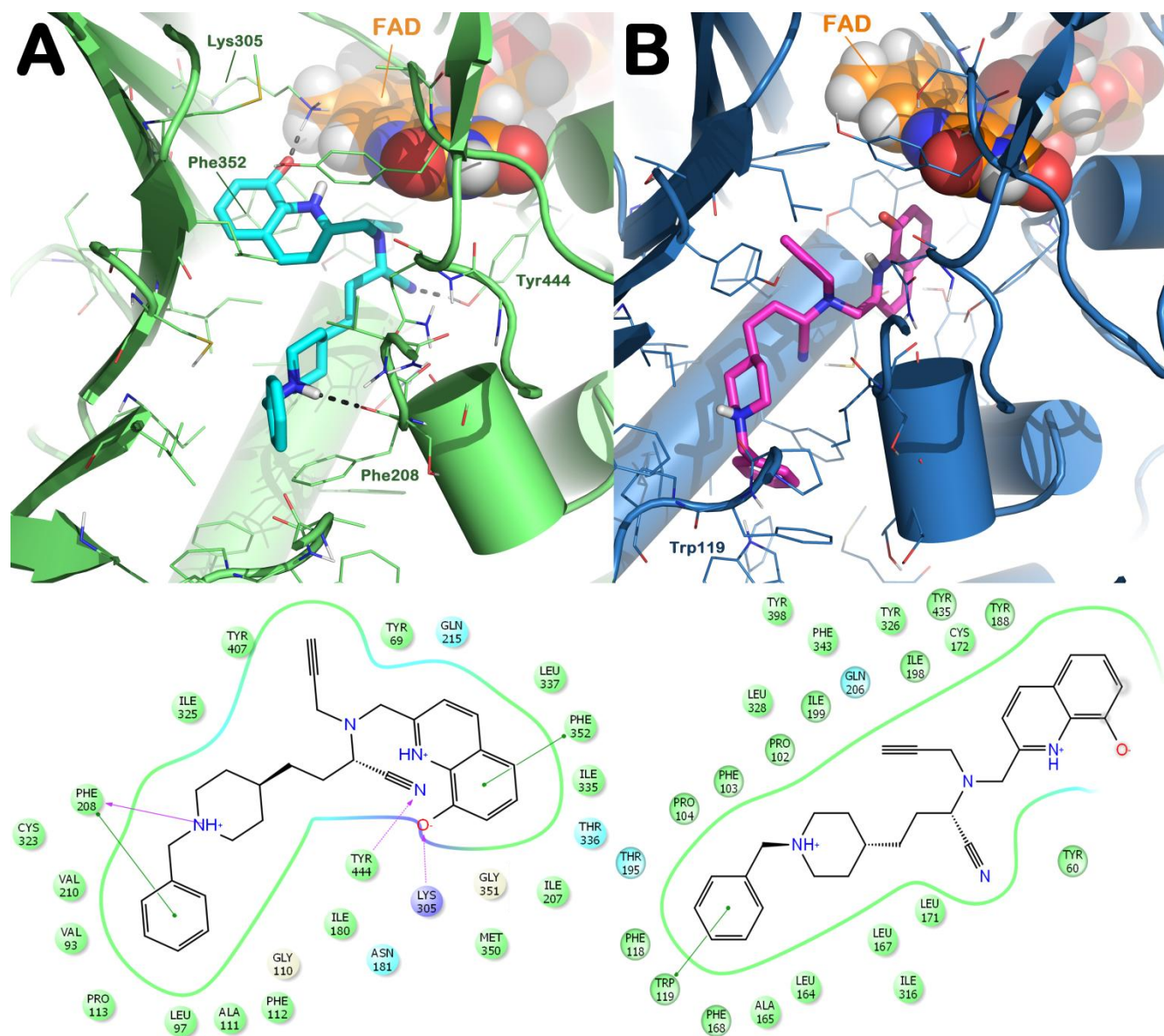


**Figure 5.** Docked pose of (*S*)-**5f** into *h*MAO-A (PDB ID: 2Z5X) (panel A) binding site and into *h*MAO-B (PDB ID: 2V5Z) (panel B). In the bottom part of the picture is represented a schematic ligand-protein interaction. The docked poses are visualized by means of PyMOL (The PyMOL Molecular Graphics System, v1.6-alpha; Schrodinger LLC, New York, NY, 2013), while the ligand-protein interaction diagram was generated by means of Maestro.

On the contrary, the IFD results obtained for (*S*)-**5f** revealed a poor affinity for MAO-B as depicted in Figure 5B. Due to the different arrangement of the enzyme active sites, (*S*)-**5f** could not engage a suitable pattern of interaction with the MAO-B binding site. In particular, the replacement of Ile335

and Ile180 (MAO-A) with Tyr326 and Leu171 (MAO-B) respectively appeared to limit cavity accessibility for our inhibitors. In addition, the replacement of Phe208 (MAO-A) with Ile199 (MAO-B) did not assure a correct accommodation of (*S*)-**5f** into MAO-B active site (Figure 5B). Consequently, the compound produced only a stacking with Trp119 that is located at the boundary of the binding pocket and no other contacts along the cleft were evident (Figure 5B). Moreover, the 8-hydroxyquinoline moiety appeared to be solvent exposed and the distance between the propargylamine and FAD is very large (8.74 Å) and not consistent with any potential covalent interaction. All these data and free binding energy calculation (GlideXP score -7.62 kcal/mol, and  $\Delta G_{\text{bind}}$  is -127.49 kcal/mol) are in line with the observed MAO-A and -B selectivity. For, the (*R*)-**5f** (Figure S1B) we obtained similar results and no stereoselective interactions with MAO-B were detected (GlideXP score -8.04 kcal/mol and the  $\Delta G_{\text{bind}}$  -130.81 kcal/mol). Similarly to the *S*-enantiomer into MAO-B with the *R*-enantiomer the distance of the propargylamine group from FAD (6.7 Å) did not assure any chance of covalent interaction thus well explaining the selectivity profile of **5f** for the two MAO isoforms.

For evaluating the influence of structural differences in MAO-A inhibition we have performed IFD studies also for **5c** for comparison with data obtained for **5f**. Compound **5c**, lacking the CN group, showed a decreased MAO-A inhibition activity when compared to **5f**, and the molecular docking output (Figure 6A) evidenced a slight different pattern of interaction with respect to **5f**. Indeed, **5c** could reproduce contacts with Lys305 and Phe208 (H-bonds), and could establish a  $\pi$ - $\pi$  stacking with Phe352, but the absence of the CN group did not allow interaction with Tyr444 and the  $\pi$ - $\pi$  stacking with Phe208 as for **5f** (Figure 6A). Moreover, the propargylamine group was found at 4.4 Å distance from the FAD molecule a larger distance than that found for **5f** (3.3 Å). All these evidences clearly demonstrate that the presence of the CN group is relevant for better interaction with MAO-A binding site (**5c** indeed showed a slight decrease of docking score value and estimated free binding energy with respect to **5f**) and for higher inhibition potency (Table 1).

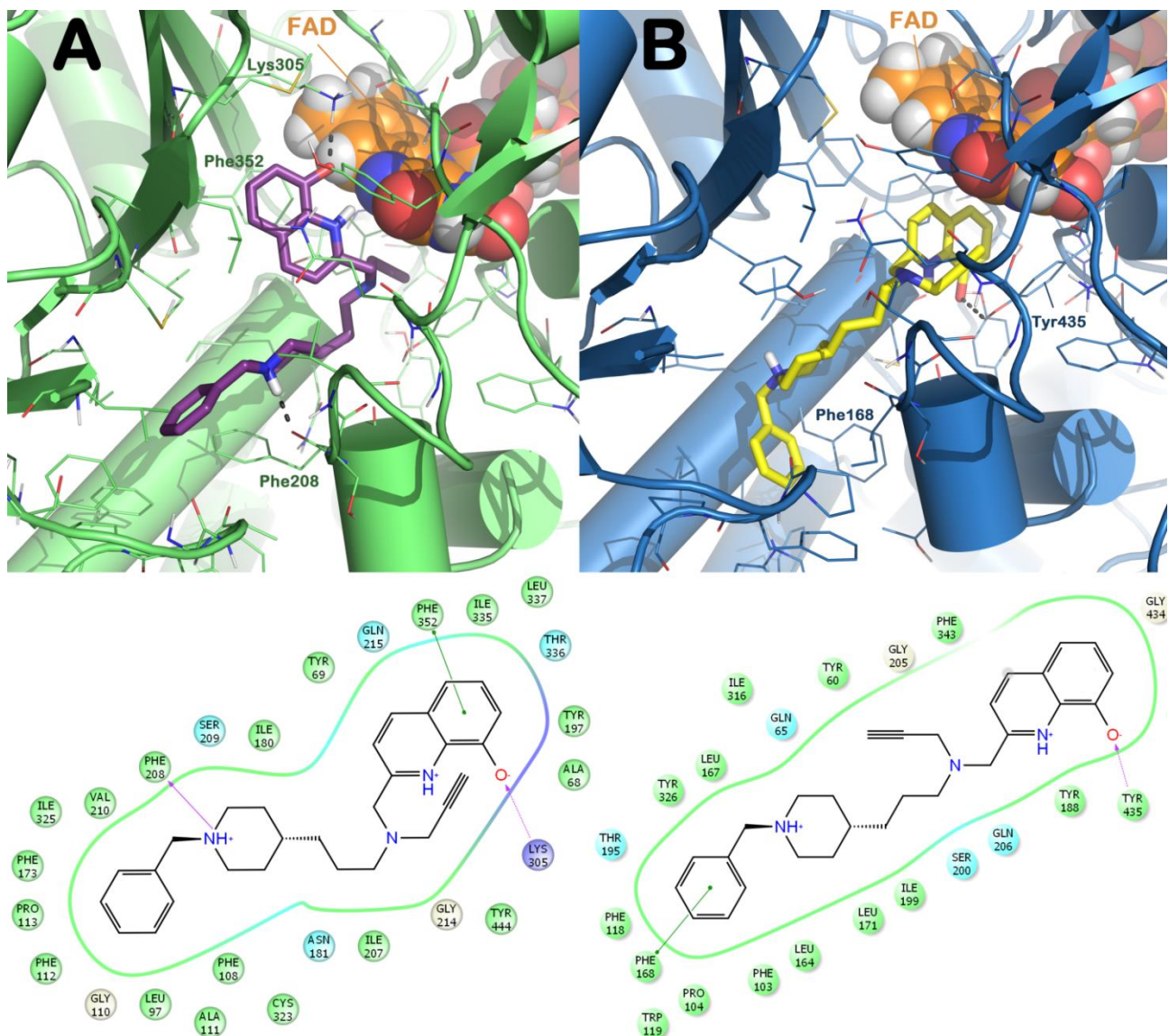


**Figure 6.** Docked pose of **5c** into *h*MAO-A (PDB ID: 2Z5X) (panel A; Docking score -9.96 kcal/mol;  $\Delta G_{\text{bind}} = -174.29$  kcal/mol) binding site and into *h*MAO-B (PDB ID: 2V5Z) (panel B; Docking score -7.56 kcal/mol;  $\Delta G_{\text{bind}} = -131.68$  kcal/mol). In the bottom part of the picture is represented a schematic ligand-protein interaction.

Similarly to **5f**, also **5c** showed a poor MAO-B inhibition potency. Our docking results (Figure 6B) showed that **5c** is able to form only a H-bond with Tyr435 and a  $\pi$ - $\pi$  stacking with Phe168 in a similar fashion to **5f**, since the stacking with aromatic residues located at the boundary of the MAO-B binding site prevented a deep accommodation of the compound into the cleft, thus precluding strong

interactions of **5c** within the active site and the propargylamine group was found at 5.8 Å from FAD. All together these features led to a decrease of docking score values and of the estimated binding affinity in line with the poor MAO-B inhibition potency of **5c** (Figure 6B).

Overall this series of compounds (**5a-f**) was found to inhibit the *h*ChEs from the micromolar to the nanomolar range and the compounds were in general more potent inhibitors of *h*BuChE than *h*AChE. Analysis of the data reported in Table 1 evidenced that *h*AChE inhibition potency of the compounds is more sensible to small variations of the structure with respect to *h*BuChE inhibition potency and this is in line with the wider gorge dimensions of the BuChE enzyme.

In order to better explain this behavior we performed IFD calculations for all the compounds within *h*AChE (PDB ID:1B41). The results (Figure 7 and 8) highlighted the importance of the length of the molecule for correct interaction with the enzyme since potency increased with the length of the compounds in both the **5a-c** and the CN containing **5d-f** sub-series. The lengthiest compounds **5c** and **5f** were indeed found to be the most potent *h*AChE inhibitors of the series since they possess the correct distance between the aromatic moieties and an appropriately positioned basic center for interacting with the peripheral anionic site (PAS), mid-gorge, and catalytic site (CAS). In addition, the length of **5f** (*S*- and *R*-enantiomer) also assured a better accommodation of the CN group into the gorge of the enzyme with respect to the **5d** and **5e** (Figure 8 and Figure S2).

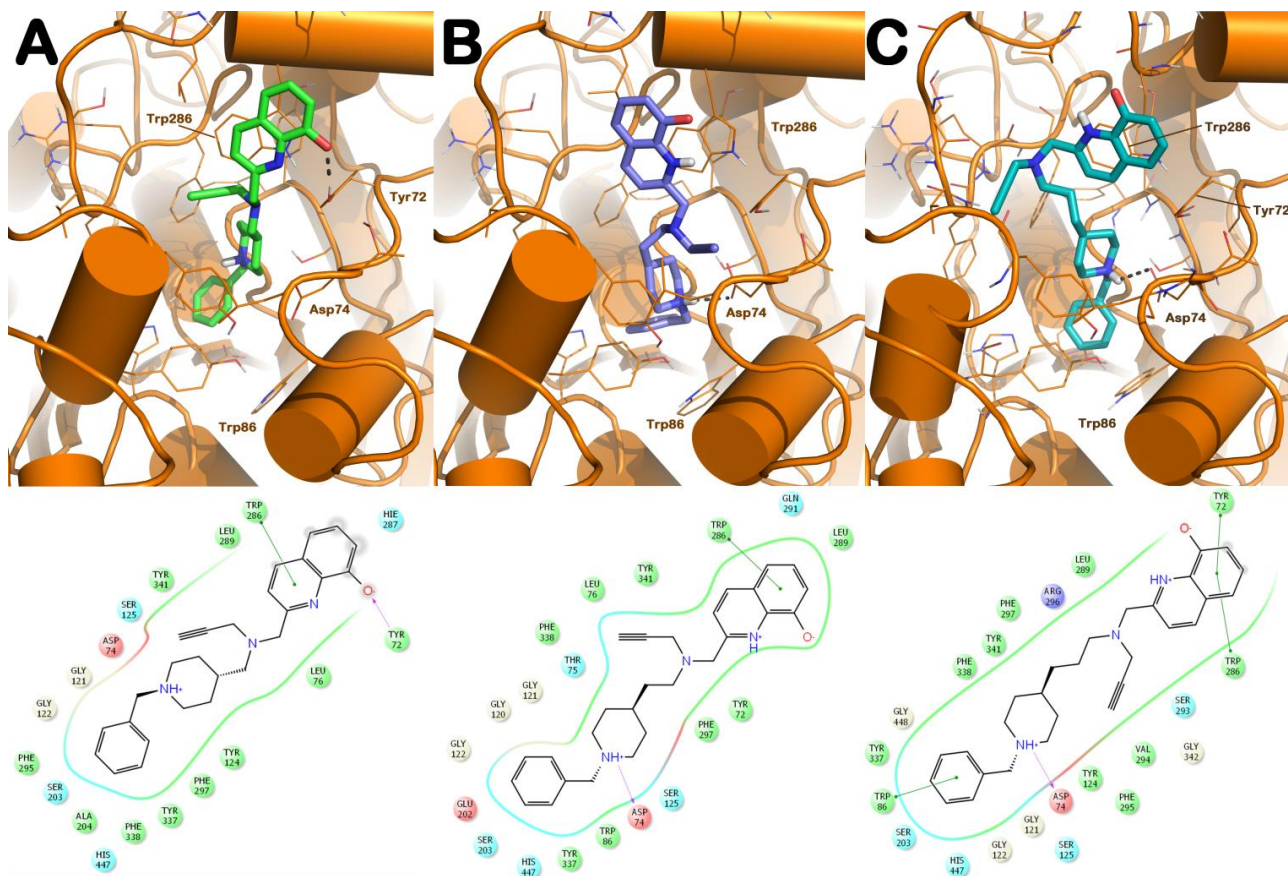


**Figure 7.** Docked poses of selected compounds (panels A-C; A: **5a**; B: **5b**; C: **5c**) into *hAChE* enzyme (PDB ID: 1B41). The pictures were generated by means of PyMOL, while the ligand-interaction diagrams were generated by means of Maestro.

In particular, the obtained binding mode of compound **5a** (Figure 7A) clearly revealed its impossibility to reach the CAS of *hAChE*. In fact, **5a** established a series of limited hydrophobic and polar contacts only with the PAS (Trp286 and Tyr72). Accordingly, the docking score and the  $\Delta G_{\text{bind}}$  of **5a** are -7.91 kcal/mol and -84.26 kcal/mol, respectively. A moderate improvement in the inhibitory activity was observed with the homologation of linker between the propargylamine moiety and piperidine group. In fact, compound **5b** displayed a better accommodation into the binding site of *hAChE* (Figure 7B), interacting by a  $\pi$ - $\pi$  stacking with Trp286 the PAS region with its 8-hydroxyquinoline moiety, and can engage a polar contact with the mid-gorge Asp74. These interactions account for the docking score and

the  $\Delta G_{\text{bind}}$  of -8.91 kcal/mol and -102.22 kcal/mol, respectively. A further homologation was beneficial for activity and **5c** strongly interacted with PAS, mid-gorge and CAS recognition sites (Figure 7C). In particular, **5c** established a double  $\pi$ - $\pi$  stacking with Trp286 and Tyr72 in the PAS region and establishes a polar contact with the mid-gorge region targeting the key residue Asp74. Notably, **5c** was also able to interact with the CAS region by a  $\pi$ - $\pi$  stacking with Trp86 by its benzyl moiety (Figure 7C). Also the docking score of -9.95 kcal/mol and the  $\Delta G_{\text{bind}}$  of -112.08 kcal/mol supported the observed improvement of affinity of **5c** vs **5a** for *hAChE*.

The same trend was observed with the introduction of CN group on the molecules **5d-f** (Figure 8). In fact, **5f** displayed the correct length and spatial arrangements of its features for appropriate interaction with *hAChE*. In fact, the CN group is perfectly tolerated in **5e** and **5f** and establishes a series of relevant polar interactions with Phe295 or/and Arg296 (backbone) as reported in Figure 8B,C and in Figure S2, accounting for the favorable docking score and  $\Delta G_{\text{bind}}$ . Notably, and in line with the  $IC_{50}$  values (Table 1), our computational analysis also revealed that the mid-gorge Asp74 is targeted by both **5f** enantiomers and by only one enantiomer of **5e**.

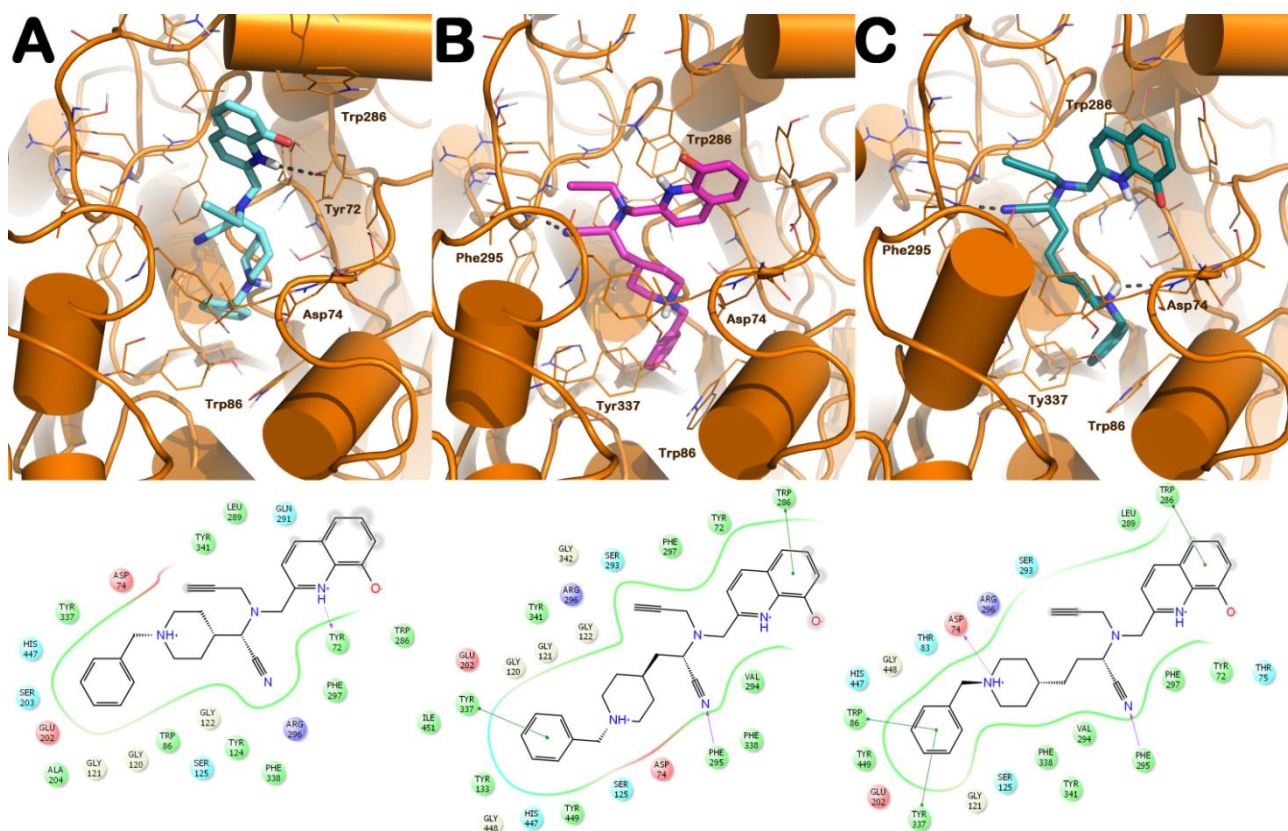


**Figure 7.** Docked poses of *S*-enantiomer of selected compounds (A-C; A: **5d**; B: **5e**; C: **5f**) into *hAChE* enzyme (PDB ID: 1B41). The docking output for the *R*-enantiomers is provided in Figure S2. The pictures were generated by means of PyMOL, while the ligand-interaction diagrams were generated by means of Maestro.

Our calculations also explained the worst *hAChE* inhibition properties of **5d** (*S*- and *R*-enantiomer) which did not establish interactions at the mid-gorge and CAS level as observed for the analogue **5a** devoid of the CN group. **5d** only interacts with PAS by a H-bond with Tyr72 by its 8-hydroxyquinoline moiety (Figure 8A and Figure S2A). Notably, a non-classical conformation of Trp286 was detected which supported the poorest affinity of **5d** for *hAChE*. Also the docking score values (*S*-enantiomer -7.58 kcal/mol; *R*-enantiomer -7.33 kcal/mol) and  $\Delta G_{\text{bind}}$  (*S*-enantiomer -79.42 kcal/mol; *R*-enantiomer -78.15 kcal/mol) are in agreement with a 6-fold lower potency with respect to **5a**. As above reported for compound **5b**, the elongation of the spacer in this scaffold improved *hAChE* inhibition potency. In fact,

**5e** (*S*- and *R*-enantiomer, Figure 8B and Figure S2B, respectively) inhibiting *hAChE* in the micromolar range revealed a better pattern of interaction than **5d**. In fact, **5e** established a series of contacts with PAS and mid-gorge, but could not reach the CAS due to the lack of appropriate length of the linker. In particular (*S*)-**5e** established a  $\pi$ - $\pi$  stacking by its aromatic moieties with Trp286 and with Tyr337 (Figure 8B). In addition, the CN group interacts with the backbone of Phe295 by a H-bond. The improvement of affinity by one order of magnitude was confirmed by the presence of a stronger pattern of interaction with *hAChE* and a good docking score (-9.46 kcal/mol) coupled to a significant  $\Delta G_{\text{bind}}$  of -109.81 kcal/mol. In addition, the *R*-enantiomer lacks the interaction with Tyr337 but it forms a H-bond with the mid-gorge site Asp74 (Figure S2B). A comparable docking score (-10.34 kcal/mol) and  $\Delta G_{\text{bind}}$  (-107.60 kcal/mol) were found for *R*-enantiomer with respect to the *S*-enantiomer.

Finally, the IFD calculation performed on **5f**, possessing the appropriate length for optimally interacting with all the key sites of *hAChE* gorge (Figures 8C and S2C), revealed a good fitting within the enzyme. In particular, (*S*)-**5f** was able to establish a double  $\pi$ - $\pi$  stacking by its 8-hydroxyquinoline and benzyl groups with Trp286 and Trp86/Tyr337, respectively. Moreover, a series of H-bonds were found with Phe295 by the cyano group, and with Asp74 by the piperidine moiety. This enantiomer showed a very high docking score (-12.93 kcal/mol) as well as the estimated free-binding energy ( $\Delta G_{\text{bind}}$  -129.67 kcal/mol). Similarly, the *R*-enantiomer (Figure S2C) was able to reproduce all the contacts found for the *S*-enantiomer (Figure 8C) with few additional contacts (H-bonds with the backbone of Arg296 by its CN group, with Tyr72 sidechain by its 8-hydroxyquinoline moiety, and a  $\pi$ - $\pi$  stacking with His447 by the benzyl moiety, Figure S2C). These additional contacts led to a significant improvement in the docking score (-14.87 kcal/mol) as well as in the  $\Delta G_{\text{bind}}$  (-146.31 kcal/mol). This strong pattern of interaction found for both **5f** enantiomers perfectly parallels and explains the *in vitro* data (Table 1). Last, but not least, all the compounds showed an excellent drug-like profile (ADME+T properties prediction) as calculated by means of QikProp [48] (Table 2).

**Table 2.** Calculated physicochemical properties for compounds presented in this study by means of QikProp application.

Cpd	SASA <sup>a</sup>	QPlogP <sup>b</sup>	QPlogS <sup>c</sup>	QPlogHERG <sup>d</sup>	%HOA <sup>e</sup>
<b>5a</b>	743.9	3.78	-3.37	-8.21	88.0
<b>5b</b>	800.9	4.84	-4.59	-8.90	95.4
<b>5c</b>	827.7	5.19	-4.91	-8.89	84.7
<b>5d</b>	757.1	3.03	-3.80	-8.23	75.2
<b>5e</b>	818.1	4.23	-5.18	-8.87	84.6
<b>5f</b>	851.7	4.50	-5.61	-8.97	84.2

The calculated properties and their recommended range according to QikProp user manual are follows: <sup>a</sup>SASA 300-1000; <sup>b</sup>QPlogP -2.00 – 6.5; <sup>c</sup>QPlogS -6.5 – 0.5; <sup>d</sup>QPlogHERG <-5; <sup>e</sup>%HOA: %human oral absorption >80% high, <25% poor.

### 2.2.3. Assessment of metal-chelating properties of **5f**

Our investigation of the relevant properties of compound **5f** as a potential DMAAD was implemented with the *in vitro* assay for establishing its metal-chelating properties. Chelating tests reported in Figure 9 allowed to understand the metal-chelating properties of **5f** evaluating the formation of metal-complexes. Indeed, the ability of **5f** to interact with metals relevant for A $\beta$  misfolding such as zinc, copper, and iron was assessed [49].

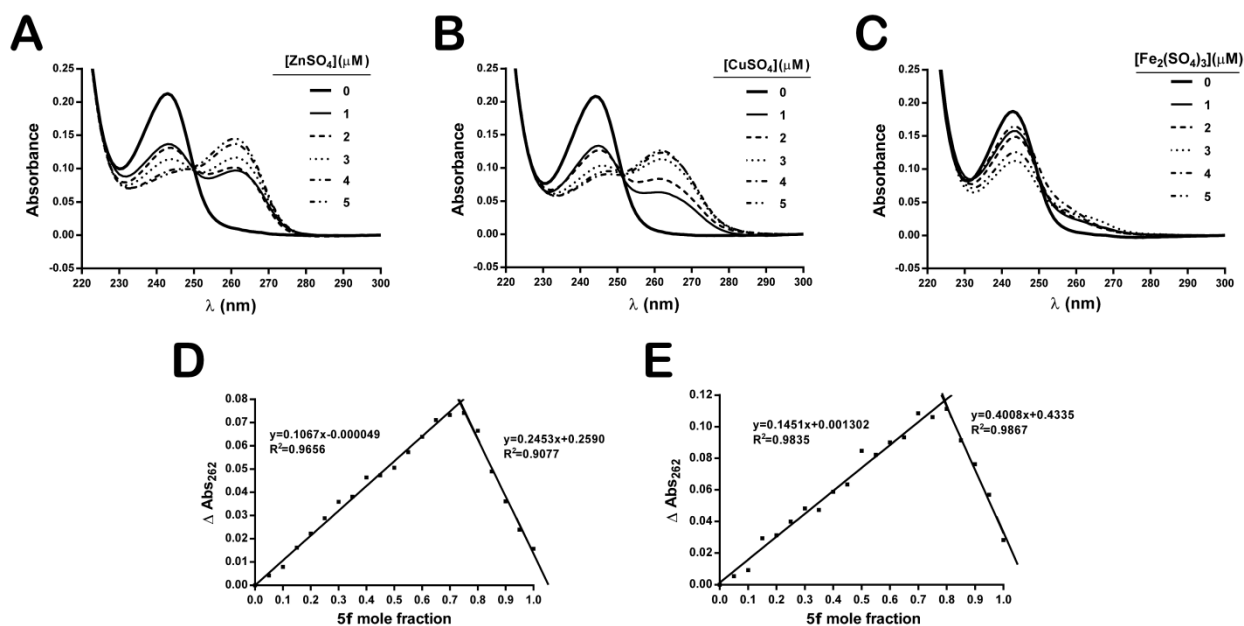


**Figure 9.** Assessment of metal-chelating properties of compound **5f**. Job's method for iron was not plotted as no significant spectral changes were observed at 262 nm after several pre-incubations as reported in the main text.

In particular, the influence of abnormally high levels of redox-active metal ions such as  $\text{Cu}^{2+}$ ,  $\text{Fe}^{2+}$  was characterized as well as the compromised regulation of redox-active metals in the promotion and formation of cytotoxic ROS and neuronal damage [50]. Moreover, the role of mentioned metals in formation and progression of aberrant  $\text{A}\beta$  species causing the misfolding of proteins and their subsequent aggregation was also established. Numerous studies have demonstrated that a surplus of metal ions such as  $\text{Cu}^{2+}$ ,  $\text{Fe}^{2+}$ ,  $\text{Zn}^{2+}$  and  $\text{Al}^{3+}$  were present in  $\text{A}\beta$  plaques of AD patients' brain [49]. Furthermore an excess of  $\text{Cu}^{2+}$  and  $\text{Zn}^{2+}$  promotes  $\text{A}\beta$  aggregation [51, 52]. For these reasons, the research with multitarget compounds additionally decorated for obtaining metal-chelating effect might provide an additional and therapeutic, rather than only symptomatological, strategy for the treatment of AD. Our *in vitro* analyses (Figure 9) reveal that **5f** is able to interact with metals. Additionally, an extinction coefficient ( $\epsilon$ ) of  $20800 \text{ M}^{-1}\cdot\text{cm}^{-1}$  was determined with **5f**, while a maximum complexation peak was detected at 262 nm. As showed in Figure 9A, **5f** displayed a spectral changes at  $10 \mu\text{M}$

forming a complex with  $\text{Zn}^{2+}$  after incubations of 15 h. Remarkably, **5f** formed a complex with  $\text{Cu}^{2+}$  (Figure 9B) after 5 minutes of incubation. On the contrary, with  $\text{Fe}^{3+}$  (Figure 9C) no significant spectral changes were observed at 262 nm after longer pre-incubations. In summary, **5f** was determined as metal-chelating agent, a stoichiometry complexation of 1:2 metal-compound with both  $\text{Cu}^{2+}$  (Figure 9D) and  $\text{Zn}^{2+}$  (Figure 9E) revealed a metal-compound ratio of 1:2.

#### 2.2.4. Evaluation of antioxidant properties of **5f**

The assessment of antioxidant properties of compound **5f** was carried out by different *in vitro* assays. Figure 10A shows the Cu(II)-chelating activity of **5f** at blocking the production of  $\text{H}_2\text{O}_2$  *in vitro* by Cu(II) and ascorbic acid using the Amplex Red reagent. This effect was in agreement with the metal-chelating properties previously observed as a stoichiometry of 1:2 Cu(II)/compound was also found. Compound **5f** also displayed oxygen radical absorbance capacity (ORAC) values equivalent to those observed with the antioxidant Trolox (Figure 10B). Lipid peroxidation induced *in vitro* by linoleic acid and 2,2'-azobis(2-amidinopropane) dihydrochloride (AAPH) (Figure 10C) was significantly reduced by **5f** though this effect was prolonged similarly ( $T_{\text{inh}}$ ) over time as that observed in the control. Finally, the radical scavenger activity of **5f** induced by 2,2-difenil-1-picrilidrazile (DPPH, Figure 10D) was observed to decrease in a dose-dependent manner, being significantly reduced when **5f** concentrations higher than 50  $\mu\text{M}$  were used.

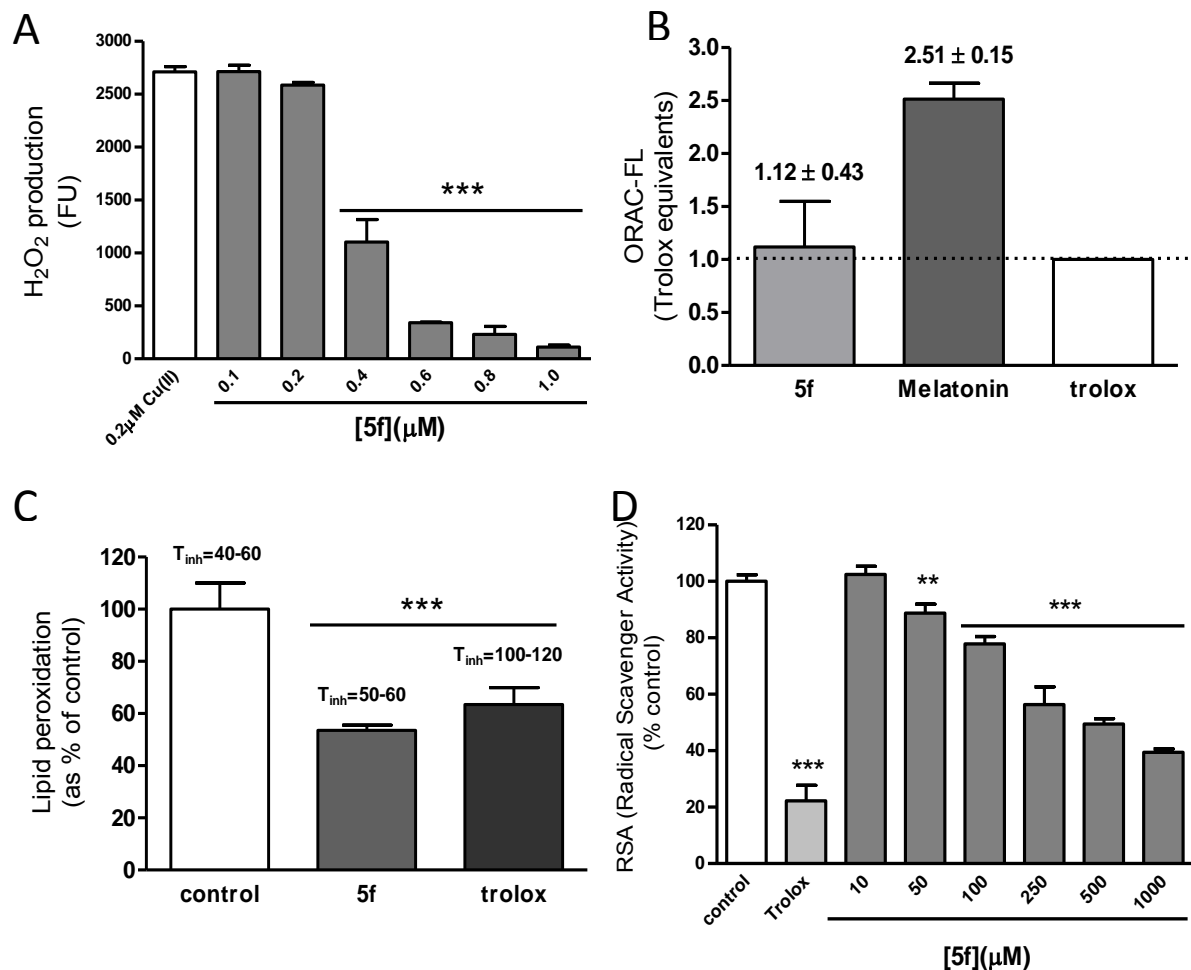


**Figure 10.** Evaluation of *in vitro* antioxidant properties of compound **5f**. A) Effect of compound **5f** on the *in vitro* production of H<sub>2</sub>O<sub>2</sub> in presence of Cu(II) and ascorbic acid expressed in fluorescence units (FU). B) ORAC-FL values of **5f** and melatonin as trolox equivalents. C) Inhibition of lipid peroxidation (LPO) by compound **5f** and trolox. Inhibition times (T<sub>inh</sub>) are expressed in minutes. D) Radical scavenger activity (RSA) induced by DPPH with compound **5f** and 50 μM trolox. Statistical analysis was performed using one-way ANOVA test followed by Bonferroni post-test. \*\*,  $p < 0.01$ , \*\*\*,  $p < 0.001$ .

### 3. Conclusion

In summary, in this study, the development of novel donepezil-related compounds (**5a-f**) characterized by a multifunctional profile is reported. Among the series of the novel chemical entities assayed, compound **5f** exhibited the most interesting profile to be further characterized as AD potential therapeutic. In fact, **5f** was defined as a mixed-type hAChE and hBuChE inhibitor of nanomolar

potency, and was also found a selective irreversible MAO-A inhibitor in the micromolar range. Molecular modeling studies were performed to rationalize the mode of action and the selectivity profile of the developed compounds. These studies evidenced the structural requirements of these donepezil-related analogues to optimally interact with the enzymes of interest. Additionally, **5f**, conceived for interacting with metals targeting the cytotoxicity derived from A $\beta$  misfolding leading to oligomers formation, was demonstrated to be able to form complexes with Zn<sup>2+</sup> and Cu<sup>2+</sup>. These data confirm **5f** metal-chelating properties which might be relevant for modulating A $\beta$  misfolding. Notably, **5f** is also endowed with relevant antioxidant properties. The calculated physico-chemical properties enrich the profile of this promising hit as it shows a drug-likeness in line with other marketed drugs. Taken together these findings will pave the way to the development of novel anti-AD based on **5f** that deserves to be further investigated as DMAAD.

#### *4. Experimental section*

##### *4.1. Chemistry*

###### *4.1.1. General procedures*

Unless otherwise specified, materials were purchased from commercial suppliers and used without further purification. Silica gel 60 (0.040 - 0.063 mm) were used for column chromatography. <sup>1</sup>H NMR, and <sup>13</sup>C NMR, spectra were recorded on a Varian INOVA-600, Varian INOVA-400 or Varian Mercury 300MHz, spectrometers by using the residual signal of the deuterated solvent as internal standard. Splitting patterns are described as singlet (s), doublet (d), triplet (t), quartet (q), quintet (p), and broad (br); the value of chemical shifts ( $\delta$ ) are given in ppm and coupling constants ( $J$ ) in Hertz (Hz). IR spectra were obtained with a Shimadzu, Model FT-IR 8400. Purity of the compounds was assessed by

HRMS, spectra were recorded on a Bruker Daltonics Bio TOF mass spectrometer. Yields refer to purified products and are not optimized. All moisture-sensitive reactions were performed under argon atmosphere using oven-dried glassware and anhydrous solvents.

#### 4.1.2. 2-(1-Benzylpiperidin-4-ylidene)acetonitrile (**8a**)

Diethyl (cyanomethyl)phosphonate (**7**). Chloroacetonitrile (3 g, 40 mmol) and triethyl phosphite (6.65 g, 40 mmol) were heated at 150 °C for 3.5 h. And the crude product was directly used in the next reactions.

A solution of diethyl (cyanomethyl)phosphonate **7** (2.13 g, 12 mmol) and K<sub>2</sub>CO<sub>3</sub> (1.66 g, 12 mmol) in 10 mL of dry THF was stirred for 15 min at rt. Then the mixture was heated to reflux for 20 min. After cooling down to rt, ketone **6a** (10 mmol of in 5 mL of dry THF) was added dropwise to this mixture and then resulting mixture was heated at reflux for 12 h. After cooling down to rt, 10% K<sub>2</sub>CO<sub>3</sub> aqueous solution was added. The reaction mixture was extracted with AcOEt three times, the organic phase were collected, dried with anhydrous Na<sub>2</sub>SO<sub>4</sub> and concentrated in vacuum to obtain the crude product which was directly used for the following reactions without further purification. Title compound was obtained as yellow oil, 92.0% yield; <sup>1</sup>H NMR (300 MHz, CDCl<sub>3</sub>) δ 7.26–7.34 (m, 5 H), 5.10 (s, 1 H), 3.55 (s, 2 H), 2.51–2.63 (m, 6 H), 2.40 (t, *J* = 5.1 Hz, 2 H).

#### 4.1.3. 3-(1-Benzylpiperidin-4-yl)acrylonitrile (**8b**).

Following the procedure described for compound **8a** the title compound was obtained as yellow oil, 95.0% yield; <sup>1</sup>H NMR (300 MHz, CDCl<sub>3</sub>) δ 7.19–7.38 (m, 5 H), 6.31 (t, *J* = 10.4 Hz, 1 H), 5.23 (d, *J* = 10.9 Hz, 1 H), 3.50 (s, 2 H), 2.89 (d, *J* = 11.7 Hz, 2 H), 2.51–2.71 (m, 1 H), 1.93–2.14 (m, 2 H), 1.62–1.77 (m, 2 H), 1.40–1.60 (m, 2 H).

#### 4.1.4. 2-(1-Benzylpiperidin-4-yl)acetonitrile (**9a**).

To a solution of compound **8a** (7.7 mmol) in 35 mL MeOH, Mg (154 mmol) and catalytic amount of I<sub>2</sub> were added while stirring at rt. The mixture was then stirred in an ice bath until the reaction mixture became gray gel. Then, conc. HCl was slowly added till the reaction became clear. 10 N NaOH was added to neutralize the pH to 8-9. The precipitate was filtered and washed with large amount of AcOEt. The filtrate was extracted with AcOEt three times, and the combined organic layers were dried with anhydrous Na<sub>2</sub>SO<sub>4</sub> and concentrated in vacuum to give the crude product which was directly used for the following reactions without further purification. Title compound was obtained as yellow oil 82% yield; <sup>1</sup>H NMR (300 MHz, CDCl<sub>3</sub>) δ 7.24–7.34 (m, 5 H), 3.55 (s, 2 H), 2.93 (d, *J* = 11.8 Hz, 2 H), 2.28 (d, *J* = 6.60 Hz, 2 H), 2.00 (t, *J* = 52.77 Hz, 2 H), 1.78 (m, 2 H), 1.68 (m, 1 H), 1.48 (m, 2 H).

#### 4.1.5. 3-(1-Benzylpiperidin-4-yl)propanenitrile (**9b**).

Following the procedure described for compound **9a** the title compound was obtained as yellow oil 87% yield; <sup>1</sup>H NMR (300 MHz, CDCl<sub>3</sub>) δ 7.19–7.37 (m, 5 H), 3.50 (s, 2 H), 2.89 (d, *J* = 11.8 Hz, 2 H), 2.35 (t, *J* = 7.3 Hz, 2 H), 1.96 (td, *J* = 11.5, 1.9 Hz, 2 H), 1.54–1.73 (m, 4 H), 1.17–1.52 (m, 3 H).

#### 4.1.6. 2-(1-Benzylpiperidin-4-yl)acetaldehyde (**10a**).

An over dried and argon-purged flask nitrile **9a** (10.0 mmol) in 20 mL of dry toluene was cooled to –78 °C, and 12 mL 1 mol/L DIBAL-H toluene solution was added dropwise to the solution. The reaction mixture was stirred at –78 °C for 1.5 h. Then 10 mL MeOH were added, and the solution was poured into 100 mL 5% H<sub>2</sub>SO<sub>4</sub> aqueous solution and then alkaline with conc. NH<sub>4</sub>OH. The precipitate was filtered and washed with AcOEt. The filtrate was extracted with AcOEt for three times. The combined organic phase was washed with brine and dried with anhydrous Na<sub>2</sub>SO<sub>4</sub>. After concentration, the crude product was purified by silica gel chromatography Hex/AcOEt, 2:1 to give pure title compound as orange oil, 87% yield; <sup>1</sup>H NMR (300 MHz, CDCl<sub>3</sub>) δ 9.76 (t, *J* = 1.9 Hz, 1 H), 7.17–7.42 (m, 5 H),

3.51 (s, 2 H), 2.88 (d,  $J = 11.2$  Hz, 2 H), 2.36 (dd,  $J = 6.7, 1.76$  Hz, 2 H), 1.60–2.15 (m, 5 H), 1.20–1.50 (m, 2 H).

#### 4.1.7. 3-(1-Benzylpiperidin-4-yl)propanal (**10b**).

Following the procedure described for compound **10a** the title compound was obtained as yellow oil, 83% yield;  $^1\text{H NMR}$  (400 MHz,  $\text{CDCl}_3$ )  $\delta$  9.76 (t,  $J = 1.6$  Hz, 1 H), 7.19–7.38 (m, 5 H), 3.44–3.53 (m, 2 H), 2.87 (d,  $J = 11.1$  Hz, 2 H), 2.43 (td,  $J = 7.5, 1.6$  Hz, 2 H), 1.92 (t,  $J = 11.8$  Hz, 2 H), 1.52–1.72 (m, 4 H), 1.16–1.35 (m, 3 H).

#### 4.1.8. 8-Hydroxyquinoline-2-carbaldehyde (**12**).

$\text{SeO}_2$  (20 mmol, 2.22 g) in 70 mL 1,4-dioxane and 1 mL water mixture were heated to 60 °C. To this solution 2-methylquinolin-8-ol **11** (1.59 g, 10 mmol) in 15 mL 1,4-dioxane was added dropwise over 30 min. The obtained mixture was heated at reflux for 12 h. After cooling down to rt, the precipitate was filtered and the filtrate was concentrated. The crude product was purified by silica gel chromatography using Hex/AcOEt, 5:1 to give 1.49 g of pure title compound as yellow solid, 86% yield;  $^1\text{H NMR}$  (600 MHz,  $\text{CDCl}_3$ ),  $\delta$  10.22 (s, 1H), 8.32 (d,  $J = 8.4$  Hz, 1H), 8.20 (br, 1H), 8.06 (d,  $J = 8.4$  Hz, 1H), 7.62 (t,  $J = 7.8$  Hz, 1H), 7.43 (d,  $J = 8.4$  Hz, 5H), 7.29–7.26(m, 1H), 7.16 (d,  $J = 7.2$  Hz, 1H).

#### 4.1.9. 8-((*tert*-Butyldimethylsilyl)oxy)quinoline-2-carbaldehyde (**13**).

To a solution of **12** (1.5 g, 8.66 mmol) and imidazole (1.3 g, 19.1 mmol) in 30 mL of dry DCM *tert*-butylchlorodimethylsilane (1.44 g, 9.53 mmol) was added while stirring at 0 °C. The mixture was allowed to warm slowly to rt for further 16 h while stirring, then 30 mL water were added. The aqueous phase was extracted with DCM three times and the combined organic phase was washed with saturated  $\text{NaHCO}_3$  solution, brine and dried with anhydrous  $\text{Na}_2\text{SO}_4$ . After concentration in vacuum, the crude

product was purified by silica gel chromatography using Hex/AcOEt, 10:1 to give 2.16 g of pure title compound as yellow oil, 87% yield, <sup>1</sup>H NMR (600 MHz, CDCl<sub>3</sub>), δ 10.22 (d, *J* = 0.6 Hz, 1H), 8.25 (d, *J* = 8.4 Hz, 1H), 7.99 (d, *J* = 8.4 Hz, 1H), 7.56-7.54 (m, 1H), 7.48 (d, *J* = 8.4 Hz, 5H), 7.25-7.24 (m, 2H), 1.09 (s, 9H), 0.32 (s, 6H).

4.1.10. *N*-((8-((*tert*-Butyldimethylsilyl)oxy)quinolin-2-yl)methyl)prop-2-yn-1-amine (**14**).

Aldehyde **13** (1.44 g, 5 mmol) and prop-2-yn-1-amine (550 mg, 10 mmol) were dissolved in 50 mL of MeOH and cooled to 0 °C. 10 drops of CF<sub>3</sub>COOH were added and the reaction mixture was stirred at 0 °C for 1 h and rt for further 2 h. Then NaBH<sub>4</sub> (380 mg, 10 mmol) were added to the reaction at 0 °C and the obtained mixture was stirred for another 1 h at rt. The reaction was quenched with 50 mL of saturated NH<sub>4</sub>Cl solution and the water phase was extracted with AcOEt for three times. The combined organic phase was washed with brine and dried with anhydrous Na<sub>2</sub>SO<sub>4</sub>. After concentrated in vacuum, the crude product was purified by silica gel chromatography using a mixture Hex/AcOEt, 2:1 to give 1.4 g of pure title compound as yellow oil, 86% yield; <sup>1</sup>H NMR (600 MHz, CDCl<sub>3</sub>), δ 8.07 (dd, *J* = 1.8 Hz, *J* = 8.4 Hz, 1H), 7.41-7.36 (m, 3H), 7.15-7.14 (m, 1H), 4.21 (d, *J* = 1.2 Hz, 2H), 3.58 (dd, *J* = 1.8 Hz, *J* = 2.4 Hz, 1H), 2.90 (br, 1H), 2.25-3.58 (d, *J* = 1.8 Hz, 1H), 1.08 (s, 9H), 0.25 (s, 6H).

4.1.11. *N*-((1-benzylpiperidin-4-yl)methyl)-*N*-((8-((*tert*-butyldimethylsilyl)oxy)quinolin-2-yl)methyl)prop-2-yn-1-amine (**15a**).

A mixture of amine **14** and 1 mmol and aldehyde **6b** (1.5 mmol) in MeOH (10 mL) was cooled at 0 °C. 3 drops of CF<sub>3</sub>COOH were added, and the reaction was stirred at 0 °C for 1 h and then kept at rt for 12 h. After that time NaBH<sub>4</sub> (3 mmol) was added at 0 °C and the reaction was stirred for 1 h at rt. 20 mL saturated NH<sub>4</sub>Cl solution were then added to quench the reaction, and water phase was extracted with AcOEt for three times. The combined organic phase was washed with brine and dried with anhydrous Na<sub>2</sub>SO<sub>4</sub>. After concentration in vacuum, the crude product was purified by silica gel chromatography

using Hex/AcOEt from 10:1 to 2:1 to obtain the pure title compound as yellow oil, 54.6% yield. The title compound was submitted to the following step without any further characterization.

4.1.12. *N*-(2-(1-benzylpiperidin-4-yl)ethyl)-*N*-((8-((*tert*-butyldimethylsilyl)oxy)quinolin-2-yl)methyl)prop-2-yn-1-amine (**15b**).

Following the procedure described for compound **15a** the title compound was obtained as yellow oil, 51.2% yield. The title compound was submitted to the following step without any further characterization.

4.1.13. *N*-(3-(1-benzylpiperidin-4-yl)propyl)-*N*-((8-((*tert*-butyldimethylsilyl)oxy)quinolin-2-yl)methyl)prop-2-yn-1-amine (**15c**).

Following the procedure described for compound **15a** the title compound was obtained as yellow oil, 46.1% yield. The title compound was submitted to the following step without any further characterization.

4.1.14. 2-(((1-Benzylpiperidin-4-yl)methyl)(prop-2-yn-1-yl)amino)methylquinolin-8-ol (**5a**).

To a solution of **15a** (0.4 mmol) in 10 mL of THF a 2 mL of a 1 M solution of TBAF in THF were added and the mixture was stirred at rt for 3 h. Then the solvent was removed, and the residue was purified by silica gel chromatography using Hex/AcOEt from 10:1 to 1:1 to obtain the pure title compound as yellow oil, 93.5% yield IR  $\nu_{\text{max}}$  = 3289, 2922, 2801, 1713, 1601, 1574, 1506, 1474, 1456, 1435, 1366, 1327, 1279, 1246, 1220, 1202, 1126, 1117, 1090, 1076, 984, 909, 833, 754, 739. <sup>1</sup>H NMR (400 MHz, CDCl<sub>3</sub>),  $\delta$  8.08 (d, *J* = 8.4 Hz, 1H), 7.62 (d, *J* = 8.4 Hz, 1H), 7.41 (t, *J* = 7.8 Hz, 1H), 7.30-7.25 (m, 5H), 7.25-7.23(m, 1H), 7.16 (d, *J* = 7.2 Hz, 1H), 3.93(s, 2H), 3.48 (s 2H), 3.40 (s 2H), 2.87 (d, *J* = 10.8 Hz, 2H), 2.44 (d, *J* = 7.2 Hz, 2H), 2.26 (d, *J* = 1.8 Hz, 1H), 1.93 (t, *J* = 11.4 Hz, 2H), 1.77 (d, *J* = 12.6 Hz, 2H), 1.53-1.50 (m, 1H), 1.21-1.15 (m, 2H); <sup>13</sup>C NMR (150 MHz, CDCl<sub>3</sub>),  $\delta$  158.1, 152.0,

138.5, 137.4, 136.4, 129.2, 128.1, 127.5, 127.2, 126.9, 121.8, 117.6, 110.0, 78.7, 73.3, 63.5, 60.7, 59.3, 53.6, 42.8, 33.7, 30.7. HRMS (ESI):  $m/z$   $[M + H]^+$  calcd for  $C_{26}H_{30}N_3O$ : 400.2383; found 400.2387.

4.1.15. 2-(((2-(1-Benzylpiperidin-4-yl)ethyl)(prop-2-yn-1-yl)amino)methyl)quinolin-8-ol (**5b**).

Following the procedure described for compound **5a** the title compound was obtained as yellow oil, 91.6% yield; IR  $\nu_{max}$  = 3302, 2911, 2797, 2787, 1713, 1574, 1506, 1474, 1454, 1435, 1396, 1366, 1327, 1248, 1200, 1150, 1123, 1086, 978, 910, 839, 754, 738.  $^1H$  NMR (400 MHz,  $CDCl_3$ ),  $\delta$  8.09(d,  $J$  = 8.4 Hz, 1H), 7.60 (d,  $J$  = 8.4 Hz, 1H), 7.40 (t,  $J$  = 7.8 Hz, 1H), 7.30-7.25 (m, 5H), 7.25-7.23 (m, 1H), 7.16 (d,  $J$  = 7.2 Hz, 1H), 3.94 (s, 2H), 3.47 (s, 2H), 3.41 (d,  $J$  = 2.4 Hz, 2H), 2.84 (d,  $J$  = 11.4 Hz, 2H), 2.62 (t,  $J$  = 7.2 Hz, 2H), 2.26 (d,  $J$  = 1.8 Hz, 1H), 1.90 (t,  $J$  = 12.0 Hz, 2H), 1.59 (d,  $J$  = 12.6 Hz, 2H), 1.46-1.44 (m, 2H), 1.31-1.25 (m, 3H);  $^{13}C$  NMR (150 MHz,  $CDCl_3$ ),  $\delta$  157.8, 152.1, 138.5, 137.5, 136.4, 129.2, 128.2, 127.5, 127.3, 126.9, 121.8, 117.6, 110.0, 78.5, 73.3, 63.5, 60.3, 53.8, 51.0, 42.4, 34.2, 33.8, 32.4, 31.6. HRMS (ESI):  $m/z$   $[M + H]^+$  calcd for  $C_{27}H_{32}N_3O$ : 414.2540; found 414.2539.

4.1.16. 2-(((3-(1-Benzylpiperidin-4-yl)propyl)(prop-2-yn-1-yl)amino)methyl)quinolin-8-ol (**5c**).

Following the procedure described for compound **5a** the title compound was obtained as yellow oil, 97.1% yield. IR  $\nu_{max}$  = 3300, 2907, 27847, 2797, 2758, 1713, 1601, 1574, 1506, 1471, 1454, 1435, 1368, 1327, 1248, 1200, 1125, 1090, 972, 910, 839, 735.  $^1H$  NMR (400 MHz,  $CDCl_3$ ),  $\delta$  8.08(d,  $J$  = 9.0 Hz, 1H), 7.60 (d,  $J$  = 8.4 Hz, 1H), 7.40(t,  $J$  = 7.8 Hz, 1H), 7.30-7.28 (m, 5H), 7.25-7.22(m, 1H), 7.16 (d,  $J$  = 7.8 Hz, 1H), 3.94(s, 2H), 3.46 (s, 2H), 3.41 (d,  $J$  = 2.4 Hz, 2H), 2.84 (d,  $J$  = 11.4 Hz, 2H), 2.57 (t,  $J$  = 7.2 Hz, 2H), 2.25 (d,  $J$  = 1.2 Hz, 1H), 2.14 (s, 1H), 1.86 (t,  $J$  = 12.0 Hz, 2H), 1.60 (d,  $J$  = 12.0 Hz, 2H), 1.52-1.50 (m, 2H), 1.26-1.18 (m, 5H);  $^{13}C$  NMR (150 MHz,  $CDCl_3$ ),  $\delta$  157.8, 152.1, 138.5, 137.5, 136.4, 129.2, 128.1, 127.5, 127.2, 126.9, 121.9, 117.6, 110.0, 78.6, 73.3, 63.5, 60.2, 53.9, 53.6, 42.4, 35.5, 34.1, 32.4, 24.7. HRMS (ESI):  $m/z$   $[M + H]^+$  calcd for  $C_{28}H_{34}N_3O$ : 428.2696; found 428.2700.

4.1.17. 2-(1-Benzylpiperidin-4-yl)-2-(((8-(tert-butyldimethylsilyloxy)quinolin-2-yl)methyl)(prop-2-ynyl)amino)acetonitrile (**17a**).

To a mixture of aldehyde **6a** (1.5 mmol) and TMSCN (2 mmol in 20 mL DCM, ZnI<sub>2</sub> (0.2 mmol) was added, and the reaction mixture was stirred for 1 h at rt the intermediate compound **16a**. After removal of the solvent amine **14** (1 mmol) in MeOH (15 mL) was added and the resulting mixture was heated to 50 °C for further 3 h. After that, MeOH was removed and the residue was purified by silica gel chromatography Hex/AcOEt from 10:1 to 2:1 to obtain pure title compounds as yellow oil 54% yield. The title compound was submitted to the following step without any further characterization.

4.1.18. 3-(1-Benzylpiperidin-4-yl)-2-(((8-(tert-butyldimethylsilyloxy)quinolin-2-yl)methyl)(prop-2-ynyl)amino)propanenitrile (**17b**).

Following the procedure described for compound **17a** the title compound was obtained as yellow oil, 31.8% yield. The title compound was submitted to the following step without any further characterization.

4.1.19. 4-(1-Benzylpiperidin-4-yl)-2-(((8-(tert-butyldimethylsilyloxy)quinolin-2-yl)methyl)(prop-2-ynyl)amino)butanenitrile (**17c**).

Following the procedure described for compound **17a** the title compound was obtained as yellow oil, 63.3% yield. The title compound was submitted to the following step without any further characterization.

4.1.20. 2-(1-Benzylpiperidin-4-yl)-2-(((8-hydroxyquinolin-2-yl)methyl)(prop-2-yn-1-yl)amino)acetonitrile (**5d**).

Following the procedure described for compound **5a** the title compound was obtained as yellow oil, 90% yield. IR  $\nu_{\max}$  = 2928, 2818, 2361, 2328, 1715, 1597, 1574, 1504, 1472, 1435, 1368, 1327, 1248,

1196, 1150, 1130, 1086, 988, 835, 758. <sup>1</sup>H NMR (400 MHz, CDCl<sub>3</sub>), δ 8.11 (d, *J* = 8.4 Hz, 1H), 7.52 (d, *J* = 9.0 Hz, 1H), 7.42 (t, *J* = 7.8 Hz, 1H), 7.30-7.22 (m, 6H), 7.16 (d, *J* = 7.2 Hz, 1H), 4.24 (d, *J* = 14.4 Hz, 1H), 3.87 (d, *J* = 14.4 Hz, 1H), 3.55 (d, *J* = 13.6 Hz, 2H), 3.49 (s, 1H), 3.43 (dd, *J* = 1.8 Hz, *J* = 16.8 Hz, 1H), 3.34 (dd, *J* = 2.4 Hz, *J* = 16.8 Hz, 1H), 2.94-2.88 (m, 2H), 2.31 (t, *J* = 2.4 Hz, 2H), 2.14-1.91 (m, 4H), 1.81-1.78 (m, 1H), 1.38-1.36 (m, 1H), 1.26-1.23 (m, 1H); <sup>13</sup>C NMR (150 MHz, CDCl<sub>3</sub>), δ 155.8, 152.0, 137.4, 137.3, 137.1, 129.3, 128.3, 127.8, 127.6, 127.3, 121.3, 117.7, 116.3, 110.4, 78.6, 74.0, 62.9, 59.5, 57.4, 52.7, 52.6, 41.5, 36.6, 29.4, 29.2. HRMS (ESI): *m/z* [M + H]<sup>+</sup> calcd for C<sub>27</sub>H<sub>29</sub>N<sub>4</sub>O: 425.2536; found 425.2335.

4.1.21. *3-(1-Benzylpiperidin-4-yl)-2-(((8-hydroxyquinolin-2-yl)methyl)(prop-2-yn-1-yl)amino)propanenitrile (5e)*

Following the procedure described for compound **5a** the title compound was obtained as yellow oil, 94.5% yield. IR  $\nu_{\max}$  = 3287, 2936, 2799, 2768, 1711, 1601, 1574, 1505, 1474, 1452, 1368, 1327, 1248, 1150, 1129, 1088, 1028, 978, 910, 839, 741. <sup>1</sup>H NMR (400 MHz, CDCl<sub>3</sub>), δ 8.05(d, *J* = 9.0 Hz, 1H), 7.46 (d, *J* = 8.4 Hz, 1H), 7.35(t, *J* = 7.8 Hz, 1H), 7.23-7.21 (m, 5H), 7.20-7.14 (m, 1H), 7.16 (dd, *J* = 1.2 Hz, *J* = 7.8 Hz, 1H), 4.17(d, *J* = 14.4 Hz, 1H), 3.93 (t, *J* = 7.8 Hz, 1H), 3.79 (d, *J* = 14.4 Hz, 1H), 3.39-3.29 (m, 3H), 3.29-3.26 (m, 1H), 2.81-2.76 (m, 2H), 2.50 (d, *J* = 1.2 Hz, 1H), 1.88-1.82 (m, 2H), 1.74-1.66 (m, 2H), 1.52-1.47 (m, 3H), 1.25-1.17 (m, 2H); <sup>13</sup>C NMR (150 MHz, CDCl<sub>3</sub>), δ 155.9, 152.0, 138.3, 137.5, 137.0, 129.2, 128.2, 127.8, 127.1, 127.0, 121.4, 117.7, 117.4, 110.5, 78.5, 74.2, 63.3, 57.0, 53.4, 53.3, 53.0, 51.6, 41.5, 32.2, 32.0, 31.6. HRMS (ESI): *m/z* [M + H]<sup>+</sup> calcd for C<sub>28</sub>H<sub>31</sub>N<sub>4</sub>O: 439.2492; found 439.2497.

4.1.21. *4-(1-Benzylpiperidin-4-yl)-2-(((8-hydroxyquinolin-2-yl)methyl)(prop-2-yn-1-yl)amino)butanenitrile (5f)*.

Following the procedure described for compound **5a** the title compound was obtained as yellow oil, 94.5% yield. yellow oil, 166.1 mg, 91.8% yield. IR  $\nu_{\max}$  =3289, 2922, 2805, 2766, 1711, 1599, 1574, 1504, 1474, 1454, 1435, 1366, 1329, 1248, 1196, 1125, 1030, 980, 910, 839, 737.  $^1\text{H}$  NMR (400 MHz,  $\text{CDCl}_3$ ),  $\delta$  8.10 (d,  $J$  = 8.6 Hz, 1H), 7.53 (d,  $J$  = 8.6 Hz, 1H), 7.41 (t,  $J$  = 7.8 Hz, 1H), 7.28-7.26 (m, 5H), 7.22-7.20 (m, 1H), 7.15 (d,  $J$  = 7.8 Hz, 1H), 4.23 (d,  $J$  = 14.4 Hz, 1H), 3.88 (d,  $J$  = 13.8 Hz, 1H), 3.81 (t,  $J$  = 7.8 Hz, 1H), 3.46-3.42 (m, 3H), 3.36-3.33 (m, 1H), 2.81 (d,  $J$  = 10.8 Hz, 2H), 2.32 (d,  $J$  = 1.8 Hz, 1H), 2.13 (s, 3H), 1.84-1.81 (m, 4H), 1.57-1.54 (m, 2H), 1.39-1.37 (m, 2H), 1.22-1.18 (m, 3H);  $^{13}\text{C}$  NMR (150 MHz,  $\text{CDCl}_3$ ),  $\delta$  156.0, 152.0, 138.4, 137.4, 137.0, 129.2, 128.1, 127.7, 127.6, 126.9, 121.5, 117.7, 117.4, 110.4, 78.5, 74.2, 57.1, 54.1, 53.6, 41.4, 35.0, 32.5, 32.2, 32.0, 28.9. HRMS (ESI):  $m/z$   $[\text{M} + \text{H}]^+$  calcd for  $\text{C}_{29}\text{H}_{33}\text{N}_4\text{O}$ : 453.2649; found 453.2652.

#### 4.2. *In vitro* biological assays.

##### 4.2.1. Monoamine oxidase inhibition

Inhibition of human recombinant MAO-A and MAO-B (Sigma-Aldrich) by the selected derivatives was performed using a fluorometric method [53]. Enzymatic reactions took place in 96-well black opaque microplates (OptiPlate-96F, PerkinElmer) in a final volume of 200  $\mu\text{L}$ . Serial dilutions of each inhibitor were pre-incubated for 30 minutes at 37  $^\circ\text{C}$  with 360 mU/mL MAO-A or 67.5 mU/mL MAO-B. Following the pre-incubations, enzymatic reactions were initiated by adding 100  $\mu\text{L}$  of a mixture solution containing 1 mM *p*-tyramine as MAO substrate, 40 U/mL horseradish peroxidase (HRP) and 25  $\mu\text{M}$  Amplex UltraRed<sup>TM</sup> reagent as final concentrations in 0.25 mM sodium phosphate (pH 7.4). The fluorescence production associated with peroxidase-coupled production of resorufin from Amplex UltraRed<sup>TM</sup> was continuously measured for at least one hour at  $\lambda_{530}(\text{exc})/\lambda_{590}(\text{em})$  in a spectrophotometric plate reader (FluoStar OPTIMA, BMG Labtech). Control experiments were carried out simultaneously by replacing the inhibitors by distilled water. In addition, the possible capacity of

compounds to modify the fluorescence generated in the reaction mixture due to non-enzymatic inhibition was determined by adding these compounds to solutions containing the Amplex UltraRed™ reagent only in phosphate buffer. Samples containing no substrate were used as blanks. Dose-response curves were plotted by using the GraphPad PRISM software (version 4.0) and IC<sub>50</sub> values were accordingly calculated. Data were expressed as mean ± S.E.M. of at least three different experiments performed in triplicate.

#### 4.2.2. Cholinesterase inhibition

Cholinesterase inhibition was assessed following a spectrophotometric method of Ellman [54], using purified human cholinesterases AChE and BuChE (Sigma-Aldrich). Enzymatic reactions took place in 96-well plates in solutions containing 0.1M phosphate buffer (pH 8.0), 0.035 U/mL AChE or 0.05 U/mL BuChE and 0.35 mM of 5,5'-dithiobis-2-nitrobenzoic acid (DTNB, Sigma-Aldrich). Inhibition curves were plotted by pre-incubating this mixture with serial dilutions of each compound for 30 minutes at 37°C. The activity in absence of compound was used as control of the 100% of enzyme activity. After pre-incubation times, substrate was added to a final concentration of 0.35 mM acetylthiocholine iodide or 0.5mM *S*-butyrylthiocholine iodide (Sigma-Aldrich) and enzymatic reactions were followed for at least 30 minutes. Changes in absorbance at  $\lambda_{405}$  were detected in a spectrophotometric plate reader (FluoStar OPTIMA, BMG Labtech) and IC<sub>50</sub> values were calculated as the compound concentration inhibiting 50% of enzymatic activity by using the GraphPad PRISM software (version 4.0). Data were expressed as the mean ± S.E.M. of at least three different experiments performed in triplicate.

#### 4.2.3. Assessment of reversibility and time-dependent inhibition

The reversibility of inhibition of human recombinant MAO-A by **5f** was determined by measuring the recovery of enzymatic activity after a rapid and large dilution of the enzyme-compound complex. To

perform so, MAO-A was pre-incubated for 30 minutes at 100-fold over the concentration required for the activity assay with 3  $\mu\text{M}$  **5f**, corresponding to 10-fold of  $\text{IC}_{50}$  value previously determined. The mixture was diluted 100-fold into reaction buffer containing 1mM *p*-tyramine. The progress curves were measured at  $\lambda_{405}$  and compared to that of samples with no inhibitor. Time-dependent inhibition of human recombinant MAO-A by **5f** was evaluated by carrying out several pre-incubations (0-240 minutes) of serial concentrations of the inhibitor with the enzyme. Dose-response curves ( $\text{IC}_{50}$ ) were determined accordingly for each pre-incubation as previously described.

#### 4.2.4. Cholinesterase kinetic assessment

To estimate the mechanism of action of **5f** inhibiting both human cholinesterases (AChE and BuChE), reciprocal plots of  $1/V$  versus  $1/[S]$  were determined using substrate concentrations ranging 0.1-2mM of acetylthiocholine iodide (ASCh) or *S*-butyrylthiocholine iodide (BuSCh), respectively. Enzyme activity was determined by using the Ellman's method [54], adding enzyme at last. The plots were assessed by a weighted least-squares analysis and slopes of reciprocal plots were plotted against **5f** concentration (0-200nM). Inhibition constants ( $K_i$ ) were estimated using the Cheng-Prusoff equation [55].

#### 4.2.5. Assessment of metal-chelating properties

Complexing studies were performed in distilled water at room temperature using a UV-VIS spectrophotometer (Lambda25, PerkinElmer). Spectral changes (220-300 nm) of 10 $\mu\text{M}$  **5f** in presence of metals  $\text{CuSO}_4$ ,  $\text{Fe}_2(\text{SO})_3$  and  $\text{ZnSO}_4$  at concentrations ranging 1-5  $\mu\text{M}$  of were detected in 1cm-quartz cells. The stoichiometry of the complexes **5f**-Cu(II)/Zn(II) was determined using the Job's method [56]. To realise so, 21 different solutions containing **5f** and biometals  $\text{CuSO}_4$  and  $\text{ZnSO}_4$  were prepared at a final sum of concentrations of both species of 10 $\mu\text{M}$ , varying the proportions of both

components between 0 and 100%. Absorbance at 262 nm was plotted versus the mole fraction of **5f** for each metal.

#### 4.2.6. Evaluation of antioxidant properties of **5f**

##### 4.2.6.1. Inhibition of lipid peroxidation (LPO).

Production of conjugated diene hydroperoxide by oxidation of linoleic acid in an aqueous dispersion was monitored at 234 nm as previously described [57]. AAPH was used as a free radical initiator. Ten microliters of 16 mM linoleic acid dispersion was added to the UV cuvette containing 0.93 mL of 0.05 M phosphate buffer pH 7.4 at 37 °C. The oxidation reaction was initiated upon the addition of 50  $\mu$ L of 40mM AAPH solution. Oxidation was carried out in the presence of aliquots (10  $\mu$ L) in the assay without antioxidant; lipid oxidation was measured in the presence of the same level of DMSO. The rate of oxidation at 37 °C was monitored by recording the increase in absorption at 234 nm caused by conjugated diene hydroperoxides.

##### 4.2.6.2. Oxygen Radical Absorbance Capacity (ORAC) assay.

The ORAC assay was performed as previously described [58]. Briefly, AAPH was used as free radical generator and trolox as standard while melatonin was used as a reference compound (both compounds, Sigma-Aldrich). Compounds **5f** and melatonin were diluted in 75 mM PBS pH 7.4 and measured at different concentrations (0.1-1  $\mu$ M). Trolox calibration was used for the standard curve. Samples were pre-incubated for 15 minutes at 37 °C with 70 nM fluorescein (Sigma-Aldrich). Upon the addition of 12 mM AAPH, the fluorescence intensity ( $\lambda_{exc} = 485$  nm,  $\lambda_{em} = 520$  nm) was monitored every minute for 1 h using a Polarstar Galaxy plate reader (BMG Labtechnologies GmbH). The area under the curve (AUC) of the fluorescence decay was calculated by subtracting AUC values for the same sample or standard from that for the net AUC values of trolox standard solutions. The ORAC value for each

tested compound was expressed as trolox equivalent ( $\mu\text{mol}$  of trolox/ $\mu\text{mol}$  of compound). The ORAC value for trolox was assigned as 1.

#### 4.2.6.3. Determination of the reducing activity of the stable radical DPPH

As previously reported [59], to an ethanolic solution of 0.1mM DPPH in absolute ethanol, an equal volume of the compounds dissolved in DMSO was added. The mixture was shaken vigorously and allowed to stand for 60 min. Then, absorbance at 517 nm was determined spectrophotometrically and the percentage of activity was calculated. All tests were undertaken on three replicates and the results were averaged.

#### 4.2.6.4. Induction of $\text{H}_2\text{O}_2$ by $\text{Cu(II)}$ and ascorbic acid

The production  $\text{H}_2\text{O}_2$  was induced *in vitro* by incubating 0.2  $\mu\text{M}$   $\text{Cu(II)}$ , 10  $\mu\text{M}$  ascorbic acid (Sigma-Aldrich). Following an incubation of 10 min at rt with different concentrations of **5f**, a mixture containing horseradish peroxidase and Amplex Red reagent was added to quantify the amount of  $\text{H}_2\text{O}_2$  produced. Distilled water was used to determine the maximum levels of  $\text{H}_2\text{O}_2$ .

### 4.3. Molecular Modeling

All calculations performed in this work were carried out on Cooler Master Centurion 5 (Intel Core i5–2500 CPU @ 3.30 GHz Quad) with Ubuntu 10.04 LTS (long-term support) operating system running Maestro 9.3 (Schrödinger, LLC, New York, NY, 2012).

#### 4.3.1. Proteins and Ligands preparation

The three-dimensional structure of the human MAO-A, MAO-B and AChE enzymes were taken from PDB (ID 2Z5X, 2V5Z, and 1B41, respectively). The co-crystallized ligands, compounds used for solving the structures and molecules of water were removed from the proteins and the resulting

structures were submitted to protein preparation wizard implemented in Maestro suite 2012 (Protein Preparation Wizard workflow 2012; <http://www.schrodinger.com/supportdocs/18/16>). Three-dimensional structure building for all compounds in this study was carried out by means of Maestro [42]. Molecular energy minimizations were performed in MacroModel [60] using the Optimized Potentials for Liquid Simulations-all atom (OPLS-AA) force field 2005 [61, 62]. The solvent effects are simulated using the analytical Generalized-Born/Surface-Area (GB/SA) model [63], and no cutoff for nonbonded interactions was selected. Polak-Ribiere conjugate gradient (PRCG) method with 1000 maximum iterations and 0.001 gradient convergence threshold was employed. All compounds reported in this paper were prepared taking into account the protonation state reported in Table S1 calculated by means of ACDlabs (ACD/pKa DB software, version 12.00; Advanced Chemistry Development, Inc., Toronto, Canada).

#### 4.3.2. Induced Fit Docking (IFD)

Molecular docking was carried out using the Schrödinger suite 2012 by applying the IFD protocol [64]. This procedure induces conformational changes in the binding site to accommodate the ligand and exhaustively identify possible binding modes and associated conformational changes by side-chain sampling and backbone minimization. The proteins and the ligands used in this step were prepared as reported in the previous paragraphs. The boxes for docking calculation was built starting from the crystallized non-covalent inhibitors for MAO enzymes, while for *h*AChE from the centre of the gorge selecting the residues Asp74 as previously reported [31, 32]. IFD includes protein side-chain flexibility in a radius of 5.0 Å around the poses found during the initial docking stage of the IFD protocol. Complexes within 30.0 kcal/mol of minimum energy structure were taken forward for redocking. The Glide redocking stage was performed by XP (Extra Precision) methods. The calculations were performed using default IFD protocol parameters. No hydrogen bonding or other constraints were used.

#### *4.3.3. Estimated free-binding energies*

The Prime/MM-GBSA method implemented in Prime software [65] consists in computing the change between the free and the complex state of both the ligand and the protein after energy minimization. The technique was used on the docking complexes herein reported. The software was used to calculate the free-binding energy ( $\Delta G_{\text{bind}}$ ) as previously reported [33, 46, 66-68].

#### *4.3.4. Predicted physicochemical properties*

QikProp application [48] was used for predicting the physicochemical properties of compounds presented in this study.

## References

- [1] A. Burns, S. Iliffe, *Dementia*, *BMJ*, 338 (2009) b75.
- [2] H.W. Querfurth, F.M. LaFerla, *Alzheimer's disease*, *N. Engl. J. Med.*, 362 (2010) 329-344.
- [3] D.S. Auld, T.J. Kornecook, S. Bastianetto, R. Quirion, *Alzheimer's disease and the basal forebrain cholinergic system: relations to beta-amyloid peptides, cognition, and treatment strategies*, *Prog. Neurobiol.*, 68 (2002) 209-245.
- [4] J. Hardy, *The amyloid hypothesis for Alzheimer's disease: a critical reappraisal*, *J. Neurochem.*, 110 (2009) 1129-1134.
- [5] A. Gella, N. Durany, *Oxidative stress in Alzheimer disease*, *Cell Adhes. Migrat.*, 3 (2009) 88-93.
- [6] D.J. Selkoe, *Alzheimer's disease results from the cerebral accumulation and cytotoxicity of amyloid beta-protein*, *J. Alzheimers Dis.*, 3 (2001) 75-80.
- [7] WHO, *Dementia: a public health priority*, in: [http://www.who.int/mental\\_health/publications/dementia\\_report\\_2012/en/](http://www.who.int/mental_health/publications/dementia_report_2012/en/), 2012.
- [8] K. Blennow, M.J. de Leon, H. Zetterberg, *Alzheimer's disease*, *Lancet*, 368 (2006) 387-403.
- [9] G. Pepeu, M.G. Giovannini, *Cholinesterase inhibitors and beyond*, *Curr. Alzheimer Res.*, 6 (2009) 86-96.
- [10] J.L. Cummings, *Treatment of Alzheimer's disease: current and future therapeutic approaches*, *Rev. Neurol. Dis.*, 1 (2004) 60-69.
- [11] J.B. Standridge, *Pharmacotherapeutic approaches to the prevention of Alzheimer's disease*, *Am. J. Geriatr. Pharmacother.*, 2 (2004) 119-132.
- [12] N. Qizilbash, J. Birks, J. Lopez Arrieta, S. Lewington, S. Szeto, *WITHDRAWN: Tacrine for Alzheimer's disease*, *The Cochrane database of systematic reviews*, (2007) CD000202.
- [13] P.B. Watkins, H.J. Zimmerman, M.J. Knapp, S.I. Gracon, K.W. Lewis, *Hepatotoxic effects of tacrine administration in patients with Alzheimer's disease*, *JAMA*, 271 (1994) 992-998.

- [14] D. Lagadic-Gossmann, M. Rissel, M.A. Le Bot, A. Guillouzo, Toxic effects of tacrine on primary hepatocytes and liver epithelial cells in culture, *Cell Biol. Toxicol.*, 14 (1998) 361-373.
- [15] C. Mount, C. Downton, Alzheimer disease: progress or profit?, *Nat. Med.*, 12 (2006) 780-784.
- [16] L. Pisani, M. Catto, F. Leonetti, O. Nicolotti, A. Stefanachi, F. Campagna, A. Carotti, Targeting monoamine oxidases with multipotent ligands: an emerging strategy in the search of new drugs against neurodegenerative diseases, *Curr. Med. Chem.*, 18 (2011) 4568-4587.
- [17] M. Sadowski, T. Wisniewski, Disease modifying approaches for Alzheimer's pathology, *Curr. Pharm. Des.*, 13 (2007) 1943-1954.
- [18] M.S. Song, D. Matveychuk, E.M. MacKenzie, M. Duchcherer, D.D. Mousseau, G.B. Baker, An update on amine oxidase inhibitors: multifaceted drugs, *Prog. Neuropsychopharmacol. Biol. Psychiatry*, 44 (2013) 118-124.
- [19] J.P. Finberg, Update on the pharmacology of selective inhibitors of MAO-A and MAO-B: focus on modulation of CNS monoamine neurotransmitter release, *Pharmacol. Ther.*, 143 (2014) 133-152.
- [20] T. Storr, K.H. Thompson, C. Orvig, Design of targeting ligands in medicinal inorganic chemistry, *Chem. Soc. Rev.*, 35 (2006) 534-544.
- [21] M.P. Cuajungco, K.Y. Faget, Zinc takes the center stage: its paradoxical role in Alzheimer's disease, *Brain Res. Brain Res. Rev.*, 41 (2003) 44-56.
- [22] D.D. Thomas, L.A. Ridnour, J.S. Isenberg, W. Flores-Santana, C.H. Switzer, S. Donzelli, P. Hussain, C. Vecoli, N. Paolucci, S. Ambs, C.A. Colton, C.C. Harris, D.D. Roberts, D.A. Wink, The chemical biology of nitric oxide: implications in cellular signaling, *Free Radic. Biol. Med.*, 45 (2008) 18-31.
- [23] T. Korcsmaros, M.S. Szalay, C. Bode, I.A. Kovacs, P. Csermely, How to design multi-target drugs, *Exp. Op. Drug Disc.*, 2 (2007) 799-808.

- [24] A. Cavalli, M.L. Bolognesi, S. Capsoni, V. Andrisano, M. Bartolini, E. Margotti, A. Cattaneo, M. Recanatini, C. Melchiorre, A small molecule targeting the multifactorial nature of Alzheimer's disease, *Angew. Chem. Int. Ed. Engl.*, 46 (2007) 3689-3692.
- [25] M.B. Youdim, J.J. Buccafusco, Multi-functional drugs for various CNS targets in the treatment of neurodegenerative disorders, *Trends Pharmacol. Sci.*, 26 (2005) 27-35.
- [26] M.L. Bolognesi, A. Cavalli, L. Valgimigli, M. Bartolini, M. Rosini, V. Andrisano, M. Recanatini, C. Melchiorre, Multi-target-directed drug design strategy: from a dual binding site acetylcholinesterase inhibitor to a trifunctional compound against Alzheimer's disease, *J. Med. Chem.*, 50 (2007) 6446-6449.
- [27] P. Camps, X. Formosa, C. Galdeano, T. Gomez, D. Munoz-Torrero, L. Ramirez, E. Viayna, E. Gomez, N. Isambert, R. Lavilla, A. Badia, M.V. Clos, M. Bartolini, F. Mancini, V. Andrisano, A. Bidon-Chanal, O. Huertas, T. Dafni, F.J. Luque, Tacrine-based dual binding site acetylcholinesterase inhibitors as potential disease-modifying anti-Alzheimer drug candidates, *Chem. Biol. Interact.*, 187 (2010) 411-415.
- [28] P. Camps, X. Formosa, C. Galdeano, D. Munoz-Torrero, L. Ramirez, E. Gomez, N. Isambert, R. Lavilla, A. Badia, M.V. Clos, M. Bartolini, F. Mancini, V. Andrisano, M.P. Arce, M.I. Rodriguez-Franco, O. Huertas, T. Dafni, F.J. Luque, Pyrano[3,2-c]quinoline-6-chlorotacrine hybrids as a novel family of acetylcholinesterase- and beta-amyloid-directed anti-Alzheimer compounds, *J. Med. Chem.*, 52 (2009) 5365-5379.
- [29] S. Butini, G. Campiani, M. Borriello, S. Gemma, A. Panico, M. Persico, B. Catalanotti, S. Ros, M. Brindisi, M. Agnusdei, I. Fiorini, V. Nacci, E. Novellino, T. Belinskaya, A. Saxena, C. Fattorusso, Exploiting protein fluctuations at the active-site gorge of human cholinesterases: further optimization of the design strategy to develop extremely potent inhibitors, *J. Med. Chem.*, 51 (2008) 3154-3170.

- [30] G. Campiani, C. Fattorusso, S. Butini, A. Gaeta, M. Agnusdei, S. Gemma, M. Persico, B. Catalanotti, L. Savini, V. Nacci, E. Novellino, H.W. Holloway, N.H. Greig, T. Belinskaya, J.M. Fedorko, A. Saxena, Development of molecular probes for the identification of extra interaction sites in the mid-gorge and peripheral sites of butyrylcholinesterase (BuChE). Rational design of novel, selective, and highly potent BuChE inhibitors, *J. Med. Chem.*, 48 (2005) 1919-1929.
- [31] M. Chioua, M. Perez, O.M. Bautista-Aguilera, M. Yanez, M.G. Lopez, A. Romero, R. Cacabelos, R.P. de la Bellacasa, S. Brogi, S. Butini, J.I. Borrell, J. Marco-Contelles, Development of HuperTacrines as Non-Toxic, Cholinesterase Inhibitors for the Potential Treatment of Alzheimer's Disease, *Mini Rev. Med. Chem.*;15(8) (2015) 648-658.
- [32] S. Butini, M. Brindisi, S. Brogi, S. Maramai, E. Guarino, A. Panico, A. Saxena, V. Chauhan, R. Colombo, L. Verga, E. De Lorenzi, M. Bartolini, V. Andrisano, E. Novellino, G. Campiani, S. Gemma, Multifunctional Cholinesterase and Amyloid Beta Fibrillization Modulators. Synthesis and Biological Investigation, *ACS Med. Chem. Lett.*, 4 (2013) 1178-1182.
- [33] S. Brogi, S. Butini, S. Maramai, R. Colombo, L. Verga, C. Lanni, E. De Lorenzi, S. Lamponi, M. Andreassi, M. Bartolini, V. Andrisano, E. Novellino, G. Campiani, M. Brindisi, S. Gemma, Disease-modifying anti-Alzheimer's drugs: inhibitors of human cholinesterases interfering with beta-amyloid aggregation, *CNS Neurosci. Ther.*, 20 (2014) 624-632.
- [34] O.M. Bautista-Aguilera, A. Samadi, M. Chioua, K. Nikolic, S. Filipic, D. Agbaba, E. Soriano, L. de Andres, M.I. Rodriguez-Franco, S. Alcaro, R.R. Ramsay, F. Ortuso, M. Yanez, J. Marco-Contelles, N-Methyl-N-((1-methyl-5-(3-(1-(2-methylbenzyl)piperidin-4-yl)propoxy)-1H-indol-2-yl)methyl)prop-2-yn-1-amine, a new cholinesterase and monoamine oxidase dual inhibitor, *J. Med. Chem.*, 57 (2014) 10455-10463.
- [35] O.M. Bautista-Aguilera, G. Esteban, M. Chioua, K. Nikolic, D. Agbaba, I. Moraleda, I. Iriepa, E. Soriano, A. Samadi, M. Unzeta, J. Marco-Contelles, Multipotent cholinesterase/monoamine oxidase

inhibitors for the treatment of Alzheimer's disease: design, synthesis, biochemical evaluation, ADMET, molecular modeling, and QSAR analysis of novel donepezil-pyridyl hybrids, *Drug Des. Dev. Ther.*, 8 (2014) 1893-1910.

[36] M.G. Kallitsakis, M. Yanez, E. Soriano, J. Marco-Contelles, D.J. Hadjipavlou-Litina, K.E. Litinas, Purine homo-N-nucleoside+coumarin hybrids as pleiotropic agents for the potential treatment of Alzheimer's disease, *Future Med. Chem.*, 7 (2015) 103-110.

[37] M. Benchekroun, L. Ismaili, M. Pudlo, V. Luzet, T. Gharbi, B. Refouvelet, J. Marco-Contelles, Donepezil-ferulic acid hybrids as anti-Alzheimer drugs, *Future medicinal chemistry*, 7 (2015) 15-21.

[38] L. Wang, G. Esteban, M. Ojima, O.M. Bautista-Aguilera, T. Inokuchi, I. Moraleda, I. Iriepa, A. Samadi, M.B. Youdim, A. Romero, E. Soriano, R. Herrero, A.P. Fernandez Fernandez, M. Ricardo Martinez, J. Marco-Contelles, M. Unzeta, Donepezil + propargylamine + 8-hydroxyquinoline hybrids as new multifunctional metal-chelators, ChE and MAO inhibitors for the potential treatment of Alzheimer's disease, *Eur. J. Med. Chem.*, 80 (2014) 543-561.

[39] S. Mann, S. Carillon, O. Breyne, A. Marquet, Total synthesis of amiclennomycin, an inhibitor of biotin biosynthesis, *Chemistry*, 8 (2002) 439-450.

[40] S. Butini, E. Guarino, G. Campiani, M. Brindisi, S.S. Coccone, I. Fiorini, E. Novellino, T. Belinskaya, A. Saxena, S. Gemma, Tacrine based human cholinesterase inhibitors: synthesis of peptidic-tethered derivatives and their effect on potency and selectivity, *Bioorg. Med. Chem. Lett.*, 18 (2008) 5213-5216.

[41] Schrödinger Suite 2012 Induced Fit Docking protocol; Glide version 5.8, Schrödinger, LLC, New York, NY, 2012; Prime version 3.1, Schrödinger, LLC, New York, NY, 2012.

[42] Maestro, version 9.3, Schrödinger, LLC, New York, NY, 2012.

[43] S. Gemma, C. Camodeca, M. Brindisi, S. Brogi, G. Kukreja, S. Kunjir, E. Gabellieri, L. Lucantoni, A. Habluetzel, D. Taramelli, N. Basilico, R. Gualdani, F. Tadini-Buoninsegni, G.

Bartolommei, M.R. Moncelli, R.E. Martin, R.L. Summers, S. Lamponi, L. Savini, I. Fiorini, M. Valoti, E. Novellino, G. Campiani, S. Butini, Mimicking the intramolecular hydrogen bond: synthesis, biological evaluation, and molecular modeling of benzoxazines and quinazolines as potential antimalarial agents, *J. Med. Chem.*, 55 (2012) 10387-10404.

[44] M. Anzini, A. Di Capua, S. Valenti, S. Brogi, M. Rovini, G. Giuliani, A. Cappelli, S. Vomero, L. Chiasserini, A. Segà, G. Poce, G. Giorgi, V. Calderone, A. Martelli, L. Testai, L. Sautebin, A. Rossi, S. Pace, C. Ghelardini, L. Di Cesare Mannelli, V. Benetti, A. Giordani, P. Anzellotti, M. Dovizio, P. Patrignani, M. Biava, Novel analgesic/anti-inflammatory agents: 1,5-diarylpyrrole nitrooxyalkyl ethers and related compounds as cyclooxygenase-2 inhibiting nitric oxide donors, *J. Med. Chem.*, 56 (2013) 3191-3206.

[45] A. Cappelli, M. Manini, S. Valenti, F. Castriconi, G. Giuliani, M. Anzini, S. Brogi, S. Butini, S. Gemma, G. Campiani, G. Giorgi, L. Mennuni, M. Lanza, A. Giordani, G. Caselli, O. Letari, F. Makovec, Synthesis and structure-activity relationship studies in serotonin 5-HT<sub>1A</sub> receptor agonists based on fused pyrrolidone scaffolds, *Eur. J. Med. Chem.*, 63 (2013) 85-94.

[46] S. Giovani, M. Penzo, S. Brogi, M. Brindisi, S. Gemma, E. Novellino, L. Savini, M.J. Blackman, G. Campiani, S. Butini, Rational design of the first difluorostatone-based PfSUB1 inhibitors, *Bioorg. Med. Chem. Lett.*, 24 (2014) 3582-3586.

[47] S.Y. Son, J. Ma, Y. Kondou, M. Yoshimura, E. Yamashita, T. Tsukihara, Structure of human monoamine oxidase A at 2.2-Å resolution: the control of opening the entry for substrates/inhibitors, *Proc. Natl. Acad. Sci. U.S.A.*, 105 (2008) 5739-5744.

[48] QikProp, version 3.5, Schrödinger, LLC, New York, NY, 2012.

[49] A.I. Bush, The metal theory of Alzheimer's disease, *J. Alzheimers Dis.*, 33 Suppl 1 (2013) S277-281.

- [50] D.J. Bonda, X. Wang, G. Perry, A. Nunomura, M. Tabaton, X. Zhu, M.A. Smith, Oxidative stress in Alzheimer disease: a possibility for prevention, *Neuropharmacol.*, 59 (2010) 290-294.
- [51] P.W. Mantyh, J.R. Ghilardi, S. Rogers, E. DeMaster, C.J. Allen, E.R. Stimson, J.E. Maggio, Aluminum, iron, and zinc ions promote aggregation of physiological concentrations of beta-amyloid peptide, *J. Neurochem.*, 61 (1993) 1171-1174.
- [52] F. Hane, Z. Leonenko, Effect of metals on kinetic pathways of amyloid-beta aggregation, *Biomolecules*, 4 (2014) 101-116.
- [53] M. Zhou, N. Panchuk-Voloshina, A one-step fluorometric method for the continuous measurement of monoamine oxidase activity, *Anal. Biochem.*, 253 (1997) 169-174.
- [54] G.L. Ellman, K.D. Courtney, V. Andres, Jr., R.M. Feather-Stone, A new and rapid colorimetric determination of acetylcholinesterase activity, *Biochem. Pharmacol.*, 7 (1961) 88-95.
- [55] Y. Cheng, W.H. Prusoff, Relationship between the inhibition constant ( $K_1$ ) and the concentration of inhibitor which causes 50 per cent inhibition ( $I_{50}$ ) of an enzymatic reaction, *Biochem. Pharmacol.*, 22 (1973) 3099-3108.
- [56] C.Y. Huang, Determination of binding stoichiometry by the continuous variation method: the Job plot, *Methods Enzymol.*, 87 (1982) 509-525.
- [57] M. Chioua, D. Sucunza, E. Soriano, D. Hadjipavlou-Litina, A. Alcazar, I. Ayuso, M.J. Oset-Gasque, M.P. Gonzalez, L. Monjas, M.I. Rodriguez-Franco, J. Marco-Contelles, A. Samadi, Alpha-aryl-N-alkyl nitrones, as potential agents for stroke treatment: synthesis, theoretical calculations, antioxidant, anti-inflammatory, neuroprotective, and brain-blood barrier permeability properties, *J. Med. Chem.*, 55 (2012) 153-168.
- [58] A. Davalos, C. Gomez-Cordoves, B. Bartolome, Extending applicability of the oxygen radical absorbance capacity (ORAC-fluorescein) assay, *J. Agric. Food Chem.*, 52 (2004) 48-54.

- [59] T. Symeonidis, M. Chamilos, D.J. Hadjipavlou-Litina, M. Kallitsakis, K.E. Litinas, Synthesis of hydroxycoumarins and hydroxybenzo[f]- or [h]coumarins as lipid peroxidation inhibitors, *Bioorg. Med. Chem. Lett.*, 19 (2009) 1139-1142.
- [60] MacroModel, version 9.9, Schrödinger, LLC, New York, NY, 2012.
- [61] W.L. Jorgensen, D.S. Maxwell, J. TiradoRives, Development and testing of the OPLS all atom force field on conformational energetics and properties of organic liquids *J. Am. Chem. Soc.*, 118 (1996) 11225-11236.
- [62] G.A. Kaminski, R.A. Friesner, J. Tirado-Rives, W.L. Jorgensen, Evaluation and reparametrization of the OPLS-AA force field for proteins via comparison with accurate quantum chemical calculations on peptides, *J. Phys. Chem. B*, 105 (2001) 6474-6487.
- [63] W.C. Still, A. Tempczyk, R.C. Hawley, T. Hendrickson, Semianalytical Treatment of Solvation for Molecular Mechanics and Dynamics, *J. Am. Chem. Soc.*, 112 (1990) 6127-6129.
- [64] W. Sherman, T. Day, M.P. Jacobson, R.A. Friesner, R. Farid, Novel procedure for modeling ligand/receptor induced fit effects, *Journal of medicinal chemistry*, 49 (2006) 534-553.
- [65] Prime, version 3.1, Schrödinger, LLC, New York, NY, 2012.
- [66] M. Brindisi, S. Gemma, S. Kunjir, L. Di Cerbo, S. Brogi, S. Parapini, S. D'Alessandro, D. Taramelli, A. Habluetzel, S. Tapanelli, S. Lamponi, E. Novellino, G. Campiani, S. Butini, Synthetic spirocyclic endoperoxides: new antimalarial scaffolds, *Med. Chem. Comm.*, 6 (2015) 357-362.
- [67] S. Giovani, M. Penzo, S. Butini, M. Brindisi, S. Gemma, E. Novellino, G. Campiani, M. Blackman, S. Brogi, Plasmodium falciparum Subtilisin-like Protease 1: Discovery of Potent Difluorostatone-based Inhibitors, *RSC Adv.*, 5(29) (2015) 22431-22448.
- [68] M. Brindisi, S. Butini, S. Franceschini, S. Brogi, F. Trotta, S. Ros, A. Cagnotto, M. Salmona, A. Casagni, M. Andreassi, S. Saponara, B. Gorelli, P. Weikop, J.D. Mikkelsen, J. Scheel-Kruger, K. Sandager-Nielsen, E. Novellino, G. Campiani, S. Gemma, Targeting Dopamine D3 and Serotonin 5-

HT1A and 5-HT2A Receptors for Developing Effective Antipsychotics: Synthesis, Biological Characterization, and Behavioral Studies, *J. Med. Chem.*, 57 (2014) 9578-9597.

## **Chapter V.**

**“Biological assessment of the novel multi-target compound DPH-4, a donepezil-propargylamine+8-hydroxyquinoline hybrid with anti-A $\beta$  aggregation, antioxidant, anti-inflammatory and anti-apoptotic properties for potential use in Alzheimer’s disease”**



**Biological assessment of the novel multi-target compound DPH-4, a donepezil-propargylamine+8-hydroxyquinoline hybrid with anti-A $\beta$  aggregation, antioxidant, anti-inflammatory and anti-apoptotic properties for potential use in Alzheimer's disease.**

Gerard Esteban<sup>1</sup>, José Marco-Contelles<sup>2</sup>, Mercedes Unzeta<sup>1</sup>

<sup>1</sup>*Institut de Neurociències i Departament de Bioquímica i Biologia Molecular. Edifici M, Facultat de Medicina. Universitat Autònoma de Barcelona (UAB), Bellaterra, Barcelona (Spain).*

<sup>2</sup>*Laboratorio de Química Médica (IQOG, CSIC), C/ Juan de la Cierva 3, 28006-Madrid (Spain).*

**Short title:** Biological assessment of DPH-4 as multi-target drug in AD treatment.

\***Corresponding authors:** Mercedes Unzeta. Neurosciences Institute and Department of Biochemistry and Molecular Biology, Universitat Autònoma de Barcelona (UAB), 08193 Bellaterra (Barcelona), Spain. Telephone: +34 93 581 1523; Fax: +34 93 581 1573. E-mail: [mercedes.unzeta@uab.es](mailto:mercedes.unzeta@uab.es)

**Authorship contributions:**

G Esteban performed the experimental part.

M Unzeta and JL Marco designed the research study.

All authors contributed to data analysis and paper drafting.

**Key Words:** Multitarget-directed ligands (MTDLs); biological assessment, anti- $\beta$ -amyloid aggregation, antioxidant, anti-inflammatory, anti-apoptotic, Alzheimer's disease therapy.

## **Abstract**

Alzheimer's disease (AD), the most common form of adult onset dementia, is an age-related neurodegenerative disorder characterised by progressive memory loss, decline in language skills and other cognitive impairments. Although its etiology is not completely known yet, several factors including  $\beta$ -amyloid deposits,  $\tau$ -protein phosphorylation, oxidative stress, excitotoxicity and neuroinflammation, metal dyshomeostasis, and deficits of neurotransmitter acetylcholine are considered to play significant roles in the pathophysiology of AD. This complex etiology may account for the failure of anti-AChE inhibitors in AD therapy, which are focused on the enhancement of the cholinergic neurotransmission in the brain. Based on the “one molecule, multiple target” paradigm, we have previously designed and synthesised a new series of MTDL molecules as donepezil-propargylamines+8-hydroxyquinoline hybrids. Among them, derivative DPH-4 exhibited the most interesting pharmacological profile. In this work, the effect of DPH-4 on  $A\beta$  aggregation, oxidative stress, inflammation, and apoptosis has been assessed. The results obtained allow to confirm DPH-4 as a multifunctional molecule with potential interest in AD therapy.

## 1. Introduction

Alzheimer's disease (AD), the most common form of adult onset dementia, is an age-related neurodegenerative disorder characterised by progressive memory loss, decline in language skills and other cognitive impairments. Although its etiology is not completely known to date, several factors including  $\beta$ -amyloid deposits,  $\tau$ -protein phosphorylation, oxidative stress (OS), excitotoxicity and neuroinflammation, metal dyshomeostasis and deficits of neurotransmitter acetylcholine (ACh) are considered to play significant roles in the pathophysiology of this disease [1]. This complex etiology may account for the failure of AChE inhibitors in the AD therapy, which effect is focused on the enhancement of the cholinergic neurotransmission in the brain by increasing the levels of ACh in the synaptic transmission [2].

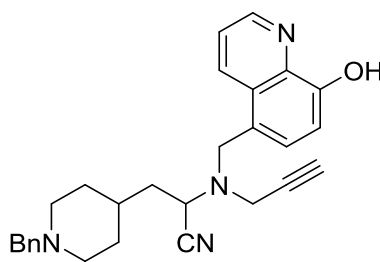
In addition, OS also appears as a major contributor in the progression of AD pathogenesis. Experimental evidence indicates that a dysregulation of the redox state strongly participates in early stage of AD by activating multiple cell signaling pathways that contribute to the initial progression of the neurodegenerative process [3]. Increased levels of oxidative markers of biomolecules including proteins, lipids, carbohydrates, and nucleic acids, have been detected in a number of studies [4]. In addition, levels of antioxidant enzymes were found to be altered in specific AD brain regions [4]. Consequently, the "OS hypothesis of AD" has emerged as a relevant factor in both the onset and progression of this disease. Aggregation and accumulation of amyloid beta protein ( $A\beta$ ) is one of the main pathological event that contributes to neuronal death in this neurodegenerative disorder. This is a metal-binding protein and metals such as iron, copper or zinc, present in brain, are able to promote and accelerate its aggregation in a situation of metal dyshomeostasis, a factor underlying AD pathology. Besides, metals are also able to generate hydrogen peroxide ( $H_2O_2$ ) when combining with  $A\beta$ , hence contributing to the formation of OS [5, 6].

Taken these facts into account, increasing levels of OS appear as a major alteration in early stages in AD pathology and are enhanced by the metals presence throughout the progression of the disease [7]. Consequently, both OS and biometal dyshomeostasis counteraction might be an appropriate potential therapeutic target for AD [8].

Based on the "one molecule, multiple target" paradigm, we have previously reported a series of new MTDL molecules, as donepezil+propargylamine+8-hydroxyquinoline-containing hybrids bearing dual ChE/MAO inhibitory activities. Moreover, these

molecules were described to exhibit strong metal-chelating properties towards biometals Cu(II), Fe(III) and Zn(II) by UV-VIS spectrometry as well as an ability to restore scopolamine-induced cognitive deficits in mice, as appealing pharmacological features in AD treatment [9].

Among the series of MTDL molecules tested, DPH-4 (Fig. 1) exhibited a promising pharmacological profile, with an additional beneficial effect on stroke condition reported to protect brain endothelial cells from damage induced by oxygen—glucose deprivation (OGD) and reoxygenation and to effectively protect against this injury in presence of A $\beta$  as a model of AD pathology [10].



**DPH4**

**Fig. 1.** Chemical structure of multi-target-directed ligand DPH-4.

Taken all these findings into account, herein we report a further biological assessment of multi-target DPH-4 as a potential drug for use in AD therapy. Its combination of inhibition of key enzymes of interest in AD, an anti-A $\beta$  aggregating effect, antioxidant behaviour, an anti-inflammatory effect and a blockade of the apoptotic pathway are fully reported in the present work. These results will allow to confirm this MTDL as a suitable candidate for its potential use in the prevention or delay of the cognitive decline present in AD pathology.

## 2. Results and discussion

### 2.1. Inhibition of human monoamine oxidases and cholinesterases by DPH-4

The activity of multi-target DPH-4 as an inhibitor of human recombinant monoamine oxidases A and B was assessed fluorometrically [11], whereas inhibition of human recombinant cholinesterases AChE and BuChE was determined by the use of Ellman's method [12].

From dose-response activities, equimolar IC<sub>50</sub> values in low micromolar range were obtained with DPH-4 as an inhibitor of both human MAO A and MAO B (3.8 and 3.0 μM, respectively) and human cholinesterases AChE and BuChE (4.0 and 7.2, respectively), as shown in Table 1. Remarkably, these values are slightly lower than those previously described using different source of enzyme [9].

In comparison to donepezil, DPH-4 exhibited was strongly more active *h*MAO A inhibitor (≥263-fold) and 5.0-fold more potent at inhibiting *h*MAO B. However, DPH-4 exhibited less inhibitory activity than multi-target M30 (103-fold and 53-fold, respectively).

As a *h*AChE inhibitor, DPH-4 was significantly less active than donepezil (444-fold) but equally potent at inhibiting *h*BuChE. Yet, DPH-4 was a potent ChE inhibitor compared to M30, inactive on these enzymes.

**Table 1.** Dose-response values (IC<sub>50</sub>, in μM) and selectivity indexes (SI) of compounds DPH-4, donepezil and M30 as human monoamine oxidases and human cholinesterases inhibitors.

<b>Compound</b>	<i>h</i> MAO A <sup>a</sup>	<i>h</i> MAO B <sup>a</sup>	SI <sup>b</sup>	<i>h</i> AChE <sup>a</sup>	<i>h</i> BuChE <sup>a</sup>	SI <sup>c</sup>
<b>DPH-4</b>	3.8 ± 0.9	3.0 ± 0.6	0.79	4.0 ± 0.8	7.2 ± 0.7	0.55
<b>Donepezil</b>	≥1000	15.2 ± 1.7	<0.015	0.009 ± 0.001	7.5 ± 0.8	0.0012
<b>M30*</b>	0.037 ± 0.01	0.057 ± 0.02	1.54	≥1000	≥1000	≥1

<sup>a</sup>Values obtained after 30 minutes of pre-incubation expressed as the mean ± S.E.M. of at least three independent experiments. <sup>b</sup>*h*MAO A selectivity index: [IC<sub>50</sub>(*h*MAO-B)]/[IC<sub>50</sub>(*h*MAO-A)]. <sup>c</sup>*h*BuChE selectivity index: [IC<sub>50</sub>(*h*AChE)]/[IC<sub>50</sub>(*h*BuChE)]. \*Values extracted from [13].

In conclusion, DPH-4 displayed an ability to inhibit human both AChE and BuChE, the main enzymes involved in AD according to the “cholinergic hypothesis” and therefore contributing to re-establish the cholinergic transmission by its inhibition. Moreover, because of the presence of a propargylamine group, DPH-4 is also able to inhibit both MAO isoforms, exhibiting a neuroprotective effect. As mentioned, all these enzymes are inhibited by DPH-4 with similar IC<sub>50</sub> values at low micromolar range, which seems of great pharmacological value in terms of pharmacokinetics and administration considerations, permitting, with a single dose, a concurrent interaction with multiple enzymes involved in AD pathology.

## 2.2. Assessment of anti-amyloid activity of DPH-4

The main histopathological hallmark of AD is the anomalous extra-neuronal deposits of  $\beta$ -amyloid protein forming the senile plaques. However, relatively weak correlations between fibrillar plaque density and dementia severity are found in AD brains whereas a correlation between soluble  $A\beta$  levels, synaptic loss and cognitive impairment was strong [14]. In this context, therapeutic strategies targeting different steps in the aggregation process of  $A\beta$  have already been performed and some of them are even being currently tested in clinical trials [15]. Therefore, the overwhelming role of  $A\beta$  aggregation and deposition in the progression of AD pathogenesis encouraged the comprehensive investigation of the potential anti-amyloid activity of multifunctional compound DPH-4.

The activity of DPH-4 against *in vitro*  $A\beta_{1-42}$  aggregation was studied by using the thioflavin T method [16]. Aggregation reactions were followed over time (0-500 minutes) in absence or presence of compounds DPH-4 or clioquinol (CQ), used as standard. As shown in Fig. 2A, a significant reduction of  $28.6 \pm 5.6$  % and  $32.1 \pm 12.2$  % of the levels of  $A\beta_{42}$  self-aggregation ( $20\mu\text{M}$ ) was observed with  $5\mu\text{M}$  DPH-4 and  $25\mu\text{M}$  CQ, respectively. When  $A\beta_{42}$  was incubated in presence of  $0.02\mu\text{M}$  *hAChE* (ratio *AChE*: $A\beta$ , 1:1000) (Fig. 2B), an increase of  $29.6 \pm 7.2$  % of the FU was detected as an activity exerted through the peripheral anion site (PAS) present in the enzyme [17]. In presence of either DPH-4 or CQ, *hAChE*-mediated  $A\beta_{42}$  aggregation was significantly decreased by  $27.7 \pm 1.8$  % and  $45.1 \pm 12.5$  %, respectively.

These results were confirmed by SDS-PAGE analysis of the assayed samples using the 6E10 antibody, which specifically binds to the *N*-terminal of  $A\beta$  peptide, and compared to control samples. As shown in Fig. E and F, the co-incubation of  $A\beta_{42}$  with DPH-4 produced a dose-dependent decrease of the highly-aggregated species (fibers and oligomers) ( $\geq 25$  KDa) from 69.3 % of signal in control samples to 61.1 % and 58.1 % with 5 and  $10\mu\text{M}$  DPH-4, respectively. However, no apparent effect was observed in the relative amount of trimers. Conversely, low-MW species (monomers and dimers) ( $< 10$  KDa) were increased dose-dependently from 22.4 % in control to 27.1 % with  $5\mu\text{M}$  and 32.3 % with  $10\mu\text{M}$  DPH-4.

In addition, the expression levels of amyloid precursor protein (APP) were also analysed in lysates of human SH-SY5Y cells treated with 0.3 to  $10\mu\text{M}$  DPH-4 for 24 hours. As shown in Fig. 2D, APP levels were significantly decreased when DPH-4 concentrations around  $2.5\mu\text{M}$  were used. This concentration range was similar to that

able to inhibit the four enzymes, AChE, BuChE and MAO (A and B) previously described.

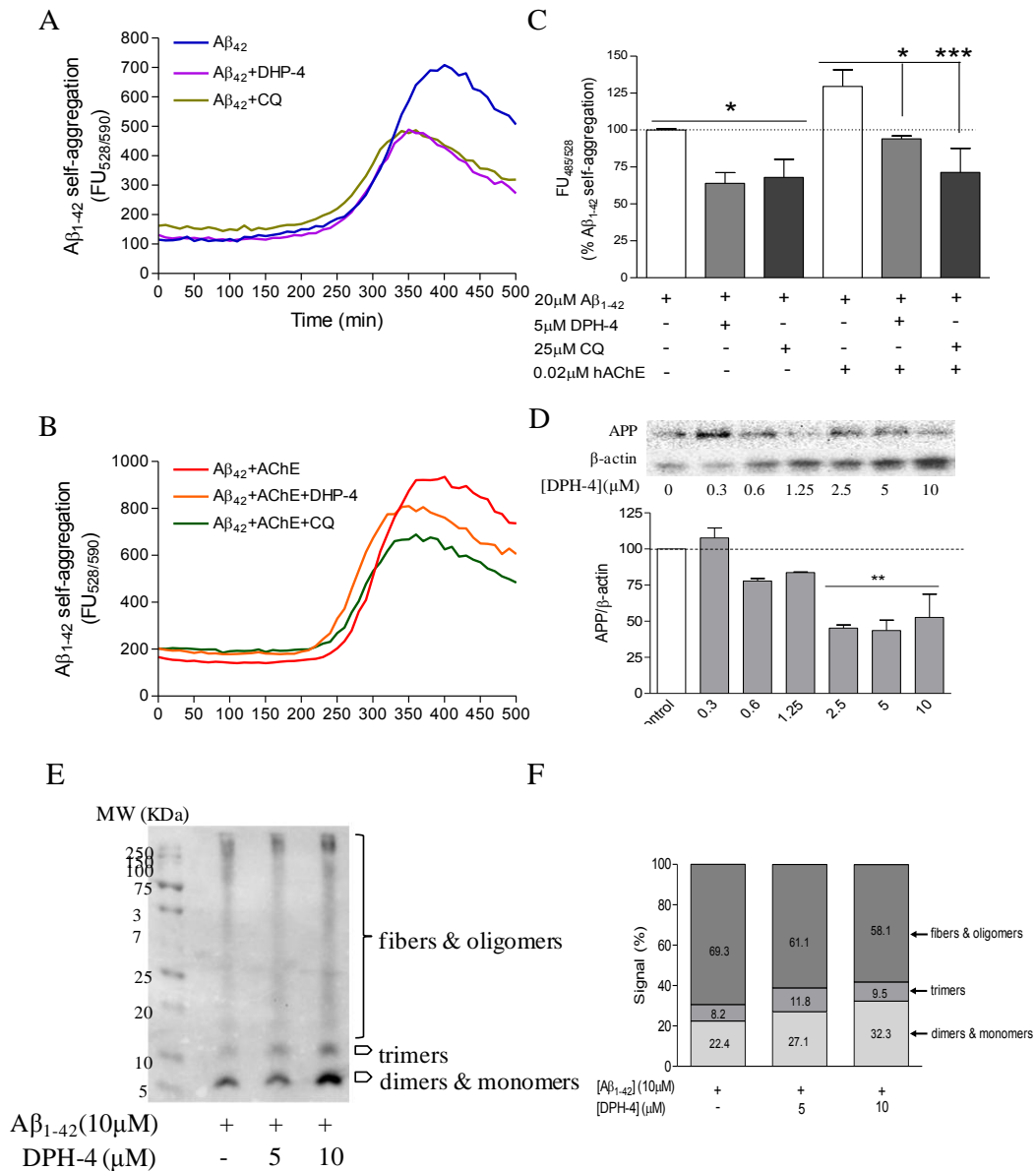


**Fig. 2.** Anti-amyloid activity of DPH-4. Effects of 5 μM DPH-4 and 25 μM CQ on both *in vitro* Aβ<sub>1-42</sub> self- (A) and hAChE-mediated (B) aggregations (20μM) by using the thioflavin T method monitored at 37°C over time. (C and D) Dose-dependent reduction of the basal APP protein levels in SH-SY5Y cells by DPH-4. Values are expressed as the mean ± S.E.M. of at least three independent experiments.

### 2.3. Assessment of the antioxidant properties of DPH-4

It has been widely reported that oxidative stress (OS) is one of the main factor that contributes to the neurodegenerative diseases [18] and it has been described that perhaps OS is the earliest feature in AD brain [19], which results from an imbalance of the pro-

oxidant/antioxidant homeostasis. In AD brain, the combination of the high metabolic rate, the low concentration of antioxidant enzymes such as glutathione peroxidase (GPx) and catalase together with the high proportion of polyunsaturated fatty acids make the brain tissue particularly susceptible to oxidative damage [20]. The role of OS in AD has been also confirmed by the significant amount of lipid peroxidation detected in brain of AD patients as well as the increased levels of 4-hydroxynonenal found in post-mortem cerebrospinal fluid of these patients [21, 22, 23]. Furthermore, ROS has been reported to mediate amyloid  $\beta$ -protein damage [24]. Thus, and considering the main involvement of OS in AD, the antioxidant properties of DPH-4 were assessed by using different experimental approaches.

First, the capacity of this multi-target compound to capture free-radical species was evaluated by the ORAC-FL (Oxygen Radical Absorbance Capacity by Fluorescence) method [25] (Fig. 3A). Trolox, an analogue of vitamin E, was used as standard and results were expressed as trolox equivalents ( $\mu\text{mol}$  of trolox/ $\mu\text{mol}$  of tested compound). Melatonin, a well-known antioxidant compound was used as standard, which exhibited an ORAC value of  $2.5 \pm 0.1$ . Compared to trolox, compound DPH-4 showed a highly significant antioxidant capacity to capturing free-radical species with an ORAC value of  $5.0 \pm 0.6$ . Next, the radical scavenger activity (RSA) of DPH-4 and trolox was measured on the scavenging activity of the stable 1,1-diphenyl-2-picrylhydrazyl (DPPH) free radical according to the method described by Brand-Williams [26] (Fig. 3B). Both DPH-4 and trolox exhibited dose-dependent scavenger activity, but no significant effect was observed with DPH-4 concentrations lower than  $100\mu\text{M}$ . Inhibition of lipid peroxidation (LP) *in vitro* was also assessed by using the water-soluble azo compound APPH (2,2'-azobis(2-amidinopropane) dihydrochloride), used as a clean and controllable source of thermally-produced alkyl peroxy free radicals, as initiator of free radical reactions of the acid oxidation of linoleic acid. As shown in Fig. 3C and 3D, both trolox and DPH-4 diminished LP by  $63.4 \pm 6.5\%$  and  $79.2 \pm 8.5\%$ , respectively with similar induction times ( $T_{\text{inh}}$ ), as representing periods in which antioxidants inhibit lipid peroxidation by reacting with APPH-derived peroxy radicals, expressed in minutes.

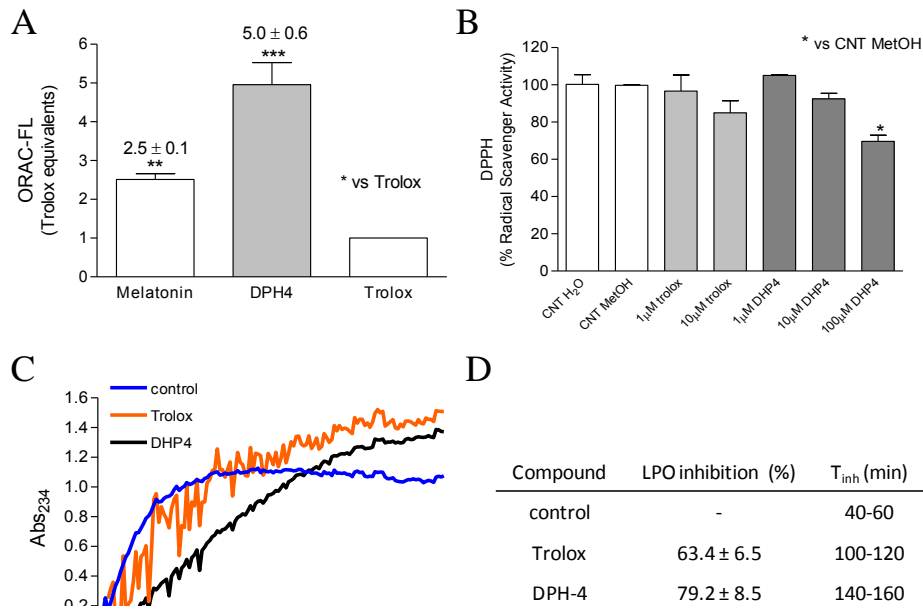


**Fig. 3.** Antioxidant activity of DPH-4 by different *in vitro* assays. (A) Oxygen radical absorbance capacity (ORAC) of DPH-4 and melatonin expressed as trolox equivalents. (B) Radical scavenger activity (RSA) of DPH-4 and trolox determined by the DPPH radical method. (C and D) Inhibition of linoleic acid lipid peroxidation (LPO, %) and inhibition time of DPH-4 and trolox using APPH as a free radical initiator. Values are expressed as the mean ± S.E.M. of at least three independent experiments.

#### 2.4. Neuroprotection of H<sub>2</sub>O<sub>2</sub>-damaged SH-SY5Y cells by DPH-4

The antioxidant properties of DPH-4 previously found by different *in vitro* assays were confirmed by the finding of potent neuroprotective properties in cell culture of human neuroblastoma SH-SY5Y cells damaged with H<sub>2</sub>O<sub>2</sub>.

Cultured SH-SY5Y cells were pre-treated with either 5 μM or 10 μM DPH-4 for one hour and treated with 250 μM or 500 μM H<sub>2</sub>O<sub>2</sub> for 24 hours. At the end of treatment times, cell viability was measured by three assays: MTT, LDH and Hoechst staining. As shown in Fig. 4A, DPH-4 was able to almost fully recover the NAD(P)H-dependent oxidoreductase activity in cells damaged with H<sub>2</sub>O<sub>2</sub> concentrations as high as 500 μM measured by MTT assay. This neuroprotection was also observed by the assessment of cytoplasmic enzyme lactate dehydrogenase (LDH) activity released into the medium (Fig. 4B). Not surprisingly, LDH activity was significantly increased after the treatment with H<sub>2</sub>O<sub>2</sub> as an indicator of cell death. However, in cells pre-treated with DPH-4, LDH activity in the medium was found significantly decreased in a dose-dependent manner. Finally, cell viability was also investigated by Hoechst 33258 staining (Fig. 4C and 4D).

The number of nuclei per field highly depleted upon the treatment with 250  $\mu\text{M}$   $\text{H}_2\text{O}_2$  for 24 hours was significantly increased when cells were pre-treated with 5  $\mu\text{M}$  DPH-4.

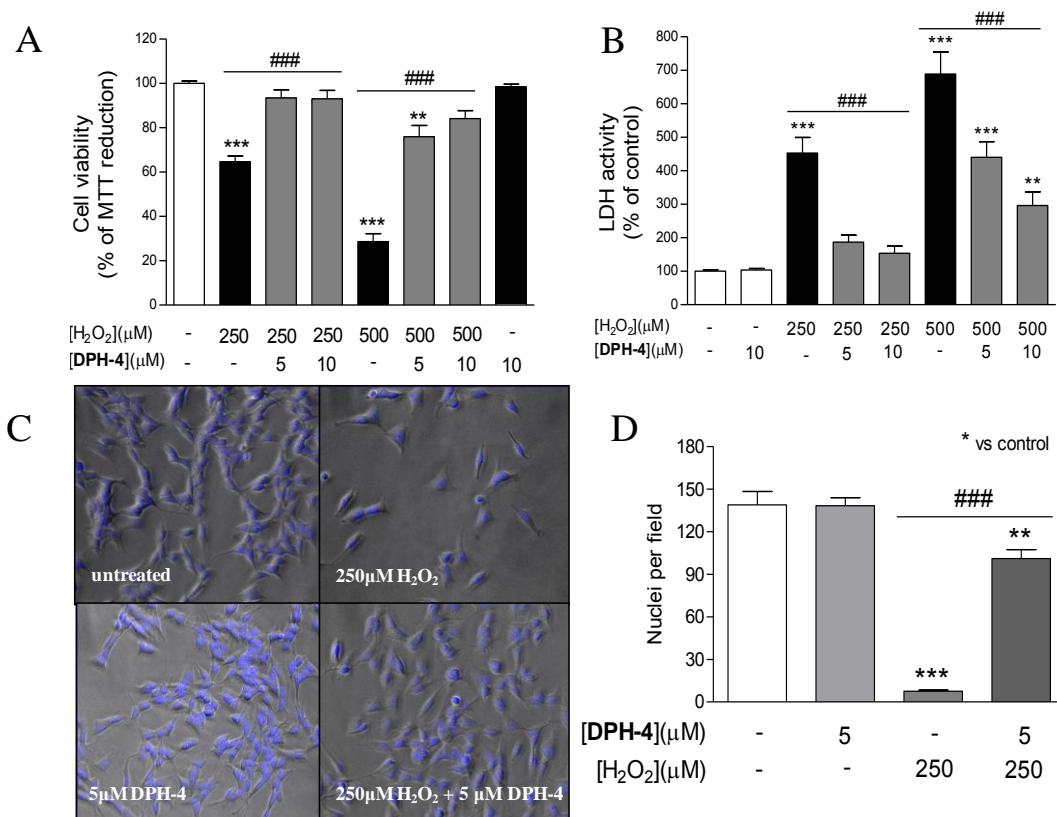


**Fig. 4.** Neuroprotective effect of DPH-4 in human SH-SY5Y cells. (A and B) Protection of DPH-4 in  $\text{H}_2\text{O}_2$ -induced toxicity in SH-SY5Y cells by MTT and LDH cell viability assays. (C and D) Hoechst staining images and quantification of nuclei of  $\text{H}_2\text{O}_2$ -damaged SH-SY5Y cells pre-treated with 5  $\mu\text{M}$  DPH-4. Values are expressed as the mean  $\pm$  S.E.M. of at least three independent experiments.

### 2.5. Prevention of ROS and $\text{O}_2^-$ generation in $\text{H}_2\text{O}_2$ -treated SH-SY5Y cells by DPH-4

The prevention of ROS formation and anion superoxide production in  $\text{H}_2\text{O}_2$ -damaged SH-SY5Y cells by DPH-4 was determined using dichlorofluorescein (DCF) and dihydroethidium (DHE) *in vitro* assays, respectively. After 3-hour co-treatment of either 250  $\mu\text{M}$  or 500  $\mu\text{M}$   $\text{H}_2\text{O}_2$  and 5  $\mu\text{M}$  or 10  $\mu\text{M}$  DPH-4, a dose-response effect was observed with DPH-4 able to significantly reduce both ROS and anion superoxide levels (Fig 5A and 5B). Interestingly, these effects were observed at compound concentrations similar to those previously determined active at inhibiting both MAO and ChE activities.

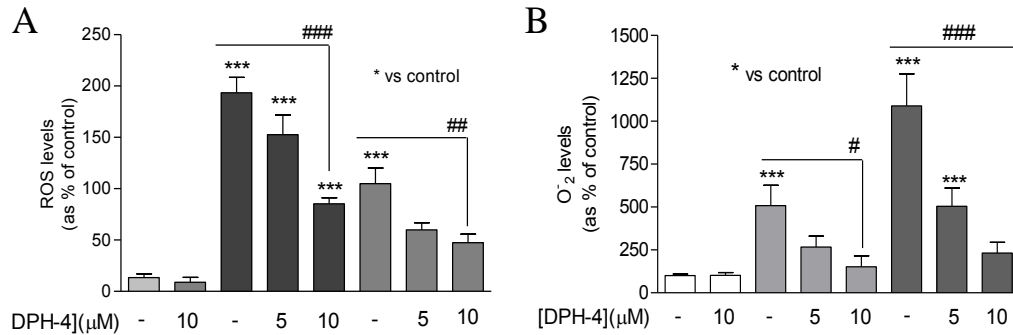


**Fig. 5.** Prevention of ROS (A) and anion superoxide (B) production in  $\text{H}_2\text{O}_2$ -treated SH-SY5Y cells pre-treated with DPH-4, detected by the use of DCF and DHE *in vitro* assays, respectively. Values are expressed as the mean  $\pm$  S.E.M. of at least three independent experiments.

### 2.6. Induction on the expression of antioxidant enzymes

In order to elucidate the mechanism of DPH-4 neuroprotection observed against  $\text{H}_2\text{O}_2$  toxicity as well as the capacity to reduce the levels of ROS and  $\text{O}_2^-$ , the expression of antioxidant enzymes superoxide dismutase-1 (SOD-1), catalase and glutathione peroxidase-1 (GPx) was studied in undamaged SH-SY5Y cells treated with an array of DPH-4 concentrations (0-10  $\mu\text{M}$ ) for 24 hours.

As shown in Fig. 6A, only in low concentrations of DPH-4 (0.62 and 1.25  $\mu\text{M}$ ) a significant increase on the expression of GPx levels was identified, an enzyme that reduces lipid hydroperoxides to alcohol and  $\text{H}_2\text{O}_2$  to water. In all compound concentrations tested, the levels of this enzyme were found higher than those untreated. Conversely, a tightly dose-dependent effect of DPH-4 in SOD-1 levels was found (Fig. 6B), which expression was significantly increased at the highest compound concentrations tested (5 and 10  $\mu\text{M}$ ). SOD-1 catalyses the dismutation of superoxide radical into either molecular oxygen (mediated by metals  $\text{Cu}^{2+}$ ,  $\text{Mn}^{3+}$ ,  $\text{Fe}^{3+}$  and  $\text{Ni}^{3+}$ ) or  $\text{H}_2\text{O}_2$  (mediated by  $\text{Cu}^+$ ,  $\text{Mn}^{2+}$ ,  $\text{Fe}^{2+}$  and  $\text{Ni}^{2+}$ ). However, although increases in the expression levels of catalase were found in all tested concentrations of DPH-4, no significant changes were observed (Fig. 6C). Catalase is an enzyme that catalyses the decomposition of  $\text{H}_2\text{O}_2$  to water and oxygen mediated by the presence of iron, which is attached to the heme group of the enzyme.

Next, the expression levels of nuclear factor (erythroid-derived 2)-like 2 (Nrf-2) in SH-SY5Y cells were studied over time (0-24 hours) upon single-dose treatment of 5  $\mu\text{M}$  DPH-4 (Fig. 6D). Nrf-2 is a transcription factor that regulates the expression of a

number of cytoprotective proteins including NAD(P)H dehydrogenase [quinone] 1 (NQO-1), glutamate cysteine ligase (GCL) or heme oxygenase-1 (HO-1). Only a significant increase of the Nrf-2 levels was observed after 8 hours of treatment with DPH-4 but the levels of this transcription factor remained higher than control from 4 hours.

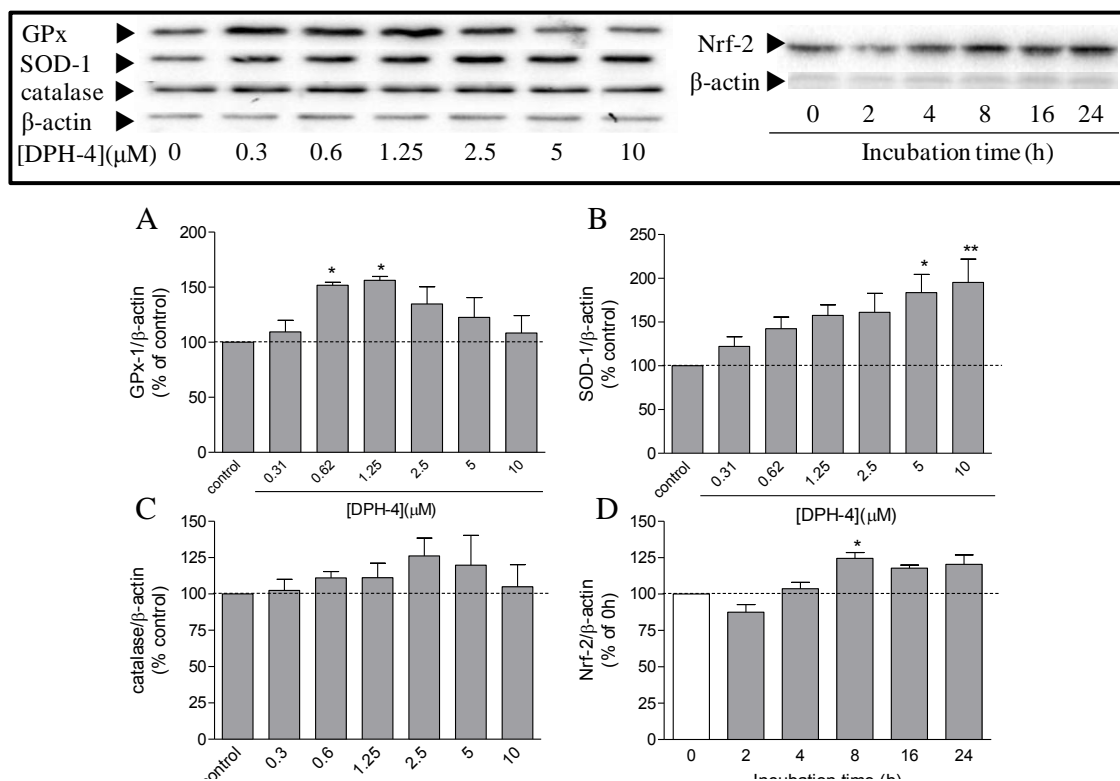


**Fig. 6.** Dose-dependent expression of antioxidant enzymes glutathione peroxidase-1 (A), superoxide dismutase-1 (B), catalase (C) and the time-dependent expression of the cellular regulator of resistance to oxidants Nrf-2(D) in SH-SY5Y cells treated with DPH-4. Values are expressed as the mean  $\pm$  S.E.M. of at least three independent experiments.

It has been reported that the presence of a propargylamine group in one molecule confers significant antioxidant potency arising from the increase in the activity of catalase, SOD-1 and GPx enzymes [27]. Moreover, the presence of a propargyl group in the DPH-4 might be responsible for its antioxidant behaviour.

### 2.7. Anti-apoptotic effect of DPH-4

Some other MTDL containing a propargyl group has been previously described to be able to maintain the mitochondrial membrane potential ( $\Psi_m$ ) and to inhibit the opening

of the permeability transition pore (PTP), hence showing an anti-apoptotic behaviour [28, 29]. In this regard, the potential inhibitory role in the apoptosis process of DPH-4, as a propargyl-containing compound, was studied. Then, SH-SY5Y cells were pre-treated with DPH-4 and lesioned with 250 $\mu$ M H<sub>2</sub>O<sub>2</sub> for 24 hours. After treatment, levels of full-length poly-(ADP-ribose) polymerase (PARP) were found significant decreased as induction of DNA damage while pre-treated cells with DPH-4 exhibited a dose-dependent increase of those levels (Fig. 7A).

Also, the levels of DEDV-directed caspase-like activity in SH-SY5Y lysates were studied (Fig. 7B). The activity of caspase, responsible for chromatin condensation and DNA fragmentation, increased by 5.5-fold in H<sub>2</sub>O<sub>2</sub>-treated samples, suggesting an activation of the caspase-like pathway under these experimental conditions. Conversely, in cells pre-treated with either 5 or 10  $\mu$ M DPH-4, those levels were significantly decreased, with a similar effect detected between the two compound concentrations tested.

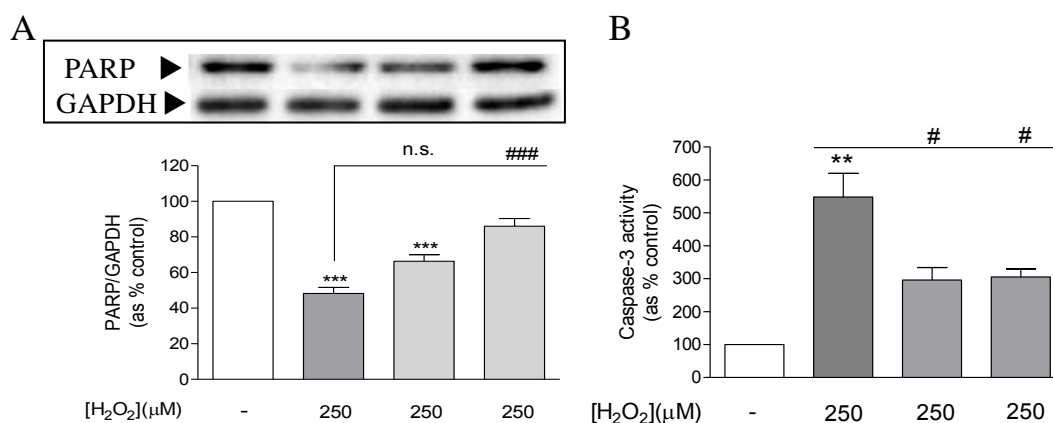


**Fig. 7.** Anti-apoptotic effect of DPH-4 in SH-SY5Y cells. (A) Increase of the expression of full-length PARP levels in H<sub>2</sub>O<sub>2</sub>-damaged SH-SY5Y cells. (B) Decrease in the activity levels of caspase-3 in H<sub>2</sub>O<sub>2</sub>-injured SH-SY5Y cell pre-treated with DPH-4. Values are expressed as the mean  $\pm$  S.E.M. of at least three independent experiments.

Altogether, these results suggest that DPH-4 exerts an anti-apoptotic activity by antagonizing the mitochondrial pathway of apoptosis, directly or indirectly. However, further experimental studies are necessary in order to elucidate the involved pathway by evaluating the levels of caspase-8, a marker of the death receptor-associated pathway, or caspase-12, as the final activated caspase of the ER-stress pathway. Overviewing all

these data, the propargyl moiety, present in the DPH-4 molecule, might be a main responsible for this antiapoptotic behaviour.

### *2.8. Anti-inflammatory activity of DPH-4*

Neuroinflammation is an early event in AD pathology and it is not a passive system activated by senile plaques (SP) and neurofibrillary tangles (NFT) once both are formed. Data from human autopsies revealed that both SP and NFTs are co-localised with activated glial cells suggesting that reactive gliosis might exert a key pathogenic role in AD [30]. A $\beta$  oligomers induce activation of astrocytes and microglia by promoting cytokines release and inflammatory mediators that affect synapses and neuronal plasticity at early stages of the disease, inducing the vascular unit dyshomeostasis, neuronal death and cognitive decline. In this context, it is essential to highlight that once initiated; inflammatory process may contribute independently to neural dysfunction and cell death, thereby establishing a self-fostering vicious cycle, by which the inflammation represents a substantial cause of further neurodegeneration [31]. In order to examine the anti-inflammatory properties of multi-target compound DPH-4, murine microglial BV-2 cell line, a well-established cell model to study inflammation, was used. Inflammation was induced in these cells by co-treating 100 ng/ml lipopolysaccharid (LPS) with 0.5 ng/ml interferon  $\gamma$  (IFN- $\gamma$ ) for 24 hours, as previously described experimental conditions. Nitric oxide (NO) is an important free radical that is involved in a number of mechanisms including the activation of NF- $\kappa$ B, an important transcription factor in iNOS gene expression in response to inflammation [32]. Under inflammatory processes, nitrite ions (NO $_2^-$ ) are released from the cells into the medium and its levels can be measured spectrophotometrically as an indicator of inflammation.

Expectedly, in BV-2 cells treated with LPS+INF $\gamma$  nitrite levels were strongly increased whereas in those pre-treated with both any of DPH-4 concentrations tested (0.01-10  $\mu$ M) or 200  $\mu$ M ibuprofen, used as an anti-inflammatory standard, NO $_2^-$  levels were significantly decreased (Fig. 8A).

In order to confirm the anti-inflammatory effect of DPH-4, the levels of cyclooxygenase-2 (COX-2), whose expression is upregulated during inflammation, were also studied under the same experimental conditions. As shown in Fig. 8B, LPS+INF- $\gamma$ -treated cells exhibited significantly increased levels of this enzyme, whose levels dose-

dependently decreased in those pre-treated with DPH-4. A significant decrease was also found with 10  $\mu$ M ibuprofen.

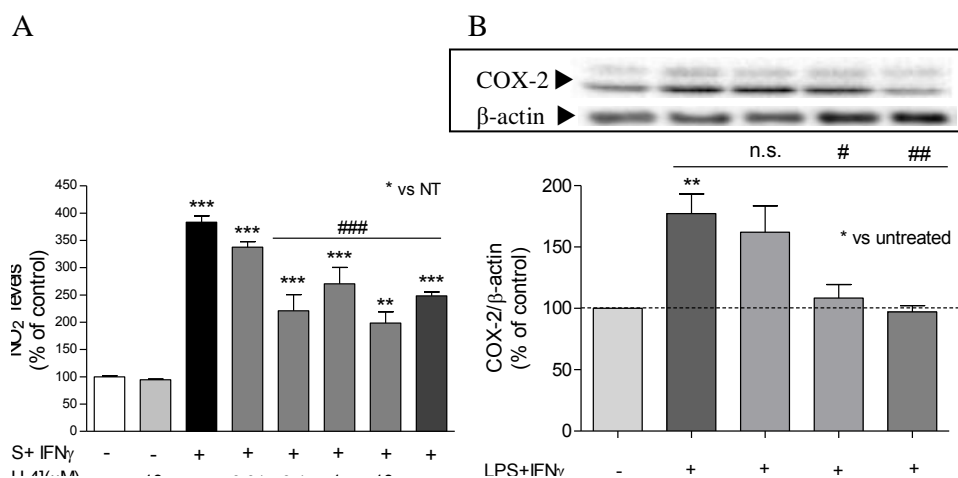


**Fig. 8.** Anti-inflammatory effect of DPH-4. (A) Decrease of the nitrite amount of LPS+INF $\gamma$ -induced inflammation in microglial BV-2 cells by DPH-4 or ibuprofen. (B) Dose-dependent reduction on the expression of COX-2 in 100 ng/ml LPS+ 0.5 ng/ml INF $\gamma$ -treated BV-2 cells pre-treated with DPH-4 or ibuprofen. Results are expressed as the mean  $\pm$  S.E.M. of at least three independent experiments. \* vs untreated. # vs LPS+INF $\gamma$ -treated.

### 3. Conclusions

The multi-target drug design is a promising therapeutic approach against the complex neurological disorder of AD. In this context, the multi-target compound DPH-4, designed as a hybrid of donepezil and M30 bearing *N*-benzylpiperidine and the pro-chelator 8-hydroxyquinoline moiety attached to a central *N*-propargylamine core [9], has been subjected to pharmacological evaluation. In this work, multiple properties with DPH-4 of potential benefit in AD therapy are reported. Among these, the initial finding of the well-balanced activity as a dual inhibitor of human ChE/MAO encouraged the exploration of further properties with this compound. Next, the ability of DPH-4 to reduce A $\beta$ <sub>1-42</sub> self- and hAChE-mediated aggregation, through the prevention of the formation of fibrillary and oligomeric species was found, revealing a potential neuroprotective effect of this compound against A $\beta$ <sub>1-42</sub>-induced neurotoxicity by reducing the formation of high-MW species and by promoting the appearance of monomers and hence non-toxic forms. The presence of oligomeric forms correlates well

with the severity of this neurological disorder [33]. Drugs able to prevent or reverse the oligomerisation and fibrillation processes of A $\beta$  show a therapeutic value in AD treatment [35]. Moreover, DPH-4 was capable to partially block AChE-dependent A $\beta$ <sub>1-42</sub> aggregation, demonstrating its interaction with the PAS and reinforcing its role in avoiding A $\beta$  aggregation. Moreover, DPH-4 showed a strong antioxidant behaviour confirmed by a wide number of different experimental approaches and furthermore being able to induce the expression of antioxidant enzymes SOD-1, GPx, catalase and the transcriptional factor Nrf-2, responsible for the expression of other cytoprotective proteins. The presence of a propargyl moiety in the structure of DPH-4 could explain its antiapoptotic behaviour. Finally, the anti-inflammatory behaviour observed by the decreasing levels of nitrite of LPS+INF $\gamma$ -induced inflammation in BV-2 cells was confirmed by the decreasing in the expression levels of COX-2.

To sum up, the findings from the present study of DPH-4, a multi-target compound with a well-balanced anti-cholinesterasic and MAO inhibition profile in addition to other remarkable pharmacological properties, prompt us to propose this molecule as a promising multi-target drug to be considered for therapeutic development against AD.

#### **4. Experimental section**

##### *Determination of human monoamine oxidase activity fluorimetrically.*

Activities of human recombinant MAO A and MAO B (Sigma-Aldrich) were performed using a fluorimetric method [11]. Tyramine hydrochloride (Sigma-Aldrich) was used as substrate for both isoforms in 96-well black opaque microplates (OptiPlate-96F, PerkinElmer) in a final volume of 200  $\mu$ l. Serial dilutions of each inhibitor were pre-incubated with 360 U/l hMAO A or 67.5 U/l hMAO B for 30 minutes at 37°C. Following the pre-incubations, enzymatic reactions were started upon the addition of 100  $\mu$ l of a mixture containing 1 mM tyramine, 40 U/l horseradish peroxidase and 25  $\mu$ M Amplex UltraRed<sup>®</sup> reagent (LifeTechnologies) in 250  $\mu$ M sodium phosphate buffer (pH 7.4), as final concentrations. The fluorescence production associated with peroxidase-coupled production of resorufin from the reagent was constantly measured for at least 1 hour at 530/590 nm spectrophotometrically (FluoStar OPTIMA, BMG Labtech). In control samples, inhibitor was replaced with distilled water. The possible capacity of compounds to modify the fluorescence generated by the reactions mixture

due to non-enzymatic inhibition was determined by adding these compounds to solutions containing the reagent and buffer only.

#### *Determination of ChE activities spectrophotometrically*

Activity of both recombinant AChE from human recombinant (*hAChE*) and human recombinant BuChE (*hBuChE*) (Sigma-Aldrich) was assessed following the spectrophotometric method of Ellman [12]. Enzymatic reactions were allowed in 96-well plates in solutions containing 0.1 M phosphate buffer (pH 8.0), 35 mU/ml *hAChE* or 50 mU/ml *hBuChE* and 0.35 mM 5,5-dithiobis-2-nitrobenzoic acid (DTNB, Sigma-Aldrich). Dose-response curves were plotted after pre-incubating the mixture with serial concentrations of each inhibitor for 30 minutes. The activity in absence of compound was used to determine the maximum enzymatic activity. Following the pre-incubations, 50  $\mu$ l of substrate were added to a final concentration of 0.35 mM acetylthiocholine iodide (ASCh) or 0.5 mM butyrylthiocholine iodide (BuSCh) (Sigma-Aldrich). Enzymatic reactions were followed for 30 minutes with both enzymes at 37°C and changes in absorbance at 405 nm were detected in a spectrophotometric plate reader (FluoStar OPTIMA, BMG Labtech). From dose-response curves, IC<sub>50</sub> values were accordingly calculated by using the GrapPad PRISM software (versions 3.0 and 4.0).

#### *Assessment of in vitro A $\beta$ self- and hAChE-mediated aggregation*

The inhibition of A $\beta$ <sub>1-42</sub> self-aggregation by compound DPH-4 was studied using the thioflavin T (ThT)-based fluorometric assay [16]. Briefly, A $\beta$ <sub>1-42</sub> peptide (Bachem AG) was pre-treated with 1,1,1,3,3,3-hexafluoro-2-propanol (HFIP, Sigma Chemicals), liquid removed by lyophilisation and kept at -20°C until use. For experiments, A $\beta$ <sub>1-42</sub> peptide was resolved in 10 mM basic phosphate buffer (PBS, pH 11.2 adjusted with NH<sub>4</sub>OH). Experiments were performed by incubating the peptides (20 $\mu$ M) with or without the compounds with 35 $\mu$ M ThT. The fluorescence intensity was monitored at 485/528 nm at 37°C every 10 minutes for at least 6 hours on a Synergy HT microplate reader (Bio-Tek). Representative figures are shown in FU and expressed as percentage of control at plateau with blanks subtracted. For A $\beta$ <sub>1-42</sub> *hAChE*-mediated aggregation, human recombinant AChE (Sigma-Aldrich) was co-incubated with the peptide at ratio A $\beta$ : AChE, 100:1 in presence of absence of compounds. The same method as previously was employed for calculations.

### *Oxygen Radical Absorbance Capacity (ORAC)*

The ORAC assay was based on the procedure previously described and partially modified by Dávalos *et al.* [25]. Briefly, was used as a free radical generator and trolox as standard and melatonin as a reference compound (Sigma-Aldrich). Test compounds were diluted in 75 mM PBS pH 7.4 and measured at eight different concentrations (0.1-1  $\mu$ M), whereas trolox calibration solutions (1-8  $\mu$ M) were prepared for the standard curve. Samples were pre-incubated 15 minutes at 37°C with 70nM fluorescein. Then, upon the addition of 12 mM APPH, fluorescence intensity at 485/520 nm was monitored every minute for 80 minutes by using a Polaris Galaxy plate reader (BMG Labtechnologies). The area under the curve (AUC) of the fluorescence decay was calculated by subtracting AUC for the sample or standard from that for the blank. A calibration curve was made from the net AUC values of trolox standard solutions. The ORAC value for each compound was expressed as trolox equivalents, in which ORAC value for trolox was assigned as 1.

### *Determination of antioxidant activity by DPPH radical method*

In a 96-well plate and a final volume of 200 $\mu$ l per well, a methanol 2,2-diphenyl-1-picrylhydrazyl (DPPH) (Sigma-Aldrich) solution at 135 $\mu$ M final concentration was added and mixed with different DPH-4 or trolox concentrations (1-100 $\mu$ M). The resulting mixture was then incubated for 2 hours at room temperature in the dark. Then, the absorbance was measured at 517 nm in a spectrophotometric plate reader (Labsystems Multiscan RC). Reactions were prepared in triplicate and the antioxidant activity was determined as the percentage of radical scavenger activity (RSA) calculated as follows:  $RSA\% = 100[(A_0 - A_i)/A_0] \times 100$ , where  $A_0$  and  $A_i$  are the DPPH absorbance in absence or presence of added compound concentration  $i$ , respectively.

### *Inhibition of linoleic acid lipid peroxidation*

Production of conjugated diene hydroperoxide by oxidation of linoleic acid in an aqueous dispersion was monitored at 234 nm. AAPH was used as a free radical generator. 10 $\mu$ l of 16 mM linoleic acid sodium salt were added to the UV-VIS cuvette containing 0.93 ml of 50 mM phosphate buffer pH 7.4 at 37°C. The oxidation reactions were initiated under air by adding 50 $\mu$ l of 40 mM APPH solution. Oxidation was

carried out in the presence of aliquots. DMSO was used to measure the lipid peroxidation without antioxidant activity. The rate of oxidation at 37°C was monitored and by recording the increase in absorption caused by conjugated diene hydroperoxides. Trolox was used as an appropriate standard.

#### *Cell culture and treatments*

Human neuroblastoma SH-SY5Y cell line was obtained from the European Collection of Cell Cultures (ECACC). Cells were grown in Dulbecco's modified Eagle medium/Ham's F-12 (DMEM/F-12) containing 15 % (v/v) FBS, non-essential aminoacids (Sigma-Aldrich), 100 U/ml penicillin, 100 µg/ml streptomycin and 2 mM l-glutamine (PAN Biotech) maintained at 37°C with 5 % CO<sub>2</sub>. Cells were seeded at a density of 250,000 cells/ml onto 24-well plates for both cell viability assays and Hoechst staining, and onto 60 mm-diameter dishes for western blot analyses. After 24 hours from seeding, cells were starved with serum-free medium overnight and then pre-treated with compounds for one hour prior to 24-hour treatments.

Murine microglial BV-2 cells were obtained from the European Collection of Cell Cultures (ECACC). Cells were grown in RPMI medium (LifeTechnologies) containing 10 % FBS and 0.1% penicillin/streptomycin at 37°C with 5 % CO<sub>2</sub>. Cells were seeded into 24-well plates at a density of 100,000 cells/ml onto collagen type-I-coated plates (BD Biosciences). Once 60-70 % confluence was reached, medium was replaced to 0.5 % FBS final concentration. After 16 hours, cells were pre-treated with compounds for 1 hour prior to 24-hour treatments.

#### *MTT reduction assay*

The mitochondrial activity of cells was measured by quantitative colorimetric assay with 3-[4,5-dimethylthiazol-2-yl]-2,5-diphenyl-tetrazolium bromide (MTT) (Sigma-Aldrich) as previously described [35]. Briefly, 50 µl of the MTT reagent were added into each well to a final concentration of 0.5 mg/ml at the end of each treatment time. Then, the plate was placed in a humidified incubator at 37°C with 5 % CO<sub>2</sub> and 95% air (v/v) for at least 30 minutes. Next, the insoluble formazan was dissolved with DMSO and colorimetric determination was carried out at 540/620 nm in a microplate reader

(Labsystems Multiscan RC). Untreated cells were used as control of 100 % cell viability.

#### *LDH release assay*

Cell viability was assessed by the quantification of lactate dehydrogenase (LDH) activity in cells using the TOX7 kit (Sigma-Aldrich). Briefly, after treatments cell media was collected and centrifuged at 800 x g for 10 minutes at 4°C to discard the dead cells. The supernatants were collected and directly used for LDH determination. The LDH mixture was first prepared by mixing equal volumes of substrate solution, LDH assay dye solution and 1X LDH assay cofactor preparation. Next, the sample media were transferred to a clean flat-bottom plate and lactate dehydrogenase assay mixture was added to each sample in a volume equal to twice that of the sample media. The plate was then covered to protect it from light and incubated at RT for 20-30 minutes. Absorbance was spectrophotometrically measured at 490/690 nm in a microplate reader (Labsystems Multiscan RC).

#### *Hoechst staining*

After treatments, cells washed with PBS (pH 7.4) and fixed with 4 % paraformaldehyde (Sigma-Aldrich) in PBS for 10 minutes at 25°C. Cell were then stained with 0.5 µg/ml Hoechst 33258 (Sigma-Aldrich) for 30 minutes at 25°C. Stained nuclei were visualised under an inverted microscope (Nikon Eclipse TE2000-E, Nikon) and quantitative image analysis was performed by counting six fields from each well. Data was expressed as the percentage of total nuclei per field relative to untreated cells.

#### *Determination of intracellular ROS and O<sub>2</sub><sup>-</sup> levels*

Intracellular accumulation of ROS levels after treatment with H<sub>2</sub>O<sub>2</sub> was assessed using 2,7-dichlorofluorescein diacetate (DCFH-DA) staining. SH-SY5Y cells were incubated with 10 µM DCFH-DA in HEPES-buffered saline solution for 20 minutes. Next, cells were washed and the basal DCF fluorescence levels were measured in a fluorimeter at 485/530 nm. Then, DPH-4 (5µM or 10µM) or vehicle was pre-incubated for 1 hour and 250µM or 500µM H<sub>2</sub>O<sub>2</sub> added for another hour. After this time, fluorescence levels were measured and basal values were subtracted. The intracellular levels of superoxide anion (O<sub>2</sub><sup>-</sup>) were monitored by the selective oxidation of dihydroethidium (DHE) to

ethidium. Cells were loaded with 10 $\mu$ M DHE for 10 minutes. Next, basal fluorescence levels were measured at 485/590 nm in a fluorimeter. Next, cells were treated with DPH-4 (5 $\mu$ M or 10 $\mu$ M) or vehicle for 30 minutes and then H<sub>2</sub>O<sub>2</sub> (250 $\mu$ M or 500 $\mu$ M) was added for an hour. Fluorescence was measured, and basal levels subtracted. In both assays, ROS and O<sub>2</sub><sup>-</sup> levels were expressed as percentage of those in non-treated cells.

#### *Western blot analysis*

For A $\beta$ <sub>1-42</sub> aggregation experiments, peptide samples were removed from the microplate at the end of the ThT aggregation assays, heated at 95°C for 2 minutes and 50 ng loaded into 10% SDS-PAGE pre-cast gels (BioRad) and electrophoresed for 1.5 hours at 100V using a running gel containing 2.5 mM Tris, 19.2 mM glycine and 0.1 % SDS pH 8.3 (Sigma-Aldrich). Resolved bands were then transferred onto a PVDF membrane using 10 mM CAPS pH 11.0 as transfer buffer and blocked in PBS pH 7.4 containing 10 % non-fat milk and 0.1 % BSA for one hour. Membranes were then incubated with mouse monoclonal anti-A $\beta$  6E10 antibody (Covance; 1:500) at 4°C overnight. Then, blots were exposed to horseradish peroxidase-conjugated rabbit anti-mouse (DAKO; 1: 2000) for one hour at room temperature. Membranes were rinsed with peroxidase/luminol solution and bands were analysed and quantified using ChemiDoc<sup>®</sup>MP Imaging System (BioRad) and ImageLab software.

For the rest of enzyme determination, cells were collected in 50 mM Tris-HCl pH 7.5 buffer containing 10 mM EDTA and 1 % (v/v) Triton X-100 after treatments. Protein concentration was determined by the Bradford protein assay. Samples were then diluted in SDS sample buffer containing 70 mM Tris-HCl, 10 %  $\beta$ -mercaptoethanol and 0.1 % (w/v) bromophenol blue. Protein samples (20-30  $\mu$ g) were heated at 96°C for 4 minutes, resolved in SDS-PAGE gels and then transferred onto nitrocellulose membranes (Whatman-Schleicher & Schuell). Transferred membranes were then blocked with 5 % (w/v) non-fat dry milk in Tris-buffered saline (TBS) containing 0.1 % (v/v) tween-20 for one hour and then incubated with primary antibodies anti-APP 20.1 (W.E. Van Nostrand, Stony Brook University, NY, USA; 1: 1000), anti-SOD-1 (SantaCruz; 1: 1000), anti-GPx-1 (Abcam; 1:1000), anti-Nrf-2 (SantaCruz; 1:1000), anti-full-length PARP (Upstate; 1:1000), anti-COX-2 (SantaCruz; 1: 1000), anti- $\beta$ -actin (Sigma-Aldrich; 1: 5000) and anti-GAPDH (glyceraldehyde-3-phosphate dehydrogenase) (Ambion-Invitrogen; 1:20000) for 16 hours at 4°C. Then, blots were exposed to

horseradish peroxidase-conjugated goat anti-rabbit (BD Biosciences; 1: 2000) or rabbit anti-mouse (DAKO; 1: 2000) for one hour at room temperature. Membranes were rinsed with peroxidase/luminol solution and bands were analysed and quantified using ChemiDoc<sup>®</sup>MP Imaging System (BioRad) and ImageLab software.

#### *DEDV-directed caspase-like activity assay*

Caspase activity in lysates from 250 $\mu$ M H<sub>2</sub>O<sub>2</sub>-treated SH-SY5Y cells for 24 hours was determined by DEVD-directed caspase-like activity method. Quantitative caspase-like activity in cell lysates were performed as previously described with minor modifications [36]. Briefly, after the indicated treatments, cells were collected and assays were performed using 25  $\mu$ g of protein in the specific buffer containing 100 mM Tris (pH 7.2–7.4), 4 mM EDTA, 4 mM EGTA, 20% sucrose, 10 mM dithiothreitol, 1 mM PMSF plus 40  $\mu$ M of the fluorogenic substrate Ac-DEVD-afc. The resulting 96-multiwell microplates were incubated at 35°C, and caspase activity was monitored for at least one hour in a BIO-TEK Synergy HT fluorimeter at 360/530 nm. For each condition, triplicates of each sample were used.

#### *Determination of nitrite content*

The nitrite content was measured in the culture medium as an indicator of the NO production process in BV-2 cells by the method of Griess following manufacturer's instructions (Molecular Probes). Briefly, after treatments, 50  $\mu$ l of medium were incubated with the equal volume of the Griess reagent and the absorbance was determined at 570 nm using a microplate reader.

#### *Statistical analysis*

Data are shown as the mean  $\pm$  S.E.M. All statistical analyses were completed using GraphPad PRISM software (versions 3.0 or 4.0). Differences were established by one-way ANOVA followed by the Bonferroni post-test with \* $p$ <0.05, \*\* $p$ <0.01 and \*\*\* $p$ <0.001.

## References

- [1] Kumar A., Singh A., Ekavali. "A review on Alzheimer's disease pathophysiology and its management: an update. *Pharmacological reports* : PR 67, 195-203. Perl, D.P., 2010. *Neuropathology of Alzheimer's disease*. The Mount Sinai journal of medicine, New York 77, 32-42.
- [2] G. Pepeu, M.G. Giovannini, *Current Alzheimer's Research* 6 (2009) 686-96.
- [3] Y. Feng, X. Wang, *Oxidative Medicine and Cellular Longevity* (2012) 472932.
- [4] R. Sultana, P. Mecocci, F. Mangialasche, R. Cecchetti, M. Baglioni, D.A. Butterfield, *Journal of Alzheimer's disease* (2011) 25-34.
- [5] A. Mark, J. Greenough, A.I. Bush, *Neurochemistry International* 62 (2013) 540-555.
- [6] A. Scott, L. Peng, A.I. Bush, *Free Radical Biology and Medicine* 62, (2013) 76-89.
- [7] D.J. Bonda *et al*, *Current Opinion on Drug Discovery and Development* 13 (2010) 235–246.
- [8] T. Storr *et al*, *Chemical Society Reviews* 35 (2006) 534-544.
- [9] L. Wang, G. Esteban, M Ojima, O.M. Bautista-Aguilera, T. Inokuchi, I. Moraleda, I. Iriepa, A. Samadi, M.B. Youdim, A. Romero, E. Soriano, R. Herrero, A.P. Fernández Fernández, R. Martínez-Murillo, J. Marco-Contelles, M. Unzeta, *European Journal of Medicinal Chemistry* 80 (2014) 543-561.
- [10] P. Sun, G. Esteban, T. Inokuchi, J. Marco-Contelles, B.B. Weksler, I.A. Romero, P.O. Couraud, M. Unzeta, M. Solé, *British Journal of Pharmacology* (2015).
- [11] M. Zhou, Z. Diwu, N. Panchuk-Voloshina, R.P. Haugland, 253 *Analytical Biochemistry* (1997) 162-168.
- [12] G.L. Ellman, A. Burkhalter, J. Ladou, *Journal of Laboratory and Clinical Medicine* 57 (1961) 813-818.
- [13] M.B. Youdim, *Experimental Neurobiology* 22 (2013) 1-10.
- [14] D.M. Walsh *et al*, *Nature* 146 (2002) 535-539.
- [15] M.B.H. Youdim, *Cell Molecular Neurobiology* 21 (2001) 555-573.
- [16] I. Bolea, J. Juárez-Jiménez, C. de los Ríos, M. Chioua, R. Pouplana, F.J. Luque, *et al*. *Journal of Medicinal Chemistry* 54 (2011) 8251-8270.

- [17] N.C. Inestrosa, A. Alvarez, C.A. Pérez, R.D. Moreno, M. Vicente, C. Linker, *et al.* *Neuron* 16 (1996) 881-891.
- [18] C.A. Rotkamp, *Free radical Biology and Medicine* 30 (2001) 447-450.
- [19] D.J. Bonda, *et al.*, *Neuropharmacology* 59 (2010) 290-294.
- [20] M.A. Smith, *et al.*, *Nature* 382 (1996) 120-121.
- [21] M.A. Lovell, *et al.*, *Neurobiology Aging* 18 (1997) 457-461.
- [22] K.S. Montine, *Journal of Neuropathology and Experimental Neurology* 56 (1997) 866-871.
- [23] D. Praticò, V. Lee, J.Q. Trojanowski, J. Rokach, G.A. Fitzgerald, *FASEB* 15 (1998) 1777-1783.
- [24] C. Behl, J.B. Davis, R. Lesley, D. Schubert, *Cell* 77 (1994) 817-827.
- [25] A. Dávalos, C. Gómez-Cordovés, B. Bartolomé, *Journal of Agriculture and Food Chemistry* 52 (2004) 48-54.
- [26] M. Musialik, G. Litwinienko, *Organic Letters* 22 (2005) 4951-4954.
- [27] M.C. Carrillo, C. Minami, K. Kitani, W. Mayurama, K. Ohashi, T. Yamamoto, M. Naoi, S. Kanai, M.B. Youdim, *Life Sciences* 67 (2000) 577-585.
- [28] M.B.H. Youdim, M. Weinstock, *Cell Molecular Neurobiology* 21 (2001) 555-573.
- [29] I. Bolea, A. Gella, M. Unzeta, *Journal of Neural Transmission* (2012).
- [30] J.M. Craft, D.M. Watterson, L.J. Van Eldik, *Glia* 53 (2006) 484-490.
- [31] M.L. Block, J.S. Hong, *Progress in Neurobiology* 76 (2005) 77-98.
- [32] H. Wilms, J. Sievers, U. Rickert, M. Rostami-Yazdi, U. Mrowietz, R.J. Lucius, *7 Neuroinflammation* (2010) 7-30.
- [33] J. Hardy, D.J. Selkoe, *Science* 297 (2002) 353-356.
- [34] T. Liu, G. Bitan, *ChemMedChem* 7 (2012) 359-374.
- [35] J.A. Plumb, R. Milroy, S.B. Kaye, *Cancer Research* 49 (1989) 4435-4440.

[36] R. Gozzelino, C. Sole, N. Llecha, M.F. Segura, R.S. Moubarak, V. Iglesias-Guimaraes, M.J. Perez-Garcia, S. Reix, J. Zhang, N. Badiola, D. Sanchis, J. Rodriguez-Alvarez, R. Trullas, V.J. Yuste, J.X. Comella, *Cell Research* 18 (2008) 1020–1036.



## **V. DISCUSSION**



## V. DISCUSSION

Alzheimer's disease (AD) is an age-linked irreversible neurodegenerative disorder characterised by a progressive loss of cholinergic neurons leading to cognitive decline. Although the etiology of AD has not been yet fully elucidated, several factors including the presence of amyloid beta peptide deposits, aggregates of hyperphosphorylated tau protein, high levels of oxidative stress, metal dyshomeostasis and neuroinflammatory processes are assumed to play a relevant role in both the onset and progression of AD pathology. The combination of all these events irrevocably lead to the selective loss of cholinergic neurons in specific brain areas producing the characteristic pathological hallmarks of AD. To date, the high number of pharmacological approaches developed against this neurological disorder have emerged long-term inefficient against its complex multifaceted nature. Amongst the few drugs approved by the FDA for the treatment of AD, the pharmacological activity of AChE inhibitors donepezil, rivastigmine and galantamine, mostly devolved upon the restoration of ACh levels in the synaptic cleft, has exhibited limited disease-modifying benefits. In this context, our group has been considering the use of the so-called multi-target-directed ligands (MTDL), based on the "one drug, multiple targets" paradigm as an innovative and enhanced approach for the treatment of AD pathology. Firstly described by Buccafusco and colleagues in 2000 (Buccafusco JJ 2000), MTDLs arise as rationally-designed compounds possessing multiple pharmacological profiles to specifically combat a disease caused by multiple pathological events such as AD. Consequently, a number of ongoing research investigations have been redirected their efforts towards this promising therapeutic strategy.

In this context, the multi-target compound ASS234, a propargylamine-containing dual ChE/MAO inhibitor, was first identified by our group as a suitable candidate for use in AD amongst several series of novel derivatives extensively screened. To date, multiple beneficial properties have been reported with this MTDL including numerous neuroprotective properties (Sanz E 2009), high permeability value to cross the BBB and penetrate into the CNS corroborated by *in*

*in vivo* experiments (Stasiak A 2014), capacity to partially reduce both A $\beta$ <sub>1-40</sub> and A $\beta$ <sub>1-42</sub> aggregations and the neurotoxicity associated to A $\beta$ <sub>1-42</sub> in human neuroblastoma SH-SY5Y cells with remarkable anti-apoptotic effect and significant antioxidant potency arising from the increase in the activity of catalase and SOD-1 enzymes. In addition, in an *in vivo* approach using transgenic APP/PS1AE9 mice administered with ASS234, both A $\beta$  plaques in cortex and activated glia were found decreased (Martínez-Murillo R, under revision).

In order to further explore the multifunctional behaviour of ASS234 as an anti-AD drug, a biochemical and structural analysis was first carried out with aims to better characterise the effects of this molecule as an inhibitor of MAO, whose involvement in depressive-like disorders as well as its increase in the expression accompanied with an induction of oxidative damage, reveal this enzyme as an AD target of interest (Esteban G 2014). From kinetic studies, ASS234 was confirmed as not only a reversible inhibitor of both cholinesterases with micromolar affinity, but also as a highly potent irreversible MAO A inhibitor similar to clorgyline. Comparatively, both PF9601N and *l*-deprenyl were endorsed as effective selective MAO B inhibitors. Although the mechanism of inactivation was found to be the alike, the selectivity of ASS234 for MAO A, indicated by the IC<sub>50</sub> values for both purified and membrane-bound protein samples, was clear and consistent with the data previously reported (Perez V 1999; Bolea I 2011). Differences observed between ASS234 and clorgyline might be attributed to the shared propynamine structure, which is larger and more hydrophobic in ASS234. The initial reversible binding parameter (K<sub>i</sub> value of 0.4  $\mu$ M) indicated that ASS234 has a slightly lower affinity for MAO A than clorgyline (K<sub>i</sub> value of 0.02  $\mu$ M), and this was also reflected in the higher K<sub>I</sub> for the irreversible reaction. Nevertheless, these data demonstrate that the addition of the donepezil moiety, which endowed ASS234 with desirable multi-target inhibitory properties in the context of AD treatment (namely ChE enzyme inhibition in the same affinity range as for MAO A), did not affect significantly the MAO inhibition properties of ASS234.

From UV-VIS spectral analysis, the irreversible modification of the MAO flavin group by ASS234 gave an absorbance profile highly similar to that found with the other propargyl MAO inhibitors. The crystal structure of human MAO B in complex with ASS234 highlighted the formation of a covalent adduct with the flavin

N5 atom which, based on the spectral changes, occurs also with the MAO A cofactor. Although the *N*-benzylpiperidine moiety was not fully visible in the electron density, the mass determinations demonstrated that ASS234 binds as the intact molecule to the MAO B active site, which ruled out the possibility that the inhibitor may undergo degradation in the cellular context. Overall, the efficacy of ASS234 as inhibitor of both the “classic” AD-targeting ChE enzymes and MAOs was fully demonstrated by this study.

Following the search of additional activities of multi-target ASS234, the potential modulation of the monoaminergic transmission and metabolism by this molecule was also investigated both *in vitro* and *in vivo* (Esteban G, under revision). As aforementioned, behavioural alterations such as depression, as featured symptoms in AD, are possibly caused by monoaminergic dysfunction. Therefore, the therapeutic use of antidepressant drugs based on the selective inhibition of MAO A, an enzyme possessing a key activity in the metabolic regulation of neurotransmitters 5-HT, NA, DA and/or on the blockage of the corresponding reuptake systems at the pre-synaptic nerve endings, may also be considered.

In this context, significant increase in the levels of 5-HT associated with a reduction in the levels of its metabolite 5-HIAA was observed as a result of irreversible inhibition of MAO A in SH-SY5Y cells treated with multi-target ASS234. Comparatively, similar, though less pronounced effects were revealed with the highly-selective MAO A inhibitor clorgyline under the same experimental conditions, revealing therefore an active effect of this multi-target to enhance 5-HT levels. Unexpectedly, DA levels were significantly decreased in PC12 cells treated with ASS234 by a possible reduction of both activity and expression of DA synthesis precursor enzymes TH and AAAD as a consequence of first-step rapidly elevated levels of DA following the blockage of MAO activity. However, ASS234, as MAO A inhibitor clorgyline, selectively modulated the levels of DA metabolites DOPAC and HVA, whose levels were decreased after incubations.

*In vivo* administration of ASS234 in freely-moving rats revealed an alteration on the extracellular monoamines levels in both hippocampus and prefrontal cortex, two highly impaired brain areas in AD. Interestingly, the effect of ASS234 differed from brain areas and dosage. In hippocampus, levels of 5-HT and NA were detected increased whereas those of DA and NA were markedly augmented in prefrontal

cortex. These differences might be attributed to the presence of metabolising enzyme in both brain areas as well as to the complexity in the monoaminergic neurochemical interactions existing in the brain. In addition, ASS234 as a multi-target compound could be modulating other neurobiological systems and therefore producing a combined pharmacological effect. These findings reinforced those previously reported in (Stasiak A 2014) increased levels of 5-HT, DA and NA in post-mortem cerebral samples of rats induced by permanent bilateral occlusion treated with ASS234 for five consecutive days. The present *in vivo* study revealed a time-dependent effect on extracellular levels of monoaminergic neurotransmitters after a single-dose subcutaneous administration of ASS234 and can be used to in-depth study the pharmacokinetics and bioavailability of the compound to reach its therapeutic target. Many factors including route of administration or the existence of active metabolites may also explain the delay on the *in vivo* effects observed with ASS234.

In AD, levels of DA and NA are diminished in cortex and hippocampus while those of 5-HT are decreased in hippocampus (Reinikainen KJ 1988), altering some behavioural symptoms including depressive-like disorder, psychosis or memory impairment related to alterations in serotonergic, catecholaminergic and cholinergic neurotransmissions (Vermeiren Y 2015). Therefore, the effects observed *in vivo* with ASS234 in addition with those previously found, confirm a reinforcement to further elucidate the underlying mechanism of action of ASS234 on the monoaminergic neurotransmission as a relevant molecule for use in AD. Compound ASS234 has been patented under US 8,999,994B2 (USA) and PCT/ES2011/070186; WO 2011/ 113988 (Spain).

Next, and with the effort to search for improved MTDLs, two series of novel compounds structurally-derived from ASS234 as multipotent donepezil-indolyl and donepezil-pyridyl hybrids were pharmacologically evaluated for their potential use in AD (Bautista-Aguilera OM 2014; Bautista-Aguilera OM 2014(2)). Among the tested compounds, a donepezil-indolyl hybrid was identified to exhibit the most interesting profile as potent MAO A inhibitor ( $IC_{50}= 5.5$  nM) moderately able to inhibit MAO B ( $IC_{50}= 150$  nM), AChE ( $IC_{50}= 190$  nM) and BuChE ( $IC_{50}= 830$  nM). Moreover, by molecular modelling studies, this compound was suggested as a

mixed-type AChE inhibitor able to span both the CAS and PAS of this enzyme. Interestingly, docking simulations revealed that the selective inhibition of MAO isoforms by propargyl-containing compounds accounts for the orientation on their propargylamine and phenyl moieties in MAO, which energetically affects the interaction with the active site. Also, a donepezil-pyridyl hybrid was recognised as a very potent human AChE inhibitor ( $IC_{50}$  = 25 nM) and moderate human BuChE inhibitor ( $IC_{50}$  = 1.2  $\mu$ M) with low selectivity toward human MAO B. Interestingly, the design and development of non-selective ChE inhibitors for use in AD seems of valuable pharmacological interest as the hydrolysis of neurotransmitter ACh may largely occur via BuChE catalysis in old AD brains as the activity levels of this enzyme have been found elevated on late-stages of the disease, similarly to MAO B. Moreover, as BuChE is also found in glial cells while recruited and activated around the plaques and tangles, the inhibition of this enzyme might provide additional benefits at reducing neuroinflammation. Suitable druglikeness profile and ADMET properties of these two novel MTDLs were confirmed by 3D-QSAR studies.

Since metal dyshomeostasis has been recently considered a key event in AD as an early factor closely related to increased levels of both oxidative stress and amyloid beta protein toxicity in AD brains, the development of metal-chelators has concurrently emerged as a novel pharmacological approach in AD. A series of newly-designed MTDLs (DPH and WMY) bearing the benzylpiperidine moiety from donepezil and the 8-hydroxyquinoline group, previously reported to possess metal-chelating properties, linked to a central *N*-propargylamine core were synthesised and pharmacologically evaluated (Wang L 2014; Wu MY 2015). Remarkably, these derivatives were identified as equimolar irreversible MAO and mixed-type ChE inhibitors in low micromolar range able to strongly complex biometals Cu (II), Zn (II) and Fe (III). In addition, an essential role for the cyano group, present only in some of these derivatives, was discovered at binding sites of AChE, BuChE and MAO A. Despite  $\alpha$ -aminonitriles have been seldom investigated as ChE inhibitors, some previous works described nitriles as MAO inhibitors, reporting that cyanide potentiates irreversible MAO inhibition (Ramadan ZB 2007). From theoretic ADMET analyses, DPH and WMY compounds exhibited proper druglikeness properties and good brain penetration capacity for CNS activity. Moreover, less toxicity than donepezil in HepG2 cells was also revealed. These

findings are of noteworthy relevance since the simultaneous administration of multiple therapeutic agents can lead to potentially lethal side effects triggered by drug-to-drug interactions. Therefore, the mentioned undesirable outcomes might be significantly reduced by the use of multi-target derivatives exhibiting low toxicity such as DPH/WMY compounds. Furthermore, these molecules also displayed well performance in terms of translational science since scopolamine-induced memory deficits were partially restored by a DPH derivative, revealing effective pharmacokinetics *in vivo*.

Once multi-target compound DPH-4 was identified from an initial pharmacological screening as an appropriate lead compound for AD, further compelling properties were revealed from subsequent investigations on this molecule (Esteban G, under preparation). As widely reported, the presence of amyloid beta protein oligomeric forms correlates well with the severity of AD. Therefore, the ability of DPH-4 to reduce both  $A\beta_{1-42}$  self- and *hAChE*-mediated aggregations by preventing the formation of both fibrillary and oligomeric species together with the reduction of high-molecular weight species into non-toxic dimers or monomers, revealed a potential neuroprotective effect of this compound against  $A\beta$ -induced neurotoxicity. Drugs capable to prevent or block the oligomerisation or fibrillation processes of amyloid beta protein have been extensively designed and developed in recent years as a convenient approach against AD. Moreover, DPH-4 significantly reduced the expression of physiological levels of APP dose-dependently in SH-SY5Y cells after 24 hour treatments. This finding is in agreement with those previously reported in a study using APP/PS1 Tg mice treated with the 8-hydroxyquinoline-containing metal-chelator M30 for nine months (Kuperschmidt L 2012). In this work, cerebral iron accumulation accompanied by a marked decrease in several AD-like phenotypes, including cerebral APP levels,  $A\beta$  levels and plaques, phospho-APP and phospho-tau were reported after treatment with M30.

Since oxidative stress is markedly considered as a determinant mediator of AD neuronal damage by the enhancement of both metal dyshomeostasis-derived

toxicity and noxious effect of A $\beta$ , the search for antioxidants has emerged as a valuable therapeutic approach for use in early stages of AD.

The outcome of the strong antioxidant capacity of DPH-4 was confirmed by a wide number of different experimental approaches. First, by an induction of the expression of antioxidant enzymes SOD-1, GPx-1, catalase and the transcriptional factor Nrf-2, responsible for the expression of other cytoprotective proteins, in undamaged SH-SY5Y as well as potential capabilities of this compound of capturing free radical species *in vitro*. Secondly, by a potent neuroprotective activity of DPH-4 against H<sub>2</sub>O<sub>2</sub>-induced toxicity in SH-SY5Y cells that was subsequently confirmed by different cell viability assays. Additionally, and although further studies are encouraged, anti-apoptotic properties were also observed with DPH-4 since increased levels of caspase-3 activity, an executioner caspase able to trigger the cleavage of other nuclear substrates such as PARP, were significantly reduced in H<sub>2</sub>O<sub>2</sub>-damaged cells in presence of DPH-4 while expression levels of full-length PARP decreased accordingly. The anti-apoptotic properties of DPH-4 might be elucidated by the presence of a propargyl moiety in its structure, a chemical group widely reported for conferring neuroprotective effects through the stabilisation of mitochondrial membrane permeability, induction of anti-apoptotic Bcl-2 and neurotrophic factors and regulation of antioxidant enzymes (Naoi M 2009). Moreover, propargylamine-containing compounds have also been reported to prevent a number of apoptotic processes including mPT-induced  $\Delta\psi_m$  reduction, mitochondrial swelling and cytochrome c release, caspase activation, condensation and fragmentation of nuclear DNA and nuclear translocation of GAPD (Naoi M 2009).

Lastly, recent research into AD pathogenesis has established that immune system-mediated actions in fact contribute to and drive AD. These insights have suggested both novel and well-defined potential therapeutic targets for AD, including microglia and several cytokines. In this concern, the anti-inflammatory behaviour of DPH-4 observed by decreasing levels of nitrites in A $\beta$ -like inflammation model induced by LPS+INF $\gamma$  in microglial BV-2 cells as well as by decreased expression levels of COX-2, revealed the potentiality of this multi-target compound in AD-occurring inflammation. Thus, additional studies *in vivo* confirming the encouraging effects revealed in this thesis with DPH-4 would

therefore prompt to propose this molecule as a promising disease-modifying drug to be considered for as an appropriate therapeutic strategy against AD.

Overall, the findings presented in this thesis robustly reinforce the suitability of MTDLs as an appropriate pharmacological approach to be used in AD therapy. Amongst all the compounds tested, multi-target DPH-4 particularly emerged as a ligand possessing a number of remarkable potential benefits for this neurological disorder including well-balanced dual AChE/MAO inhibition, strong metal-chelating activity, neuroprotective and anti-apoptotic properties, potent antioxidant capacities and anti-inflammatory action.

## **VI. CONCLUSIONS**



## VI. CONCLUSIONS

The results obtained in this thesis allow to draw the following conclusions:

1. Multi-target compound ASS234 is confirmed as a highly-selective irreversible MAO A inhibitor able to inhibit both purified and membrane-bound forms of the enzyme similarly by covalently interacting with the flavin N5 atom.
2. Compound ASS234 is able to modulate the monoaminergic neurotransmission in both SH-SY5Y cells and *in vivo* in freely-moving rats.
3. Newly-synthesized multi-targets based on the hybridization of indolyl-donepezil and pyridyl-donepezil moieties exhibited appropriate profiles as dual MAO/ChE inhibitors for further design and development of new improved derivatives for use in Alzheimer's disease.
4. First-time reported  $\alpha$ -aminonitriles as MTDLs (DPH) able to display an equimolar inhibitory profile inhibiting MAO/ChE exhibit higher affinities with longer carbon chain linker and a cyano group.
5. Structurally modified multi-target DPH compounds potently increase the selectivity as ChE inhibitors.
6. The MTDL DPH-6 is identified as a moderate equimolar dual MAO/ChE inhibitor with strong metal-chelating properties to complex copper, iron and zinc, exhibiting low toxicity levels and able to restore cognitive deficits in scopolamine-treated mice.
7. Metal-chelator DPH-4 is selected as a multifunctional molecule for use in Alzheimer's disease exhibiting potent antioxidant capacity, anti-A $\beta$  aggregation activity, anti-apoptotic and anti-inflammatory properties.
8. The compound DPH-4 has been identified as a promising MTDL exhibiting multiple potential disease-modifying properties for use in Alzheimer's disease therapy.



## **VII. REFERENCES**



**VII. REFERENCES**

- Acevedo KM, Hung YH, Dalziel AH, Li QX, Laughton K, Wikhe K, Rembach A, Roberts B, Masters CL, Bush AI, Camakaris J. 2011. 'Copper promotes the trafficking of the amyloid precursor protein.', *J. Biol. Chem.*, 286: 8252-62.
- Adem A, . 1993. 'The next generation of cholinesterase inhibitors.' *Acta Neurol Scand Suppl.*, 149: 10-12.
- Adem A, Jossan SS, Orelund L. 1989. 'Tetrahydroaminoacridine inhibits human and rat brain monoamine oxidase.', *Neurosci Lett.*, 107: 313-17.
- Adlard PA, Bica L, White AR, et al. . 2011. 'Metal ionophore treatment restores dendritic spine density and synaptic protein levels in a mouse model of Alzheimer's disease.', *PLoS One*, 6: e17669.
- Adlard PA, Cherny RA, Finkelstein DI, et al. 2008. 'Rapid restoration of cognition in Alzheimer's transgenic mice with 8-hydroxy quinoline analogs is associated with decreased interstitial Aβ.', *Neuron.*, 59: 43-55.
- Adlard PA, Parncutt JM, Finkelstein DI, Bush AI. 2010. 'Cognitive loss in zinc transporter-3 knock-out mice: a phenocopy for the synaptic and memory deficits of Alzheimer's disease? ', *J Neurosci*: 1631-36.
- Adlard PA, West AK, Vickers JC. 1998. 'Increased density of metallothionein I/II-immunopositive cortical glial cells in the early stages of Alzheimer's disease.', *Neurobiol. Dis*: 349-56.
- Adolfsson O, Pihlgren M, Toni N, et al. 2012. 'An effector-reduced anti-beta-amyloid (Aβ) antibody with unique abeta binding properties promotes neuroprotection and glial engulfment of abeta. ', *J Neurosci*, 32: 9677-89.
- AFFiRiS AG, . 'Clinical and immunological activity, safety and tolerability of different doses/ formulations of AFFITOPE AD02 in early Alzheimer's disease. '.
- Agarwal KN. 2001. 'Iron and the brain: neurotransmitter receptors and magnetic resonance spectroscopy.', *Br. J. Nutr.*, 85: S147-S50.
- Aguzzi A, Barres BA, Bennett ML, . 2013. 'Microglia: scapegoat, saboteur, or something else? ', *Science*, 339.
- Akao Y, et al. 2002. 'Mitochondrial permeability transition mediates apoptosis induced by N-methyl(R)salsolinol, an endogenous neurotoxin, and is inhibited by Bcl-2 and Rasagiline, N-Propargyl-1(R)-aminoindan.', *J. Neurochem.*, 82: 913-23.
- Akk G, Steinbach JH. 2005. 'Galantamine activates muscle-type nicotinic acetylcholine receptors without binding to the acetylcholine-binding site.', *J Neurosci.*, 25: 1992-2001.
- Ali FE, Separovic F, Barrow CJ, Cherny RA, Fraser F, Bush AI, Masters CL, Barnham KJ., 'Methionine regulates copper/hydrogen peroxide oxidation products of Aβ. ', *J. Pept. Sci.*, 11: 353-60.
- Alies B, Eury H, Bijani C, Rechinat L, Faller P, Hureau C.; . 2011. 'pH-dependent, Cu(II) coordination to amyloid-beta peptide: impact of sequence alterations, including the H6R and D7N familial mutations.', *Inorg. Chem.*, 50: 11192-201.

- Aliev G, Li Y, Palacios HH, and Obrenovich ME. 2011. Oxidative stress induced mitochondrial DNA deletion as a hallmark for the drug development in the context of the cerebrovascular diseases. *Recent Pat Cardiovasc. Drug Discov.* 6 (3): 222-241
- Allard P, Alafuzoff I, Carlsson A, Eriksson K, Ericson E, Gottfries CG, and Marcusson JO. 1990. Loss of dopamine uptake sites labeled with [3H]GBR-12935 in Alzheimer's disease. *Eur. Neurol.* 30 (4): 181-185.
- Alonso AC, Zaidi T, Grundke-Iqbal I, and Iqbal K. 1994. Role of abnormally phosphorylated tau in the breakdown of microtubules in Alzheimer disease. *Proc. Natl. Acad. Sci. U. S. A* 91 (12): 5562-5566.
- Alzheimer's Association: Alzheimer's disease facts and. 2012. 'Alzheimer's association: Alzheimer's disease facts and figures.', *Alzheimer's Dement*, 2012: 131-68.
- Ambree O, Richter H, Sachser N, Lewejohann L, Dere E, de Souza Silva MA, Herring A, Keyvani K, Paulus W, and Schabitz WR. 2009. Levodopa ameliorates learning and memory deficits in a murine model of Alzheimer's disease. *Neurobiol. Aging* 30 (8): 1192-1204.
- Amit T, Avramovich-Tirosh Y, Youdim MBH, Mandel S, . 'Targeting multiple Alzheimer's disease etiologies with multimodal neuroprotective and neurorestorative iron chelators. ', *FASEB J.*: 1296-305.
- An WL, Bjorkdahl C, Liu R, Cowburn RF, Winblad B, Pei JJ. 2005. 'Mechanism of zinc-induced phosphorylation of p70 S6 kinase and glycogen synthase kinase 3beta in SH-SY5Y neuroblastoma cells.', *J. Neurochem.*: 1104-15.
- Anderson MC, Hasan F, McCrodden JM, Tipton KF. . 1993. 'Monoamine oxidase inhibitors and the cheese effect.', *Neurochem. Res.*: 1145-49.
- Andrasi E, Farkas E, Scheibler H, Reffy A, Bezur LAI. 'Zn, Cu, Mn and Fe levels in brain in Alzheimer's disease.', *Arch. Gerontol. Geriatr.*, 21: 89-97.
- Arai H, Kosaka K, and Iizuka R. 1984. Changes of biogenic amines and their metabolites in postmortem brains from patients with Alzheimer-type dementia. *J. Neurochem.* 43 (2): 388-393.
- Arai H, Ichimiya Y, Kosaka K, Moroji T, and Iizuka R. 1992. Neurotransmitter changes in early- and late-onset Alzheimer-type dementia. *Prog. Neuropsychopharmacol. Biol. Psychiatry* 16 (6): 883-890.
- Arendt T, Brückner MK, Lange M, and et al. 1992. 'Changes in acetylcholinesterase and butyrylcholinesterase in Alzheimer's disease resemble embryonic development—a study of molecular forms.', *Neurochem Int.*, 21: 381-96.
- Arendt T, Bigl V. 1986. 'Alzheimer plaques and cortical cholinergic innervation.', *Neuroscience*, 17: 277-79
- Atwood CS, Perry G, Zeng H, Kato Y, Jones WD, Ling KQ, Huang X, Moir RD, Wang D, Sayre LM, Smith MA, Chen SG, Bush AI. 2004. 'Copper mediates dityrosine cross-linking of Alzheimer's amyloid-beta.', *Biochemistry*,: 560-68.
- Atwood CS, Scarpa RC, Huang X, Moir RD, Jones WD, Fairlie DP, Tanzi RE, Bush AI,. 2000. 'Characterization of copper interactions with Alzheimer amyloid beta

- peptides: identification of an attomolar-affinity copper binding site on amyloid beta1-42. ', *J. Neurochem.*, 75: 1219-33.
- Avila M, Balsa MD, Fernandez-Alvarez E, Tipton KF, Unzeta M. 1993. 'The effect of side chain substitution at positions 2 and 3 of the heterocyclic ring of N-acetylenic analogues of tryptamine as monoamine oxidase inhibitors.', *Biochem Pharmacol.*, 45: 2231-37.
- Ayton S, Lei P, and Bush AI. 2013. Metallostasis in Alzheimer's disease. *Free Radic. Biol. Med.* 62: 76-89.
- Badiola N, Alcalde V, Pujol A, Munter LM, Multhaup G, Lleo A, Coma M, Soler-Lopez M, Aloy P., . 2013. 'The proton-pump inhibitor lansoprazole enhances amyloid beta production. ', *PLoS One*, 8: e58837.
- Ballard C, Perry EK. . 2003. 'The role of butyrylcholinesterase in Alzheimer's disease.', *Giacobini E, editor. Butyrylcholinesterase: Its Function And Inhibitors. London, UK: Martin Dunitz*: 123-34.
- Balsa D, Fernandez-Alvarez E, Tipton KF, Unzeta M. 1991. 'Monoamine oxidase inhibitory potencies and selectivities of 2-[N-(2-propynyl)-aminomethyl]-1-methyl indole derivatives.', *Biochem Soc Trans.*, 19: 215-18.
- Bar Am O, Amit T, Youdim MB. 2004. 'Contrasting neuroprotective and neurotoxic actions of respective metabolites of anti-Parkinson drugs rasagiline and selegiline.', *Neurosci Lett.*, 355: 169-72.
- Bar-Am O, Weinreb O, Amit T, and Youdim MB. 2005. Regulation of Bcl-2 family proteins, neurotrophic factors, and APP processing in the neurorescue activity of propargylamine. *FASEB J.* 19 (13): 1899-1901.
- Barnham KJ, Masters CL, Bush AI., . 2004. 'Neurodegenerative diseases and oxidative stress. ', *Nat. Rev. Drug Discovery*, 3: 205-14.
- Barnham KJ, McKinstry WJ, Multhaup G, Galatis D, Morton CJ, Curtain CC, Williamson NA, White AR, Hinds MG, Norton RS, Beyreuther K, Masters CL, Parker MW, Cappai R, . 2003. 'Structure of the Alzheimer's disease amyloid precursor protein copper binding domain: a regulator of neuronal copper homeostasis. ', *J. Biol. Chem.*, 278: 17401-07.
- Barone P, Fernandez H, Ferreira J, Mueller T, Saint-Hilaire M, Stacy M, et al. 2013. 'Safinamide as an add-on therapy to a stable dose of a single dopamine agonist: results from a randomized, placebocontrolled, 24-week multicenter trial in early idiopathic Parkinson disease (PD) patients (MOTION Study).', *Neurology.*, 80.
- Bartus RT, Dean RL, Beer B, Lippa AS. 1982. 'The cholinergic hypothesis of geriatric memory dysfunction.', *Science*: 408-14.
- Bartus RT. 2000. 'On neurodegenerative diseases, models, and treatment strategies: lessons learned and lessons forgotten a generation following the cholinergic hypothesis. ', *Exp Neurol.*: 495-529.
- Bartzokis G, Tishler TA. 2000. 'MRI evaluation of basal ganglia ferritin iron and neurotoxicity in Alzheimer's and Huntington's disease.', *Cell. Mol. Biol.*, 46: 821-33.
- Baur JA, Sinclair DA. 2006. 'Therapeutic potential of resveratrol: the in vivo evidence. ', *Nat. Rev. Drug Discov.*, 5: 493-506.

- Bayer TA, Jäkälä P, Hartmann T, Havas L, McLean C, Culvenor JG, Li QX, Masters CL, Falkai P, Beyreuther K. 1999. 'Alpha-synuclein accumulates in Lewy bodies in Parkinson's disease and dementia with Lewy bodies but not in Alzheimer's disease beta-amyloid plaque cores.', *Neurosci Lett.*, 266: 213-16.
- Beard J. 2003. 'Iron deficiency alters brain development and functioning.'1468S-72S.
- Benkler C, Offen D, Melamed E, Kupersmidt L, Amit T, Mandel S, Youdim MB, and Weinreb O. 2010. Recent advances in amyotrophic lateral sclerosis research: perspectives for personalized clinical application. *EPMA. J.* 1 (2): 343-361.
- Bertram L, Tanzi RE. 'Thirty years of Alzheimer's disease genetics: the implications of systematic meta-analyses.', *Nat. Rev.*, 768-78.
- Besser L, Chorin E, Sekler I, Silverman WF, Atkin S, Russell JT, Hershfinkel M. 2009. 'Synaptically released zinc triggers metabotropic signaling via a zinc-sensing receptor in the hippocampus', *J. Neurosci.*: 2890-901.
- Besser, L.; Chorin, E.; Sekler, I.; Silverman, W. F.; Atkin, S.; Russell, J. T.; and M. Hershfinkel. 2009. 'Synaptically released zinc triggers metabotropic signaling via a zinc-sensing receptor in the hippocampus', *J. Neurosci.*: 2890-901.
- Biesold D, Inanami O, Sato A, Sato Y. 1989. 'Stimulation of the nucleus basalis of Meynert increases cerebral cortical blood flow in rats.', *Neurosci Lett.*, 98: 39-44.
- Birkmayer W, Riederer P. 1984. 'Deprenyl prolongs the therapeutic efficacy of combined L-DOPA in Parkinson's disease.', *Adv Neurol.*, 40: 475-81.
- Birkmayer W. 1983. 'Deprenyl (selegiline) in the treatment of Parkinson's disease.', *Acta Neurol Scand Suppl.*, 95: 103-05.
- Birks J., and Harvey R.J. 2006. 'Donepezil for dementia due to Alzheimer's disease', *Cochrane Database Syst Rev*, 1.
- Birks JS, Grimley-Evans J. 'Rivastigmine for Alzheimer's disease (Review)', *The Cochrane Collaboration*: 1-206.
- Bishop NA, Lu T, Yankner BA. 'Neural mechanisms of ageing and cognitive decline.', *Nature.*, 464:.
- Bitan G, Kirkitadze MD, Lomakin A, Vollers SS, Benedek GB, Teplow DB. 2003. 'Amyloid beta -protein (Abeta) assembly: Abeta 40 and Abeta 42 oligomerize through distinct pathways.', *Proc Natl Acad Sci U S A*, 100: 330-35.
- Blazquez L, De Juan D, Ruiz-Martinez J, Emparanza JI, Saenz A, Otaegui D, Sistiaga A, Martinez-Lage P, Lamet I, Samaranch L, Buiza C, Etxeberria I, Arriola E, Cuadrado E, Urdaneta E, Yanguas J, Lopez de Munain A. 'Genes related to iron metabolism and susceptibility to Alzheimer's disease in Basque population.', *Neurobiol. Aging*, 28: 1941-43.
- Blennow K, de Leon MJ, Zetterberg H. 2006. 'Alzheimer's Disease', *Lancet*, 368: 387-403.
- Bohrmann B, Baumann K, Benz J, Gerber F, Huber W, Knoflach F, et al. 2012. 'Gantenerumab: a novel human anti-beta-amyloid antibody demonstrates sustained cerebral amyloid- $\beta$  binding and elicits cell-mediated removal of human amyloid- $\beta$ .', *J Alzheimers Dis.*, 28: 49-69.
- Bolea I, Gella A, Monjas L, Pérez C, Rodríguez-Franco MI, Marco-Contelles J, Samadi A, Unzeta M. 2013. 'Multipotent, permeable drug ASS234 inhibits A $\beta$  aggregation,

- possesses antioxidant properties and protects from A $\beta$ -induced apoptosis in vitro.', *Curr Alzheimer Res*: 797-808.
- Bolea I, Gella A, Monjas L, Pérez C, Rodríguez-Franco MI, Marco-Contelles J, Samadi A, Unzeta M. 2013. 'Multipotent, permeable drug ASS234 inhibits A $\beta$  aggregation, possesses antioxidant properties and protects from A $\beta$ -induced apoptosis in vitro.', *Curr Alzheimer Res*: 797-808.
- Bolea I, Juárez-Jiménez J, de Los Ríos C, Chioua M, Pouplana R, Luque FJ, Unzeta M, Marco-Contelles J, Samadi A. 2011. 'Synthesis, biological evaluation, and molecular modeling of donepezil and N-[5-(benzyloxy)-1-methyl-1H-indol-2-yl)methyl]-N-methylprop-2-yn-1-amine hybrids as new multipotent cholinesterase/monoamine oxidase inhibitors for the treatment of Alzheimer's disease.', *J Med Chem.*, 54: 8251-70.
- Bolognesi ML, Bartolini M, Tarozzi A, Morroni F, Lizzi F, et al. 2011. 'Multitargeted drugs discovery: balancing anti-amyloid and anticholinesterase capacity in a single chemical entity. ', *Bioorg Med Chem Lett*, 21: 2655-58.
- Bolognesi ML, Cavalli A, Luca-Valgimigli L, Bartolini M, Rosini M, Andrisano V, Recanatini M, Melchiorre C. . 2007. 'MultiTarget-Directed Drug Design Strategy: From a Dual Binding Site Acetylcholinesterase Inhibitor to a Trifunctional Compound against Alzheimer's Disease.', *J. Med. Chem.*: 6446-49. .
- Bolognesi ML, Cavalli A, Melchiorre C., 2009. 'Memoquin: a multi-targetdirected ligand as an innovative therapeutic opportunity for Alzheimer's disease.', *Neurotherapeutics*, 6: 152-62.
- Bolte TJ, Cunningham MC, and Benes FM. 1998. Neonatal raphe lesions increase dopamine fibers in prefrontal cortex of adult rats. *Neuroreport* 9 (8): 1811-1815.
- Bomfim TR, Forny-Germano L, Sathler LB, Brito-Moreira J, Houzel JC, Decker H, et al. 2012. 'An anti-diabetes agent protects the mouse brain from defective insulin signaling caused by Alzheimer's disease associated Abeta oligomers. ', *J Clin Invest*, 122: 1339-53.
- Bonda DJ, Wang X, Perry G, Smith MA, Zhu X., 2010. 'Mitochondrial dynamics in Alzheimer disease: opportunities for future treatment strategies. ', *Drugs and Aging*, 27: 1-12.
- Bondareff W, Mountjoy CQ, Roth M, Rossor MN, Iversen LL, Reynolds GP, and Hauser DL. 1987. Neuronal degeneration in locus ceruleus and cortical correlates of Alzheimer disease. *Alzheimer Dis. Assoc. Disord.* 1 (4): 256-262.
- Boom A, Authelet M, Dedecker R, Frederick C, Van Heurck R, Daubie V, Leroy K, Pochet R, Brion JP. . 2009. 'Bimodal modulation of tau protein phosphorylation and conformation by extracellular Zn<sup>2+</sup> in human-tau transfected cells. ', *Biochim. Biophys. Acta*: 1058-67.
- Borchardt T, Schmidt C, Camarkis J, Cappai R, Masters CL., and Multhaup G Beyreuther K. 2000. 'Differential effects of zinc on amyloid precursor protein (APP) processing in copperresistant variants of cultured Chinese hamster ovary cells.', *Cell Mol Biol*: 785-95.

- Borghain R, Szasz J, Stanzione P, Meshram C, Bhatt M, Chirilineau D, et al. 2014. 'Randomized trial of safinamide add-on to levodopa in Parkinson's disease with motor fluctuations. ', *Mov Disord.*, 29: 229-37.
- Boureau YL, and Dayan P. 2011. Opponency revisited: competition and cooperation between dopamine and serotonin. *Neuropsychopharmacology* 36 (1): 74-97.
- Braak H, Braak E. 1994. 'Morphological criteria for the recognition of Alzheimer's disease and the distribution pattern of cortical changes related to this disorder.', *Neurobiol. Aging*, 15: 355-56.
- Bromberg-Martin ES, and Hikosaka O. 2009. Midbrain dopamine neurons signal preference for advance information about upcoming rewards. *Neuron* 63 (1): 119-126.
- Brown KL, Cosseau C, Gardy JL, Hancock RE. 'Complexities of targeting innate immunity to treat infection. ', *Trends Immunol*, 28: 260-66.
- Brunden KR, Trojanowski JQ, and Lee VM. 2009. Advances in tau-focused drug discovery for Alzheimer's disease and related tauopathies. *Nat. Rev. Drug Discov.* 8 (10): 783-793.
- Brunden KR, Zhang B, Carroll J, et al. 2010. 'Epothilone D improves microtubule density, axonal integrity, and cognition in a transgenic mouse model of tauopathy', *J Neurosci*, 30: 13861-66.
- Bruno MA, Leon WC, Fragoso G, Mushynski WE, Almazan G, and Cuello AC. 2009. Amyloid beta-induced nerve growth factor dysmetabolism in Alzheimer disease. *J Neuropathol. Exp. Neurol.* 68 (8): 857-869.
- Bullock R, Lane R. 2007. 'Executive dyscontrol in dementia, with emphasis on subcortical pathology and the role of butyrylcholinesterase.', *Curr Alzheimer Res.*, 4: 277-93.
- Bush AI, and Tanzi RE. 2008. Therapeutics for Alzheimer's disease based on the metal hypothesis. *Neurotherapeutics.* 5 (3): 421-432.
- Bush AI, Multhaup G, Moir RD, Williamson TG, Small DH, Rumble B, Pollwein P, Beyreuther K, Masters CL. 1993. A novel zinc (II) binding site modulates the function of the beta A4 amyloid protein precursor of Alzheimer's disease. ', *J. Biol. Chem.*: 16109-12.
- Bush AI, Pettingell Jr WH, de Paradis M, Tanzi RE, Wasco W. 1994a. The amyloid beta-protein precursor and its mammalian homologues: evidence for a zinc-modulated heparin-binding superfamily., *J. Biol. Chem.*: 26618-21.
- Bush AI, Pettingell Jr WH, Paradis MD, Tanzi RE. . 1994b. 'Modulation of A beta adhesiveness and secretase site cleavage by zinc. ', *J. Biol. Chem.*: 12152-58.
- Bush AI, Pettingell WH, Multhaup G, de Paradis M, Vonsattel JP, Gusella JF, Beyreuther K, Masters CL, Tanzi RE 1994c. 'Rapid induction of Alzheimer Abeta amyloid formation by zinc.', *Science*: 1464-67.
- Bush AI. 2003. The metallobiology of Alzheimer's disease. *Trends Neurosci.*, 26: 207-14.
- Butterfield DA, Reed T, Perluigi M, De Marco C, Coccia R, Cini C, Sultana R., 2006. 'Elevated protein-bound levels of the lipid peroxidation product, 4-hydroxy-2-nonenal, in brain from persons with mild cognitive impairment.', *Neuroscience Letters*.

- Caccia C, Maj R, Calabresi M, Maestroni S, Faravelli L, Curatolo L, et al. 2006. 'Safinamide: from molecular targets to a new antiParkinson drug.', *Neurology.*, 67: S18-23.
- Cappai R, Kong G, McKinstry W, Galatis D, Adams J, Bellingham S, Camakaris J, Curtain C, Williamson N, White A, . 2004. 'Structural and functional analysis of the Alzheimer's disease amyloid precursor protein copper binding domain.', *Neurobiol. Aging*, 25: s60-s60.
- Capurro V, Busquet P, Lopes JP, Bertorelli R, Tarozzo G, Bolognesi ML, Piomelli D, Reggiani A, Cavalli A.,. 2013. 'Pharmacological Characterization of Memoquin, a MultiTarget Compound for the Treatment of Alzheimer's Disease', *PLoS One*, 8: e56870.
- Castellani RJ, Lee HG, Zhu X, Nunomura A, Perry G, Smith MA.,. 2006. 'Neuropathology of Alzheimer disease: pathognomonic but not pathogenic.' *Acta Neuropathologica*, 111: 503-09.
- Cattaneo A, Capsoni S, and Paoletti F. 2008. Towards non invasive nerve growth factor therapies for Alzheimer's disease. *J. Alzheimers. Dis.* 15 (2): 255-283.
- Cattaneo C, Caccia C, Marzo A, Maj R, Fariello RG. 2003. 'Pressor response to intravenous tyramine in healthy subjects after safinamide, a novel neuroprotectant with selective, reversible monoamine oxidase B inhibition. ', *Clin Neuropharmacol.*, 26: 213-17.
- Cavalli A, Bolognesi ML, Capsoni S, Andrisano V, Bartolini M, Margotti E, Cattaneo A, Recanatini M, Melchiorre C. 'A small molecule targeting the multifactorial nature of Alzheimer's disease.', *Angew Chem Int Ed Engl.*, 46: 3689-92.
- Cavalli A, Bolognesi ML. 2012. 'Multitargeted Drugs for Treatment of Alzheimer's Disease ', *Polypharmacology in Drug Discovery*: 441–58.
- Chan-Palay V, and Asan E. 1989. Alterations in catecholamine neurons of the locus coeruleus in senile dementia of the Alzheimer type and in Parkinson's disease with and without dementia and depression. *J. Comp Neurol.* 287 (3): 373-392.
- Chazot PL, . . 2007. 'Safinamide for the treatment of Parkinson's disease, epilepsy and restless legs syndrome.', *Curr Opin Investig Drugs.*, 8: 570-79.
- Cherny RA, Atwood CS, Xilinas ME, Gray DN, Jones WD, McLean CA, Barnham KJ, Volitaskis I, Fraser F, Kim YH, Huang X, Goldstein LE, Moir RD, Lim JT, Beyreuther K, Zheng H, Tanzi RE, Masters CL, Bush AI. . 2001. 'Treatment with a copper–zinc chelator markedly and rapidly inhibits beta-amyloid accumulation in Alzheimer's disease transgenic mice. ', *Neuron*: 665-76.
- Chester DS, DeWall CN, Derefinko KJ, Estus S, Peters JR, Lynam DR, and Jiang Y. 2015. Monoamine oxidase A (MAOA) genotype predicts greater aggression through impulsive reactivity to negative affect. *Behav. Brain Res.* 283: 97-101.
- Christensen H, Maltby N, Jorm AF, Creasey H, Broe GA.,. 1992. 'Cholinergic 'blockade' as a model of the cognitive deficits in Alzheimer's disease.', *Brain*, 115: 1681-99.
- Cifariello A, Pompili A, Gasbarri A.,. 2008. '5-HT(7) receptors in the modulation of cognitive processes', *Behav. Brain Res.*, 195: 171-79.
- Ciro A, Park J, Burkhard G, and et al. 2012. 'Biochemical differentiation of cholinesterases from normal and Alzheimer's disease cortex', *Curr Alzheimer Res*, 9: 138-43.

- Citron M, Oltersdorf T, Haass C, McConlogue L, Hung AY, Seubert P, Vigo-Pelfrey C, Lieberburg I, Selkoe DJ. 1992. 'Mutation of the beta-amyloid precursor protein in familial Alzheimer's disease increases beta-protein production.', *Nature*, 360: 672-74.
- Claxton A, Baker LD, Wilkinson CW, Trittschuh EH, Chapman D, Watson GS, Cholerton B, Plymate SR, Arbuckle M, Craft S. 'Sex and ApoE genotype differences in treatment response to two doses of intranasal insulin in adults with mild cognitive impairment or Alzheimer's disease. ', *J. Alzheimers Dis.* 787-97.
- Cole GM, Teter B, Frautschy SA. 2007. 'Neuroprotective effects of curcumin.', *Adv Exp Med Biol*, 595: 197-212.
- Collingwood JF, Mikhaylova A, Davidson M, Batich C, Streit WJ, Terry J, Dobson J., 2005. 'In situ characterization and mapping of iron compounds in Alzheimer's disease tissue.', *J. Alzheimers Dis.*, 267-72.
- Connor JR, Menzies St SL, Martin SM, Mufson EJ., . 1992. 'A histochemical study of iron, transferrin, and ferritin in Alzheimer's diseased brains.', *J. Neurosci. Res.*, 31: 75-83.
- Coric V, van Dyck CH, Salloway S, et al. . 2012. 'Safety and tolerability of the gamma-secretase inhibitor Avagacestat in a phase 2 study of mild to moderate Alzheimer disease. ', *Arch Neurol*, 69: 1430-40.
- Cortes R, Probst A, and Palacios JM. 1988. Decreased densities of dopamine D1 receptors in the putamen and hippocampus in senile dementia of the Alzheimer type. *Brain Res.* 475 (1): 164-167.
- Corrigan FM, Reynolds GP, Ward NI. . 1993. 'Hippocampal tin, aluminum and zinc in Alzheimer's disease.', *Biometals*: 149-54.
- Corrigan FM, Reynolds GP, Ward NI. . 1993. 'Hippocampal tin, aluminum and zinc in Alzheimer's disease.', *Biometals*: 149-54.
- Coulson EJ, Paliga K, Beyreuther K, Masters CL., 2000. 'What the evolution of the amyloid protein precursor supergene family tells us about its function.', *Neurochem.*, 36: 175-84.
- Crouch PJ, Barnham KJ. 2012. 'Therapeutic redistribution of metal ions to treat Alzheimer's disease.', *Acc Chem Res.*, 45: 1604-11.
- Crouch PJ, Blake R, Duce JA, Ciccotosto GD, Li QX, Barnham KJ, Curtain CC, Cherny RA, Cappai R, Dyrks T, Masters CL, Trounce IA. 2005. 'Copper-dependent inhibition of human cytochrome c oxidase by a dimeric conformer of amyloid-beta(1-42).', *J. Neurosci.*, 25: 672-79.
- Crouch PJ, Savva MS, Hung LW, et al. 2011. 'The Alzheimer's therapeutic PBT2 promotes amyloid- $\beta$  degradation and GSK3 phosphorylation via a metal chaperone activity', *J Neurochem*, 119: 220-30.
- Crouch PJ, Tew DJ, Du T, Nguyen DN, Caragounis A, Filiz G, Blake RE, Trounce IA, Soon CP, Laughton K, Perez KA, Li QX, Cherny RA, Masters CL, Barnham KJ, White AR. . 2009. 'Restored degradation of the Alzheimer's amyloid-beta peptide by targeting amyloid formation. ', *J. Neurochem.*: 1198-207.

- Cuajungco MP, Faget KY. 2003. 'Zinc takes the center stage: Its paradoxical role in Alzheimer's disease', *Brain Res Brain Res Rev*: 44-56.
- Curtain CC, Ali FE, Volitaskis I, Cherny RA, Norton RS, Beyreuther K, Barrow CJ, Masters CL, Bush AI, Barnham KJ. 2001. 'Alzheimer's disease amyloid-beta binds copper and zinc to generate an allosterically ordered membrane-penetrating structure containing superoxide dismutase-like subunits. ', *J. Biol. Chem.*, 276: 20466-2047.
- Cutillas B, Ambrosio S, and Unzeta M. 2002. Neuroprotective effect of the monoamine oxidase inhibitor PF 9601N [N-(2-propynyl)-2-(5-benzyloxy-indolyl) methylamine] on rat nigral neurons after 6-hydroxydopamine-striatal lesion. *Neurosci. Lett.* 329 (2): 165-168.
- Czirr E, Wyss-Coray T. 2012. 'The immunology of neurodegeneration.', *J Clin Invest*: 1156-63.
- Da Prada M, Zürcher G, Wüthrich I, Haefely WE 1988. 'On tyramine, food, beverages and the reversible MAO inhibitor moclobemide', *J Neural Transm Suppl*: 31-56.
- Da Prada M, Zürcher G, Wüthrich I, Haefely WE 1988. 'On tyramine, food, beverages and the reversible MAO inhibitor moclobemide', *J Neural Transm Suppl*: 31-56.
- Daikhin Y, Yudkoff M. 'Compartmentation of brain glutamate metabolism in neurons and glia', *J Nutr.*, 130: 1026S-31S.
- Dajas-Bailador FA, Heimala K, Wonnacott S 'The allosteric potentiation of nicotinic acetylcholine receptors by galantamine is transduced into cellular responses in neurons: Ca<sup>2+</sup> signals and neurotransmitter release.', *Mol Pharmacol.*, 1217-26.
- Damante CA, Osz K, Nagy Z, Pappalardo G, Grasso G, Impellizzeri G, Rizzarelli E, Sovago I. 2009. 'Metal loading capacity of Abeta N-terminus: a combined potentiometric and spectroscopic study of zinc(II) complexes with Abeta(1-16), its short or mutated peptide fragments and its polyethylene glycol-ylated analogue. ', *Inorg. Chem*: 10405-15.
- Danscher G, Jensen KB, Frederickson CJ, Kemp K, Andreasen A, Juhl S, Stoltenberg M, Ravid R., 1997. 'Increased amount of zinc in the hippocampus and amygdala of Alzheimer's diseased brains: a proton-induced X-ray emission spectroscopic analysis of cryostat sections from autopsy material.', *J. Neurosci. Methods*: 53-59.
- Danscher, G.; Jensen, K. B.; Frederickson, C. J.; Kemp, K.; Andreasen, A.; Juhl, and M.; Ravid S.; Stoltenberg, R. 1997. 'Increased amount of zinc in the hippocampus and amygdala of Alzheimer's diseased brains: a proton-induced X-ray emission spectroscopic analysis of cryostat sections from autopsy material.', *J. Neurosci. Methods*: 53-59.
- Darreh-Shori T, Brimijoin S, Kadir A, and et al. 2006. 'Differential CSF butyrylcholinesterase levels in Alzheimer's disease patients with the ApoE epsilon4 allele, in relation to cognitive function and cerebral glucose metabolism.', *Neurobiol Dis.*, 24: 326-33.
- Darreh-Shori T, Forsberg A, Modiri N, and et al. 'Differential levels of apolipoprotein E and butyryl-cholinesterase show strong association with pathological signs of Alzheimer's disease in the brain in vivo. ', *Neurobiol Aging.*, 32: 23-20.

- Darreh-Shori T, Soininen H, . . 2010. 'Effects of cholinesterase inhibitors on the activities and protein levels of cholinesterases in the cerebrospinal fluid of patients with Alzheimer's disease: A review of recent clinical studies.', *Curr Alzheimer Res*, 7: 67-73.
- Darvesh S, Grantham DL, and Hopkins DA. 1998. 'Distribution of butyrylcholinesterase in the human amygdala and hippocampal formation', *J Comp Neurol.*, 393.
- Darvesh S, MacKnight C, and Rockwood K. 2001. ' Butyrylcholinesterase and cognitive function', *Int Psychogeriatr.*, 13: 461-64.
- Darvesh S, MacKnight C, Rockwood K. . 2001. 'Butyrylcholinesterase and cognitive function', *Int Psychogeriatr.*, 13: 461-64.
- Das UN. 2007. 'Acetylcholinesterase and butyrylcholinesterase as possible markers of low-grade systemic inflammation', *Med Sci Monit*, 12: RA214-RA21.
- Davies P, Maloney AJ. 1976. 'Selective loss of central cholinergic neurons in Alzheimer's disease. ', *Lancet*: 1403.
- De Colibus CL, Li M, Binda C, Lustig A, Edmondson DE, and Mattevi A. 2005. Three-dimensional structure of human monoamine oxidase A (MAO A): relation to the structures of rat MAO A and human MAO B. *Proc. Natl. Acad. Sci. U. S. A* 102 (36): 12684-12689.
- De Domenico I, McVey-Ward D, Kaplan J., . 2008. 'Regulation of iron acquisition and storage: consequences for iron-linked disorders', *Nature Reviews Molecular Cell Biology*, 9: 72-81.
- De Strooper B, Beullens M, Contreras B, Levesque L, Craessaerts K, Cordell B, Moechars D, Bollen M, Fraser P, George-Hyslop PS, Van Leuven F., 1997. 'Phosphorylation, subcellular localization, and membrane orientation of the Alzheimer's disease-associated presenilins.', *J Biol Chem.*, 272: 3590-98.
- Deibel MA, Ehmann WD, Markesbery WR. . 1996. 'Copper, iron, and zinc imbalances in severely degenerated brain regions in Alzheimer's disease: possible relation to oxidative stress. ', *J. Neurol. Sci.*: 137-42.
- Deibel MA, Ehmann WD, Markesbery WR., . 1996. 'Copper, iron, and zinc imbalances in severely degenerated brain regions in Alzheimer's disease: possible relation to oxidative stress. ', *J. Neurol. Sci.*: 137-42.
- Deibel, M. A.; Ehmann, W. D.; Markesbery, W. R. . 1996. 'Copper, iron, and zinc imbalances in severely degenerated brain regions in Alzheimer's disease: possible relation to oxidative stress. ', *J. Neurol. Sci.*: 137-42.
- Del Pino J, Ramos E, Bautista Aguilera OM, Marco-Contelles J, Romero A. 2014. 'Wnt Signaling Pathway, a Potential Target for Alzheimer's Disease Treatment, is Activated by a Novel Multitarget Compound ASS234', *CNS Neurosc Ther*: 568-70.
- Détári L, Rasmusson DD, Semba K., 1999. 'The role of basal forebrain neurons in tonic and phasic activation of the cerebral cortex.', *Prog Neurobiol.*, 58: 249-77.
- Deutsch JA. 1971. The cholinergic synapse and the site of memory. *Science* 174 (4011): 788-794.
- Di GS, Eleuteri S, Paleologou KE, Yin G, Zweckstetter M, Carrupt PA, and Lashuel HA. 2010. Entacapone and tolcapone, two catechol O-methyltransferase inhibitors, block

- fibril formation of alpha-synuclein and beta-amyloid and protect against amyloid-induced toxicity. *J. Biol. Chem.* 285 (20): 14941-14954.
- Diamant S, Podoly E, Friedler A, Ligumsky H, Livnah O, and Soreq H. 2006. Butyrylcholinesterase attenuates amyloid fibril formation in vitro. *Proc. Natl. Acad. Sci. U. S. A* 103 (23): 8628-8633.
- Dickey CA, Kamal A, Lundgren K, Klosak N, Bailey RM, Dunmore J, Ash P, Shoraka S, Zlatkovic J, Eckman CB, Patterson C, Dickson DW, Nahman Jr. NS, Hutton M, Burrows F, Petrucelli L., 2007. 'The high-affinity HSP90-CHIP complex recognizes and selectively degrades phosphorylated tau client proteins. ', *J. Clin. Invest.*, 117: 648-58.
- Dickerson BC, Salat DH, Greve DN, Chua EF, Rand-Giovannetti E, Rentz DM, Bertram L, Mullin K, Tanzi RE, Blacker D, Albert MS, and Sperling RA. 2005. Increased hippocampal activation in mild cognitive impairment compared to normal aging and AD. *Neurology* 65 (3): 404-411.
- Diez M, Danner S, Frey P, Sommer B, Staufenbiel M, Wiederhold KH, and Hokfelt T. 2003. Neuropeptide alterations in the hippocampal formation and cortex of transgenic mice overexpressing beta-amyloid precursor protein (APP) with the Swedish double mutation (APP23). *Neurobiol. Dis.* 14 (3): 579-594.
- Dobson J, Batich C. 2004. 'A potential iron-based mechanism for enhanced deposition of amyloid plaques due to cognitive stimulation in Alzheimer disease.', *J Neuropathol Exp Neurol.*, 63: 674-75.
- Doody R.S., Dunn J.K., Clark C.M., Farlow M., Foster N.L, Liao T., *et al.* 2001. 'Chronic donepezil treatment is associated with slowed cognitive decline in Alzheimer's disease.', *Dementi Geriat Cogn Disord*: 295-300.
- Doody RS, Tariot PN, Pfeiffer E, Olin JT, Graham SM. 2007. 'Meta-analysis of six-month memantine trials in Alzheimer's disease.', *Alzheimers Dement.*, 3.
- Doody RS, Thomas RG, Farlow M, Iwatsubo T, Vellas B, Joffe S, *et al.* 2014. 'Alzheimer's Disease Cooperative Study Steering Committee; Solanezumab study group. Phase 3 trials of solanezumab for mild-to-moderate Alzheimer's disease.', *N Engl J Med.*, 370: 311-21.
- Dragoni S, Materozzi G, Pessina F, Frosini M, Marco JL, Unzeta M, Sgaragli G, Valoti M. 2007. 'CYP-dependent metabolism of PF9601N, a new monoamine oxidase-B inhibitor, by C57BL/6 mouse and human liver microsomes.', *J Pharm Pharm Sci.*, 10: 473-85.
- Duce JA, Bush AI 2010. 'Biological metals and Alzheimer's disease: Implications for therapeutics and diagnostics. ', *Prog Neurobiol Aging.*: 1-18.
- Duce JA, Tsatsanis A, Cater MA, James SA, Robb E, Wikhe K, Leong SL, Perez K, Johanssen T, Greenough MA, Cho HH, Galatis D, Moir RD, Masters CL, McLean C, Tanzi RE, Cappai R, Barnham KJ, Ciccotosto GD, Rogers JT, Bush AI,. 2010. 'Iron-export ferroxidase activity of beta-amyloid precursor protein is inhibited by zinc in Alzheimer's disease', *Cell*: 857-67.
- Duce JA, Tsatsanis A, Cater MA, James SA, Robb E, Wikhe, Leong SL K, Perez K, Johanssen T, Greenough MA, Cho, Galatis D HH, Moir RD, Masters CL, McLean

- C, Tanzi RE, and Barnham KJ Cappai R, Ciccotosto GD, Rogers JT, Bush AI. 2010. 'Iron-export ferroxidase activity of beta-amyloid precursor protein is inhibited by zinc in Alzheimer's disease', *Cell*: 857-67.
- Eckenroth BE, Steere AN, Chasteen ND, Everse SJ, Mason AB,. 2011. 'How the binding of human transferrin primes the transferrin receptor potentiating iron release at endosomal pH', *Proc. Natl. Acad. Sci. USA*, 108: 13089-94.
- Edmondson DE, Binda C, and Mattevi A. 2007. Structural insights into the mechanism of amine oxidation by monoamine oxidases A and B. *Arch. Biochem. Biophys.* 464 (2): 269-276.
- Egaña JT, Zambrano C, Nuñez MT, Gonzalez-Billault C, Maccioni RB.. 2003. 'Iron-induced oxidative stress modifies tau phosphorylation patterns in hippocampal cell cultures.', *Biometals*.
- EnVivo Pharmaceuticals, Inc. 'Safety, tolerability, pharmacokinetics of EVP-0962 and effects of EVP-0962 on cerebral spinal fluid amyloid concentrations in healthy subjects and in subjects with mild cognitive impairment or early Alzheimer's disease'.
- Eriksen JL, Sagi SA, Smith TE, Weggen S, Das P, McLendon DC, Ozols VV, Jessing KW, Zavitz KH, Koo EH, Golde TE.. 2003. 'NSAIDs and enantiomers of flurbiprofen target gamma-secretase and lower Abeta 42 in vivo.', *J. Clin. Invest.*, 112: 440-49.
- Evin G, Weidemann A. 2002. 'Biogenesis and metabolism of Alzheimer's disease Abeta amyloid peptides.', *Peptides*, 23: 1285-97.
- Ewbank JJ, Barnes TM, Lakowski B, Lussier M, Bussey H, Hekimi S. 1997. 'Structural and functional conservation of the Caenorhabditis elegans timing gene clk-1. ', *Science*: 980-83.
- Faller P, Hureau C, and Berthoumieu O. 2013. Role of metal ions in the self-assembly of the Alzheimer's amyloid-beta peptide. *Inorg. Chem.* 52 (21): 12193-12206.
- Faux NG, Ritchie CW, Gunn AP, Rembach A, Tsatsanis A, Bedo J, Harrison J, Lannfelt L, Blennow K, Zetterberg H, Ingelsson M, Masters CL, Tanzi RE, Cummings JL, Herd CM, Bush AI. 2010. 'PBT2 rapidly improves cognition in Alzheimer's disease: additional phase II analyses.', *J. Alzheimers Dis.*: 509-16.
- Feng Y, Wang X. 2012. 'Antioxidant therapies for Alzheimer's disease.', *Oxid Med Cell Longev.*, 2012: 472932.
- Fibiger HC. 1991. 'Cholinergic mechanisms in learning, memory and dementia: a review of recent evidence.', *Trends Neurosci.*, 14: 220-23.
- Figueiredo CP, Clarke JR, Ledo JH, Ribeiro FC, Costa CV, Melo HM, Mota-Sales AP, Saraiva LM, Klein WL, Sebollela A, De Felice FG, Ferreira ST. 2013. 'Memantine rescues transient cognitive impairment caused by high-molecular-weight aβ oligomers but not the persistent impairment induced by low-molecular-weight oligomers.', *J Neurosci.*, 33: 9626-34.
- Filip V, and Kolibas E. 1999. Selegiline in the treatment of Alzheimer's disease: a long-term randomized placebo-controlled trial. Czech and Slovak Senile Dementia of Alzheimer Type Study Group. *J. Psychiatry Neurosci.* 24 (3): 234-243.

- Filiz G, Caragounis A, Bica L, Du T, Masters CL, Crouch PJ, White AR. 2008a. 'Clioquinol inhibits peroxide-mediated toxicity through up-regulation of phosphoinositol-3-kinase and inhibition of p53 activity.', *Int. J. Biochem. Cell Biol.*: 1030–42.
- Filiz G, Price KA, Caragounis A, Du T, Crouch PJ, White AR. 2008b. 'The role of metals in modulating metalloprotease activity in the AD brain.', *Eur. Biophys. J.* : 315-21.
- Finberg JP, Youdim MB. . 2002. 'Pharmacological properties of the antiParkinson drug rasagiline; modification of endogenous brain amines, reserpine reversal, serotonergic and dopaminergic behaviours.', *Neuropharmacology.*, 43: 1110-18.
- Fornai F, et al. 1999. 'Striatal dopamine metabolism in monoamine oxidase B-deficient mice: a brain dialysis study.', *J. Neurochem.*: 2434-40.
- Forman MS, Trojanowski JQ, Lee VM,. 2004. 'Neurodegenerative diseases: a decade of discoveries paves the way for therapeutic breakthroughs.', *Nat Med.*, 10: 1055-63.
- Fowler JS, et al. . 1987. 'Mapping human brain monoamine oxidase A and B with <sup>11</sup>C-labeled suicide inactivators and PET.', *Science* 481-85.
- Frederickson CJ, Giblin LJ, Balaji RV, Masalha R, Zeng Y, Lopez EV, Koh JY, Chorin U, Besser L, Hershfinkel M, Li Y, Thompson RB, Krezel A. 2006. 'Synaptic release of zinc from brain slices: factors governing release, imaging, and accurate calculation of concentration', *J. Neurosci. Methods*: 19-29.
- Frederickson, C. J. 1989. 'Neurobiology of zinc and zinc-containing neurons', *Int. Rev. Neurobiol*: 145-238.
- Frederickson, C. J.; Giblin 3rd L. J.; Balaji, R. V.; Masalha, R.; Zeng, Y.; Lopez, E., J. Y.; Chorin V.; Koh, U.; Besser, L.; Hershfinkel, M.; Li, Y.; Thompson, R. B., and A. Krezel. 2006. 'Synaptic release of zinc from brain slices: factors governing release, imaging, and accurate calculation of concentration', *J. Neurosci. Methods*: 19-29.
- Frolich L, Ashwood T, Nilsson J, Eckerwall G. 'Effects of AZD3480 on cognition in patients with mild-to-moderate Alzheimer's disease: a phase IIb dose-finding study', *J Alzheimers Dis*, 24: 363-74.
- Fuchs E, Czeh B, Kole MH, Michaelis T, and Lucassen PJ. 2004. Alterations of neuroplasticity in depression: the hippocampus and beyond. *Eur. Neuropsychopharmacol.* 14 Suppl 5: S481-S490.
- Fujii T, Mori Y, Tominaga T, Hayasaka I, Kawashima K,. 1997. 'Maintenance of constant blood acetylcholine content before and after feeding in young chimpanzees.', *Neurosci Lett*, 227: 21-24.
- Fukuda M, Kanou F, Shimada N, Sawabe M, Saito Y, Murayama S, Hashimoto M, Maruyama N, Ishigami A,. 2009. 'Elevated levels of 4-hydroxynonenal-histidine Michael adduct in the hippocampi of patients with Alzheimer's disease.', *Biomed Res.*, 30.
- Fukushima T, Makamura A, Iwakami N, et al. 2011. 'T-817MA, a neuroprotective agent, attenuates the motor and cognitive impairments associated with neuronal degeneration in P301L tau transgenic mice.', *Biochem Biophys Res Commun*, 407: 730-34.
- Fukuto TR. 1990. 'Mechanism of action of organophosphorus and carbamate insecticides', *Environ Health Perspect*, 87: 245-54.

- Fuxe K, Canals M, Torvinen M, Marcellino D, Terasmaa A, Genedani S, Leo G, Guidolin D, Diaz-Cabiale Z, Rivera A, Lundstrom L, Langel U, Narvaez J, Tanganelli S, Lluís C, Ferre S, Woods A, Franco R, and Agnati LF. 2007. Intramembrane receptor-receptor interactions: a novel principle in molecular medicine. *J. Neural Transm.* 114 (1): 49-75.
- Gaczynska M, Osmulski PA, Ward WF,. 2001. 'Caretaker or undertaker? The role of the proteasome in aging.', *Mech Ageing Dev.*, 122: 235-54.
- Gal S, Zheng H, Fridkin M, Youdim MB 2005. ' Novel multifunctional neuroprotective iron chelator-monoamine oxidase inhibitor drugs for neurodegenerative diseases. In vivo selective brain monoamine oxidase inhibition and prevention of MPTP-induced striatal dopamine depletion.', *J Neurochem Int.*: 79-88.
- Galasko DR, Graff-Radford N, May S, Hendrix S, Cottrell BA, Sagi SA, Mather G, Laughlin M, Zavitz KH, Swabb E, Golde TE, Murphy MP, Koo EH. 2007. 'Safety, tolerability, pharmacokinetics, and Abeta levels after short-term administration of R-flurbiprofen in healthy elderly individuals.', *Alzheimer Dis. Assoc. Disord.*, 21: 292-99.
- Galasko DR, Peskind E, Clark CM, Quinn JF, Ringman JM, Jicha GA, Cotman C, Cottrell B, Montine TJ, Thomas RG, Aisen P.. 2012. 'Antioxidants for Alzheimer disease: a randomized clinical trial with cerebrospinal fluid biomarker measures.', *Arch Neurol.*, 69: 836-41.
- Gerald Z, Ockert W. . 2013. 'Alzheimer's disease market: hope deferred.', *Nat Rev Drug Discov*, 12: 19-20.
- Geula C, and Mesulam M. 'Special properties of cholinesterases in the cerebral cortex of Alzheimer's disease.', *Brain Res*, 498: 185-89.
- Giacobini E. 2001. 'Selective inhibitors of butyrylcholinesterase: a valid alternative for therapy of Alzheimer's', *Drugs Aging*: 891-98.
- Giacobini E. 2003. *Butyrylcholinesterase: Its function and inhibitors.*
- Giommarelli C, Zuco V, Favini E, Pisano C, Dal Piaz F, De Tommasi N, Zunino F.. 2010. 'The enhancement of antiproliferative and proapoptotic activity of HDAC inhibitors by curcumin is mediated by Hsp90 inhibition. ', *Cell Mol. Life Sci.*, 67: 995-1004.
- Glenner GG1, Murphy MA. 1989. 'Amyloidosis of the nervous system.', *J Neurol Sci.*, 94: 1-28.
- Goedert M, Klug A, Crowther RA,. 2006. 'Tau protein, the paired helical filament and Alzheimer's disease.', *J Alzheimers Dis.*, 9: 195-207.
- Goedert M, and Jakes R. 2005. Mutations causing neurodegenerative tauopathies. *Biochim. Biophys. Acta* 1739 (2-3): 240-250.
- Golde TE, Petrucelli L, Lewis J. 'Targeting A $\beta$  and tau in Alzheimer's disease, an early interim report', *Exp Neurol.*, 252-66.
- Gomes LM, Vieira RP, Jones MR, Wang MC, Dyrager C, Souza-Fagundes EM, Da Silva JG, Storr T, Beraldo H. 2014. '8-Hydroxyquinoline Schiff-base compounds as antioxidants and modulators of copper-mediated A $\beta$  peptide aggregation.', *J Inorg Biochem.*, 139: 106-16.

- Gong CX, and Iqbal K. 2008. Hyperphosphorylation of microtubule-associated protein tau: a promising therapeutic target for Alzheimer disease. *Curr. Med. Chem.* 15 (23): 2321-2328.
- Gonzalez-Burgos I, and Feria-Velasco A. 2008. Serotonin/dopamine interaction in memory formation. *Prog. Brain Res.* 172: 603-623.
- Goodman L. 'Alzheimer's disease; a clinico-pathologic analysis of twentythree cases with a theory on pathogenesis.', *J. Nerv. Mental Dis.*
- Gottfries CG. 1986. Monoamines and myelin components in aging and dementia disorders. *Prog. Brain Res.* 70: 133-140.
- Gozes I. 'NAP (davunetide) provides functional and structural neuroprotection.', *Curr. Pharm. Des.*, 17: 1040-44.
- Grant WB, Campbell A, Itzhaki RF, Savory J., 2002. 'The significance of environmental factors in the etiology of Alzheimer's disease.', *J Alzheimers Dis*, 4: 179-89.
- Gravius A, Laszy J, Pietraszek M, Saghy K, Nagel J, Chambon C, Wegener N, Valastro B, Danysz W, Gyertyan I., 2011. 'Effects of 5-HT6 antagonists, Ro- 4368554 and SB-258585, in tests used for the detection of cognitive enhancement and antipsychotic-like activity. ', *Behav. Pharmacol.*, 22: 122-35.
- Greenblatt HM, Kryger G, Lewis T, Silman I, Sussman JL. 1999. 'Structure of acetylcholinesterase complexed with (-)-galanthamine at 2.3 Å resolution.', *FEBS Lett.* 321-26.
- Gregoire L, Jourdain VA, Townsend M, Roach A, Di Paolo T. 2013. 'Safinamide reduces dyskinesias and prolongs L-DOPA antiparkinsonian effect in parkinsonian monkeys.', *Parkinsonism Relat Disord.*, 19: 508-14.
- Grossi C, Francese S, Casini A, Rosi MC, Luccarini I, Fiorentini A, Gabbiani C, Messori L, Moneti G, Casamenti F. 2009. 'Clioquinol decreases amyloid-beta burden and reduces working memory impairment in a transgenic mouse model of Alzheimer's disease.', *J. Alzheimers Dis.*: 423-40.
- Group., Parkinson Study. 2002. 'A controlled trial of rasagiline in early Parkinson disease: the TEMPO Study', *Arch Neurol.*, 59: 1937-43.
- Guglielmotto M, Giliberto L, Tamagno E, Tabaton M 2010. 'Oxidative stress mediates the pathogenic effect of different Alzheimer's disease risk factors.', *Front Aging Neurosci*, 2, 3.
- Guillozet AL, Smiley JF, Mash DC, and et al. 1997. 'Butyrylcholinesterase in the life cycle of amyloid plaques', *Ann Neurol.*, 42: 909-18.
- Hardy JA, Higgins GA. 1992. 'Alzheimer's disease: the amyloid cascade hypothesis.', *Science*, 256: 184-85.
- Hartter DE, Barnea A. 1988. 'Evidence for release of copper in the brain: depolarization-induced release of newly taken-up 67 copper.', *Synapse*, 2: 412-15.
- Harvey RJ, Skelton-Robinson M, Rossor MN., 2003. 'The prevalence and causes of dementia in people under the age of 65 years', *J Neurol Neurosurg Psych*, 74: 1206-09.

- Hasan F, McCrodden JM, Kennedy NP, Tipton KF. . 1988. 'The involvement of intestinal monoamine oxidase in the transport and metabolism of tyramine.', *J. Neural Transm.*: 1-9.
- Hayashi T, Shishido N, Nakayama K, Nunomura A, Smith MA, Perry G, Nakamura M., 2007. 'Lipid peroxidation and 4-hydroxy-2-nonenal formation by copper ion bound to amyloid-beta peptide. ', *Free Radical Biology and Medicine*, 43: 1552-59.
- Heinonen EH, Anttila MI, Lammintausta RA. 1994. 'Pharmacokinetic aspects of l-deprenyl (selegiline) and its metabolites.', *Clin Pharmacol Ther.*, 56: 742-49.
- Heinonen EH, Rinne UK, Tuominen J. 1989. 'Selegiline in the treatment of daily fluctuations in disability of parkinsonian patients with long-term levodopa treatment.', *Acta Neurol Scand Suppl.*, 126: 113-18.
- Henry G, Williamson D, and Tampi RR. 2011. Efficacy and tolerability of antidepressants in the treatment of behavioral and psychological symptoms of dementia, a literature review of evidence. *Am. J. Alzheimers. Dis. Other Demen.* 26 (3): 169-183.
- Heppner FL, Ransohoff RM, and Becher B. 2015. Immune attack: the role of inflammation in Alzheimer disease. *Nat. Rev. Neurosci.* 16 (6): 358-372.
- Herreman A, Hartmann D, Annaert W, Saftig P, Craessaerts K, Serneels L, Umans L, Schrijvers V, Checler F, Vanderstichele H, Baekelandt V, Dressel R, Cupers P, Huylebroeck D, Zwijsen A, Van Leuven F, De Strooper B., 1999. 'Presenilin 2 deficiency causes a mild pulmonary phenotype and no changes in amyloid precursor protein processing but enhances the embryonic lethal phenotype of presenilin 1 deficiency.', *Proc Natl Acad Sci U S A.*, 96: 11872-77.
- Hershey LA, Hershey CO, Varnes A, Songmongkolrit T, Strain WH.,. 1984. "Quantitation, localization and variations of brain zinc with aging by instrumental neutron activation analysis." In, 325-34.
- Hershey, L. A.; Hershey, C. O.; Varnes, A.; Songmongkolrit, T.; Strain, W. H. 1984. "Quantitation, localization and variations of brain zinc with aging by instrumental neutron activation analysis." In, 325-34.
- Hilt D, Gawryl M, Koenig G, et al.. 'Positive effects on cognition and clinical function in mild to moderate Alzheimer's disease patients with a selective alpha-7 nicotinic partial agonists: interpretation of effects based on a PK/PD model.', *J Nutr Health Aging*, 819: 25.
- Hirst WD, Stean TO, Rogers DC, Sunter D, Pugh P, Moss SF, Bromidge SM, Riley G, Smith DR, Bartlett S, Heidbreder CA, Atkins AR, Lacroix LP, Dawson LA, Foley AG, Regan CM, Upton N., . 2006. 'SB-399885 is a potent, selective 5-HT<sub>6</sub> receptor antagonist with cognitive enhancing properties in aged rat water maze and novel object recognition models.', *Eur. J. Pharmacol.*, 553: 109-19.
- Hoke DE, Tan JL, Ilaya NT, Culvenor JG, Smith SJ, White AR, Masters CL, Evin GM. 2007. 'In vitro gamma-secretase cleavage of the Alzheimer's amyloid precursor protein correlates to a subset of presenilin complexes and is inhibited by zinc. ', *FEBS J*: 5544-57.

- Hopt A, Korte S, Fink H, Panne U, Niessner R, Jahn R, Kretschmar H, Herms J., . 2003. 'Methods for studying synaptosomal copper release. ', *J. Neurosci. Methods*, 128: 159-72.
- Hou L, Zagorski MG. 2006. 'NMR reveals anomalous copper(II) binding to the amyloid Abeta peptide of Alzheimer's disease. ', *J. Am. Chem. Soc.*, 128: 9260-61.
- Howes MJ, and Perry E. 2011. The role of phytochemicals in the treatment and prevention of dementia. *Drugs Aging* 28 (6): 439-468.
- Hu M, Schurdak ME, Puttfarcken PS, El Kouhen R, Gopalakrishnan M, Li J. 2007. 'High content screen microscopy analysis of A beta 1-42-induced neurite outgrowth reduction in rat primary cortical neurons: neuroprotective effects of alpha 7 neuronal nicotinic acetylcholine receptor ligands.', *Brain Res.*, 1151: 227-35.
- Huang TH, Yang DS, Fraser PE, Chakrabartty A., 2000. 'Alternate aggregation pathways of the Alzheimer beta-amyloid peptide. An in vitro model of preamyloid.', *J Biol Chem.*, 275: 36436-40.
- Huang XT, Qian ZM, He X, Gong Q, Wu KC, Jiang LR, Lu LN, Zhu ZJ, Zhang HY, Yung WH, and Ke Y. 2014. Reducing iron in the brain: a novel pharmacologic mechanism of huperzine A in the treatment of Alzheimer's disease. *Neurobiol. Aging* 35 (5): 1045-1054.
- Huang X, Atwood CS, Hartshorn MA, Multhaup G, Goldstein, Scarpa RC LE, Cuajungco MP, Gray DN, Lim J, Moir RD., and Bush AI Tanzi RE. 1999. 'The A beta peptide of Alzheimer's disease directly produces hydrogen peroxide through metal ion reduction', *Biochemistry* 7609-16.
- Huang X, Cuajungco MP, Atwood CS, Hartshorn MA, Tyndall, Hanson GR JD, Stokes KC, Leopold M, Multhaup G., Scarpa RC Goldstein LE, Saunders AJ, Lim J, Moir RD., Bowden EF Glabe C, Masters CL, Fairlie DP, Tanzi RE, Bush, and AI. 1999. 'Cu(II) potentiation of alzheimer abeta neurotoxicity. Correlation with cell-free hydrogen peroxide production and metal reduction', *J Biol Chem*: 37111-16.
- Huang X, Dai J, Huang C, Zhang Q, Bhanot O, Pelle E.,. 2007. 'Deferoxamine synergistically enhances iron-mediated AP-1 activation: a showcase of the interplay between extracellular-signal-regulated kinase and tyrosine phosphatase.', *Free Radic. Res.*, 41: 1135-42.
- Iannuzzi C, Irace G, and Sirangelo I. 2015. The effect of glycosaminoglycans (GAGs) on amyloid aggregation and toxicity. *Molecules*. 20 (2): 2510-2528.
- Ibach B, Haen E, Marienhagen J, Hajak G. . 2005. 'Clioquinol treatment in familial early onset of Alzheimer's disease: a case report.', *Pharmacopsychiatry*: 178-79.
- Imbimbo BP. 2009. 'Why did tarenflurbil fail in Alzheimer's disease? ', *J. Alzheimers Dis*. 757-60.
- Islam K, Levy E. 1997. 'Carboxyl-terminal fragments of beta-amyloid precursor protein bind to microtubules and the associated protein tau. ', *Am. J. Pathol*, 151: 265-71.
- Iversen LL, Rossor MN, Reynolds GP, Hills R, Roth M, Mountjoy CQ, Foote SL, Morrison JH, and Bloom FE. 1983. Loss of pigmented dopamine-beta-hydroxylase positive cells from locus coeruleus in senile dementia of Alzheimer's type. *Neurosci. Lett*. 39 (1): 95-100.

- Jang J, Surh Y. . 2003. 'Protective effect of resveratrol on beta-amyloid-induced oxidative PC12 cell death.', *Free Radic. Biol. Med.*, 34: 1100-10.
- Jenner P. 2004. Preclinical evidence for neuroprotection with monoamine oxidase-B inhibitors in Parkinson's disease. *Neurology* 63 (7 Suppl 2): S13-S22.
- Jiang H, Wang X, Huang L, Luo Z, Su T, Ding K, Li X. 2011. 'Benzenediol-berberine hybrids: Multifunctional agents for Alzheimer's disease. ', *Bioorg. Med. Chem*: 7228-35.
- Jiao Y, Han DX, Yang P. . 2005. 'Molecular modeling of the inhibitory mechanism of copper(II) on aggregation of amyloid beta-peptide.', *Sci. China Ser.*, 48.
- Jiao Y, Yang P. 2007. 'Mechanism of copper(II) inhibiting Alzheimer's amyloid beta-peptide from aggregation: a molecular dynamics investigation.', *J. Phys. Chem*, 111: 7646-55.
- Jin L, Wu WH, Li QY, Zhao YF, Li YM,. 2011. 'Copper inducing A $\beta$ 42 rather than A $\beta$ 40 nanoscale oligomer formation is the key process for A $\beta$  neurotoxicity.', *Nanoscale.*, 3: 4746-51.
- Jin M, Shepardson N, Yang T, Chen G, Walsh D, Selkoe DJ,. 2011. 'Soluble amyloid beta-protein dimers isolated from Alzheimer cortex directly induce Tau hyperphosphorylation and neuritic degeneration.', *Proc Natl Acad Sci U S A.*, 108: 5819-24.
- Jonassen T, Larsen PL, Clarke CF. 2001. 'A dietary source of coenzyme Q is essential for growth of long-lived *Caenorhabditis elegans* clk-1 mutants.', *Proc. Natl. Acad. Sci. USA*: 421-26.
- Jonsson T, Atwal JK, Steinberg S, Snaedal J, Jonsson PV, Bjornsson S, et al. 2012. 'A mutation in APP protects against Alzheimer's disease and age-related cognitive decline. ', *Nature*, 488: 96-99.
- Kalinin S, Polak PE, Lin SX, Sakharkar AJ, Pandey SC, and Feinstein DL. 2012. The noradrenaline precursor L-DOPS reduces pathology in a mouse model of Alzheimer's disease. *Neurobiol. Aging* 33 (8): 1651-1663.
- Karran E, Marc Mercken M, De Strooper B,. 2011. 'The amyloid cascade hypothesis for Alzheimer's disease: an appraisal for the development of therapeutics', *Nature Reviews Drug Discovery*, 10: 698-712.
- Kaseda S, Nomoto M, Iwata S. 1999. 'Effect of selegiline on dopamine concentration in the striatum of a primate.', *Brain Res.*, 815: 44-50.
- Kaur D, Yantiri F, Rajagopalan S, Kumar J, Mo JQ, Boonplueang R, Viswanath V, Jacobs R, Yang L, Beal MF, DiMonte D, Volitaskis I, Ellerby L, Cherny RA, Bush AI, Andersen JK. 2003. ' Genetic or pharmacological iron chelation prevents MPTP-induced neurotoxicity in vivo: a novel therapy for Parkinson's disease. ', *Neuron*: 899-909.
- Kazuno AA, Munakata K, Nagai T, Shimozono S, Tanaka M, Yoneda M, Kato N, Miyawaki A, and Kato T. 2006. Identification of mitochondrial DNA polymorphisms that alter mitochondrial matrix pH and intracellular calcium dynamics. *PLoS. Genet.* 2 (8): e128.

- Kawahara M, Mizuno D. 2014. 'Crosstalk between metals and neurodegenerative diseases.', *Nihon Eiseigaku Zasshi.*, 69: 155-65.
- Kayed R, Head E, Thompson JL, McIntire TM, Milton SC, Cotman CW, Glabe CG, . 2003. 'Common structure of soluble amyloid oligomers implies common mechanism of pathogenesis. ', *Science*, 300: 486-89.
- Keller JN, Schmitt FA, Scheff SW, Ding Q, Chen Q, Butterfield DA, Markesbery WR. 'Evidence of increased oxidative damage in subjects with mild cognitive impairment. ', *Neurology*, 64: 1152-56.
- Kennedy BP, et al. . 2003. 'Early and persistent alterations in prefrontal cortex MAO A and B in Alzheimer's disease.', *J. Neural Transm.*: 789-801.
- Khalil M, Teunissen C, and Langkammer C. 2011. Iron and neurodegeneration in multiple sclerosis. *Mult. Scler. Int.* 2011: 606807.
- Khatoun S, Grundke-Iqbal I, Iqbal K.,. 1994. 'Levels of normal and abnormally phosphorylated tau in different cellular and regional compartments of Alzheimer disease and control brains. ', *FEBS Lett*, 351: 80-84.
- Kidani Y, Naga S, Koike H. 1974. 'Mass spectrophotometry of 5-chloro-7-iodo-8-quinolinol metal chelates.', *Jpn. Analyst* 1375-78.
- King MV, Marsden CA, Fone KC., . 2008. 'A role for the 5-HT(1A), 5-HT4 and 5- HT6 receptors in learning and memory.', *Trends Pharmacol. Sci.*, 29: 482-92.
- Kirkwood TB, . 2003. 'The most pressing problem of our age.', *BMJ*, 326: 1297-99.
- Kitani K, Minami C, Maruyama W, Kanai S, Ivy GO, Carrillo MC. 2000. 'Common properties for propargylamines of enhancing superoxide dismutase and catalase activities in the dopaminergic system in the rat: implications for the life prolonging effect of (-)deprenyl.', *J Neural Transm Suppl.*, 60: 139-56.
- Kitano H. 2007. 'A robustness-based approach to systems-oriented drug design.', *Nat Rev Drug Discov.*, 6: 202-10.
- Kitazawa M, Yamasaki TR, and LaFerla FM. 2004. Microglia as a potential bridge between the amyloid beta-peptide and tau. *Ann. N. Y. Acad. Sci.* 1035: 85-103.
- Kitazawa M, Cheng D, Laferla FM. . 2009. 'Chronic copper exposure exacerbates both amyloid and tau pathology and selectively dysregulates cdk5 in a mouse model of AD. ', *J. Neurochem*, 108: 1550-60.
- Knoll J. 2000. '(-)Deprenyl (Selegiline): past, present and future.
- Kodama H, Murata Y, Kobayashi M., . 1999. 'Clinical manifestations and treatment of Menkes disease and its variants.', *Pediatr. Int.*, 41: 423-29.
- Koren P, Diver-Haber A, Adunsky A, Rabinowitz M, and Hershkowitz M. 1993. Uptake of serotonin into platelets of senile dementia of the Alzheimer type patients. *J. Gerontol.* 48 (3): B93-B96.
- Kumar S, Walter J. 2011. 'Phosphorylation of amyloid beta (A $\beta$ ) peptides – A trigger for formation of toxic aggregates in Alzheimer's disease', *Aging*, 3: 803-12.
- Kuperstein F, Yavin E. 2003. 'Pro-apoptotic signaling in neuronal cells following iron and amyloid beta peptide neurotoxicity. ', *J. Neurochem*, □□: 114-25.
- Lacor PN. 2007. Advances on the understanding of the origins of synaptic pathology in AD. *Curr. Genomics* 8 (8): 486-508.

- Lambert JC. 2013. 'Meta-analysis of 74,046 individuals identifies 11 new susceptibility loci for Alzheimer's disease', *Nature Genetics*, 45: 1452-58.
- Lambert MP, Barlow AK, Chromy BA, Edwards C, Freed R, Liosatos M, Morgan TE, Rozovsky I, Trommer B, Viola KL, Wals P, Zhang C, Finch CE, Krafft GA, Klein WL,. 1998. 'Diffusible, nonfibrillar ligands derived from Abeta1-42 are potent central nervous system neurotoxins.', *Proc Natl Acad Sci USA*, 95: 6448-53.
- Lanctot KL, Herrmann N, Ganjavi H, Black SE, Rusjan PM, Houle S, and Wilson AA. 2007. Serotonin-1A receptors in frontotemporal dementia compared with controls. *Psychiatry Res.* 156 (3): 247-250.
- Lannfelt L, Blennow K, Zetterberg H, Batsman S, Ames D, Harrison J, Masters CL, Targum S, Bush AI, Murdoch R, Wilson J, Ritchie CW. 2008. 'PBT2-201-EURO study group. Safety, efficacy, and biomarker findings of PBT2 in targeting Abeta as a modifying therapy for Alzheimer's disease: a phase IIa, double-blind, randomised, placebo-controlled trial. ', *Lancet Neurol.*: 779-86.
- Lee CY, Landreth GE. 2010. 'The role of microglia in amyloid clearance from the AD brain. ', *J Neural Transm*, 117:
- Lee MG, Hassani OK, Alonso A, Jones BE,. 2005. 'Cholinergic basal forebrain neurons burst with theta during waking and paradoxical sleep.', *J Neurosci.*, 25: 4365-69.
- Lee HP, Zhu X, Casadesus G, Castellani RJ, Nunomura A, Smith MA, Lee H-g, Perry G 2010. 'Antioxidant approaches for the treatment of Alzheimer's disease. ', *Expert Rev Neurother*: 1201-08.
- Lee YJ, Jeong SY, Karbowski M, Smith CL, Youle RJ,. 2004. 'Roles of the mammalian mitochondrial fission and fusion mediators Fis1, Drp1, and Opa1 in apoptosis. ', *Mol Bio Cell*, 15: 5001-11.
- Lei P, Ayton S, Bush AI, Adlard PA. 2011. 'GSK-3 in neurodegenerative diseases.', *Int. J. Alzheimers Dis.* : 189246.
- Lei P, Ayton S, Finkelstein DI, Adlard PA, Masters CL, Bush AI,. 2010. 'Tau protein: relevance to Parkinson's disease. ', *Int. J. Biochem. Cell Biol.*, 42:
- Lei P, Ayton S, Finkelstein DI, Spoerri L, Ciccotosto GD, Wright DK, Wong BX, Adlard PA, Cherny RA, Lam LQ, Roberts BR, Volitakis I, Egan GF, McLean CA, Cappai R, Duce JA, Bush AI. 2012. 'Tau deficiency induces parkinsonism with dementia by impairing APP-mediated iron export.', *Nat. Med*: 291-95.
- Lei P, Ayton S, Finkelstein DI, Spoerri L, Ciccotosto GD, Wright DK, Wong BX, Adlard PA, Cherny RA, Lam LQ, Roberts BR, Volitakis I, Egan GF, McLean CA, Cappai R, Duce JA, Bush AI. 2012. 'Tau deficiency induces parkinsonism with dementia by impairing APP-mediated iron export.', *Nat. Med*: 291-95.
- LeVine H, Ding Q, Walker JA, Voss RS, Augelli-Szafran CE. 2009. 'Clioquinol and other hydroxyquinoline derivatives inhibit Abeta(1-42) oligomer assembly. ', *Neurosci. Lett.*: 99-103.
- LeVine H. 1993. 'Thioflavine T interaction with synthetic Alzheimer's disease beta-amyloid peptides: detection of amyloid aggregation in solution.', *Protein Sci.*, 2: 404-10.

- Levy-Lahad E, Lahad A, Wijsman EM, Bird TD, Schellenberg GD,. 1995. 'Apolipoprotein E genotypes and age of onset in early-onset familial Alzheimer's disease.', *Ann Neurol.*, 38: 678-80.
- Li C, Wang J, Zhou B. 2010. ' The metal chelating and chaperoning effects of clioquinol: insights from yeast studies. ', *J. Alzheimers Dis.*: 1249-62.
- Liao J, Norgaard-Pedersen B, and Brodbeck U. 1993. Subunit association and glycosylation of acetylcholinesterase from monkey brain. *J. Neurochem.* 61 (3): 1127-1134.
- Lin R, Chen X, Li W, Han Y, Liu P, Pi R 2008. 'Exposure to metal ions regulates mRNA levels of APP and BACE1 in PC12 cells: Blockage by curcumin', *Neurosci Lett*: 344-47.
- Ling Y, Morgan K, and Kalsheker N. 2003. Amyloid precursor protein (APP) and the biology of proteolytic processing: relevance to Alzheimer's disease. *Int. J. Biochem. Cell Biol.* 35 (11): 1505-1535.
- Lipton SA, . 2006. 'Paradigm shift in neuroprotection by NMDA receptor blockade: memantine and beyond.', *Nat Rev Drug Discov.*, 5: 160-70.
- Liu W, Xu Z, Deng Y, Xu B, Wei Y, Yang T. 2013. 'Protective effects of memantine against methylmercury-induced glutamate dyshomeostasis and oxidative stress in rat cerebral cortex.', *Neurotox Res.*, 24: 320-37.
- Loeffler DA, Connor JR, Juneau PL, Snyder BS, Kanaley L, DeMaggio AJ, Nguyen H, Brickman CM, LeWitt PA., . 1995. 'Transferrin and iron in normal, Alzheimer's disease, and Parkinson's disease brain regions.', *J. Neurochem.*, 65: 710-24.
- Loewi O. 1921. 'Uberhumerole ubertragbarkeit der herznervenwirkung', *I Mitteilung Pflugers Arch*, 189: 239-42.
- Long DD, Armstrong SR, Beattie DT, Choi SK, Fatheree PR, Gendron RA, Genov D, Goldblum AA, Humphrey PP, Jiang L, Marquess DG, Shaw JP, Smith JA, Turner SD, Vickery RG., . 2012. 'Discovery, oral pharmacokinetics and in vivo efficacy of velusetrag, a highly selective 5-HT(4) receptor agonist that has achieved proof-of-concept in patients with chronic idiopathic constipation.', *Bioorg. Med. Chem. Lett.*, 22: 6048-52.
- Lovell MA, Robertson JD, Teesdale WJ, Campbell JL, Markesbery WR. 1998. ' Copper, iron and zinc in Alzheimer's disease senile plaques. ', *J. Neurol. Sci.*: 47-52.
- Lovell MA, Xiong S, Xie C, Davies PL, Markesbery WR., 2004. 'Induction of hyperphosphorylated tau in primary rat cortical neuron cultures mediated by oxidative stress and glycogen synthase kinase-3.', *J. Alzheimers Dis.*, □: 659-71.
- Lu C, Guo Y, Yan J, Luo Z, Luo HB, Yan M., 2013. 'Design, synthesis, and evaluation of multitarget-directed resveratrol derivatives for the treatment of Alzheimer's disease', *J. Med. Chem.*, 56: 5843-59.
- Ma QF, Hu J, Wu WH, Liu HD, Du JT, Fu Y, Wu YW, Lei P, Zhao YF, Li YM., . 2006. 'Characterization of copper binding to the peptide amyloid-beta(1-16) associated with Alzheimer's disease. ', *Biopolymers*, 83: 20-31.
- Ma QF, Li YM, Du JT, Kanazawa K, Nemoto T, Nakanishi H, Zhao YF, . 2005. 'Binding of copper(II) ion to an Alzheimer's tau peptide as revealed by MALDI-TOF MS, CD, and NMR. ', *Biopolymers*, 79: 74-85.

- Ma X, Tan C, Zhu D, Gang DR, and Xiao P. 2007. Huperzine A from *Huperzia* species--an ethnopharmacological review. *J. Ethnopharmacol.* 113 (1): 15-34.
- Ma QL, Zuo X, Yang F, Ubada OJ, Gant DJ, Alaverdyan M, Teng E, Hu S, Chen PP, Maiti P, Teter B, Cole GM, Frautschy SA., . 2013. 'Curcumin suppresses soluble tau dimers and corrects molecular chaperone, synaptic, and behavioral deficits in aged human tau transgenic mice.', *J. Biol. Chem.*, 288: 4056-65.
- Magaki S, Raghavan R, Mueller C, Oberg KC, Vinters HV, Kirsch WM.,. 2007. 'Iron, copper, and iron regulatory protein 2 in Alzheimer's disease and related dementias. ', *Neurosci. Lett.*: 72-76.
- Maher-Edwards G, Dixon R, Hunter J, Gold M, Hopton G, Jacobs G, Williams P.,. 2011. 'SB-742457 and donepezil in Alzheimer disease: a randomized, placebocontrolled study. ', *Int. J. Geriatr. Psychiatry*, 26: 536-44.
- Maher-Edwards G, Zvartau-Hind M, Hunter AJ, Gold M, Hopton G, Jacobs G, Davy M, Williams P., . 2010. 'Double-blind, controlled phase II study of a 5-HT<sub>6</sub> receptor antagonist, SB-742457, in Alzheimer's disease. ', *Curr. Alzheimer Res.*, 7: 374-85.
- Mahley RW, Weisgraber KH, Huang Y.,. 2006. 'Apolipoprotein E4: a causative factor and therapeutic target in neuropathology, including Alzheimer's disease.', *Proc Natl Acad Sci USA*, 103: 5644-51.
- Malar DS, Devi KP. 2014. 'Dietary polyphenols for treatment of Alzheimer's disease: future research and development.', *Curr Pharm Biotechnol.*, 15: 330-42.
- Mandelkow EM, and Mandelkow E. 1998. Tau in Alzheimer's disease. *Trends Cell Biol.* 8 (11): 425-427.
- Mancino AM, Hindo SS, Kochi A, Lim MH. . 2009. 'Effects of clioquinol on metal-triggered amyloid-beta aggregation revisited. ', *Inorg. Chem.*: 9596-98.
- Mantyh PW, Ghilardi JR, Rogers S, DeMaster E, Allen CJ, Stimson ER, Maggio JE.,. 1993. 'Aluminum, iron, and zinc ions promote aggregation of physiological concentrations of beta-amyloid peptide.', *J. Neurochem.*, 61: 1171-74.
- Martignoni E, Blandini F, Petraglia F, Pacchetti C, Bono G, and Nappi G. 1992. Cerebrospinal fluid norepinephrine, 3-methoxy-4-hydroxyphenylglycol and neuropeptide Y levels in Parkinson's disease, multiple system atrophy and dementia of the Alzheimer type. *J. Neural Transm. Park Dis. Dement. Sect.* 4 (3): 191-205.
- Matlack KES, Tardiff DF, Narayan P, Hamamichi S, Caldwell KA, Caldwell GA, Lindquist S. 2014. 'Clioquinol promotes the degradation of metal-dependent amyloid- $\beta$  (A $\beta$ ) oligomers to restore endocytosis and ameliorate A $\beta$  toxicity ', *PNAS*, 111: 4013-18.
- Mattson MP. 2004. Pathways towards and away from Alzheimer's disease. *Nature* 430 (7000): 631-639.
- Mattson MP. 1997. 'Cellular actions of beta-amyloid precursor protein and its soluble and fibrillogenic derivatives.', *Physiol Rev.*, 77: 1081-132.
- Matthews KL, Chen CP, Esiri MM, Keene J, Minger SL, and Francis PT. 2002. Noradrenergic changes, aggressive behavior, and cognition in patients with dementia. *Biol. Psychiatry* 51 (5): 407-416.

- Matsubayashi K, Fukuyama H, Akiguchi I, Kameyama M, Imai H, and Maeda T. 1986. Localization of monoamine oxidase (MAO) in the rat peripheral nervous system--existence of MAO-containing unmyelinated axons. *Brain Res.* 368 (1): 30-35.
- Mazanetz MP, and Fischer PM. 2007. Untangling tau hyperphosphorylation in drug design for neurodegenerative diseases. *Nat. Rev. Drug Discov.* 6 (6): 464-479.
- Meadowcroft MD, Connor JR, Smith MB, Yang QX,. 2009. 'MRI and histological analysis of beta-amyloid plaques in both human Alzheimer's disease and APP/PS1 transgenic mice.', *J. Magn. Reson. Imaging*, 29: 997-1007.
- Meltzer HY, Mills R, Revell S, Williams H, Johnson A, Bahr D, Friedman JH.,. 2010. 'Pimavanserin, a serotonin(2A) receptor inverse agonist, for the treatment of parkinson's disease psychosis. ', *Neuropsychopharmacology*, 35: 881-92.
- Meraz-Rios MA, Toral-Rios D, Franco-Bocanegra D, Villeda-Hernandez J, and Campos-Pena V. 2013. Inflammatory process in Alzheimer's Disease. *Front Integr. Neurosci.* 7: 59.
- Mercken M, Takahashi H, Honda T, Sato K, Murayama M, Nakazato Y, Noguchi K, Imahori K, Takashima A,. 1996. 'Characterization of human presenilin 1 using N-terminal specific monoclonal antibodies: Evidence that Alzheimer mutations affect proteolytic processing.', *FEBS Lett.*, 389: 297-303.
- Merle U, Schaefer M, Ferenci P, Stremmel W., . 2007. 'Clinical presentation, diagnosis and long-term outcome of Wilson's disease: a cohort study.', *Gut*, 56: 115-20.
- Mesulam M, Guillozet A, Shaw P, and et al. 2002. 'Widely spread butyrylcholinesterase can hydrolyze acetylcholine in the normal and Alzheimer brain.', *Neurobiol Dis*, 9: 88-93.
- Meunier J, Ieni J, Maurice T,. . 2006. 'The anti-amnesic and neuroprotective effects of donepezil against amyloid beta25-35 peptide-induced toxicity in mice involve an interaction with the sigma 1 receptor', *Br J Pharm*, 149: 998-1012.
- Migliore L, Coppedè F. 2009. 'Environmental-induced oxidative stress in neurodegenerative disorders and aging.', *Mutat Res.*: 73-84.
- Miguel-Hidalgo JJ, Alvarez XA, Cacabelos R, Quack G.. 'Neuroprotection by memantine against neurodegeneration induced by beta-amyloid(1-40).', *Brain Res.*, 958: 210-21.
- Miller LM, Wang Q, Telivala TP, Smith RJ, Lanzirotti A, Miklossy J. 2006. 'Synchrotron-based infrared and X-ray imaging shows focalized accumulation of Cu and Zn co-localized with beta-amyloid deposits in Alzheimer's disease.', *J. Struct. Biol.*: 30-37.
- Minicozzi V, Stellato F, Comai M, Serra MD, Potrich C, MeyerKlaucke W, Morante S., . 2008. 'Identifying the minimal copper- and zinc-binding site sequence in amyloid-beta peptides.', *J. Biol. Chem.*, 283: 10784-92.
- Mo ZY, Zhu YZ, Zhu HL, Fan JB, Chen J, Liang Y. . 2009. 'Low micromolar zinc accelerates the fibrillization of human tau via bridging of Cys-291 and Cys-322. ', *J. Biol. Chem.*: 34648-57.
- Molnar P, Nadler JV. 2001. 'Lack of effect of mossy fiber-released zinc on granule cell GABA(A) receptors in the pilocarpine model of epilepsy.', *J. Neurophysiol.*: 1932-40.

- Morales I, Guzman-Martinez L, Cerda-Troncoso C, Farias GA, and Maccioni RB. 2014. Neuroinflammation in the pathogenesis of Alzheimer's disease. A rational framework for the search of novel therapeutic approaches. *Front Cell Neurosci.* 8: 112.
- Moreira PI, Nunomura A, Nakamura M, Takeda A, Shenk JC, Aliev G, Smith MA, Perry G,.. 'Nucleic acid oxidation in Alzheimer disease.', *Free Radic Biol Med.*; 1493-505.
- Moriguchi S, Marszalec W, Zhao X, Yeh JZ, Narahashi T. 2003. 'Potentiation of N-methyl-D-aspartate-induced currents by the nootropic drug nefiracetam in rat cortical neurons.', *J Pharmacol Exp Ther.*, 307: 160-67.
- Moszczynska A, Fitzmaurice P, Ang L, Kalasinsky KS, Schmunk GA, Peretti FJ, Aiken SS, Wickham DJ, Kish SJ. 'Why is parkinsonism not a feature of human methamphetamine users?', *Brain.*, 127: 363-70.
- Mousavi M, Hellstrom-Lindahl E. 2009. 'Nicotinic receptor agonists and antagonists increase sAPPalpha secretion and decrease Abeta levels in vitro.', *Neurochem Int*, 54: 237-44.
- Multhaup G, Schlicksupp A, Hesse L, Behr D, Ruppert T, Masters CL, Beyreuther K,.. 'The amyloid precursor protein of Alzheimer's disease in the reduction of copper(II) to copper(I)', *Science*.
- Muñoz P, Zavala G, Castillo K, Aguirre P, Hidalgo C, Nuñez M. 2006. 'Effect of iron on the activation of the MAPK/ERK pathway in PC12 neuroblastoma cells', *Biol. Res*, 39: 189-90.
- Nakamura M, Shishido N, Nunomura A, Smith MA, Perry G, Hayashi Y, Nakayama K, Hayashi T., 2007. 'Three histidine residues of amyloid-beta peptide control the redox activity of copper and iron.', *Biochemistry*, 46: 12737-43.
- Narahashi T, Moriguchi S, Zhao X, Marszalec W, and Yeh JZ. 2004. 'Mechanisms of action of cognitive enhancers on neuroreceptors.', *Biol Pharm Bull*, 27: 1701-6.
- Nelson PT, Alafuzoff I, Bigio EH, et al. 2012. 'Correlation of Alzheimer disease neuropathologic changes with cognitive status: a review of the literature.', *J. Neuropathol. Exp. Neurol.*, 71: 362-81.
- Nguyen T, Hamby A, Massa SM. 2005. 'Clioquinol down-regulates mutant huntingtin expression in vitro and mitigates pathology in a Huntington's disease mouse model. ', *Proc. Natl. Acad. Sci. USA*: 11840-45.
- Nicotra A, Pierucci F, Parvez H, Senatori O. 2004. 'Monoamine oxidase expression during development and aging. ', *Neurotoxicology*: 155-65.
- Nielsen JA, Mena EE, Williams IH, Nocerini MR, Liston D. 1989. 'Correlation of brain levels of 9-amino-1,2,3,4-tetrahydroacridine (THA) with neurochemical and behavioral changes.', *Eur J Pharmacol.*, 173:.
- Nitzan YB, Sekler I, Frederickson CJ, Coulter DA, Balaji RV, Liang SL, Margulis A, Hershinkel M, Silverman WF. 2003. 'Clioquinol effects on tissue chelatable zinc in mice. ', *J. Mol. Med.*: 637-44.

- Nochi S, Asakawa N, and Sato T. 1995. Kinetic study on the inhibition of acetylcholinesterase by 1-benzyl-4-[(5,6-dimethoxy-1-indanon)-2-yl]methylpiperidine hydrochloride (E2020). *Biol. Pharm. Bull.* 18 (8): 1145-1147.
- Nunomura A, Perry G, Pappolla MA, Friedland RP, Hirai K, Chiba S, Smith MA,. 2000. 'Neuronal oxidative stress precedes amyloid-beta deposition in Down syndrome.', *Journal of Neuropathology and Experimental Neurology*, 59: 1011-17.
- O'Carroll AM, Fowler CJ, Phillips JP, Tobbia I, Tipton KF. . 1983. 'The deamination of dopamine by human brain monoamine oxidase. Specificity for the two enzyme forms in seven brain regions.', *Naunyn Schmiedeberg's Arch. Pharmacol.*: 198-202.
- O'Carroll AM, Tipton KF, Sullivan JP, Fowler CJ, Ross SB. 1987. 'Intra- and extrasynaptosomal deamination of dopamine and noradrenaline by the two forms of human brain monoamine oxidase. Implications for the neurotoxicity of N-methyl-4-phenyl-1,2,3,6- tetrahydropyridine in man.', *Biogenic Amines*: 165-78.
- Odetti P, Angelini G, Dapino D, Zaccheo D, Garibaldi S, Dagna-Bricarelli F, Piombo G, Perry G, Smith M, Traverso N, Tabaton M,. 1998. 'Early glycooxidation damage in brains from Down's syndrome.', *Biochemical and Biophysical Research Communications*, □□□: 849-51.
- Ohtsuka K, Ohishi N, Eguchi G, Yagi K. 1982. 'Degeneration of retinal neuroblasts by chinoform–ferric chelate.', *Experientia*: 120-22.
- Olanow CW, Rascol O, Hauser R, Feigin PD, Jankovic J, Lang A, et al. 2009. 'A double-blind, delayed-start trial of rasagiline in Parkinson's disease. ', *N Engl J Med.*, 361: 1268-78.
- Ollis DL, Cheah E, Cygler M, Dijkstra B, Frolow F, Franken SM, Harel M, Remington SJ, Silman I, Schrag J, Sussman JL, Verschueren KHG, Goldman A,. 1992. 'The  $\alpha/\beta$  hydrolase fold', *Protein Eng*, 5: 197-211.
- Opar A. 2008. 'Mixed results for disease-modification strategies for Alzheimer's disease', *Nat Rev Drug Discov.*, 7: 717-18.
- Palfreyman MG, et al. . 1985. 'Inhibition of monoamine oxidase selectively in brain monoamine nerves using the bioprecursor (E)- $\beta$ -fluoromethylene-m-tyrosine (MDL 72394), a substrate for aromatic L-amino acid decarboxylase. ', *Neurochem.*: 1850-60.
- Pålhagen S, Heinonen E, Hägglund J, Kaugesaar T, Mäki-Ikola O, Palm R; Swedish Parkinson Study Group. 2006. 'Selegiline slows the progression of the symptoms of Parkinson disease.', *Neurology.*, 66: 1200-06.
- Palmer AM, Francis PT, Benton JS, Sims NR, Mann DM, Neary D, Snowden JS, and Bowen DM. 1987. Presynaptic serotonergic dysfunction in patients with Alzheimer's disease. *J. Neurochem.* 48 (1): 8-15.
- Panayi AE, Spyrou NM, Iversen BS, White MA.,. 2002. 'Determination of cadmium and zinc in Alzheimer's brain tissue using inductively coupled plasma mass spectrometry', *J. Neurol. Sci.*: 1-10.
- Panayi, A. E.; Spyrou, N. M.; Iversen, B. S.; White, M. A. 2002. 'Determination of cadmium and zinc in Alzheimer's brain tissue using inductively coupled plasma mass spectrometry', *J. Neurol. Sci.* : 1-10.

- Paoletti P, Ascher P, Neyton J. 1997. 'High-affinity zinc inhibition of NMDA NR1–NR2A receptors', *J. Neurosci.*: 5711-25.
- Paoletti, P.; Ascher, P.; Neyton, J. 1997. 'High-affinity zinc inhibition of NMDA NR1–NR2A receptors', *J. Neurosci.*: 5711-25.
- Park IH, Jung MW, Mori H, Mook-Jung I. 2001. 'Zinc enhances synthesis of presenilin 1 in mouse primary cortical culture.', *Biochem. Biophys. Res. Commun.*: 680-88.
- Park MH, Lee SJ, Byun HR, Kim Y, Oh YJ, Koh JY, Hwang, J. J. 2011. 'Clioquinol induces autophagy in cultured astrocytes and neurons by acting as a zinc ionophore.', *Neurobiol. Dis.*: 242-51.
- Parsons CG1, Danysz W, Bartmann A, Spielmans P, Frankiewicz T, Hesselink M, Eilbacher B, Quack G. 1999. 'Amino-alkyl-cyclohexanes are novel uncompetitive NMDA receptor antagonists with strong voltage-dependency and fast blocking kinetics: in vitro and in vivo characterization.', *Neuropharmacology.*, 38: 85-108.
- Parvizi J, Van Hoesen GW, and Damasio A. 2001. The selective vulnerability of brainstem nuclei to Alzheimer's disease. *Ann. Neurol.* 49 (1): 53-66.
- Patat A, Parks V, Raje S, Plotka A, Chassard D, Le Coz F., . 2009. 'Safety, tolerability, pharmacokinetics and pharmacodynamics of ascending single and multiple doses of lecozotan in healthy young and elderly subjects. ', *Br. J. Clin. Pharmacol.*, 67: 299-308.
- Pei JJ, An WL, Zhou XW, Nishimura T, Norberg J, Benedikz E, Gotz J, Winblad B. 2006. 'P70 S6 kinase mediates tau phosphorylation and synthesis.', *FEBS Lett.*: 107-14.
- Percy M, Moalem S, Garcia A, Somerville MJ, Hicks M, Andrews D, Azad A, Schwarz P, Beheshti Zavareh R, Birkan R, Choo C, Chow V, Dhaliwal S, Duda V, Kupferschmidt AL, Lam K, Lightman D, Machalek K, Mar W, Nguyen F, Rytwinski PJ, Svava E, Tran M, Wheeler K, Yeung L, Zanibbi K, Zener R, Ziraldo M, Freedman M. 'Involvement of ApoE E4 and H63D in sporadic Alzheimer's disease in a folate-supplemented Ontario population.', *J. Alzheimers Dis.*, 14: 69-84.
- Perez V, Marco JL, Fernandez-Alvarez E, Unzeta M. 1996. 'Kinetic studies of N-allenic analogues of tryptamine as monoamine oxidase inhibitors.', *J Pharm Pharmacol.*, 48: 718-22.
- Perez V, and Unzeta M. 2003. PF 9601N [N-(2-propynyl)-2-(5-benzyloxy-indolyl) methylamine], a new MAO-B inhibitor, attenuates MPTP-induced depletion of striatal dopamine levels in C57/BL6 mice. *Neurochem. Int.* 42 (3): 221-229.
- Perl DP. 2010. 'Neuropathology of Alzheimer's disease. ', *Mt Sinai J. Med. (New York)*, 77: 32-42.
- Perrone L, Mothes E, Vignes M, Mockel A, Figueroa C, Miquel MC, Maddelein ML, Faller P. . 2010. 'Copper transfer from Cu-Abeta to human serum albumin inhibits aggregation, radical production and reduces Abeta toxicity.', *ChemBioChem*, 11: 110-18.
- Perry G, Mulvihill P, Manetto V, Autilio-Gambetti L, and Gambetti P. 1987. Immunocytochemical properties of Alzheimer straight filaments. *J. Neurosci.* 7 (11): 3736-3738.

- Perry E, McKeith I, and Ballard C. 2003. 'Butyrylcholinesterase and progression of cognitive deficits in dementia with Lewy bodies.', *Neurology*, □□: 1852-53.
- Perry EK, Perry RH, Blessed G, and et al. 1978. 'Changes in brain cholinesterases in senile dementia of Alzheimer type.', *Neuropathol Appl Neurobiol.*, 4: 273-77.
- Perry VH, Nicoll JA, Holmes C., 2010. 'Microglia in neurodegenerative disease. ', *Nat Rev Neurol*, 6: 193-201.
- Petersen RB, Nunomura A, Lee HG, Casadesus G, Perry G, Smith MA, Zhu X., 2007. 'Signal transduction cascades associated with oxidative stress in Alzheimer's disease. ', *Journal of Alzheimer's Disease*, 11: 143-52.
- Petousi N, and Robbins PA. 2014. Human adaptation to the hypoxia of high altitude: the Tibetan paradigm from the pregenomic to the postgenomic era. *J. Appl. Physiol (1985. )* 116 (7): 875-884.
- Pinessi L, Rainero I, De GT, Gentile S, Portaleone P, and Bergamasco B. 1987. Biogenic amines in cerebrospinal fluid and plasma of patients with dementia of Alzheimer type. *Funct. Neurol.* 2 (1): 51-58.
- Pratico D, Uryu K, Leight S, Trojanoswki JQ, Lee VM, . 2001. 'Increased lipid peroxidation precedes amyloid plaque formation in an animal model of Alzheimer amyloidosis.', *Journal of Neuroscience*, 21: 4183-87.
- Praticò D. 2008. 'Evidence of oxidative stress in Alzheimer's disease brain and antioxidant therapy: lights and shadows.', *Ann N Y Acad Sci.*, 1147: 70-78.
- Price DL, Bonhaus DW, McFarland K., 2012. 'Pimavanserin, a 5-HT<sub>2A</sub> receptor inverse agonist, reverses psychosis-like behaviors in a rodent model of Alzheimer's disease. ', *Behav. Pharmacol.*, 23: 426-33.
- Priel T, Aricha-Tamir B, Sekler, I. . 2007. 'Clioquinol attenuates zinc-dependent beta-cell death and the onset of insulinitis and hyperglycemia associated with experimental type I diabetes in mice.', *Eur. J. Pharmacol*, 565.
- Prodan CI, Ross ED, Stoner JA, Cowan LD, Vincent AS, and Dale GL. 2011. Coated-platelet levels and progression from mild cognitive impairment to Alzheimer disease. *Neurology* 76 (3): 247-252.
- Przuntek H, Conrad B, Dichgans J, Kraus PH, Krauseneck P, Pergande G, Rinne U, Schimrigk K, Schnitker J, Vogel HP. 1999. 'SELEDO: a 5-year long-term trial on the effect of selegiline in early Parkinsonian patients treated with levodopa.', *Eur J Neurol*, 6: 141-50.
- Qian J, Noebels JL. 2005. 'Visualization of transmitter release with zinc fluorescence detection at the mouse hippocampal mossy fibre synapse.', *J. Physiol*: 747-58.
- Qian, J.; Noebels, J. L. 2005. ' Visualization of transmitter release with zinc fluorescence detection at the mouse hippocampal mossy fibre synapse.', *J. Physiol*: 747-58.
- Qizilbash N, Whitehead A, Higgins J, et al. 1998. 'Cholinesterase inhibition for Alzheimer's disease: a meta-analysis of the tacrine trials', *Journal of the American Medical Association*, 280: 1777-82.
- Qizilbash N., Whitehead A., Higgins J., et al. 1998. 'Cholinesterase inhibition for Alzheimer's disease: a meta-analysis of the tacrine trials', *Journal of the American Medical Association*, 280: 1777-82.

- Rafii MS, Aisen PS. 2015. 'Advances in Alzheimer's disease drug development.', *BMC Med.*, 13: 62.
- Raman B, Ban T, Yamaguchi K, Sakai M, Kawai T, Naiki H, Goto Y. □□□□. 'Metal ion-dependent effects of clioquinol on the fibril growth of an amyloid □ peptide.', *J. Biol. Chem.*: 16157-62.
- Rammes G, Rupprecht R, Ferrari U, Zieglgänsberger W, Parsons CG. 2001. 'The N-methyl-D-aspartate receptor channel blockers memantine, MRZ 2/579 and other amino-alkyl-cyclohexanes antagonise 5-HT(3) receptor currents in cultured HEK-293 and N1E-115 cell systems in a non-competitive manner.', *Neurosci Lett.*, 306: 81-84.
- Rascol O, Brooks DJ, Melamed E, Oertel W, Poewe W, Stocchi F, et al. 2005. 'Rasagiline as an adjunct to levodopa in patients with Parkinson's disease and motor fluctuations (LARGO, Lasting effect in Adjunct therapy with Rasagiline Given Once daily, study): a randomised, double-blind, parallel-group trial.', *Lancet.*, 365: 947-54.
- Ratia M, Gimenez-Llort L, Camps P, Munoz-Torrero D, Perez B, Clos MV, and Badia A. 2013. Huprine X and huperzine A improve cognition and regulate some neurochemical processes related with Alzheimer's disease in triple transgenic mice (3xTg-AD). *Neurodegener. Dis.* 11 (3): 129-140.
- Reinikainen KJ, Paljarvi L, Huuskonen M, Soininen H, Laakso M, and Riekkinen PJ. 1988. A post-mortem study of noradrenergic, serotonergic and GABAergic neurons in Alzheimer's disease. *J. Neurol. Sci.* 84 (1): 101-116.
- Religa D, Stroyk D, Cherny RA, Volitakis I, Haroutunian V, Winblad B, Naslund J, Bush AI., 2006. 'Elevated cortical zinc in Alzheimer disease.', *Neurology*: 69-75.
- Religa, D.; Stroyk, D.; Cherny, R. A.; Volitakis, I.; Haroutunian, V.; Winblad, and J.; Bush B.; Naslund, A. I. 2006. 'Elevated cortical zinc in Alzheimer disease.', *Neurology*: 69-75.
- Reznick AZ, Gershon D. 1979. 'The effect of age on the protein degradation system in the nematode *Turbatrix aceti*.', *Mech Ageing Dev.*, 11: 403-15.
- Richard T, Pawlus AD, Iglésias M, Pedrot E, Waffo-Teguo P, Mérillon J, Monti J. . 2011. 'Neuroprotective properties of resveratrol and derivatives.', *Ann. N. Y. Acad. Sci.*, 1215: 103-08.
- Riederer P, and Laux G. 2011. MAO-inhibitors in Parkinson's Disease. *Exp. Neurobiol.* 20 (1): 1-17.
- Robert PH, and Benoit M. 2008. Neurochemistry of cognition: serotonergic and adrenergic mechanisms. *Handb. Clin. Neurol.* 88: 31-40.
- Robertson IH. 2013. A noradrenergic theory of cognitive reserve: implications for Alzheimer's disease. *Neurobiol. Aging* 34 (1): 298-308.
- Rodriguez JJ, Noristani HN, Verkhatsky A., . 2012. 'The serotonergic system in ageing and Alzheimer's disease. ', *Prog. Neurobiol.*, 99: 15-41.
- Rogers JT, Randall JD, Cahill CM, Eder PS, Huang X, Gunshin, Leiter L H, McPhee J, Sarang SS, Utsuki T, Greig NH., and Tanzi RE Lahiri DK, Bush AI, Giordano T, Gullans SR. 2002. 'An iron-responsive element type II in the 5-untranslated region of the Alzheimer's amyloid precursor protein transcript.

- Rogers J, Webster S, Lue LF, Brachova L, Civin WH, Emmerling M, Shivers B, Walker D, McGeer P, . 1996. 'Inflammation and Alzheimer's disease pathogenesis.', *Neurobiol. Aging*, 17: 681-86.
- Rosenmann, H. 2013. 'Immunotherapy for targeting tau pathology in Alzheimer's disease and tauopathies. ', *Curr. Alzheimer Res.*, □□: 217-28.
- Rosini M, Simoni E, Milelli A, Minarini A, Melchiorre C,. 2014. 'Oxidative stress in Alzheimer's disease: Are we connecting the dots?', *J Med Chem.*, 57: 2821-31.
- Rottkamp CA, Raina AK, Zhu XW, Gaier E, Bush AI, Atwood CS, Chevion M, Perry G, Smith MA ., . 2001. 'Redox-active iron mediates amyloid-b toxicity. ', *Free Radic. Biol. Med*, 30: 447-50.
- Ruiz, A.; Walker, M. C.; Fabian-Fine, R.; Kullmann, D. M. . 2004. 'Endogenous zinc inhibits GABA(A) receptors in a hippocampal pathway', *J. Neurophysiol.*: 1091-96.
- Sagi Y, Weinstock M, Youdim MB. 2003. 'Attenuation of MPTP-induced dopaminergic neurotoxicity by TV3326, a cholinesterase-monoamine oxidase inhibitor.', *J Neurochem*: 290-97.
- Samadi A, Valderas C, de los Ríos C, Bastida A, Chioua M, González-Lafuente L, Colmena I, Gandía L, Romero A, del Barrio L, Martín-de-Saavedra MD, López MG, Villarroya M, Contelles JM. 2011. 'Cholinergic and neuroprotective drugs for the treatment of Alzheimer and neuronal vascular diseases. II. Synthesis, biological assessment, and molecular modelling of new tacrine analogues from highly substituted 2-aminopyridine-3-carbonitriles.', *Bioorg. Med. Chem.*: 122-33.
- Sample I, 2007. 'New Alzheimer's drugs might help prevent glaucoma', *The Guardian*.
- Samudralwar DL, Diprete CC, Ni BF, Ehmann WD, Markesbery WR., . 1995. 'Elemental imbalances in the olfactory pathway in Alzheimer's disease.', *J. Neurol. Sci.*: 139-45.
- Samudralwar, D. L.; Diprete, C. C.; Ni, B. F.; Ehmann, W. D.; Markesbery, W., and R. 1995. 'Elemental imbalances in the olfactory pathway in Alzheimer's disease.', *J. Neurol. Sci.*: 139-45.
- Sanz E, Quintana A, Hidalgo J, Marco JL, and Unzeta M. 2009. PF9601N [N-(2-propynyl)-2-(5-benzyloxy-indolyl) methylamine] confers MAO-B independent neuroprotection in ER stress-induced cell death. *Mol. Cell Neurosci.* 41 (1): 19-31.
- Sanz E, Romera M, Bellik L, Marco JI, and Unzeta M. 2004. Indolalkylamines derivatives as antioxidant and neuroprotective agents in an experimental model of Parkinson's disease. *Med. Sci. Monit.* 10 (12): BR477-BR484.
- Sanz E, Quintana A, Battaglia V, Toninello A, Hidalgo J, Ambrosio S, Valoti M, Marco JL, Tipton KF, Unzeta M. 2008. 'Anti-apoptotic effect of Mao-B inhibitor PF9601N [N-(2-propynyl)-2-(5-benzyloxy-indolyl) methylamine] is mediated by p53 pathway inhibition in MPP+-treated SH-SY5Y human dopaminergic cells.', *J Neurochem.*, 105: 2404-17.
- Sanz E, Quintana A, Hidalgo J, Marco JL, Unzeta M. 2009. 'PF9601N [N-(2-propynyl)-2-(5-benzyloxy-indolyl) methylamine] confers MAO-B independent neuroprotection in ER stress-induced cell death.', *Mol Cell Neurosci.*, 41: 19-31.

- Saura J, Kettler R, Da PM, and Richards JG. 1992. Quantitative enzyme radioautography with 3H-Ro 41-1049 and 3H-Ro 19-6327 in vitro: localization and abundance of MAO-A and MAO-B in rat CNS, peripheral organs, and human brain. *J. Neurosci.* 12 (5): 1977-1999.
- Saura J, Nadal E, van den Berg B, Vila M, Bombi JA, and Mahy N. 1996. Localization of monoamine oxidases in human peripheral tissues. *Life Sci.* 59 (16): 1341-1349.
- Sayre LM, Perry G, Harris PL, Liu Y, Schubert KA, Smith MA.,. 2000. ' In situ oxidative catalysis by neurofibrillary tangles and senile plaques in Alzheimer's disease: a central role for bound transition metals.', *J. Neurochem*
- Sayre LM, Perry G, Harris PL, Liu Y, Schubert KA, Smith MA.,. 2000. ' In situ oxidative catalysis by neurofibrillary tangles and senile plaques in Alzheimer's disease: a central role for bound transition metals.', *J. Neurochem.*
- Scarr E, Gibbons AS, Neo J, Udawela M, and Dean B. 2013. Cholinergic connectivity: it's implications for psychiatric disorders. *Front Cell Neurosci.* 7: 55.
- Schapira AH, Fox S, Hauser R, Jankovic J, Jost W, Kulisevsky J, et al. 2013. 'Safinamide add on to L-dopa: a randomized, placebo-controlled 24-week global trial in patients with Parkinson's disease and motor fluctuations (SETTLE).', *Neurology.*, 80.
- Scheper W, Hoozemans JJ. 2009. 'Endoplasmic reticulum protein quality control in neurodegenerative disease: the good, the bad and the therapy.', *Curr Med Chem.*, 16: 615-26.
- Schipper HM, Bennett DA, Liberman A, Bienias JL, Schneider JA, Kelly J, Arvanitakis Z.,. 2006. 'Glial heme oxygenase-1 expression in Alzheimer disease and mild cognitive impairment. ', *Neurobiology of Aging*, 27: 252-61.
- Schlief ML, Craig AM, Gitlin JD., . 2005. 'NMDA receptor activation mediates copper homeostasis in hippocampal neurons. ', *J. Neurosci.*, 25: 239-46.
- Schliebs R. 2005. 'Basal forebrain cholinergic dysfunction in Alzheimer's disease--interrelationship with beta-amyloid, inflammation and neurotrophin signaling.', *Neurochem Res.*, 30: 895-908.
- Schlief ML, West T, Craig AM, Holtzman DM, Gitlin JD.'Role of the Menkes copper-transporting ATPase in NMDA receptor-mediated neuronal toxicity. ', *Proc. Natl. Acad. Sci. USA*, 103: 14919-24.
- Schubert D, Chevion M. 1995. 'The role of iron in beta amyloid toxicity.', *Biochem. Biophys. Res. Commun.*, 216: 702-07.
- Schubert D, Behl C, Lesley R, Brack A, Dargusch R, Sagara Y, Kimura H.,. 1995. 'Amyloid peptides are toxic via a common oxidative mechanism.', *Proc Natl Acad Sci U S A.*, 14: 1989-93.
- Schultz W. 2007. Behavioral dopamine signals. *Trends Neurosci.* 30 (5): 203-210.
- Schulz K, Kroner A, David S. 2012. 'Iron efflux from astrocytes plays a role in remyelination.', *J. Neurosci.*, 32: 4841-47.
- Selkoe DJ. 1994. 'Alzheimer's disease: a central role for amyloid. ', *J. Neuropathol. Exp. Neurol.*, 53: 438-47.

- Selkoe DJ, Schenk D. 2003. 'Alzheimer's disease: molecular understanding predicts amyloid-based therapeutics.', *Annu Rev Pharmacol Toxicol.*, 43: 545-84.
- Seeman P, Caruso C, Lasaga M. 2008. 'Memantine agonist action at dopamine D2High receptors.', *Synapse.*, 62: 149-53.
- Serrano-Pozo A, Qian J, Monsell SE, et al., 2013. 'Examination of the clinicopathologic continuum of Alzheimer disease in the autopsy cohort of the National Alzheimer Coordinating Center. ', *J. Neuropathol. Exp. Neurol.*, 72: 1182-92.
- Shan WJ, Huang L, Zhou Q, Meng FC, Li XS. 2011. 'Synthesis, biological evaluation of 9-N-substituted berberine derivatives as multi-functional agents of antioxidant, inhibitors of acetylcholinesterase, butyrylcholinesterase and amyloid- $\beta$  aggregation.', *Eur. J. Med. Chem.*: 5885-93.
- Sharma M, Gupta Y. 'Chronic treatment with trans resveratrol prevents intracerebroventricular streptozotocin induced cognitive impairment and oxidative stress in rats.', *Life Sci.*, 71: 2489-98.
- Shen F, Smith JA, Chang R, Bourdet DL, Tsuruda PR, Obedencio GP, Beattie DT., . 2011. '5-HT(4) receptor agonist mediated enhancement of cognitive function in vivo and amyloid precursor protein processing in vitro: a pharmacodynamic and pharmacokinetic assessment. ', *Neuropharmacology*, 61: 69-79.
- Shin RW, Iwaki T, Kitamoto T, Sato Y, Tateishi J.,. 1992. 'Massive accumulation of modified tau and severe depletion of normal tau characterize the cerebral cortex and white matter of Alzheimer's disease: demonstration using the hydrated autoclaving method. ', *Am. J. Pathol.* 937-45.
- Shoffner JM. 1997. 'Oxidative phosphorylation defects and Alzheimer's disease.', *Neurogenetics.*, 1: 13-19.
- Siek GC, Katz LS, Fishman EB, and et al. 1990. 'Molecular forms of acetylcholinesterase in subcortical areas of normal and Alzheimer disease brain.', *Biol Psychiatry*, 27: 573-80.
- Silvestri L, Camaschella C. 2008. ' A potential pathogenetic role of iron in Alzheimer's disease', *J Cell Mol Med* 1548-50.
- Smith DP, Smith DG, Curtain CC, Boas JF, Pilbrow JR, Ciccotosto GD, Lau TL, Tew DJ, Perez KA, Wade JD, Bush AI, Drew SC, Separovic F, Masters CL, Cappai R, Barnham KJ. 'Copper-mediated amyloid-beta toxicity is associated with an intermolecular histidine bridge.', *J. Biol. Chem.*
- Smith MA, Harris PL, Sayre LM, Perry G.,. 1997. 'Iron accumulation in Alzheimer disease is a source of redox-generated free radicals. ', *Proc. Natl. Acad. Sci. USA*, 94: 9866-68.
- Smith A, Giunta B, Bickford PC, Fountain M, Tan J, and Shytle RD. 2010. Nanolipidic particles improve the bioavailability and alpha-secretase inducing ability of epigallocatechin-3-gallate (EGCG) for the treatment of Alzheimer's disease. *Int. J. Pharm.* 389 (1-2): 207-212.
- Smith MA, Hirai K, Hsiao K, Pappolla MA, Harris PL, Siedlak SL, Tabaton M, Perry G.,. 1998. 'Amyloid-beta deposition in Alzheimer transgenic mice is associated with oxidative stress.', *Journal of Neurochemistry*, 70: 2212-15.

- Snape MF, Misra A, Murray TK, De Souza RJ, Williams JL, Cross AJ, Green AR. 1999. 'A comparative study in rats of the in vitro and in vivo pharmacology of the acetylcholinesterase inhibitors tacrine, donepezil and NXX-066.', *Neuropharmacology.*, 38: 181-93.
- Song MS, Rauw G, Baker GB, Kar S. 2008. 'Memantine protects rat cortical cultured neurons against beta-amyloid-induced toxicity by attenuating tau phosphorylation.', *Eur J Neurosci.*, 28: 1989-2002.
- Soreq H, and Seidman S. 2001. Acetylcholinesterase--new roles for an old actor. *Nat. Rev. Neurosci.* 2 (4): 294-302.
- Stasiak A, Mussur M, Unzeta M, Samadi A, Marco-Contelles JL, Fogel WA. 2014. 'Effects of novel monoamine oxidases and cholinesterases targeting compounds on brain neurotransmitters and behavior in rat model of vascular dementia.', *Curr Pharm Des.*, 20: 161-71.
- Stocchi F, Borgohain R, Onofri M, Schapira AH, Bhatt M, Lucini V, et al. 2012. 'A randomized, double-blind, placebo-controlled trial of safinamide as add-on therapy in early Parkinson's disease patients.', *Mov Disord.*, 27: 106-12.
- Stoltenberg M, Bruhn M, Sondergaard C, Doering, P, West MJ, Larsen A, Troncoso JC, Danscher G. 2005. 'Immersion autometallographic tracing of zinc ions in Alzheimer beta-amyloid plaques.', *Histochem. Cell Biol.*: 605-11.
- Storga D, Vrecko K, Birkmayer JG, and Reibnegger G. 1996. Monoaminergic neurotransmitters, their precursors and metabolites in brains of Alzheimer patients. *Neurosci. Lett.* 203 (1): 29-32.
- Strolin-Benedetti M, Dostert P, Tipton KF. 1992. 'Developmental aspects of the monoamine-degrading enzyme monoamine oxidase.', *Dev. Pharmacol. Ther.*: 191-200.
- Struble RG, Cork LC, Whitehouse PJ, Price DL,. 1982. 'Cholinergic innervation in neuritic plaques.', *Science*, 216: 413-15.
- Su XY, Wu WH, Huang ZP, Hu J, Lei P, Yu CH, Zhao YF, Li YM. 2007. 'Hydrogen peroxide can be generated by tau in the presence of Cu(II).', *Biochem. Biophys. Res. Commun.*, 358: 661-65.
- Suh SW, Jensen KB, Jensen MS, Silva DS, Kesslak PJ, Danscher G, Frederickson J. . 2000. 'Histochemically-reactive zinc in amyloid plaques, angiopathy, and degenerating neurons of Alzheimer's diseased brains.', *Brain Res.*: 274-78.
- Sultana R, Butterfield DA. 'Role of oxidative stress in the progression of Alzheimer's disease.', *J Alzheimers Dis*, 19: 341-53.
- Sultana R, Mecocci P, Mangialasche F, Cecchetti R, Baglioni M, Butterfield DA,. 2011. 'Increased protein and lipid oxidative damage in mitochondria isolated from lymphocytes from patients with Alzheimer's disease: insights into the role of oxidative stress in Alzheimer's disease and initial investigations into a potential biomarker for this dementing disorder.', *J Alzheimers Dis.*,.
- Sussman JL, Harel M, Frolow F, Oefner C, Goldman A, Toker L, and Silman I. 1991. Atomic structure of acetylcholinesterase from *Torpedo californica*: a prototypic acetylcholine-binding protein. *Science* 253 (5022): 872-879.

- Swardfager W, Lanctot K, Rothenburg L, Wong A, Cappell J, Herrmann N., 2010. 'A meta-analysis of cytokines in Alzheimer's disease.', *Biol Psychiatry*, 68: 930-41.
- Sweet RA, Hamilton RL, Healy MT, Wisniewski SR, Henteleff R, Pollock BG, Lewis DA, and DeKosky ST. 2001. Alterations of striatal dopamine receptor binding in Alzheimer disease are associated with Lewy body pathology and antemortem psychosis. *Arch. Neurol.* 58 (3): 466-472
- Syme CD, Nadal RC, Rigby SEJ, Viles JH. 2004. 'Copper binding to the amyloid-beta (A $\beta$ ) peptide associated with Alzheimer's disease: folding, coordination geometry, pH dependence, stoichiometry, and affinity of A $\beta$ -(1-28): insights from a range of complementary spectroscopic techniques. ', *J. Biol. Chem.*, 279: 18169-77.
- Tamura Z, Yoshioka M, Imanari T, Fukaya J, Kusaka J. . 1973. 'Identification of green pigment and analysis of clioquinol in specimens from patients with subacute myelo-optico-neuropathy.', *Clin. Chim. Acta*: 13-20.
- Tanzi RE, Vaula G, Romano DM, Mortilla M, Huang TL, Tupler RG, Wasco W, Hyman BT, Haines JL, Jenkins BJ, et al. 'Assessment of amyloid beta-protein precursor gene mutations in a large set of familial and sporadic Alzheimer disease cases', *Am. J. Hum. Genet.*, 51: 273-82.
- Tateishi J. 2000. 'Subacute myelo-optico-neuropathy: clioquinol intoxication in humans and animals.', *Neuropathology*: S20-S24.
- Tatton WG, et al, . 2002. 'Propargylamines induce antiapoptotic new protein synthesis in serum- and nerve growth factor (NGF)-withdrawn, NGF-differentiated PC-12 cells.', *J. Pharmacol. Exp. Ther.*, 301: 753-64.
- Thies W, Beiler L. 2013. 'Alzheimer's disease: Facts and figures ', *Alzheimer Dement*, 9: 208-15.
- Thies W, Bleiler L. 2012. 'Alzheimer's association: Alzheimer's disease facts and figures.', *Alzheimer's Dement*, 2012: 131-68.
- Tohgi H, Abe T, Takahashi S, Kimura M, Takahashi J, and Kikuchi T. 1992. Concentrations of serotonin and its related substances in the cerebrospinal fluid in patients with Alzheimer type dementia. *Neurosci. Lett.* 141 (1): 9-12.
- Touchon J, Bergman H, Bullock R, Rapatz G, Nagel J, Lane R. 2006. 'Response to rivastigmine or donepezil in Alzheimer's patients with symptoms suggestive of concomitant Lewy body pathology.', *Curr Med Res Opin*, 22: 49-59.
- Tougu V, Karafin A, Palumaa P., 2008. 'Binding of zinc(II) and copper(II) to the full-length Alzheimer's amyloid-beta peptide.', *J. Neurochem*, 104: 1249-59.
- Traynelis SF, Burgess MF, Zheng F, Lyuboslavsky P, Powers JL. 1998. 'Control of voltage-independent zinc inhibition of NMDA receptors by the NR1 subunit.', *J. Neurosci.*: 6163-75.
- Traynelis, S. F.; Burgess, M. F.; Zheng, F.; Lyuboslavsky, P.; Powers, J. L. 1998. 'Control of voltage-independent zinc inhibition of NMDA receptors by the NR1 subunit.', *J. Neurosci.* : 6163-75.

- Treiber C, Simons A, Strauss M, Hafner M, Cappai R, Bayer TA, Multhaup G. 2004. 'Clioquinol mediates copper uptake and counteracts copper efflux activities of the amyloid precursor protein of Alzheimer's disease.', *J. Biol. Chem.*: 51958-64.
- Tremblay R, Chakravarthy B, Hewitt K, Tauskela J, Morley P, Atkinson T, Durkin JP. 'Transient NMDA receptor inactivation provides long-term protection to cultured cortical neurons from a variety of death signals.', *J Neurosci.*, 20: 7183-92.
- Tsang D, Ho KP, Wen HL. 1986. 'Ontogenesis of multiple forms of monoamine oxidase in rat brain regions and liver. ', *Dev. Neurosci.*: 243-50.
- Tsubaki T, Honma Y, Hoshi M. . 1971. 'Neurological syndrome associated with clioquinol.', *Lancet*: 696-97.
- Trojanowski JQ, Schmidt ML, Shin RW, Bramblett GT, Rao D, and Lee VM. 1993. Altered tau and neurofilament proteins in neuro-degenerative diseases: diagnostic implications for Alzheimer's disease and Lewy body dementias. *Brain Pathol.* 3 (1): 45-54.
- Truchot L, Costes SN, Zimmer L, Laurent B, Le BD, Thomas-Anterion C, Croisile B, Mercier B, Hermier M, Vighetto A, and Krolak-Salmon P. 2007. Up-regulation of hippocampal serotonin metabolism in mild cognitive impairment. *Neurology* 69 (10): 1012-1017.
- Tucker RP. 1990. The roles of microtubule-associated proteins in brain morphogenesis: a review. *Brain Res. Brain Res. Rev.* 15 (2): 101-120.
- Uchida Y, Takio K, Titani K, Ihara, Y, Tomonaga M. . 1991. 'The growth inhibitory factor that is deficient in the Alzheimer's disease brain is a 68 amino acid metallothionein-like protein. ', *Neuron*, 7.
- van Eersel J, Bi M, Ke YD, Hodges JR, Xuereb JH, Gregory GC, Halliday GM, Gotz J, Kril JJ, Ittner LM. 'Phosphorylation of soluble tau differs in Pick's disease and Alzheimer's disease brains., 116: 1243-51.
- van Ham TJ, Breitling R, Swertz MA, Nollen EA,. 2009. 'Neurodegenerative diseases: Lessons from genome-wide screens in small model organisms.', *EMBO Mol Med.*, 1: 360-70.
- van Stegeren AH. 2008. The role of the noradrenergic system in emotional memory. *Acta Psychol. (Amst)* 127 (3): 532-541.
- Vargas JY, Fuenzalida M, and Inestrosa NC. 2014. In vivo activation of Wnt signaling pathway enhances cognitive function of adult mice and reverses cognitive deficits in an Alzheimer's disease model. *J. Neurosci.* 34 (6): 2191-2202.
- Vellas B, Sol O, Snyder PJ, et al. . 2011. 'EHT 0202 in Alzheimer's disease: a 3-month, randomized, placebo-controlled, doubleblind study.', *Curr Alzheimer Res*, 8: 203-2012.
- Vogt, K.; Mellor, J.; Tong, G.; Nicoll, R. 2000. 'The actions of synaptically released zinc at hippocampal mossy fiber synapses', *Neuron*: 187-96.
- Vogels OJ, Broere CA, ter Laak HJ, ten Donkelaar HJ, Nieuwenhuys R, Schulte BP,. 1990. 'Cell loss and shrinkage in the nucleus basalis Meynert complex in Alzheimer's disease.', *Neurobiol Aging.*, 11: 3-13.

- von Bernhardt R, Eugén J. 2012. 'Alzheimer's disease: redox dysregulation as a common denominator for diverse pathogenic mechanisms.', *Antioxid Redox Signal.*, 16: 974-1031.
- Wadia JS, et al. 1998. 'Mitochondrial membrane potential and nuclear changes in apoptosis caused by serum and nerve growth factor withdrawal: time course and modification by (-)-deprenyl. ', *J. Neurosci.*, 18: 932-47.
- Wang CY, Wang T, Zheng W, Zhao BL, Danscher G, Chen YH, Wang ZY 2010. 'Zinc overload enhances APP cleavage and Abeta deposition in the Alzheimer mouse brain. ', *PLoSOne*, 5.
- Wang X, Su B, Siedlak SL, Moreira PI, Fujioka H, Wang Y, Casadesus G, Zhu X,. 2008. 'Amyloid-beta overproduction causes abnormal mitochondrial dynamics via differential modulation of mitochondrial fission/fusion proteins.', *Proc Natl Acad Sci USA*, 105: 19318-23.
- Wang X, Su B, Zheng L, Perry G, Smith MA, Zhu X,. 2009. 'The role of abnormal mitochondrial dynamics in the pathogenesis of Alzheimer's disease. ', *Journal of Neurochemistry*, 109: 153-59.
- Wang X.D., Chen X.Q., Yang H.H., Hu G.Y. 1999. 'Comparison of the effects of cholinesterase inhibitors on [3H] MK-801 binding in rat cerebral cortex ', *Neurosci Lett*, 272: 21-24.
- Weidemann A, Eggert S, Reinhard FB, Vogel M, Paliga K, Baier G, Masters CL, Beyreuther K, Evin G,. 2002. 'A novel epsilon-cleavage within the transmembrane domain of the Alzheimer amyloid precursor protein demonstrates homology with Notch processing.', *Biochemistry*, 41: 2825-35.
- Weinstock M, Bejar C, Wang RH, Poltyrev T, Gross A, Finberg JP, Youdim MB. 2000a. 'TV3326, a novel neuroprotective drug with cholinesterase and monoamine oxidase inhibitory activities for the treatment of Alzheimer's disease', *J Neural Transm Suppl*: 157-69.
- Weinstock M, Goren T, Youdim MB. 2000b. 'Development of a novel neuroprotective drug (TV3326) for the treatment of Alzheimer's disease, with cholinesterase and monoamine oxidase inhibitory activities. ', *Drug Dev Res*: 216-22.
- Weinstock M, Poltyrev T, Bejar C, Youdim MB. 2002. 'Effect of TV3326, a novel monoamine-oxidase cholinesterase inhibitor, in rat models of anxiety and depression. ', *Psychopharmacology (Berl)*: 318-24.
- Wessler I, Kirkpatrick CJ. 2008. 'Acetylcholine beyond neurons: the non-neuronal cholinergic system in humans.', *Br J Pharmacol.*, 154: 1558-71.
- Westlund KN, Denney RM, Kochersperger LM, Rose RM, Abell CW. . 'Distinct monoamine oxidase A and B populations in primate brain.', *Science*: 181-83.
- White AR, Du T, Loughton KM, Volitaskis I, Sharples RA, Xilinas ME, Hoke DE, Holsinger RMD, Evin G, Cherny RA, Hill AF, Barnham KJ, Li QX, Bush AI, Masters CL. . 2006. 'Degradation of the Alzheimer disease amyloid beta-peptide by metal-dependent up-regulation of metalloprotease activity. ', *J. Biol. Chem.*: 17670-80.

- White AR, Multhaup G, Maher F, Bellingham S, Camakaris J, Zheng H, Bush AI, Beyreuther K, Masters CL, Cappai R. . 1999. 'The Alzheimer's disease amyloid precursor protein modulates copper-induced toxicity and oxidative stress in primary neuronal cultures. ', *J. Neurosci.*,
- Wilkinson D, Murray J. 2001. 'Galantamine: a randomized, double-blind, dose comparison in patients with Alzheimer's disease.', *Int J Geriatr Psychiatry.* 852-57.
- Willard LB, Hauss-Wegrzyniak B, Danysz W, Wenk GL. 2000. 'The cytotoxicity of chronic neuroinflammation upon basal forebrain cholinergic neurons of rats can be attenuated by glutamatergic antagonism or cyclooxygenase-2 inhibition.', *Exp Brain Res.*, 134: 58-65.
- Woodhouse A, Dickson TC, Vickers JC. 2007. 'Vaccination strategies for Alzheimer's disease: A new hope?', *Drugs Aging.*, 24: 107-19.
- Wright CI, Geula C, Mesulam MM. 1993. 'Neurological cholinesterases in the normal brain and in Alzheimer's disease: relationship to plaques, tangles, and patterns of selective vulnerability.', *Ann Neurol.*, 34: 373-84.
- Wu RM, Chiueh CC, Pert A, Murphy DL. 1993. 'Apparent antioxidant effect of l-deprenyl on hydroxyl radical formation and nigral injury elicited by MPP+ in vivo.', *Eur J Pharmacol.*, 243: 241-47.
- Wu W, Lei P, Liu Q, Hu J, Gunn AP, Chen M, Rui Y, Su X, Xie Z, Zhao Y, Bush AI, Li Y. 2008. 'Sequestration of copper from beta-amyloid promotes selective lysis by cyclen-hybrid cleavage agents.', *J. Biol. Chem.*, 283: 31657-64.
- Xie W, Stribley JA, Chatonnet A, Wilder PJ, Rizzino A, McComb RD, Taylor P, Hinrichs SH, and Lockridge O. 2000. Postnatal developmental delay and supersensitivity to organophosphate in gene-targeted mice lacking acetylcholinesterase. *J. Pharmacol. Exp. Ther.* 293 (3): 896-902.
- Yamamoto A, Shin RW, Hasegawa K, Naiki H, Sato H., and Kitamoto T Yoshimasu F. 2002. 'Iron (III) induces aggregation of hyperphosphorylated tau and its reduction to iron(II) reverses the aggregation: Implications in the formation of neurofibrillary tangles of Alzheimer's disease', *J Neurochem*: 1137-47.
- Yang Y, Ma D, Wang Y, Jiang T, Hu S, Zhang M, Yu X, Gong CX., 2013. 'Intranasal insulin ameliorates tau hyperphosphorylation in a rat model of type 2 diabetes. ', *J. Alzheimers Dis.*, 33: 329-38.
- Yang Y, Yang J, and Jiang Q. 2014. The protective effect of huperzine A against hepatic ischemia reperfusion injury in mice. *Transplant. Proc.* 46 (5): 1573-1577.
- Yao R, Lu X, Guan Q, Zheng L, Lu X, Ruan B. 2013. 'Synthesis and biological evaluation of some novel resveratrol amide derivatives as potential anti-tumor agents. ', *Eur. J. Med. Chem.*, 62: 222-31.
- You H, Tsutsui S, Hameed S, Kannanayakal TJ, Chen L, Xia P, Engbers JDT, Lipton SA, Stys PK, Zamponi GW. 'Ab neurotoxicity depends on interactions between copper ions, prion protein, and N-methylD-aspartate receptors. ', *Proc. Natl. Acad. Sci. USA*, 109: 1737-42.

- Youdim MB. 2013. Multi target neuroprotective and neurorestorative anti-Parkinson and anti-Alzheimer drugs ladostigil and m30 derived from rasagiline. *Exp. Neurobiol.* 22 (1): 1-10.
- Youdim MBH, Edmonson D, Tipton KF. 2006. 'The therapeutic potential of monoamine oxidase inhibitors.', *Nature Reviews*, 7: 295-309.
- Youdim MBH, Maruyama W, Naoi M. 2005. 'Neuropharmacological, neuroprotective and amyloid precursor processing properties of selective MAO-B inhibitor antiparkinsonian drug, rasagiline. ', *Drugs Today*, 41: 369-91.
- Youdim MBH, Weinstock M. 2004. 'Therapeutic applications of selective and non-selective inhibitors of monoamine oxidase A and B that do not cause significant tyramine potentiation. ', *Neurotoxicology*: 243-50.
- Yu WH, Lukiw WJ, Bergeron C, Niznik HB, Fraser PE. 2001. 'Metallothionein III is reduced in Alzheimer's disease.', *Brain Res.*
- Zhang B, Carroll J, Trojanowski JQ, et al. 2012. 'The microtubule-stabilizing agent, epothilone D, reduces axonal dysfunction, neurotoxicity, cognitive deficits, and Alzheimer-like pathology in an interventional study with aged tau transgenic mice.', *J Neurosci*, 1432: 3601-11.
- Zhang H, Zou K, Tesseur I, and Wyss-Coray T. 2005. Small molecule tgf-beta mimetics as potential neuroprotective factors. *Curr. Alzheimer Res.* 2 (2): 183-186.
- Zhao YJ, Wee HL, Au WL, Seah SH, Luo N, Li SC, Tan LC. 2011. 'Selegiline use is associated with a slower progression in early Parkinson's disease as evaluated by Hoehn and Yahr Stage transition times.', *Parkinsonism Relat Disord.*, 17: 194-97.
- Zheng H, Fridkin M, Youdim MBH. 2014. 'From Single Target to Multitarget/Network Therapeutics in Alzheimer's Therapy', *Pharmaceuticals*, 7: 113-35.
- Zheng H, Gal S, Weiner LM, Bar-Am O, Warshawsky A., and Youdim MB Fridkin M. 2005. 'Novel multifunctional neuroprotective iron chelator-monoamine oxidase inhibitor drugs for neurodegenerative diseases: in vitro studies on antioxidant activity, prevention of lipid peroxide formation and monoamine oxidase inhibition.', *J Neurochem* 68-78.
- Zheng H, Youdim MB, Fridkin M,. . 2010. 'Site-activated chelators targeting acetylcholinesterase and monoamine oxidase for Alzheimer's therapy ', *ACS Chem Biol*, 5: 605-10.
- Zhou LX, Du JT, Zeng ZY, Wu WH, Zhao YF, Kanazawa K, Ishizuka Y, Nemoto T, Nakanishi H, Li YM,. 2007. 'Copper(II) modulates in vitro aggregation of tau peptide'. *Peptides* 28(11):2229-34.
- Zhu W, Xie W, Pan T, Xu P, Fridkin M, Zheng H, Jankovic, and Youdim MB J, Le W 2007. 'Prevention and restoration of lactacystin-induced nigrostriatal dopamine neuron degeneration by novel brain-permeable iron chelators.', *FASEB J*: 3835-44.
- Zhu X, Lee HG, Perry G, Smith MA,. 2007. 'Alzheimer disease, the two-hit hypothesis: an update.', *Biochimica et Biophysica Acta*, 1772: 494-502.
- Zhukareva V, Vogelsberg-Ragaglia V, Van Deerlin VM, Bruce J, Shuck T, Grossman M, Clark CM, Arnold SE, Masliah E, Galasko DR, Trojanowski JQ, Lee VMY,.. 2001.

- 'Loss of brain tau defines novel sporadic and familial tauopathies with frontotemporal dementia.' *Ann. Neurol.*, 49: 165-75.
- Zigler Jr JS, Jernigan Jr HM, Garland D, Reddy VN.. 'The effects of "oxygen radicals" generated in the medium on lenses in organ culture: inhibition of damage by chelated iron. ', *Arch. Biochem. Biophys.*, 241: 163-72.

## **VIII. ANNEXES**



## **Annex I**

“Synthesis, biological assessment and molecular modelling of new multipotent MAO and cholinesterase inhibitors as potential drugs for the treatment of Alzheimer’s disease”





## Short communication

# Synthesis, biological assessment and molecular modeling of new multipotent MAO and cholinesterase inhibitors as potential drugs for the treatment of Alzheimer's disease

Abdelouahid Samadi<sup>a,\*</sup>, Mourad Chioua<sup>a</sup>, Irene Bolea<sup>b</sup>, Cristóbal de los Ríos<sup>c,d</sup>, Isabel Iriepa<sup>d</sup>, Ignacio Moraleda<sup>d,c</sup>, Agatha Bastida<sup>e</sup>, Gerard Esteban<sup>b</sup>, Mercedes Unzeta<sup>b</sup>, Enrique Gálvez<sup>d</sup>, José Marco-Contelles<sup>a,\*</sup>

<sup>a</sup> Laboratorio de Radicales Libres y Química Computacional (IQOG, CSIC), C/Juan de la Cierva 3, 28006 Madrid, Spain

<sup>b</sup> Departament de Bioquímica i Biologia Molecular, Facultat de Medicina, Universitat Autònoma de Barcelona, 08193 Bellaterra, Barcelona, Spain

<sup>c</sup> Instituto Teófilo Hernando, Fundación de Investigación Biomédica, Hospital Universitario de la Princesa, C/Diego de León, 62, 28006-Madrid, Spain

<sup>d</sup> Departamento de Química Orgánica, Universidad de Alcalá, Ctra. Madrid-Barcelona, Km. 33,6, 28871, Alcalá de Henares, Madrid, Spain

<sup>e</sup> Departamento de Química Bioorgánica (IQOG, CSIC), C/Juan de la Cierva 3, 28006-Madrid, Spain

## ARTICLE INFO

## Article history:

Received 23 March 2011

Received in revised form

16 May 2011

Accepted 19 May 2011

Available online 26 May 2011

## Keywords:

Pyridines

Naphthyridines

Multipotent molecules

AChE

BuChE

MAO-A

MAO-B

Kinetic analysis

Inhibition mechanism

Molecular modeling

Alzheimer's disease

## ABSTRACT

The synthesis, biological evaluation and molecular modeling of new multipotent inhibitors of type **I** and type **II**, able to simultaneously inhibit monoamine oxidases (MAO) as well as acetylcholinesterase (AChE) and butyrylcholinesterase (BuChE), is described. Compounds of type **I** were prepared by sequential reaction of 2,6-dichloro-4-phenylpyridine-3,5-dicarbonitrile (**14**) [or 2,6-dichloropyridine-3,5-dicarbonitrile (**15**)] with prop-2-yn-1-amine (or *N*-methylprop-2-yn-1-amine) and 2-(1-benzylpiperidin-4-yl)alkylamines **22–25**. Compounds of type **II** were prepared by Friedländer type reaction of 6-amino-5-formyl-2-(methyl(prop-2-yn-1-yl)amino)nicotinonitriles **32** and **33** with 4-(1-benzylpiperidin-4-yl)butan-2-one (**31**). The biological evaluation of molecules **1–11** showed that most of these compounds are potent, in the nanomolar range, and selective AChEI, with moderate and equipotent selectivity for MAO-A and MAO-B inhibition. Kinetic studies of compound **8** proved that this is a *Ee*AChE mixed type inhibitor ( $IC_{50} = 16 \pm 2$ ;  $K_i = 12 \pm 3$  nM). Molecular modeling investigation on compound **8** confirmed its dual AChE inhibitory profile, binding simultaneously at the catalytic active site (CAS) and at the peripheric anionic site (PAS). In overall, compound **11**, as a potent and selective dual AChEI, showing a moderate and selective MAO-A inhibitory profile, can be considered as an attractive multipotent drug for further development on two key pharmacological targets playing key roles in the therapy of Alzheimer's disease.

© 2011 Elsevier Masson SAS. All rights reserved.

## 1. Introduction

Alzheimer's disease (AD) is an age-related neurodegenerative process characterized by a progressive memory loss, decline in language skills and other cognitive impairments [1]. Although the etiology of AD is not known, amyloid- $\beta$  ( $A\beta$ ) deposits [2],  $\tau$ -protein

aggregation, oxidative stress [3] and low levels of acetylcholine [4] are thought to play significant roles in the pathophysiology of the disease [5]. The cholinergic theory [6] suggests that the loss of cholinergic neurons in AD results in a deficit of acetylcholine (ACh) in specific brain regions that mediate learning and memory functions [7]. Consequently, a number of acetylcholinesterase inhibitors (AChEI) such as tacrine [8], rivastigmine [9], donepezil [10] and galanthamine [11] have been developed, but with limited therapeutic benefits, mainly due to the multifactorial nature of AD. The multi-target-directed ligand (MTDL) approach, based on the "one molecule, multiple target" paradigm [12], has been the subject of increasing attention by many research groups, which have developed a number of compounds acting simultaneously on different receptors implicated in AD [13]. In this context, alterations in other neurotransmitter systems, especially the serotonergic and

\* Corresponding authors. Tel.: +34 91 5622900.

E-mail addresses: [samadi@iqog.csic.es](mailto:samadi@iqog.csic.es) (A. Samadi), [mchioua@iqog.csic.es](mailto:mchioua@iqog.csic.es) (M. Chioua), [irene.bolea@campus.uab.cat](mailto:irene.bolea@campus.uab.cat) (I. Bolea), [cristobal.delosrios@uam.es](mailto:cristobal.delosrios@uam.es) (C. de los Ríos), [isabel.iriempa@uah.es](mailto:isabel.iriempa@uah.es) (I. Iriepa), [ignacio.moraleda@uah.es](mailto:ignacio.moraleda@uah.es) (I. Moraleda), [agatha.bastida@iqog.csic.es](mailto:agatha.bastida@iqog.csic.es) (A. Bastida), [gerardo.esteban@uab.cat](mailto:gerardo.esteban@uab.cat) (G. Esteban), [mercedes.unzeta@uab.cat](mailto:mercedes.unzeta@uab.cat) (M. Unzeta), [enrique.galvez@uah.es](mailto:enrique.galvez@uah.es) (E. Gálvez), [jlmarco@iqog.csic.es](mailto:jlmarco@iqog.csic.es) (J. Marco-Contelles).

dopaminergic, are also thought to be responsible for the observed behavioral disturbances [14,15]. Monoamine oxidase (MAO; EC 1.4.3.4) is an important target to be considered for the treatment of AD, as catalyzes the oxidative deamination of a variety of biogenic and xenobiotic amines, with the concomitant production of hydrogen peroxide [16]. MAO is a FAD-containing enzyme bound to mitochondrial outer membrane of neuronal, glial and other cells [17]. MAO exists as two isozymes: MAO-A and MAO-B, showing different substrate specificity, sensitivity to inhibitors, and amino-acid sequences. MAO-A preferentially oxidizes norepinephrine and serotonin, and is selectively inhibited by chlorgyline, while MAO-B preferentially deaminates  $\beta$ -phenylethylamine and is irreversibly inhibited by l-deprenyl [18]. X-ray crystal structures of human MAO-A [19] and MAO-B [20] have been reported.

With these ideas in mind, and based on our previous work in the synthesis and biological evaluation of MAO inhibitors (MAOI) [21] and AChE inhibitors (AChEI) [22], we have now designed new multipotent MAO and ChE inhibitors (**I** and **II**, Chart 1) for the potential treatment of AD. This approach has been previously analyzed with success by other laboratories [23–26]. What is new and original in our strategy is that the design of our molecules based on a conjunctive approach that combines for the first time the *N*-benzyl piperidine and the *N*-propargylamine moieties present in the AChE inhibitor donepezil [10], and PF9601N, a well known MAOI [21], respectively, connected through an appropriate linker to a central pyridine (or 1,8-naphthyridine) ring (Chart 1). In this preliminary communication, we report the synthesis and pharmacological evaluation of polyfunctionalized pyridines **1–8**, naphthyridines **9–11** (Table 1), and the identification of compound **11**, as a potent, in the nanomolar range, and selective dual AChEI, showing a moderate and selective MAO-A inhibitory profile.

## 2. Results and discussion

### 2.1. Chemistry

Type **I** compounds (Chart 1) were prepared by sequential reaction of 2,6-dichloro-4-phenylpyridine-3,5-dicarbonitrile (**14**) [27] (or 2,6-dichloropyridine-3,5-dicarbonitrile (**15**) [28]) with commercially available prop-2-yn-1-amine (or *N*-methylprop-2-yn-1-amine) and 2-(1-benzylpiperidin-4-yl)alkylamines **22–25** (Chart 2). Compounds of type **II** were prepared by Friedländer type reaction of 6-amino-5-formyl-2-(methyl(prop-2-yn-1-yl)amino)nicotinonitriles **32** and **33** with 4-(1-benzylpiperidin-4-yl)butan-2-one (**31**) (Supplementary data).

The *in vitro* activity of these new molecules against *Ee*AChE and eqBuChE was determined using Ellman's method [29] (Supplementary data) with tacrine and donepezil as reference compounds (Table 1). From these data some interesting SAR can be obtained. The IC<sub>50</sub> values suggest that most of these molecules are

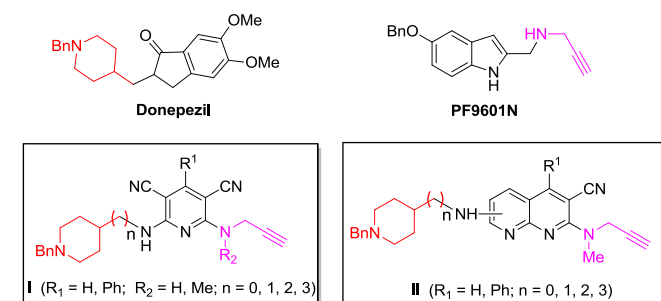


Chart 1. General structure of PF9601N, and the MAO and ChE inhibitors **I** and **II**.

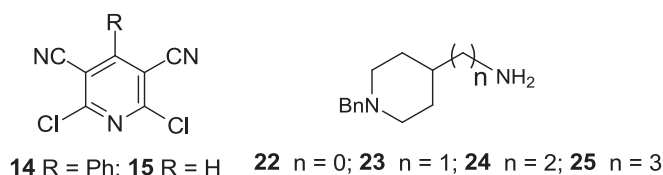


Chart 2. Structure of precursors: Pyridines **14,15**, and amines **22–25**.

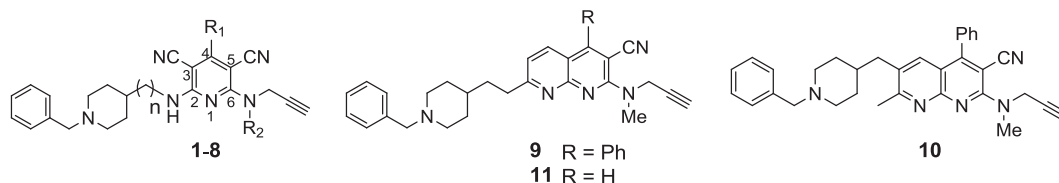
potent, in the nanomolar range, and selective *Ee*AChE inhibitors, the most potent are compounds **3**, **4**, **6**, and **8** [IC<sub>50</sub> (*Ee*AChE) = 13–16 nM], which are more potent than tacrine, but equipotent with donepezil for the *Ee*AChE inhibition.

All compounds are less potent than the reference compounds for BuChE inhibition, except compound **4**, 4-fold more potent than donepezil. Regarding the effect of the linker, for compounds **1–4** bearing a phenyl group at C4 and a methyl group at N(C6), the inhibition of both *Ee*AChE and eqBuChE increases on going from *n* = 0 to *n* = 2 or 3. For the same length in the linker (*n* = 0), changing only the methyl group by hydrogen (compare compound **1** with **5**), the *Ee*AChE inhibitory potency decreases 3.3-fold, while both compounds remain inactive for eqBuChE inhibition. Similarly, for the same length in the linker (*n* = 2), changing only the phenyl at C4 by a hydrogen (compare compound **3** with **6**), the *Ee*AChE inhibitory potency remains similar, affording the most potent AChEI (**6**) in this series [IC<sub>50</sub> (*Ee*AChE) = 13 nM], while the eqBuChE potency is reduced, becoming around 3-fold less potent. Very interestingly, the substitution of the methyl group in compound **6** by a hydrogen, with the same length (*n* = 2), results in the potent, but completely selective *Ee*AChEI **8**. However, this potency is lost in inhibitor **7** bearing the same type of substituent, the length of the linker being now *n* = 0. Note also that for *n* = 2, compound **3** with the functional couple Ph(C-4)/N(C-6)Me is equipotent with compound **8** bearing the functional couple H(C-4)/N(C-6)H for the inhibition of *Ee*AChE. Definitely, compound **4** with the longest length (*n* = 3), bearing a phenyl group at C4 and a methyl group at N(C6) remains as the most potent eqBuChE inhibitor [IC<sub>50</sub> (eqBuChE) = 230 nM].

Based on our previous work on the area [30], and in order to evaluate the presumed critical effect of the pyridine ring in compounds **1–8** on the biological activity, we prepared naphthyridine derivatives **9–11** [31] (Table 1). According to the observed IC<sub>50</sub> values (Table 1), these three compounds are also potent and selective AChEI, the most potent is compound **11** [IC<sub>50</sub> = 37 nM], while compound **10** shows the worst inhibitory potency for both enzymes.

To determine the type of the *Ee*AChE inhibition mechanism on these compounds, a kinetic study was carried out with inhibitor **8** [IC<sub>50</sub> (*Ee*AChE) = 16 ± 2 nM; IC<sub>50</sub> (eqBuChE) > 100000 nM] (Supplementary data). The type of inhibition was established from the analysis of Lineweaver–Burk reciprocal plots (Fig. 1) showing both increasing slopes (lower *V*<sub>max</sub>) and intercepts (higher *K*<sub>m</sub>) with higher inhibitory concentration. This suggests a mixed-type inhibition [32]. The graphical analysis of steady-state inhibition data for compound **8** is shown in Fig. 1. A *K*<sub>i</sub> value of 12.2 nM was estimated from the slopes of double reciprocal plots versus compound **8** concentrations.

Based on these results, compound **8** was analyzed in order to investigate the possible interactions between the inhibitor and the amino acid residues on the catalytic active site (CAS), and in the peripheral anionic site (PAS) of AChE. Ligand docking studies were performed with AUTODOCK VINA [33] using a single catalytic subunit of *Ee*AChE (PDB: 1C2B) (Supplementary data). The docking procedure was applied to the whole protein target (“blind docking”). To account for side chain flexibility during docking, flexible

**Table 1**Inhibition of AChE from *Electrophorus electricus* (EeAChE), equine serum butyrylcholinesterase (eqBuChE) and monoamineoxidase (MAO-A and MAO-B) by compounds **1–11**.<sup>a</sup>

Compound	R <sub>1</sub>	R <sub>2</sub>	n	IC <sub>50</sub> (nM)		Selectivity BuChE/AChE	IC <sub>50</sub> (μM)		Selectivity MAO-B/MAO-A
				EeAChE	EqBuChE		MAO-A	MAO-B	
<b>1</b>	Ph	Me	0	1200 ± 200	>100 000	>83	>100	>100	>1
<b>2</b>	Ph	Me	1	270 ± 52	5000 ± 700	18.5	>100	>100	>1
<b>3</b>	Ph	Me	2	16 ± 2	1110 ± 30	69.4	>100	>100	>1
<b>4</b>	Ph	Me	3	14 ± 1	230 ± 30	16.4	>100	>100	>1
<b>5</b>	Ph	H	0	4000 ± 100	>100 000	>25	25 ± 1	>100	>4
<b>6</b>	H	Me	2	13 ± 1	3100 ± 300	238.5	>100	>100	>1
<b>7</b>	H	H	0	530 ± 70	>100 000	>188	>100	>100	>1
<b>8</b>	H	H	2	16 ± 2	>100 000	>6250	>100	>100	>1
<b>9</b>				53 ± 3	3500 ± 350	66	>100	32 ± 3	>0.32
<b>10</b>				2300 ± 300	>100 000	>34	>100	97 ± 24	>1
<b>11</b>				37 ± 4	1990 ± 270	54	41 ± 7	>100	>2.4
<b>tacrine</b>				27 ± 2	5.2 ± 0.2	0.19	40 ± 10	>100	>2.5
<b>donepezil</b>				13.4 ± 0.9	840 ± 50	63	>100	15 ± 2	>0.15

<sup>a</sup> Values are expressed as mean ± standard error of the mean of at least three different experiments in quadruplicate.

torsions in the ligand were assigned, and the acyclic dihedral angles were allowed to rotate freely. In the docking simulation, the pose with the lowest docking energy was selected as the best solution. The “blind docking” of the **8**-EeAChE molecules was successful as indicated by the statistically significant scores. Fig. 2 shows the complex of EeAChE with ligand **8**. As can be seen, docking results indicate that the cyano group makes hydrogen bonding with residue Ser203 in the catalytic triad, playing an important role in the molecular recognition as well as in the inhibition process. The pyridine nitrogen of compound **8** is likely to form a hydrogen interaction with the OH Tyr337 side chain, located in the constricted region in the gorge. Additionally, inhibitor **8** seems to stabilize through  $\pi$ - $\pi$  stacking interactions between the phenyl group and the indole ring of Trp286 in the PAS. Therefore, ligand **8** is a dual EeAChEI, able to simultaneously interact with both, the

CAS and PAS of the enzyme, a result that is in good agreement with its mixed-type inhibition profile [34]: the pyridine moiety of this inhibitor binds at the CAS, while the linker spans the active-site gorge, and the phenyl ring binds at the PAS [35].

Finally, and in order to test their multipotent profile, compounds **1–11** have been evaluated as MAO-A and MAO-B inhibitors (Table 1) (Supplementary data). These results show that pyridines **2, 3, 6** and **7** are inactive, and pyridines **1, 4, 8**, and naphthyridine **10** are poor MAO inhibitors. Only pyridine **5** (IC<sub>50</sub> = 25 ± 1 μM) and naphthyridine **11** (IC<sub>50</sub> = 41 ± 7 μM) were moderate, in the micromolar range, selective MAO-A inhibitors, while pyridine **9** showed selective MAO-B inhibition activity (IC<sub>50</sub> = 32 ± 3 μM). Thus, the substitution of a phenyl at C4 in compound **9** by a hydrogen in inhibitor **11** drives the MAO selectivity from MAO-B to MAO-A, with the potency remaining similar. In general, the

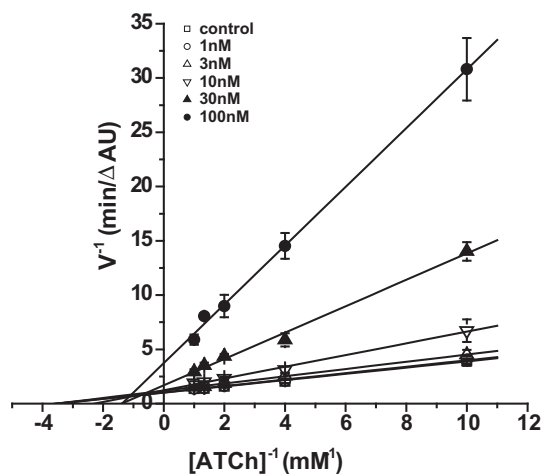


**Fig. 1.** Steady-state inhibition of AChE hydrolysis of acetylthiocholine (ATCh) by compound **8**. Lineweaver–Burk reciprocal plots of initial velocity and substrate concentrations (0.1–1 mM) are presented. Lines were derived from a weighted least-squares analysis of data.

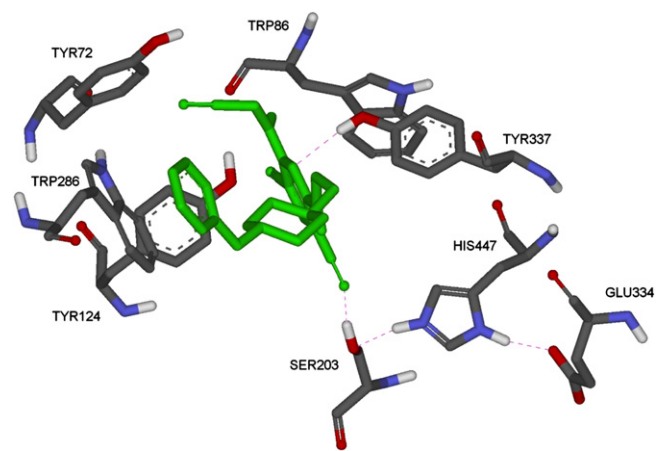


**Fig. 2.** Binding mode of **8** on EeAChE as the outcome of docking simulations. The compound is rendered as sticks and illustrated in green. The hydrogen bonds are represented in dashed yellow lines. (For interpretation of the references to colour in this figure legend, the reader is referred to the web version of this article.)

naphthyridine core seems to be a more promising hit. However, no clear SAR can be deduced from these results, and a careful molecular modeling analysis in progress should possibly afford the keys in order to rationalize the observed inhibition trends.

### 3. Conclusions

To sum up, compounds **1–11**, designed as hybrids from donepezil and PF9601N, bearing *N*-benzyl piperidine and propargylamine moieties attached to a central pyridine or naphthyridine ring, have been synthesized and subjected to pharmacological evaluation. The biochemical results clearly identify compound **8**, and particularly, **11** as multipotent drugs showing strong and selective AChE inhibitory activity [(IC<sub>50</sub> = 37 ± 4 nM)], and moderate, but selective MAO-A inhibitory profile [(IC<sub>50</sub> = 41 ± 7 μM)]. We conclude that the most sensitive moiety to modulate AChE inhibition is the length of the spacer, which would control the dual interaction of these molecules with both CAS and PAS sites, improving inhibition when both binding sites are spatially targeted at the same time. Compared to tacrine, compound **11** is equipotent for the AChE and MAO-A inhibition, less potent for the inhibition of BuChE and more potent for the inhibition of MAO-B. Compared to donepezil, compound **11** is less potent for the inhibition of AChE, BuChE, and MAO-B, and more potent for the inhibition of MAO-A. Comparing the two pyridine derivatives **9** and **2**, with the same length in the linker, compound **9** (linker: CH<sub>2</sub>CH<sub>2</sub>) is 5-fold less potent than inhibitor **2** (linker: CH<sub>2</sub>NH) for the inhibition of *Ee*AChE, and 1.4-fold less active for the inhibition of *eq*BuChE. Conversely, regarding MAO inhibition, while pyridine **2** was inactive, naphthyridine **9** showed a moderate, but selective MAO-B inhibitory profile. The pharmacological profile of compound **11**, as well as the fact that it is a readily available compound in a short synthetic sequence, in good chemical yields, prompts us to select it as a lead-compound for further optimization in our current research programme targeted to the preparation of new molecules for the potential treatment of AD. Work is now in progress and will be reported in due course.

### Acknowledgments

A. Samadi thanks CSIC for a I3P-post-doc contract. M. Chioua thanks ISCI (MICINN) for a “Sara Borrell” post-doctoral contract. J. Marco-Contelles thanks MICINN (SAF2006-08764-CO2-01, SAF2009-07271) and CAM (S/SAL-0275-2006) financial support. C. de los Ríos thanks ISCI for a “Miguel Servet” contract and financial support (Fundación CIEN and “Miguel Servet Program”).

### Appendix. Supplementary data

Supplementary data associated with this article can be found, in the online version, at doi:10.1016/j.ejmech.2011.05.048.

### References

- [1] M. Goedert, M.G. Spillantini, *Science* 314 (2006) 777–781.
- [2] A. Castro, A. Martínez, *Curr. Pharm. Des.* 12 (2006) 4377–4387.
- [3] A. Gella, N. Durany, *Cell. Adh. Migr.* 3 (2009) 88–93.
- [4] L. Cummings, *J. Rev. Neurol. Dis.* 1 (2004) 60–69.
- [5] E. Scarpini, P. Scheltens, H. Feldman, *Lancet Neurol.* 2 (2003) 539–547.
- [6] E.K. Perry, B.E. Tomlinson, G. Blessed, K. Bergmann, P.H. Gibson, R.H. Perry, *British Med. J.* (1978) 1457–1459.
- [7] V.N. Talesa, *Mech. Ageing Dev.* 122 (2001) 1961–1969.
- [8] K.L. Davis, P. Powchick, *Lancet* 345 (1995) 625–630.
- [9] C.M. Spencer, S. Noble, *Drugs Aging* 13 (1998) 391–400.
- [10] E.L. Barner, S.L. Gray, *Ann. Pharmacother.* 32 (1998) 70–77.
- [11] J.J. Sramek, E.J. Frackiewicz, N.R. Cutler, *Expert Opin. Invest. Drugs* 9 (2000) 2393–2402.
- [12] D. Muñoz-Torrero, P. Camps, *Curr. Med. Chem.* 13 (2006) 399–422.
- [13] A. Cavalli, M.L. Bolognesi, A. Minarini, M. Rosini, V. Tumiatto, M. Recanatini, C. Melchiorre, *J. Med. Chem.* 51 (2008) 347–372.
- [14] M. García-Alloza, F.J. Gil-Bea, M. Díez-Ariza, C.P. Chen, P.T. Francis, B. Lasheras, M. Ramirez, *J. Neuropsychologia* 43 (2005) 442–449.
- [15] A.V. Terry, J.J. Buccafusco, C. Wilson, *Behav. Brain Res.* 195 (2008) 30–38.
- [16] M.B.H. Youdim, J.P.M. Finberg, K.F. Tipton, in: U. Tredelenburg, N. Weiner (Eds.), *Monoamine Oxidase*, Springer-Verlag, Berlin, 1988, pp. 119–192.
- [17] J. Mitoma, A. Ito, *J. Bio. Chem.* 111 (1992) 20–24.
- [18] T.P. Singer, in: F. Müller (Ed.), *Chemistry and Biochemistry of Flavoenzymes*, Vol III, CRC Press, Boca Raton, FL, USA, 1990, pp. 437–470.
- [19] S.Y. Son, A. Ma, Y. Kondou, M. Yoshimura, E. Yamashita, T. Tsukihara, *Proc. Natl. Acad. Sci. USA* 105 (2008) 5739–5744.
- [20] C. Binda, P. Newton-Vinson, F. Hubalek, N. Restelli, D.E. Edmondson, A. Mattevi, *Nat. Struct. Biol.* 2 (2002) 22–26.
- [21] V. Pérez, J.L. Marco, E. Fernández-Álvarez, M. Unzeta, *Brit. J. Pharmacol.* 127 (1999) 869–876.
- [22] C. de los Ríos, J. Egea, J. Marco-Contelles, R. León, A. Samadi, I. Iriepa, I. Moraleda, E. Gálvez, A.G. García, M.G. López, M. Villarroya, A. Romero, *J. Med. Chem.* 53 (2010) 5129–5143.
- [23] H. Zheng, M.B.H. Youdim, M. Fridkin, *J. Med. Chem.* 52 (2009) 4095–4098.
- [24] J. Sterling, Y. Herzig, T. Goren, N. Finkelstein, D. Lerner, W. Goldenberg, I. Miskolczi, S. Molnar, F. Rantal, T. Tamas, G. Toth, A. Zagyva, A. Zekany, G. Lavian, A. Gross, R. Friedman, M. Razin, W. Huang, B. Kraiss, M. Chorev, M.B. Youdim, M. Weinstock, *J. Med. Chem.* 45 (2002) 5260–5279.
- [25] C. Brühlmann, F. Ooms, P.-A. Carrupt, B. Testa, M. Catto, F. Leonetti, C. Altomare, A. Carotti, *J. Med. Chem.* 44 (2001) 3195–3198.
- [26] D.M. Fink, M.G. Palermo, G.M. Bores, F.P. Huger, B.E. Kurys, M.C. Merriman, G.E. Olsen, W. Petko, G.J. O'Malley, *Bioorg. Med. Chem. Lett.* 6 (1996) 625–630.
- [27] (a) C. Peinador, M.C. Veiga, J. Vilar, J.M. Quintela, *Heterocycles* 38 (1994) 1299–1305;  
(b) A.G. E.Merck, DE1182896; 1963, *Chem. Abstr.* 62 (1965) 4013a Patent.
- [28] (a) A. Duindam, V.L. Lishinsky, D.J. Sikkema, *Synth. Commun.* 23 (1993) 2605–2609;  
(b) D.V. Vilarelle, C. Peinador, J.M. Quintela, *Tetrahedron* 60 (2004) 275–283.
- [29] G.L. Ellman, K.D. Courtney, B.J. Andres, R.M. Featherstone, *Biochem. Pharmacol.* 7 (1961) 88–95.
- [30] J. Marco-Contelles, R. León, C. de los Ríos, A. Samadi, M. Bartolini, V. Andrisano, O. Huertas, X. Barril, F.J. Luque, M.I. Rodríguez-Franco, B. López, M.G. López, A.G. García, M.C. Carreiras, M. Villarroya, *J. Med. Chem.* 52 (2009) 2724–2732.
- [31] Compounds **9** and **11** were prepared by Friedländer type reaction of 6-amino-5-formyl-2-(methyl(prop-2-yn-1-yl)amino)-4-phenylnicotinonitrile (**32**) with 4-(1-benzylpiperidin-4-yl)butan-2-one (**31**), while compound **10** was obtained as the only product in a similar reaction between 6-amino-5-formyl-2-(methyl(prop-2-yn-1-yl)amino)nicotinonitrile (**33**) and ketone **31** (Supplementary data).
- [32] A. Rampa, A. Bisi, F. Belluti, S. Gobbi, P. Valenti, V. Andrisano, V. Cavrini, A. Cavalli, M. Recanatini, *Bioorg. Med. Chem.* 8 (2000) 497–506.
- [33] O. Trott, A.J. Olson, *J. Comput. Chem.* 31 (2010) 455–461.
- [34] D. Alonso, I. Dorransoro, L. Rubio, P. Muñoz, E. García-Palomero, M. Del Monte, A. Bidon-Chanal, M. Orozco, F.J. Luque, A. Castro, M. Medina, A. Martínez, *Bioorg. Med. Chem.* 13 (2005) 6588–6597.
- [35] N.C. Inestrosa, A. Álvarez, C.A. Pérez, R.D. Moreno, M. Vicente, C. Linker, O.I. Casanueva, C. Soto, J. Garrido, *J. Neuron* 16 (1996) 881–891.

## **Annex II**

“A therapeutic approach to cerebrovascular diseases based on indole-substituted hydrazides and hydrazines able to interact with human vascular adhesion protein-1, monoamine oxidases (A and B), AChE and BuChE”.



# A therapeutic approach to cerebrovascular diseases based on indole substituted hydrazides and hydrazines able to interact with human vascular adhesion protein-1, monoamine oxidases (A and B), AChE and BuChE

Gerard Esteban · Irene Bolea · Ping Sun ·  
Montse Solé · Abdelouahid Samadi ·  
José Marco-Contelles · Mercedes Unzeta

Received: 14 October 2012 / Accepted: 2 December 2012 / Published online: 21 December 2012  
© Springer-Verlag Wien 2012

**Abstract** Herein, we report the biological evaluation of a series of indole substituted hydrazides and hydrazines throughout the assessment of their multipotent inhibitory potency towards monoamine oxidase (MAO) A and B, semicarbazide-sensitive amine oxidase/vascular adhesion protein-1 (SSAO/VAP-1), and the cholinesterases, acetylcholinesterase (AChE) and butyrylcholinesterase (BuChE). Hydrazine **JL72** (3-(3-hydrazinylpropyl)-1H-indole) showed a potent, reversible and non-time-dependent inhibition of MAO-A, which suggests its capacity in restoring serotonergic neurotransmission being devoid of the side effects observed for classic MAO-A inhibitors. In addition, **JL72** behaved as a moderate BuChE inhibitor. Finally, both hydrazines and hydrazides derivatives showed high affinity towards SSAO/VAP-1. Among them, **JL72** behaved as a noncompetitive and the most potent inhibitor ( $IC_{50} = 0.19 \pm 0.04 \mu\text{M}$ ), possessing also a significant anti-inflammatory activity. The combined inhibition of SSAO/VAP-1, MAO (A and B), AChE and BuChE appear as an important therapeutic target to be considered in the treatment of cerebrovascular and neurological disorders such as Alzheimer's disease.

**Keywords** Hydrazine · Hydrazide · Monoamine oxidase · Vascular adhesion protein-1 · Acetylcholinesterase · Butyrylcholinesterase

## Abbreviations

Ach	Acetylcholine
AChE	Acetylcholinesterase
AChEI	Acetylcholinesterase inhibitor
AD	Alzheimer's disease
BuChE	Butyrylcholinesterase
CAA	Cerebral amyloid angiopathy
DTNB	5,5'-Dithiobis-2-nitrobenzoic acid
5-HT	5-Hydroxytryptamine
MAO	Monoamine oxidase
MAOI	Monoamine oxidase inhibitor
MTT	3-(4,5-Dimethylthiazol-2-yl)-2,5-diphenyltetrazolium bromide
MA	Methylamine
SSAO/VAP-1	Semicarbazide sensitive amine oxidase/vascular adhesion protein-1

## Introduction

Alzheimer's disease (AD) is a progressive neurodegenerative disorder of the central nervous system, associated with cognitive impairment and dementia (Goedert and Spillantini 2006).  $\beta$ -Amyloid ( $A\beta$ ) accumulation in the brain parenchyma produces senile plaques, a characteristic hallmark of AD and also produces the vascular deposits of cerebral amyloid angiopathy (CAA) (Castro et al. 2006). CAA is present in most cases of AD and it is characterised by the deposition of  $A\beta$  in the tunica media and adventitia of leptomeningeal vessels and intracortical microvessels, thus producing the degeneration of vascular smooth muscle

---

This manuscript is dedicated to the memory of Dr. Eldiberto M. Fernández-Álvarez (1928–1996).

---

G. Esteban · I. Bolea · P. Sun · M. Solé · M. Unzeta (✉)  
Departament de Bioquímica i Biologia Molecular,  
Facultat de Medicina, Universitat Autònoma de Barcelona,  
Bellaterra, 08193 Barcelona, Spain  
e-mail: mercedes.unzeta@uab.cat

A. Samadi · J. Marco-Contelles  
Laboratorio de Química Médica (IQOG, CSIC),  
C/Juan de la Cierva 3, 28006 Madrid, Spain

cells and endothelial cells (Vinters et al. 1988). The fact that AD and cerebrovascular diseases share risk factors supports the common view that there is a link between vascular degeneration and AD. It has been suggested that the accumulation of A $\beta$  in the vessel wall causes the functional deterioration of the blood brain barrier, which is essential for the correct transport and clearance of A $\beta$  from parenchyma (Deane et al. 2004; Zlokovic 2005).

Semicarbazide-sensitive amine oxidase, also called vascular adhesion protein-1 (SSAO/VAP-1, E.C 1.4.3.21) is a multifunctional enzyme involved in the metabolic deamination of primary amines, the functions of which depend on the tissue where it is expressed (Jalkanen and Salmi 2008). SSAO/VAP-1 shows some overlap with monoamine oxidase [E.C.1.4.3.4], which is responsible of the primary, secondary and tertiary amine metabolism in human brain. MAO is present in most mammalian tissues and exists as two distinct enzymatic isoforms, MAO-A and MAO-B, based on their substrate and inhibitor specificities (Johnston 1968). SSAO/VAP-1 is a circulating and membrane-bound ectoenzyme, present in vascular tissue localised in two different types of cells such as smooth muscle cells and endothelial cells being these involved in the leukocyte and neutrophil recruitment through its SSAO catalytic activity (Koskinen et al. 2004). Alterations of SSAO/VAP-1 levels in human plasma have been related to several pathological situations, such as AD (Ferrer et al. 2002) and ischaemic stroke, where abnormally high plasma VAP-1/SSAO activity has been found in patients with certain vascular and/or inflammatory conditions with bad prognosis (Hernández-Guillamon et al. 2012, 2010). In this context, the inhibition of SSAO/VAP-1 and/or MAO-A and MAO-B activities, appears as an important therapeutic target to be used in the treatment of these cerebrovascular disorders. On the other hand, low levels of acetylcholine (ACh) (Geula and Mesulam 1999) are thought to play significant roles in the pathophysiology of AD (Perry et al. 1977). The cholinergic theory of AD suggests that the selective loss of cholinergic neurons in this disorder results in a deficit of ACh in specific brain regions that mediate learning and memory functions (Davies and Maloney 1976). However, alterations in other neurotransmitter systems, especially the serotonergic and dopaminergic, are also thought to be responsible for the behavioral disturbances observed in patients with AD (García-Alloza et al. 2005; Terry et al. 2008). Thus, in addition to cholinesterase enzymes (acetylcholinesterase, AChE and butyrylcholinesterase, BuChE) and SSAO/VAP-1, monoamine oxidases also (MAO; EC 1.4.3.4) appear as an important target to be considered for the treatment of specific features of this complex and multifactorial disease.

Herein, we report the biological evaluation (MAO-A, MAO-B, SSAO/VAP-1, AChE and BuChE inhibitory

profile) of a number of indole substituted hydrazides and hydrazines. These compounds were designed and synthesized for the first time by Prof. Fernández-Álvarez's laboratory in the IQOG (CSIC, Madrid, Spain) as potential *in vitro* bovine MAO inhibitors (Alemany et al. 1966, 1975; Bernabé et al. 1971; Monge et al. 1985). In the present work, we have found that some of them and especially **JL72** (3-(3-hydrazinylpropyl)-1*H*-indole) are able to interact with human SSAO/VAP-1, MAO (A and B), as well as AChE and BuChE, showing an interesting pharmacological profile and suggesting their potential to be used in the therapy of cerebrovascular and cognitive decline disorders.

## Materials and methods

### HUVEC and HUVEC hSSAO/VAP-1 cell culture

These cell lines were prepared in our laboratory as previously described (Sole et al. 2011). Cells were cultured in M199 (Invitrogen), supplemented with 5 % FBS, 1.2 mM L-glutamine and antibiotics (50 U/ml penicillin/0.05 mg/ml streptomycin). The selected antibiotic geneticin (G418) was added at a final concentration of 100  $\mu$ g/ml to maintain the SSAO/VAP-1 expression in HUVEC hSSAO/VAP-1 cells. Cells were maintained in an incubator at 37 °C, 5 % CO<sub>2</sub>, and were subcultured every 5–7 days.

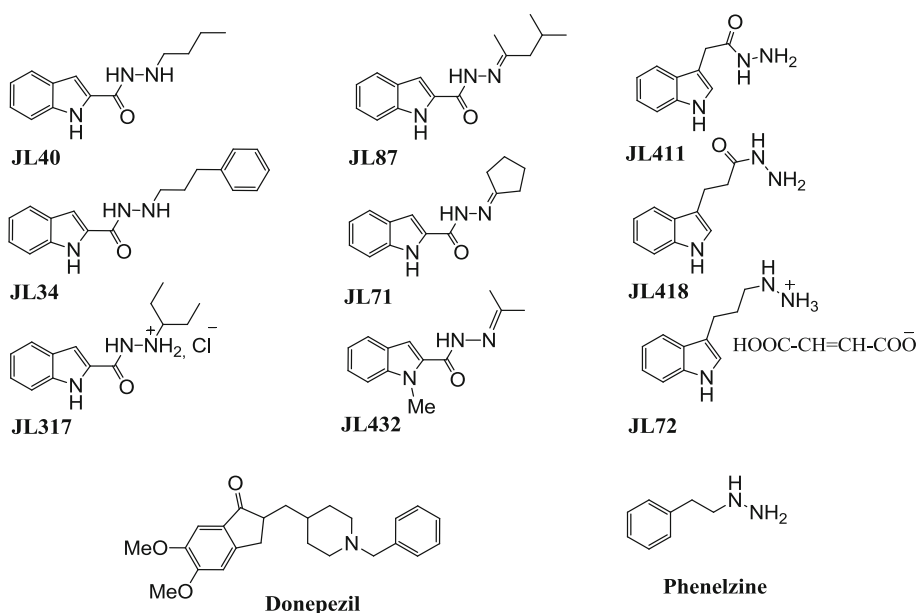
### Chemistry

The indole substituted hydrazides and hydrazines **JL34**, **JL40**, **JL71**, **JL87**, **JL317**, **JL432**, **JL72**, **JL411**, and **JL418** (Fig. 1) were synthesized and purified according to the methods described in the literature (Alemany et al. 1966, 1975; Bernabé et al. 1971; Monge et al. 1985).

### Inhibition experiments of MAO (A and B) and SSAO/VAP-1

Mitochondria from rat liver homogenates were used as source for MAO activities (Gómez et al. 1986). The inhibitory activity of the compounds towards MAO-A and MAO-B was determined as previously described (Fowler and Tipton 1981), using [<sup>14</sup>C]-labelled substrates (Perkin Elmer, USA). For comparative purposes, **phenelzine** was used as reference compound. MAO-B activity was determined towards 20  $\mu$ M [<sup>14</sup>C]-phenylethylamine (PEA) (2.5 mCi/mmol) and MAO-A activity towards [<sup>14</sup>C]-(5-hydroxy-triptamine) (5-HT) 100  $\mu$ M (0.5 mCi/mmol). SSAO/VAP-1 activity was measured towards [<sup>14</sup>C]-benzylamine 100  $\mu$ M (2 mCi/mmol) using microsomes from bovine lung as source (Lizcano et al. 1996). Inhibition

**Fig. 1** Structures of the indole substituted hydrazides and hydrazines, and the reference compounds **donepezil** and **phenelzine**



curves were made by pre-incubating the enzyme with at least nine concentrations of each compound for 30 min in 50 mM phosphate buffer (pH 7.2). A sample without compound was always present to determine the 100 % enzyme activity. The reaction was carried out at 37 °C adding 25  $\mu$ L of substrate in a final volume of 225  $\mu$ L and stopped by the addition of 100  $\mu$ L in 2 M citric acid. Radiolabelled aldehyde products were extracted into toluene/ethyl acetate (1:1, v/v) containing 0.6 % (w/v) 2,5-diphenyloxazole before liquid scintillation counting (Tri-Carb 2810TR). The inhibition curves were expressed in percentage of total activity and the  $IC_{50}$  values were calculated by using the GraphPad Prism program (Prism 3.0, GraphPad Software Inc). Total protein was measured by the method of Bradford (1976) using bovine–serum albumin as standard. Data are the mean  $\pm$  SEM of at least three different experiments realised in triplicate.

#### Inhibition experiments of AChE and BuChE

To assess the inhibitory activity of the compounds towards AChE (E.C.3.1.1.7) and BuChE (E.C.3.1.1.8), we followed a spectrophotometric method (Ellman et al. 1961), using purified AChE from *Electrophorus electricus* (Type V–S), or BuChE from equine serum (lyophilized powder) (Sigma-Aldrich, Madrid, Spain). For comparative purposes, **donepezil** was used as reference compound. The reaction took place in 96-well plates in a final volume of 300  $\mu$ L in 0.1 M phosphate-buffered solution (pH 8.0) containing 0.035 U/ml AChE or 0.05 U/ml BuChE and 0.35 mM of 5,5'-dithiobis-2-nitrobenzoic acid (DTNB, Sigma-Aldrich, Madrid, Spain). Inhibition curves were made by pre-incubating this mixture with serial dilutions of

each compound for 20 min. The activity in the absence of compounds was always performed to determine the 100 % of enzyme activity. After the mentioned pre-incubation period, 0.35 mM acetylthiocholine iodide or 0.5 mM butyrylthiocholine iodide (Sigma-Aldrich) were added, allowing five more minutes of incubation, where the DTNB produces the yellow anion 5-thio-2-nitrobenzoic acid along with the enzymatic degradation of both substrates. Changes in absorbance were detected at 405 nm in a spectrophotometric plate reader (FluoStar OPTIMA, BMG Labtech). Compounds inhibiting AChE or BuChE activity would reduce the colour generation, thus,  $IC_{50}$  values were calculated as the concentration of compound that produces 50 % AChE or BuChE activity inhibition. Data are expressed as mean  $\pm$  SEM of at least three different experiments in triplicate.

#### Reversibility and time-dependence inhibition studies

To study the nature of the MAO-A enzymatic inhibition exerted by **JL72**, the derivative with the most interesting pharmacological profile, the activity of the enzyme was determined in the presence and in the absence of the inhibitor before and after three consecutive washings with buffer. Enzyme samples were preincubated for 30 min at 37 °C with 100 nM **JL72** or 40 nM clorgyline, the latter used as control of irreversible inhibition. Samples were then washed with 50 mM phosphate buffer (pH 7.2) and centrifuged at 25,000g for 10 min at 4 °C consecutively three times. Finally, total protein was measured and MAO-A activity was determined as described above. We next evaluated the time-dependence inhibition of the reaction. Samples of enzyme plus **JL72** at the indicated concentration range ( $10^{-9}$  to

$10^{-3}$  M), were preincubated for 0, 30, 60, 120, and 180 min before MAO-A activity determination as described above.

#### Kinetic analysis of MAO-A and SSAO/VAP-1 inhibition

To obtain estimates of the mechanism of action of **JL72** on MAO-A and SSAO/VAP-1, reciprocal plots of  $1/V$  versus  $1/[S]$  were constructed at different concentration of the substrate 5-HT (10–500  $\mu\text{M}$ ) for MAO-A and benzylamine (10–200  $\mu\text{M}$ ) for SSAO/VAP-1, as previously described (Fowler and Tipton 1981). The plots were assessed by a weighted least-squares analysis. Data analysis was performed with GraphPad Prism 3.0 software. Slopes of the reciprocal plots were then plotted against the concentration of **JL72** (0–1  $\mu\text{M}$  for SSAO and 50–500  $\mu\text{M}$  for MAO-A) to evaluate  $K_i$  data.

#### Leukocyte (THP-1)-endothelial (HUVEC) cell adhesion assay

HUVEC and HUVEC transfected hSSAO/VAP-1 monolayers were prepared, as previously reported (Sole et al. 2011). For leukocyte adhesion assays, cells were pre-treated with **JL72** or **phenelzine** at 10  $\mu\text{M}$  for 1 h. Then, 1 mM methylamine (MA), a SSAO/VAP-1 specific substrate, was added to the media for the next 24 h. At the end of the treatment, calcein/AM-dyed THP-1 cells were added to the HUVEC monolayer, and were allowed to bind to the endothelial cells for 30 min at 37 °C. After this period, plates were successively washed in order to discard non-bound THP-1 cells. Leukocyte-binding ability was determined by the emitted fluorescence of bound THP-1 cells, measured at ex/em 495/530 nm. Non-treated cells were used as control.

## Results and discussion

### MAO-A, MAO-B and SSAO enzymatic inhibition

The indole substituted hydrazines and hydrazides were first evaluated as inhibitors of MAO-A and MAO-B (from rat liver mitochondria), and SSAO (from bovine lung microsomes). Values were compared with the inhibition exerted by the reference compound **phenelzine** (Table 1). Although compounds **JL87**, **JL71**, **JL432**, **JL411**, **JL418** were not active for MAO-A, compounds **JL40**, **JL34**, **JL317** showed a significant MAO-A inhibitory profile, acting in the micromolar range ( $IC_{50} = 3.3 \pm 0.9$  to  $80.3 \pm 14.7 \mu\text{M}$ ) (Table 1). Interestingly, **JL72** showed the highest potency ( $IC_{50} = 0.12 \pm 0.03 \mu\text{M}$ ) and gave a similar value than that observed for the reference

compound **phenelzine** ( $IC_{50} = 0.13 \pm 0.02 \mu\text{M}$ ). Interestingly, we observed that only compounds **JL40** and **JL317** were able to interact with both MAO-A and MAO-B enzymes. Conversely, all analysed compounds showed high affinity towards SSAO/VAP-1 enzyme, showing  $IC_{50}$  values ranging from  $0.19 \pm 0.04 \mu\text{M}$  for **JL72** to  $79.2 \pm 10.5 \mu\text{M}$  for **JL40**.

From the structure–activity relationship (SAR) study some conclusions can be drawn. First of all, and comparing compounds bearing a substituent at the indole C2 position, it is clear that the *N'*-alkylidene-1*H*-indole-2-carbohydrazides **JL87**, **JL71**, and **JL432** are very weak towards MAO-A, but moderate towards MAO-B inhibitors, while the *N'*-alkyl-1*H*-indole-2-carbohydrazides **JL34** and **JL317** are moderate and selective MAO-A inhibitors. Also note that the substitution of a methyl by a phenyl group in **JL40** to render **JL34** increases the inhibitory effect on MAO-A, but strongly drops its inhibitory potency on MAO-B. Comparing with compounds bearing substituents at C3 position of the indole ring, such as **JL411** and **JL418** the presence of the carbonyl group loses the inhibitory activity drastically in both MAO-A and MAO-B isoforms. On the other hand, **JL72** is the only compound that does not have carbonyl group in its molecule. This could be the structural feature responsible for the facilitation of the interaction with the active centre showing its high inhibitory potency towards MAO-A and MAO-B comparing with the rest of molecules. It is worth to remark the high selectivity of **JL72** towards MAO-A, comparing with MAO-B.

Concerning the effects on SSAO inhibition, very surprisingly, the presence of such substituents on the C2 and C3 position does not affect the inhibitory activity of these compounds. Among them, the most potent are **JL34**, **JL411**, **JL418** and **JL72**, the more active being 3-(3-hydrazinylpropyl)-1*H*-indole (**JL72**). It is worth to remark that the presence of the indole ring in all these hydrazine analogs can induce the inhibitory interaction towards MAO-A because of the similarity towards serotonin, its specific substrate. Furthermore, they could act as potential pharmacological agents stimulating the monoaminergic and catecholaminergic transmission, showing the **JL72** the highest affinity towards MAO-A inhibition. The potency of **JL72** as SSAO inhibitor, suggests that this compound may also possess a good anti-inflammatory profile.

### AChE and BuChE inhibition

To complete the study of the biological profile of the indole substituted hydrazides and hydrazines, the inhibitory activity against AChE (from *Electrophorus electricus*, EeAChE) and BuChE (from equine serum, eqBuChE) was determined by using Ellmans method (Ellman et al. 1961) and compared with that of the reference compound

**Table 1** *Ee*AChE, *eq*BuChE, rMAO-A, rMAO-B and bSSAO/VAP-1 Inhibitory activities of indole substituted hydrazides and hydrazines **JL34**, **JL40**, **JL71**, **JL87**, **JL317**, **JL432**, **JL72**, **JL411**, and **JL418**

Compound	IC <sub>50</sub> (μM) <sup>a</sup>				
	rMAO-A	rMAO-B	bSSAO/VAP-1	<i>Ee</i> AChE	<i>eq</i> BuChE
<b>JL40</b>	80.3 ± 14.7	5.0	79.2 ± 10.5	>100	>100
<b>JL34</b>	3.3 ± 0.9	>100	10.6 ± 0.4	86.4 ± 15.8	>100
<b>JL317</b>	5.5 ± 1.5	33.2	45.8 ± 4.3	>100	16.1 ± 1.1
<b>JL87</b>	>100	47.1	31.6 ± 8.1	>100	>100
<b>JL71</b>	>100	84.0	29.7 ± 8.5	>100	49.2 ± 11.3
<b>JL432</b>	>100	54.3	37.2 ± 5.5	>100	>100
<b>JL411</b>	>100	>100	13.3 ± 2.9	>100	>100
<b>JL418</b>	>100	>100	17.2 ± 4.2	>100	>100
<b>JL72</b>	0.12 ± 0.03	>100	0.19 ± 0.04	46.3 ± 2.9	25.3 ± 6.5
<b>Phenelzine</b>	0.13 ± 0.02	2.3 ± 0.41	0.011 ± 0.002	>100	>100
<b>Donepezil</b>	>100	>100	–	0.022 ± 0.003	3.6 ± 0.53

<sup>a</sup> Values are expressed as the mean ± SEM of at least three independent experiments performed in triplicate

**donepezil**. The obtained IC<sub>50</sub> values are summarised in Table 1. According to these values, the derivatives are poor inhibitors of *Ee*AChE, with the exception of **JL34** and **JL72** that showed activity in the micromolar range (IC<sub>50</sub> = 86.4 ± 15.8 μM and 46.3 ± 2.9 μM, respectively). Nevertheless, these values are very far from the IC<sub>50</sub> value determined for **donepezil** (Table 1), one of the most potent AChE inhibitors used in AD therapy. Similar trends were observed when the inhibitory potency was determined towards *eq*BuChE. In this case, only compounds **JL317**, **JL71** and **JL72** proved to be active in the micromolar range showing IC<sub>50</sub> from 16.1 ± 1.0 μM to 49.2 ± 11.3 μM, being the most potent 3-(3-hydrazinylpropyl)-1*H*-indole (**JL 317**), almost equipotent with **donepezil**. Note that, whereas compounds **JL317** and **JL71** are selective towards *eq*BuChE, **JL72** is almost equipotent for both enzymes.

Concerning the SAR study, the best inhibitor for both enzymes (*Ee*AChE and *eq*BuChE) is the indole hydrazine **JL72**, bearing the substituent at C3 position on the indole ring. Taking all these results into account, **JL72** (3-(3-hydrazinylpropyl)) was selected as the most interesting compound to follow up with its biological evaluation as an indole-2-carbohydrazone able to interact with five different enzymatic systems, all of them involved in Alzheimer's disease pathology.

#### Reversibility and time-dependence inhibition

To study the type of inhibition of **JL72**, the most potent inhibitor of the series, towards MAO-A, we analysed the reversibility/irreversibility of the binding. We observed that **JL72** reversibly inhibited MAO-A, since the inhibition was significantly reverted (from 34.1 to 19.1 %) after three

consecutive washings and centrifugations with buffer (Fig. 2a). Clorgyline was used under the same experimental conditions for comparative purposes and, in agreement with data reported in literature, behaves as an irreversible inhibitor. The reversibility of MAO-A inhibition by **JL72** was also confirmed by the time-dependent inhibition analysis (Fig. 2b), where identical inhibition was observed in spite of the different periods of incubation-time (0–180 min). The observed slight shift of the curve from zero time could be explained by the small delay in adding the substrate. This was considered not significant, since the time-independent inhibition was confirmed by finding similar inhibitory behavior at the other analysed times. Thus, these results allowed us to conclude that **JL72** behaves as a reversible and non time-dependent inhibitor of MAO-A.

In this regard, and because of the structural similarity with serotonin, a specific MAO-A substrate, **JL72** can be considered a potent inhibitor of this MAO isoform with potential benefit in restoring and enhancing the serotonergic transmission altered in depression and other psychological disorders.

#### Kinetic analysis of SSAO and MAO-A

To gain further insight into the kinetic behavior of this family of compounds on SSAO and MAO-A, a kinetic study was carried out with **JL72**, the most promising compound investigated. Graphical analysis of the reciprocal to Lineweaver–Burk plots (Fig. 3), showed increased slopes (decreased  $V_{\max}$ ) and constant  $K_m$  values in both enzymes analysed, indicating that **JL72** behaves as a noncompetitive inhibitor and thus it binds to a different site from the active site in both MAO-A and SSAO enzymes.

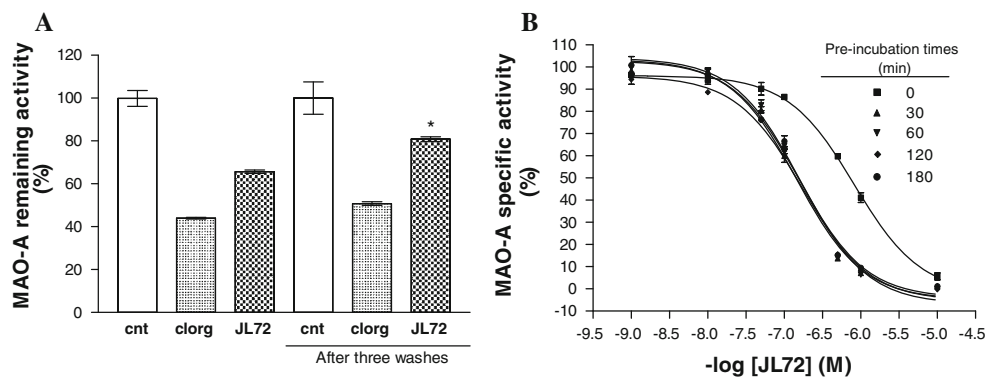


**Fig. 2** Reversibility studies of MAO-A inhibition by **JL72**. **a** MAO-A was inhibited at 100 nM **JL72** and 40 nM clorgyline for 30 min. Then, three consecutive washings were performed with buffer. **b** Time-dependence inhibition was studied at several times of pre-

incubation (0–180 min) of MAO-A with **JL72**. Data are the mean  $\pm$  SEM of four independent experiments in triplicate. \* $p < 0.05$  versus non-washed

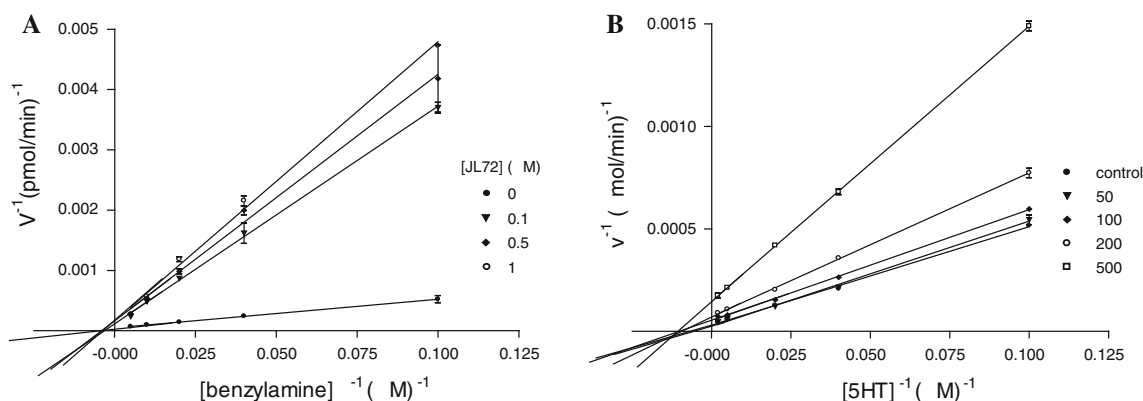


**Fig. 3** Kinetic behavior of SSAA and MAO-A inhibition by **JL72**. **a** Double reciprocal plots (Lineweaver–Burk transformation) of SSAA inhibition by **JL72** towards (10–200  $\mu$ M). **b** Double reciprocal

plots (Lineweaver–Burk transformation) of MAO-A inhibition by **JL72** towards 5-HT as a substrate (10–500  $\mu$ M). Data are the mean  $\pm$  SEM of three different experiments

Replots of the slope versus concentration of **JL72**, gave an estimate of the inhibition constant  $K_i$  towards MAO-A of  $163.2 \pm 12.1$  and  $60.8 \pm 12.5$  nM towards SSAA. These results confirm the high inhibitory potency of **JL72** towards both MAO-A and SSAA.

#### Inhibition of SSAA activity in HUVEC hSSAA/VAP-1 cells by **JL72** and phenelzine

The toxicity of **JL72** and **phenelzine** on HUVEC transfected hSSAA/VAP-1 cells was assessed as a previous step to determine their inhibitory behavior. Thus, the viability of cells treated with **JL72** and **phenelzine** at concentration range of (0.1–100  $\mu$ M) was analysed after 30-min pre-incubation by the MTT method (Mosmann 1983). **Phenelzine** did not affect cell viability at all concentrations assayed, whereas 10  $\mu$ M **JL72** induced a loss of cell viability of the 20 %. Thus, the concentrations used were always lower than 10  $\mu$ M. Then, in order to determine the enzymatic inhibition of hSSAA/VAP-1 expressed in

HUVEC cells, treatments with **JL72** and **phenelzine** at concentrations of 0.1, 1 and 10  $\mu$ M for 30 min were carried out. SSAA/VAP-1 activity was determined in cell lysates radiometrically as previously stated in “**Materials and methods**”, and expressed as percentage activity compared to non-treated cells. A complete inhibitory effect was observed at concentrations higher than 1  $\mu$ M in both cases (Fig. 4), showing that both compounds behave as potent SSAA inhibitors on HUVEC human transfected hSSAA/VAP-1 cells model.

#### Leukocyte (THP-1)-endothelial (HUVEC) cell adhesion assay

Concerning cerebrovascular diseases, where the inflammation is one of the most significant factors involved, finding a molecule capable of inhibiting leukocyte adhesion to the endothelial wall has an important therapeutic value. The high inhibitory potency of **JL72** towards SSAA enzymatic activity ( $IC_{50} = 0.19 \pm 0.04$  nM) led us to

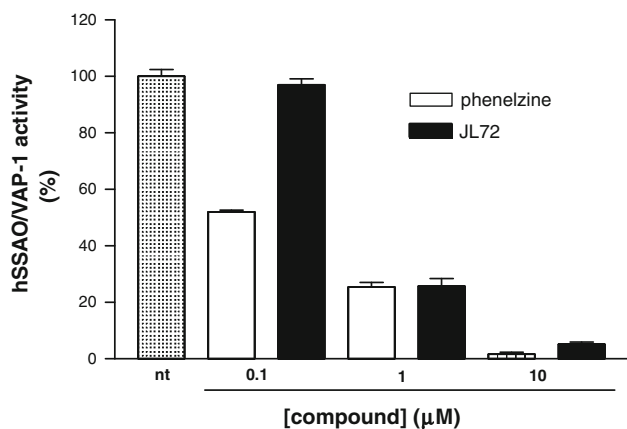


**Fig. 4** HUVEC hSSAO/VAP-1 lysates were treated with **JL72** and **phenelzine** (0.1, 1 and 10 μM) for 30 min. SSAO activity was radiometrically measured and expressed as percentage activity compared to non-treated cells. Data are the mean ± SEM of three independent experiments

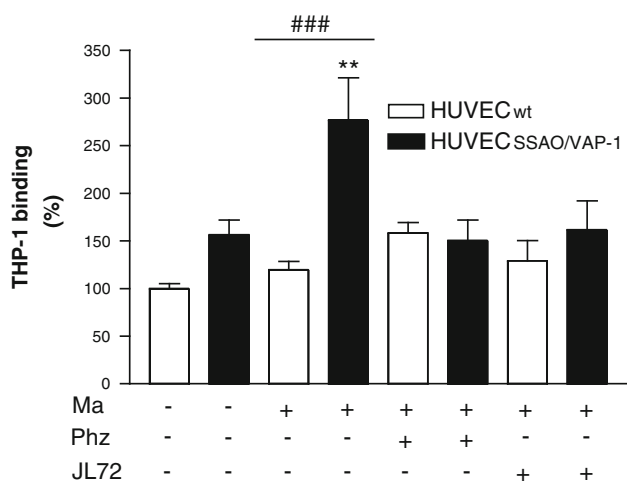


**Fig. 5** Leukocyte (THP-1)-endothelial (HUVEC) cell adhesion assay. Higher THP-1 adhesion was observed in hSSAO/VAP-1 cells treated with MA compared to WT cells. As shown in the figure, both **phenelzine** and **JL72** significantly reduced THP-1 adhesion after MA addition in hSSAO/VAP-1 cells. Data are the mean ± SEM of five independent experiments \*\* $p < 0.01$  compared to non-treated hSSAO/VAP-1 cells, and ### $p < 0.001$  versus non-treated cells

consider whether this molecule can possess a potential anti-inflammatory effect. Consequently, endothelial HUVEC wild type cells, that do not express SSAO/VAP-1, and transfected hSSAO/VAP-1 cells were cultured as described in “Materials and methods”. When cells were treated with methylamine (MA), a specific substrate of SSAO/VAP-1, the adhesion of leukocytes significantly increased when compared with the HUVEC wild type cells. One of the functions of this multifunctional enzyme through its catalytic action is to mediate the leukocyte-adhesion in inflammatory processes (Salmi et al. 1993). As expected, this effect disappears when transfected cells were

pre-treated with **JL72** or **Phenelzine**, confirming the anti-inflammatory effect of these drugs on inhibiting the SSAO/VAP-1 activity (Fig. 5).

## Conclusion

To sum up, some of the hydrazides and hydrazines studied here show a wide enzymatic inhibitory profile towards the two MAO isoforms, SSAO/VAP-1 and both AChE and BuChE, all them involved in Alzheimer’s disease pathology. Among them, **JL34**, **JL317**, and **JL72**, are good and selective MAO-A inhibitors, thus possible modulators of the monoaminergic neurotransmission. In this regard, these molecules could act as potential antidepressant, and behavior enhancers, especially **JL72** a highly potent and selective MAO-A inhibitor. Then, **JL72**, may be able to stimulate the serotonergic, catecholaminergic and noradrenergic transmission. Some other derivatives, such as **JL34**, **JL411**, **JL418**, and **JL72** were potent and selective inhibitors of SSAO/VAP-1. The involvement of this multifunctional enzyme in different pathologies, especially regarding Alzheimer and stroke (Ferrer et al. 2002; Hernandez-Guillamon et al. 2010, 2012), suggest that inhibitors of this enzyme can be a good therapeutic approach to solve these neurological disorders. Furthermore, the fact that **JL72** is able to block the leukocytes adhesion in human endothelial cells, transfected with human SSAO/VAP-1, confers to this molecule an additional anti-inflammatory profile. On the other hand, **JL317**, **JL71** and **JL72** were moderate and selective BuChE inhibitors. Only the hydrazine **JL72** showed a moderate non selective AChE inhibitory behavior. According to the Cholinergic hypothesis of Alzheimer’s disease (Geula and Mesulam 1999), the cholinergic transmission is affected in this disorder. The IC<sub>50</sub> values of **JL72**, herein, reported show that this compound could be able to restore cholinergic transmission by inhibiting AChE and at the same time to inhibit BuChE present in glia and both involved in Alzheimer’s pathology. Recently it has been reported that the hydrazine type **phenelzine**, besides its antidepressant profile, it has a neuroprotective effect on neurons and astrocytes against formaldehyde-induced toxicity (Song et al. 2010). On the other hand **phenelzine** provided robust neuroprotection in the gerbil model of transient forebrain ischaemia (Wood et al. 2006).

Herein, we report a new hydrazine, **JL72**, that behaves as a multitarget ligand able to modulate monoaminergic transmission and besides showing an anti-inflammatory profile, both pathways known to be altered in neurological disorders. Further experimental work should be done to definitively confirm the neuroprotective effect of this novel hydrazine, **JL72**. The interesting pharmacological profile

of **JL72**, together with the observation of a significant anti-inflammatory activity, suggests that **JL72** is a promising lead compound for further development of drugs to be used in the therapy of cerebrovascular and neurological diseases.

**Acknowledgments** A. Samadi thanks the CSIC for I3P post-doctoral contract, J. Marco-Contelles and M. Unzeta thank the MICIN for grants: SAF2006-08764-C02-01, SAF2009-07271, SAF2012-33304, and (COST, EU) Action CM-1103 for support.

## References

- Alemay A, Bernabé M, Elorriaga C, Fernández-Alvarez E, Lora-Tamayo M, Nieto O (1966) Potential psychotropic agents. I. Synthesis of 1-(2-indolylcarbonyl)-2-alkylhydrazines, 1-(3-indolylcarbonyl)-2-alkylhydrazines and 1-(3-indolylacetyl)-2-alkylhydrazines, and measurement, in vitro, of their monoamine oxidase inhibitory activity. *Bull Soc Chim Fr* 8:2486–2497
- Alemay A, Fernández-Álvarez E, Hernández-Sánchez M (1975) Enzyme inhibitors. X. Preparation and in vitro study of N2-substituted 2-(N-methylindolyl) and 2-(N-benzylindolyl) carbonylhydrazides as monoamine oxidase inhibitors. *An Quím* 71:406–411
- Bernabé M, Fernández-Álvarez E, Lora-Tamayo M, Nieto O (1971) Potential psychotropic drugs. V. Monoamine oxidase inhibitors. Preparation and study of some indolyl-3 alkyl-hydrazines. *Bull Soc Chim Fr* 5:1882–1887
- Bradford MM (1976) A rapid and sensitive method for the quantitation of microgram quantities of protein utilizing the principle of protein-dye binding. *Anal Biochem* 72:248–254
- Castro A, Martínez A (2006) Targeting beta-amyloid pathogenesis through acetylcholinesterase inhibitors. *Curr Pharm Des* 12:4377–4387
- Davies P, Maloney AJ (1976) Selective loss of central cholinergic neurons in Alzheimer's disease. *Lancet* 2:1403
- Deane R, Wu Z, Sagare A, Davis J, Du YS, Hamm K, Xu F, Parisi M, LaRue B, Hu HW, Spijkers P, Guo H, Song X, Lenting PJ, Van Nostrand WE, Zlokovic BV (2004) LRP/amyloid beta-peptide interaction mediates differential brain efflux of Abeta isoforms. *Neuron* 43:333–344
- Ellman GL, Courtney KD, Andres V Jr, Feather-Stone RM (1961) A new and rapid colorimetric determination of acetylcholinesterase activity. *Biochem Pharmacol* 7:88–95
- Ferrer I, Lizcano JM, Hernández M, Unzeta M (2002) Overexpression of semicarbazide sensitive amine oxidase in the cerebral blood vessels in patients with Alzheimer's disease and cerebral autosomal dominant arteriopathy with subcortical infarcts and leukoencephalopathy. *Neurosci Lett* 321:21–24
- Fowler CJ, Tipton KF (1981) Concentration dependence of the oxidation of tyramine by the two forms of rat liver mitochondrial monoamine oxidase. *Biochem Pharmacol* 30:3329–3332
- García-Alloza M, Gil-Bea FJ, Díez-Ariza M, Chen CP, Francis PT, Lasheras B, Ramirez MJ (2005) Cholinergic-serotonergic imbalance contributes to cognitive and behavioral symptoms in Alzheimer's disease. *Neuropsychologia* 43:442–449
- Geula C, Mesulam MM (1999) Cholinergic systems in Alzheimer's disease. In: Terry RD, Katzman R, Bick K, Sisodia SS (eds) *Alzheimer disease*, 2nd edn. Lippincott Williams & Wilkins, Philadelphia, PA, pp 69–292
- Goedert M, Spillantini MG (2006) A century of Alzheimer's disease. *Science* 314:777–781
- Gomez N, Unzeta M, Tipton KF, Anderson MC, O'Carroll AM (1986) Determination of monoamine oxidase concentrations in rat liver by inhibitor binding. *Biochem Pharmacol* 35:4467–4472
- Hernandez-Guillamon M, García-Bonilla L, Solé M, Sosti V, Parés M, Campos M, Ortega-Aznar A, Domínguez C, Rubiera M, Ribó M, Quintana M, Molina CA, Alvarez-Sabín J, Rosell A, Unzeta M, Montaner J (2010) Plasma VAP-1/SSAO activity predicts intracranial hemorrhages and adverse neurological outcome after tissue plasminogen activator treatment in stroke. *Stroke* 41:1528–1535
- Hernandez-Guillamon M, Solé M, Delgado P, García-Bonilla L, Giralt D, Boada C, Penalba A, García S, Flores A, Ribó M, Alvarez-Sabín J, Ortega-Aznar A, Unzeta M, Montaner J (2012) VAP-1/SSAO plasma activity and brain expression in human hemorrhagic stroke. *Cerebrovasc Dis* 33:55–63
- Jalkanen S, Salmi M (2008) VAP-1 and CD73, endothelial cell surface enzymes in leukocyte extravasation. *Arterioscler Thromb Vasc Biol* 28:18–26
- Johnston JP (1968) Some observations upon a new inhibitor of monoamine oxidase in brain tissue. *Biochem Pharmacol* 17:1285–1297
- Koskinen K, Vainio PJ, Smith DJ, Pihlavisto M, Ylä-Herttuala S, Jalkanen S, Salmi M (2004) Granulocyte transmigration through the endothelium is regulated by the oxidase activity of vascular adhesion protein-1 (VAP-1). *Blood* 103:3388–3395
- Lizcano JM, Fernández de Arriba A, Tipton KF, Unzeta M (1996) Inhibition of bovine lung semicarbazide-sensitive amine oxidase (SSAO) by some hydrazine derivatives. *Biochem Pharmacol* 52:187–195
- Monge A, Palop JA, Goni T, Martínez A, Fernández-Alvarez E (1985) About the synthesis of (1,2) diazepinoindole derivatives from ethyl 2-(1-methylindole)acetate, 2-indole- and 3-indoleacetohydrazones. *J Heterocyclic Chem* 22:1445–1451
- Mosmann T (1983) Rapid colorimetric assay for cellular growth and survival: application to proliferation and cytotoxicity assays. *J Immunol Methods* 65:55–63
- Perry EK, Gibson PH, Blessed G, Perry RH, Tomlinson BE (1977) Neurotransmitter enzyme abnormalities in senile dementia. Choline acetyltransferase and glutamic acid decarboxylase activities in necropsy brain tissue. *J Neurol Sci* 34:247–265
- Salmi M, Kalimo K, Jalkanen S (1993) Induction and function of vascular adhesion protein-1 at sites of inflammation. *J Exp Med* 178:2255–2260
- Solé M, Unzeta M (2011) Vascular cell lines expressing SSAO/VAP-1: a new experimental tool to study its involvement in vascular diseases. *Biol Cell* 103:543–557
- Song MS, Baker GB, Dursun SM, Todd KG (2010) The antidepressant phenelzine protects neurons and astrocytes against formaldehyde-induced toxicity. *J Neurochem* 114:1405–1413
- Terry AV Jr, Buccafusco JJ, Wilson C (2008) Cognitive dysfunction in neuropsychiatric disorders: selected serotonin receptor subtypes as therapeutic targets. *Behav Brain Res* 195:30–38
- Vinters HV, Pardridge WM, Secor DL, Ishii N (1988) Immunohistochemical study of cerebral amyloid angiopathy. II. Enhancement of immunostaining using formic acid pretreatment of tissue sections. *Am J Pathol* 133:150–162
- Wood PL, Khan MA, Moskal JR, Todd KG, Tanay VA, Baker G (2006) Aldehyde load in ischemia-reperfusion brain injury: neuroprotection by neutralization of reactive aldehydes with phenelzine. *Brain Res* 1122:184–190
- Zlokovic BV (2005) Neurovascular mechanisms of Alzheimer's neurodegeneration. *Trends Neurosci* 28:202–208

### **Annex III**

“Catecholaminergic and cholinergic systems of mouse brain are modulated by LMN diet, rich in theobromine, polyphenols and polyunsaturated fatty acids”.





Cite this: DOI: 10.1039/c5fo00052a

## Catecholaminergic and cholinergic systems of mouse brain are modulated by LMN diet, rich in theobromine, polyphenols and polyunsaturated fatty acids

Laura Fernández-Fernández,<sup>†a</sup> Gerard Esteban,<sup>†a</sup> Mercedes Giralt,<sup>b</sup> Tony Valente,<sup>a,c</sup> Irene Bolea,<sup>a</sup> Montse Solé,<sup>a</sup> Ping Sun,<sup>a</sup> Susana Benítez,<sup>a</sup> José Ramón Morelló,<sup>d</sup> Jordi Reguant,<sup>d</sup> Bartolomé Ramírez,<sup>d</sup> Juan Hidalgo<sup>b</sup> and Mercedes Unzeta<sup>\*a</sup>

The possible modulatory effect of the functional LMN diet, rich in theobromine, polyphenols and polyunsaturated fatty acids, on the catecholaminergic and cholinergic neurotransmission, affecting cognition decline during aging has been studied. 129S1/SvImJ mice were fed for 10, 20, 30 and 40 days with either LMN or control diets. The enzymes involved in catecholaminergic and cholinergic metabolism were determined by both immunohistological and western blot analyses. Noradrenalin, dopamine and other metabolites were quantified by HPLC analysis. Theobromine, present in cocoa, the main LMN diet component, was analysed in parallel using SH-SY5Y and PC12 cell lines. An enhanced modulatory effect on both cholinergic and catecholaminergic transmissions was observed on 20 day fed mice. Similar effect was observed with theobromine, besides its antioxidant capacity inducing SOD-1 and GPx expression. The enhancing effect of the LMN diet and theobromine on the levels of acetylcholine-related enzymes, dopamine and specially noradrenalin confirms the beneficial role of this diet on the "cognitive reserve" and hence a possible reducing effect on cognitive decline underlying aging and Alzheimer's disease.

Received 14th January 2015,  
Accepted 25th February 2015

DOI: 10.1039/c5fo00052a

www.rsc.org/foodfunction

### Introduction

Aging is a highly complex process that can affect multiple organs and induce changes that will disturb the correct functioning of the organism over time, leading to different pathologies.<sup>1</sup> In this respect, neurological disorders such as Alzheimer's disease (AD), are deeply related to the aging process<sup>2,3</sup> and research in this area is becoming promising especially regarding the implications for both public health and social policies.

AD is a progressive neurodegenerative disorder characterized by memory loss and cognitive impairment. AD is a multi-

factorial disease in which oxidative stress, mitochondrial dysfunction, inflammation, metal dyshomeostasis, accumulation of miss-folded proteins, deficit of cholinergic transmission or apoptosis, among others play an important role.<sup>4,5</sup>

AD histological hallmarks such as the deposition of  $\beta$ -amyloid protein or the neurofibrillary tangle formation have been widely reported.<sup>6,7</sup> However, the correlation between the biological measurement of the pathology markers that are shown in the brain at middle age and the real loss of cognitive function that appears at advanced life stages has not yet been found. This gap between symptoms and pathology has been explained by the "cognitive reserve" theory, in which a set of variables such as education, training, intelligence or mental stimulation allow the brain to adapt or mask the pathology, maintaining the cognition in spite of the neuronal loss. It has been hypothesised that these key elements of "cognitive reserve" normalize the otherwise declining noradrenergic system during aging, and therefore the optimization of noradrenergic activity may reduce the risk of AD.<sup>8</sup>

The complexity of AD is corroborated by the fact that currently no drug is able to prevent this neurodegenerative process. To date, only five drugs have been approved by the Food and Drug Administration to enhance cholinergic trans-

<sup>a</sup>Institute of Neurosciences, and Department of Biochemistry and Molecular Biology, Faculty of Medicine, Universitat Autònoma de Barcelona, Bellaterra, Barcelona, Spain. E-mail: Mercedes.unzeta@uab.es; Fax: +34 93 581 3861; Tel: +34 93 581 1624

<sup>b</sup>Institute of Neurosciences, and Department of Cellular Biology, Physiology and Immunology, Faculty of Biosciences, Universitat Autònoma de Barcelona, Bellaterra, Barcelona, Spain

<sup>c</sup>Biomedical Research Institute of Barcelona (IIBB), Spanish National Research Council (CSIC), Institut d'Investigacions Biomèdiques August Pi i Sunyer (IDIBAPS), Department of Brain Ischemia and Neurodegeneration, Barcelona, Spain

<sup>d</sup>La Morella Nuts SA, Reus, Tarragona, Spain

<sup>†</sup>Both authors contributed equally.

mission related to cognitive deficits associated with AD,<sup>9</sup> leaving a vast majority of other potential AD targets nearly unaffected by current therapies.

Diet has been extensively reported to play an important role in cognition<sup>10</sup> and at present, there is mounting evidence that certain components of diet intake, especially those exhibiting antioxidant properties, could be beneficial for preventing and delaying neurodegenerative disorders such as AD.<sup>11,12</sup> Fish, vitamins and methionine-rich proteins have been identified to confer protection against AD.<sup>13</sup>

In this regard, polyphenolic compounds present in dry fruits, nuts and almonds, wine, tea, berry fruits, cocoa and fish oils, have shown anti-aging and neuroprotective effects.<sup>14</sup> All of them are potent antioxidant agents that could be useful as a nutritional approach against the oxidative stress and inflammation associated with AD.<sup>15</sup> Therefore, diet supplementation may offer an alternative or supplementary therapy to the use of acetylcholinesterase inhibitors.

It has been previously reported that LMN cream intake, [Patent ref WO2007063158 A2], based on cocoa, hazelnuts, polyphenols, vegetable oils rich in polyunsaturated fatty acids and flours rich in soluble fiber, is able to reduce the cardiovascular risk factors that are underlying AD.<sup>16</sup> Moreover, the LMN diet has been described as an inductor of neurogenesis in the adult mouse brain by promoting the proliferation and differentiation of neuronal cells in both the olfactory bulb and the hippocampus, being the latest one of the most highly affected brain regions in AD.<sup>17</sup>

Besides, the LMN diet is able to decrease the behavioural deterioration caused by aging in both wild type and in Tg2576 mice and diminish the A $\beta$  plaque formation. LMN also reduces the A $\beta$  (1–40 and 1–42) plasma levels in adult mice.<sup>18</sup> Taking all these results into account, the increasing importance of polyphenols as human dietary supplements playing a potential role in ameliorating the cognitive impairment during aging and neurological disorders is corroborated.

The objective of the present work was to evaluate the possible modulatory effect of the LMN diet on both cholinergic and catecholaminergic systems in 129S1/SvImJ mice fed for 10, 20, 30 and 40 days by immunodetection and high-performance liquid chromatography (HPLC) approaches.

## Results

### AChE and ChAT immunohistochemical analysis in the striatum of LMN fed mice

The effect of the LMN diet on AChE and ChAT as the main enzymes involved in acetylcholine (ACh) metabolism has been studied since ACh is a depleted neurotransmitter in AD. Fig. 1 shows representative immunohistochemistry images for AChE and ChAT in basal ganglia (striatum) of 4-month old 129S1/SvImJ mice fed with the LMN diet for 10, 20, 30 and 40 days. The LMN diet induced a decrease of the AChE levels immunostaining in the striatum at early times, which was significantly different at 20 day feeding. However, AChE levels were reestab-

lished at longer times. In contrast, ChAT levels showed an opposite pattern, being increased at 20 days and returning to normal values afterwards.

### Immunohistochemical quantification of TH expression in basal ganglia of LMN fed mice

The effect of the diet on the TH expression, as a key enzyme in the synthetic pathways of catecholamines DA and NA was analysed. TH expression was determined in the catecholaminergic circuits of both striatum and substantia nigra as shown in Fig. 2. The corresponding quantification of the immunofluorescence signal showed a significant increase of TH expression in the catecholaminergic fibers of the striatum at 20 and 30 day feeding. In the substantia nigra, a progressive increase of the TH expression was observed in the neurons and fibers of catecholaminergic circuits. It was significant at 30 and 40 day feeding. The different periods of time observed on the expression of TH in the striatum and substantia nigra could be explained by the fact that different components of the LMN diet are probably not processed by the gastro-intestinal track with the same efficacy and furthermore, they can cross the blood–brain barrier with different accessibilities and hence to reach the selected cerebral locations at different rates.<sup>19</sup>

### LMN cream modulates COMT expression in the hippocampus

The expression of Catechol-O-Methyl Transferase (COMT) was analysed in the hippocampus of 129S1/SvImJ mice fed with the LMN diet for 10, 20, 30 and 40 days. This brain region is involved in memory and learning processes and it is severely affected in AD. As shown in Fig. 3, the highest COMT expression was observed at 20 days while it progressively decreased at longer times.

### HPLC analysis of the catecholaminergic neurotransmitters DA and NA in the striatum

The levels of DA, NA, their metabolites DOPAC and HVA, and 5HIAA were determined by HPLC in basal nuclei of 4-month old mice fed with the LMN diet for 10, 20, 30 or 40 days. Fig. 4 shows an increase in the levels of DA and NA at 20 day feeding. In the case of their metabolites DOPAC and HVA, the same trend was observed. However, no effect on the levels of the serotonin metabolite 5-HIAA was detected.

### Theobromine, the main component of the LMN cream shows similar antioxidant effects on SH-SY5Y cells

It was also analyzed the antioxidant effect of theobromine (TBr) and compared to that of LMN cream. Theobromine is present in cocoa, the main component of LMN cream. Fig. 5a shows a similar protective effect of both the LMN cream and TBr on SH-SY5Y cells lesioned with 150  $\mu$ M H<sub>2</sub>O<sub>2</sub> for 24 h. Protection was observed in all doses, the highest effect being detected with 10  $\mu$ g ml<sup>-1</sup> LMN cream. An increase in the protein levels of the antioxidant enzymes Superoxide Dismutase-1 (SOD-1) (Fig. 5b) and Glutathione Peroxidase (GPx) (Fig. 5c) was observed after TBr and LMN cream treatment without H<sub>2</sub>O<sub>2</sub> addition.

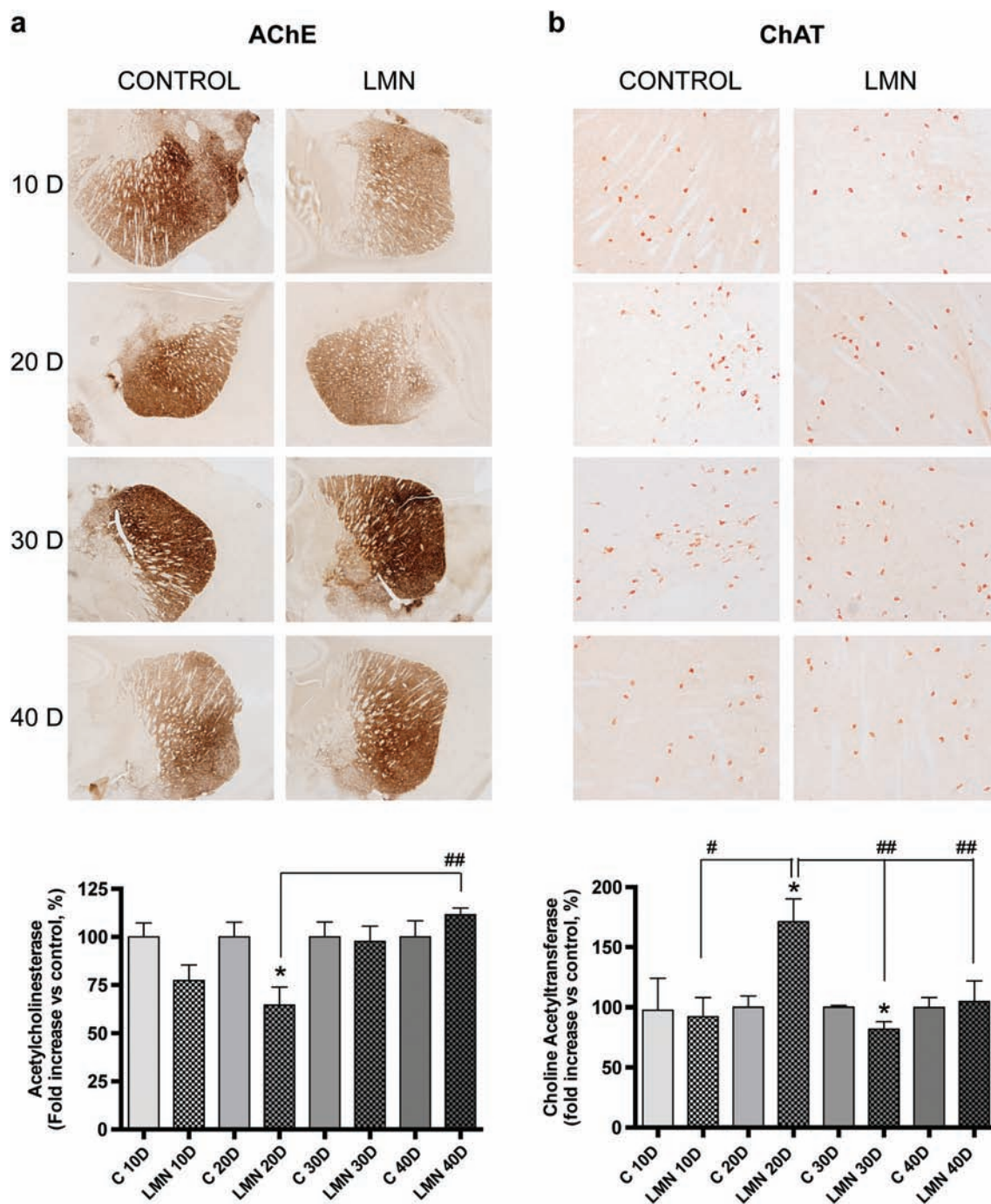


**Fig. 1** Immunohistochemical analysis of AChE and ChAT in the striatum of 129S1/SvImJ mice fed with the LMN diet. (a) Representative images for acetylcholinesterase (AChE, 2x) and (b) for choline acetyltransferase (ChAT, 10x) immunohistochemistry in basal nuclei of 4-month old 129S1/SvImJ mice fed with the control or the LMN diet for 10 ( $n = 4$ ), 20 ( $n = 4$ ), 30 ( $n = 4$ ) or 40 ( $n = 4$ ) days. Graphs at the bottom show the IHC quantifications carried out in 10x images. Data are related to each representative control. \* $p < 0.05$  vs. its own control (C), by Student's  $t$ -test; # $p < 0.05$ , ## $p < 0.01$  by one-way ANOVA and the addition of Newman–Keuls multiple comparison test.

In order to corroborate this antioxidant effect, Nrf2 activation, the transcription factor that activates the gene expression of these antioxidant enzymes, was determined after LMN or TBr treatments without the addition of  $H_2O_2$ . Fig. 5d

shows representative images for Nrf2 immunofluorescence analysis in LMN or TBr-treated SH-SY5Y cells for 24 h. These results clearly show a translocation of Nrf2 to the nucleus as a response to LMN and TBr treatments.

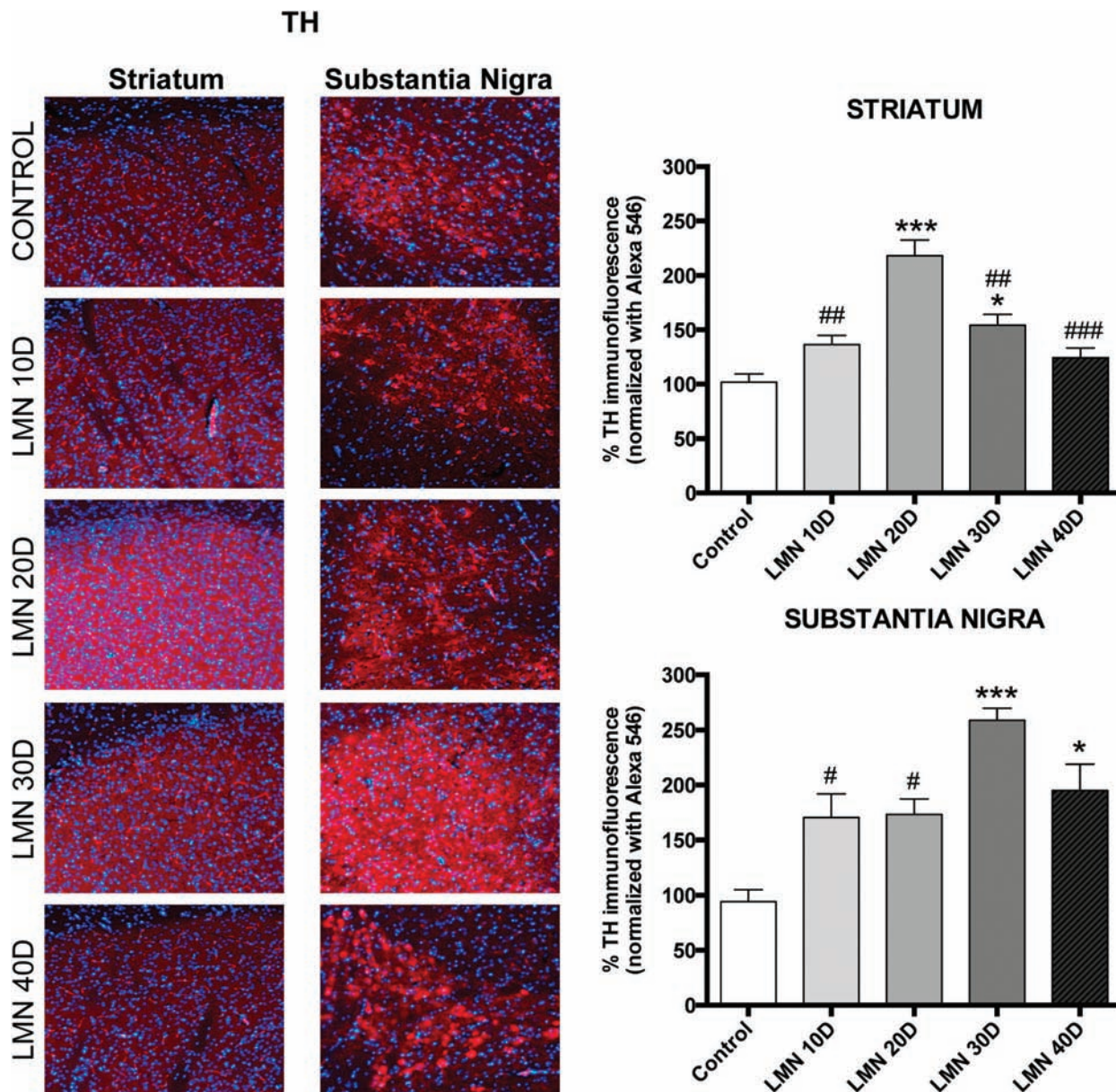


**Fig. 2** Quantification of TH expression in nucleus basalis of the LMN fed mice. Representative images for tyrosine hydroxylase (TH) immunofluorescence in the striatum and substantia nigra of 4-month old 129S1/SvImJ mice fed with the LMN diet for 10 ( $n = 4$ ), 20 ( $n = 4$ ), 30 ( $n = 4$ ) or 40 ( $n = 4$ ) days. Graphs show the quantification for each brain area. \* $p < 0.05$ , \*\*\* $p < 0.001$  vs. control diet fed animals; # $p < 0.05$ , ## $p < 0.01$ , ### $p < 0.001$  vs. LMN 20D in striatum or vs. LMN 30D in substantia nigra, by one-way ANOVA and the addition of Tukey's multiple comparison test.

### Theobromine as a modulator of catecholaminergic metabolism in undifferentiated PC12 cells

Undifferentiated PC12 cells, derived from rat pheochromocytoma adrenal medulla, were treated with TBr (1–100  $\mu\text{M}$ ) for 24 h and catecholamine levels were subsequently quantified by HPLC-ED analysis. Broadly, the levels of NA, L-DOPA, DA and DOPAC increased after treatments with all concentrations of TBr used (Table 1). However, no changes were observed in 3-MT or HVA levels.

Significant increase in the levels of NA (60.6%), DOPAC (65.3%) and DA (78.5%) were only detected at 10  $\mu\text{M}$  TBr

*versus* non-treated cells. These results are in agreement with those previously determined in the mice fed with LMN for 20 days.

## Discussion

The main component of the LMN cream is cocoa that contains a large amount of polyphenols, natural substances that are present in plants, coloured fruits and vegetables as well as in olive oil, tea and red wine. This wide family of natural products

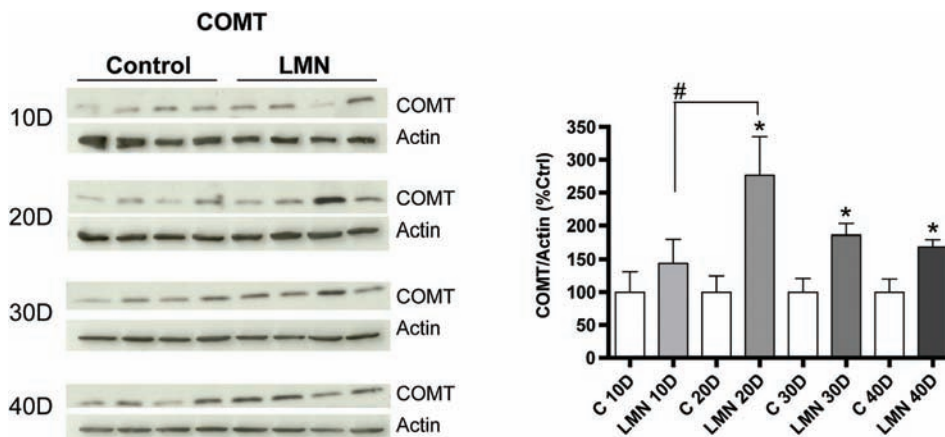


**Fig. 3** Quantification of COMT in the hippocampus from LMN fed mice. Representative western blots for catechol-*O*-methyltransferase (COMT) in hippocampi from 4-month old mice fed with the control or the LMN diet for 10 ( $n = 3$ ), 20 ( $n = 4$ ), 30 ( $n = 4$ ) or 40 ( $n = 4$ ) days. Graph shows the data corresponding to the western blot densitometric analysis. \* $p < 0.05$  vs. its respective control by Student's *t*-test. # $p < 0.05$  by one-way ANOVA and the addition of Newman–Keuls multiple comparison test.

contains flavonoids, the largest group of polyphenols including subclasses of flavones, isoflavones, flavonols, or flavans, among others. Because of their antioxidant properties, some of them are able to promote physiological benefits especially regarding the cognitive function and memory impairment.<sup>20</sup> The most abundant polyphenol present in green tea, the EGCG, also present in the LMN cream, has been reported to possess beneficial effects on cancer and cardiovascular function, with anti-inflammatory and antioxidant properties.<sup>21</sup> Furthermore, the importance of long-chain polyunsaturated fatty acids in neural development and neurodegeneration has been widely reported,<sup>22</sup> such as omega-3, present in dry fruits like hazelnuts, one of the LMN cream components.

According to the cholinergic hypothesis of AD, this neurological disorder is characterized by a loss of cholinergic neurons present in nucleus basalis, responsible for learning and memory functions.

Moreover, the existing gap between symptoms and pathology in AD has been explained by the concept of “cognitive reserve” in which both cognition and memory are maintained despite the progress in the pathology. Cognitive reserve has been hypothesized to help people to avoid greater brain pathology and it has been considered a preventive factor for dementia. Compensatory adjustments, such as an enhancement on the noradrenergic transmission, have been proposed to be involved.<sup>8</sup> Regarding nutritional aspects, some authors report that the Mediterranean diet does not support a beneficial effect on cognitive function, irrespective of educational level, which is the strongest indicator of cognitive reserve.<sup>23</sup> These results are in contrast with other studies which conclude that the Mediterranean diet is associated with lower risk of dementia.<sup>24</sup> In line with this, other authors have provided support for the hypothesis that cognitive reserve moderates the relationship between brain structure and cognition at middle age well before the onset of dementia.<sup>25</sup>

Neurotransmitters NA, DA and ACh are considered neuro-modulators released by neurons, whose cell bodies are found in specific nuclei in the brainstem. The function of many brain regions can be influenced through their wide spread projections. Dopaminergic neurons innervate the striatum, pre-frontal cortex and hippocampus. Noradrenalin has multiple effects on cellular excitability, intracellular cascades or synaptic plasticity of its target neurons. It is also able to enhance/block excitatory responses to glutamate depending on its concentration. The effect of NA on synaptic plasticity in the hippocampus promotes long-term potentiation (LTP) in both dentate gyrus through the action on  $\beta$ -receptors and in the pre-frontal cortex improving working memory in primates.<sup>26</sup>

In this respect, the search for some natural products able to modulate cholinergic and noradrenergic systems could help delaying the loss of cognition. In this work, adult male 129S1/SvImJ mice were selected as a mid-age model in which strengthening of this neurotransmission could have beneficial effects during aging.

Basal nuclei, containing striatum, were selected as a rich area in both cholinergic as well as catecholaminergic terminals. The expression of both ChAT and AChE, the two main enzymes involved in the ACh metabolism, was modulated after LMN diet intake. The increase of ChAT expression indicates a stimulation of ACh synthesis, a neurotransmitter that is diminished in AD. Furthermore, the expression of AChE, the enzyme responsible for ACh degradation at the synaptic cleft, was significantly decreased after LMN feeding. Taken together, these results strongly suggest that the LMN diet shows a beneficial modulatory effect on the stimulation of cholinergic transmission.

The previous results were correlated with the increasing TH expression in the dopaminergic fibers of both striatum and substantia nigra. This is the key enzyme responsible for the regulation of the catecholamine synthesis pathway, which

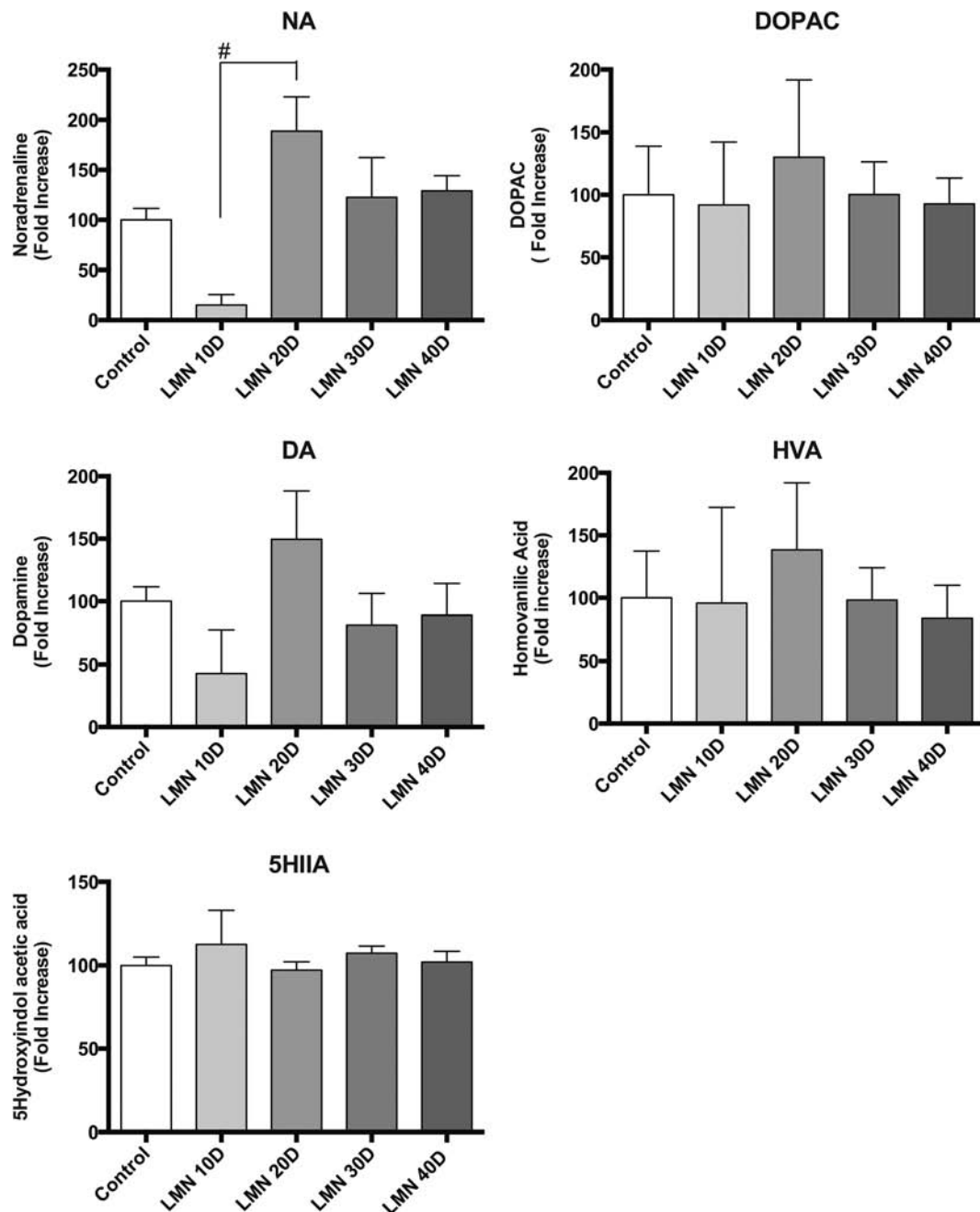
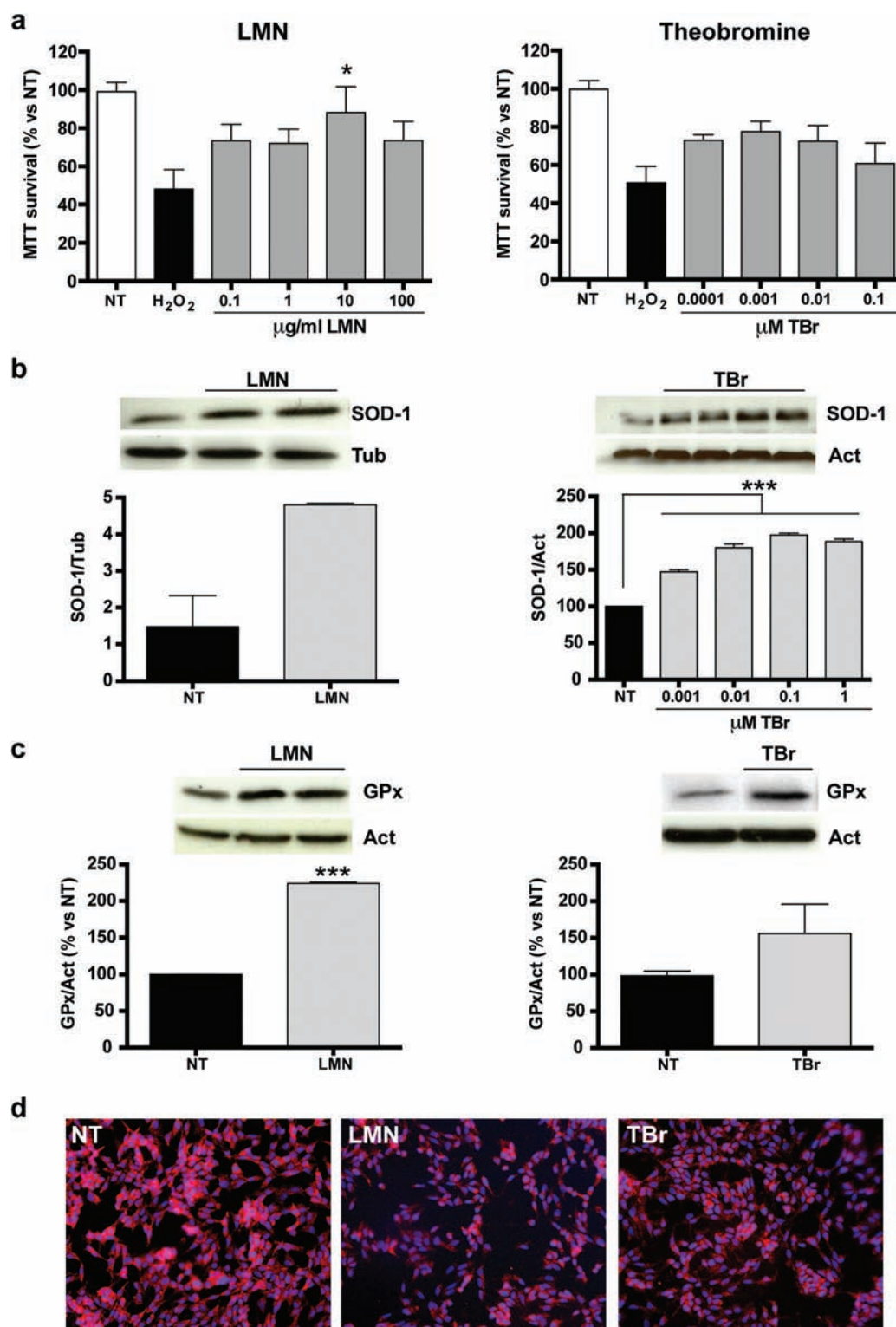


Fig. 4 HPLC analysis of catecholaminergic neurotransmitters: DA and NA in the striatum. Quantification of noradrenaline (NA), dopamine (DA), the metabolites DOPAC and HVA and 5-HIAA in basal nuclei of 4-month old mice fed with the LMN diet for 10 ( $n = 3$ ), 20 ( $n = 4$ ), 30 ( $n = 4$ ) or 40 ( $n = 4$ ) days. Data are related to each respective control.  $^{\#}p < 0.05$  by one-way ANOVA and the addition of Bonferroni's multiple comparison test.

controls reward-induced neurotransmitter change in cognitive brain regions and learning processes.<sup>27</sup> Therefore, the LMN diet enhances the dopaminergic system and consequently, catecholamine production. COMT is the enzyme responsible for dopamine metabolism rendering HVA after its catalytic action on DOPAC, a metabolite of DA generated by both aldehyde dehydrogenase and monoamine oxidase activities. The increased expression of COMT in the hippocampus, the specific area related to memory and cognition, strongly con-

firms the stimulatory effect of the LMN diet on catecholamine metabolism. All these data obtained by immunohistological assays were corroborated by the metabolite quantification by HPLC analysis. The levels of NA, DA and their metabolites were also found to be increased in PC12 cells treated with TBr.

The antioxidant properties of the LMN cream previously reported<sup>17,28</sup> were also observed with TBr. This main component of cocoa is able to stimulate the Nrf2 activation, a transcription factor responsible for the expression of both SOD-1



**Fig. 5** Antioxidant effects of the LMN cream and its main component, theobromine, in SH-SY5Y cells. (a) SH-SY5Y cells were pretreated for 24 h with the LMN cream or with theobromine (TBr) and then lesioned with 150  $\mu$ M hydrogen peroxide (H<sub>2</sub>O<sub>2</sub>) for 1 h. Cell viability was determined by the MTT method. Data are the mean  $\pm$  S.E.M. of three independent experiments. \* $p$  < 0.05 vs. H<sub>2</sub>O<sub>2</sub> by one-way ANOVA and the addition of Newman–Keuls multiple comparison test. (b, c) Effect of the LMN diet (0.1  $\mu$ g ml<sup>-1</sup>) or TBr (0.001–1  $\mu$ M) on the expression of Superoxide Dismutase-1 (SOD-1, b) or Glutathione Peroxidase (GPx, c) in 72 h-treated SH-SY5Y. Tubulin (Tub) or  $\beta$ -actin (Act) was used as loading control. Graphs represent the western blot quantification of three independent experiments. \*\*\* $p$  < 0.001 by one-way ANOVA and the addition of Tukey's multiple comparison test (TBr in SOD-1 analysis) or by Student's  $t$ -test (LMN treatment in GPx analysis). (d) Representative images for Nrf2 immunofluorescence analysis in LMN or TBr-treated SH-SY5Y cells for 24 h. Red staining represents Nrf2 whereas nuclei are stained in blue (DAPI).

**Table 1** Modulation of the levels of catecholaminergic neurotransmitters in PC12 cell lysates treated with theobromine<sup>a</sup>

Metabolite	NT	[Theobromine] ( $\mu\text{M}$ )		
		1	10	100
Noradrenalin	100.0 $\pm$ 6.6	151.8 $\pm$ 15.5	160.6 $\pm$ 22.8*	138.2 $\pm$ 12.0
L-DOPA	100.0 $\pm$ 14.3	131.1 $\pm$ 7.9	135.8 $\pm$ 27.1	104.8 $\pm$ 9.7
DOPAC	100.0 $\pm$ 5.1	105.0 $\pm$ 11.4	165.3 $\pm$ 23.5*	120.6 $\pm$ 9.3
Dopamine	100.0 $\pm$ 4.3	142.6 $\pm$ 21.5	178.5 $\pm$ 35.0*	124.9 $\pm$ 16.8
HVA	100.0 $\pm$ 4.4	83.1 $\pm$ 4.3	92.7 $\pm$ 5.9	96.2 $\pm$ 6.2
3-MT	100.0 $\pm$ 6.7	123.8 $\pm$ 16.6	119.8 $\pm$ 10.5	113.8 $\pm$ 11.4

<sup>a</sup> PC12 cells were treated for 24 h with theobromine (TBr) (1–100  $\mu\text{M}$ ). The levels of the catecholamines were quantified by HPLC analysis. Values are expressed as the mean of the percentage increase from at least four independent experiments; \* $p < 0.05$  vs. NT.

and GPx by themselves, in the absence of any oxidant contaminant.

All these results suggest that TBr may be one of the main components responsible for the modulatory effects on catecholaminergic and cholinergic observed with the LMN cream. The effects observed only in a short-time window could be explained by the activation of compensatory mechanisms that need to be further elucidated.

Only male mice were used in this study due to their homogeneity. However, since females also experience aging and show higher AD prevalence, further studies carried out in females would also be interesting in order to confirm these results.

## Experimental

### Animals and diets

Mice were bred under controlled temperature and light conditions and were fed with control diet prior to the experiments. Animal care and experimental procedures were performed in accordance with European Community Council Directive 86/609/ECC. Four-month 129S1/SvImJ adult male mice were fed either with control diet (Harlan Global Diet 2014, Mucedola SRL, Milano, Italy) or control diet supplemented with the LMN cream (LMN diet, Harlan Global Diet 2014 containing 9.27% LMN cream, Mucedola SRL, Milano Italy) for 10, 20, 30 or 40 days. The LMN cream consists of a mixture containing at least one ingredient from each of the following four groups: dry fruits, cocoa, vegetable oils rich in unsaponifiable lipids and flours rich in soluble fibers [Patent ref WO2007063158 A2]. After predetermined feeding periods, all mice were killed by decapitation and their brains were immediately removed. Right hemispheres were dissected into regions and frozen in liquid nitrogen at  $-80$  °C for subsequent western blot and HPLC analyses. Left hemispheres were fixed in 4% paraformaldehyde (PFA) for 24 hours. Then, tissue was cryoprotected in 30% sucrose/PBS solution for 48 hours at 4 °C, frozen in dry ice and cut into sagittal sequential 30  $\mu\text{m}$  sections using a

Leica cryostat. These sagittal slices were used for immunohistochemistry and histological techniques.

### Cell lines and treatments

Human neuroblastoma SH-SY5Y cells were purchased and cultured as previously described.<sup>18</sup> PC12 cell line was purchased from the American Type Culture Collection (ATCC) and grown in DMEM containing 7% FBS, 7% foetal horse serum (FHS), 1.14 mM HEPES pH 6.8, 60 U ml<sup>-1</sup> penicillin and 60  $\mu\text{g}$  ml<sup>-1</sup> streptomycin. Both cell lines were maintained at 37 °C under a saturating humidity atmosphere containing 5% CO<sub>2</sub>.

For treatments, both SH-SY5Y and PC12 cells were seeded at a density of  $2.5 \times 10^4$  cells mL<sup>-1</sup> in full media onto collagen type I (BD Biosciences)-coated plates until 70–80% confluence was reached. Before treatments, full medium was replaced by 1% FBS-medium overnight except for HPLC analysis. Both theobromine (TBr) and the LMN cream were dissolved in PBS at 37 °C and added to the media for desired times. Non-toxic TBr concentrations (1, 10 or 100  $\mu\text{M}$ ) were used for 24 h. At the end of each treatment, cells were collected in PBS, centrifuged at 3000g for 5 minutes and the pellets resuspended in 100  $\mu\text{L}$  of homogenization solution (0.25 M HClO<sub>4</sub>, 100  $\mu\text{M}$  sodium bisulfate and 250  $\mu\text{M}$  EDTA). Samples were sonicated for 10 seconds on ice and lysates kept at  $-80$  °C for at least 24 h prior to the HPLC analysis.

### Histochemistry and immunohistochemistry

The brain sections were permeabilized in PBS-0.3% Triton X-100 for 30 min and blocked in PBS-Triton X-100 containing 10% FBS, 0.2 M glycine and 1% BSA for 10 minutes. Afterwards, the slides were incubated with goat anti-Choline Acetyltransferase (ChAT, 1 : 200, Millipore AB144P) overnight at 4 °C, washing with PBS-Triton X-100 and incubated with donkey anti-goat HRP (1 : 200; Thermo PA 1-28664) for 1 or 2 hours at room temperature. After washing, sections were incubated with the streptavidin–HRP (1 : 1250; Sigma, S5512) for one hour and developed with DAB/H<sub>2</sub>O<sub>2</sub> (0.5 mg/0.22  $\mu\text{l}$  ml<sup>-1</sup>; Sigma). Acetylcholinesterase (AChE) histochemistry was performed according to the Geneser-Jensen procedure.<sup>29</sup>

Quantification of ChAT and AChE was carried out in the striatum. Brain sections from 4 animals per group were used and pictures were taken at 2 $\times$  and 10 $\times$  magnifications using the software ACT-1 version 2.70 (Nikon Corporation). They were examined with a Nikon Eclipse 90i microscope interfaced to a DXM 1200F camera. Three to five pictures per section were evaluated and quantified in 10 $\times$  images using image analysis software ImageJ.

### Immunofluorescence

For tyrosine hydroxylase (TH) immunohistochemistry, the brain sections were rinsed in PBS, treated with 2% H<sub>2</sub>O<sub>2</sub> in methanol for 15 minutes, rinsed in PBS-0.5% Triton X-100, blocked with 10% of normal goat serum in PBS-0.5% Triton X-100 and incubated overnight at 4 °C with polyclonal rabbit anti-TH (1 : 1000; Millipore). After rinsing in PBS-0.5% Triton X-100, sections were incubated for 2 h at room temperature

with goat anti-rabbit Alexa 546 (1 : 500; Molecular Probes). Finally, the sections were counterstained with DAPI and after being washed in PBS, were mounted in Mowiol medium (Sigma-Aldrich). For quantification of TH immunofluorescence, photographs of four sequential histological sections per animal were acquired with a Zeiss Axio observer Z1 microscope (Carl Zeiss) and a digital camera (QImaging Retiga Exi, QImaging). Using ImageJ software and Paxinos brain mouse atlas, the striatum and substantia nigra areas were delimited (striatum: lateral 1.32 to 2.04 mm; substantia nigra: lateral 0.84 to 1.68 mm) and relative TH immunofluorescence densitometry was obtained for each individual section, as well as for relative Alexa 546 immunofluorescence. The quantification of TH immunofluorescence was obtained by its normalization with Alexa 546 tissue background.

SH-SY5Y cells fixed in 4% PFA were incubated with the primary antibody against Nrf2 (1 : 100; Santa Cruz) diluted in PBS containing 0.2% gelatin, 0.1% Triton X-100, 20 mM glycine and 5% FBS overnight at 4 °C. Secondary anti-rabbit conjugated to Alexa Fluor® 594 (1 : 1000; Invitrogen) and 0.5 mg ml<sup>-1</sup> Hoechst were then incubated for 1 h at room temperature and cells were mounted in Fluorescent Mounting Medium (Dako). Preparations were observed under a Nikon Eclipse TE 2000-E inverted fluorescence microscope with a Hamamatsu C-4742-80-12AG camera and Metamorph® Imaging System software.

### Western blot analysis

SH-SY5Y cells were lysed in RIPA buffer, centrifuged at 3000g for 10 min at 4 °C and the supernatants were kept at -80 °C until their use. Protein concentration was determined using Bradford reagent (Bio-Rad). Twenty-five µg of total protein extract were resolved by SDS-PAGE according to standard protocols. Primary antibodies used were: Catechol-*O*-Methyl Transferase (COMT) (1 : 1000; Santa Cruz), Superoxide Dismutase-1 (SOD-1) (1 : 1000; Santa Cruz), Glutathione Peroxidase (GPx) (1 : 1000, Abcam), β-tubulin (1 : 50 000; Sigma) and β-actin (1 : 40 000; Sigma). Secondary antibodies used were horseradish peroxidase-conjugated goat anti-mouse IgG (1 : 2000; Dako) or goat anti-rabbit IgG (1 : 1000; BD Biosciences). Densitometry analyses were performed using Quantity One® software (Bio-Rad) following manufacturer's instructions.

### Cell viability analysis

Cell viability was determined by the MTT [3-(4,5-dimethylthiazol-2-yl)-2,5-diphenyltetrazolium bromide] reduction assay. MTT solution was added at a final concentration of 0.5 mg ml<sup>-1</sup> for 45 min. DMSO was used to dissolve the formazan blue precipitate formed, which was quantified at 560–620 nm using a microplate reader (Labsystems Multiskan RC).

### Determination of catecholamine levels by HPLC

Catecholamine levels were determined by HPLC coupled to an electrochemical detector. The mobile phase consisting of 0.1 M citric acid, 0.05 mM EDTA and 1.2 mM sodium octylsul-

phate (SOS) was adjusted at pH 2.75 with triethylamine (TEA). Acetonitrile was added to reach 10% (v/v). Elution was performed at a flow rate of 1 mL per minute. A Coulochem 5100A Electrochemical Detector (ESA) with a Model 5011 dual-electrode analytical cell with porous graphite electrodes was used. The potential of the electrodes 1 and 2 was set at 70.05 V and +0.4 V, respectively.

PC12 cell lysates were thawed and centrifuged at 12 000g for 10 min at 4 °C. Next, 20 µL of each sample supernatant was injected into the HPLC system for analysis. Catecholamine analysis was performed at room temperature (20–25 °C). The level of metabolites was expressed in pg of metabolite per mg of protein.

Frozen samples from basal nuclei were homogenized in RIPA buffer. After that, samples were split into two parts and diluted (1 : 1) in homogenization solution containing 2000 pg ml<sup>-1</sup> of 3,4-dihydroxybenzylamine (DHBA) as an internal standard for catecholamine determination and 4000 pg ml<sup>-1</sup> of NW-5-met-5HT as an internal standard for serotonin determination. After homogenization, the samples were sonicated and centrifuged (15 000g, 10 min, 4 °C) and supernatants were injected into the HPLC system for analysis of 3,4-dihydroxyphenylacetic acid (DOPAC), noradrenalin (NA), homovanillic acid (HVA), dopamine (DA), serotonin (5-HT) and serotonin metabolite 5-hydroxyindoleacetic acid (5HIAA). DHBA was used as an internal standard.

### Statistics

Graphs were plotted and data were analysed using the Graph-Pad Prism 4.02 software. Values of *p* < 0.05 were considered to be statistically significant.

## Conclusions

At present, there are few reports on the beneficial effect of nutrients on the stimulation of cholinergic and catecholaminergic transmission.<sup>30</sup> In this work, we report for the first time the enhancement of cholinergic and catecholaminergic transmissions, both of which are highly impaired in neurodegenerative disorders such as AD, by some natural nutrients present in the LMN cream. These results will give an insight into the possible contribution of the LMN cream in the “cognitive reserve”<sup>8</sup> and its beneficial effect on the cognitive decline related to aging and neurological disorders.

## Acknowledgements

The present study was supported by the Spanish Ministry of Industry (CDTI) through the following projects: Project CENIT (MET-DEV-FUN); Programa Ingenio 2010, Programa INCOMES and a grant from the Chinese Scholarship Council (P. S.).

## References

- 1 H. H. Dodge, C. N. Wang, C. C. Chang and M. Ganguli, *Neurology*, 2011, **77**, 722–730.
- 2 S. A. Villeda, J. Luo, K. I. Mosher, B. Zou, M. Britschgi, G. Bieri, T. M. Stan, N. Faingerg, Z. Ding, A. Eggel, K. M. Lucin, E. Czirr, J. S. Park, S. Couillard-Després, L. Aigner, G. Li, E. R. Peskind, J. A. Kaye, J. F. Quinn, D. R. Galakso, S. S. Xie, T. A. Rando and T. Wyss-Coray, *Nature*, 2011, **477**, 90–94.
- 3 Z. U. Khan, E. Martín-Montañez, I. Navarro-Lobato and E. C. Muly, *Prog. Mol. Biol. Transl. Sci.*, 2014, **122**, 1–29.
- 4 X. Huang, R. D. Moir and R. E. Tanzi, *Ann. N. Y. Acad. Sci.*, 2004, **1012**, 153–163.
- 5 R. H. Swerdlow and S. M. Khan, *Exp. Neurol.*, 2009, **218**, 308–315.
- 6 J. P. Blass, L. Ko and H. M. Wisniewski, *Psychiatr. Clin. North Am.*, 1991, **14**, 397–420.
- 7 G. G. Glenner and M. A. Murphy, *J. Neurol. Sci.*, 1989, **94**, 1–28.
- 8 I. H. Robertson, *Neurobiol. Aging*, 2013, **34**, 298–308.
- 9 P. Davies and A. J. Maloney, *Lancet*, 1976, **2**, 1403.
- 10 F. Gomez-Pinilla, *Nat. Rev. Neurosci.*, 2008, **9**, 568–578.
- 11 E. Exposito, D. Rotilo, V. Di Matteo, C. Di Giulio, M. Cacchio and S. Algeri, *Neurobiol. Aging*, 2001, **2**, 719–735.
- 12 C. Ramassamy, *Eur. J. Pharmacol.*, 2006, **545**, 51–64.
- 13 B. N. Ramesh, T. S. Rao, A. Prakasam, K. Sambamurti and K. S. Rao, *J. Alzheimers Dis.*, 2010, **19**, 1123–1139.
- 14 J. Joseph, G. Cole, E. Head and D. Ingram, *J. Neurosci.*, 2009, **29**, 12795–12801.
- 15 J. A. Joseph, B. Shukitt-Hale, G. Casadesus and D. Fisher, *Neurochem. Res.*, 2005, **30**, 927–935.
- 16 R. Sola, R. M. Valls, G. Godàs, G. Perez-Busquets, J. Ribalta, J. Girona, M. Heras, A. Cabré, A. Castro, G. Domenech, F. Torres, L. Masana, N. Anglés, J. Reguant, B. Ramírez and J. M. Barriach, *PLoS One*, 2012, **7**, e31103.
- 17 T. Valente, J. Hidalgo, I. Bolea, B. Ramirez, N. Anglés, J. Reguant, J. R. Morelló, C. Gutiérrez, M. Boada and M. Unzeta, *J. Alzheimers Dis.*, 2009, **18**, 849–865.
- 18 L. Fernandez-Fernandez, M. Solé, I. Bolea, T. Valente, J. C. E. Serrano, M. Jové, B. Ramirez, N. Anglés, J. Reguant, J. R. Morello, R. Pamplona, M. Portero-Otin and M. Unzeta, in *Diet and Nutrition in Dementia and Cognitive Decline*, ed. C. R. Martin and V. R. Preedy, Elsevier Inc., 2014, ch. 78, pp. 847–858.
- 19 Y. Gao, M. H. Tschöp and S. Luquet, *Cell Metab.*, 2014, **19**, 173–175.
- 20 D. Buterfield, A. Castegna, C. Pocernich, J. Drake, G. Scapagnini and V. Calabrese, *J. Nutr. Biochem.*, 2002, **13**, 444.
- 21 J. V. Higdon and B. Frei, *Crit. Rev. Food Sci. Nutr.*, 2003, **43**, 89–143.
- 22 C. I. Janssen and A. J. Kiliaan, *Progr. Lipid Res.*, 2014, **53**, 1–17.
- 23 E. Kesse-Guyot, V. A. Andreeva, C. Lassale, M. Ferry, C. Jeandel, S. Hercberg, P. Galan and SU.VI.MAX 2 Research Group, *Am. J. Clin. Nutr.*, 2013, **97**, 369–376.
- 24 I. Lourida, M. Soni, J. Thompson-Coon, N. Purandare, I. A. Lang, O. C. Ukoummunne and D. J. Llewellyn, *Epidemiology*, 2013, **24**, 479–489.
- 25 E. Vuoksima, M. S. Panizzon, C. H. Chen, L. T. Eyler, C. Fennema-Notestine, M. J. Fiecas, B. Fischl, C. E. Franz, M. D. Grant, A. J. Jak, M. J. Lyons, M. C. Neale, W. K. Thompson, M. T. Tsuang, H. Xian, A. M. Dale and W. S. Kremen, *Neuropsychologia*, 2013, **51**, 1124–1131.
- 26 J. S. Sara, *Nat. Rev. Neurosci.*, 2009, **10**, 211–223.
- 27 A. Fallon, E. Shearman and H. Sershen, *Neurochem. Res.*, 2007, **32**, 1772–1782.
- 28 L. Fernandez-Fernandez, G. Comes, I. Bolea, T. Valente, J. Ruiz, P. Murtra, B. Ramirez, N. Anglés, J. Reguant, J. R. Morelló, M. Boada, J. Hidalgo, R. M. Escorihuela and M. Unzeta, *Behav. Brain Res.*, 2012, **228**, 261–271.
- 29 F. A. Geneser-Jensen, *Z. Zellforsch. Mikrosk. Anat.*, 1972, **131**, 481–495.
- 30 J. A. Joseph, B. Shukitt-Hale and G. Casadesus, *Am. J. Clin. Nutr.*, 2005, **81**, 313S–316S.

#### **Annex IV**

“Protective effect of the multitarget compound DPH-4 on human SSAO/VAP-1-expressing hCMEC/D3 cells under oxygen-glucose deprivation conditions, an *in vitro* experimental model of cerebral ischemia”



**Protective effect of the multitarget compound DPH-4 on human SSAO/VAP-1-expressing hCMEC/D3 cells under oxygen-glucose deprivation conditions, an in vitro experimental model of cerebral ischemia**

P. Sun<sup>1</sup>, G. Esteban<sup>1</sup>, T. Inokuchi<sup>2</sup>, J. Marco-Contelles<sup>3</sup>, B.B. Weksler<sup>4</sup>, I.A. Romero<sup>5</sup>, P.O. Couraud<sup>6</sup>, M. Unzeta<sup>1\*</sup>, M. Solé<sup>1\*</sup>

<sup>1</sup>Institut de Neurociències i Departament de Bioquímica i Biologia Molecular. Edifici M, Facultat de Medicina. Universitat Autònoma de Barcelona (UAB), Bellaterra, Barcelona (Spain)

<sup>2</sup>Division of Chemistry and Biotechnology, Graduate School of Natural Science and Technology, Okayama University, 3.1.1 Tsushima-Naka, Kita-ku, Okayama 700-8530 (Japan)

<sup>3</sup>Instituto de Química Orgánica General (CSIC); 3, Juan de la Cierva, 28006-Madrid (Spain)

<sup>4</sup>Department of Medicine, Division of Hematology-Oncology, Weill Cornell Medical College, New York, NY 10065 (USA)

<sup>5</sup>Department of Life, Health and Chemical Sciences, Open University, Milton Keynes (UK)

<sup>6</sup>Institut Cochin, INSERM U1016, CNRS UMR 8104, Université Paris Descartes, Sorbonne Paris Cité, Paris (France)

**Short title:** DPH-4 as a multitarget compound for AD and stroke treatment

\* **Corresponding authors:** Montse Solé and Mercedes Unzeta. Neurosciences Institute and Department of Biochemistry and Molecular Biology, Universitat Autònoma de Barcelona (UAB), 08193 Bellaterra, Barcelona (Spain). Telephone: +34 93 581 1624; Fax: +34 93 581 1573. E-mail: [montserrat.sole@uab.cat](mailto:montserrat.sole@uab.cat), [mercedes.unzeta@uab.es](mailto:mercedes.unzeta@uab.es)

**Authorship contributions:**

P Sun and G Esteban performed the research study

M Unzeta and M Solé designed the research study, and contributed to data analysis

T Inokuchi provided compound DPH-4

J Marco-Contelles designed compound DPH-4

BB Weksler, IA Romero and PO Couraud provided the hCMEC/D3 cellular model

All authors contributed to drafting and revising the manuscript, and accepted the final manuscript

**Key Words:** Multitarget-directed ligands (MTDLs); stroke; blood-brain barrier (BBB); semicarbazide-sensitive amine oxidase/vascular adhesion protein-1 (SSAO/VAP-1); inflammation.

This article has been accepted for publication and undergone full peer review but has not been through the copyediting, typesetting, pagination and proofreading process which may lead to differences between this version and the Version of Record. Please cite this article as doi: 10.1111/bph.13328

## Abstract

### BACKGROUND AND PURPOSE

Stroke and Alzheimer's disease (AD) are related pathologies in which the cerebrovascular system is involved. Semicarbazide-sensitive amine oxidase/vascular adhesion protein-1 (SSAO/VAP-1), increased in both stroke and AD patients' plasma, contributes to the vascular damage. During inflammation its enzymatic activity mediates leukocyte recruitment into the injured tissue, inducing damage in the blood-brain barrier (BBB) and neuronal tissue. We hypothesized that through the alteration of cerebrovascular function, SSAO/VAP-1 might play a role in the stroke-AD transition. Therefore, the protective effect on the BBB of the novel multitarget-directed ligand (MTDL) DPH-4, initially designed for AD therapy, was evaluated.

### EXPERIMENTAL APPROACH

A human microvascular brain endothelial cell line expressing the human SSAO/VAP-1 (hCMEC/D3 hSSAO/VAP-1) was generated, as SSAO/VAP-1 expression is lost in cultured cells. To simulate ischemic damage, oxygen and glucose deprivation (OGD) and reoxygenation conditions were established in these cells. The protective role of DPH-4 was then evaluated in the presence of methylamine as an SSAO/VAP-1 substrate and/or  $\beta$ -amyloid ( $A\beta$ ).

### KEY RESULTS

Under these conditions, DPH-4 was able to protect brain endothelial cells from OGD and reoxygenation-induced damage, as well as to decrease SSAO-dependent leukocyte adhesion. DPH-4 was also effective against the damage induced by OGD and reoxygenation in the presence of  $A\beta$  as a model of AD pathology.

**CONCLUSIONS AND IMPLICATIONS:** These results allow us to conclude that the multitarget compound DPH-4 might provide a therapeutic benefit to delay the onset and/or progression of these two linked neurological pathologies.

### Abbreviations

$A\beta$ , beta amyloid peptide; AD, Alzheimer's disease; ADME, absorption, distribution, metabolism and excretion; BBB, blood-brain barrier; bFGF, basic Fibroblast Growth Factor; Dep, deprenyl; DMSO, dimethylsulfoxide; FBS, foetal bovine serum; G418, Geneticine; hCMEC/D3, human cerebral microvascular endothelial cells/D3; HUVEC, human umbilical vein endothelial cells; MA, methylamine; MAO, monoamine oxidase; MTDL, multitarget-directed ligand; OGD, oxygen-glucose deprivation; PBS, phosphate-buffered saline; SC, semicarbazide; SMC, smooth muscle cells; SSAO/VAP-1, semicarbazide sensitive amine oxidase/vascular adhesion protein 1; WT, wild type.

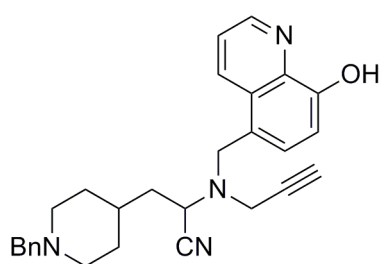
## Introduction

Increasing evidence suggests that the neurovasculature plays an important role in the onset and progression of neurological disorders like Alzheimer's disease (AD) (Zlokovic, 2008; Grammas, 2011; Marchesi, 2014). In this regard, the concept of "neurovascular unit", integrated by neurons, astrocytes and vascular cells, constitutes a functional unit able to maintain the homeostasis of the brain microenvironment (Iadecola, 2010). Stroke is a vascular disorder and the second leading cause of death worldwide with higher incidence in elderly people. Inflammation and oxidative stress accumulated during human aging worsen the vascular damage following a stroke incident (DiNapoli *et al.*, 2008), and the immune system may contribute to infarct progression (Iadecola and Anrather, 2011). In fact, the observation that a high percentage of patients having suffered stroke subsequently developed AD, suggests that a strong link between these two pathologies exists. In this sense, hypoxia and ischemic injury induce the up-regulation of BACE-1 that increases  $\beta$ -amyloid (A $\beta$ ) formation (Guglielmotto *et al.*, 2009). In addition, endothelial cells activated by hypoxia during stroke produce free radical species, which induce the expression of adhesion molecules such as the vascular adhesion protein 1 (VAP-1) that mediates the leukocytes recruitment, which infiltrate through the blood-brain barrier (BBB) into the injured tissue, inducing tissue damage by their release of cytokines.

VAP-1 is a homodimeric glycoprotein with enzymatic function that binds leukocytes through its semicarbazide-sensitive amine oxidase (SSAO, E.C 1.4.3.21) activity (Smith *et al.*, 1998; Jalkanen and Salmi, 2008). As an enzyme, SSAO/VAP-1 metabolizes primary amines producing aldehydes, hydrogen peroxide, and ammonia, which are able to induce cellular damage when overproduced (Yu and Deng, 1998). SSAO/VAP-1, either present at the cell membrane or in a soluble form, released into blood plasma, is altered in several human pathologies (Kurkijarvi *et al.*, 1998; Boomsma *et al.*, 2003) including AD (Ferrer *et al.*, 2002; Hernández *et al.*, 2005) and cerebral ischemia (Airas *et al.*, 2008). The mediators that induce these alterations in the SSAO/VAP-1 levels are still unknown, but it is believed that increased SSAO/VAP-1 levels may contribute to the physiopathology in these diseases (Conklin *et al.*, 1998; Solé *et al.*, 2008), constituting therefore a potential therapeutic target. In addition, increased human plasma SSAO activity is a strong predictor of parenchymal haemorrhages in ischemic stroke patients following tissue plasminogen activator (tPA) treatment (Hernández-Guillamón *et al.*, 2010). On the other hand, plasma SSAO activity, also elevated in haemorrhagic stroke patients, predicts neurological outcome (Hernández-Guillamón *et al.*, 2012). Altogether, these data suggest that SSAO/VAP-1 may contribute to the association between stroke and the progression to AD through the alteration of cerebrovascular tissue function.

AD is a complex disease for which therapy has been long focused on one of its multiple pathological signs, the depletion of basal forebrain cholinergic neurons with a subsequent decrease in the cholinergic transmission (Perry *et al.*, 1977; Geula and Mesulam 1999). At present, no drug has been able to successfully prevent or cure the neurodegenerative process of AD. The Food and Drug Administration (US)-approved drugs for the treatment of AD are based on the cholinergic hypothesis of AD and therefore, aimed to increase the cholinergic transmission to recover cognitive function. To date, only four drugs (rivastigmine, galantamine, donepezil and memantine) have been approved by the FAD for the treatment of AD (Birks and Harvey, 2006). Among them, donepezil has shown some temporary efficacy, but fails to reverse the cognitive decline. In the search for more effective therapies, the "one drug, multiple target" strategy, also called multitarget-directed ligand (MTDL) approach, might be more appropriate (Buccafusco and Terry, 2000; Youdim and Buccafusco, 2005;

Bolea *et al.*, 2013; León *et al.* 2013). This strategy suggests the use of compounds with multiple activities for different biological targets (Cavalli *et al.*, 2008). In this context, we recently designed a novel series of derivatives based on the hybridisation of selected moieties from donepezil, propargylamine and 8-hydroxyquinoline (DPH), that were synthesised and pharmacologically evaluated for the potential prevention and treatment of AD (Wang *et al.*, 2014). They behaved as dual inhibitors of cholinesterase (AChE and BuChE) and monoamine oxidase (MAO A and MAO B) activities, both altered in AD, for the potential prevention and treatment of this neurological disorder. Among them, hybrid DPH-4 showed strong biometal-chelating properties *vs*  $\text{Cu}^{2+}$  and  $\text{Fe}^{2+}$ , good ADMET properties and brain penetration capacity, as well as a significant decrease in scopolamine-induced learning deficits in healthy adult mice (Wang *et al.*, 2014). Additionally, compound DPH-4 (Fig 1) inhibited bovine SSAO activity in the low micromolar range ( $\text{IC}_{50} = 2.8 \pm 0.7 \mu\text{M}$ ).



**DPH-4**

EeAChE  $\text{IC}_{50} = 5.5 \pm 0.5 \mu\text{M}$     rat MAO A  $\text{IC}_{50} = 9.7 \pm 1.5 \mu\text{M}$

eqBuChE  $\text{IC}_{50} = 6.1 \pm 0.6 \mu\text{M}$     rat MAO B  $\text{IC}_{50} = 12.4 \pm 2.5 \mu\text{M}$

(Wang, L 2014, Eur. J. Med Chem)

**Figure 1. Structure of the multifunctional compound DPH-4.** DPH-4 inhibits AChE (Ee, electric eel), BuChE (eq, equine), MAO (A and B) enzymes, showing biometal-chelating properties, as described in the corresponding publication.

Taking into account that stroke and AD are related pathologies and that one can trigger the progression of the other, the aim of this work was to analyse whether the beneficial effect of DPH-4, previously observed in an experimental model of AD (Wang *et al.*, 2014), could also exhibit a protective effect on a new *in vitro* experimental model of cerebral ischemia that uses human cerebral microvascular endothelial cells as a model of the BBB expressing the human SSAO/VAP-1 protein (hCMEC/D3 hSSAO/VAP-1). Obtaining SSAO/VAP-1-expressing cells was an essential preliminary step as the expression of this protein is lost in cultured cells.

## Methods

### *Cell culture and transfection:*

The human cerebral microvascular endothelial cell line hCMEC/D3 was obtained from coauthors from the Institut COCHIN (Paris, France) as previously described (Weksler *et al.*, 2005) as a model of the BBB. hCMEC/D3 cells were cultured as recommended, on  $150 \mu\text{g mL}^{-1}$  collagen type I (Rat Tail, Corning)-coated plates in EBM-2 (Lonza) medium supplemented with 5% FBS (Fetal Bovine Serum, Life Technologies),  $1.4 \mu\text{M}$  Hydrocortisone (Sigma),  $5 \mu\text{g mL}^{-1}$  Ascorbic Acid (Sigma), 1% Chemically Defined Lipid Concentrate (Life Technologies), 10 mM HEPES (Life Technologies) and  $1 \text{ ng}\cdot\text{mL}^{-1}$  human bFGF (Fibroblast Growth Factor-basic, Sigma). Human SSAO/VAP-1-expressing human umbilical vein endothelial cells (HUVEC hSSAO/VAP-1) and rat smooth muscle cells (SMC) (A7r5 hSSAO/VAP-1) were previously developed in our group, and cultured as described (Solé and Unzeta, 2011; Solé *et al.*, 2007). THP-1 monocytic cells were obtained from the American Type Culture Collection (ATCC) and grown in RPMI 1640 medium (Life Technologies) supplemented with 10% FBS. All cells were maintained at  $37 \text{ }^\circ\text{C}$  in a humidified atmosphere containing 5%  $\text{CO}_2$ . Geneticine (G418,  $100 \mu\text{g mL}^{-1}$ ; Invitrogen) was added to the culture medium of HUVEC and SMC cells to ensure the hSSAO/VAP-1 DNA maintenance.

In order to obtain the hCMEC/D3 cell line stably expressing the human SSAO/VAP-1, wild type (WT), hCMEC/D3 cells were transfected with a PcDNA3.1(+) vector containing the human SSAO/VAP-1 cDNA (Solé *et al.*, 2007) using the Fugene® HD transfection reagent (Roche) according to the manufacturer's conditions. After transfection, cells were selected by the addition of G418 antibiotic ( $800 \mu\text{g mL}^{-1}$ ) for 1-2 months. Then, cells were diluted to allow the formation of monoclonal colonies in the presence of  $200 \mu\text{g mL}^{-1}$  G418, an antibiotic concentration that was used thereafter for cell maintenance. Cell colonies were amplified and checked for SSAO/VAP-1 expression and activity before being frozen.

### *Cell lysates and concentrated culture medium:*

Cells were collected and homogenized in 50 mM Tris-HCl (pH 7.5), containing 1% Triton X-100, 10 mM EDTA and a protease inhibitor cocktail (Sigma) (1:100) and were sonicated for 10 sec. To obtain concentrated culture medium samples, culture media were collected after cell treatments and centrifuged at  $4400 g$  for 10 min to eliminate dead cells and debris. Then media samples were lyophilized by evaporation in a Refrigerated CentriVap Concentrator (Labconco) and reconstituted in a smaller, known volume of distilled water to obtain ten-fold concentrated culture medium.

### *Sub-cellular fractionations:*

Membrane-enriched preparations were obtained by homogenization of cells in 10 mM HEPES, 1.5 mM  $\text{MgCl}_2$  and 10 mM KCl buffer at pH 7.9, containing protease inhibitor cocktail. After centrifugation at  $2000 g$  for 15 min at  $4 \text{ }^\circ\text{C}$ , the resulting supernatant was ultracentrifuged at  $100000 g$  (Sorvall Discorvery M120 SE) for 30 min at  $4 \text{ }^\circ\text{C}$  to separate the soluble cytosolic fraction from the pellet containing the membrane-enriched fraction.

Lipid raft-enriched fractions were obtained by scraping the cells in PBS, recovering them by centrifugation for 5 min at  $800 g$  and then reconstituting the pellet in  $450 \mu\text{L}$  of 50 mM Tris-HCl, 150 mM NaCl, 1 mM EDTA and 1% Brij 98 buffer at pH 7.2, containing protease inhibitor cocktail. After 15 min incubation at  $37 \text{ }^\circ\text{C}$  under continuous agitation, samples were

centrifuged for 10 min at 2000 g to discard nuclei. The supernatants were mixed with 450  $\mu\text{L}$  of 90% sucrose in Tris-HCl buffer to obtain 45% sucrose fractions, which were deposited at the bottom of ultracentrifuge tubes. Two additional fractions of 35% (2 mL) and 5% (0.8 mL) sucrose were added to the former to generate a sucrose gradient, and then the samples were centrifuged for 19 h at 120000 g. Ten 370  $\mu\text{L}$ -fractions were recovered and analysed by western blot to identify the lipid raft and soluble membrane-enriched fractions.

#### ***OGD model and cell treatment:***

Combined oxygen and glucose deprivation (OGD) and reoxygenation have been used as an experimental approach to ischemic stroke. For HUVEC hSSAO/VAP-1 cells, the ischemic condition was carried out by subjecting the cells to a 24 h OGD followed by a 7 h reoxygenation, as previously described (Sun *et al.*, 2014). For WT and hSSAO/VAP-1 hCMEC/D3 cells, the OGD treatment was performed in glucose-free DMEM (Life Technologies) after washing cells with glucose-free PBS, and then introducing the cells into a temperature-controlled ( $37\pm 1$  °C) Invivo<sub>2</sub> hypoxia workstation (RUSKINN) containing a gas mixture composed of 5% CO<sub>2</sub>, 95% N<sub>2</sub> and 0.5% O<sub>2</sub>. Control cells were maintained in DMEM (5 mM glucose) in the incubator under normoxic conditions (5% CO<sub>2</sub>/95% air). In experiments including reoxygenation, cells that have undergone OGD were returned to normoxia conditions after replacing glucose-free DMEM by serum-free DMEM (5 mM glucose) and adding the same treatments present during OGD. In experiments analysing release of soluble SSAO/VAP-1, DMEM was not replaced for the reoxygenation period, but glucose was added into OGD plates.

For cell viability and adhesion assays, HUVEC hSSAO/VAP-1 were seeded at 53200 cells mL<sup>-1</sup>, hCMECs were seeded at 50000 cells/mL, and both were grown for 48 h before the addition of treatments for another 24 h. For immunoblot analysis, cells were seeded at 60000 cells mL<sup>-1</sup>, and grown to 80% - 90% confluence before treatments. MA (methylamine), SC (semicarbazide), A $\beta_{1-40}$ D (A $\beta_{1-40}$  peptide containing the Dutch mutation, Anaspec), and/or DPH-4 (Wang *et al.*, 2014) were added into DMEM before OGD starting. In the reoxygenation process, the compounds were maintained at the same concentrations as during OGD. For the preparation of A $\beta_{1-40}$ D, it was pretreated with 1,1,1,3,3,3-hexa-fluoro-2-propanol (HFIP, Sigma-Aldrich) for more than 4 h but less than 6 h, then aliquoted, evaporated at room temperature, and stored at -80 °C until using, then dissolved in sterile PBS containing 0.1% ammonium hydroxide.

#### ***Cell viability assay:***

MTT [3-(4, 5-dimethylthiazol-2-yl)-2, 5-diphenyltetrazolium bromide] reduction assay was employed to evaluate the cell viability. Briefly, at the end of the treatments, cells were incubated with 0.5 mg mL<sup>-1</sup> MTT for 3 h in HUVECs and for 1.5 h in hCMECs at 37 °C. The medium was then replaced by dimethylsulfoxide (DMSO) to dissolve the blue formazan precipitate, and color was spectrophotometrically quantified at 560 nm and 620 nm in a microplate reader (Labsystems multiscan RC) (Plumb *et al.*, 1989).

#### ***Antibodies and western blot analysis:***

The antibodies used were: rabbit anti-VAP-1 (abcam, 1:1000), rabbit anti-bovine SSAO (1:1000) (Lizcano *et al.*, 1998), rabbit anti-VCAM-1 (Epitomics, 1:1000), rabbit anti-ICAM-1 (GeneTex, 1:1000), rabbit anti-P-selectin (BioVision, 1:1000), rabbit anti-E-selectin (Santa Cruz, 1:500), rabbit anti-IGF1-R (insulin-like growth factor 1 receptor) (Santa Cruz Biotechnology, 1:1000), mouse anti-Flotillin (BD Biosciences, 1:1000), mouse anti-GAPDH

(glyceraldehyde-3-phosphate dehydrogenase) (Ambion-Invitrogen, 1:40000); mouse anti-Tf Rec (ZYMED, 1:1000), HRP (horseradish peroxidase)-conjugated anti-rabbit IgG (BD Biosciences, 1:2000), HRP anti-mouse IgG (Dako, 1:2000). Equal amounts of protein (20 µg per lane) determined by the Bradford method, or equal volumes of media (45 µL per lane) were separated by SDS/PAGE and transferred onto nitrocellulose membranes. Membranes were blocked for 1 h with TBS/0.1%-Tween buffer containing 5% (w/v) non-fatty milk and incubated overnight at 4 °C with the corresponding primary antibodies. After incubation with the secondary antibodies, blots were developed using ECL® Chemoluminescent detection reagents and High Performance Chemiluminescence Films (GE Healthcare). The ImageJ software was used to quantify the western blot signals.

#### ***SSAO enzymatic activity determination:***

For SSAO activity determinations, cells were collected and homogenized in 100 mM Tris-HCl, pH 9, and containing protease inhibitors cocktail. Enzymatic activity was determined radiochemically by using a modification of the Otsuka and Kobayashi method (Otsuka *et al.*, 1964). Briefly, [<sup>14</sup>C]-benzylamine hydrochloride (100 µM and 2 mCi mmol<sup>-1</sup>, American Radiolabeled Chemicals) was used as substrate, and 1 µM Dep (deprenyl) was added to avoid monoamine oxidase (MAO) B interference. A 30-min inhibitory pre-treatment of samples was performed at 37 °C with 1 µM Dep or Dep plus DPH-4. Reactions were performed at 37 °C for 120 min in 100 mM Tris-HCl buffer, pH 9.0, adding 25 µL of substrate to the 200 µL of reaction. Eighty to a hundred µg of HUVEC hSSAO/VAP-1 or hCMEC/D3 hSSAO/VAP-1 cell lysates were used in each reaction. Reaction was stopped by adding 100 µL of 2 M citric acid. The [<sup>14</sup>C]-aldehyde products were extracted into 4 mL of toluene/ethylacetate (1:1, v/v) solution containing 0.6% (w/v) of diphenyloxazole. The amount of [<sup>14</sup>C]-aldehyde was quantified using a Tri-Carb 2810TR liquid scintillation counter (Perkin Elmer) and the Quanta Smart 3.0 software (Perkin Elmer).

#### ***Adhesion assays:***

THP-1 monocytes were labelled with 1 µM calcein-AM, and at the end of treatments, endothelial cells were incubated with the calcein-AM-labelled THP-1 cells (2.5×10<sup>5</sup> per well in 24-well plates) for 30 min at 37 °C. Then, unbound monocytes were removed by turning over the plates onto absorbent paper, carefully adding FBS-free RPMI 1640 medium to the plates with an auto-pipette, and repeating the washing for at least three times. The fluorescence intensity was measured using a fluorescence microplate reader ( $\lambda_{ex}/\lambda_{em}$ : 495/530 nm). Results are represented as the percentage of fluorescence intensity, referring values to those obtained for the non-treated cells.

#### ***Analysis of Data:***

Results are given as mean ± SEM of independent experiments. Statistical analysis was performed by one-way ANOVA and further Newman-Keuls multiple comparison test. P<0.05 was considered to be statistically significant. Statistical analyses and graphic representations were obtained with the Graph-Pad Prism 6.0 software.

## **Results**

### ***Generation and characterization of the human SSAO/VAP-1-expressing hCMEC/D3 cell line.***

In order to obtain a brain endothelial cell model to study *in vitro* the role of SSAO/VAP-1 in cerebrovascular tissue, the immortalized human brain endothelial cell line hCMEC/D3

(Weksler *et al.*, 2005) was stably transfected with human SSAO/VAP-1 cDNA. This step was necessary because SSAO/VAP-1 expression is lost in cultured cells (El Hadri *et al.*, 2002). After selection and amplification of G418-resistant cells, different clones were analysed for SSAO activity and expression (Fig. 2a,b). Clones 1 and 2 showed the highest SSAO enzymatic activity using benzylamine as specific substrate, as well as the highest protein expression of SSAO by western blot analysis. The activity levels observed were significantly higher than those obtained with previously generated HUVECs (H) or A7r5 smooth muscle (SMC) SSAO/VAP-1-transfected cell lines (Solé and Unzeta, 2011; Solé *et al.*, 2007).

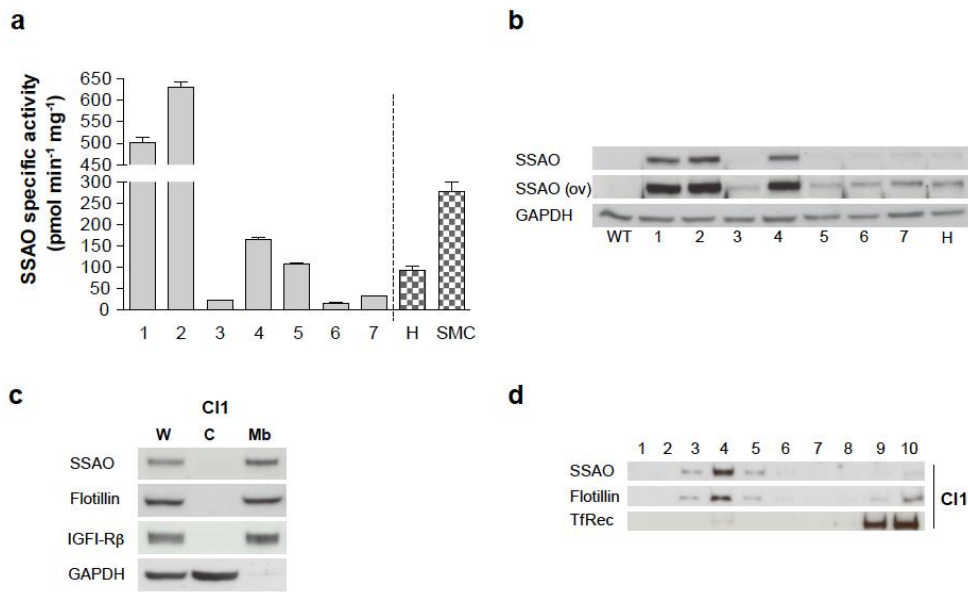


**Figure 2. Characterization of the hCMEC/D3 cell line stably transfected with human SSAO/VAP-1.** (a) SSAO specific activity (expressed as pmol min<sup>-1</sup> mg<sup>-1</sup> of protein) of the antibiotic-selected and amplified positive clones (1 - 7). HUVEC endothelial (H) or A7r5 smooth muscle (SMC) SSAO/VAP-1-transfected cell lines are shown for comparison. (b) SSAO/VAP-1 protein visualization by western blot corresponding to the same clones than in a. The overexposure (ov) of the SSAO western blot is shown to highlight the weaker bands. GAPDH was used as loading control. WT, wild type (non-transfected cells). (c) The transfected SSAO protein is located in the membrane fraction, and absent from the cytosol in clone 1 cells, shown as example. Flotillin and IGF1-Rβ were used as membrane-positive markers; GAPDH was used as cytosolic marker. W, whole fraction; C, cytosolic fraction; Mb, membrane fraction. (d) The transfected SSAO is located in the lipid raft fractions of the cell membrane; clone 1 is shown as example. Flotillin was used as raft-positive protein and transferrin receptor (Tf Rec) was used as marker of the soluble membrane fraction.

The correct sub-cellular localization of the expressed SSAO/VAP-1 protein was checked by two distinct cell fractionation procedures. On one hand, the membrane and cytosolic fractions were separated and their subsequent analysis by western blot showed that SSAO/VAP-1 expression is associated with the membrane fraction, while it is absent in the cytosol (Fig 2c). Furthermore, SSAO/VAP-1 was located in the lipid rafts regions as revealed by its presence in flotillin-containing fractions, a characteristic raft-positive protein (Fig 2d). The presence of other amine oxidases was also assessed in both WT and SSAO/VAP-1-expressing cells showing an absence of MAO B and a moderate MAO A activity with slightly increased

levels in SSAO/VAP-1-expressing cells compared to WT (data not shown).

*Effect of OGD and reoxygenation on the cell viability of WT and hSSAO/VAP-1-expressing hCMEC/D3 cells, and influence of SSAO activity.*

Both WT and hSSAO/VAP-1 hCMEC/D3 cells underwent OGD for different time periods (1 to 24 h). This treatment induced a decrease in cell viability reaching 50% of cell death after 24 h of OGD exposition. No differences between both cell types were observed at any of the analysed time-points (Fig 3a).

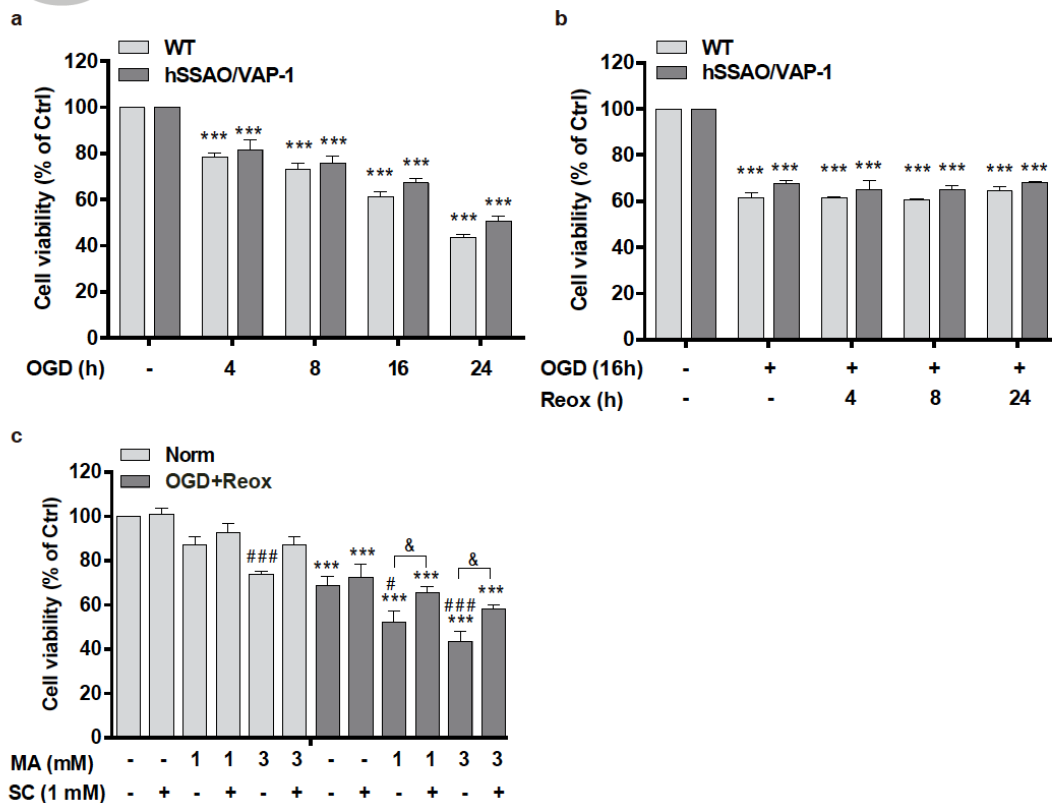


**Figure 3. Effect of OGD, OGD with reoxygenation, and methylamine (MA) on cell viability of wild type (WT) and human SSAO/VAP-1-transfected hCMEC/D3 cells (hCMEC/D3 hSSAO/VAP-1).** Different duration of OGD (a) or 16 h-OGD with different duration of reoxygenation (b) induces WT and hSSAO/VAP-1-transfected hCMEC/D3 cell death. MTT reduction assay was used to assess cell viability under the different assayed conditions. Cells without OGD were maintained under normoxia conditions, and are considered control cells (Ctrl). The metabolism of MA under 16 h-OGD plus 24 h of reoxygenation condition (OGD+Reox) (c) induces a reduction of cell viability in hSSAO/VAP-1-expressing hCMEC/D3 cells, which is partially prevented by the SSAO activity inhibitor semicarbazide (SC). MA (1 mM or 3 mM) and SC (1 mM) were added before OGD and maintained during reoxygenation. Control cells are non-treated cells in normoxia (Norm). Data are expressed as mean  $\pm$  SEM of at least 3 independent experiments. \*\*\* $P < 0.001$  versus control of the corresponding cell type. # $P < 0.05$  and ### $P < 0.001$  versus non-treated hSSAO/VAP-1-expressing hCMEC/D3 cells in the corresponding condition (Norm or OGD+Reox); & $P < 0.05$  between the indicated treatments. Statistical analyses were performed by a one-way ANOVA test and the addition of Newman-Keuls multiple comparison test.

A 16h OGD treatment inducing 40% cell death was selected to further study the effect of different reoxygenation times (4 to 24 h) after OGD. Results shown in Fig 3b revealed that the addition of reoxygenation did not increase cell death following OGD treatment. In order to assess whether the SSAO catalytic activity vs methylamine (MA) as specific substrate could contribute to the vascular damage under these conditions, a 16 h OGD with 24 h reoxygenation treatment was selected. SSAO/VAP-1-expressing cells were incubated in the presence of MA (1 and 3 mM) and/or semicarbazide (SC, 1 mM) under the OGD with reoxygenation conditions selected. Fig 3c shows that the presence of MA enhanced the loss of cell viability induced by OGD with re-oxygenation in a dose-dependent manner, which was partially recovered by SC, a specific SSAO inhibitor. These results confirm that the SSAO catalytic activity enhances the cell death induced by OGD with reoxygenation conditions.

*OGD with reoxygenation induces the release of soluble SSAO/VAP-1 into the culture media by hCMEC/D3 hSSAO/VAP-1 cells.*

The soluble SSAO/VAP-1 form derives from the membrane-bound protein by a shedding process that may be activated under some pathological conditions (Abella *et al.*, 2004; Sun *et al.*, 2014). In order to assess whether stroke can induce SSAO/VAP-1 release by human brain endothelial cells, concentrated culture media of SSAO/VAP-1-expressing cells subjected to different periods of OGD and OGD with reoxygenation were analysed using TNF- $\alpha$  as positive control (Fig 4a).

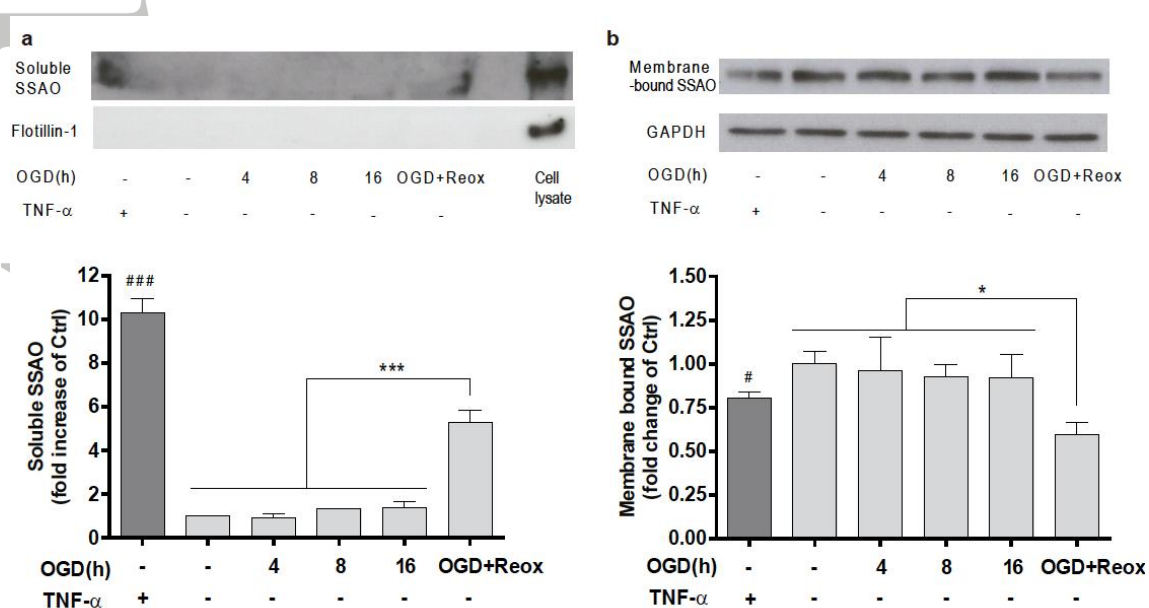


**Figure 4. OGD with reoxygenation induces the release of soluble SSAO to the culture media by hCMEC/D3 hSSAO/VAP-1 cells.** (a) Presence of soluble SSAO/VAP-1 in ten-fold concentrated culture media corresponding to TNF- $\alpha$  treatment (24 h in normoxia, 100 ng mL<sup>-1</sup>), different OGD times and 16 h-OGD with 24 h-reoxygenation (OGD+Reox). TNF- $\alpha$  was used as positive control of SSAO/VAP-1 release. Flotillin-1 was used as control of cell debris absence in the media. (b) Presence of membrane-bound SSAO/VAP-1 in hCMEC/D3 hSSAO/VAP-1 cell lysates under the same experimental conditions than in a. The presence of membrane-bound SSAO was normalized to the GAPDH levels. Non-treated cells or media under normoxia conditions were considered control samples (Ctrl). Data in graphs represent

the western blot quantifications and are expressed as mean  $\pm$  SEM of data obtained from 3 independent experiments. \* $P$ <0.05 and \*\*\* $P$ <0.001 as indicated; # $P$ <0.05 and ### $P$ <0.001 versus control cells, by a one-way ANOVA test and the addition of Newman-Keuls multiple comparison test.

The western blot results showed soluble SSAO/VAP-1 release into the medium occurred after 16 h OGD and 24 h reoxygenation by contrast to OGD only. This result correlated with the loss of signal observed in the membrane-bound form, obtained by analysing the cell lysates under the same experimental conditions (Fig 4b).

*DPH-4 attenuates the cell death induced by the SSAO-mediated methylamine metabolism in both normoxia and OGD with reoxygenation conditions in a dose-dependent manner.*

In order to determine a possible protective effect of DPH-4 in the stroke conditions, the above established experimental model with hSSAO/VAP-1-expressing hCMEC/D3 cells was compared with a peripheral endothelial model using hSSAO/VAP-1-expressing HUVEC cells, in the same conditions previously described (Sun *et al.*, 2014). Both endothelial cell lines were pre-incubated with DPH-4 (1  $\mu$ M) prior to addition of MA (3 mM) and subjected to OGD and re-oxygenation. A significant loss of cell viability was observed in the presence of MA (Fig. 5a,b) in normoxia as well as an enhancement of cell toxicity induced by OGD and reoxygenation.

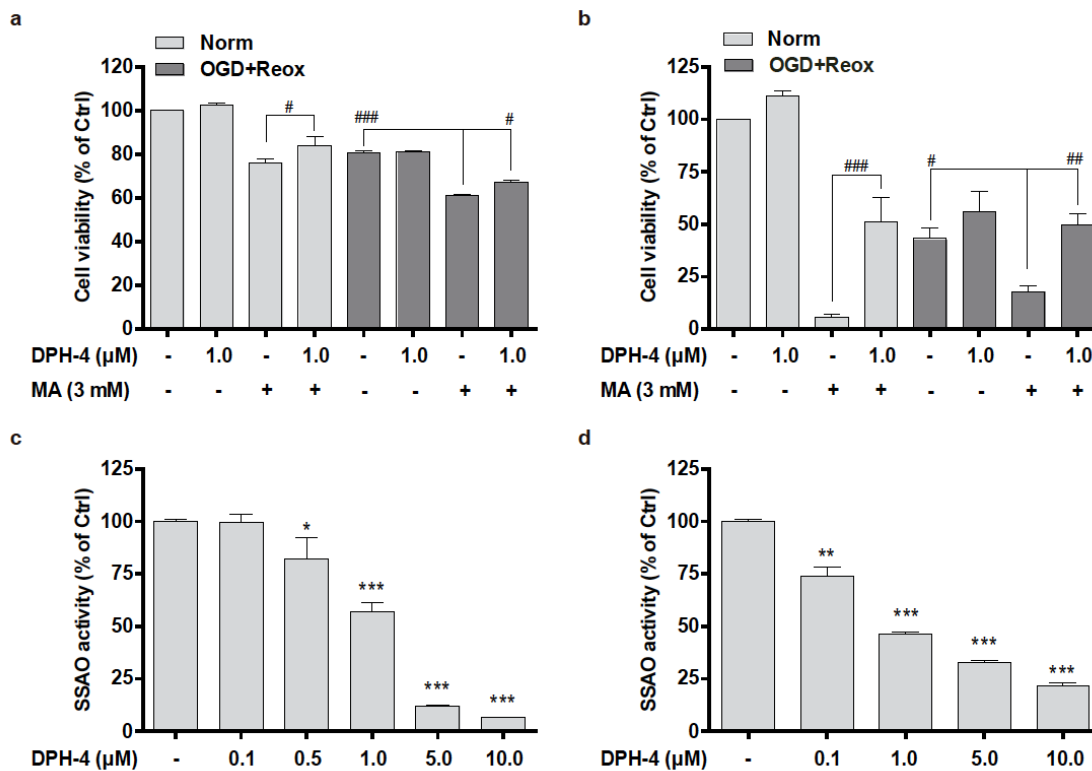


**Figure 5. DPH-4 attenuates the cell death induced by the metabolism of methylamine in normoxia or in OGD with reoxygenation conditions in different endothelial cell types.** MTT reduction assay was used to determine the cell viability of hCMEC/D3 hSSAO/VAP-1 cells subjected to 16 h-OGD with 24 h-reoxygenation (a), and HUVEC hSSAO/VAP-1 cells

subjected to 24 h-OGD with 7 h-reoxygenation (b). MA (3 mM) and DPH-4 (1  $\mu$ M) were added before OGD and maintained during reoxygenation. Non-treated endothelial cells under normoxia were used as control (Ctrl) cells. The SSAO activity inhibiting capacity of DPH-4 was determined by investigating SSAO activity remaining in hCMEC/D3 hSSAO/VAP-1 cell lysates after being incubated with DPH-4 (0.1-10  $\mu$ M) for 30 min (c), or by evaluating SSAO activity present in HUVEC hSSAO/VAP-1 cell lysates from DPH-4 (0.1-10  $\mu$ M)-treated cells for 24 h (d). SSAO activity was analyzed by radiometric method, using  $^{14}$ C-benzylamine as substrate. A non-treated cell lysate was considered the control (Ctrl) sample. Data in graphs are expressed as mean  $\pm$  SEM and represent data obtained from 3 independent experiments. \* $P$ <0.05, \*\* $P$ <0.01 and \*\*\* $P$ <0.001 versus non-treated samples; # $P$ <0.05, ## $P$ <0.01 and ### $P$ <0.001 as indicated, by a one-way ANOVA test and the addition of Newman-Keuls multiple comparison test.

The effect of MA was higher in HUVECs (Fig 5b) than in hCMEC/D3 cells (Fig 5a), revealing a greater resistance of the latter although showing higher SSAO/VAP-1 expression and activity levels (see Fig 2). Interestingly, the loss of cell viability was partially restored in both cell types in the presence of DPH-4, although the protective effect was surprisingly more significant in HUVECs (Fig 5b), reaching 50% recovery in normoxia and almost 100% under OGD with reoxygenation conditions, than in hCMEC/D3 (Fig 5a), which showed less cell toxicity with MA. These results confirmed the protective effect of DPH-4 on human brain endothelial cells expressing SSAO/VAP-1 in this experimental stroke model. The protective behaviour of DPH-4 might be explained by the SSAO activity inhibition, since it is clearly evidenced in the presence of MA. Thus, different concentrations of DPH-4 (0.1-10  $\mu$ M) were used to determine the inhibition of SSAO activity using  $^{14}$ C-benzylamine as substrate in both hSSAO/VAP-1-expressing hCMEC/D3 (Fig 5c) and HUVEC (Fig 5d) cells. Results revealed that DPH-4 inhibited SSAO activity with a rough IC<sub>50</sub> value of 1  $\mu$ M in both endothelial cell types from different vascular origin.

In order to determine whether this effect was concentration-dependent, we performed the same analysis using the hCMEC/D3 and different concentrations of DPH-4 (Fig 6).

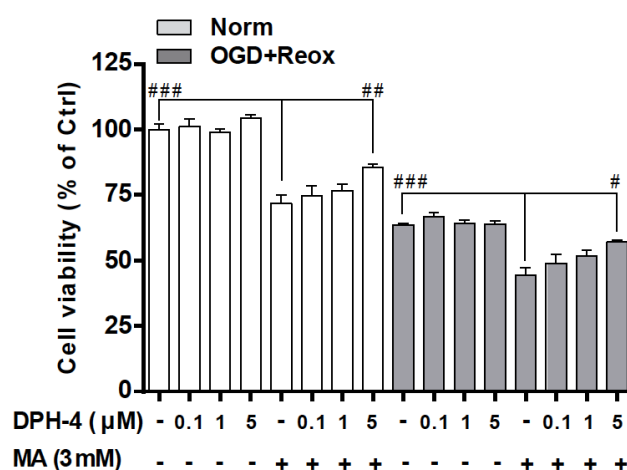


**Figure 6. Dose response effect of DPH-4 on hCMEC/D3 cell viability under OGD with reoxygenation.** MTT reduction assay was used to determine the cell viability of hSSAO/VAP-1-expressing hCMEC/D3 cells subjected to normoxia (Norm) or 16 h-OGD with 24 h-reoxygenation (OGD+Reox). MA (3mM) and DPH-4 (0.1, 1 and 5  $\mu$ M) were

added before OGD and maintained during reoxygenation. Data in graph are expressed as mean  $\pm$  SEM and represent data obtained from 3 independent experiments. <sup>#</sup> $P < 0.05$ , <sup>##</sup> $P < 0.01$  and <sup>###</sup> $P < 0.001$  as indicated, by a one-way ANOVA test and the addition of Newman-Keuls multiple comparison test.

These results showed that the 5  $\mu$ M concentration of DPH-4 was the most effective in protecting hCMEC/D3 cells from OGD and reoxygenation when MA was present. No effect was observed in the absence of MA.

*DPH-4 shows an anti-inflammatory activity preventing MA-induced leukocyte binding to hSSAO/VAP-1-expressing hCMEC/D3 cells subjected to OGD.*

BBB dysfunction and the occurrence of haemorrhages after stroke have been associated with leukocyte adhesion to brain endothelium and subsequent transmigration into the injured tissue. Because SSAO/VAP-1 mediates leukocyte extravasation, the anti-inflammatory behaviour of DPH-4 was assessed in hSSAO/VAP-1-expressing hCMEC/D3 cells under normoxia and OGD conditions as well as in the presence of MA by quantifying the binding of calcein-AM-labelled THP-1 leukocytes to the endothelial cells (Fig 7). The presence of MA induced an increase of leukocyte adhesion to the endothelium in hSSAO/VAP-1-expressing cells after short OGD (5 h, Fig 7a), long OGD (16 h, Fig 7b) and OGD with reoxygenation (16 h + 24 h, Fig 7c), while no effect was observed in WT cells after MA treatment, indicating that this inflammatory behaviour was induced by the catalytic action of SSAO with MA as substrate. This effect was prevented when cells were incubated in presence of DPH-4 in all the conditions assayed.

Accepted

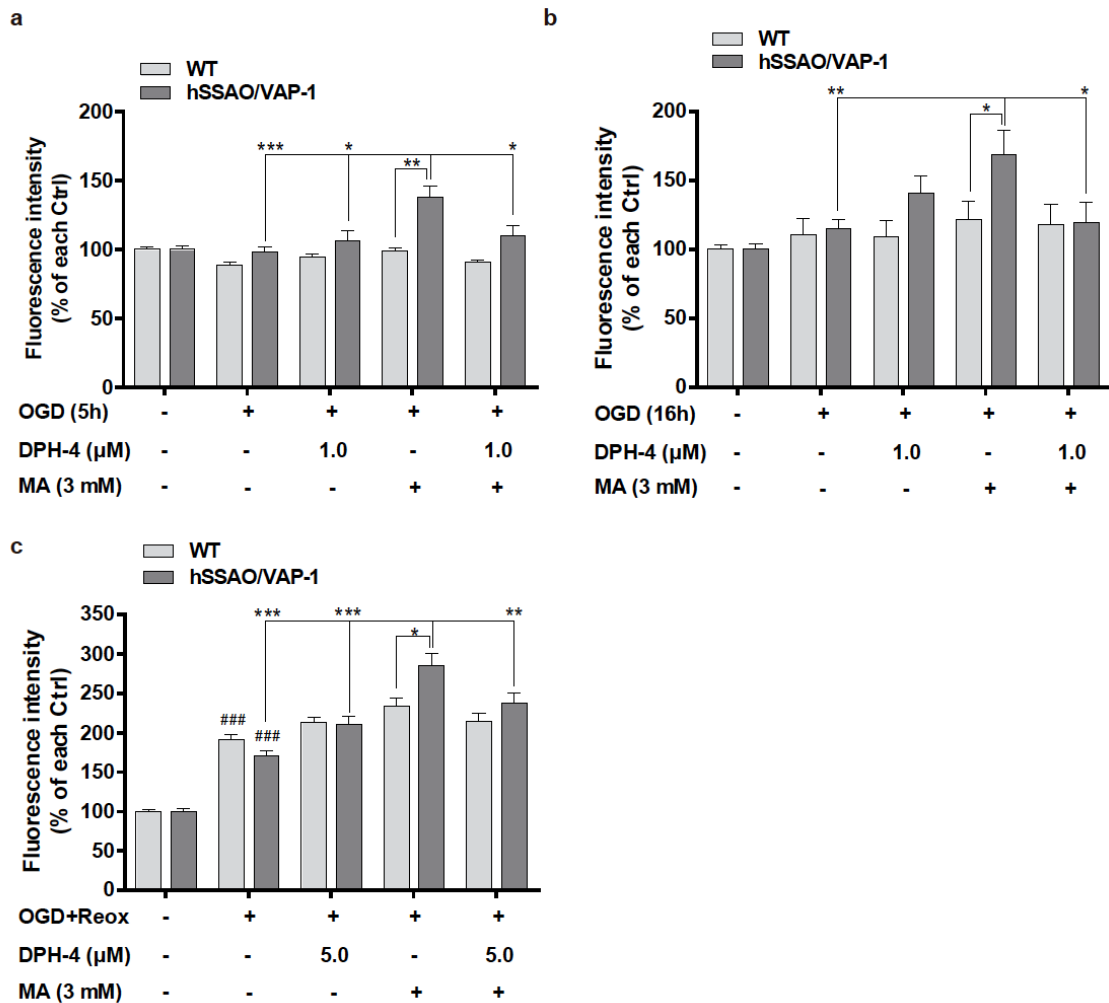


**Figure 7. DPH-4 prevents increased leukocyte adhesion to endothelial cells under different OGD conditions in presence of the SSAO substrate.** Leukocyte-endothelium adhesion assay was performed to analyze the anti-inflammatory effect of DPH-4 against SSAO mediated pro-inflammatory action. WT and hSSAO/VAP-1-expressing hCMEC/D3 cells treated with MA (3 mM) or/and DPH-4 (1 or 5 μM) undergo 5 h-OGD (a), 16h-OGD (b) or 16h-OGD with 24 h-reoxygenation (OGD+Reox, c) and the binding of calcein-AM-labelled THP-1 leukocytes on these cells was quantified. Non-treated cells under normoxia conditions were considered as control (Ctrl) for each type of cells. Data are expressed as mean ± SEM of three independent experiments. \* $P < 0.05$ , \*\* $P < 0.01$  and \*\*\* $P < 0.001$  versus hCMEC/D3 hSSAO/VAP-1 treated with MA under OGD conditions; ### $P < 0.001$  versus control of the corresponding cell type, by a one-way ANOVA and the addition of Newman-Keuls multiple comparison test.

In order to analyse whether other adhesion proteins would be involved in this adhesion process after OGD + reoxygenation, we also measured SSAO/VAP-1, VCAM-1, ICAM-1, P-selectin and E-selectin levels in SSAO/VAP-1-expressing hCMEC/D3 cells (Figure 8). ICAM-1 and E-selectin showed very low expression levels with no changes among the performed treatments (data not shown). SSAO/VAP-1 and VCAM-1 displayed similar behaviour, being decreased after the OGD + reox treatment and with no changes among the pharmacological treatments under these conditions. P-selectin showed non-significant changes after OGD + reox or other treatments.

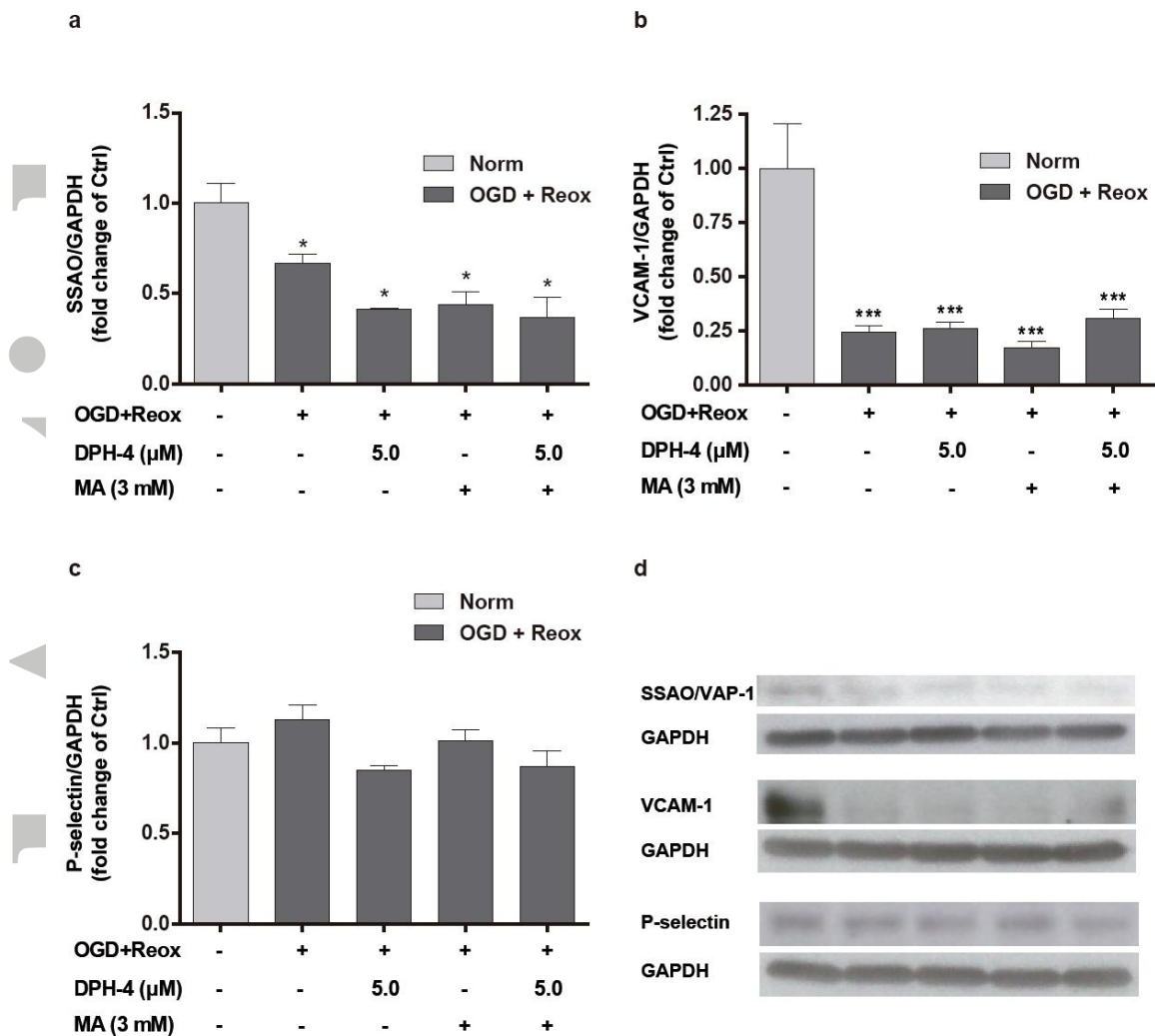


**Figure 8. Effect of DPH-4 on the response of other adhesion molecules to the OGD with reoxygenation stimulus and its role on the leukocyte adhesion on hCMEC/D3 endothelial cells.** Presence of membrane-bound SSAO/VAP-1 (a), VCAM-1 (b) and P-selectin (c) in hCMEC/D3 hSSAO/VAP-1 cell lysates subjected to 16 h-OGD with 24 h-reoxygenation (OGD+Reox) in the presence of DPH-4 (5  $\mu\text{M}$ ) and MA (3 mM). (d) Representative western blots. The presence of each protein was normalized to the GAPDH levels. Non-treated cells were considered control samples (Ctrl). Data in graphs represent the western blot quantifications and are expressed as mean  $\pm$  SEM of data obtained from at least 2 independent experiments. \* $P$ <0.05, \*\*\* $P$ <0.001 vs Ctrl, by a one-way ANOVA test and the addition of Newman-Keuls multiple comparison test.

*DPH-4 protects against cell death caused by the co-treatment of SSAO substrate methylamine (MA) and  $A\beta_{1-40}$ D in hCMEC/D3 hSSAO/VAP-1 cells under OGD with reoxygenation.*

In order to determine whether the presence of  $A\beta$  and SSAO/VAP-1 promoted vascular damage under ischemic conditions, as we previously described in normoxia (Solé *et al.*, 2015), cells under normoxia and OGD with reoxygenation were incubated in the presence of  $A\beta_{1-40}$ D and cell viability was determined. Both the co-treatment of MA with  $A\beta_{1-40}$ D (Fig

9a), and the 24 h pre-treatment with A $\beta$ <sub>1-40</sub>D (Fig 9b) induced an increased loss of the cell viability compared to that induced by either treatment under OGD with reoxygenation. The addition of DPH-4 in the presence of both treatments significantly increased cell viability; similar results were obtained when SC was used (data not shown).

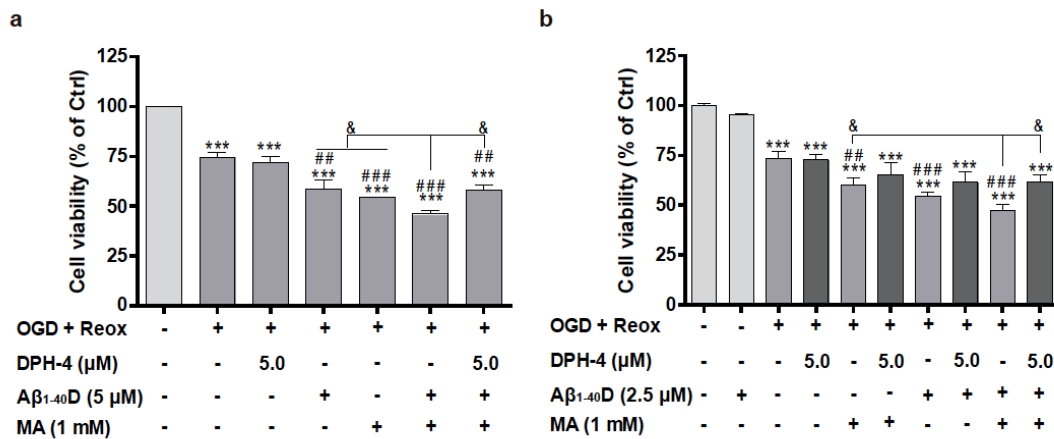


**Figure 9. DPH-4 protects against cell death caused by the co-treatment of SSAO activity and A $\beta$ <sub>1-40</sub>D in hCMEC/D3 hSSAO/VAP-1 cells under OGD with reoxygenation.** MTT reduction assay was used to evaluate the cell viability of hCMEC/D3 hSSAO/VAP-1 cells subjected to 16h-OGD with 24 h-reoxygenation (OGD+Reox) in the presence of A $\beta$ <sub>1-40</sub> containing the Dutch mutation (A $\beta$ <sub>1-40</sub>D, 2.5 or 5  $\mu$ M), MA (1 mM) or/and DPH-4 (5  $\mu$ M). (a) A $\beta$ <sub>1-40</sub>D (5  $\mu$ M), MA and DPH-4 were added at the same time before OGD. (b) A 24 h pre-treatment was performed with A $\beta$ <sub>1-40</sub>D (2.5  $\mu$ M) and cells were then subjected to 8 h-OGD with 24 h-reoxygenation. All treatments were maintained during reoxygenation. Non-treated cells under normoxia were considered as control (Ctrl). Data are expressed as mean  $\pm$  SEM of three independent experiments. \*\*\* $P$ <0.001 versus Ctrl; ## $P$ <0.05 and ### $P$ <0.001 versus non-treated cells under OGD+Reox; & $P$ <0.05 as indicated, by a one-way ANOVA test and the addition of Newman-Keuls multiple comparison test.

## Discussion & Conclusions

Cerebral hypoperfusion, atherosclerosis, oxidative stress, vascular A $\beta$  deposition or a failure of its clearance are insults that can disturb the transport of nutrients across the BBB. These alterations can lead to an acute and big failure of the cerebrovascular function due to brain ischemia or haemorrhage, contributing to the cognitive decline and dementia. Moreover, a deep meta-analysis recently reported that stroke significantly and independently increases the risk for AD and in turn, the risk of intracerebral haemorrhage (Zhou *et al.*, 2015). Furthermore, both hypoxia and ischemic injury induce the up-regulation of BACE 1 and increase the A $\beta$  generation (Guglielmotto *et al.*, 2009) confirming a link between AD and stroke.

Although the pathogenesis of AD is not yet fully understood, there is a clear consensus in describing it as a multifactorial disease caused by several agents, including BBB dysfunction. At present, it is widely accepted that a more effective therapy for the multifactorial nature of AD would result from the development of molecules aimed to interact with several or all the systems altered in this disorder. Among them, hybrid DPH-4 emerged as an interesting compound able to dually inhibit cholinesterase and monoamine oxidase activities with metal

chelating properties and hence, to show a great therapeutic interest for AD treatment (Wang *et al.*, 2014).

Because of the SSAO/VAP-1 alteration in AD (Ferrer *et al.*, 2002) and stroke (Hernández-Guillamón *et al.*, 2010), and due to its high expression in cerebrovascular tissue, we hypothesized that this protein could be a potential link and therapeutic target for both pathologies. However, the expression of some proteins is lost when cells are cultured, as it is the case for SSAO/VAP-1; therefore, we report for the first time the preparation of a human brain endothelial-immortalized cell line derived from the hCMEC/D3 cell line (Weksler *et al.*, 2005), that stably expresses the human SSAO/VAP-1 gene. The hCMEC/D3 hSSAO/VAP-1 cell line was characterized and compared with previously developed endothelial and smooth muscle cell lines expressing SSAO/VAP-1 (Solé and Unzeta, 2011; Solé, *et al.*, 2007). Then, we established a new experimental model of stroke consisting of subjecting these brain endothelial cells to OGD and reoxygenation conditions. The hCMEC/D3 cell line is the first stable well differentiated and well characterized human brain endothelial cell line (Weksler *et al.*, 2005) in terms of expression of endothelial markers, up-regulation of adhesion molecules in response to inflammatory cytokines, as well as BBB characteristics, so it was chosen as an accepted BBB cellular model (Weksler *et al.*, 2013), instead of peripheral endothelial HUVEC cells, because genes expressed by cerebral endothelial cells are important and distinct in several processes as vasculo- and angiogenesis (VEGF), immunoregulation (decorin, IL6) or have growth-supporting properties (BDNF, transforming growth factor- $\beta$ ) (Kalmann *et al.*, 2002). Although this cell line is a good approximation to a BBB model, it has some limitations and co-cultures including neurons and glia would be a better physiologic model.

Under OGD with reoxygenation conditions, cell viability was observed to be significantly decreased in the presence of MA, the main physiological SSAO/VAP-1 substrate, and restored when cells were pre-incubated in the presence of semicarbazide, a specific SSAO/VAP-1 inhibitor. These results confirmed that this enzyme plays an important role enhancing endothelial cell death under ischemia. Moreover, under these hypoxic conditions, membrane-bound SSAO/VAP-1 is released due to an increase in its shedding, likely resulting from the activation of metalloproteinase 2 (MMP-2) (Sun *et al.*, 2014). This soluble form of the enzyme may be also able to contribute to the vascular cell damage through its catalytic activity, as previously described by some of us (Hernández *et al.*, 2006). At the concentrations assayed, DPH-4 inhibits about 50% of the SSAO/VAP-1 activity. DPH-4 pre-treatment shows a dose-dependent protective effect on hSSAO/VAP-1-expressing hCMEC/D3 cells in the presence of MA in both normoxia and in OGD with reoxygenation conditions. This protection was found to be even more significant when the same experiment was carried out on hSSAO/VAP-1-expressing HUVEC cells. This different behaviour might be explained because cerebral endothelial cells are somewhat protected from cell death by the SV40T antigen that was used to in their immortalization, so are more hardy under difficult conditions. However, a different sensitivity of both cells to the toxicities generated by SSAO activity cannot be ruled out.

The beneficial effect of DPH-4 was also noticeable in terms of inflammation, since it significantly reduced the leukocyte adhesion to the endothelia subjected to different OGD conditions in the presence of MA, as a result of its inhibitory effect on the SSAO/VAP-1 activity. In this regard, the participation of other adhesion molecules cannot be ruled out, but it would be more likely to happen after the OGD + Reox stimulus, where both the WT and the SSAO/VAP-1-expressing cells increase the leukocyte adhesion, rather than in response to MA treatment, where leukocyte adhesion increases only in SSAO-expressing cells.

Moreover, although the western blot results show mainly a reduction of the membrane-bound form of these adhesion molecules, especially SSAO/VAP-1 and VCAM-1, it is worth to point out that both proteins can be shed to generate a soluble form, as we demonstrate for SSAO/VAP-1. As it is known the soluble SSAO/VAP-1 contributes to the adhesion process through the generation of H<sub>2</sub>O<sub>2</sub> and probably other unknown mechanisms. Therefore, it is reasonable to think that VCAM-1 could show a similar behaviour. This anti-inflammatory effect may also contribute to the protective effect observed in this experimental model of stroke.

In addition, when A $\beta$ <sub>1-40</sub>D treatment was introduced in this experimental model of ischemia simulating a pre-existing AD pathology, DPH-4 showed a protective effect on the synergic damage induced by MA and A $\beta$ <sub>1-40</sub>D. These results allow us to conclude that A $\beta$ <sub>1-40</sub>D together with the catalytic action of SSAO/VAP-1 induces more vascular damage under OGD with reoxygenation conditions, and that the protective effect of DPH-4 is higher than that observed using each toxic molecule separately.

To sum up, herein we report for the first time that DPH-4, a new MTDL hybrid, designed by juxtaposition of selected pharmacophoric groups present in donepezil, propargylamine, and 8-hydroxyquinoline, protects hCMEC/D3 hSSAO/VAP-1 cells under hypoxia conditions through its inhibitory and anti-inflammatory effect on SSAO/VAP-1. In the context of the close relationship between AD and stroke, and the involvement of SSAO/VAP-1 in both diseases, DPH-4 could be considered as a promising multivalent drug with potential therapeutic interest to be used in both neurological pathologies.

### **Funding**

This study was supported by the MINECO (Spanish Ministry of Economy and Competitiveness): projects SAF2006-08764-C02-01, SAF2009-07271 and SAF2012-33304.

### **Conflict of Interests**

The authors declare that they have no conflict of interest.

## References

- Abella A, García-Vicente S, Viguerie N, Ros-Baró A, Camps M, Palacín M *et al.*, (2004). Adipocytes release a soluble form of VAP-1/SSAO by a metalloprotease-dependent process and in a regulated manner. *Diabetologia* 47: 429-438.
- Airas L, Lindsberg PJ, Karjalainen-Lindsberg ML, Mononen I, Kotisaari K, Smith DJ *et al.*, (2008). Vascular adhesion protein-1 in human ischaemic stroke. *Neuropathol Appl Neurobiol* 34: 394-402.
- Birks J, Harvey RJ (2006). Donepezil for dementia due to Alzheimer's disease. *Cochrane Database Sys Rev* 1:CD001190.
- Bolea I, Gella A, Unzeta M (2013). Propargylamine-derived multitarget-directed ligands: fighting Alzheimer's disease with monoamine oxidase inhibitors. *J Neural Transm* 120: 893-902.
- Boomsma F, Bhaggoe UM, van der Houwen AM, van den Meiracker AH (2003). Plasma semicarbazide-sensitive amine oxidase in human (patho)physiology. *Biochim Biophys Acta* 1647: 48-54.
- Buccafusco JJ, Terry AV Jr (2000). Multiple central nervous system targets for eliciting beneficial effects on memory and cognition. *J Pharmacol Exp Ther* 295: 438-446.
- Cavalli A, Bolognesi ML, Minarini A, Rosini M, Tumiatti V, Recanatini M *et al.*, (2008). Multi-target-directed ligands to combat neurodegenerative diseases. *J Med Chem* 51: 347-372.
- Conklin DJ, Langford SD, Boor PJ (1998). Contribution of serum and cellular semicarbazide-sensitive amine oxidase to amine metabolism and cardiovascular toxicity. *Toxicol Sci* 46: 386-392.
- DiNapoli VA, Huber JD, Houser K, Li X, Rosen CL (2008). Early disruptions of the blood-brain barrier may contribute to exacerbated neuronal damage and prolonged functional recovery following stroke in aged rats. *Neurobiol Aging* 29: 753-64.
- El Hadri K, Moldes M, Mercier N, Andreani M, Pairault J, Fève B (2002). Semicarbazide sensitive amino oxidase in vascular smooth muscle cells; differentiation-dependent expression and role in glucose uptake. *Arterioscler Thromb Vasc Biol* 22: 89-94.
- Ferrer I, Lizcano JM, Hernández M, Unzeta M (2002). Overexpression of semicarbazide sensitive amine oxidase in the cerebral blood vessels in patients with Alzheimer's disease and cerebral autosomal dominant arteriopathy with subcortical infarcts and leukoencephalopathy. *Neurosci Lett* 321: 21-24.
- Geula C, Mesulam MM (1999) in *Alzheimer disease*, Cholinergic system in Alzheimer disease, eds Terry RD, Katzman R, Bick KL, Sisodia SS (Lippincott, Williams, and Wilkins, Philadelphia), Ed 2, pp 269-292.
- Grammas P (2011). Neurovascular dysfunction, inflammation and endothelial activation: implications for the pathogenesis of Alzheimer's disease. *J Neuroinflammation* 8, 26.

Guglielmotto M, Aragno M, Autelli R, Giliberto L, Novo E, Colombatto S *et al.*, (2009). The up-regulation of BACE1 mediated by hypoxia and ischemic injury: role of oxidative stress and HIF1 alpha. *J Neurochem* 108: 1045-1056.

Hernández M, Esteban M, Szabo P, Boada M, Unzeta M (2005). Human plasma semicarbazide sensitive amine oxidase (SSAO), beta-amyloid protein and aging. *Neurosci Lett* 384: 183-187.

Hernández M, Solé M, Boada M, Unzeta M (2006). Soluble semicarbazide sensitive amine oxidase (SSAO) catalysis induces apoptosis in vascular smooth muscle cells. *Biochim Biophys Acta* 1763: 164-173.

Hernández-Guillamón M, García-Bonilla L, Solé M, Sosti V, Parés M, Campos M *et al.*, (2010). Plasma VAP-1/SSAO activity predicts intracranial hemorrhages and adverse neurological outcome after tissue plasminogen activator treatment in stroke. *Stroke* 41: 1528-1535.

Hernández-Guillamón M, Solé M, Delgado P, García-Bonilla L, Giralt D, Boada C *et al.*, (2012). VAP-1/SSAO plasma activity and brain expression in human hemorrhagic stroke. *Cerebrovasc Dis* 33: 55-63.

Iadecola C (2010). The overlap between neurodegenerative and vascular factors in the pathogenesis of dementia. *Acta Neuropathol* 120: 287-296.

Iadecola C, Anrather J (2011). The immunology of stroke: from mechanisms to translation. *Nat Medicine* 17: 796-808.

Jalkanen S, Salmi M (2008). VAP-1 and CD73, endothelial cell surface enzymes in leukocyte extravasation. *Arterioscler Thromb Vasc Biol* 28: 18-26.

Kallmann BA, Wagner S, Hummel V, Buttman M, Bayas A, Tonn JC *et al.*, (2002). Characteristic gene expression profile of primary human cerebral endothelial cells. *FASEB J* 16: 589-591.

Kurkijärvi R, Adams DH, Leino R, Möttönen T, Jalkanen S, Salmi M (1998). Circulating form of human vascular adhesion protein-1 (VAP-1): increased serum levels in inflammatory liver diseases. *J Immunol* 161: 1549-1557.

León R, García, AG, Marco-Contelles J (2013). Recent advances in the multitarget-directed ligands approach for the treatment of Alzheimer's disease. *Med Res Rev* 33: 139-189.

Lizcano JM, Tipton KF, Unzeta M (1998). Purification and characterization of membrane-bound semicarbazide-sensitive amine oxidase (SSAO) from bovine lung. *Biochem J* 331: 69-78.

Marchesi VT (2014). Alzheimer's disease and CADASIL are heritable, adult-onset dementias that both involve damaged small blood vessels. *Cell Mol Life Sci* 71: 949-955.

Otsuka S, Kobayashi Y (1964). Radioisotopic assay for monoamine oxidase determinations in human plasma. *Biochem Pharmacol* 13: 995-1006.

Perry EK, Perry RH, Blessed G, Tomlinson BE (1977). Necropsy evidence of central cholinergic deficits in senile dementia. *Lancet* 1:189.

Plumb JA, Milroy R, Kaye SB (1989). Effects of the pH dependence of 3-(4,5-dimethylthiazol-2-yl)-2,5-diphenyl-tetrazolium bromide-formazan absorption on chemosensitivity determined by a novel tetrazolium-based assay. *Cancer Res* 49: 4435-4440.

Smith DJ, Salmi M, Bono P, Hellman J, Leu T, Jalkanen S (1998). Cloning of vascular adhesion protein 1 reveals a novel multifunctional adhesion molecule. *J Exp Med* 188: 17-27.

Solé M, Hernández M, Boada M, Unzeta M (2007). Characterization of A7r5 cell line transfected in a stable form by hSSAO/VAP-1 gene (A7r5 hSSAO/VAP-1 cell line). *J Neural Transm* 114: 763-767.

Solé M, Hernández-Guillamón M, Boada M, Unzeta M (2008). p53 phosphorylation is involved in vascular cell death induced by the catalytic activity of membrane-bound SSAO/VAP-1. *Biochim Biophys Acta* 1783: 1085-1094.

Solé M, Unzeta M (2011). Vascular cell lines expressing SSAO/VAP-1: a new experimental tool to study its involvement in vascular diseases. *Biol Cell* 103: 543-557.

Solé M, Miñano AJ, Unzeta M (2015). A cross-talk between A $\beta$  and endothelial SSAO/VAP-1 accelerates vascular damage and A $\beta$  aggregation related to CAA-AD. *Neurobiol Aging* 36: 762-775.

Sun P, Solé M, Unzeta M (2014). Involvement of SSAO/VAP-1 in oxygen-glucose deprivation-mediated damage using the endothelial hSSAO/VAP-1-expressing cells as experimental model of cerebral ischemia. *Cerebrovasc Dis* 37: 171-180.

Wang L, Esteban G, Ojima M, Bautista-Aguilera OM, Inokuchi T, Moraleda I *et al.*, (2014). Donepezil + propargylamine + 8-hydroxyquinoline hybrids as new multifunctional metal-chelators, ChE and MAO inhibitors for the potential treatment of Alzheimer's disease. *Eur J Med Chem* 80: 543-561.

Weksler BB, Subileau EA, Perrière N, Charneau P, Holloway K, Leveque M *et al.*, (2005). Blood-brain barrier-specific properties of a human adult brain endothelial cell line. *FASEB J* 19: 1872-1874.

Weksler BB, Romero IA, Couraud PO (2013). The hCMEC/D3 cell line as a model of the human blood brain barrier. *Fluids Barriers CNS* 10: 16.

Youdim MB, Buccafusco JJ (2005). CNS targets for multi-functional drugs in the treatment of Alzheimer's and Parkinson's diseases. *J Neural Transm* 112: 519-537.

Yu PH, Deng YL (1998). Endogenous formaldehyde as a potential factor of vulnerability of atherosclerosis: involvement of semicarbazide-sensitive amine oxidase-mediated methylamine turnover. *Atherosclerosis* 140: 357-363.

Zlokovic BV (2008). The blood-brain barrier in health and chronic neurodegenerative disorders. *Neuron* 57: 178-201.

Zhou J, Yu JT, Wang HF, Meng SF, Tan CC, Wang J *et al.*, (2015). Association between stroke and Alzheimer's disease: systematic review and meta-analysis. *J Alzheimers Dis* 43: 479-489.